

VOLUME 80

DECEMBER 16, 1976

NUMBER 26

JPCHAx

---

THE JOURNAL OF

PHYSICAL

CHEMISTRY

---



PUBLISHED BIWEEKLY BY THE AMERICAN CHEMICAL SOCIETY



# Tape Recordings for Lab Professionals

## ☐ **TLC—Best for Drug Abuse Screening**

Low-cost alternative to immunoassays

## ☐ **Microcomputers in Biochemistry Research**

New computers make possible hitherto impossible measurements

## ☐ **Data Analysis in the Lab**

Today and tomorrow in chem lab data analysis methods

## ☐ **Use of Enzymes in Immunology**

Detection of bound and free antigen without separation

## ☐ **Elemental Analysis of Blood: Cancer Patients & Controls**

Detailed comparisons, plus evaluation of analytical methods used

## ☐ **Polarographic Analysis in Drug Development**

D.P.P. assays of drugs in biological fluids

## ☐ **Bioanalysis with Membrane Electrode Probes**

Recent advances in electrode development

## ☐ **In Vivo Electrochemistry for Monitoring Drugs**

Reveals drug's chemical fate in the brain

## ☐ **Detection of Lipids & Amines in Biological Samples**

Chemical ionization mass spec speeds assay of closely related chemicals

## ☐ **Pulse Polarography Analysis in Environmental Toxicology**

Solves tough problems in human and animal poisoning

## ☐ **New Developments in Measurement of Proteins**

Light scattering of immune complexes provides a specific method for proteins in body fluids

## ☐ **Direct Determination of Drugs in Plasma & Urine**

Non-chromatographic procedure uses chemical ionization mass spec & stable isotope labeling

## ☐ **DSC: New Developments in Clinical Analysis**

Differential Scanning Calorimetry—a new analytical tool

## ☐ **Serum Electrolytes Using Vidicon Flame Spectrometry**

Fast, simultaneous determination of sodium, potassium, and calcium

## ☐ **Enthalpimetric Analysis of Immunological Reactions**

Thermometric enthalpy titration may revolutionize serological analysis

## ☐ **Clinical Application of Titration Calorimetry**

Thermochemical methods look very promising for clinical work

## ☐ **GC Determination of Apomorphine in Urine**

Study of apomorphine metabolism

## ☐ **Metals in Liver & Kidney Tissue by AA**

AA determination of copper, zinc, magnesium, and calcium

## ☐ **Bromazepam in Blood by Electron Capture GLC**

A sensitive, specific assay

## ☐ **Drug Analysis by Direct Multiple-Ion Detection**

Unique computerized system analyses drugs without use of GC

## ☐ **Thermochemical Analysis in Clinical Chemistry**

Total protein content in biological material can be determined with a precision of better than 0.6%

## ☐ **Amperometric Measurement of Enzyme Reactions**

Enzyme reactions are monitored by amperometric measurement of substrate depletion, product formation

## ☐ **Homovanillic Acid by GC-MS**

A simple procedure for HVA in urine

## ☐ **Kinetic Assay of Enzyme Activity**

Centrifugal fast analyzer provides data at output rate suitable for direct input into small computer

## ☐ **Automated Photochemical Analysis of Phenothiazines**

Samples were assayed by this system at the rate of 20 per hour

## ☐ **Automation in Clinical Medicine**

A Bureau of Standards colloquium

## ☐ **Analysis of Trace Elements**

Sensitive, reliable analytical methods are needed for trace elements

## ☐ **Electrochemical Approaches to Clinical Instrumentation**

Precise, accurate, highly specific analyses using ultramicro samples

## ☐ **Standardization of Protein & Enzyme Assays**

Biuret reaction as standard for measuring total serum protein

## ☐ **Pharmacologic Studies Using GC-MS**

Utility of GC-MS is emphasized in a report of two pharmacologic studies

## ☐ **Method Evaluation Studies in Clinical Analyses**

Method evaluation studies on precision and accuracy of lab methods

### ORDER FROM:

American Chemical Society  
1155 16th St., N.W.  
Washington, D.C. 20036  
ATTN: Dept. AP

PRICE: \$8.95 per title, includes visual materials. CASSETTES ONLY CHECK TITLES DESIRED  
(Allow 4 to 6 weeks for delivery)

Name \_\_\_\_\_

Address \_\_\_\_\_

# THE JOURNAL OF PHYSICAL CHEMISTRY

**BRYCE CRAWFORD, Jr.,** *Editor*  
**STEPHEN PRAGER,** *Associate Editor*  
**ROBERT W. CARR, Jr.,** **C. ALDEN MEAD,** *Assistant Editors*

**EDITORIAL BOARD:** C. A. ANGELL (1973–1977), F. C. ANSON (1974–1978), V. A. BLOOMFIELD (1974–1978), J. R. BOLTON (1976–1980), L. M. DORFMAN (1974–1978), H. L. FRIEDMAN (1975–1979), H. L. FRISCH (1976–1980), W. A. GODDARD (1976–1980), E. J. HART (1975–1979), W. J. KAUZMANN (1974–1978), R. L. KAY (1972–1976), D. W. McCLURE (1974–1978), R. M. NOYES (1973–1977), W. B. PERSON (1976–1980), J. C. POLANYI (1976–1980), S. A. RICE (1976–1980), F. S. ROWLAND (1973–1977), R. L. SCOTT (1973–1977), W. A. STEELE (1976–1980), J. B. STOTHERS (1974–1978), W. A. ZISMAN (1972–1976)

*Published by the*  
**AMERICAN CHEMICAL SOCIETY**  
**BOOKS AND JOURNALS DIVISION**  
D. H. Michael Bowen, Director

Editorial Department: Charles R. Bertsch,  
Head; Marianne C. Brogan, Associate  
Head; Celia B. McFarland, Joseph E.  
Yurvati, Assistant Editors

Graphics and Production Department:  
Bacil Guiley, Head

Research and Development Department:  
Seldon W. Terrant, Head

Advertising Office: Centcom, Ltd., 50 W.  
State St., Westport, Conn. 06880.

© Copyright, 1976, by the American  
Chemical Society. No part of this publication  
may be reproduced in any form without  
permission in writing from the American  
Chemical Society.

Published biweekly by the American  
Chemical Society at 20th and Northampton  
Sts., Easton, Pennsylvania 18042. Second  
class postage paid at Washington, D.C. and  
at additional mailing offices.

## Editorial Information

**Instructions for authors** are printed in  
the first issue of each volume. Please conform  
to these instructions when submitting man-  
uscripts.

**Manuscripts for publication** should be  
submitted to *The Journal of Physical  
Chemistry*, Department of Chemistry, Uni-  
versity of Minnesota, Minneapolis, Minn.  
55455. Correspondence regarding **accepted  
papers and proofs** should be directed to the  
Editorial Department at the ACS Easton  
address.

**Page charges** of \$60.00 per page are as-  
sessed for papers published in this journal.  
Ability to pay does not affect acceptance or  
scheduling of papers.

**Bulk reprints or photocopies** of indi-  
vidual articles are available. For information  
write to Business Operations, Books and  
Journals Division at the ACS Washington  
address.

Requests for **permission to reprint**  
should be directed to Permissions, Books and  
Journals Division at the ACS Washington  
address. The American Chemical Society and  
its Editors assume no responsibility for the  
statements and opinions advanced by con-  
tributors.

## Subscription and Business Information

1976 Subscription rates—including surface  
postage

	U.S.	PUAS	Canada, Foreign
Member	\$24.00	\$29.75	\$30.25
Nonmember	96.00	101.75	102.25
Supplementary material	15.00	19.00	20.00

**Air mail and air freight** rates are avail-  
able from Membership & Subscription Ser-  
vices, at the ACS Columbus address.

**New and renewal subscriptions** should  
be sent with payment to the Office of the  
Controller at the ACS Washington address.

**Changes of address** must include both old  
and new addresses with ZIP code and a recent  
mailing label. Send all address changes to the  
ACS Columbus address. Please allow six  
weeks for change to become effective. **Claims**  
for missing numbers will not be allowed if loss  
was due to failure of notice of change of ad-  
dress to be received in the time specified; if

claim is dated (a) North America—more than  
90 days beyond issue date, (b) all other for-  
eign—more than 1 year beyond issue date; or  
if the reason given is “missing from files”.  
Hard copy claims are handled at the ACS  
Columbus address.

**Microfiche subscriptions** are available  
at the same rates but are mailed first class to  
U.S. subscribers, air mail to the rest of the  
world. Direct all inquiries to Business Oper-  
ations, Books and Journals Division, at the  
ACS Washington address or call (202) 872-  
4444. **Single issues** in hard copy and/or mi-  
crofiche are available from Special Issues  
Sales at the ACS Washington address. Cur-  
rent year \$4.75. Back issue rates available  
from Special Issues Sales. **Back volumes** are  
available in hard copy and/or microform.  
Write to Special Issues Sales at the ACS  
Washington address for further information.  
**Microfilm** editions of ACS periodical pub-  
lications are available from volume 1 to the  
present. For further information, contact  
Special Issues Sales at the ACS Washington  
address. **Supplementary material** must be  
ordered directly from Business Operations,  
Books and Journals Division, at the ACS  
Washington address.

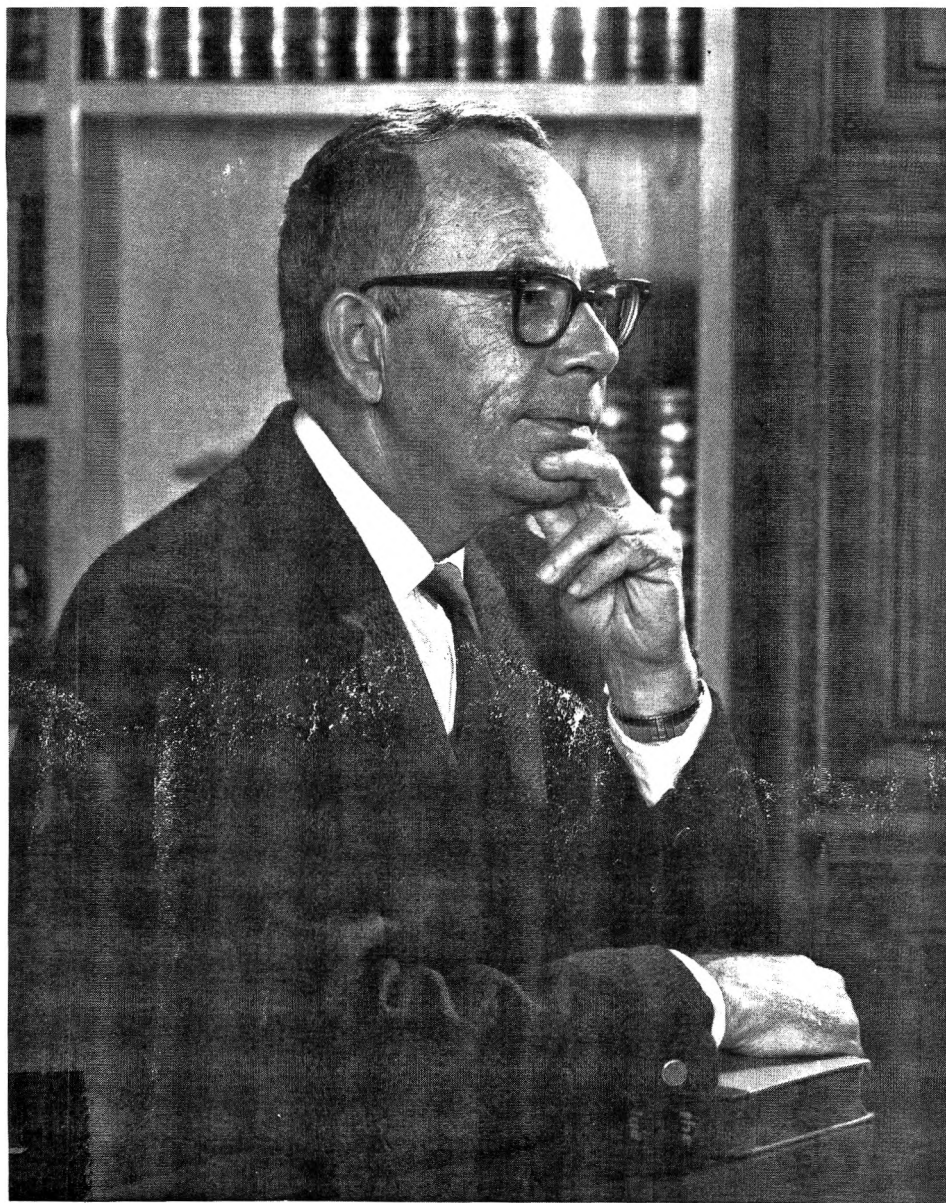
	U.S.	PUAS, Canada	Other Foreign
Microfiche			
Photocopy	\$2.50	\$3.00	\$3.50
1–7 pages	4.00	5.50	7.00
8–20 pages	5.00	6.50	8.00

Orders over 20 pages are available only on  
microfiche, 4 × 6 in., 24X, negative, silver  
halide. Orders must state photocopy or mi-  
crofiche if both are available. Full biblio-  
graphic citation including names of all au-  
thors and prepayment are required. Prices  
are subject to change.

American Chemical Society  
1155 16th Street, N.W.  
Washington, D.C. 20036  
(202) 872-4600

Member & Subscription Services  
American Chemical Society  
P.O. Box 3337  
Columbus, Ohio 43210  
(614) 421-7230

Editorial Department  
American Chemical Society  
20th and Northampton Sts.  
Easton, Pennsylvania 18042  
(215) 258-9111





*The Editors join with his former students and  
research associates in dedicating this issue  
of The Journal of Physical Chemistry to*

**Joe L. Franklin, Jr.**

*on the occasion of his seventieth year*

## JOE L. FRANKLIN JR.

Only rarely does one encounter a man whose professional contributions and achievements span a gap as wide as that from petroleum refining technology to fundamental chemical physics and, at the same time, whose warm and friendly personality endears him to those fortunate to have been associated with him. Such a man is Professor J. L. Franklin. To many chemists, chemical engineers, and chemical physicists he has been advisor, colleague, teacher, and valued friend, and to all who know him he has been, by his personal example, an inspiration. Because so many areas of physical chemistry, both applied and fundamental, as well as many of its practitioners, owe so much to his guidance and stimulation, it is very appropriate that this issue of *The Journal of Physical Chemistry* be dedicated to him during his first year of formal retirement.

Although Joe Franklin is often thought of as a Texan, it should be recorded here that he is actually a native son of Natchez, Mississippi who later became a naturalized Texan. His higher education at the University of Texas resulted in a B.S. in 1929 and an M.S. in 1930 in chemical engineering. During 1930–1931 he was a Fellow at the Massachusetts Institute of Technology and in the following year returned to the University of Texas to pursue graduate study in physical chemistry, under Professor E. P. Schoch, for which he was awarded the Ph.D. in 1934.

His first position after receiving the Ph.D. was that of Research Chemist with the Humble Oil and Refining Company in Baytown, Texas. For the next 29 years, with the exception of a leave of absence during 1957–1958, spent as a guest scientist at the National Bureau of Standards, he was engaged in the research and development effort of this company. Advancing through the ranks of the Refining Technical and Research Division, he became Assistant Section Head in 1936, Section Head in 1938, Assistant Division Head in 1945 and Research Associate in 1947. This latter post was held until 1963 when he accepted the Chair of Robert A. Welch, Professor of Chemistry at Rice University. Now in his first year of formal retirement from this latter position, he has just recently celebrated his seventieth birthday.

For the first 15 years with the Humble Oil and Refining Company, Professor Franklin was involved principally in petroleum refining technology and chemical engineering. During this time he became more and more devoted to scientific fundamentals and to the goal of understanding petroleum technology on the basis of these fundamentals. Probably the turning point in his career was reached in 1949, as reflected by the nature of two of his papers that appeared that year in *Industrial and Engineering Chemistry*. One paper, of an applied nature, and of considerable significance to petroleum refining, dealt with the propane dewaxing of paraffin distillates; the other, of more fundamental interest, introduced the Franklin group-equivalent method of estimating the standard enthalpies and free energies of formation of organic compounds. His papers after 1949 reveal a departure from active participation in applied research and a total dedication to fundamental science. During the next few years he extended the group-equivalent method to include gaseous free radicals and ions and began the fundamental studies of gaseous ion chemistry for which he is best known.

Several joint papers with F. H. Field in 1953 on the thermochemical properties of gaseous ions marked the beginning of a collaboration of many years, which, in addition to producing a large quantity of high quality research papers, resulted in the appearance in 1957 of their well-known book, "Electronic Impact Phenomena and the Properties of Gaseous Ions". The widely known studies of ion-molecule reactions, in which the writer was privileged to participate, began in 1956 and played a very significant role in opening an area of research that has become a very active one in physical chemistry. Professor Franklin's intense interest in ion-molecule reactions continues to this day and such studies remain one of his major activities.

It was a loose-knit group of co-workers in gaseous ion chemistry at Humble during the latter part of the 1950's because there were few, if indeed any, administrative bonds cementing the members. Only near the end of the Humble period did Professor Franklin's name appear in the same box on the company organization chart with any of his co-workers. Yet, despite the lack of administrative ties—and probably due much more to Professor Franklin than the rest of us realized at the time—the group of collaborators not only held together and produced significant work but actually grew. J. H. Futrell began participation in the ion-chemistry studies in 1958 and M. S. B. Munson in 1960. The existence of such a group for a prolonged period in an industrial research laboratory can only have been due to the personality of the man to whom this issue of *The Journal of Physical Chemistry* is dedicated.

Such character and achievement do not go unnoticed and it was really no surprise when in 1963 Franklin was offered and accepted the post of Robert A. Welch Professor of Chemistry at Rice University. Characteristically, he lost no time, after moving to Rice, in getting his research program under way. Not only did he continue in the area of research he had left at Humble, but expanded his efforts to include many new areas. Since 1963, with numerous graduate students and post-doctoral fellows, many of whom are authors of papers in this issue, he had produced very significant work in the following areas: ion-molecule reactions; energetics of gaseous ions; kinetic energies of ions formed in fragmentation processes; reactions in electric discharges; photoelectron spectroscopy; and kinetics of hydrocarbon combustion. Although he is now formally retired, none of his friends expects to notice any decline in his research output.

Quite characteristically, Professor Franklin has been generous with his time and experience to scientific organizations also, and of course is a member of many. He served for many years as a member of the Advisory Board for *Advances in Petroleum Chemistry and Refining* and on the Advisory Committees of Research Projects 50 and 54 of the American Petroleum Institute. He was one of the founders of the American Society for Mass Spectrometry and served as its first president during 1969–1970.

The achievements of J. L. Franklin have been recognized by the American Chemical Society in the form of the Southwest Regional Award in 1962 and the Southeast Texas Section Award in 1970. Also recognizing his accomplishments has been the American Institute of Chemical Engineers through the South Texas Section Publication Award in 1949 and the



Distinguished Service Award in 1962. In 1973 he was named a Distinguished Alumnus of the University of Texas.

At the 1975 meeting in Houston, the American Society for Mass Spectrometry dedicated a Symposium to him and arranged to have a lecture by a distinguished scientist in each of the areas in which Professor Franklin has been active. The collected papers of this symposium were published in an issue of the *International Journal of Mass Spectrometry and Ion Physics*. Not surprisingly, however, the number of colleagues, collaborators, and good friends of Joe Franklin were in considerable excess of the number of papers that could be scheduled at the Franklin Symposium in 1975. Following this

meeting several of us decided the dedication of an issue of *The Journal of Physical Chemistry* would be a fitting way of expressing our fondness and esteem for a man who has so significantly influenced our profession and our lives. At least one author of each paper in this issue is a person who has worked closely in one capacity or another with Professor Franklin and we present these papers as a token of our deep appreciation to him.

F. W. Lampe  
The Pennsylvania State University

THE JOURNAL OF  
PHYSICAL CHEMISTRY

---

Volume 80, Number 26 December 16, 1976

JPCA 80(26) 2811-2928 (1976)

ISSN 0022-3654

Hydrogen-Atom Initiated Decomposition of Monosilane . . .	<b>E. R. Austin and F. W. Lampe*</b>	2811
Ion-Molecule Reactions of Cyclic Borazine Cations. Thermodynamic and Kinetic Considerations . . . . .	<b>Anthony J. DeStefano and Richard F. Porter*</b>	2818
A Time-Resolved Study of the Unimolecular Fragmentation of Some $C_6H_6^+$ Molecular Ions . . . . .	<b>Paul P. Dymerski and Alex. G. Harrison*</b>	2825
On the Measurements of Vibrational Intensity in the Photoelectron Spectra of Oxygen for the Ionic Ground State . . . . .	<b>P. Natalis</b>	2829
High-Pressure Mass Spectra and Gaseous Ion Chemistry of Metal Acetylacetonates . . . . .	<b>Steven M. Schildcrout</b>	2834
Identification of Bacteria Using Linear Programmed Thermal Degradation Mass Spectrometry. The Preliminary Investigation . . . . .	<b>Terence H. Risby and Alfred L. Yergey*</b>	2839
Arrival Time Distributions in High Pressure Mass Spectrometry. 5. Effect of $E/P$ on Measured Apparent Heats and Entropies of Reaction . . . . .	<b>G. G. Meisels,* R. K. Mitchum, and J. P. Freeman</b>	2845
Thermochemistry of Alkyl Ions . . . . .	<b>Alan Goren and Burnaby Munson*</b>	2848
The Nominal Butyl Ester Ion in the Mass Spectra of Long-Chain $n$ -Alkyl Esters . . . . .	<b>Seymour Meyerson,* E. S. Kuhn, Imre Puskas, and E. K. Fields</b>	2855
The Thermochemistry of $C_2H_4O^+$ Ions . . . . .	<b>John L. Holmes,* J. K. Terlouw, and F. P. Lossing*</b>	2860
Thermodynamic Properties of Dilute Sulfuric Acid and the Potential of the Lead Sulfate-Lead Electrode . . . . .	<b>Kenneth S. Pitzer</b>	2863
Unimolecular Thermal Decomposition Reactions of Gaseous Carbonium Ions . . . . .	<b>M. Meot-Ner and F. H. Field*</b>	2865
Consistency between Kinetics and Thermodynamics . . . . .	<b>M. Boudart</b>	2869
Terminal Ions in Weak Atmospheric Pressure Plasmas. Applications of Atmospheric Pressure Ionization to Trace Impurity Analysis in Gases . . . . .	<b>M. W. Siegel and W. L. Fite*</b>	2871
Collision Induced Singlet to Triplet Transition of Methylene. 2. Numerical Tests of Two Theories . . . . .	<b>Kenneth C. Kulander and John S. Dahler*</b>	2881
Application of a Modified Elastic Spectator Model to Proton Transfer Reactions in Polyatomic Systems . . . . .	<b>M. L. Vestal,* A. L. Wahrhaftig, and J. H. Futrell</b>	2892





Titles from the series currently available:

**Chemical Thermodynamics, Vol. 1**  
Senior Reporter: Prof. M. L. McGlashan  
362 pages Cloth (1973) \$30.25

**Molecular Spectroscopy, Vol. 3**  
Senior Reporters: Prof. D. A. Long, Prof.  
D. J. Millen, Dr. R. F. Barrow  
(1973-74 literature)  
602 pages Cloth (1975) \$66.00

**Theoretical Chemistry**, Vol. 2  
Senior Reporter: Prof. R. N. Dixon  
200 pages Cloth (1975) \$27.50

Title	No. Copies	Price
		Total _____
<input type="checkbox"/> Enclosed is my check for \$ _____ <input type="checkbox"/> Bill me		
Postage at 40 cents per copy if other than U.S. or Canada.		
Name _____		
Address _____		
City _____	State _____	Zip _____

Reactions of Saturated Hydrocarbons in the Presence of Deuterium on Evaporated Iron Films . . . . .	<b>Robert S. Dowie, Charles Kemball, and David A. Whan*</b>	2900
A Study of the Mechanism of ( <sup>2</sup> P) Carbon Ion Reactions with Benzene at 1.0–12 eV . . . . .	<b>Richard D. Smith and James J. DeCorpo*</b>	2904
Role of Impact Parameters in Branching Reactions. Chemical Accelerator Study of the Reactions of Kr <sup>+</sup> with Methane . . . . .	<b>J. R. Wyatt, L. W. Strattan, and P. M. Hierl*</b>	2911
Rate Constants at 297 K for Proton-Transfer Reactions with HCN and CH <sub>3</sub> CN. Comparisons with Classical Theories and Exothermicity . . . . .	<b>G. I. Mackay, L. D. Betowski, J. D. Payzant, H. I. Schiff, and D. K. Bohme*</b>	2919
Photoelectron Spectra of 1,2-Dibromo-1,1-difluoroethane, 1,2-Bromochloroethane, and 1,2-Dichloro-, 1,2-Dibromo-, and 1,2-Diodotetrafluoroethane . . . . .	<b>F. T. Chau and C. A. McDowell*</b>	2923

There is no supplementary material for this issue.

\* In papers with more than one author, the asterisk indicates the name of the author to whom inquiries about the paper should be addressed.

#### COPIES OF THIS ISSUE

Copies of this issue may be purchased for \$4.75 each. Send orders to Business Operations, American Chemical Society, 1155 Sixteenth St., N.W., Washington, D.C. 20036. Payment must be sent with the order.



## AUTHOR INDEX

- |                        |                       |                       |                          |
|------------------------|-----------------------|-----------------------|--------------------------|
| Austin, E. R., 2811    | Fite, W. L., 2871     | Mackay, G. I., 2919   | Schiff, H. I., 2919      |
| Betowski, L. D., 2919  | Freeman, J. P., 2845  | McDowell, C. A., 2923 | Schildcrout, S. M., 2834 |
| Bohme, D. K., 2919     | Futrell, J. H., 2892  | Meisels, G. G., 2845  | Siegel, M. W., 2871      |
| Boudart, M., 2869      | Goren, A., 2848       | Meot-Ner, M., 2865    | Smith, R. D., 2904       |
| Chau, F. T., 2923      | Harrison, A. G., 2825 | Meyerson, S., 2855    | Strattan, L. W., 2911    |
| Dahler, J. S., 2881    | Hierl, P. M., 2911    | Mitchum, R. K., 2845  | Terlouw, J. K., 2860     |
| DeCorpo, J. J., 2904   | Holmes, J. L., 2860   | Munson, B., 2848      | Vestal, M. L., 2892      |
| DeStefano, A. J., 2818 | Kemball, C., 2900     | Natalis, P., 2829     | Wahrhaftig, A. L., 2892  |
| Dowie, R. S., 2900     | Kuhn, E. S., 2855     | Payzant, J. D., 2919  | Whan, D. A., 2900        |
| Dymerski, P. P., 2825  | Kulander, K. C., 2881 | Pitzer, K. S., 2863   | Wyatt, J. R., 2911       |
| Field, F. H., 2865     | Lampe, F. W., 2811    | Porter, R. F., 2818   | Yergey, A. L., 2839      |
| Fields, E. K., 2855    | Lossing, F. P., 2860  | Puskas, I., 2855      |                          |
|                        |                       | Risby, T. H., 2839    |                          |

# THE JOURNAL OF PHYSICAL CHEMISTRY

Registered in U. S. Patent Office © Copyright, 1976, by the American Chemical Society

VOLUME 80, NUMBER 26 DECEMBER 16, 1976

## Hydrogen-Atom Initiated Decomposition of Monosilane

E. R. Austin and F. W. Lampe\*

Davey Laboratory, Department of Chemistry, The Pennsylvania State University,  
University Park, Pennsylvania 16802 (Received February 6, 1976)

Publication costs assisted by the U.S. Energy Research and Development Administration

The H-atom initiated decomposition of  $\text{SiH}_4$  at room temperature produces mainly  $\text{H}_2$ ,  $\text{Si}_2\text{H}_6$ , and a solid deposit with trace amounts of  $\text{Si}_3\text{H}_8$  and  $\text{Si}_4\text{H}_{10}$  appearing later as secondary products. The initial reaction appears to be nearly completely described by a gas-phase conversion of  $\text{SiH}_4$  to  $\text{Si}_2\text{H}_6$  and  $\text{H}_2$  but the secondary gas-phase reactions are strongly influenced by surface reactions involving silicon hydride polymer. Detailed studies of the H-D distribution in the disilane product of an equimolar mixture of  $\text{SiH}_4$  and  $\text{SiD}_4$  show conclusively that the disilane is formed by insertion reactions of  $\text{SiH}_2$ ,  $\text{SiHD}$ , and  $\text{SiD}_2$  radicals into  $\text{SiH}_4$  and  $\text{SiD}_4$  and that combination of  $\text{SiH}_3$  and  $\text{SiD}_3$  radicals play virtually no role.

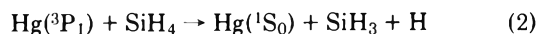
### Introduction

The decomposition of gaseous monosilane at room temperature is known to be initiated by the attack of atoms and free radicals according to

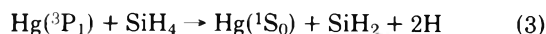


in which  $\text{R} = \text{H}$ ,<sup>2-5</sup>  $\text{D}$ ,<sup>3,5-7</sup>  $\text{CH}_3$ ,<sup>8-11</sup>  $\text{CF}_3$ ,<sup>12,13</sup>  $\text{C}_2\text{H}_5$ ,<sup>14</sup> and  $\text{C}_3\text{H}_7$ .<sup>14</sup> As a result of these recently reported studies,<sup>2-14</sup> Arrhenius parameters for (1a) have been well established. In the determination of the Arrhenius parameters of (1a), attention has generally been concentrated either on the formation of  $\text{RH}$  or on the disappearance of  $\text{R} \cdot$ ; comparatively little attention<sup>4</sup> has been given to the details of the reactions of the  $\text{SiH}_3$  radicals formed and to the formation of stable products containing silicon.

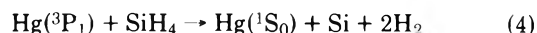
The decomposition of monosilane is also known to be induced by mercury( $^3\text{P}_1$ ) photosensitization.<sup>15-19</sup> There is no doubt that one of the elementary reactions of monosilane with excited mercury atoms is that shown by



Moreover, it is clear that (2) is followed rapidly by (1a) (for  $\text{R} = \text{H}$ ), so that one interaction of  $\text{Hg}(^3\text{P}_1)$  with  $\text{SiH}_4$  yields two  $\text{SiH}_3$  radicals and an  $\text{H}_2$  molecule. Quantum yields<sup>17,18</sup> of products of the mercury photosensitized decomposition indicate strongly that (2) cannot be the only elementary reaction between  $\text{Hg}(^3\text{P}_1)$  and  $\text{SiH}_4$ . Other reactions that have been suggested<sup>17,18</sup> are

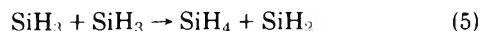


and



although nitric oxide scavenging studies<sup>19</sup> suggest that (3) is probably not very important, if it occurs at all.

The major silicon-containing gaseous product of both the H-atom (D-atom) sensitized and  $\text{Hg}(^3\text{P}_1)$ -sensitized decomposition of monosilane is disilane. This product clearly is formed in the H-atom initiated system by further reactions of the  $\text{SiH}_3$  radicals produced in (1a), and in  $\text{Hg}(^3\text{P}_1)$  photosensitization from further reactions of the Si-containing products of (2)–(4). The isotopic disilanes formed when H atoms are generated in the presence of equimolar amounts of  $\text{SiH}_4$  and  $\text{SiD}_4$  have been reported<sup>4</sup> to consist predominantly of isomers containing even numbers of H and D atoms. This observation led to the suggestion<sup>4</sup> that the mechanism of disilane formation from silyl radicals is that shown in



and



In addition to disilane, very small amounts of trisilane, tetrasilane, and a solid polymeric silicon hydride are formed as products of the mercury photosensitized decomposition<sup>15,17-19</sup> of monosilane. The literature is not clear with regard to for-



mation of silicon-containing gaseous products and solid polymer in the free-radical induced decompositions of monosilane, i.e., (1a). However, disilane is known to be formed as a result of H-atom attack on  $\text{SiH}_4$  and it has been reported<sup>14</sup> that solid polymer is formed in the ethyl and propyl radical initiated decompositions of monosilane.

This paper describes a mass-spectrometric study of the hydrogen-atom initiated decomposition of monosilane in which attention is centered on the further reactions of the silyl radicals produced by process 1.

## Experimental Section

Silyl radicals were generated by mercury photosensitization of hydrogen-monosilane mixtures which in all cases consisted of about 95% hydrogen. The quenching cross sections<sup>18,20</sup> for mercury resonance radiation suggest that under these conditions more than 94% of the  $\text{Hg}(^3\text{P}_1)$  atoms which are quenched by collision react with hydrogen, thereby forming hydrogen atoms. Reported values of rate constants of hydrogen atom reactions<sup>5,6</sup> indicate that all the atomic hydrogen formed will react with monosilane via (1) to form silyl radicals. Therefore reactions 2 and 3 can play only a minor role in the generation of silyl radicals.

The reactions were carried out in a photolysis cell containing a pinhole leak leading into the ionization region of a Bendix Model 14-101 time-of-flight mass spectrometer. A diagram of the apparatus is shown in Figure 1. The total length of the photolysis cell is 12.9 cm. The cylindrical section, which comprises 95% of the total volume, has a diameter of 1.90 cm and the total volume of the photolysis cell is 32.9  $\text{cm}^3$ . The diameter of the pinhole leak is  $2.1 \times 10^{-3}$  cm and the foil thickness is  $3.3 \times 10^{-3}$  cm. The photolysis cell is connected via 0.25-in. diameter stainless steel and 6-mm diameter pyrex tubing to a large reservoir (5–12 l.) containing the reactants. Reactant gases are at all times contained in both the reservoir and the photolysis cell and flow continuously through the pinhole leak into the ion source. The flow rates are such that over the course of an experiment (typically 20–25 min) the pressure decrease in the reservoir is of the order of 3% or less.

Photolysis products are formed and contained only in the photolysis cell. Since they flow through the pinhole into the ion source, their concentrations in the cell will increase with time of irradiation until their formation rates in the cell are equal to their loss rate from the cell. For a chemically stable product, leakage from the cell through the pinhole is the sole loss process determining this steady-state concentration and the rate of approach to it. For a product which reacts further, leakage through the pinhole represents only one of two or more loss channels.

The nature of the flow through the pinhole is an important experimental parameter in our experiments and some discussion is warranted. Over the range of pressures employed in our experiments (10–30 Torr) the ratio of the pinhole diameter to mean free path is in the range of 0.7–2. One would expect<sup>21</sup> the flow to be in the transition region between molecular and viscous flow but closer to molecular flow. In molecular flow the leakage rate of a substance from the cell should be first order in concentration and the first-order rate constant should be inversely proportional to the square root of the mass. If the flow is viscous all substances present should leak from the cell at the same rate. We have investigated the kinetic nature of the cell leakage by carrying out the mercury photosensitization of 95:5  $\text{H}_2$ - $\text{C}_2\text{H}_4$  mixtures to produce the two well-known stable products of this reaction,<sup>22</sup> namely,  $\text{C}_2\text{H}_6$

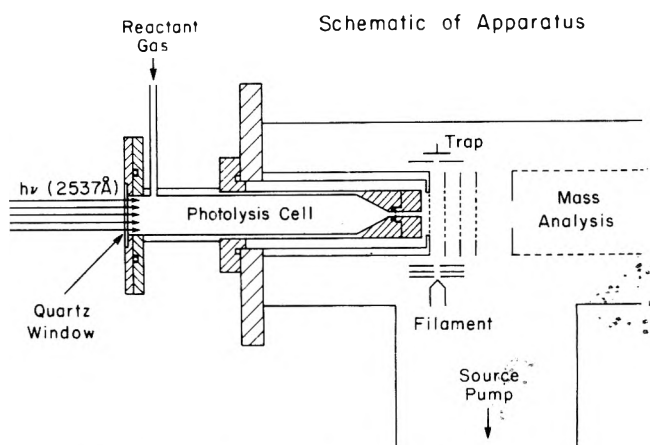


Figure 1. Schematic diagram of the apparatus.

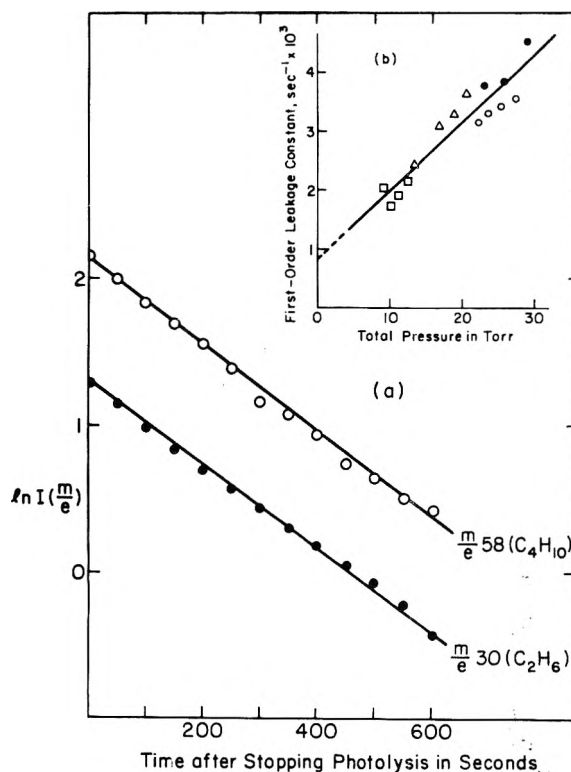


Figure 2. Flow rate out of photolysis cell: (a) Decay of  $\text{C}_4\text{H}_{10}^+$  (○) and  $\text{C}_2\text{H}_6^+$  (●) as a function of time due to leakage of  $\text{C}_4\text{H}_{10}$  and  $\text{C}_2\text{H}_6$  from the cell; (b) First-order rate constant for leakage from the cell as a function of total pressure.

and  $\text{C}_4\text{H}_{10}$ . We then studied the leakage of these products that occurs when the irradiation was stopped by following the decay in the ion currents of their respective parent ions, namely,  $m/e$  30 and  $m/e$  58. A typical result at a total pressure of ~20 Torr is shown in Figure 2a.

The ion currents at  $m/e$  30 and 58 are proportional to the concentrations of  $\text{C}_2\text{H}_6$  and  $\text{C}_4\text{H}_{10}$ , respectively, in the photolysis cell. The linearity of the plots of the logarithm of the ion current vs. time indicate that the leakage of the minor constituents of the cell contents (95% of the gas is  $\text{H}_2$ ) is first order in their concentration as would be the case if molecular flow obtained. On the other hand, the identical slopes of the lines in Figure 2a indicate that the first-order rate constant for leakage from the cell is independent of mass as would be the case for viscous flow through the pinhole. Identical results

were obtained for the flow rates of  $\text{SiH}_4$  (32 amu) and  $\text{Si}_2\text{H}_6$  (62 amu) from the cell. The first-order rate constant so determined from experiments with  $\text{Si}_2\text{H}_6$  varies linearly with the total pressure as shown in Figure 2b. The value obtained by extrapolation to zero pressure is that predicted from the pinhole size and the theory of molecular effusion.

These results show that in any given experiment the leakage of the low concentration constituents of the gas mixture, namely, any constituent other than hydrogen, will be first order in the concentration of that constituent. Moreover, the first-order rate constants for flow out of the cell will be the same for all substances, i.e., all substances will flow out of the cell at the same rate. This latter fact simplifies the kinetic analysis of the experiments but somewhat complicates the calibration of the mass spectrometer. The fact that all substances flow at the same rate from the high-pressure region (photolysis cell at 10–30 Torr) into the low pressure region (ion source at  $\sim 10^{-5}$  Torr) results in a concentration of the higher-mass substances along the center line of the system as the molecules travel the 2 cm distance from the exit of the pinhole to the ionization region. In other words the orifice acts as a molecular separator. The practical effect is that calibration of ion currents in terms of photolysis cell concentrations could not be made using pure compounds (i.e.,  $\text{SiH}_4$  and  $\text{Si}_2\text{H}_6$ ) but rather had to be made with the compounds admixed with  $\text{H}_2$  at the concentration levels characteristic of the experiments.

The source of 2537-Å radiation was a General Electric 4-W G4T4/1 germicidal lamp. Measurements of the initial rate of formation of  $n\text{-C}_4\text{H}_{10}$  indicate the mercury-photosensitized formation rate of hydrogen atoms in our experiments to be  $6.7 \times 10^{13}$  atoms  $\text{cm}^{-3} \text{s}^{-1}$ .

Monosilane, purchased from the Matheson Co., was purified by fractionation on a vacuum line prior to use. Disilane was prepared by the reduction of  $\text{Si}_2\text{Cl}_6$  (Peninsular Chemical Co.) with  $\text{LiAlH}_4$  (Alfa Inorganics) using bis[2-(2-methoxyethoxy)ethyl] ether as solvent. Similarly,  $\text{SiD}_4$  was prepared by the reduction of  $\text{SiCl}_4$  (Peninsular Chemical Co.) with  $\text{LiAlD}_4$  (Alfa Inorganics). Hydrogen and deuterium obtained from Matheson were passed through several traps immersed in liquid nitrogen and then stored in reservoir bulbs on the vacuum line. Ethylene and  $n$ -butane were Phillips Research Grade and with the exception of a freeze-pump-thaw cycle on the vacuum line were used as received. Dimethyldichlorosilane was purchased from Applied Science Laboratories, Inc. and was used as received.

## Results and Discussion

1. *General Nature of the Reaction.* Illumination of the reaction cell containing  $\text{H}_2$  (96%)– $\text{SiH}_4$  (4%)– $\text{Hg}$  ( $10^{-3}$  Torr) mixtures with 2537-Å radiation results mainly in the formation of  $\text{Si}_2\text{H}_6$  and depletion of  $\text{SiH}_4$ , as evidenced by the time dependence of the mass spectrum of the mixture. At longer illumination times the appearance of ions with  $m/e$  in the 84–92 range and above 110 suggest that small amounts of  $\text{Si}_3\text{H}_8$  and even smaller amounts of  $\text{Si}_4\text{H}_{10}$  are produced. Stoichiometry demands that  $\text{H}_2$  also be formed but this is not detectable with the excess of  $\text{H}_2$  employed. Experiments in which the  $\text{H}_2$  is replaced by  $\text{D}_2$  show clearly the formation of HD at rates equivalent to that of  $\text{Si}_2\text{H}_6$ . In addition to the above volatile products, a solid polymeric substance  $(\text{SiH}_x)_n$  is observed to deposit on the wall and quartz window of the reaction vessel.

In Figure 3 is shown the time dependences of the concentrations of  $\text{SiH}_4$  and  $\text{Si}_2\text{H}_6$  (both relative to the initial con-

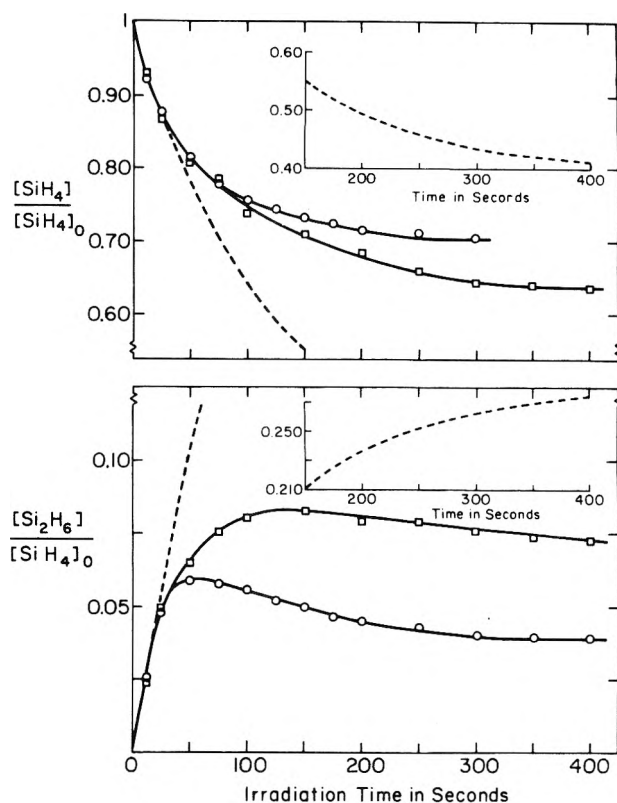


Figure 3. Formation of  $\text{Si}_2\text{H}_6$  and consumption of  $\text{SiH}_4$  by  $\text{Hg}(^3\text{P}_1)$  photosensitization of  $\text{H}_2$ – $\text{SiH}_4$  mixtures: (○) stainless steel walls; (□) pyrex walls.

centration of  $\text{SiH}_4$ ) for two cells, one with pyrex walls and the other with stainless steel walls. For irradiation times greater than 50 s the concentration–time behavior in the two cells is significantly different. However, the initial slopes or rates of both the depletion of  $\text{SiH}_4$  and the formation of  $\text{Si}_2\text{H}_6$  are independent of the nature of the cell walls. A third cell prepared by packing the stainless steel cell with quartz wool showed identical results with respect to initial rates of depletion of  $\text{SiH}_4$  and formation of  $\text{Si}_2\text{H}_6$ . A fourth cell prepared by presilanation of the pyrex walls with  $(\text{CH}_3)_2\text{SiCl}_2$  gave completely different results, however. In this cell the initial rate of depletion of  $\text{SiH}_4$  was reduced from that of the above three cells by a factor of about 2, while the initial rate of formation of  $\text{Si}_2\text{H}_6$  was reduced by a factor of about 7. The initial rates and their ratios in the various cells are shown in Table I.

The results in Table I show that in a freshly cleaned cell whose walls do not contain adsorbed silanes the initial rates of depletion of  $\text{SiH}_4$  and formation of  $\text{Si}_2\text{H}_6$  are independent of the nature and area of surfaces. The simple stoichiometry of



would require the ratio of initial rates to be 2. The values of this ratio for the first three vessels in Table I clearly show that in these cells the predominant chemical reaction is conversion of  $\text{SiH}_4$  to  $\text{Si}_2\text{H}_6$ . In the cell with initially silanated walls, however, the situation is significantly different. The greatly increased ratio of  $\text{SiH}_4$  depletion rate to  $\text{Si}_2\text{H}_6$  formation rate indicates that most of the  $\text{SiH}_4$  consumed does not produce  $\text{Si}_2\text{H}_6$  or any other volatile product but results instead in increased polymer formation on the walls. The lowered depletion rate of  $\text{SiH}_4$  in the silanated vessel is probably due to some

TABLE I: Effect of Vessel Surfaces on Initial Rates

Nature of cell walls	$-R_0$ (SiH <sub>4</sub> ) <sup>a</sup> s <sup>-1</sup> × 10 <sup>3</sup>	$R_0$ (Si <sub>2</sub> H <sub>6</sub> ) <sup>b</sup> s <sup>-1</sup> × 10 <sup>3</sup>	$-R_0$ (SiH <sub>4</sub> )/ $R_0$ (Si <sub>2</sub> H <sub>6</sub> )
Stainless steel	5.8	2.7	2.1
Pyrex	5.4	2.4	2.2
Stainless steel packed with quartz wool	5.4	2.6	2.1
Pyrex treated with (CH <sub>3</sub> ) <sub>2</sub> SiCl <sub>2</sub>	2.5	0.38	6.7

<sup>a</sup>  $-R_0(\text{SiH}_4) = -(1/[\text{SiH}_4]_0)(d[\text{SiH}_4]/dt)_0$ . <sup>b</sup>  $R_0(\text{Si}_2\text{H}_6) = (1/[\text{SiH}_4]_0)(d[\text{Si}_2\text{H}_6]/dt)_0$ .

evolution of SiH<sub>4</sub> from the walls. In confirmation of this we have observed that "dirty" cells (prepared by carrying out a normal irradiation of a H<sub>2</sub>-SiH<sub>4</sub>-Hg mixture) immediately evolve SiH<sub>4</sub> when following evacuation to 10<sup>-6</sup> Torr they are filled with H<sub>2</sub> and Hg and irradiated. No SiH<sub>4</sub> evolution occurs, however, until irradiation is begun. This was also observed by Niki and Mains<sup>17</sup> but unlike these authors we did not observe any evolution of Si<sub>2</sub>H<sub>6</sub> from the vessel walls when H<sub>2</sub>-Hg mixtures were irradiated in such "dirty" cells.

The dotted curves in Figure 3 show the relative concentration-time behavior that is expected in this flow system, given the initial rates, the cell leakage constant, and the assumption that the following conditions obtain: (1) the light intensity transmitted by the cell window is independent of time; (2) the sole loss channel for Si<sub>2</sub>H<sub>6</sub> is leakage through the pinhole (i.e., Si<sub>2</sub>H<sub>6</sub> is a stable product). The steady-state values of the relative concentrations, i.e.

$$\xi = [\text{SiH}_4]/[\text{SiH}_4]_0$$

and

$$\eta = [\text{Si}_2\text{H}_6]/[\text{SiH}_4]_0$$

with these assumptions are 0.395 and 0.281, respectively, and the insets to Figure 3 show the calculated approach to these values. The departures of the observed values of  $\xi$  and  $\eta$  from the dotted curves and then failure to reach anything near the calculated steady-state values shows that the above assumptions are not correct.

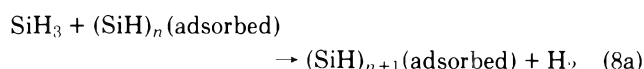
The rapid negative deviations of observed values of  $\eta$  from the dotted curve in Figure 3 indicate that either the incident light intensity decreases rapidly with time or that Si<sub>2</sub>H<sub>6</sub> is not a chemically stable product in this system or both. The positive departures of  $\xi$  from the corresponding dotted curve suggests that the light intensity decreases with time or that secondary reactions in the system reform SiH<sub>4</sub> or both.

A brown solid polymer is, in fact, observed to be deposited on the quartz window of the cell. Repeated photolyses of freshly introduced reactant mixtures, following evacuation of the cell but not cleaning of the window, show successive reductions in initial rates. Cleaning of the quartz window with KOH solution restores the initial rates to the values shown in Table I. Spectrophotometric measurements of the transmission of the cell window when clean and after an irradiation confirm the successive initial rate studies. It must, therefore, be concluded that during an experiment the light intensity incident on the reaction mixture decreases continually because of polymer buildup on the window. This effect will contribute to the departure of the observed values of  $\xi$  and  $\eta$  from the dotted curves of Figure 3. On the basis of the reported rate constants for reactions of H atoms<sup>2,5-7</sup> and SiH<sub>2</sub> radicals<sup>24</sup>

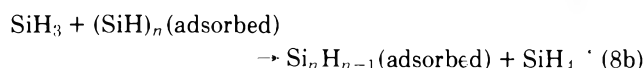
with SiH<sub>4</sub> and Si<sub>2</sub>H<sub>6</sub>, it has to be concluded that even at the low concentrations involved significant amounts of Si<sub>2</sub>H<sub>6</sub> must react with H atoms and SiH<sub>2</sub> radicals before flowing out of the cell. This chemical removal of Si<sub>2</sub>H<sub>6</sub> from the cell will contribute to the deviation of  $\eta$  from the dotted curve. Moreover, it has been reported<sup>4</sup> that about 1/3 of the reactions of H atoms with Si<sub>2</sub>H<sub>6</sub> produce SiH<sub>4</sub> and this will contribute to the positive deviation of  $\xi$  from the dotted curve.

It is also to be noted in Figure 3 that after about 50 s of irradiation the formation rate of Si<sub>2</sub>H<sub>6</sub> and the depletion rate of SiH<sub>4</sub> are reduced more in the stainless steel cell than in the pyrex cell. One major reason for this difference in the two cells is that polymer buildup on the quartz window is observed to be significantly greater in the stainless steel cell. Thus after 1250 s of irradiation the incident light intensity in the stainless steel cell has been reduced by 55% while in the pyrex cell the reduction after 1250 s is only 23%.

The above reductions in incident light intensity account for only about 2/3 of the differences between the two cells seen in Figure 3. It is likely that reactions of free radicals with the silanated surfaces produced by the reaction account for the remaining differences. That such reactions exist are confirmed by the initial rate studies in the vessel with the presilanated surface (cf. Table I). For the concentrations and total pressures used, the rate constants for the reactions of H atoms<sup>2,5,7</sup> and SiH<sub>2</sub> radicals<sup>24</sup> with SiH<sub>4</sub> and Si<sub>2</sub>H<sub>6</sub> indicate that most of these reactive radicals will react in the gas phase before they can reach the wall. On the other hand, in this system SiH<sub>3</sub> radicals formed by (1a) will react only with each other by (5). Since their concentration is low (we estimate about 10<sup>11</sup>-10<sup>12</sup> per cm<sup>3</sup>), this reaction will be sufficiently slow for appreciable numbers of them to collide with the surfaces of the vessel. The simplest (but by no means unique) rationalization of this surface effect is that subsequent to polymer buildup on the walls, SiH<sub>3</sub> radicals react on the walls by



and



The consumption of SiH<sub>3</sub> by (8a) and (8b) will reduce the rate of formation of Si<sub>2</sub>H<sub>6</sub> since they will compete with (5). The slowing of the depletion rate of SiH<sub>4</sub> is contributed to by (8b). If polymer builds up more rapidly on the walls of the stainless steel vessel than in the pyrex vessel walls (as suggested but not proven by the relative rates of buildup on the quartz window) then the differences in the two cells in Figure 3 can be accounted for. It is worth repeating, however, that while the incident light intensity effect has been demonstrated, the occurrence of (8a) and (8b) is only a rationalization. Further, we do not know in which cell the buildup of polymer is more rapid although buildup on the quartz window is more rapid in the stainless steel cell.

2. *The Formation of Disilane from Silyl Radicals.* With the large [H<sub>2</sub>]/[SiH<sub>4</sub>] ratios used, i.e., 20-25, about 95% of the Hg(<sup>3</sup>P<sub>1</sub>) atoms react with H<sub>2</sub> to produce H atoms.<sup>20</sup> At the total pressures of our experiments, i.e., 10-30 Torr, essentially all of these H atoms will react with SiH<sub>4</sub> (or Si<sub>2</sub>H<sub>6</sub> in the later stages) by



before they can undergo a third-body stabilized recombina-

tion<sup>25</sup> or before they can reach the wall. The formation of  $\text{Si}_2\text{H}_6$  arises from further reaction of the  $\text{SiH}_3$  radicals with each other. On the basis of mass spectrometric analyses of the disilane formed in the reaction of H atoms with an equimolar mixture of  $\text{SiH}_4$  and  $\text{SiD}_4$ , it has been suggested<sup>4</sup> that direct recombination of  $\text{SiH}_3$  radicals does not occur; rather it is proposed that the disproportionation (5) is followed by insertion of the resulting  $\text{SiH}_2$  radical into the Si-H bond of  $\text{SiH}_4$  (6). We have studied in some detail the protium-deuterium isotopic composition of the  $\text{Si}_2\text{H}_n\text{D}_{6-n}$  product of the  $\text{Hg}(^3\text{P}_1)$  photosensitized decomposition of a 96:2:2  $\text{H}_2$ - $\text{SiH}_4$ - $\text{SiD}_4$  mixture. Our results confirm the conclusion of Pollock, Sandhu, Jodhan, and Strausz<sup>4</sup> that the dominant mode of formation of disilane is the sequence (5)-(6). However, our results differ in that we find significant quantities of  $\text{Si}_2\text{H}_5\text{D}$  and  $\text{Si}_2\text{HD}_5$  in the products.

The mass spectrum of the  $\text{H}_2$ - $\text{SiH}_4$ - $\text{SiD}_4$  mixture in the region  $m/e$  56-68 and at 50-eV ionizing energy was scanned repeatedly as a function of irradiation time for up to 430 s. It was found that within an average deviation of  $\pm 4\%$  the mass spectrum in this region was independent of irradiation time. The fractional abundance of a few representative ions as a function of irradiation time is shown in Figure 4a. The 50-eV mass spectrum of the  $\text{Si}_2\text{H}_n\text{D}_{6-n}$  product in this mass range, corrected for the presence of  $^{29}\text{Si}$  (4.70%) and  $^{30}\text{Si}$  (3.08%), is shown in Table II. It is clear from this spectrum that  $\text{Si}_2\text{HD}_5$  is definitely formed, since  $m/e$  67 cannot be anything but a parent molecule-ion. Moreover, since the spectrum is independent of irradiation time,  $\text{Si}_2\text{HD}_5$  is a primary product of the reaction, i.e., it does not result from reaction of previously formed  $\text{Si}_2\text{D}_6$  with H atoms.

We attempted to use the published mass spectra of deuterated disilanes<sup>26</sup> to calculate, from the spectrum in Table II, the distribution of  $\text{Si}_2\text{H}_n\text{D}_{6-n}$  in the disilane product. This attempt had to be given up because the extensive fragmentation corrections resulted in large negative amounts of  $\text{Si}_2\text{H}_6$ . Probably the major reason for this difficulty is a significantly different fragmentation pattern in our mass spectrometer as compared with that used by Ring et al.<sup>26</sup>

The method finally used was to determine mass spectra of the  $m/e$  56-68 region at a series of ionizing electron energies near the ionization potential of  $\text{Si}_2\text{H}_6$ . These spectra were then extrapolated to the electron energy corresponding to the disappearance of the most abundant ion known to consist only of fragment ions. The spectrum at this electron energy must be comprised solely of the parent ions  $\text{Si}_2\text{H}_n\text{D}_{6-n}^+$ . Inspection of Table II reveals that  $m/e$  60 is the most intense ion that is composed only of fragment ions and so its intensity must vanish before the parent-ion intensities do. The ions at  $m/e$  67 and  $m/e$  68, on the other hand, consist only of parent ions. These facts suggest that a useful method of extrapolation is to plot the ratios of ion intensities at various  $m/e$  values to that of  $m/e$  68 (or  $m/e$  67) as a function of ionizing energy. The extrapolated threshold energy of the ion-current ratio  $i_{60}/i_{68}$  is then the maximum ionizing energy at which the mass spectrum is composed solely of parent ions.

Figure 4 shows a plot of the ion currents of all parent ions and  $m/e$  60 relative to the ion current at  $m/e$  68 as a function of nominal electron energy in the range 12.5-13.8 eV. A linear extrapolation of the  $i_{60}/i_{68}$  ratio yields a nominal electron energy of 11.0 eV for the disappearance from the spectrum of all fragments. This is to be compared with the lowest appearance potential of a fragment ion from disilane of 10.85 eV.<sup>23</sup> The mass spectrum corresponding to the presence of only the parent ions  $\text{Si}_2\text{H}_n\text{D}_{6-n}^+$  is then given by the values

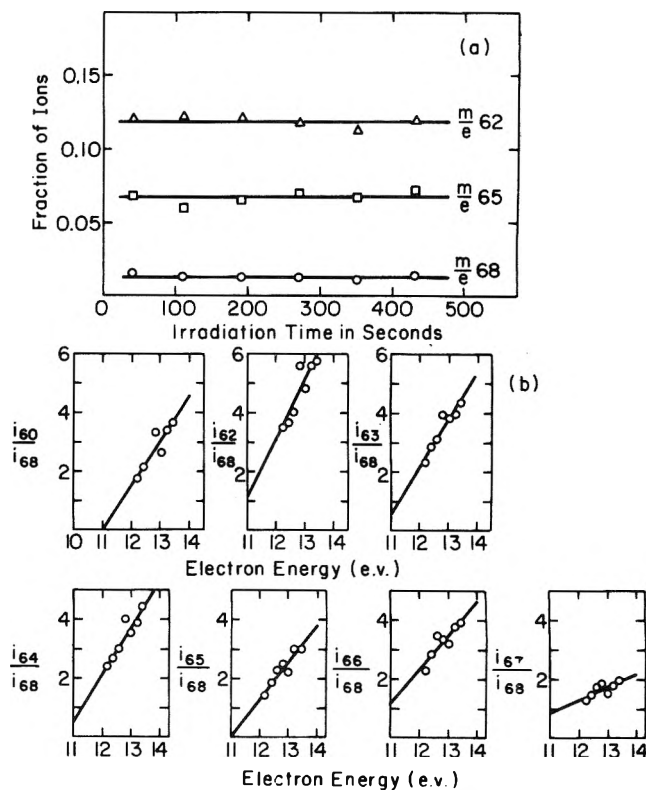


Figure 4. Mass spectra of  $\text{Si}_2\text{H}_n\text{D}_{6-n}$  product: (a) Fractional abundance of product ions as a function of irradiation time; (b) Dependence of ion intensities relative to ( $m/e$  68) as a function of electron energy.

TABLE II: 50-eV Monoisotopic Mass Spectrum of  $\text{Si}_2\text{H}_n\text{D}_{6-n}$  Product from H-Atom Initiated Decomposition of an Equimolar  $\text{SiH}_4$ - $\text{SiD}_4$  Mixture

$m/e$	Ions	Rel abundance ( $\pm 4\%$ )
56	$\text{Si}_2^+$	42.9
57	$\text{Si}_2\text{H}^+$	36.6
58	$\text{Si}_2\text{H}_2^+ + \text{Si}_2\text{D}^+$	76.0
59	$\text{Si}_2\text{H}_3^+ + \text{Si}_2\text{HD}^+$	54.3
60	$\text{Si}_2\text{H}_4^+ + \text{Si}_2\text{H}_2\text{D}^+ + \text{Si}_2\text{D}_2^+$	98.0
61	$\text{Si}_2\text{H}_5^+ + \text{Si}_2\text{H}_3\text{D}^+ + \text{Si}_2\text{HD}_2^+$	72.2
62	$\text{Si}_2\text{H}_6^+ + \text{Si}_2\text{H}_4\text{D}^+ + \text{Si}_2\text{H}_2\text{D}_2^+ + \text{Si}_2\text{D}_3^+$	88.7
63	$\text{Si}_2\text{H}_5\text{D}^+ + \text{Si}_2\text{H}_3\text{D}_2^+ + \text{Si}_2\text{HD}_3^+$	100.0
64	$\text{Si}_2\text{H}_4\text{D}_2^+ + \text{Si}_2\text{H}_2\text{D}_3^+ + \text{Si}_2\text{D}_4^+$	73.3
65	$\text{Si}_2\text{H}_3\text{D}_3^+ + \text{Si}_2\text{HD}_4^+$	44.0
66	$\text{Si}_2\text{H}_2\text{D}_4^+ + \text{Si}_2\text{D}_5^+$	35.6
67	$\text{Si}_2\text{HD}_5^+$	22.6
68	$\text{Si}_2\text{D}_6^+$	8.42

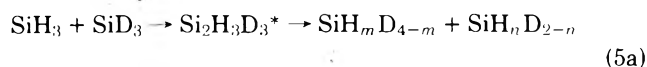
of the ion-current ratios of Figure 4 extrapolated to 11.0 eV. The ion currents in Figure 4 have not been corrected for  $^{29}\text{Si}$  and  $^{30}\text{Si}$  isotopes. It should be pointed out that the slight variation of  $i_{67}/i_{68}$  with electron energy in Figure 4 is due to a considerably greater abundance of isotopic fragment ions (i.e.,  $^{29}\text{Si}^{28}\text{SiD}_5^+$  and  $^{30}\text{Si}^{28}\text{SiD}_4^+$ ) in  $m/e$  67 than in  $m/e$  68 (i.e.,  $^{30}\text{Si}^{28}\text{SiD}_5^+$ ).

The purely parent-ion mass spectrum (i.e., at 11.0 eV), corrected for the presence of  $^{29}\text{Si}$  and  $^{30}\text{Si}$ , is shown in Table III. Since the ionization cross sections do not vary significantly with deuterium substitution, the relative abundances in Table III represent the distribution of  $\text{Si}_2\text{H}_n\text{D}_{6-n}$  in the disilane

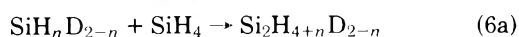
TABLE III:  $^{28}\text{Si}$  Mass Spectrum of  $\text{Si}_2\text{H}_n\text{D}_{6-n}$  Product at 11 eV

( <i>m/e</i> )	Ion	Rel abundance
62	$\text{Si}_2\text{H}_6^+$	$90 \pm 26$
63	$\text{Si}_2\text{H}_5\text{D}^+$	$43 \pm 11$
64	$\text{Si}_2\text{H}_4\text{D}_2^+$	$37 \pm 15$
65	$\text{Si}_2\text{H}_3\text{D}_3^+$	$3 \pm 13$
66	$\text{Si}_2\text{H}_2\text{D}_4^+$	$100 \pm 16$
67	$\text{Si}_2\text{HD}_5^+$	$66 \pm 11$
68	$\text{Si}_2\text{D}_6^+$	$74 \pm 16$

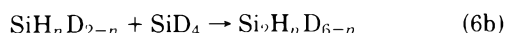
product. Despite the necessarily large uncertainties in relative abundances, it is clear from Table III that  $\text{Si}_2\text{H}_3\text{D}_3$  is virtually absent. If disilane was formed by the simple association of silyl radicals one would expect this molecule to be one of the dominant products. The simplest explanation of its absence in  $\text{SiH}_3\text{-SiD}_3$  reaction is that association of silyl radicals does not occur; instead, as proposed by Pollack, Sandhu, Jodhan, and Strausz,<sup>4</sup> a disproportionation



is followed by insertion



or

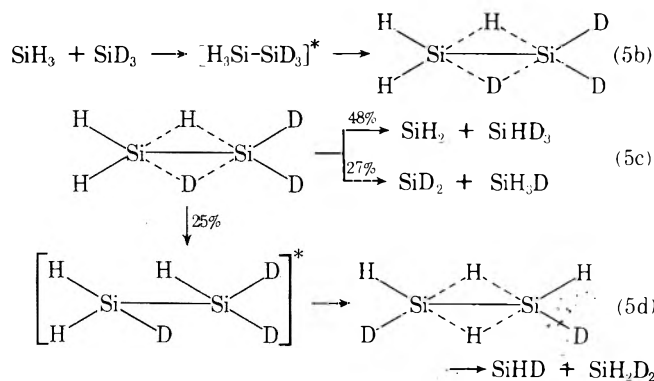


in which the indices have the possible values:  $m = 0-4$  and  $n = 0-2$ . Clearly  $\text{Si}_2\text{H}_3\text{D}_3$  cannot be formed by this mechanism and it is therefore in accord with the facts shown in Table III. The formation of large amounts of  $\text{Si}_2\text{H}_5\text{D}$  and  $\text{Si}_2\text{HD}_5$ , as indicated in Table III, appears to be at variance with the very brief statement of Pollock, Sandhu, Jodhan, and Strausz<sup>4</sup> concerning their results for the  $\text{SiH}_3\text{-SiD}_3$  reaction. However, the demonstrated virtual absence of  $\text{Si}_2\text{H}_3\text{D}_3$  is a striking confirmation of their suggestion that  $\text{SiH}_3$  radicals form  $\text{Si}_2\text{H}_6$  essentially exclusively by the disproportionation-insertion mechanism, (5) and (6).

Assuming that the rate constants for insertion of  $\text{SiH}_n\text{D}_{2-n}$  into an Si-H bond of  $\text{SiH}_4$  is independent of  $n$  and that the same is true of insertion into an Si-D bond of  $\text{SiD}_4$ , the data of Table III indicate that the relative steady-state concentrations of  $\text{SiH}_2$ ,  $\text{SiHD}$ , and  $\text{SiD}_2$  in the equimolar  $\text{SiH}_4\text{-SiD}_4$  mixtures are given as:

$$[\text{SiH}_2]:[\text{SiHD}]:[\text{SiD}_2] = 100 \pm 22:53 \pm 19:56 \pm 15$$

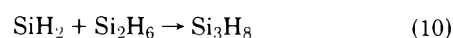
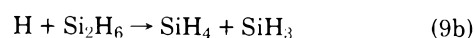
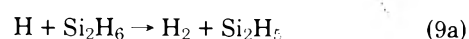
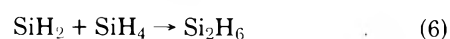
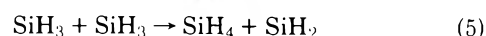
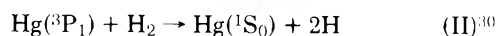
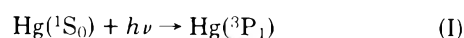
Despite the large uncertainties, these results suggest that the attack of H atoms on  $\text{SiH}_4$  to form  $\text{SiH}_3$  radicals is about twice as fast as that on  $\text{SiD}_4$  to produce  $\text{SiD}_3$  radicals. This is in accord with the corresponding rate constant ratio of 2-2.5 as reported by Laupert, Potzinger, Mihelcic, and Schubert.<sup>27</sup> The rather low abundance of  $\text{SiHD}$  indicates that break-up of the energy-rich intermediate in (5a) is not statistical, i.e., H and D atoms are not completely equivalent in the energy-rich intermediate. Nonetheless the presence of significant amounts of  $\text{SiHD}$  indicates that some intramolecular randomization of H and D occurs in the energy-rich silyl radical association complex. The mechanism of silylene radical formation may be pictured<sup>29</sup> as



The observed scrambling of H and D must occur in a primary process, as shown, since the H-D distribution in the disilane product is independent of reaction time (Figure 4a).

3. Overall Mechanism and Kinetic Considerations. Following formation by (5) and (6),  $\text{Si}_2\text{H}_6$  will react with the H atoms<sup>4</sup> to form  $\text{SiH}_4$  and  $\text{Si}_4\text{H}_{10}$ , and with the  $\text{SiH}_2$  radicals to form  $\text{Si}_3\text{H}_8$ . In the flow system used in this study the partial pressure of  $\text{Si}_2\text{H}_6$  reaches at most 0.08 Torr in a total pressure of about 20 Torr. Consequently, the products of the conversion of  $\text{Si}_2\text{H}_6$  by these secondary processes are present at such low concentrations that quantitative determination is precluded. Nonetheless, at the longer irradiation times, ion currents at *m/e* values consistent with  $\text{Si}_3\text{H}_8$  and  $\text{Si}_4\text{H}_{10}$  were detected.

Neglecting the effect of polymer buildup on the walls, the overall conversion may be represented by the following reaction scheme:



The reactions of  $\text{Hg}(^3\text{P}_1)$  with  $\text{SiH}_4$  and  $\text{Si}_2\text{H}_6$  are considered negligible because of the large excess of  $\text{H}_2$ . Despite this large excess, it is not likely at the temperature of our experiment, namely, 300 K, that  $\text{SiH}_2$  radicals will react with  $\text{H}_2$ ,<sup>24</sup> and this possible reaction has also been neglected in the scheme. Finally, we do not account for further reactions of  $\text{Si}_2\text{H}_5$  and  $\text{Si}_3\text{H}_8$ ; since the concentration of these substances are very low they are not likely to influence the observed kinetics.

In a kinetic description of the time dependence of the concentrations of  $\text{SiH}_4$  and  $\text{Si}_2\text{H}_6$  in the photolysis cell, we must include the rates of leakage of both substances out of the cell into the mass spectrometer and the rate of flow of  $\text{SiH}_4$  into the cell from the reservoir. As shown in the Experimental Section, the rates of leakage out of the cell occur with the same first-order constant  $\lambda$ . In addition, measurement of the rate of replenishment of  $\text{SiH}_4$  in the cell, following termination of an irradiation, shows that this process occurs also with the same first-order constant  $\lambda$ .

Treating this reaction scheme with the usual steady-state assumption for the concentrations of  $\text{Hg}(^3\text{P}_1)$ , H,  $\text{SiH}_3$ , and  $\text{SiH}_2$ , and with introduction of the relative concentrations  $\xi$



and  $\eta$ , defined earlier leads in a straightforward way to the coupled rate equations

$$-\frac{d\xi}{dt} = \lambda(\xi - 1) + \left(\frac{I_a}{[\text{SiH}_4]_0}\right) \left[ \frac{2 - (2\alpha\gamma - \omega)\frac{\eta}{\xi} - 3\alpha\gamma\omega\left(\frac{\eta}{\xi}\right)^2}{\left(1 + \gamma\frac{\eta}{\xi}\right)\left(1 + \omega\frac{\eta}{\xi}\right)} \right] \quad (11)$$

$$\frac{d\eta}{dt} = \frac{I_a}{[\text{SiH}_4]_0} \left[ \frac{1 - [(2 - \alpha)\gamma + \omega]\frac{\eta}{\xi} - (2 + \alpha)\gamma\omega\left(\frac{\eta}{\xi}\right)^2}{\left(1 + \gamma\frac{\eta}{\xi}\right)\left(1 + \omega\frac{\eta}{\xi}\right)} \right] - \lambda\eta \quad (12)$$

in which  $I_a$  is the rate of absorption of light and  $\alpha$ ,  $\gamma$ , and  $\omega$  are rate constant ratios defined as follows:

$$\alpha = k_{9a}/(k_{9a} + k_{9b})$$

$$\gamma = (k_{9a} + k_{9b})/k_0$$

$$\omega = k_{10}/k_6$$

In the limit of zero time,  $\xi \rightarrow 1$  and  $\eta \rightarrow 0$ . Hence it may be seen that (11) and (12) yield the limiting initial rate ratio of 2 as required by the stoichiometry.

Numerical integration of (11) and (12) yields results for  $\xi$  and  $\eta$  that are fairly insensitive to the physically real range of  $\alpha$ , i.e., 0 to 1. Assuming the value of  $\alpha = 0.34^4$  comparison of the numerically integrated expressions for  $\xi$  and  $\eta$  with the experimental data for the pyrex cell leads to ranges of values for  $\gamma$  and  $\omega$  that are interdependent. The simultaneous maximum values of  $\gamma$  and  $\omega$  obtained are  $\gamma = \omega = 2.5$ .

These are to be compared with the reported value for  $\gamma$  of 7.1<sup>27</sup> and an extrapolated value of  $6.4 \pm 2.4$ ,<sup>28</sup> for  $\omega$ . Thus our measured rates of formation of  $\text{Si}_2\text{H}_6$  and depletion of  $\text{SiH}_4$ , described in terms of the above mechanism, yield only semiquantitative agreement with reported rate constant ratios. Incorporation of the time dependence of  $I_a$  does not significantly improve this semiquantitative agreement.

We believe the reason for the lack of quantitative agreement, with respect to the rate constant ratios, is that the mechanism shown is an incomplete description of the secondary reactions. The mechanism appears to be a correct description of the primary reactions, as judged by the results of Table I and the limiting forms of (11) and (12) as  $t$  tends to zero. However, in this primary reaction region we cannot obtain information about  $\gamma$  and  $\omega$ . We can only obtain information about  $\gamma$  and  $\omega$  at later times when the secondary reactions 9a, 9b, and 10 are significant; but it is just at these later

times when surface reactions involving adsorbed polymeric silicon hydrides also become significant. Since the details of these surface reactions are not clear, we cannot incorporate them into a quantitative kinetic description. Their omission, however, renders the mechanism incomplete so that quantitative evaluation of  $\gamma$  and  $\omega$  from our data is precluded.

**Acknowledgment.** This work was supported by the U.S. Energy Research and Development Administration under Contract No. ER(11-1)-3416. We also thank the National Science Foundation for providing funds to assist in the original purchase of the time-of-flight mass spectrometer.

## References and Notes

- (1) U.S. Energy Research and Development Administration Document No. C00-3416-22.
- (2) K. Y. Choo, P. P. Gaspar, and A. P. Wolf, *J. Phys. Chem.*, **79**, 1752 (1975).
- (3) J. A. Cowfer, K. P. Lynch, and J. V. Michael, *J. Phys. Chem.*, **79**, 1139 (1975).
- (4) T. L. Pollock, H. S. Sandhu, A. Jodhan, and O. P. Strausz, *J. Am. Chem. Soc.*, **95**, 1017 (1973).
- (5) P. Potzinger, L. C. Glasgow, and B. Reimann, *Z. Naturforsch. A*, **29**, 493 (1974).
- (6) D. Mihelcic, P. Potzinger, and R. N. Schindler, *Ber. Bunsenges. Phys. Chem.*, **78**, 82 (1974).
- (7) K. OBi, H. S. Sandhu, H. E. Gunning, and O. P. Strausz, *J. Phys. Chem.*, **76**, 3911 (1972).
- (8) E. R. Morris and J. C. J. Thynne, *J. Phys. Chem.*, **73**, 3294 (1969).
- (9) O. P. Strausz, E. Jakubowski, H. S. Sandhu, and H. E. Gunning, *J. Chem. Phys.*, **51**, 552 (1969).
- (10) R. E. Berkley, I. Safarik, H. E. Gunning, and O. P. Strausz, *J. Phys. Chem.*, **77**, 1734 (1973).
- (11) H. E. O'Neal, S. Pavlou, T. Lubin, M. A. Ring, and L. Batt, *J. Phys. Chem.*, **75**, 3945 (1971).
- (12) E. R. Morris and J. C. J. Thynne, *Trans. Faraday Soc.*, **66**, 183 (1970).
- (13) E. Jakubowski, H. S. Sandhu, H. E. Gunning, and O. P. Strausz, *J. Chem. Phys.*, **52**, 4242 (1970).
- (14) R. E. Berkeley, I. Safarik, O. P. Strausz, and H. E. Gunning, *J. Phys. Chem.*, **77**, 1741 (1973).
- (15) H. J. Emeléus and K. Stewart, *Trans. Faraday Soc.*, **32**, 1577 (1936).
- (16) D. White and E. G. Rochow, *J. Am. Chem. Soc.*, **76**, 3897 (1954).
- (17) H. Niki and G. J. Mains, *J. Phys. Chem.*, **68**, 304 (1964).
- (18) M. A. Nay, G. N. C. Woodall, O. P. Strausz, and H. E. Gunning, *J. Am. Chem. Soc.*, **87**, 179 (1965).
- (19) E. Kamaratos and F. W. Lampe, *J. Phys. Chem.*, **74**, 2267 (1970).
- (20) J. G. Calvert and J. N. Pitts, "Photochemistry", Wiley, New York, N.Y., 1966, p 74.
- (21) S. Dushman, "Scientific Foundations of Vacuum Technique", Wiley, New York, N.Y., 1949, Chapter 2.
- (22) E. W. R. Steacie, "Atomic and Free Radical Reactions", Reinhold, New York, N.Y., 1954, pp 434 ff.
- (23) P. Potzinger and F. W. Lampe, *J. Phys. Chem.*, **73**, 3912 (1969).
- (24) P. John and J. H. Purnell, *J. Chem. Soc., Faraday Trans. 1*, **69**, 1455 (1973).
- (25) S. W. Benson, "The Foundations of Chemical Kinetics", McGraw-Hill, New York, N.Y., 1960.
- (26) M. A. Ring, G. D. Beverly, F. H. Koester, and R. P. Hollandsworth, *Inorg. Chem.*, **8**, 2033 (1969).
- (27) R. Laupert, P. Potzinger, D. Mihelcic, and V. Schubert, private communication.
- (28) P. P. Gaspar and P. Markus, *Chem. Commun.*, 1331 (1970).
- (29) We thank one of the reviewers for this suggestion.
- (30) We neglect here the possible formation of  $\text{HgH}$ . We are interested predominantly in initial reaction rates and under such circumstances the formation of this compound cannot play a significant role.

## Ion-Molecule Reactions of Cyclic Borazine Cations. Thermodynamic and Kinetic Considerations

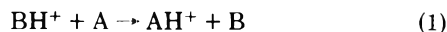
Anthony J. DeStefano and Richard F. Porter\*

Department of Chemistry, Cornell University, Ithaca, New York 14853 (Received June 18, 1976)

Borazine cations ( $BH^+$ ) formed by 10.2-eV photon impact of borazine, *B*-trimethylborazine, and *N*-trimethylborazine react with their molecular precursors by proton transfer. Second-order rate constants for the reaction  $BH^+ + BH \rightarrow BH_2^+ + B$  at 300 K are  $1.3 \pm 0.2 \times 10^{-9}$ ,  $6.5 \pm 1 \times 10^{-10}$ , and  $3.5 \pm 1.5 \times 10^{-10} \text{ cm}^3 \text{ molecule}^{-1} \text{ s}^{-1}$ , respectively. *B*-Trimethylborazine and *N*-trimethylborazine transfer a proton from exocyclic methyl groups indicating that the free radical formed (*B*) has the odd electron localized on a carbon atom. From a comparative rate study of reactions of  $H_3B_3N_3H_3^+$  with a series of organic molecules, the proton affinity of the *B*-borazinyl radical ( $H_2B_3N_3H_3$ ) is found to be  $193 \pm 2 \text{ kcal mol}^{-1}$ . The dissociation energy of borazine to form  $H_2B_3N_3H_3$  and H is  $112 \pm 3 \text{ kcal mol}^{-1}$ . In the borazine and *B*-trimethylborazine systems the intermediate borazinium ion ( $BH_2^+$ ) undergoes proton transfer and condensation reactions with the precursor borazine molecule. Some of the mechanistic details of these reactions are unraveled by studies of selectively deuterated species. The relevance of this study to the photochemical behavior of borazines is discussed.

### Introduction

Current research in gas phase ion-molecule chemistry encompasses areas of interest from organic reaction mechanisms<sup>1,2</sup> to astrochemistry.<sup>3,4</sup> The pioneering work of Franklin and co-workers<sup>5</sup> has played an important role in establishing ion-molecule chemistry as a viable field of research. With the development of ion cyclotron resonance and high pressure mass spectrometric techniques it is now possible to obtain kinetic and thermodynamic data for proton transfer reactions of complex molecules in the gas phase. Our work in this area has been limited largely to inorganic systems, especially compounds containing boron.<sup>6,7</sup> In this present paper we discuss results of an ion-molecule study of three borazine cations derived from borazine, *N*-trimethylborazine, and *B*-trimethylborazine. A consequence of this work is information on the nature of borazine radicals produced in these reactions. We consider a reaction of the type



where *B* refers to a borazine radical produced in the reaction and *A* may be either a borazine molecule or a second reagent. Ideally thermochemical data for gas phase ion-molecule reactions are obtained from equilibrium measurements. Since it is virtually impossible to achieve conditions for a gas phase equilibrium for (1) involving a highly reactive intermediate (*B*), we will necessarily be limited, for thermochemical measurements, to the method of relative proton transfer rates. We feel this procedure has validity because of the availability of reliable proton affinity data for a number of reference organic compounds and accurate ionization energies of boron compounds from photoionization and photoelectron measurements.

In the experiments described in this paper the reactant ions are generated by photon impact at 10.2 eV (the hydrogen  $\alpha$  line). Under these reaction conditions only the parent ion of a borazine molecule is formed. Photoelectron spectra have been reported for the three borazines investigated.<sup>8</sup> These spectra indicate that for a photon energy of 10.2 eV the borazine molecular ions will be formed in their ground electronic

states. Rate constant measurements were obtained using borazine samples diluted with an excess of an inert bath gas. This procedure facilitates measurements of borazine source pressures in the micron range.

### Experimental Section

The mass spectrometer and photon impact ion source used in this study have been previously described and will only be discussed briefly.<sup>7</sup> The reaction chamber consisted of a 0.375-in. cubical cavity in a  $0.75 \times 0.50 \times 0.40$  in. block of Type 304 stainless steel. Light entered the source through a  $0.030 \times 0.250$  in. slit centered 0.477 in. from the base of the cavity. This slit was covered by a 1-mm thick LiF window held in place with Dow Corning 732 RTV adhesive. The source was equipped a repeller which maintained a field strength of  $14.8 \text{ V cm}^{-1}$  unless otherwise noted. The ion exit slit was  $0.003 \times 0.250$  in. The ion drawout potential was 400 V negative with respect to the reaction chamber, and the ion acceleration potential was held at +2000 V. The light source was a hydrogen resonance lamp similar to that described by Ausloos,<sup>9,10</sup> and was powered by a Ratheon Model PGM-10 microwave power generator. Under normal operating conditions the principle source of radiation was the 10.2-eV Lyman  $\alpha$  line of hydrogen. The LiF window used is an effective filter for radiation above 11.9 eV<sup>9</sup> and in test experiments with xenon (ionization potential = 12.1 eV),<sup>11</sup> Xe<sup>+</sup> was not detectable.

Borazine was prepared by the reduction of *B*-trichloroborazine (Alfa Inorganics) with  $NaBH_4$  using triethylene glycol-dimethyl ether as solvent, according to the method of Hohnstedt and Haworth.<sup>12</sup> *B*-Trideuterioborazine was prepared by the reaction of borazine with deuterium gas in the presence of  $DBF_2$ .<sup>13</sup> Mass spectral analysis showed the boron sites of borazine to be better than 98% deuterated. *N*-Trimethylborazine was prepared from  $CH_3NH_3Cl$  and  $NaBH_4$  under a helium atmosphere using  $NaBH_4$  dried 1,2-dimethoxyethane as solvent by a method similar to that of Beachley.<sup>14</sup> *B*-Trimethylborazine and  $(CD_3)_3B_3N_3H_3$  were prepared by the reaction of *B*-trichloroborazine with  $CH_3MgI$  and  $CD_3MgI$ , respectively, following the procedure of Haworth and Hohnstedt.<sup>15</sup>

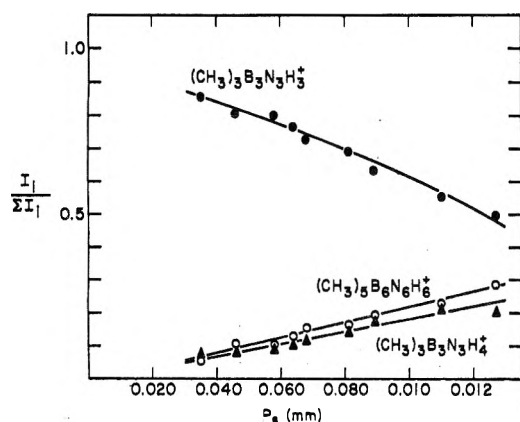
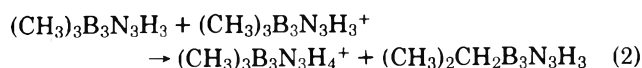


Figure 1. Effect of source pressure on the intensities of the ions in the mass spectra of  $(\text{CH}_3)_3\text{B}_3\text{N}_3\text{H}_3$ . Sample composition  $\text{Ar}-(\text{CH}_3)_3\text{B}_3\text{N}_3\text{H}_3 = 12:1$ .

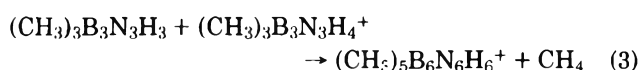
Methane, ethyl acetate, acetone, isobutylene, ethyl formate, dimethyl ether, acetonitrile, and benzene- $d_6$  were obtained from commercial sources.

### Chemistry of the *B*-Trimethylborazine Cation and *B*-Trimethylborazinium Ion

Radiation from the  $\text{H}_2$  resonance lamp at 10.2 eV is sufficient to ionize *B*-trimethylborazine (ionization potential = 9.5 eV)<sup>8</sup> without fragmentation. The diluent gases methane and argon (ionization potentials 12.7 and 15.8 eV, respectively)<sup>11</sup> were not ionized by the lamp radiation. At low source pressures only the parent ion of  $(\text{CH}_3)_3\text{B}_3\text{N}_3\text{H}_3$  was observed, but as the pressure was increased the species  $(\text{CH}_3)_3\text{B}_3\text{N}_3\text{H}_4^+$  (borazinium ion) and  $(\text{CH}_3)_5\text{B}_6\text{N}_6\text{H}_6^+$  appeared. Figure 1 shows the effect of source pressure on the relative intensities of these ions in a mixture of  $(\text{CH}_3)_3\text{B}_3\text{N}_3\text{H}_3$  and Ar. As the source pressure was increased the intensities of the species  $(\text{CH}_3)_3\text{B}_3\text{N}_3\text{H}_4^+$  and  $(\text{CH}_3)_5\text{B}_6\text{N}_6\text{H}_6^+$  both increased relative to the intensity of the parent ion. The rate of increase of the  $(\text{CH}_3)_5\text{B}_6\text{N}_6\text{H}_6^+$  ion is seen to be close to that for  $(\text{CH}_3)_3\text{B}_3\text{N}_3\text{H}_4^+$ . Figure 2 illustrates the effect of repeller voltage on the relative intensities of the ions in this system. The ratio  $I_{(\text{CH}_3)_5\text{B}_6\text{N}_6\text{H}_6^+}/I_{(\text{CH}_3)_3\text{B}_3\text{N}_3\text{H}_4^+}$  decreased as the residence time was decreased (by an increase in the repeller voltage). These observations infer that  $(\text{CH}_3)_5\text{B}_6\text{N}_6\text{H}_6^+$  is formed in the source at some time later than  $(\text{CH}_3)_3\text{B}_3\text{N}_3\text{H}_4^+$ , supporting a consecutive reaction scheme involving the reaction



followed by



This mechanism is similar to that proposed earlier<sup>7</sup> for the  $\text{H}_3\text{B}_3\text{N}_3\text{H}_3$  system in which the borazinium ion is intermediate to the formation of the B-N linked  $\text{H}_5\text{B}_6\text{N}_6\text{H}_6^+$ .

Further data regarding the reaction mechanism were obtained from studies with  $(\text{CD}_3)_3\text{B}_3\text{N}_3\text{H}_3$ . Shown in Figure 3 is a pressure-intensity profile of the ionic species in this system. The ionic species in the high mass region was  $(\text{CD}_3)_5\text{B}_6\text{N}_6\text{H}_6^+$  (the species  $(\text{CD}_3)_5\text{B}_6\text{N}_6\text{H}_5\text{D}^+$  occurred to

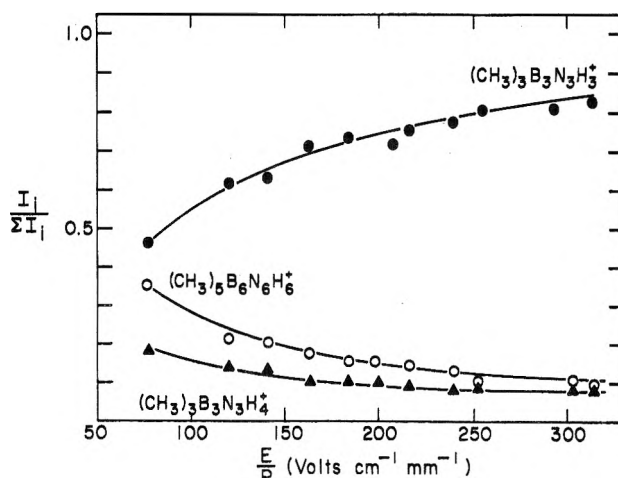


Figure 2. Effect of repeller voltage on the relative intensities of the ions in the  $(\text{CH}_3)_3\text{B}_3\text{N}_3\text{H}_3$  system. Sample composition  $\text{Ar}-(\text{CH}_3)_3\text{B}_3\text{N}_3\text{H}_3 = 12:1$ .

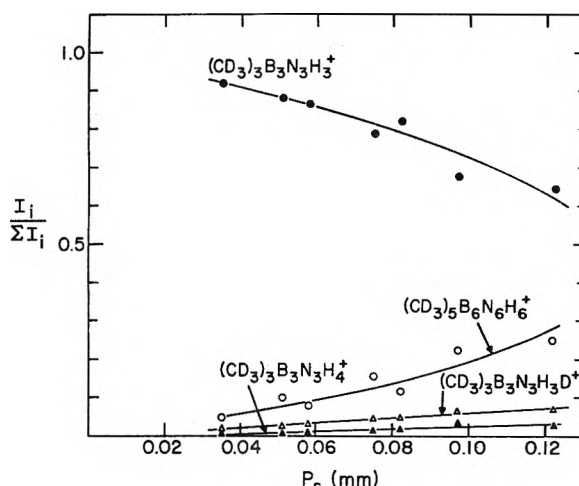
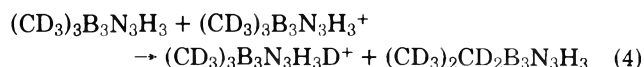
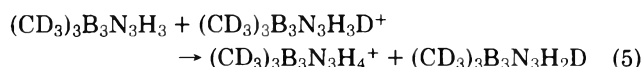


Figure 3. Pressure-intensity profile of the ionic species in the  $(\text{CD}_3)_3\text{B}_3\text{N}_3\text{H}_3$  system. Sample composition  $\text{Ar}-(\text{CD}_3)_3\text{B}_3\text{N}_3\text{H}_3 = 20.3:1$ .

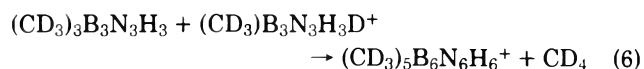
a negligible extent). An ionic species corresponding to the adduct of  $(\text{CD}_3)_3\text{B}_3\text{N}_3\text{H}_4^+$  and  $(\text{CD}_3)_3\text{B}_3\text{N}_3\text{H}_3$  occurred at pressures above that shown in Figure 3. Shown in Figure 4 is a plot of the ratio  $I_{(\text{CD}_3)_3\text{B}_3\text{N}_3\text{H}_4^+}/I_{(\text{CD}_3)_3\text{B}_3\text{N}_3\text{H}_3\text{D}^+}$  vs.  $(\text{CD}_3)_3\text{B}_3\text{N}_3\text{H}_3$  pressure observed for a  $\text{CH}_4-(\text{CD}_3)_3\text{B}_3\text{N}_3\text{H}_3$  mixture. This ratio decreased with decreasing  $(\text{CD}_3)_3\text{B}_3\text{N}_3\text{H}_3$  pressure, indicating that deuteron transfer occurred from an exocyclic methyl group. The proposed reaction scheme is deuteron transfer



followed by proton transfer



Once formed the ions  $(\text{CD}_3)_3\text{B}_3\text{N}_3\text{H}_3\text{D}^+$  and  $(\text{CD}_3)_3\text{B}_3\text{N}_3\text{H}_4^+$  react to form  $(\text{CD}_3)_5\text{B}_6\text{N}_6\text{H}_6^+$  and small intensities of  $(\text{CD}_3)_5\text{B}_6\text{N}_6\text{H}_5\text{D}^+$  through the processes



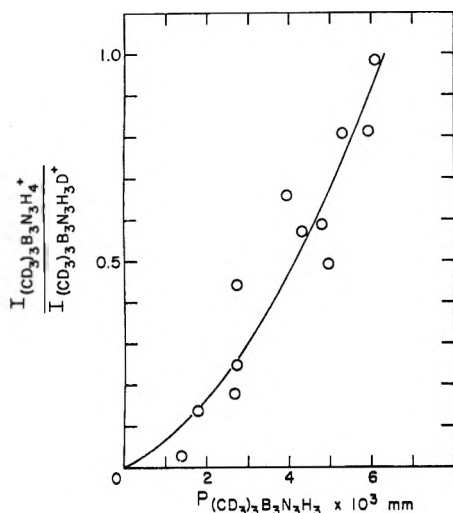
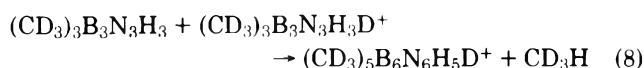
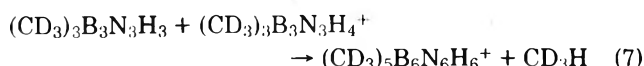


Figure 4. Effect of source pressure on the  $I_{(\text{CD}_3)_3\text{B}_3\text{N}_3\text{H}_4^+}/I_{(\text{CD}_3)_3\text{B}_3\text{N}_3\text{H}_3\text{D}^+}$  ratio in the mass spectra of  $(\text{CD}_3)_3\text{B}_3\text{N}_3\text{H}_3$ . Sample composition  $\text{CH}_4-(\text{CD}_3)_3\text{B}_3\text{N}_3\text{H}_3 = 21:1$ .



The absence of noticeable intensities of  $(\text{CD}_3)_5\text{B}_6\text{N}_6\text{H}_5\text{D}^+$  under conditions where the intensity of  $(\text{CD}_3)_3\text{B}_3\text{N}_3\text{H}_3\text{D}^+$  is higher than that of  $(\text{CD}_3)_3\text{B}_3\text{N}_3\text{H}_4^+$  is an indication that the deuterium added in reaction 4 is subsequently removed in reaction 6.

### Kinetic Treatment

Rate data for the disappearance of a borazine cation ( $\text{BH}^+$ ) were treated assuming pseudo-first-order kinetics. With this assumption the integrated bimolecular rate expression becomes

$$-\ln [I_{(\text{BH}^+)}/\Sigma I_i] = k(n_{\text{BH}})\tau \quad (9)$$

where  $\tau$  is the residence time of the ions in the source and  $n_{\text{BH}}$  is the density of the borazine in the source at a temperature of 295 K. At low source pressures (less than 0.1 mm) the free flight residence time,  $\tau_{\text{ff}}$ , calculated from electrostatic considerations, yielded concordant rate constants for the ion-molecule reactions of borazine.<sup>7</sup> The free flight residence time is given by

$$\tau_{\text{ff}} = (2dm/eE)^{1/2} \quad (10)$$

where  $d$  is the distance from the center of the light entrance slit to the ion exit slit measured in centimeters,  $m$  is the mass of the primary ion,  $e$  is the electrostatic charge in esu, and  $E$  is the electric field in statvolts per centimeter. At pressures much above 0.1 mm collisional effects on ion mobility become major factors in defining  $\tau$  and the free flight expression is no longer valid. Table I lists rate constants for the disappearance of the  $(\text{CH}_3)_3\text{B}_3\text{N}_3\text{H}_3^+$  calculated from measurements at different  $E/P$  values using  $\tau_{\text{ff}}$ . It is noted that the rate constant is essentially invariant over this range of residence times (repeller voltage changes at constant pressure).

On treating the kinetics of the *B*-trimethylborazine system according to the above mechanism the proton transfer step is equivalent to the overall rate of disappearance of the parent

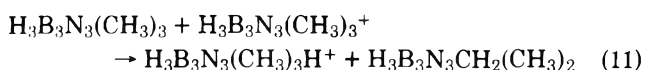
TABLE I: Bimolecular Rate Constants for the Reaction  $(\text{CH}_3)_3\text{B}_3\text{N}_3\text{H}_3 + (\text{CH}_3)_3\text{B}_3\text{N}_3\text{H}_3^+ \rightarrow \text{Products}$  at Various  $E/P$  Ratios<sup>a</sup>

$E/P$ , V $\text{cm}^{-1} \text{ mm}^{-1}$	$I_{(\text{CH}_3)_3\text{B}_3\text{N}_3\text{H}_3^+}/\Sigma I_i$	$k \times 10^{10} \text{ cm}^3$ $\text{molecule}^{-1} \text{ s}^{-1}$
163	0.730	6.0
184	0.736	5.5
198	0.742	6.2
216	0.765	6.2
239	0.777	5.9
303	0.810	6.0
314	0.828	5.3
		$k = 5.9 \pm 0.3 \times 10^{-10}$

<sup>a</sup> Sample composition  $\text{Ar}-(\text{CH}_3)_3\text{B}_3\text{N}_3\text{H}_3 = 12:1$ .

ions. Reactions 5 and 6 are treated as parallel reactions involving the same ionic intermediate  $(\text{CD}_3)_3\text{B}_3\text{N}_3\text{H}_3\text{D}^+$ . Shown in Table II are rate constants for the disappearance of  $(\text{CH}_3)_3\text{B}_3\text{N}_3\text{H}_3^+$  at various pressures for samples of  $(\text{CH}_3)_3\text{B}_3\text{N}_3\text{H}_3$  in methane and argon. The two sets of rate constants do not differ significantly and yield an averaged value of  $k = 6.5 \pm 1 \times 10^{-10} \text{ cm}^3 \text{ molecule}^{-1} \text{ s}^{-1}$ .

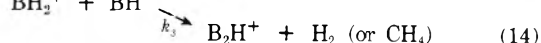
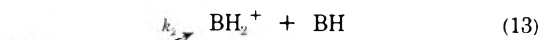
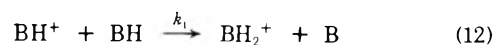
The only reaction observed in the *N*-trimethylborazine system is the proton transfer reaction



where protonation occurs from an exocyclic methyl group. Shown in Table III are rate constant data for  $\text{H}_3\text{B}_3\text{N}_3(\text{CH}_3)_3^+$  disappearance in samples of  $\text{H}_3\text{B}_3\text{N}_3(\text{CH}_3)_3$  in methane and argon. The two sets of data yield an averaged value for the rate constant of  $k(11) = 3.5 \pm 1.5 \times 10^{-10} \text{ cm}^3 \text{ molecule}^{-1} \text{ s}^{-1}$ . This value is somewhat lower than that reported previously<sup>7</sup> but was measured in a regime where the source pressure was better defined.

It should be noted that rate constants calculated for the borazines in diluents such as  $\text{H}_2$  and  $\text{He}$  are somewhat higher than the actual rate constants.<sup>7</sup> At the low source pressures used in this study (generally less than 0.1 mm) gas flow from the ion exit slit is primarily effusive, leading to density adjustment of the two gases. Thus the partial pressure of the borazine in the source is actually higher than that assumed from the sample composition and measured source pressure. For  $\text{Ar}$  and  $\text{CH}_4$  diluents the effect is not as great and the corrections to the rate constants are in general less than the random errors inherent in these measurements.

Similarities in the reactions of the borazine<sup>7</sup> and *B*-trimethylborazine cations with their molecular precursors may be noted. In both of these systems the simplest kinetic scheme may be described by the following reactions



Hydrogen or methane is a product in (14) when  $\text{BH}$  is borazine or *B*-trimethylborazine, respectively. CNDO calculations<sup>7</sup> indicate that the most stable structure for  $\text{BH}_2^+$  is one with equivalent hydrogens bound to a nitrogen site. We visualize the first step in the reaction for *B*-trideuterioborazine as

**TABLE II: Bimolecular Rate Constants for the Reaction  $(\text{CH}_3)_3\text{B}_3\text{N}_3\text{H}_3 + (\text{CH}_3)_3\text{B}_3\text{N}_3\text{H}_3^+ \rightarrow \text{Products}$  at Various Pressures for  $(\text{CH}_3)_3\text{B}_3\text{N}_3\text{H}_3\text{-CH}_4$  and  $(\text{CH}_3)_3\text{B}_3\text{N}_3\text{H}_3\text{-Ar}$  Mixtures**

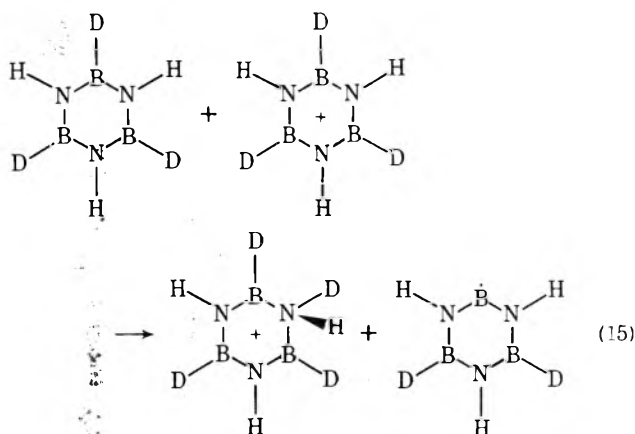
$P_s, \text{mm}^a$	$I_{(\text{CH}_3)_3\text{B}_3\text{N}_3\text{H}_3^+}/\Sigma I_i$	$k \times 10^{10}{}^b$	$P_s, \text{mm}^c$	$I_{(\text{CH}_3)_3\text{B}_3\text{N}_3\text{H}_3^+}/\Sigma I_i$	$k \times 10^{10}{}^b$
0.038	0.905	6.9	0.035	0.869	5.3
0.046	0.890	6.6	0.46	0.810	6.0
0.052	0.877	6.6	0.064	0.770	5.3
0.064	0.831	7.6	0.081	0.690	6.0
0.080	0.801	7.3	0.089	0.635	6.7
$k = 7.0 \pm 0.4 \times 10^{-10}$			$k = 5.9 \pm 0.5 \times 10^{-10}$		

<sup>a</sup> Sample composition  $\text{CH}_4\text{-(CH}_3)_3\text{B}_3\text{N}_3\text{H}_3 = 23:1$ .  $P_s$  = total source pressure. <sup>b</sup>  $\text{cm}^3 \text{ molecule}^{-1} \text{ s}^{-1}$ . <sup>c</sup> Sample composition  $\text{Ar-(CH}_3)_3\text{B}_3\text{N}_3\text{H}_3 = 16.4:1$ .

**TABLE III: Bimolecular Rate Constants for the Reaction  $\text{H}_3\text{B}_3\text{N}_3(\text{CH}_3)_3 + \text{H}_3\text{B}_3\text{N}_3(\text{CH}_3)_3^+ \rightarrow \text{H}_3\text{B}_3\text{N}_3(\text{CH}_3)_3\text{H}^+ + \text{H}_3\text{B}_3\text{N}_3(\text{CH}_3)_2\text{CH}_2$  at Various Pressures for  $\text{H}_3\text{B}_3\text{N}_3(\text{CH}_3)_3\text{-CH}_4$  and  $\text{H}_3\text{B}_3\text{N}_3(\text{CH}_3)_3\text{-Ar}$  Mixtures**

$P_s, \text{mm}^a$	$I_{\text{H}_3\text{B}_3\text{N}_3(\text{CH}_3)_3^+}/\Sigma I_i$	$k \times 10^{10}{}^b$	$P_s, \text{mm}^c$	$I_{\text{H}_3\text{B}_3\text{N}_3(\text{CH}_3)_3^+}/\Sigma I_i$	$k \times 10^{10}{}^b$
0.035	0.960	2.6	0.035	0.934	3.7
0.043	0.955	2.4	0.038	0.914	4.5
0.053	0.927	3.2	0.051	0.908	3.6
0.063	0.901	3.7	0.060	0.894	3.5
0.076	0.859	4.5	0.077	0.826	4.7
$k = 3.3 \pm 0.8 \times 10^{-10}$			$k = 4.0 \pm 0.5 \times 10^{-10}$		

<sup>a</sup> Sample composition  $\text{CH}_4\text{-H}_3\text{B}_3\text{N}_3(\text{CH}_3)_3 = 19.5:1$ .  $P_s$  = total source pressure. <sup>b</sup>  $\text{cm}^3 \text{ molecule}^{-1} \text{ s}^{-1}$ . <sup>c</sup> Sample composition  $\text{Ar-H}_3\text{B}_3\text{N}_3(\text{CH}_3)_3 = 16.4:1$ .

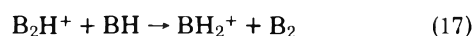


In this labeled system proton or deuteron transfer from the intermediate borazinium ion may occur. Thus reaction 13 is observable. Rate constants obtained for reaction 12 do not show a dependence on field strength or source pressure over a range of experimental conditions. However, the kinetics of the branching steps (reactions 13 and 14) are more complicated. It is observed in reactions with  $\text{D}_3\text{B}_3\text{N}_3\text{H}_3$  and  $(\text{CD}_3)_3\text{B}_3\text{N}_3\text{H}_3$  that the deuteron transferred initially is subsequently eliminated in reaction 14. This indicates that the deuteron added to the borazine in the initial step does not achieve immediate equivalence with the H atom at the nitrogen site. Thus at low BH pressures (in the regime where the average number of  $\text{BH}^+ \text{-BH}$  collisions is near one) reactions 13 and 14 may be viewed as two pathways by which an excited  $\text{BH}_2^+$  is deactivated. Treatment of reactions 13 and 14 as competitive reactions leads to the expression

$$k_2/k_3 = I_{\text{BH}_2^+}/I_{\text{BH}^+} \quad (16)$$

which serves as a measure of the relative rates of (13) and (14). Shown in Table IV are  $k_2/k_3$  ratios observed over a range of

pressures for  $\text{H}_3\text{B}_3\text{N}_3\text{H}_3$  and  $(\text{CH}_3)_3\text{B}_3\text{N}_3\text{H}_3$ . The averaged value of  $k_2/k_3 = 0.85 \pm 0.15$  obtained for  $(\text{CH}_3)_3\text{B}_3\text{N}_3\text{H}_3$  in Ar was higher than the value of  $0.54 \pm 0.10$  obtained for  $\text{H}_3\text{B}_3\text{N}_3\text{H}_3$ . The kinetics at higher BH pressures is complicated both by the reaction of the deactivated  $\text{BH}_2^+$  and the possible reaction of  $\text{B}_2\text{H}^+$  to form  $\text{BH}^+$  through the process



### Proton Affinity of the $\text{H}_2\text{B}_3\text{N}_3\text{H}_3$ Radical

In this section we consider the results of a kinetic study for reaction 1 involving proton transfer from the borazine cation ( $\text{BH}^+$ ) to a neutral base (A). In general, if process 1 is exothermic the rates for these reactions tend to be fast and the bimolecular rate constants fall in the range of  $10^{-10}$  to  $10^{-9} \text{ cm}^3 \text{ molecule}^{-1} \text{ s}^{-1}$  unless there is an activation energy. If  $k(1)$  is significantly less than  $10^{-10} \text{ cm}^3 \text{ molecule}^{-1} \text{ s}^{-1}$  it is possible to infer that process 1 requires an activation energy and is probably endothermic. Thus by measuring the rate constants for reaction 1 for different species A and knowing the proton affinity of each A,  $\text{PA(A)}$ , we can set boundaries on  $\text{PA(B)}$ . The organic bases selected for study include ethyl acetate, acetone, isobutylene, ethyl formate, diethyl ether, acetonitrile, and benzene- $d_6$ . The proton affinities of these substances have recently been determined from thermochemical data now available.<sup>16</sup> By using selectively deuterated species it is possible to determine if proton transfer is occurring by reaction 1. This is important since in most cases the neutral species A is also ionized under our experimental conditions and can undergo subsequent ion-molecule reactions.

Experimental observations of photon impact studies involving borazine are summarized in Table V. The protonation of borazine by a borazine cation has been studied previously.<sup>7</sup> The relatively large rate constant for this reaction,  $k = 1.3 \times 10^{-9} \text{ cm}^3 \text{ molecule}^{-1} \text{ s}^{-1}$  ( $k = 1.9 \times 10^{-9} \text{ cm}^3 \text{ molecule}^{-1} \text{ s}^{-1}$  in  $\text{CH}_4$ ), indicates that  $\text{PA(B)} < \text{PA(BH)}$ . The proton affinity



TABLE IV: Data for the Calculation of  $k_2/k_3$  for  $\text{H}_3\text{B}_3\text{N}_3\text{H}_3$  and  $(\text{CH}_3)_3\text{B}_3\text{N}_3\text{H}_3$  at Low Pressures

$P_{\text{H}_3\text{B}_3\text{N}_3\text{H}_3} \times 10^3, \text{ mm}^a$	$I_{\text{BH}_2^+}/I_{\text{B}_2\text{H}^+}$	$P_{(\text{CH}_3)_3\text{B}_3\text{N}_3\text{H}_3} \times 10^3, \text{ mm}^b$	$I_{\text{BH}_2^+}/I_{\text{B}_2\text{H}^+}$
1.8	0.64	3.9	0.76
2.5	0.46	4.9	0.87
3.3	0.55	5.3	0.76
		5.7	0.76
		6.8	0.87
		7.4	0.94
$I_{\text{BH}_2^+}/I_{\text{B}_2\text{H}^+} = 0.54 \pm 0.1$		$I_{\text{BH}_2^+}/I_{\text{B}_2\text{H}^+} = 0.85 \pm 0.1$	

<sup>a</sup> Sample composition Ar- $\text{H}_3\text{B}_3\text{N}_3\text{H}_3 = 51:1$ . <sup>b</sup> Sample composition Ar- $(\text{CH}_3)_3\text{B}_3\text{N}_3\text{H}_3 = 12:1$ .

TABLE V: Reaction Sequences Involving Borazine

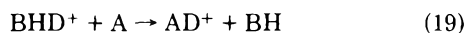
Reaction mixture	Reaction composition	Pressure range, mm	Reaction sequence	Pertinent observations	PA- ( $\text{H}_2\text{B}_3\text{N}_3\text{H}_3$ ), kcal/mol
$\text{D}_3\text{B}_3\text{N}_3\text{H}_3\text{-CH}_4$	1:12.3	0.038–0.078	$\text{D}_3\text{B}_3\text{N}_3\text{H}_3 + \text{D}_3\text{B}_3\text{N}_3\text{H}_3^+ \rightarrow \text{D}_3\text{B}_3\text{N}_3\text{H}_3\text{D}^+ + \text{D}_2\text{B}_3\text{N}_3\text{H}_3$	Occur $k = 1.3 \times 10^{-9}$ <sup>a</sup>	$<199 \pm 3$ <sup>b</sup>
$\text{H}_3\text{B}_3\text{N}_3\text{H}_3\text{-CH}_4$	1:28.6	0.028–0.090	$\text{H}_3\text{B}_3\text{N}_3\text{H}_3 + \text{H}_3\text{B}_3\text{N}_3\text{H}_3^+ \rightarrow \text{H}_3\text{B}_3\text{N}_3\text{H}_4^+ + \text{H}_2\text{B}_3\text{N}_3\text{H}_3$		
$\text{C}_2\text{H}_5\text{CO}_2\text{CH}_3\text{-D}_3\text{B}_3\text{N}_3\text{H}_3\text{-CH}_4$	1:1.33:15.7	0.040–0.086	$\text{C}_2\text{H}_5\text{CO}_2\text{CH}_3 + \text{D}_3\text{B}_3\text{N}_3\text{H}_3^+ \rightarrow \text{C}_2\text{H}_5\text{CO}_2\text{CH}_3\text{D}^+ + \text{D}_2\text{B}_3\text{N}_3\text{H}_3$	Occurs $k > 2 \times 10^{-10}$	$<198.0$ <sup>c</sup>
$\text{CH}_3\text{COCH}_3\text{-D}_3\text{B}_3\text{N}_3\text{H}_3\text{-CH}_4$	1:3:25.5	0.026–0.072	$\text{CH}_3\text{COCH}_3 + \text{D}_3\text{B}_3\text{N}_3\text{H}_3^+ \rightarrow \text{CH}_3\text{COCH}_3\text{D}^+ + \text{D}_2\text{B}_3\text{N}_3\text{H}_3$	Occurs $k > 3 \times 10^{-10}$	$<194.6$
$i\text{-C}_4\text{H}_8\text{-D}_3\text{B}_3\text{N}_3\text{H}_3\text{-CH}_4$	1:1.8:23.8	0.035–0.073	$i\text{-C}_4\text{H}_8 + \text{D}_3\text{B}_3\text{N}_3\text{H}_3^+ \rightarrow \text{C}_4\text{H}_8\text{D}^+ + \text{D}_2\text{B}_3\text{N}_3\text{H}_3$	Occurs $k > 5 \times 10^{-11}$	193.0
$\text{HCO}_2\text{C}_2\text{H}_5\text{-D}_3\text{B}_3\text{N}_3\text{H}_3\text{-CH}_4$	1:9.8:48	0.037–0.096	$\text{HCO}_2\text{C}_2\text{H}_5 + \text{D}_3\text{B}_3\text{N}_3\text{H}_3^+ \rightarrow \text{HCO}_2\text{C}_2\text{H}_5\text{D}^+ + \text{D}_2\text{B}_3\text{N}_3\text{H}_3$	May occur $k < 3 \times 10^{-11}$ <sup>c</sup>	191.2
$\text{HCO}_2\text{C}_2\text{H}_5\text{-D}_3\text{B}_3\text{N}_3\text{H}_3\text{-CH}_4$	1:1.78	0.025	$\text{HCO}_2\text{C}_2\text{H}_5 + \text{D}_3\text{B}_3\text{N}_3\text{H}_3^+ \rightarrow \text{HCO}_2\text{C}_2\text{H}_5\text{D}^+ + \text{D}_2\text{B}_3\text{N}_3\text{H}_3$		191.2
$\text{CH}_3\text{OCH}_3\text{-D}_3\text{B}_3\text{N}_3\text{H}_3\text{-CH}_4$	3.5:1	0.008–0.013	$\text{CH}_3\text{OCH}_3 + \text{D}_3\text{B}_3\text{N}_3\text{H}_3^+ \rightarrow \text{CH}_3\text{OCH}_3\text{D}^+ + \text{D}_2\text{B}_3\text{N}_3\text{H}_3$	Not observed ( $k < 3 \times 10^{-11}$ )	$>190.1$
$\text{CH}_3\text{CN-D}_3\text{B}_3\text{N}_3\text{H}_3$	1.58:1	0.010–0.032	$\text{CH}_3\text{CN} + \text{D}_3\text{B}_3\text{N}_3\text{H}_3^+ \rightarrow \text{CH}_3\text{DCN}^+ + \text{D}_2\text{B}_3\text{N}_3\text{H}_3$	Not observed	$>187.3$
$\text{C}_6\text{D}_6\text{-H}_3\text{B}_3\text{N}_3\text{H}_3$	1:33	0.008–0.048	$\text{C}_6\text{D}_6 + \text{H}_3\text{B}_3\text{N}_3\text{H}_3^+ \rightarrow \text{C}_6\text{D}_6\text{H}^+ + \text{D}_2\text{B}_3\text{N}_3\text{H}_3$	Not observed	$>183.4$

<sup>a</sup> Units for bimolecular rate constants =  $\text{cm}^3 \text{ molecule}^{-1} \text{ s}^{-1}$ . <sup>b</sup> Proton affinity of  $\text{H}_3\text{B}_3\text{N}_3\text{H}_3$  between 2-butyne ( $198 \pm 2$  kcal/mol) and  $\text{NH}_3$  (200.7 kcal/mol).<sup>6c,16</sup> <sup>c</sup> All other proton affinity data from ref 16.

of borazine has previously been determined<sup>6c</sup> to be between that of 2-butyne ( $198 \pm 2$  kcal/mol<sup>-1</sup>)<sup>6c</sup> and  $\text{NH}_3$  (200.7 kcal/mol<sup>-1</sup>).<sup>16</sup> In  $\text{C}_2\text{H}_5\text{CO}_2\text{CH}_3\text{-D}_3\text{B}_3\text{N}_3\text{H}_3$ ,  $\text{CH}_3\text{COCH}_3\text{-D}_3\text{B}_3\text{N}_3\text{H}_3$ , and  $i\text{-C}_4\text{H}_8\text{-D}_3\text{B}_3\text{N}_3\text{H}_3$  mixtures ion-molecule reactions result in the formation of the species  $\text{C}_2\text{H}_5\text{CO}_2\text{CH}_3\text{D}^+$ ,  $\text{CH}_3\text{COCH}_3\text{D}^+$ , and  $\text{C}_4\text{H}_8\text{D}^+$ , respectively. Approximate rate constants for reaction 1 were obtained from the relationship

$$k_{\text{AD}^+} = k_{\text{BH}^+} \left( \frac{P_{\text{BH}}}{P_{\text{A}}} \right) \left( \frac{I_{\text{AD}^+}}{I_{\text{BHD}^+}} \right) \quad (18)$$

assuming a competitive reaction scheme for  $\text{BH}^+$  disappearance. These rate constants are only approximate since they do not take into account any ion-molecule reactions involving the species  $\text{AD}^+$  or  $\text{BHD}^+$  other than reaction 13, but they do serve to indicate the relative rates of these reactions. The reaction



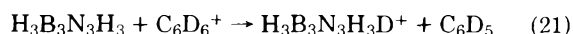
does not contribute significantly to  $\text{AD}^+$  formation since  $\text{PA}(\text{BH}) > \text{PA}(\text{A})$  for all cases except perhaps ethyl acetate. Samples of ethyl formate and  $\text{D}_3\text{B}_3\text{N}_3\text{H}_3$  were run with and without the methane diluent. In the samples without methane a small intensity of  $\text{HCO}_2\text{C}_2\text{H}_5\text{D}^+$  was observed, while in samples with  $\text{CH}_4$  the intensity of  $\text{HCO}_2\text{C}_2\text{H}_5\text{D}^+$  was not

detectable above the noise level of the instrument. No deuteration of the neutral organic species was observed in  $\text{CH}_3\text{OCH}_3\text{-D}_3\text{B}_3\text{N}_3\text{H}_3$  or  $\text{CH}_3\text{CN-D}_3\text{B}_3\text{N}_3\text{H}_3$  mixtures.

The  $\text{C}_6\text{D}_6\text{-H}_3\text{B}_3\text{N}_3\text{H}_3$  system is of some interest in the sense that neither reaction



nor



is observed. This implies that  $\text{PA}(\text{H}_2\text{B}_3\text{N}_3\text{H}_3) > \text{PA}(\text{C}_6\text{D}_6)$  and  $\text{PA}(\text{C}_6\text{D}_5) > \text{PA}(\text{H}_3\text{B}_3\text{N}_3\text{H}_3)$ . The proton affinity of  $\text{C}_6\text{D}_5$  may be obtained from the heats of formation of  $\text{H}^+$ ,  $\text{C}_6\text{D}_5$ , and  $\text{C}_6\text{D}_6^+$  (366, 72, and 233 kcal mol<sup>-1</sup>, respectively).<sup>11</sup> This calculation gives  $\text{PA}(\text{C}_6\text{D}_5) = 205$  kcal mol<sup>-1</sup>. Thus we note  $\text{PA}(\text{H}_3\text{B}_3\text{N}_3\text{H}_3) < 205$  kcal mol<sup>-1</sup>. It may also be noted that while in the benzene system  $\text{PA}(\text{C}_6\text{H}_5) > \text{PA}(\text{H}_2\text{B}_3\text{N}_3\text{H}_3)$  in the analogous borazine system  $\text{PA}(\text{H}_3\text{B}_3\text{N}_3\text{H}_3) > \text{PA}(\text{H}_2\text{B}_3\text{N}_3\text{H}_3)$ .

The accumulation of information on reaction sequences involving the borazine cation as a proton donor (Table V) indicates that the proton affinity of  $\text{H}_2\text{B}_3\text{N}_3\text{H}_3$  is greater than those of benzene, acetonitrile, dimethyl ether, and ethyl formate but less than those of borazine, ethyl acetate, and acetone. Using  $\text{PA}(\text{HCO}_2\text{C}_2\text{H}_5) = 191.2$  kcal mol<sup>-1</sup> and PA-

(CH<sub>3</sub>COCH<sub>3</sub>) = 194.6 kcal mol<sup>-1</sup> we obtain PA(H<sub>2</sub>B<sub>3</sub>N<sub>3</sub>H<sub>3</sub>) 193 ± 2 kcal mol<sup>-1</sup>.

Strictly speaking the occurrence or nonoccurrence of reaction 1 is assumed to be a direct reflection of the proton affinity of BH<sup>+</sup>, that is,  $\Delta G^\circ(1) = \Delta H^\circ(1) = \text{PA}(\text{B}) - \text{PA}(\text{A})$ . This expression tacitly assumes  $\Delta S^\circ(1) \approx 0$ . The entropy changes occurring in these proton transfer reactions are usually quite small (less than 1 eu) and often very difficult to measure. As noted by Kebarle<sup>16</sup> exceptions to this rule occur in cases of internal hydrogen bonding, creation of restricted internal rotation, or large changes of rotational symmetry numbers.<sup>16,17</sup> The easiest of these to predict are entropy changes due to changes of rotational symmetry numbers. With this correction, the condition for occurrence of reaction 1 becomes  $\text{PA}(\text{B}) \leq \text{PA}(\text{A}) + RT \ln(3\sigma_{\text{A}}/\sigma_{\text{AH}^+})$  since  $\sigma_{\text{BH}^+} = 6$  and  $\sigma_{\text{B}} = 2$ . This correction term contributes less than 1.2 kcal mol<sup>-1</sup> to PA(B) in all cases except for A = H<sub>3</sub>B<sub>3</sub>N<sub>3</sub>H<sub>3</sub> and C<sub>6</sub>D<sub>6</sub> where the corrections are 1.7 and 2.0 kcal mol<sup>-1</sup>, respectively. These additions to PA(B) are in general small compared to the error limits imposed by the experimental system.

### Stability of the H<sub>2</sub>B<sub>3</sub>N<sub>3</sub>H<sub>3</sub> Radical

From measurements of the proton affinity of H<sub>2</sub>B<sub>3</sub>N<sub>3</sub>H<sub>3</sub> we may now calculate the dissociation energy for the process



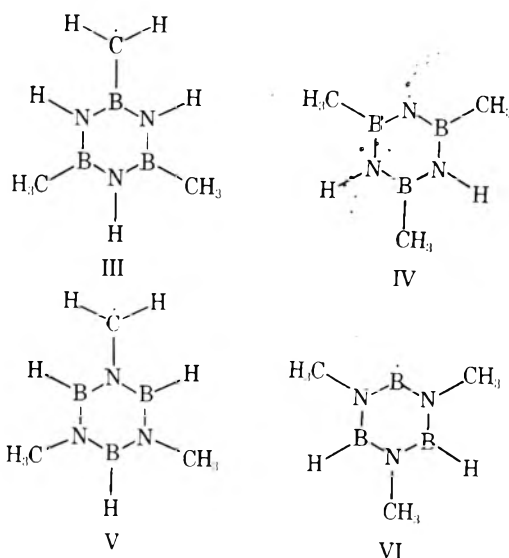
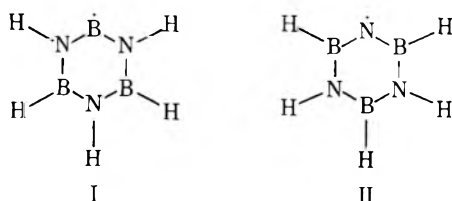
From the appropriate thermochemical cycle  $\Delta E$  for reaction 22 is given by

$$\Delta E(22) = \text{PA}(\text{H}_2\text{B}_3\text{N}_3\text{H}_3) + \text{IP}(\text{H}_3\text{B}_3\text{N}_3\text{H}_3) - \text{IP}(\text{H}) \quad (23)$$

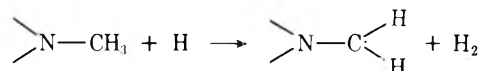
Using  $\text{IP}(\text{H}_3\text{B}_3\text{N}_3\text{H}_3) = 10.1$  eV from photoelectron data<sup>8,18-20</sup> and  $\text{IP}(\text{H}) = 13.595$  eV, we obtain  $\Delta E(22) = 112 \pm 3$  kcal mol<sup>-1</sup> where the uncertainty is primarily in PA(H<sub>2</sub>B<sub>3</sub>N<sub>3</sub>H<sub>3</sub>). In these calculations we have assumed that zero point energy corrections involving differences in D and H are sufficiently small to be neglected within the experimental uncertainties. Using the heat of formation of borazine based on solution calorimetry ( $\Delta H_f^\circ = 198$  kcal mol<sup>-1</sup>)<sup>21</sup> and  $\Delta H_f^\circ = 52$  kcal mol<sup>-1</sup> for H(g) we obtain for the borazynyl radical  $\Delta H_f^\circ = -138$  kcal mol<sup>-1</sup>.

### Discussion

Results of these experiments and earlier work have shown that the cations of borazine, *B*-trimethylborazine, and *N*-trimethylborazine undergo a rapid bimolecular proton transfer reaction with their precursor molecules. This implies that in each case PA(borazine radical) < PA(borazine molecule). From ion-molecule studies with selectively deuterated borazines it is possible to infer the structure of the radicals formed in these reactions. From the three systems investigated we find that I is favored over II, III is favored over IV, and V



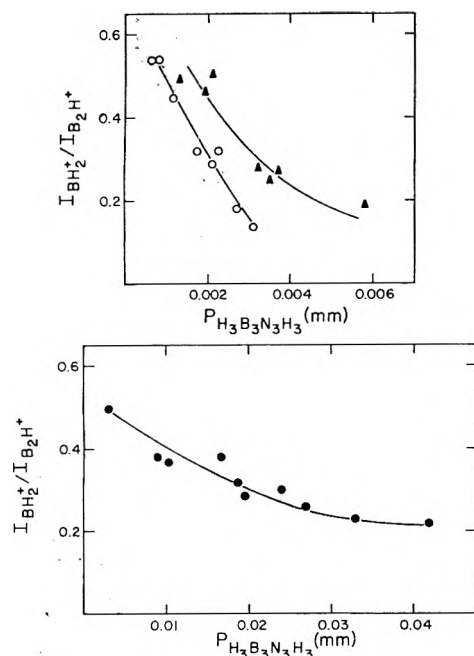
is favored over VI. More indirectly these conclusions for structures III and V are supported by photochemical evidence. The stable product of the Hg-photosensitized reaction of *N*-trimethylborazine in hydrogen is a dimer of V with C-C linkage.<sup>22</sup> No evidence for a B-B linked product was obtained. In similar studies with *B*-trimethylborazine the stable product is a dimer of III with C-C linkage; N-N linked dimers are not observed.<sup>23</sup> Photochemical studies with *N*-trimethylborazine show that radical formation results from H abstraction through the reaction



We can assume therefore that the C-H bond dissociation energy in this compound is probably less than that for H<sub>2</sub> (104 kcal mol<sup>-1</sup>). Based on our determined value of the energy needed to dissociate an N-B bond in borazine (112 kcal mol<sup>-1</sup>), it follows that hydrogen abstraction from borazine by thermalized H atoms is a thermodynamically unfavorable reaction.

The intermediate borazinium ion (BH<sub>2</sub><sup>+</sup>) formed in the borazine and *B*-trimethylborazine systems reacts in a scheme indicated by eq 13 and 14. Studies with partially deuterated borazines show that reaction 13 involves a genuine proton transfer process and that the proton transferred in the initial step of the reaction sequence is subsequently eliminated in reaction 14. These studies also indicate that the proton transferred from the borazine cation is bound to the nitrogen site in BH<sub>2</sub><sup>+</sup>, but that it does not achieve immediate equivalence with the second H bound to nitrogen. The branching ratio  $k_2/k_3$ , measured after a small number of BH<sub>2</sub><sup>+</sup>-BH collisions have occurred, is taken as a measure of the deactivation rate of BH<sub>2</sub><sup>+</sup>. For borazine this corresponds to about one in three collisions and for *B*-trimethylborazine about one in two collisions.

For the borazine system,  $I_{\text{BH}_2^+}/I_{\text{B}_2\text{H}^+}$  ratios approach the same value (0.55 ± 0.1) at low source pressures irrespective of the diluent gas used (rare gases, CH<sub>4</sub>, SF<sub>6</sub>). Shown in Figure 5 are plots of this ratio for pure borazine and for SF<sub>6</sub>-H<sub>3</sub>B<sub>3</sub>N<sub>3</sub>H<sub>3</sub> mixtures. In all cases the  $I_{\text{BH}_2^+}/I_{\text{B}_2\text{H}^+}$  ratio decreased as the source pressure was increased. This is a further indication that BH<sub>2</sub><sup>+</sup> is a precursor to B<sub>2</sub>H<sup>+</sup> formation. For SF<sub>6</sub>-H<sub>3</sub>B<sub>3</sub>N<sub>3</sub>H<sub>3</sub> mixtures the value of the  $I_{\text{BH}_2^+}/I_{\text{B}_2\text{H}^+}$  ratio was essentially identical with that observed for the pure bo-



**Figure 5.** Effect of borazine source pressure on  $I_{BH_2^+}/I_{B_2H^+}$  ratio. Top: (O) sample composition  $SF_6-H_3B_3N_3H_3 = 58:1$ ; (▲) sample composition  $SF_6-H_3B_3N_3H_3 = 30.4:1$ . Bottom: pure borazine sample.

razine system at low source pressures. The rapid decrease at the higher source pressures (Figure 5) is due in part to the increase in residence times of the  $BH_2^+$  ions.

A condensation reaction (reaction 14) does not contribute significantly to the kinetic analysis of ion-molecule reactions in the *N*-trimethylborazine system. Such a process would require elimination of a methyl bound to N. Reaction 13 most probably occurs but is not directly observable with partially deuterated species since the deuteron transferred in the pri-

mary step is presumably bound to a N site in the intermediate borazinium ion. Equivalence of two H's in the intermediate could be achieved only if the proton added were bound to the B site.

**Acknowledgments.** We are grateful for support of this work by the National Science Foundation through Grant No. CHE76-02477.

## References and Notes

- (1) S. G. Lias and P. Ausloos, "Ion-Molecule Reactions", American Chemical Society, Washington, D.C., 1975.
- (2) J. L. Beauchamp in "Interactions between Ions and Molecules", P. Ausloos, Ed., Plenum Press, New York, N.Y., 1975, p 413.
- (3) E. E. Ferguson, ref 2, p 313.
- (4) A. Dalgarno, ref 2, p 341.
- (5) See other papers in this volume.
- (6) (a) J. J. Solomon and R. F. Porter, *J. Am. Chem. Soc.*, **94**, 1443 (1972); (b) R. F. Porter and J. J. Solomon, *ibid.*, **93**, 56 (1971); (c) L. D. Betowski, J. J. Solomon, and R. F. Porter, *Inorg. Chem.*, **11**, 424 (1972); (d) R. C. Pierce and R. F. Porter, *ibid.*, **14**, 1087 (1975).
- (7) A. DeStefano and R. F. Porter, *Inorg. Chem.*, **14**, 2882 (1975).
- (8) J. Kroner, D. Proch, W. Fuss, and H. Boch, *Tetrahedron*, **28**, 1585 (1972).
- (9) P. Ausloos and S. G. Lias, *Radiat. Res. Rev.*, **1**, 75 (1968).
- (10) R. Gorden, R. E. Rebert, and P. Ausloos, *Natl. Bur. Stand. (U.S.), Tech. Note*, **496** (1963).
- (11) J. L. Franklin, J. G. Dillard, H. M. Rosenstock, J. T. Herron, K. Draxl, and F. H. Field, *Natl. Stand. Ref. Data Ser., Natl. Bur. Stand.*, **No. 26** (1969).
- (12) L. F. Hohnstedt and D. T. Haworth, *J. Am. Chem. Soc.*, **82**, 89 (1960).
- (13) A. J. DeStefano and R. F. Porter, *Inorg. Chem.*, in press.
- (14) O. T. Beachley, Jr., *Inorg. Chem.*, **8**, 981 (1969).
- (15) D. T. Haworth and L. F. Hohnstedt, *J. Am. Chem. Soc.*, **82**, 3860 (1960).
- (16) R. Yamdagni and P. Kebarle, *J. Am. Chem. Soc.*, **98**, 1320 (1976).
- (17) R. Yamdagni and P. Kebarle, *J. Am. Chem. Soc.*, **95**, 3504 (1973).
- (18) D. C. Frost, F. G. Herring, C. A. McDowell, and T. A. Stenhouse, *Chem. Phys. Lett.*, **5**, 291 (1970).
- (19) C. R. Brundle, M. B. Robins, and N. A. Kuebler, *J. Am. Chem. Soc.*, **94**, 1466 (1972).
- (20) D. R. Lloyd and N. Lynaugh, *Phil. Trans. Roy. Soc., London Ser. A*, **268**, 97 (1970).
- (21) B. C. Smith, L. Thakur, and M. A. Wassef, *J. Chem. Soc. A*, 1616 (1967).
- (22) L. J. Turbini, T. J. Mazanec, and R. F. Porter, *J. Inorg. Nucl. Chem.*, **37**, 1129 (1975).
- (23) G. A. Kline, M. S. Thesis, Cornell University, Ithaca, N. Y., 1976.

## A Time-Resolved Study of the Unimolecular Fragmentation of Some $C_6H_6^+$ Molecular Ions

Paul P. Dymerski and Alex. G. Harrison\*

Department of Chemistry, University of Toronto, Toronto, Canada M5S 1A1 (Received June 29, 1976)

Publication costs assisted by the National Research Council of Canada

The unimolecular fragmentation reactions of the molecular ions of 1,5-hexadiyne, 1,4-hexadiyne, 2,4-hexadiyne, and benzene have been studied by time-resolved mass spectrometry using ion-trapping techniques. Extensive fragmentation of the molecular ions of 1,5-hexadiyne and 1,4-hexadiyne is observed over the time period from 5 to 500  $\mu$ s. However, over the same time period, no fragmentation of the 2,4-hexadiyne molecular ion is observed and only a very small extent of fragmentation of the benzene molecular ion is observed. From curve fitting of the decay curves for the molecular ion intensities it is concluded that the observed fragmentation does not arise from reaction of a single state with a characteristic half-life, but rather that several states are involved. Sample calculations show that a decay curve arising from many reacting states (or in the limit a continuum of states) can be fitted adequately by a three-state function and that it is not possible to determine the number of reactive states from curve fitting if several (or many) states are involved.

### Introduction

The fragmentation reactions following electron impact or photon impact ionization of polyatomic molecules usually are considered to be a set of competing and consecutive unimolecular decomposition reactions. On the assumption that the excitation and subsequent internal energy transfer processes rapidly lead to an equilibrium distribution of excited ions among all the possible quantum states, the rates of the fragmentation reactions can be calculated by suitable application of the absolute rate theory.<sup>1</sup> The most widely used formulation has been the quasiequilibrium theory (QET) of mass spectra whose status has been reviewed.<sup>2,3</sup>

If one assumes that a large number of states (of differing energies) are populated by the initial ionization process, the energy randomization and fragmentation model assumed by the QET leads to a large range (or, in the limit, a continuum) of reaction rates or ion lifetimes. At the other extreme, if one assumes population of only a few isolated states capable of fragmentation, only a small number of reaction rates or ion lifetimes should be observed. The evidence<sup>2,3</sup> to date indicates that for polyatomic molecules ionized by electron impact the real situation lies closer to the first assumption than the second. It has long been recognized that a direct study of the kinetics of fragmentation processes could provide, in principle, crucial evidence relevant to this question.

However, such direct studies are difficult, not only because it is difficult to vary the reaction time over a significant range with conventional mass spectrometers, but also because the major part of the fragmentation reaction normally is complete in a time interval shorter than the minimum ion source residence times of conventional mass spectrometers.

The first experimental approach to such studies was to vary ion source residence times (over a limited range) to obtain "decay curves" for metastable ion abundances.<sup>4-9</sup> In a number of cases linear regions have been observed in these curves which have been interpreted in terms of discrete rate constants or ion lifetimes, although in several cases conflicting results have been obtained for the same reaction. Rosenstock<sup>10</sup> has reviewed this work and concluded that none of the conclusions concerning discrete lifetimes are valid, primarily

because the data are not sufficiently precise. More recent studies by Ottinger,<sup>11,12</sup> in which the ion source residence time could be varied between  $10^{-8}$  and  $10^{-5}$  s with good time resolution, led to the conclusion that the fragmentation reactions leading to metastable ions involved a large number rather than a few discrete ion half-lives.

The first direct study of the kinetics of ion fragmentation in the ion source was carried out by Meyer and Harrison<sup>13</sup> who studied the fragmentation of the toluene molecular ion (loss of H) over the time range from 2 to 20  $\mu$ s using a pulsed ion source. They interpreted their results in terms of a fast reaction which was complete before observations could be made and a slow reaction with an apparent discrete rate constant, thus suggesting fragmentation from an discrete state with a single half-life. Subsequently Vestal<sup>12</sup> has reported that the results can be accommodated within the framework of the quasi-equilibrium theory although the details of the calculations have not been reported. More recently, Buttrill<sup>14</sup> has used time-resolved photoionization mass spectrometry to study the fragmentation of the toluene molecular ion over the time range from 70 to 200  $\mu$ s and has concluded that only three discrete states are involved in the fragmentation (loss of H) of toluene molecular ions formed by photoionization between 1053 and 1026 Å. This conclusion has been challenged by Lifshitz<sup>15</sup> who has suggested that the data are consistent with a distribution of lifetimes if the rate coefficient for the fragmentation is a slowly increasing function of the internal energy above the threshold.

Recently, Gross and Aerni<sup>16</sup> observed that in the mass spectrum of 1,5-hexadiyne obtained with a conventional magnetic deflection mass spectrometer (ion source residence time  $\sim 1$   $\mu$ s) the  $m/e$  78 molecular ion was the major ion in the 70-eV mass spectrum while in the low-pressure ion cyclotron resonance mass spectrum (cell residence time  $\sim 10^{-3}$  s) the  $m/e$  77 ( $M^+ - H$ ) ion was the major ion in the mass spectrum. These results indicate an unusually large extent of fragmentation at reaction times greater than  $10^{-6}$  s and it was suggested<sup>16</sup> that this fragmentation might involve an isolated state of the molecular ion. The large amount of fragmentation apparently occurring over a time range accessible by time-

resolved mass spectrometry led us to carry out a kinetic study of the fragmentation of the molecular ion of 1,5-hexadiyne in an attempt to obtain more detailed information concerning the slow fragmentation reaction. Since there have been suggestions<sup>17</sup> of extensive structural isomerizations of  $C_6H_6^+$  ions we also have studied benzene, 1,4-hexadiyne, and 2,4-hexadiyne.

### Experimental Section

**Instrumental.** The ion-trapping technique used to vary the reaction time has been described previously<sup>18</sup> with respect to its use in the study of bimolecular ion-molecule reactions. The mode of operation in the present study of unimolecular ion fragmentation reactions was essentially the same except that much lower ion source concentrations ( $<1 \times 10^{11}$  molecule  $cm^{-3}$ ) were used to avoid complications from bimolecular processes. Briefly, ionization of the sample of interest was accomplished by a 1- $\mu s$  pulse of electrons with nominal mean energies ranging from 15 to 70 eV. The ions produced were trapped in the negative space charge of the continuous low energy ( $\sim 5$  eV) electron beam until ejected for mass analysis by a 5- $\mu s$  pulse (3.5-V amplitude) applied to the repeller electrode. Trapping times, i.e., the delay time between the two pulses, were varied from 0 to 1.0 ms.

For unimolecular reactions the total reaction time is the sum of the trapping time plus the flight time of the ions out of the ionization chamber to the point where they reach the ion acceleration region. This latter time was determined by applying a deflection pulse to one-half of the split focus electrode in the ion gun as described previously<sup>19</sup> and observing the recorded ion signal as a function of the delay time between the onset of the repeller pulse and the short duration deflection pulse. Under the present operating conditions the mean flight time was 5.4  $\mu s$  for ions of  $m/e$  78 with a total spread of  $\sim 2 \mu s$ . This mean time was added to the measured trapping times to obtain the total reaction time.

**Materials.** The 1,5-hexadiyne, 2,4-hexadiyne, and benzene were commercially available samples. 1,4-Hexadiyne was prepared by the method of Gensler et al.<sup>20</sup> and purified by glc before use.

**Treatment of Data.** After normalization, the experimental data are obtained as the fraction of the total ionization for each ionic species as a function of time after the initial ionization process. Our desire was to obtain, if possible, the number of states active in the fragmentation of the  $C_6H_6^+$  molecular ion in each system and the population and mean lifetime of each state. To this end the experimental decay curves were fitted to the relations

$$f(n) = 1 + \sum_{i=1}^n \{A_i \exp(-k_i t) - A_i\} \quad (1)$$

$$f(n') = 1 + \sum_{i=1}^{n'-1} \{A_i \exp(-k_i t) - A_i\} - A_{n'} \quad (2)$$

where  $f(n)$  or  $f(n')$  is the fractional ion current observed as  $C_6H_6^+$ ,  $n$  or  $n'$  is the total number of states considered, and  $A_i$  is the population of the  $i$ th state fragmenting with a characteristic rate constant  $k_i$ . Equation 2 differs from eq 1 by including a state (or states), with total population  $A_{n'}$ , which has reacted completely before observations can be made. Curve fitting was carried out to determine the minimum number of parameters required to reproduce the experimental data employing the boundary condition of  $f = 1$  at  $t = 0$  using a non-linear least-squares computer program.<sup>21</sup>

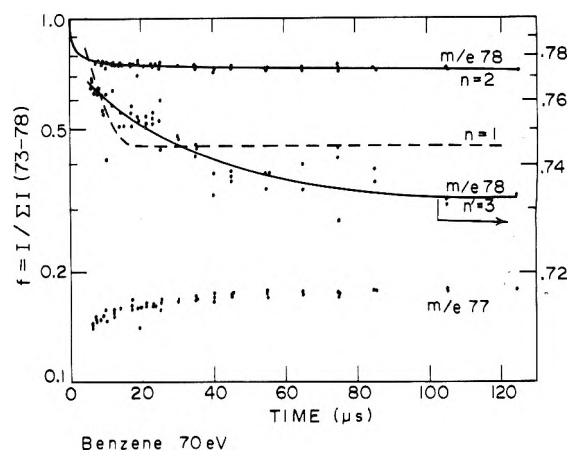


Figure 1. Ion signals in benzene as function of reaction time. Solid lines are computer fits as described in text.

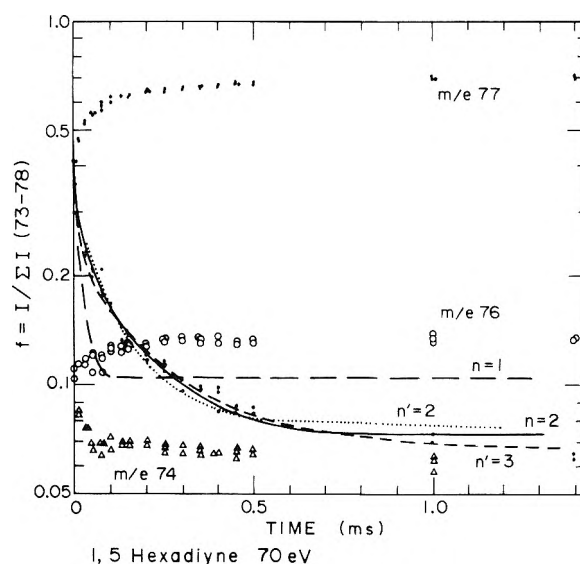


Figure 2. Ion signals in 1,5-hexadiyne as a function of reaction time. Solid lines are computer fits to  $m/e$  78 decay, see text.

### Results and Discussion

**Benzene.** Typical results for the benzene system at 70-eV electron energy are shown in Figure 1. Only a very small amount of fragmentation ( $\sim 3\%$ ) of the benzene molecular ion is observed at times greater than 5  $\mu s$ . The experimental decay curve shows considerable scatter but is best fit by eq 2 with  $n' = 3$  indicating an apparent minimum of two reactive states with half-lives in the measurable range. At lower electron energies ( $<20$  eV) the scatter in the experimental data was too great, because of decreased ion signals, to detect any fragmentation over the accessible time range.

**1,5-Hexadiyne.** Typical experimental results obtained at 70 eV for the 1,5-hexadiyne system are shown in Figure 2. In agreement with the more qualitative observations of Gross and Aerni<sup>16</sup> we observe that the  $C_6H_6^+$  molecular ion, which comprises  $\sim 40\%$  of the total ionization at the shortest observable time (5–6  $\mu s$ ), decreases rapidly in importance with increasing reaction time and, at long times, accounts for only 6–7% of the total ionization. The major portion of the fragmentation occurs over the first 500  $\mu s$  with  $C_6H_5^+$  ( $m/e$  77) being the main decomposition product.

As is shown in Figure 2, it was found that the total decay



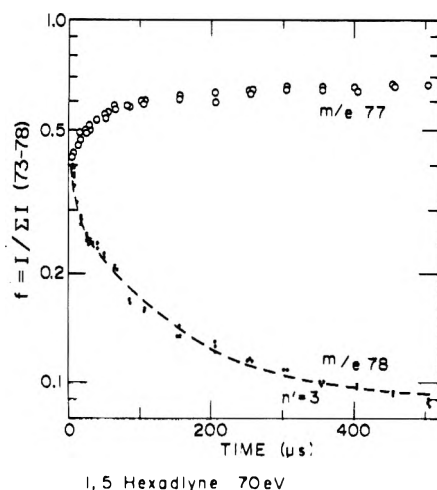


Figure 3. Ion signals in 1,5-hexadiyne as a function of reaction time. Data of Figure 2 on an expanded scale.

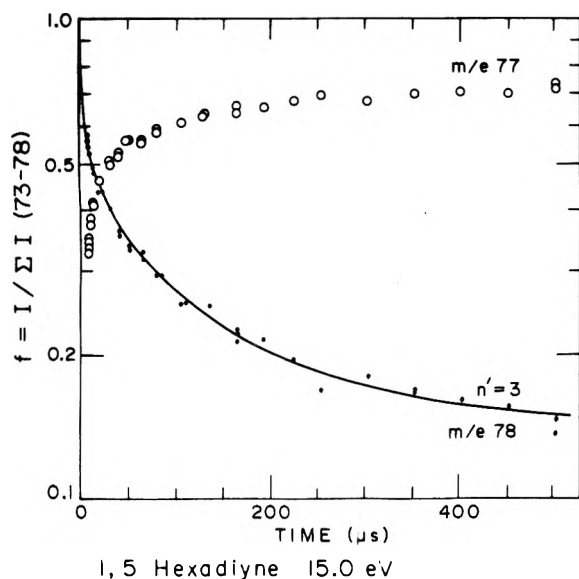


Figure 4. Ion signals in 1,5-hexadiyne as a function of reaction time, 15.0 eV. Solid line is a computer fit to  $m/e$  78 decay, see text.

curve could not be fitted by eq 1 with  $n = 1$  or by eq 2 with  $n' = 2$ , clearly eliminating the possibility that a single isolated state with a characteristic fragmentation rate constant is responsible for the observed fragmentation. However, it should be noted that the experimental results for reaction times less than  $300 \mu s$  were fitted satisfactorily assuming a single reactive state with a half-life in the accessible time range. This observation indicates that extreme caution must be exercised in the interpretation of decay curves which cover only a short time interval. Over the complete reaction time examined the decay curve is well fitted by eq 2 with  $n' = 3$ . The fit is shown in Figure 2 and, more clearly, in Figure 3 which presents the results covering the first  $500 \mu s$  on an expanded time scale.

At 15-eV nominal electron energy results very similar to the 70-eV results were obtained as shown by the data in Figure 4. In particular, the extent of fragmentation over the observable time is similar to that at 70 eV and the experimental data are well fitted by eq 2 with  $n' = 3$ . The significance of these fits will be discussed in detail below.

**1,4-Hexadiyne.** Typical results obtained for 1,4-hexadiyne at 70- and 15.1-eV nominal electron energy are shown in

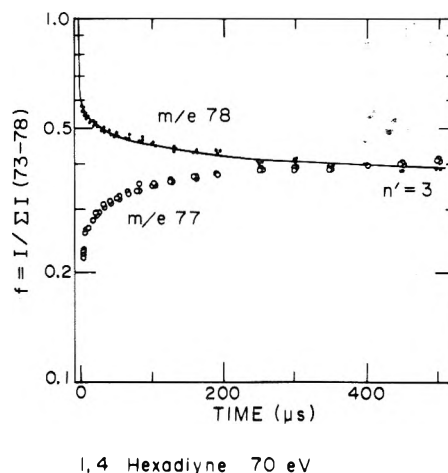


Figure 5. Ion signals in 1,4-hexadiyne as a function of reaction time, 70 eV.

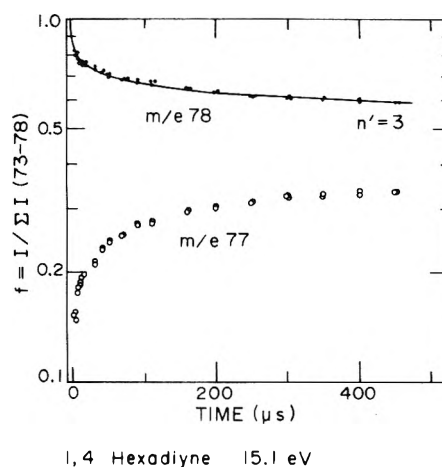


Figure 6. Ion signals in 1,4-hexadiyne as a function of reaction time, 15.1 eV.

Figures 5 and 6. A significant decrease in the  $C_6H_6^{+}$  ion signal with a concomitant increase in the  $C_6H_5^{+}$  ion signal is observed over the first  $300 \mu s$  following ionization, although the extent of slow fragmentation is considerably less than that observed for 1,5-hexadiyne. These observations are in accord with the qualitative observations of Gross et al.<sup>22</sup> who found significant differences in the conventional mass spectrum and ICR mass spectrum but less than was observed for 1,5-hexadiyne. As for the two systems discussed above the experimental decay curves are best fitted by eq 2 with  $n' = 3$ .

**2,4-Hexadiyne.** The mass spectrum of 2,4-hexadiyne was recorded at trapping times from 0 to  $100 \mu s$ . No changes in the relative  $C_6H_6^{+}$  and  $C_6H_5^{+}$  ion intensities were observed over this time range indicating that the fragmentation reactions were essentially complete in a time shorter than  $5 \mu s$ . This again is consistent with the results of Gross et al.<sup>22</sup> who observed no differences in the ICR and conventional mass spectra.

**Significance of Results.** The experimental decay curves for the  $m/e$  78 molecular ion in 1,5-hexadiyne, 1,4-hexadiyne, and, with less certainty because of the small extent of reaction, benzene, which have been determined over the time range from 6 to  $1000 \mu s$ , clearly cannot be explained in terms of a single reactive state with a single characteristic fragmentation rate constant. As discussed above, in all cases the experimental

TABLE I: Parameters of Generated Decay Curve and Computer Fit

10-term generation $A(n) = 0.05$		2-state fit		3-state fit	
$n$	$k(n)$ ( $\times 10^{-4}$ )	$k(n)$ ( $\times 10^{-4}$ )	$A(n)$	$k(n)$ ( $\times 10^{-4}$ )	$A(n)$
1	0.1	0.83	0.24	0.66	0.23
2	0.3	23.1	0.21	11.0	0.17
3	0.5			>50	0.06
4	0.7				
5	1.0	$\sigma(I) = 0.92\%$		$\sigma(I) = 0.47\%$	
6	4.0				
7	8.0				
8	10.0				
9	50.0				
10	100.0				

decay curves can be satisfactorily fitted by eq 2 with  $n' = 3$ . This appears to imply at least three discrete reactive states, one (or more) which has reacted completely before observations can be made and two reactive states which have lifetimes within the time range of observation. However, it is necessary to enquire whether this is a unique solution and whether the conclusions as to the number of distinctive reactive states is justified. To test this we have generated a decay curve with ten discrete states with equal populations and characteristic rate coefficients as detailed in Table I. The decay curve generated in this fashion is displayed as points in Figure 7. We have attempted to fit this decay curve by eq 1 and 2. As shown in Figure 7 eq 1 with  $n = 1$  does not give a satisfactory fit, however, eq 1 with  $n = 2$  and eq 2 with  $n' = 3$  both give satisfactory fits to the generated decay curve. The calculated curve for  $n' = 3$  is shown in Figure 7 while the relevant parameters for the two-state fit and the three-state fit are given in Table I. For both fits the  $\sigma(I)$ 's in Table I are the sums of the standard deviations of the "experimental" points from the computed curve. These are satisfactorily small and less than would result from the scatter of data anticipated in an actual experiment.

The above results show that a decay curve resulting from fragmentation reactions involving many states (or, in the limit, a continuum of states) can be fitted satisfactorily by an expression involving at most three reactive states, even when the decay curves have been established over a wide range of time. Consequently, the three reactive states abstracted by the least-squares method from the present results have no fundamental significance beyond establishing that the results cannot be explained in terms of a single reactive state with a characteristic rate coefficient. The results provide no evidence that a limited number of discrete states are involved in the slow fragmentation reactions observed and, therefore, provide no evidence contradicting the multistate assumption usually applied in QET considerations of the mass spectra of polyatomic molecules.

This shortcoming of the curve-fitting technique should be even more pronounced when the range of times over which the decay curves are established is limited. Thus we would suggest that the earlier studies<sup>13,14</sup> of the fragmentation of the toluene molecular ion, which were interpreted in terms of a limited number of discrete states with characteristic lifetimes, are of doubtful validity in providing evidence as to the number of states involved since the decay curves were established over

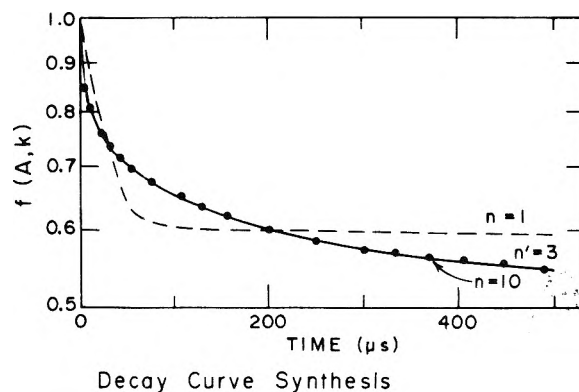


Figure 7. Computer fit of generated decay curve: (●) generated curve. Lines show the computer generated fit.

a relatively short time range. The problem is perhaps best illustrated by the present results for 1,5-hexadiyne where the data for reaction times  $< 300 \mu s$  can be fitted satisfactorily by a single-state expression although the entire curve cannot be so fitted.

Finally, some comment on the unusually large extent of fragmentation of the 1,5-hexadiyne and 1,4-hexadiyne molecular ions at times longer than a few microseconds seems in order. Gross and Aerni<sup>16</sup> have reported an ionization potential of 1,5-hexadiyne of  $\sim 10.0$  eV, in agreement with the onset of ionization in the photoelectron spectrum.<sup>23</sup> They observed that the appearance potential of the  $C_6H_5^+$  fragment ion varied from 10.5 eV at short ion source residence times to 10.2 eV at long residence times (ICR), indicative of a substantial kinetic shift<sup>24</sup> and suggesting a very slow rise in the  $k(E)$  vs. internal energy curve for the fragmentation reaction forming  $C_6H_5^+$ . The loss of a hydrogen atom from the benzene molecular ion also shows a very slowly rising  $k(E)$  curve.<sup>2,25</sup> Examination of the photoelectron spectrum of 1,5-hexadiyne<sup>23</sup> shows that a large fraction of the total ionization occurs in the energy region from 10 to 11 eV and thus covers the energy range appropriate for fragmentation. This, coupled with a very slowly rising  $k(E)$  curve, could give rise to the large extent of slow fragmentation observed. A similar rationalization could be advanced for the 1,4-hexadiyne system although the parameters involved are not known. On the other hand, the thermochemical threshold for formation of  $C_6H_5^+$  from benzene is  $\sim 13$  eV<sup>26</sup> and an examination of the photoelectron spectrum of benzene indicates that there is very little ionization in this energy region. Thus the extent of slow fragmentation of benzene should be small. Similar arguments probably also apply to the 2,4-hexadiyne system.

**Acknowledgments.** The authors are indebted to the National Research Council of Canada for financial support and to Professor M. L. Gross for helpful correspondence.

## References and Notes

- (1) H. M. Rosenstock, M. B. Wallenstein, A. L. Wahrhaftig, and H. Eyring, *Proc. Natl. Acad. Sci. U.S.A.*, **38**, 667 (1952).
- (2) M. L. Vesal in "Fundamental Processes in Radiation Chemistry", P. Ausloos, Ed., Wiley-Interscience, New York, N.Y., 1969.
- (3) A. L. Wahrhaftig in "Mass Spectrometry", A. Maccoll, Ed., M.T.P. International Review of Science, Butterworths, London, 1972.
- (4) J. A. Hipple, *Phys. Rev.*, **71**, 594 (1947).
- (5) J. Mornign, *Bull. Soc. Chim. Belg.*, **70**, 291 (1961).
- (6) N. D. Coggeshall, *J. Chem. Phys.*, **37**, 2167 (1962).
- (7) J. C. Schug, *J. Chem. Phys.*, **40**, 1283 (1964).
- (8) G. A. Muccini, W. H. Hamill, and R. Barker, *J. Phys. Chem.*, **68**, 261 (1964).

- (9) C. Lifshitz and M. Shapiro, *J. Chem. Phys.*, **45**, 4242 (1966).
- (10) H. M. Rosenstock, *Adv. Mass Spectrom.*, **4**, 523 (1968).
- (11) O. Osberghaus and Ch. Ottinger, *Phys. Lett.*, **16**, 121 (1965).
- (12) Ch. Ottinger, *Z. Naturforsch. A*, **22**, 20 (1967).
- (13) F. Meyer and A. G. Harrison, *J. Chem. Phys.*, **43**, 1778 (1965).
- (14) S. E. Buttrill, *J. Chem. Phys.*, **61**, 619 (1974); **62**, 1603 (1975).
- (15) C. Lifshitz, *J. Chem. Phys.*, **62**, 1602 (1975).
- (16) M. L. Gross and R. J. Aerni, *J. Am. Chem. Soc.*, **95**, 7875 (1973).
- (17) J. Momigny, L. Brakier, and J. D'Or, *Bull. Cl. Sci. Acad. R. Belg.*, **48**, 1002 (1962); J. Momigny, *Mem. Soc. R. Sci. Liege, Ser. 5*, **13**, 1 (1964).
- (18) A. A. Herod and A. G. Harrison, *Int. J. Mass Spectrom. Ion Phys.*, **4**, 415 (1970).
- (19) T. W. Shannon, F. Meyer, and A. G. Harrison, *Can. J. Chem.*, **43**, 159 (1965).
- (20) W. J. Gensler, A. P. Mahadevan, and J. Casella, *J. Am. Chem. Soc.*, **78**, 163 (1956).
- (21) P. R. Bevington, "Data Reduction and Error Analysis for the Physical Sciences", McGraw-Hill, New York, N.Y., 1969, pp 232-246.
- (22) M. L. Gross, G. A. Gallup, J. A. R. Samson, and J. Gardner. Paper presented at the 22nd Annual Conference on Mass Spectrometry, Philadelphia, Pa., May 1974.
- (23) P. Bischof, R. Gleiter, H. Hopf, and F. T. Lenich, *J. Am. Chem. Soc.*, **97**, 5467 (1975).
- (24) W. A. Chupka and J. Berkowitz, *J. Chem. Phys.*, **32**, 1546 (1960).
- (25) B. Andlauer and Ch. Ottinger, *J. Chem. Phys.*, **55**, 1471 (1971); *Z. Naturforsch. A*, **27**, 293 (1972).
- (26) H. M. Rosenstock, J. T. Larkins, and J. A. Walker, *Int. J. Mass Spectrom. Ion Phys.*, **11**, 309 (1973).

## On the Measurements of Vibrational Intensity in the Photoelectron Spectra of Oxygen for the Ionic Ground State

P. Natalis

*Institut de Chimie, Université de Liège, Sart Tilman, B-4000 Liège, Belgium (Received June 8, 1976)*

About 40 experimental values of the photoelectron intensity  $I(v')$ , with  $v' = 0$  to 6 (normalized to  $I(v' = 1)$  equal to 100) for the O<sub>2</sub><sup>+</sup>, X<sup>2</sup>Π<sub>g</sub> photoelectron vibrational series, are gathered or calculated from literature data, compared, and discussed. These data are analyzed taking into account, insofar as possible, the types of analyzer used, the instrumental conditions, the character of the uv light, and the possible intensity corrections. As a result it is shown that information on Franck-Condon factors for the direct ionization process alone is difficult to obtain from the presently available vibrational photoelectron intensity data because of frequent perturbation of autoionization process(es).

### Introduction

In a preceding paper<sup>1</sup> we have gathered and analyzed numerous experimental data scattered in the literature concerning the vibrational intensities of the photoelectron band corresponding to the ground ionic state of nitrogen and carbon monoxide. We were considering the ionization processes and the Franck-Condon factors (FCF) associated with the transition from neutral to ionic ground states of these molecules. A similar study is presented here for oxygen. All photoelectron spectroscopic intensity data available, to our knowledge, for the vibronic transitions O<sub>2</sub><sup>+</sup>, X<sup>2</sup>Π<sub>g</sub> ( $v' = 0$  to 6) ← O<sub>2</sub>, X<sup>3</sup>Σ<sub>g</sub><sup>-</sup> ( $v'' = 0$ ) will be examined and discussed.

One of the purposes of this work is to see to what extent the measurement of photoelectron intensities, corresponding to the distribution of ions in various vibrational levels of the ground ionic state, can be considered as a reliable way of determining the FCF's associated to the vibronic transitions for direct ionization. It is well known that, using suitable photon energies, it is possible to populate ionic states of many molecules by an autoionization process as well as by direct ionization. Experimental investigations by photoelectron spectroscopy have already shown that this is indeed observed for diatomic molecules such as N<sub>2</sub>, CO, and NO, and this is also the case for the ground ionic state of O<sub>2</sub><sup>+</sup>, X<sup>2</sup>Π<sub>g</sub> examined here.

A second point of interest is to see if instrumental effects and/or operating conditions have to be invoked to explain discrepancies between some experimental results published

in the literature, or between experimental data and theoretical calculations. As a matter of fact, the data have been obtained under various experimental conditions differing mainly by the wavelength of the uv light used, its possible degree of polarization (when using synchrotron radiation and/or monochromators), and the type of instrument employed to analyze the photoelectron energies. For instance, one must be aware of photoelectron angular distribution effects which may not be taken into account in the same way if different types of analyzer are utilized, depending upon the electron ejection angle with respect to the photon beam direction.

In this work, we propose a critical analysis of photoelectron intensity data for the vibrational distribution of O<sub>2</sub><sup>+</sup> in its ground ionic state X<sup>2</sup>Π<sub>g</sub>. This study will be limited to the energy region corresponding to the direct ionization which spreads over six vibrational levels. About 40 series of values of vibrational peak intensities  $I(v')$ , with  $v' = 0$  to 6 (normalized to  $I(v' = 1)$  equal to 100), obtained under various conditions, are listed in Table I. The  $v' = 6$  vibrational peak has been included here because it is usually highly populated when autoionization is present. Other vibrational levels, up to  $v' = 20$ , not considered here, may also be populated, in some cases, due to autoionization. A few values are directly taken from literature data, and one series of values is an unpublished result from this laboratory. The types of instrument used as well as particular operating conditions are mentioned whenever this information is available and useful for the discussion.

TABLE I: Photoelectron Current Intensities  $I(v')$  for  $v' = 0, 2, 3, 4, 5$ , and  $6$  (Normalized to  $I(v' = 1)$  Equal to 100) for the Vibronic Transitions  $O_2^+, X^2\Pi_g(v') \leftarrow O_2, X^2\Sigma_g^- (v'' = 0)$  Obtained with Different Uv Lines and under Various Experimental Conditions

Photon wavelength, Å	Vibrational quantum number $\nu'$						Type of analyzer	Remark	Ref.		
	0	1	2	3	4	5				6	
304	54.9	100	81.3	31.5	7.6			Electrostatic cylindrical mirror	<i>a</i>	2, 3	
584	53	100	98	57				Retarding potential plane electrodes		4	
	50	100	97	57				Retarding potential plane electrodes		5	
	43	100	92	45	14			Retarding potential plane electrodes		6	
	40	100	90	40	10			Retarding potential slotted grid		7	
	43	100	93	43	14			Retarding potential spherical electrodes		8	
	56	100	104	65	33	15		Retarding potential spherical electrodes	<i>b</i>	9	
	47	100	94	53	22			Retarding potential spherical electrodes		10	
	43	100	88	38	14			127° electrostatic		11	
	44	100	91	44	15			127° electrostatic		12	
	47	100	92	45				127° electrostatic		13	
	46	100	95	49	15	2		127° electrostatic		14	
	46	100	91	46	14			Electrostatic parallel plates		15	
	44	100	93	48	16	3		Electrostatic parallel plates		16	
	46.4	100	94.0	45.2	13.8	1.4		Electrostatic cylindrical mirror	<i>a</i>	2	
	736	63	100	71	25	4			180° magnetic	<i>c</i>	17
59		100	97	76	65	76	100	Retarding potential spherical electrodes	<i>d</i>	10	
48		100	90	71	65	78	95	Electrostatic hemispherical elect	<i>d</i>	18	
57		100	86	68	63	75	93	Electrostatic hemispherical elect	<i>d</i>	19	
58		100	98	69	74	76	95	Electrostatic spherical sectors	<i>d, e</i>	20	
53		100	96	68	51	47	59	Electrostatic spherical sectors	<i>d, f</i>	20	
68		100	79	55	72	76	81	127° electrostatic		21	
56		100	97	75	69	73	94	Electrostatic parallel plates		16	
54		100	93	72	67	74	89	Electrostatic parallel plates	<i>g</i>	16	
49		100	93	76	73	92	114	Electrostatic cylindrical mirror	<i>a</i>	22	
819.9		52	100	104	65	30	26	19	Electrostatic parallel plates	<i>g</i>	16
826.0		50	100	93	61	19	25	25	Electrostatic parallel plates	<i>g</i>	16
832.3		45	100	96	71	60	16	20	Electrostatic parallel plates	<i>g</i>	16
839.0		50	100	122	70	65	50	13	Electrostatic parallel plates	<i>g</i>	16
839.1		73	100	92	100	181	123	100	Retarding potential spherical electrodes	<i>b, h</i>	9
845.9	78	100	104	78	31	37	19	Electrostatic parallel plates	<i>g</i>	16	
853.2	54	100	91	43	27	25	36	Electrostatic parallel plates	<i>g</i>	16	
939.2	48	100	65	8	31	84	<i>i</i>	Retarding potential plane electrodes	<i>h</i>	23	
947.5	20	100	194	30	80	<i>i</i>		Retarding potential plane electrodes	<i>h</i>	23	
965.5	60	100	60	220	<i>i</i>			Retarding potential plane electrodes	<i>h</i>	23	
972.9	57	100	157	<i>i</i>				Retarding potential plane electrodes	<i>h</i>	23	
978	47	100	84	<i>i</i>				Retarding potential plane electrodes	<i>h</i>	23	

TABLE I (Continued)

Photon wavelength, Å	Vibrational quantum number $v'$							Type of analyzer	Remark	Ref.
	0	1	2	3	4	5	6			
983.3	53	100	133	<i>i</i>				Retarding potential plane electrodes	<i>h</i>	23
993.5	34	100	<i>i</i>					Retarding potential plane electrodes	<i>h</i>	23
1004.0	10	100	<i>i</i>					Retarding potential plane electrodes	<i>h</i>	23

<sup>a</sup>Monochromator; electrons emitted at 54° 44' of the photon beam direction. <sup>b</sup>Probably overestimated values because obtained from deconvolution of an incompletely resolved spectrum. <sup>c</sup>Incompletely resolved spectrum. <sup>d</sup>Data uncorrected for some contribution of the 744-Å line from the neon discharge used as a light source. <sup>e</sup>Electrons emitted at 90°. <sup>f</sup>Electrons emitted at 20°. <sup>g</sup>Synchrotron and monochromator. <sup>h</sup>Autoionization contribution only. <sup>i</sup>From this  $v'$  value and above, no vibrational level is accessible because of insufficient photon energy.

## Results and Discussion

Generally speaking, the data of Table I show that the series of vibrational peaks for O<sub>2</sub><sup>+</sup>, X<sup>2</sup>Π<sub>g</sub> extends over the energy range which can be expected for a direct Franck-Condon transition when photons of 584 or 304 Å from a helium discharge are used. On the contrary, when using other uv lines of suitable and sufficient energy, in particular the one at 736 Å from a neon discharge, the series definitely includes the sixth level which, as indicated in Table I, is usually highly populated. This occurs when autoionization is contributing to the ionization process. Most of the works having been performed with rare gases resonance lines at 584 Å (He I), 304 Å (He II), and 736 Å (Ne I), the following discussion will be divided into four sections, in which the results obtained at 584, 304, and 736 Å, and then with other lines corresponding to resonant absorptions of O<sub>2</sub>, will be successively examined.

(1) 584 Å. If one examines the 15 series of values of  $I(v')$  at 584 Å, with  $v' = 0, 2, 3$ , and 4 (also  $v' = 5$  in four cases), considering the types of instrument, one notices a rather satisfactory agreement between the results obtained with seven analyzers of various types: either 127° electrostatic,<sup>12-14</sup> parallel plates electrostatic,<sup>15,16</sup> cylindrical mirror,<sup>2</sup> or retarding potential with spherical electrodes.<sup>8</sup> Values obtained from these works are close to each other within rather narrow limits,  $\pm 1$  to  $\pm 2.5$ , and give  $I(v' = 0) = 43-47$ ,  $I(v' = 1) = 100$  (normalization),  $I(v' = 2) = 91-95$ ,  $I(v' = 3) = 44-49$ , and  $I(v' = 4) = 14-16$ . Moreover, in three cases<sup>2,14,16</sup> out of the seven mentioned above, a value of 1.4 to 3 is given for  $I(v' = 5)$ .

Three other series of values are somewhat different from the preceding ones. A first one is obtained by means of a 127° electrostatic analyzer<sup>11</sup> which gives two values smaller than the above average: 88 for  $I(v' = 2)$  instead of 91-95 and 38 for  $I(v' = 3)$  instead of 43-47. A second series is provided by a retarding potential spherical analyzer<sup>10</sup> which gives values higher than the above average for  $I(v' = 3)$  and  $I(v' = 4)$ , 53 and 22, respectively. Values obtained from ref 7 are also somewhat smaller than the above average. No explanation of the differences observed in these three cases can be brought. Apart from these discrepancies, it can be concluded, from the analysis of the preceding data, that there is no significant instrumental effect on the series of  $I(v')$  values obtained with the various types of analyzer examined above.

On the contrary, two other series of values are considerably different from the above average. The first one is provided by a 180° magnetic analyzer<sup>17</sup> which gives a much higher value of  $I(v' = 0)$  and much lower values for  $I(v' = 2, 3$ , and 4). The second series comes from a spherical retarding potential analyzer<sup>9</sup> which gives much higher values for  $I(v' = 3, 4$ , and 5). It is to be noticed, however, that in both cases the estimation

of intensities is difficult because of the incomplete resolution of the photoelectron band. Even in the case<sup>9</sup> where the values result from deconvolution of the photoelectron band, an important uncertainty is to be expected, in particular on the intensity measurement of peaks of high  $v'$  value because of errors accumulation due to successive corrections. Therefore, the results observed in these two cases cannot be significantly compared to the other ones discussed above and, on the other hand, no possible instrumental effect between both instruments can be evidenced.

Finally, two other works,<sup>4,5</sup> among the oldest ones and performed by means of retarding potential analyzers with plane electrodes, are still to be mentioned for completeness. Both give the same results although rather different from the average discussed above, with higher values for  $I(v' = 0)$  and  $I(v' = 3)$  (see Table I). These results may not be the most reliable since a more recent work<sup>6</sup> also obtained by means of a retarding potential analyzer with plane electrodes, gives results in agreement with those obtained on other instruments.

From another point of view, in the case of the various types of analyzer examined in this work, no discrimination due to a possible angular distribution effect on photoelectron intensities corresponding to ions formed in various vibronic states is observed. This is shown by the results obtained from a spherical retarding potential analyzer,<sup>8</sup> the geometry of which provides an isotropic electron collection, and from a cylindrical mirror analyzer<sup>2</sup> operating at a particular electron ejection angle of 54° 44',<sup>24</sup> both instruments being free from angular distribution effects. Values given in both cases are within limits of  $\pm 2$ , compared to those obtained by means of other instruments which analyze photoelectrons at right angle with respect to the light beam direction.

It should also be mentioned that error limits are rarely provided in these photoelectron intensity data. They are given in two cases,<sup>2,14</sup> are of the order of  $\pm 2-3$ , and are mentioned as standard deviations from the mean of a number of results. More generally, these limits may possibly, in the absence of other indication, be considered as an order of magnitude of the uncertainty on the kind of data discussed here. Further information on this point would be useful and the authors should be more aware of this.

As a general result of the above discussion, the whole body of data compared in this study provides a series of values of  $I(v' = 0-5)$  at 584 Å which does not seem to depend on neither the type of analyzer, nor possible angular distribution effects, within rather short limits of uncertainty of the order of  $\pm 2$ .

Now the question is: how can this series of "best" experimental values be compared to that of theoretically calculated

FCF's? Several authors<sup>25-27</sup> have calculated FCF's for the transition  $O_2^+, X^2\Pi_g(v') \leftarrow O_2, X^3\Sigma_g^-(v'')$  using a Morse potential. Later, by use of better values of molecular constants,<sup>28</sup> better FCF data have been obtained<sup>29</sup> in agreement with similar calculations performed by the same authors<sup>29</sup> using an RKR instead of a Morse potential. The admitted values now found in the literature<sup>30,31</sup> for the series of calculated FCF's for the vibronic transitions  $O_2^+, X^2\Pi_g(v') \leftarrow O_2, X^3\Sigma_g^-(v'' = 0)$  are: 51.7, 100.0, 79.6, 33.7, 8.17, and 1.14, with  $v' = 0-5$ . They are to be compared to the "best", after our above analysis, series of experimental photoelectron intensity values:  $45 \pm 2$ , 100 (normalization),  $93 \pm 2$ ,  $46 \pm 2.5$ ,  $15 \pm 1$ , and  $2.2 \pm 0.8$ . As a consequence, it is clearly evidenced that there is no satisfactory agreement between calculated and experimental data. The disagreement is seen in the whole range of  $v' = 0$  to 5 and is especially important for high  $v'$  data (4 and 5) for which experimental values amount to twice as much as the calculated ones. This disagreement has been recently mentioned.<sup>2</sup> As a conclusion the photoionization of  $O_2$  by 584-Å photons cannot be due to a single direct ionization process, but the possibility of an autoionization process is also to be considered to account for the experimental observations. On the other hand, indications of autoionization seem to be present in the 590-Å range in the photoionization cross section.<sup>32</sup> In addition, another fundamental reason of the observed difference might also be considered in the variation of the transition matrix element with vibrational state, as was pointed out in the case of  $H_2$ .<sup>33</sup>

(2) 304 Å. At this wavelength only one series of values of  $I(v')$  for  $v' = 0$  to 4, can be found.<sup>2</sup> These values, with a mentioned uncertainty of  $\pm 2$  to 3, are in quite satisfactory agreement with calculated FCF's.<sup>30,31</sup> Therefore this indicates<sup>2</sup> that the direct transition  $O_2^+, X^2\Pi_g(v' = 0 \text{ to } 4) \leftarrow O_2, X^3\Sigma_g^-(v'' = 0)$  is the only one to be considered at 304 Å. At this wavelength, no particular structure shows up in the photoionization curve.

(3) 736 Å. In Table I, nine series of values are reported for the first photoelectronic  $O_2$  band at 736 Å, in the 12-13-eV energy range, i.e., in the region corresponding to the direct ionization toward the ground state  $X^2\Pi_g$  of  $O_2^+$ . It has now long been recognized<sup>34,35</sup> that at this particular wavelength,  $O_2$  is photoionized by direct ionization and by autoionization, and that the observed vibrational peak intensities result from the combination of the transitions due to both types of processes.

Experimentally measured values of peak intensities account for this situation and are very different from calculated FCF values for the single direct vibronic transitions, therefore indicating the quantitative importance of the autoionization process with respect to the direct ionization. This aspect of the phenomenon has been theoretically examined.<sup>36,37</sup> In this case also, however, a small part of the difference might also be due to a variation of the transition matrix element with vibrational state, as mentioned before in the  $H_2$  case.<sup>33</sup>

The data reported at 736 Å are difficult to analyze because the works at this wavelength have been performed, except in two cases,<sup>16,22</sup> with uv light from undispersed discharge lamps. As a consequence of this and because of the energy difference between the 736- and 744-Å lines and between the  $O_2^+, X^2\Pi_g$  vibrational levels, there is a contribution of the 744-Å line to the 736-Å photoelectron band, except if the resolution is sufficient to separate both 736- and 744-Å spectra. The latter condition is fulfilled in one case,<sup>21</sup> which showed that the 744-Å line produces ionization of  $O_2$  only by a direct process as was already mentioned in another study.<sup>38</sup> For most works

examined here, it is not possible to evaluate quantitatively the 744-Å contribution to the reported "736-Å" data, because of lack of information on the relative intensity of both lines. However, a rough estimate can be made from the indication<sup>10,19,21</sup> that the 744-Å line amounts to about 25% of the 736-Å in usual operating discharge conditions. The major part of the reported "736-Å" data is indeed due to the 736-Å line, and in any case the 744-Å contribution to the  $v' = 4, 5$ , and 6 vibrational peaks particularly discussed below is small.

Now looking at the 736-Å values in Table I, it may be surprising that, notwithstanding the above consideration, the 736-Å values appear only somewhat more scattered than in the studies made at 584 Å. For example, three works performed by means of hemispherical<sup>18,19</sup> or spherical sectors<sup>20</sup> electrostatic analyzers give values of  $I(v' = 0, 2, \text{ and } 4)$  in agreement within limits of  $\pm 5$  or 6 instead of  $\pm 2$  at 584 Å.

On the other hand, an important angular distribution effect on photoelectron intensities is observed, since measurements realized at a photoelectron ejection angle of  $20^\circ$  instead of  $90^\circ$  by means of a spherical sectors electrostatic analyzer<sup>20</sup> show a substantial reduction of intensities for  $v' = 4, 5$ , and 6 levels. This angular distribution effect also definitely shows up when results obtained by means of instruments analyzing at right angle to the photon beam direction are compared to those from analyzers free from this effect, cylindrical mirror with electron ejection angle of  $54^\circ 44'$ <sup>22</sup> and spherical retarding potential.<sup>10</sup> In both latter cases, an increase of  $I(v' = 6)$  intensity,<sup>10,22</sup> and also possibly of  $I(v' = 5)$ <sup>22</sup> is noticed. Since the analyzers sampling electrons from the ionization region at  $90^\circ$  collect electrons produced by autoionization and corresponding to  $v' = 5$  and 6 less than those corresponding to  $v' < 5$ , there is thus a marked angular distribution effect on vibrational levels populated by autoionization. This effect should be evidenced by a change in the value of the asymmetry parameter  $\beta$  as a function of  $v'$  and has been experimentally shown at 736 Å.<sup>38</sup>

Similarly, two other studies<sup>39,40</sup> of the asymmetry parameter variation with the type of ionization process, direct ionization and autoionization, for the  $O_2^+, X^2\Pi_g$  photoelectron band at 736 Å, also showed that kind of effect. Both works<sup>39,40</sup> are in agreement in reporting  $\beta$  values different from zero for  $v' = 0$  to 3 vibrational levels populated by direct ionization and values of about zero for  $v' > 4$  levels, as can be expected for autoionizing vibronic transitions.<sup>20</sup> In this respect measurements performed with the synchrotron polarized radiation would be informative since the photoelectron intensities obtained with polarized light are dependent on the  $\beta$  asymmetry parameter. Such an experiment has been made at 736 Å with a parallel plate electrostatic analyzer using either the unpolarized light from a discharge lamp or the polarized light from a synchrotron.<sup>16</sup> The two series of vibrational intensity values obtained with both kinds of light are in very good agreement, only differing by  $\pm 1$  or  $\pm 2$ , which presumably indicates no light polarization effect on the vibrational distribution of  $O_2^+$  ions produced at 736 Å in the ground ionic state. This result is somewhat surprising, considering the nonzero value of the  $\beta$  parameter for the first four vibrational levels, as measured by others<sup>38-40</sup> unless the expected effect be masked by a 744-Å contribution to the measured intensities.

Finally, considering possible instrumental effects, data obtained for  $O_2^+$  ground state at 736 Å with a parallel plate electrostatic analyzer<sup>16</sup> are in fair agreement with those provided by hemispherical<sup>18,19</sup> or spherical sectors<sup>20</sup> electrostatic analyzers, in spite of the previous remarks on the 744-Å line contribution present in the latter three cases<sup>18-20</sup> and not in



the former one when a monochromatized light is used.<sup>16</sup> On the contrary, other data from a 127° electrostatic analyzer<sup>21</sup> give higher  $I(v' = 0)$  and lower  $I(v' = 2 \text{ and } 3)$  values than those discussed previously<sup>16,18-20</sup> and consequently this does not preclude the possibility of an instrumental effect in the last case.<sup>21</sup>

(4) *Other Lines.* Photoionization studies of O<sub>2</sub> by means of uv lines other than usual rare gases resonance lines having energies corresponding to autoionization states have been reported in several works.<sup>9,16,23</sup> In such photon energy conditions, as shown by photoelectron intensity data of Table I, the vibrational population of O<sub>2</sub><sup>+</sup> ions in the ground ionic state appears very different from line to line, and from calculated FCF's for direct ionization. This observation can be expected since the FCF's associated to the transition from a neutral autoionizing state toward the ground ionic state depend on molecular constants specific of this electronically excited neutral state, which are different from those of the neutral ground state. This behavior has been predicted<sup>37,41</sup> and discussed in the literature. We shall only make here, as in the case of N<sub>2</sub> and CO previously studied,<sup>1</sup> a few remarks which are also of application in the case of O<sub>2</sub>.

The data of Table I have been obtained with three different types of instruments, i.e., retarding potential with spherical<sup>9</sup> or plane<sup>23</sup> electrodes and parallel plate electrostatic<sup>16</sup> analyzers. Except in one case, at 839.0–839.1 Å, measurements have been made at different wavelengths in the three works and, as a result, a comparison of the data from the point of view of possible instrumental effects cannot be made. One may admit, hopefully, that there is no important effect of this kind since none was found at 584 Å and possibly not much at 736 Å, as shown in the previous sections. The only case where a comparison could be attempted is at 839.0 and 839.1 Å (O<sub>2</sub> absorption line belonging to the I series,  $v = 2$  progression resonance<sup>42</sup>). Table I shows that the values of  $I(v')$  with  $v' = 2$  to 6 are very different in the two works. This dramatic difference could hardly, at first sight, be explained by the light bandpass width used in the two experiments which is practically the same, 1.7<sup>16</sup> and 1.6 Å.<sup>9</sup> However, as shown in the N<sub>2</sub> case,<sup>1</sup> different bandpass widths give very different photoelectron intensity distributions, which indicates that a vibrational population is extremely sensitive to the part of the autoionizing region covered by the bandpass width of the light beam. This is to be expected if more than one autoionizing level overlap in the energy region considered.

Two other reasons prevent one from making a significant comparison of the data of both works. First, the data of ref 9 represent the part of the photoelectron spectrum only due to autoionization, the other one due to direct ionization having been removed by data manipulation involving the direct and autoionization cross sections. Secondly, there is a large uncertainty in the values of the 839.1 Å series<sup>9</sup> because they have been obtained by deconvolution of an incompletely resolved spectrum and consequently high  $v'$  intensity values must be affected by a large uncertainty because of accumulation of errors due to successive corrections. For this reason data recorded at other wavelengths in ref 9 have been omitted in Table I and are not considered in the present discussion.

At higher wavelengths than those reported in the two preceding works, i.e., in the 970–1000-Å range, the O<sub>2</sub><sup>+</sup>, X<sup>2</sup>Π<sub>g</sub> vibrational progression is limited to three or two peaks only,<sup>23</sup> as shown from Table I. In such conditions, higher vibrational levels are inaccessible because of an insufficient photon energy. Moreover, as in ref 9, data of ref 23 also represent only the autoionization contribution to the photo-

electron band examined. Two additional remarks are to be made in this last case. The first one is that the intensity measurements may be affected by large errors when the photoelectron energy is close to zero. The authors<sup>23</sup> were aware of this point and corrected their data by using a suitable collecting efficiency curve. The second point is that, near the ionization threshold, large variations of photoionization cross sections can occur and may be responsible for the usually observed high value for the intensity of the vibrational peak closest to zero energy.

All the above remarks explain why a comparison of the data obtained at photon energies corresponding to autoionizing levels is difficult, or even impossible, if experimental conditions are not as closely as possible reproduced.

## Conclusion

The present analysis of O<sub>2</sub><sup>+</sup>, X<sup>2</sup>Π<sub>g</sub> photoelectron vibrational intensity data leads to a conclusion similar to that previously<sup>1</sup> drawn for the N<sub>2</sub><sup>+</sup> and CO<sup>+</sup> ground state.

First, the information broadly scattered in the literature was gathered and analyzed from the point of view of measurement reliability to obtain the "best" usable photoelectron vibrational intensity values to be compared with calculated FCF's. Such an analysis requires the consideration of the possible effects of differences in the types of analyzer used, the operating conditions, the mode of uv excitation, and the intensity corrections.

Secondly, taking into account the probable uncertainty in the "best" data, it is shown that, at 584 Å, the vibrational population of the O<sub>2</sub><sup>+</sup>, X<sup>2</sup>Π<sub>g</sub> ground state does not only correspond to a direct ionization process alone. Autoionization is a frequently met perturbing process at the wavelengths used in the available studies examined here. In addition a possible effect due to a variation of the transition matrix element with vibrational level is to be considered and could possibly account for the observed differences when small, or part of them when large, between theory and experiment. Further experimental investigation in well-defined operating conditions would be useful in the present case of O<sub>2</sub>, such as in N<sub>2</sub> and CO.

NOTE ADDED IN PROOF: While this paper was in press, new values of vibrational intensities in O<sub>2</sub><sup>+</sup>, X<sup>2</sup>Π<sub>g</sub> obtained using a cylindrical mirror analyzer calibrated for relative luminosity have been published.<sup>43</sup> These values, 46.7 ± 1.8, 100.0 ± 5.0, 91.6 ± 3.2, 46.1 ± 2.1, and 15.4 ± 0.5 for  $I(v' = 0-4)$ , are in excellent agreement with those obtained from the analysis reported in the present work.

*Acknowledgment.* I gratefully acknowledge Professor J. W. Taylor and Dr. J. A. Kinsinger, University of Wisconsin, and Professor C. E. Brion, University of British Columbia, for fruitful discussions and comments about some of the data included in this paper. I also thank Professor J. E. Collin for a useful discussion, Dr. J. Delwiche for his collaboration, and Dr. G. Caprace for her help in carefully reading the manuscript. The Belgian "Fonds de la Recherche Fondamentale Collective" and "Fonds National de la Recherche Scientifique" are acknowledged for their financial support.

## References and Notes

- (1) P. Natalis, J. Delwiche, G. Caprace, J. E. Collin, M.-J. Hubin, and M.-Th. Praet, *J. Electron Spectrosc. Relat. Phenom.*, in press.
- (2) J. L. Gardner and J. A. R. Samson, *J. Chem. Phys.*, **61**, 5472 (1974).
- (3) J. L. Gardner and J. A. R. Samson, *J. Chem. Phys.*, **62**, 4460 (1975).
- (4) J. Berkowitz, H. Ehrhardt, and T. Tekaas, *Z. Phys.*, **200**, 69 (1967).

- (5) R. Spohr and E. Von Puttkamer, *Z. Naturforsch. A*, **22**, 705 (1967).
- (6) H. Hotop, Thesis, University of Freiburg, 1971, cited in ref 13.
- (7) D. C. Frost, C. A. McDowell, and D. A. Vroom, *Proc. R. Soc. London, Ser. A*, **296**, 566 (1967).
- (8) W. C. Price in "Molecular Spectroscopy", P. Hepple, Ed., London, 1968, p 221.
- (9) J. L. Bahr, A. J. Blake, J. H. Carver, J. L. Gardner, and V. Kumar, *J. Quant. Spectrosc. Radiat. Transfer*, **11**, 1853 (1971).
- (10) J. E. Collin, J. Delwiche, and P. Natalis in "Electron Spectroscopy", D. A. Shirley, Ed., North Holland Publishing Co., Amsterdam, 1972, p 401.
- (11) D. W. Turner, *Proc. R. Soc. London, Ser. A*, **307**, 15 (1968).
- (12) O. Edqvist, E. Lindholm, L. E. Selin, and L. Asbrink, *Phys. Script.*, **1**, 25 (1970).
- (13) R. G. Dromey, J. D. Morrison, and J. B. Peel, *Chem. Phys. Lett.*, **23**, 30 (1973).
- (14) D. S. C. Yee, W. B. Stewart, C. A. McDowell, and C. E. Brion, *J. Electron Spectrosc. Relat. Phenom.*, **7**, 93 (1975).
- (15) J. D. H. Eland and C. J. Danby, *J. Phys. E.*, **1**, 406 (1968).
- (16) J. A. Kinsinger and J. W. Taylor, *Int. J. Mass Spectrom. Ion Phys.*, **11**, 461 (1973).
- (17) D. W. Turner and D. P. May, *J. Chem. Phys.*, **45**, 471 (1966).
- (18) G. R. Branton, D. C. Frost, T. Makita, C. A. McDowell, and I. A. Stenhouse, *Phil. Trans. R. Soc. London, Ser. A*, **268**, 77 (1970).
- (19) J. Delwiche, P. Natalis, and J. E. Collin, unpublished result.
- (20) T. A. Carlson, *Chem. Phys. Lett.*, **9**, 23 (1971).
- (21) W. C. Price, A. W. Potts, and D. G. Streets in "Electron Spectroscopy", D. A. Shirley, Ed., North-Holland Publishing Co., Amsterdam 1972, p 187.
- (22) J. A. R. Samson and J. L. Gardner, *Can. J. Phys.*, **53**, 1948 (1975).
- (23) K. Tanaka and I. Tanaka, *J. Chem. Phys.*, **59**, 5042 (1973).
- (24) J. A. R. Samson, *J. Opt. Soc. Am.*, **59**, 356 (1969).
- (25) M. E. Wacks, *J. Chem. Phys.*, **41**, 930 (1964).
- (26) M. Halmann and I. Laulicht, *J. Chem. Phys.*, **43**, 1503 (1965).
- (27) R. W. Nicholls, *J. Phys. B*, **1**, 1192 (1968).
- (28) G. L. Bhale and P. R. Rao, *Proc. Indian Acad. Sci.*, **67A**, 350 (1968).
- (29) R. K. Asundi and C. V. S. Ramachandrarao, *Chem. Phys. Lett.*, **4**, 89 (1969).
- (30) P. H. Krupenie, *J. Phys. Chem. Ref. Data*, **1**, 423 (1972).
- (31) D. L. Albritton, A. L. Schmeltekopf, and R. N. Zare, "Diatomic Intensity Factors", Wiley, New York, N.Y., to be published.
- (32) L. C. Lee, R. W. Carlson, D. L. Judge, and M. Ogawa, *J. Quant. Spectrosc. Radiat. Transfer*, **13**, 1023 (1973).
- (33) Y. Itikawa, *J. Electron Spectrosc. Relat. Phenom.*, **2**, 125 (1973).
- (34) W. C. Price in "Molecular Spectroscopy", Institute of Petroleum, London, 1969, p 221.
- (35) J. E. Collin and P. Natalis, *Int. J. Mass Spectrom. Ion Phys.*, **2**, 231 (1969).
- (36) A. L. Smith, *J. Quant. Spectrosc. Radiat. Transfer*, **10**, 1129 (1970).
- (37) A. L. Smith, *Phil. Trans. R. Soc. London*, **A268**, 169 (1970).
- (38) R. Morgenstern, A. Niehaus, and M. W. Ruf, VII ICPEAC Conference, Amsterdam, 1971, p 167.
- (39) T. A. Carlson, G. E. McGuire, A. E. Jonas, K. L. Cheng, C. P. Anderson, C. C. Lu, and B. P. Pullen in "Electron Spectroscopy", D. A. Shirley, Ed., North Holland Publishing Co., Amsterdam, 1972, p 207.
- (40) V. B. Miliyev and F. I. Vilesov, *Usp. Foton.*, **4**, 3 (1974).
- (41) A. J. Blake, J. L. Bahr, J. H. Carver, and V. Kumar, *Phil. Trans. R. Soc. London*, **A268**, 159 (1970).
- (42) F. M. Matsunaga and K. Watanabe, *Sci. Light (Tokyo)*, **16**, 31 (1967).
- (43) J. L. Gardner, J. A. R. Samson, *J. Electron Spectrosc. Relat. Phenom.*, **8**, 469 (1976).

## High-Pressure Mass Spectra and Gaseous Ion Chemistry of Metal Acetylacetonates

Steven M. Schildcrout

Department of Chemistry, Youngstown State University, Youngstown, Ohio 44555 (Received February 17, 1976)

Publication costs assisted by the Petroleum Research Fund and Youngstown State University

With ion-source pressures up to 0.01 Torr, mass spectra have been obtained for 16 bis and tris acetylacetonates and hexafluoroacetylacetonates of various group 3A and transition metals. For each complex except aluminum hexafluoroacetylacetonate, positive ions containing two or more metal atoms make important contributions to the spectra. The dependence of the spectra upon sample pressure, temperature, repeller potential, and ionizing energy indicates that these ions are products of reaction between metal-containing fragment ions and the neutral monomeric complex. The polynuclear ions typically contain unfragmented ligands, with the oxidation state of the metal being that commonly found in its condensed-phase chemistry. The occurrence or absence of charge-transfer reaction permits in each case confirmation or prediction of the relative ionization energies of the complex and its neutral fragments.

### Introduction

Studies of gaseous ion-neutral reactions have only recently been extended to metal complexes. Müller and co-workers have used high-pressure mass spectrometry to investigate reactions involving a variety of organometallic complexes,<sup>1</sup> and we have used this technique to determine the ion-neutral reactions in ferrocene and their rates.<sup>2</sup> Ion cyclotron resonance spectrometry has been used to study metal carbonyls<sup>3,4</sup> and to confirm our results<sup>2</sup> on the relative reaction rates in the ferrocene system.<sup>5</sup> The success of these methods with these simpler compounds suggests applying such methods to other important classes of metal complexes.

The volatility of many  $\beta$ -diketonate chelates of metals has facilitated their study by mass spectrometry. Low abundances of ions with masses greater than the molecular mass of the

parent complex were reported by Macdonald and Shannon in the mass spectra of several acetylacetonates. They considered them to result from ionization and fragmentation of neutral polymers in the ion source, but the possibility of ion-neutral reactions was not discounted.<sup>6</sup> Formation of such polynuclear ions in a mass spectrometer has since been attributed also to reaction upon evaporation of the metal complex<sup>7</sup> and to the existence of gaseous polymeric precursors in the cases of some alkaline-earth chelates.<sup>8,9</sup>

The present work was undertaken to determine the effects of sample pressure, temperature, ionizing energy, and ion residence time in the source upon the formation of positive polynuclear ions in a series of metal  $\beta$ -diketonates. Thus the possibility of ion-neutral reactions could be distinguished from that of dissociative ionization of polymers, and the preferential formation of certain types of polynuclear ions

could be rationalized. The complexes studied are the acetylacetonates  $M(\text{acac})_2$  where  $M$  is Mn, Co, Ni, Cu, Zn, and Cd;  $M(\text{acac})_3$  where  $M$  is V, Cr, Mn, Fe, Co, Rh, Al, and Ga; and the hexafluoroacetylacetonates  $\text{Cu}(\text{hfac})_2$  and  $\text{Al}(\text{hfac})_3$ .<sup>10</sup>

### Experimental Section

All compounds were purchased commercially. The solid samples were held under vacuum in the inlet before introduction to the ion source of a CEC (DuPont) 21-491 mass spectrometer previously described.<sup>2</sup> Unless otherwise noted the ionizing energy was 70 eV and the ion-repeller potential was +2.2 V relative to the ion-source block. Metal complexes were introduced via a direct probe inlet heated to produce sufficient vapor pressure. Ion-source temperature was held near the maximum probe temperature for each sample. Spectra were scanned up to  $m/e \sim 1100$ .

Ion composition is inferred from mass number and natural isotopic abundances for multiplet peaks due to polyisotopic metals and  $^{13}\text{C}$  in the ligands. Liquids for mass reference were introduced via a heated batch inlet.

Although it was not possible to reliably determine the pressures in the ion source for the complexes, pressure changes were indicated by an ionization gauge in the analyzer region of the instrument and by measurements of total ion current. In previous work<sup>2</sup> it was determined that the present conditions give maximum sample pressures of about  $10^{-2}$  Torr in the ion source.

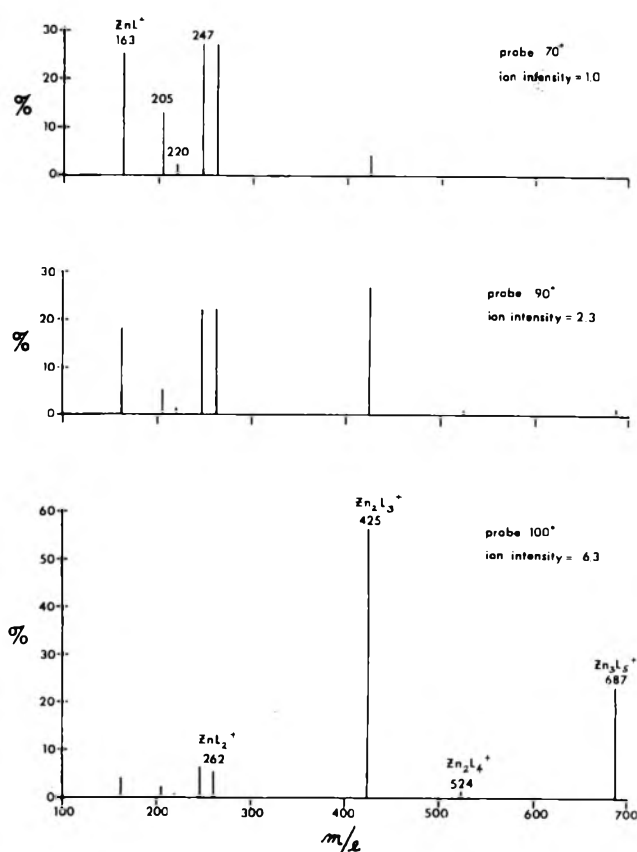
### Results

For each complex investigated except  $\text{Al}(\text{hfac})_3$ , substantial contributions to the high-pressure mass spectra are made by ions containing two or more metal atoms. In many cases a peak due to such an ion is the most intense in the high-pressure spectrum but is minor or absent in the normal low-pressure spectrum of the same complex. An example of this is shown in Figure 1 for  $\text{Zn}(\text{acac})_2$ , where  $m/e$  425 from  $\text{Zn}_2(\text{acac})_3^+$  becomes the base peak as pressure increases. The maximum relative abundances of selected polynuclear ions are given in Table I for comparison among the various complexes.

Spectra were measured for ion-repeller potentials varying from 2 to 9 V at fixed high pressure for  $\text{Cu}(\text{acac})_2$ ,  $\text{Cu}(\text{hfac})_2$ ,  $\text{Zn}(\text{acac})_2$ ,  $\text{Co}(\text{acac})_3$ , and  $\text{Al}(\text{acac})_3$ . Significant decreases in the relative abundances of the polynuclear ions as the potential was increased (ion residence time in the source decreased) were observed in each case and indicate that these ions originate from ion-neutral reactions rather than from primary processes. The low-pressure spectrum of  $\text{Cr}(\text{acac})_3$  showed no significant change as repeller potential was varied, indicating that these variations do not cause an instrumental mass-discrimination effect. Similar results in the case of ferrocene were shown to be caused by ion-neutral reactions.<sup>2</sup>

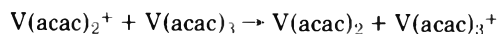
### Discussion

More detailed results for each of the complexes, including results of variation of ionizing energy for the two copper complexes and of variation of probe and source temperatures, are given and discussed in this section. Mass numbers refer to the most intense peak in the case of a polyisotopic multiplet. Relative ionic abundances are percentages of the total metal-containing ion current in a given mass spectrum, where all isotopic variations for a given species are considered, i.e., these are monoisotopic values. The complexes are considered in the order listed in Table I; the tris complexes are followed by the bis.



**Figure 1.** Monoisotopic mass spectra of  $\text{Zn}(\text{acac})_2$  at ionizing energy 70 eV, source temperature 135 °C, repeller potential 2.2 V. For each spectrum, total ion intensity (which should be roughly proportional to sample pressure) is given in arbitrary units, relative to that of the first spectrum.

$\text{V}(\text{acac})_3$ . A slight contamination of the sample by  $\text{VO}(\text{acac})_2$  is suggested by the low-pressure spectrum, which otherwise is consistent with a previous 50-eV spectrum,<sup>11</sup> with  $\text{V}(\text{acac})_2^+$  as the base peak. As the probe temperature increases to 140 °C and the sample pressure increases, all ions with masses below that of  $\text{V}(\text{acac})_3^+$   $m/e$  348 decreases in abundance while that of  $\text{V}(\text{acac})_3^+$  has increased from about 16 to 50%. This suggests charge transfer from fragment ions to the parent molecule with

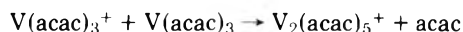


being likely. Occurrence of such a reaction implies its exothermicity, so  $\text{V}(\text{acac})_2$  should have an ionization energy greater than the 7.7 eV found for  $\text{V}(\text{acac})_3$ .<sup>12</sup>

The most important binuclear ion is  $\text{V}_2(\text{acac})_5^+$  at  $m/e$  597 with abundances up to 17% at the higher pressures. This ion consists of two V atoms in the same formal oxidation state (III) as that in the parent molecule. A condensation reaction



cannot be distinguished here from a process such as



Elimination of a neutral fragment as in the latter reaction is not presumed to be necessary, since excess energy may be absorbed internally by the metal-containing ion. This was shown to be so in a condensation process, analogous to the former reaction, occurring in ferrocene.<sup>2,3</sup>

Minor contributions to the high-pressure spectra are from

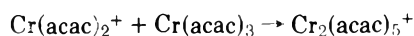
TABLE I: Maximum Relative Abundances of Nonprimary Ions in the High-Pressure Mass Spectra of Metal Complexes <sup>a, b</sup>

Parent complex ML <sub>3</sub> or ML <sub>2</sub> III      II	ML <sub>3</sub> <sup>+</sup> IV	M <sub>2</sub> L <sub>2</sub> <sup>+</sup> I, II	M <sub>2</sub> L <sub>3</sub> <sup>+</sup> II	M <sub>2</sub> L <sub>4</sub> <sup>+</sup> II, III	M <sub>2</sub> L <sub>5</sub> <sup>+</sup> III	M <sub>3</sub> L <sub>4</sub> <sup>+</sup> I, II, II	M <sub>3</sub> L <sub>5</sub> <sup>+</sup> II
V(acac) <sub>3</sub>	s				m		
Cr(acac) <sub>3</sub>				m	s		
Mn(acac) <sub>3</sub>	s		w	w	s		
Fe(acac) <sub>3</sub>				m	s		
Co(acac) <sub>3</sub>	s		m	s	w		
Rh(acac) <sub>3</sub>	s	w			m		
Al(acac) <sub>3</sub>					m		
Al(hfac) <sub>3</sub>							
Ga(acac) <sub>3</sub>			w		m		
Mn(acac) <sub>2</sub>			m	m			m
Co(acac) <sub>2</sub>		w	s	w		w	m
Ni(acac) <sub>2</sub>		m	s			w	m
Cu(acac) <sub>2</sub>		w	s			s	
Cu(hfac) <sub>2</sub>		m	m			m	
Zn(acac) <sub>2</sub>			s	w			s
Cd(acac) <sub>2</sub>			s				m

<sup>a</sup> Apparent oxidation states of the metal are shown below each general formula. <sup>b</sup> s = strong, more than 30% of total abundance for metal-containing ions; m = medium, between 10 and 30%; w = weak, less than 10%.

V<sub>2</sub>O(acac)<sub>3</sub><sup>+</sup>, V<sub>2</sub>O<sub>2</sub>(acac)<sub>3</sub><sup>+</sup> which reacts further at higher pressure, and V<sub>2</sub>O(acac)<sub>4</sub><sup>+</sup>.

Cr(acac)<sub>3</sub>. The low-pressure spectrum consists predominantly (nearly 50%) of Cr(acac)<sub>2</sub><sup>+</sup> and is consistent with previous reports.<sup>6,11</sup> As pressure increases with the probe heating to 125 °C, Cr<sub>2</sub>(acac)<sub>5</sub><sup>+</sup>, *m/e* 599, reaches 40% abundance, giving the base peak. Its formation is analogous to that of V<sub>2</sub>(acac)<sub>5</sub><sup>+</sup> discussed above. Cr<sub>2</sub>(acac)<sub>4</sub><sup>+</sup> reaches an abundance of 10% while the primary ions Cr(acac)<sup>+</sup> and Cr(acac)<sub>2</sub><sup>+</sup> decrease in abundance. The molecular ion Cr(acac)<sub>3</sub><sup>+</sup> remains nearly constant at 20%, indicating that charge transfer does not occur and that the ionization energy of 7.9 eV for Cr(acac)<sub>3</sub><sup>12</sup> is greater than the ion-electron recombination energy for either Cr(acac)<sup>+</sup> or Cr(acac)<sub>2</sub><sup>+</sup>.



seems important here, as with the vanadium analogue.

Mn(acac)<sub>3</sub>. The base peak in the low-pressure spectrum is due to Mn(acac)<sub>2</sub><sup>+</sup>, and a large contribution is made also by Mn(acac)<sup>+</sup>, in agreement with previous results.<sup>11</sup> With the ion source at 185 °C, and the probe heating to 150 °C all ions with masses below that of the parent at *m/e* 352 decrease in relative abundance with Mn(acac)<sub>2</sub><sup>+</sup> reacting more slowly than the others. Mn(acac)<sub>3</sub><sup>+</sup> increases from 6 to 35% abundance, indicating formation by charge transfer, possibly from Mn(acac)<sub>2</sub><sup>+</sup>. This is consistent with the lower ionization energy of Mn(acac)<sub>3</sub><sup>11,12</sup> compared to that of Mn(acac)<sub>2</sub>.<sup>13</sup>

As sample pressure rises Mn<sub>2</sub>(acac)<sub>3</sub><sup>+</sup> at *m/e* 407 increases to 8%, then decreases in abundance at higher pressures where Mn<sub>2</sub>(acac)<sub>5</sub><sup>+</sup> becomes the base peak at more than 50% abundance. Other binuclear ions at the higher pressures are Mn<sub>2</sub>(acac)<sub>4</sub><sup>+</sup> up to 7% and Mn<sub>2</sub>(acac)<sub>4</sub>C<sub>3</sub>H<sub>5</sub>O<sup>+</sup> up to 2% at *m/e* 563. The latter may be derived from Mn<sub>2</sub>(acac)<sub>5</sub><sup>+</sup> by loss of ketene. A very weak peak corresponds to Mn<sub>3</sub>(acac)<sub>6</sub><sup>+</sup>.

Fe(acac)<sub>3</sub>. Agreement with previous low-pressure spectra<sup>6,11</sup> is found, with Fe(acac)<sub>2</sub><sup>+</sup> giving the base peak. There is no growth in Fe(acac)<sub>3</sub><sup>+</sup> as the pressure increases (ion source 175 °C, probe heating to 155 °C), which is consistent with Fe(acac)<sub>3</sub> having a larger ionization energy<sup>11,12</sup> than Fe(acac)<sub>2</sub>.<sup>13</sup>

Macdonald and Shannon reported the heavy ions 0.06% Fe<sub>2</sub>O(acac)<sub>3</sub><sup>+</sup> at *m/e* 425, 0.6% Fe<sub>2</sub>(acac)<sub>4</sub><sup>+</sup> at *m/e* 508, and 0.2% Fe<sub>2</sub>(acac)<sub>5</sub><sup>+</sup> at *m/e* 607.<sup>6</sup> The first of these is now observed at 3% at moderate pressure with a decrease at higher pressure. The second now reaches a maximum of 15% before its abundance drops, and Fe<sub>2</sub>(acac)<sub>5</sub><sup>+</sup> grows to over 70% at higher pressure. At these pressures 3% of Fe<sub>2</sub>(acac)<sub>4</sub>C<sub>3</sub>H<sub>5</sub>O<sup>+</sup> at *m/e* 565 is observed, analogous to the results with Mn(acac)<sub>3</sub>.

To determine possible effects of evaporation temperature upon the mass spectrum, a low-pressure spectrum of Fe(acac)<sub>3</sub> with the probe at 100 °C was compared to one with the probe at 170 °C where the loaded sample had just been depleted and the pressure had dropped. The agreement of the spectra indicates that the heavy ions are formed as a function of sample pressure and not of the temperature at which the sample is evaporated in the probe inlet. Their formation by ion-neutral reaction is thus further indicated.

Co(acac)<sub>3</sub>. Spectra were obtained with the ion source at 160 °C and the probe heating to 160 °C. Good agreement is found with previous low-pressure results,<sup>6,11</sup> with Co(acac)<sup>+</sup>, Co(acac)<sub>4</sub>H<sub>4</sub>O<sub>2</sub><sup>+</sup>, and Co(acac)<sub>2</sub><sup>+</sup> of comparable abundance. These all decrease as the pressure increases, and Co(acac)<sub>3</sub><sup>+</sup> increases to 30% before dropping. As with Mn(acac)<sub>3</sub>, formation of this ion by charge transfer is consistent with the relative ionization energies of the bis and tris cobalt complexes.<sup>11,13</sup>

Binuclear ions previously reported are 2.5% Co<sub>2</sub>(acac)<sub>3</sub><sup>+</sup> and 1.2% Co<sub>2</sub>(acac)<sub>4</sub><sup>+</sup>.<sup>6</sup> The first of these is now found up to 10% and the second dominates at the highest pressures with 80%. This is the only complex studied where M<sub>2</sub>L<sub>4</sub><sup>+</sup> is so abundant. It is a mixed-valence ion, and might be expected for a metal such as cobalt which has stable neutral acetylacetonates of both Co(II) and Co(III). Other polynuclear ions now observed are up to 5% Co<sub>2</sub>(acac)<sub>5</sub><sup>+</sup>, 0.2% Co<sub>3</sub>(acac)<sub>5</sub><sup>+</sup>, and 2% Co<sub>4</sub>(acac)<sub>7</sub><sup>+</sup> assigned by approximate mass number, *m/e* 929. This last ion suggests comparison with solid tetrameric [Co(acac)<sub>2</sub>]<sub>4</sub>, where metal atoms share ligand oxygen atoms.<sup>14</sup> In this case, formation of the ion from a gaseous neutral polymer cannot be excluded since the low abundance makes the repeller-variation results inconclusive.

$Rh(acac)_3$ . With a source temperature and a maximum probe temperature of 200 °C, there appeared to be significant thermal decomposition. This is evidenced by high intensities of ions assigned to acetylacetone, which may protonate the complex to cause  $HRh(acac)_3^+$  at  $m/e$  401 to dominate the high-pressure spectra with up to 42% abundance.  $H_2(acac)^+$  is observed at the higher pressures. A metallic-appearing residue with a weight about 10% that of the original sample was found in the sample tube after heating in the mass spectrometer.

At high pressures  $Rh(acac)_3^+$  increases to 70%, in proportion to total ion current, implying its formation by charge transfer from fragment ions of the complex or of acetylacetone.  $Rh_2(acac)_5^+$  reaches a maximum of 30%. Less than 2% of  $Rh_2(acac)_2^+$  and  $Rh_3(acac)_7^+$  are detected. A previously reported spectrum<sup>6</sup> includes only ions with one Rh atom.

$Al(acac)_3$ . In their spectrum of this compound, Macdonald and Shannon reported  $Al_2(acac)_5^+$  at 8%.<sup>6</sup> This is now observed to nearly 30% at high pressures with the ion source at 210 °C and probe heating to 150 °C. The only precursor ion with sufficient low-pressure abundance to form this is  $Al(acac)_2^+$ , which would then form the adduct with a molecule of  $Al(acac)_3$ . This type of reaction appears common to all the tris complexes so far discussed.

Since  $Al(acac)_3^+$  is not observed as a secondary ion,  $Al(acac)_2$  must have an ionization energy less than that of  $Al(acac)_3$ .<sup>11,12</sup>

A study of temperature variation, as described above for  $Fe(acac)_3$ , shows the spectrum of  $Al(acac)_3$  to be nearly invariant with respect to both probe temperature and source temperature at low pressure. Formation of  $Al_2(acac)_5^+$  is therefore attributed to a pressure effect (ion-neutral reaction) rather than a temperature effect.

A very low abundance of  $Al(acac)_3CH_3CO^+$  is observed, in agreement with the previous work,<sup>6</sup> but its origin could not be determined.

$Al(hfac)_3$ . No ion with more than one Al atom is detected with the ion source at 140 °C and probe increasing to 80 °C. The low-pressure spectrum agrees well with a previous report.<sup>15</sup> As with  $Al(acac)_3$ , no secondary  $Al(hfac)_3^+$  is observed, so  $Al(hfac)_2$  must have a lower ionization energy than  $Al(hfac)_3$ .<sup>12,15</sup> The predominant metal-containing ion at all pressures is the primary  $Al(hfac)_2^+$ . Small amounts of  $HAL(hfac)_3^+$  and ions which may result from addition of ligand fragments to the metal complex are observed at the higher pressures.

$Ga(acac)_3$ . The low-pressure spectrum is dominated (nearly 90%) by  $Ga(acac)_2^+$ . As pressure increases with the probe heating to 130 °C and the source at this temperature,  $Ga_2(acac)_5^+$  increases to 23% with a corresponding decrease in  $Ga(acac)_2^+$ . The molecular ion  $Ga(acac)_3^+$  is nearly constant at 5%, indicating that the bis complex has a lower ionization energy than the tris. Minor secondary ions observed are 0.3%  $Ga_2(acac)_3O^+$  containing Ga(III) and 0.2%  $Ga_2(acac)_3^+$ , which has nominally Ga(II), but may be considered mixed valence with Ga(I) and Ga(III) as with the gallium "dihalides",  $Ga_2X_4$ .<sup>16</sup>

$Mn(acac)_2$ . Macdonald and Shannon reported that this complex gave 0.02%  $Mn_2(acac)_2^+$  and 0.2%  $Mn_2(acac)_3^+$ .<sup>6</sup> We find no evidence of the former, but do find the latter at a maximum of 24%. The abundance of  $Mn_2(acac)_3^+$  decreases as the pressure continues to rise and the tertiary ion  $Mn_3(acac)_5^+$  grows to 15% with source and probe at 190 °C. As with the tris manganese complex, mixed-valence  $Mn_2(acac)_4^+$  is observed as a secondary ion, up to 11% in this case. Minor

heavy ions include 4%  $Mn_2(acac)_3C_3H_5O^+$  and 6%  $Mn_3(acac)_4C_3H_5O^+$ . These have analogues in the  $Mn(acac)_3$  spectra already discussed. All primary ions decrease in abundance as the pressure increases.

For  $Mn(acac)_2$  and all other bis complexes studied,  $ML_2^+$  is not observed as a secondary ion, indicating that the  $ML_2$  complexes have higher ionization energies than the ion-electron recombination energies of their abundant fragments.

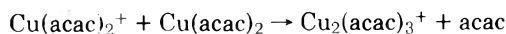
$Co(acac)_2$ . It was necessary to hold the sample under vacuum for several hours at room temperature to avoid excessive interference from acetylacetone in the spectra. Both the source temperature and maximum probe temperature were 195 °C. Agreement with previous low-pressure spectra<sup>6,13</sup> is good. Dicobalt ions previously reported are 0.4%  $Co_2(acac)_3^+$  and a trace of  $Co_2(acac)_4^+$ .<sup>6</sup> These are now found at 47 and 7%, respectively, at high pressure. They are obtained also from  $Co(acac)_3$ . Other heavy ions are  $Co_2(acac)_2^+$  at 2%,  $Co_3(acac)_4^+$  at 3%, and  $Co_3(acac)_5^+$  at 15%. This last ion occurs in greater abundance than it does from  $Co(acac)_3$ . A strong pressure-dependence suggests it is a tertiary ion resulting from stepwise reaction of a primary ion such as  $Co(acac)^+$  or  $Co(acac)_2^+$  with two molecules of  $Co(acac)_2$ . In this case involvement of neutral polymers may be ruled out according to results of an infrared spectroscopic study of the matrix-isolated vapor of  $Co(acac)_2$ , which showed that at sublimation temperatures near those used here, the vapor is monomeric.<sup>17</sup>

As with  $Mn(acac)_2$ , the most abundant secondary and tertiary ions from  $Co(acac)_2$  are those where the metal atoms are in the same oxidation state as in the neutral complex,  $Co(II)$ .

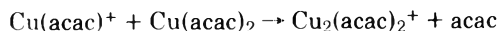
$Ni(acac)_2$ . The dinuclear species  $Ni_2(acac)_2^+$  and  $Ni_2(acac)_3^+$  reported by Macdonald and Shannon at 0.3 and 0.4%, respectively,<sup>6</sup> are now observed at maxima of 13 and 49%, respectively. This abundance of  $Ni_2(acac)_3^+$  occurs at the maximum probe temperature and source temperature of 170 °C after  $Ni_2(acac)_2^+$  and the primary ions have decreased in abundance. Heavier ions observed are 4%  $Ni_3(acac)_4^+$ , 16%  $Ni_3(acac)_5^+$  containing Ni(II), 2%  $Ni_3(acac)_7^+$ , and 8%  $Ni_4(acac)_8^+$  at  $m/e$  1024. This last ion suggests a tetrameric vapor, but Fackler et al. concluded that  $Ni(acac)_2$  is monomeric as a vapor<sup>17</sup> although it is trimeric in the solid state and in hydrocarbon solution.<sup>14</sup> The polynuclear ions are therefore taken to be products of gaseous ion-neutral reactions.

$Cu(acac)_2$ . In agreement with a previous spectrum<sup>6</sup> the base peak at low pressure is due to  $Cu(acac)_2^+$  at 27%. Slightly more than 1% abundance was reported<sup>6</sup> for  $Cu_2(acac)_2^+$  and for  $Cu_2(acac)_3^+$ . With the ion source at 210 °C and the probe heating to 185 °C,  $Cu_2(acac)_2^+$  rises to 8% and  $Cu_2(acac)_3^+$ , with Cu(II), has its maximum at 35%. Other heavy ions are 1.5%  $Cu_2(acac)_2C_4H_4O_2^+$  at  $m/e$  408 corresponding to loss of methyl radical from  $Cu_2(acac)_3^+$ , 1%  $Cu_3(acac)_3^+$ , and 43%  $Cu_3(acac)_4^+$  which is considered to have two atoms of Cu(II) and one of Cu(I). The trinuclear Cu(II) ion  $Cu_3(acac)_5^+$  is not found, although its analogue is of significant abundance for the bis complexes of other metals. The greater tendency of copper to exist as Cu(I) accounts for formation of  $Cu_3(acac)_4^+$  rather than  $Cu_3(acac)_5^+$ . The abundance of  $Cu_3(acac)_4^+$  has a much greater pressure dependence than does  $Cu_2(acac)_3^+$ , as expected if the former is tertiary and the other is secondary. The vapor of this complex also has been found monomeric.<sup>17</sup>

A comparison of spectra at 70 and 15 eV for fixed pressure shows  $Cu_2(acac)_3^+$  at a nearly constant ratio to  $Cu(acac)_2^+$  suggesting that



accounts for at least part of the production of  $\text{Cu}_2(\text{acac})_3^+$ . The same precursor may give rise to  $\text{Cu}_2(\text{acac})_2\text{C}_4\text{H}_4\text{O}_2^+$  since this ion has an appearance potential near that of  $\text{Cu}_2(\text{acac})_3^+$ . Similar considerations imply  $\text{Cu}_2(\text{acac})_2^+$  has an appearance potential at least as great as that of  $\text{Cu}(\text{acac})^+$ , suggesting the possibility of



The difficulty of maintaining constant sample pressure and the loss in sensitivity at low ionizing energy prevent the obtaining of quantitative appearance potentials for secondary ions.

**$\text{Cu}(\text{hfac})_2$ .** The green crystals used are the diaquo complex,<sup>18</sup> but evidence of hydrated ions in the mass spectrum decreased at the higher probe temperatures. The source was at 115 °C and the probe was as high as 80 °C. The low-pressure spectrum is similar to that previously reported<sup>15</sup> with  $\text{CuC}_4\text{HO}_2\text{F}_3^+$ , corresponding to loss of  $\text{CF}_3$  from  $\text{Cu}(\text{hfac})^+$ , as the base peak at  $m/e$  201. Heavy ions at the high pressures are analogous to those found for  $\text{Cu}(\text{acac})_2$ .  $\text{Cu}_2(\text{hfac})_4^+$  grows to 13%,  $\text{Cu}_2(\text{hfac})_3^+$  to 20%, and  $\text{Cu}_3(\text{hfac})_2^+$  to 13%. The ion at  $m/e$  678, corresponding to loss of  $\text{CF}_3$  from  $\text{Cu}_2(\text{hfac})_3^+$ , grows to 6%.

A spectrum at 14 eV shows  $\text{Cu}_2(\text{hfac})_3^+$  to be of similar appearance potential to  $\text{Cu}(\text{hfac})_2^+$ , implying formation of the dinuclear ion by a process analogous to that suggested above for  $\text{Cu}_2(\text{acac})_3^+$ .

If  $\text{Cu}_3(\text{hfac})_5^+$  forms, it would not be detected since its  $m/e$  of 1224 puts it beyond the upper mass limit of this instrument. Its absence is predicted by analogy with  $\text{Cu}(\text{acac})_2$ .

**$\text{Zn}(\text{acac})_2$ .** Several of the spectra of this complex are shown in Figure 1. The low-pressure spectrum is in agreement with a previous report,<sup>6</sup> which includes no ion heavier than  $\text{Zn}(\text{acac})_2^+$ . High intensities of the  $\text{Zn}(\text{II})$  ions  $\text{Zn}_2(\text{acac})_3^+$  and  $\text{Zn}_3(\text{acac})_5^+$  are now obtained at high pressure.  $\text{Zn}_2(\text{acac})_4^+$  increases to 2%. Fackler et al. determined that  $\text{Zn}(\text{acac})_2$  sublimes as a monomer,<sup>17</sup> so, again, evidence is strong that the polynuclear ions are products of gaseous ion-neutral reactions.

**$\text{Cd}(\text{acac})_2$ .** The white solid left a brown residue after heating to 200 °C. The spectra with the ion source at 255 °C showed large amounts of acetylacetone, as evidenced by intense peaks at  $m/e$  43 and 101 for  $\text{CH}_3\text{CO}^+$  and  $\text{H}_2(\text{acac})^+$ , respectively. Considering only the metal-containing ions, at low pressure the primary ions include 32%  $\text{Cd}(\text{acac})_2^+$ , 14%  $\text{Cd}(\text{acac})\text{C}_4\text{H}_4\text{O}_2^+$ , and 49%  $\text{Cd}(\text{acac})^+$ . These all react at higher pressures to produce up to 38%  $\text{Cd}_2(\text{acac})_3^+$  and 13%  $\text{Cd}_3(\text{acac})_5^+$ . There is growth in  $\text{HCd}(\text{acac})_2^+$  to 30% at high pressure, which is apparently caused by the presence of acetylacetone in the ion source, as with  $\text{Rh}(\text{acac})_3$  already discussed.

## Conclusions

Of the 16 complexes investigated, only  $\text{Al}(\text{hfac})_3$  shows no polynuclear ions in the high-pressure mass spectra. Ion-neutral reactions producing polynuclear ions, usually with no fragmentation within the ligand, occur readily in all other cases.

The formation of secondary  $\text{ML}_3^+$  from tris complexes is observed when the ionization energy of the complex is less than the recombination energy of its fragment ions, as for  $\text{Mn}(\text{acac})_3$  and  $\text{Co}(\text{acac})_3$  but not  $\text{Fe}(\text{acac})_3$ . Thus where direct measurements are not available, the complex is predicted to have a lower ionization energy than its fragments when charge transfer is observed, as for  $\text{V}(\text{acac})_3$  and  $\text{Rh}(\text{acac})_3$  but not for all other complexes studied.

Formulas for readily produced polynuclear ions are most simply correlated with expected oxidation states of the metal atoms. Thus  $\text{M}_2\text{L}_3^+$  and  $\text{M}_3\text{L}_5^+$ , which contain  $\text{M}(\text{II})$ , are abundant with the bis complexes while  $\text{M}_2\text{L}_5^+$ , with  $\text{M}(\text{III})$ , characterizes the tris complexes. Less-abundant and mixed-valence ions are similarly rationalized in specific cases. Consideration of oxidation states and their changes has been useful also in interpreting the unimolecular fragmentation mechanisms of many of these complexes as deduced from low-pressure mass spectra.<sup>6</sup>

The formation of the polynuclear ions does not appear to involve a transition state with significant restructuring about the metal in the neutral complex. The octahedral tris complexes typically have reactivities comparable to those of the bis complexes, whether the latter are planar,<sup>17</sup> as  $\text{Ni}(\text{acac})_2$  and  $\text{Cu}(\text{acac})_2$ , or tetrahedral,<sup>17</sup> as  $\text{Co}(\text{acac})_2$  and  $\text{Zn}(\text{acac})_2$ . The small effect of structural differences can be understood if reaction is determined mainly by kinetic, rather than thermodynamic, effects. By polarization theory<sup>19</sup> the interaction of an ion with the induced dipole of the neutral molecule increases with the polarizability of the molecule. The low polarizability expected for  $\text{Al}(\text{hfac})_3$  relative to the other complexes is consistent with its low reactivity.

**Acknowledgment.** Acknowledgment is made to the donors of the Petroleum Research Fund, administered by the American Chemical Society, for partial support of this research.

## References and Notes

- (1) J. Müller and W. Goll, *J. Organometal. Chem.*, **69**, C23 (1974), and preceding papers in the series.
- (2) S. M. Schildcrout, *J. Am. Chem. Soc.*, **95**, 3846 (1973).
- (3) R. C. Dunbar, J. F. Ennever, and J. P. Fackler, Jr., *Inorg. Chem.*, **12**, 2734 (1973).
- (4) M. S. Foster and J. L. Beauchamp, *J. Am. Chem. Soc.*, **97**, 4808 (1975).
- (5) M. S. Foster and J. L. Beauchamp, *J. Am. Chem. Soc.*, **97**, 4814 (1975).
- (6) C. G. Macdonald and J. S. Shannon, *Aust. J. Chem.*, **19**, 1545 (1966).
- (7) J. R. Majer and R. Perry, *Chem. Commun.*, 454 (1969).
- (8) J. E. Schwarberg, R. E. Sievers, and R. W. Moshier, *Anal. Chem.*, **42**, 1828 (1970).
- (9) R. Belcher, C. R. Cranley, J. R. Majer, W. I. Stephen, and P. C. Uden, *Anal. Chim. Acta*, **60**, 109 (1972).
- (10) The conjugate base of acetylacetone or 2,4-pentanedione is represented as  $\text{acac}^-$ , and that of 1,1,1,5,5,5-hexafluoro-2,4-pentanedione is represented as  $\text{hfac}^-$ .
- (11) G. M. Bancroft, C. Reichert, and J. B. Westmore, *Inorg. Chem.*, **7**, 870 (1968).
- (12) S. M. Schildcrout, R. G. Pearson, and F. E. Stafford, *J. Am. Chem. Soc.*, **90**, 4006 (1968).
- (13) C. Reichert and J. B. Westmore, *Inorg. Chem.*, **8**, 1012 (1969).
- (14) J. P. Fackler, Jr., *Prog. Inorg. Chem.*, **7**, 361 (1966).
- (15) C. Reichert, G. M. Bancroft, and J. B. Westmore, *Can. J. Chem.*, **48**, 1362 (1970).
- (16) F. A. Cotton and G. Wilkinson, "Advanced Inorganic Chemistry", 3d ed, Interscience, New York, N.Y., 1972, p 279.
- (17) J. P. Fackler, Jr., M. L. Mittelman, H. Weigold, and G. M. Barrow, *J. Phys. Chem.*, **72**, 4631 (1968).
- (18) J. A. Bertrand and R. I. Kaplan, *Inorg. Chem.*, **5**, 489 (1966).
- (19) G. Gioumousis and D. P. Stevenson, *J. Chem. Phys.*, **29**, 294 (1958).



## Identification of Bacteria Using Linear Programmed Thermal Degradation Mass Spectrometry. The Preliminary Investigation

Terence H. Risby

*Department of Chemistry, Pennsylvania State University, University Park, Pennsylvania 16802*

and Alfred L. Yergey\*

*Scientific Research Instruments Corporation, 6707 Whitestone Road, Baltimore, Maryland 21207 (Received May 20, 1976)*

*Publication costs assisted by Scientific Research Instruments Corporation*

A novel process for the identification of bacteria has been developed. The process makes use of evolution patterns of molecular fragments generated during the well-controlled thermal degradation of bacterial cells. The process has been shown to be effective in distinguishing ten well-characterized bacterial organisms from each other and in grouping known members of the same genus together. The reproducibility of the method has been demonstrated.

### Introduction

The identification of bacterial organisms is important for a set of human problems which range from maximizing food production to controlling and preventing disease. The methods commonly used for bacteria identification depend upon the nature of the organisms, the time available for the task, and the degree of identification required. Classical physical methods of identification include morphological differences detected by microscopy and enhanced by staining techniques.<sup>1</sup> This type of identification, while fairly rapid, is unsatisfactory for the speciation of most organisms. Biochemical methods used for identification are based on the ability of organisms to ferment specific sugars, or on other characteristic chemical reactions.<sup>1</sup> These methods, although generally specific, require at least 1.5 days for the reactions to be carried to a point satisfactory for identification. Some of the newer chemical techniques used for the identification of bacteria to the strain level are immunofluorescence, radio-antibody analysis, and serology.<sup>2</sup> All of these methods are so specific that they have no general applicability and can be used only when the identification is nearly complete.

Modern physical approaches to bacterial identification fall into two broad classes: thermal methods such as microcalorimetry<sup>3</sup> and pyrolysis methods including use of a gas chromatograph<sup>4-8</sup> and/or a mass spectrometer to analyze the pyrolysate.<sup>9-11</sup> Other thermal analytical methods such as thermogravimetry, differential thermal analysis, and thermogravimetry-mass spectrometry, while used for polymer analysis, have found little or no application to bacteria analysis.<sup>12-14</sup> Pyrolysis gas chromatography is the most widely used physical method at this time, and bacterial identifications based on its use are frequently dependent upon characteristic ratios of the heights of peaks in a gas chromatogram rather than upon the existence of characteristic peaks.<sup>7</sup> The use of mass spectrometer with or without a gas chromatograph to analyze directly the products of a pyrolysis carried out in or near the ion source results in some improvement in identification of organisms. Nevertheless, all these methodologies employ isothermal pyrolysis, which means the bacteria identification is based upon the analysis of the complex mixture of cellular degradation products produced at a single temperature.

The purpose of this investigation is to test the feasibility of identifying bacterial organisms through the use of a new methodology. The methodology is based on the hypothesis that a sample of complex biological materials will decompose in an orderly and reproducible manner when heated gradually. The hypothesis of a sequence of characteristic reactions occurring reproducibly in complex materials has been validated in a study of the hydrosulfurization of bituminous coals.<sup>15</sup> This hypothesis has not been previously tested for the more complex materials represented by bacterial cells. The results of such decomposition processes in bacteria are expected to be a sequence of characteristic molecular fragments that could be monitored mass spectrometrically to produce temperature-dependent profiles of the masses of the decomposition products. Because of the temperature dependence of the mass profiles, it was felt the bacterial cell decomposition products having the same molecular weight might evolve at different temperatures. This anticipated separation of decomposition product masses resulting from sequential degradations, absent in isothermal pyrolysis, represents a parameter for identifying bacterial organisms that has not been available previously. It was thought that these temperature-dependent profiles of specific ion intensities could be characteristic of the organisms being pyrolyzed and could therefore be used to identify them. In addition, it was thought that some of the profiles from known different but taxonomically related species could be used for the classification of organisms.

### Experimental Section

**Apparatus.** A standard Scientific Research Instruments Biospect chemical ionization quadrupole mass spectrometer was used to obtain the mass spectra. The instrumental conditions used were: 1 Torr of methane reagent gas, 0.1-mA emission current, and 160 °C source temperature. Consistent sensitivity and resolution for the mass range in this work was established using a mixture of methylstearate (protonated parent ion,  $m/e$  299) and chromium tris(1,1,1-trifluoro)-2,4-pentanedionate (protonated parent ion,  $m/e$  512).

The solids probe used to introduce samples into the chemical ionization source was heated by a linear temperature programmer. A temperature ramp of 20 °C/min operating between ambient and 400 °C was used for all of the work re-

ported here. Control of the probe tip temperature was effected by a feedback loop between the power source and a thermocouple junction at the probe tip.

Data were recorded using a Systems Industries (Sunnyvale, Calif.) System 150 mass spectrometry data system. Scan conditions used in the mass range 250–750 amu were as follows: data acquisition times: 3 ms/amu from 250 to 350 amu, 10 ms/amu from 351 to 450 amu, 20 ms/amu from 451 to 750 amu; time between scans 1 s; time per scan 8.3 s.

Because the source temperature is maintained at 160 °C, and the rate of temperature increase is 20 °C/min, it is apparent that a linear temperature increase in the sample does not hold over the entire temperature range. The nonlinear portion of temperature increase is very reproducible and, because the time per scan is known and constant, it can be shown that after approximately the sixtieth scan, a linear relationship between temperature and scan number is obtained.

**Organisms.** Table I lists ten organisms obtained from American Type Culture Collection (ATCC), Rockville, Md., along with the accession number of each organism. These ten organisms were prepared at the ATCC by using a 10% inoculation of 250-ml nutrient broth, culturing for 24 h, harvesting the organisms, spinning down the cells, washing in 0.1 M phosphate buffer, and lyophilizing for 18 h in two vials. Upon receipt, the vials were stored at 4 °C. Samples for analysis were prepared by opening a sample vial, extracting a portion of dried cells with a flamed spatula, placing the cells onto a flamed watch glass, replugging the sample vial, placing the vial into a flamed test tube, and sealing the tube with a sterile gauze swatch. Only one sample vial was open in the room at a time, and all items in contact with the cells were flamed between openings.

The sample of *Citrobacter freundii* used in the reproducibility studies was obtained from Dr. Frank Kocka, Billings Hospital, Chicago, Ill. Cells for analysis were obtained by streaking plates of trypticase-soy-5% sheep blood agar plates (Bioquest lot no. K4ZMMA). After approximately 18-h growth at 37 °C, each plate was divided into three sections by scoring with a sterile loop. The growth in each sector was harvested by scraping the cells from the agar and placing the cells into approximately 1 ml of methanol in conical tubes. The tubes containing the cells were stored at 4 °C. The concentration of cells in the tubes was determined by using McFarland nephelometer standards and the concentrations were shown to be greater than  $3 \times 10^7$  cells/cm<sup>3</sup>, the most optically dense standard available.

**Analysis.** The samples consisted of either slightly moist lyophilized cellular material ( $3 \times 10^7$  cells, 10–100 µg of dry material) placed into a capillary or a suspension of cells in methanol drawn into an approximately 6-µl sample tube by touching the surface of the suspension with the sample tube. A lower limit of the amount of cellular material in a 6-µl aliquot of the suspension was estimated to be  $2 \times 10^7$  cells. Solvent was removed by pumping at approximately 0.1 Torr at ambient temperature.

The capillary sample tubes were introduced into the chemical ionization source in the tip of the solids probe. A run was initiated immediately after the probe was seated by starting the temperature programmer and the computer data acquisition. Data taking was terminated when the temperature reached 400 °C (150 scans), by which time the material had evolved from the probe tip.

After a run was completed, the data stored by the computer could be displayed in a variety of formats shown schematically

**TABLE I: Organisms Used in the Characterization Process**

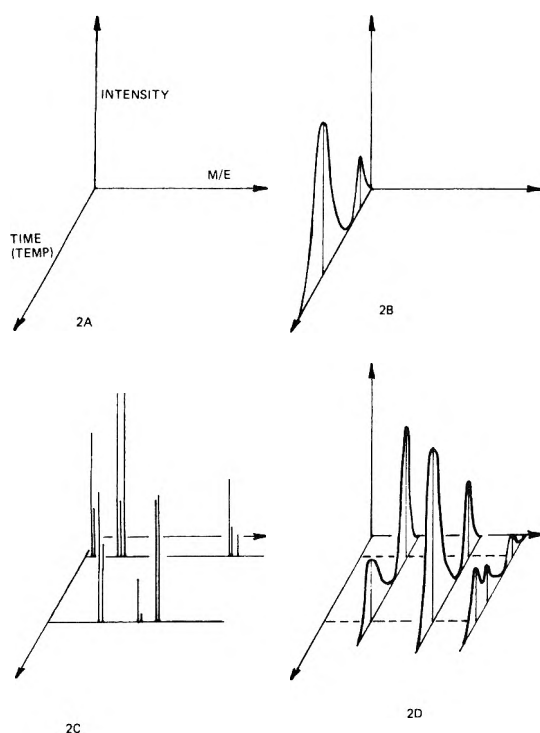
Organism	ATTC no.	Sequence no.
<i>Pseudomonas putida</i>	12633	1
<i>Pseudomonas putida</i>	15073	2
<i>Pseudomonas fluorescens</i>	13525	3
<i>Escherichia coli</i>	4147	4
<i>Escherichia coli</i>	11775	5
<i>Bacillus megaterium</i>	14581	6
<i>Bacillus subtilis</i>	6051	7
<i>Arthrobacter oxydans</i>	14358	8
<i>Arthrobacter globiformis</i>	8010	9
<i>Erwinia amylovora</i>	15580	10

in Figure 1. The objective of the data analysis was to find those temperature/time dependent specific ion plots, Figure 1D, that would be characteristic of particular bacteria. Selecting those ions to be used in making specific ion plots was done by selecting mass spectra (Figure 1C) from several prominent points in the total ion plot (Figure 1B). Candidate ions for specific ion temperature/time profiles were those ions significantly higher than the background intensity. A table was made by combining the list of candidate ions from each of the organisms studied. Specific ion profiles were then prepared for each of the organisms at all of the mass numbers contained in the summary table of candidate ions. Study of these specific ion profiles was undertaken to find those that were judged to have the greatest ability to distinguish and classify bacteria.

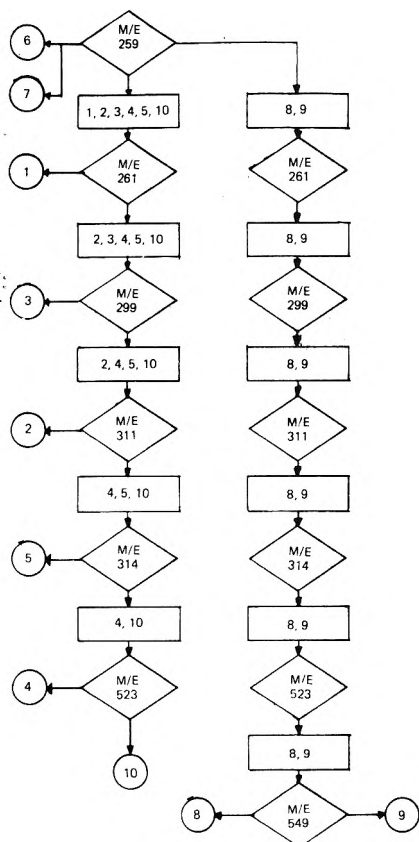
## Results and Discussion

A total of 77 ions from all of the organisms studied were found to have intensities significantly greater than background levels. These 77 ions were used as candidate ions and specific ion temperature/time profiles were produced for each of these masses for the ten bacterial organisms in Table I. Those profiles that could be used as characterizers of the organisms were then selected. Because the purpose of this study was to demonstrate the possibility of identifying bacteria by the use of particular specific ion temperature/time profiles, it was decided to limit the search of the 770 profiles to the finding of a single profile for each of the bacteria in Table I that would distinguish that bacterial strain from all others in the table. This limitation is a reasonable one because the organisms listed in Table I are taxonomically quite diverse in that five genera are represented, but at the same time several genera are represented by several species e.g. *Pseudomonas* and several species are represented by two strains, i.e., *Pseudomonas putida* and *Escherichia coli*. If the degree of differentiation is great enough that the use of a single profile can be used to distinguish intraspecific strains, then, at the level of a feasibility study, use of a single profile to distinguish between species and genera is acceptable. The considerably more demanding task of finding multiple characterizing profiles for each organism is left to future work when computer-assisted sorting methods can be applied to the data.

Figure 2 is a flow chart that shows how a set of characteristic specific ion profiles are used to distinguish the bacteria in Table I from each other. At *m/e* 259, six organisms are seen to be inseparable from each other, two separate from the remaining eight but not from each other, and two are completely distinguishable. Figure 3 shows the temperature/time profile for the *m/e* 259 ion of all ten organisms numbered from top

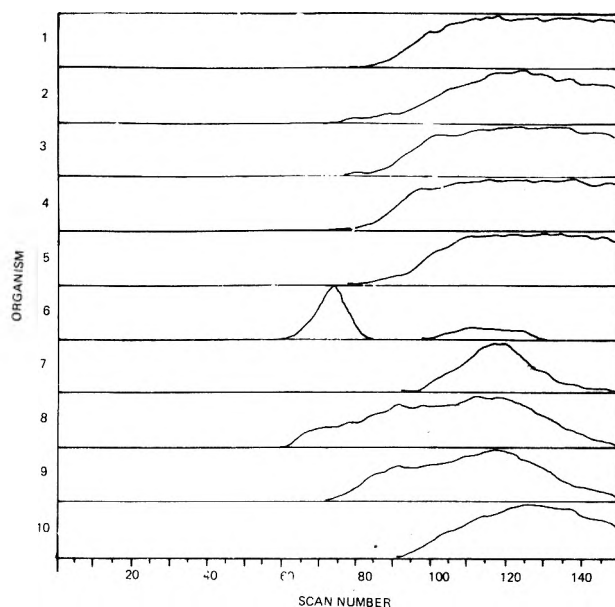


**Figure 1.** Data formats: (A) data axes; (B) total ion plot; (C) sequential mass spectra; (D) specific ion plots (temperature/time profile).

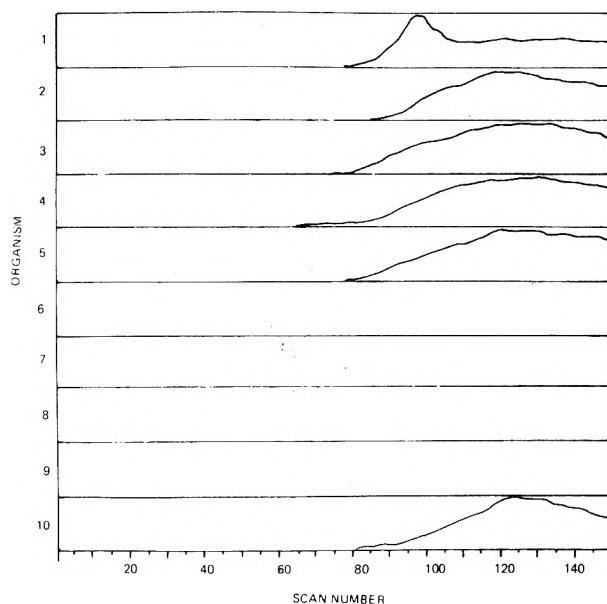


**Figure 2.** Flow chart for differentiating 10 bacteria using temperature/time profiles.

to bottom as they are numbered in Table I. The basis for Figure 2 is readily seen. Referring back to Figure 2, it is seen that  $m/e$  261 (Figure 4) allows organism one to be separated



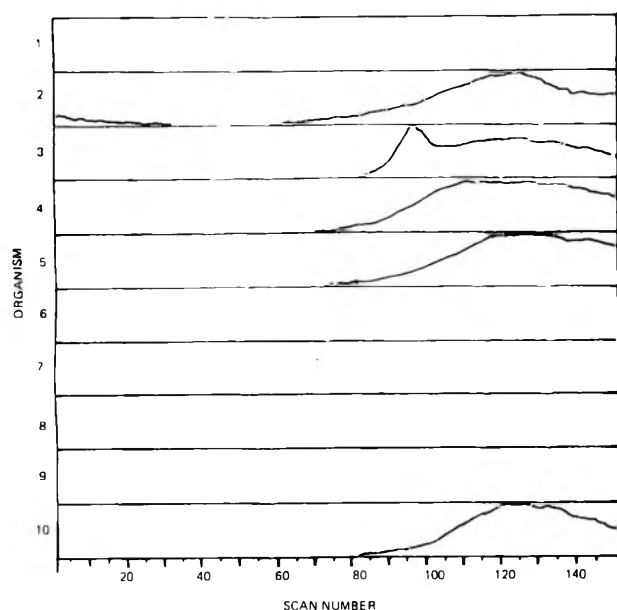
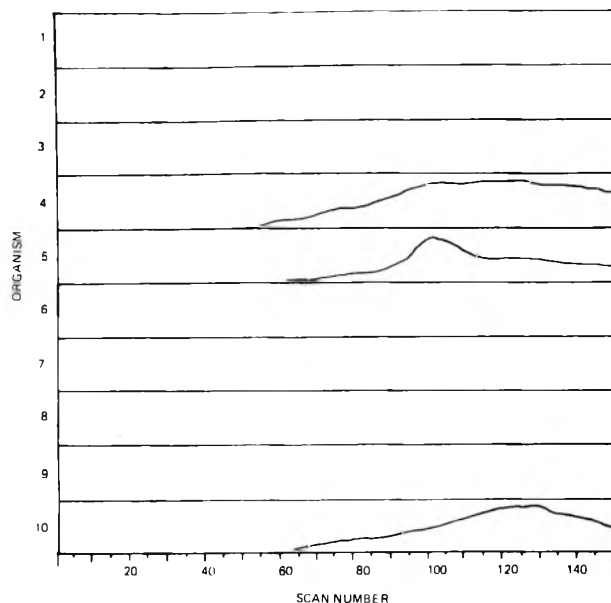
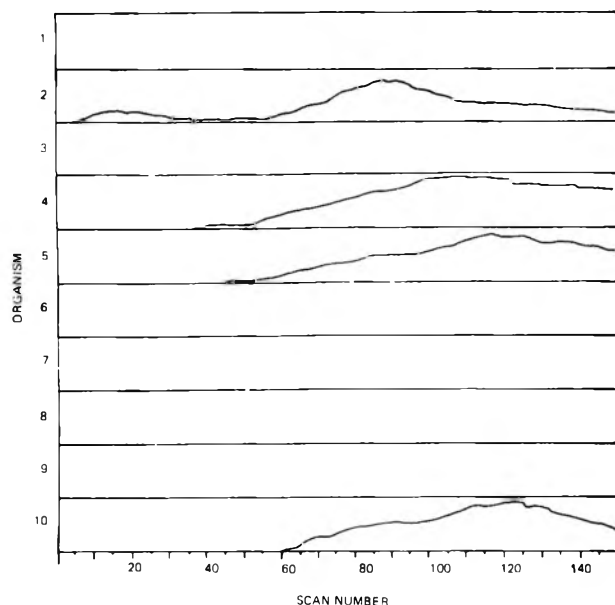
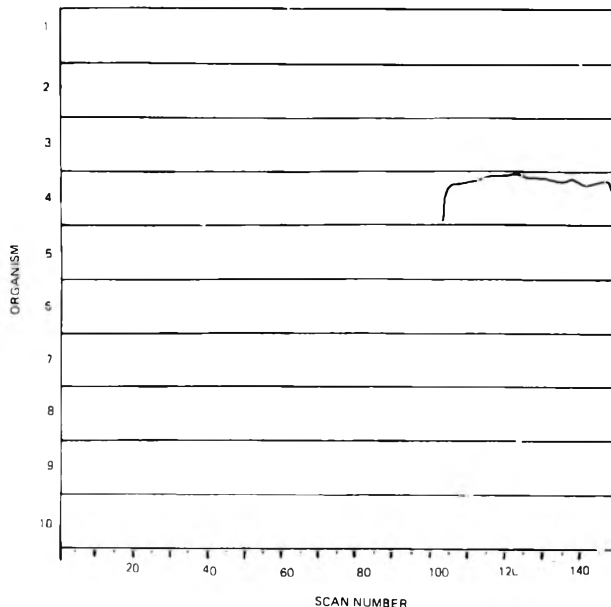
**Figure 3.** Profiles of ions at  $m/e$  259.



**Figure 4.** Profiles of ions at  $m/e$  261.

from the other five in its subgroup. For the sake of clarity, only those organisms being differentiated at a particular mass number have ion profiles illustrated at that mass number. The remaining five temperature/time dependent profiles required for differentiation are shown in Figures 5–9. Note that the differentiating features of the profiles chosen are those that have sharp maxima, or maxima that are displaced to temperatures different from the rather broad maximum that occurs in the region of the 120th scan (approximately 300 °C). All of the differentiating characteristics of the profiles shown in Figures 3–9 occur above the 160 °C temperature that is the beginning of linear dependence of temperature on time.

In addition to distinguishing the ten organisms from each other, the specific ion temperature/time profiles can be used to obtain a posteriori, the normal taxonomic relationships between the organisms. Figure 10 is a flow chart that shows the grouping. The profiles at  $m/e$  259 produce separations into

Figure 5. Profiles of ions at  $m/e$  299.Figure 7. Profiles of ions at  $m/e$  314.Figure 6. Profiles of ions at  $m/e$  311.Figure 8. Profiles of ions at  $m/e$  523.

three groups: organisms 8 and 9 known to be of the same genus, organisms 1, 2, 3, 4, 5, and 10 known to have three genera among its members, and organisms 6 and 7 known to belong to the same genus. The profiles at  $m/e$  276 (Figure 11) separates the species *Erwinia* organisms from the other five in the large group. The profiles at  $m/e$  308 (Figure 12) are used to group the known members of genus *Bacillus* together. In light of the great differences between the profiles of the two *Bacillus* organisms at  $m/e$  259, and in fact at many other masses not shown here, this seems to be an excellent choice. The profiles at  $m/e$  313 show a large resemblance between the known members of genus *Escherichia* and differences between the three known members of genus *Pseudomonas*. The combination of separation at  $m/e$  313 and resemblance at  $m/e$  259 is used as the means of grouping the three *Pseudomonas* organisms of this study.

The most likely source of error in using a temperature/time profile at a particular mass number is the potential presence of plasticizers in the samples. Control of experimental conditions was such that other contaminants or systematic errors were not likely to contribute to erroneous results, however, the almost ubiquitous presence of plasticizers in a laboratory could have resulted in their being in the sample. These plasticizers could produce profiles that are apparently characteristic of a bacterial organism, but in fact are characteristic of the history of the sample. Care was taken that no plastic materials contacted the organisms used in this work after they were received. Since all of the organisms were grown under identical conditions, it would be expected that any plasticizer contamination would be uniformly present in all the bacteria, thus a particular specific ion plot would not show the amount of characteristic behavior seen in Figures 3–9 and 11–13.

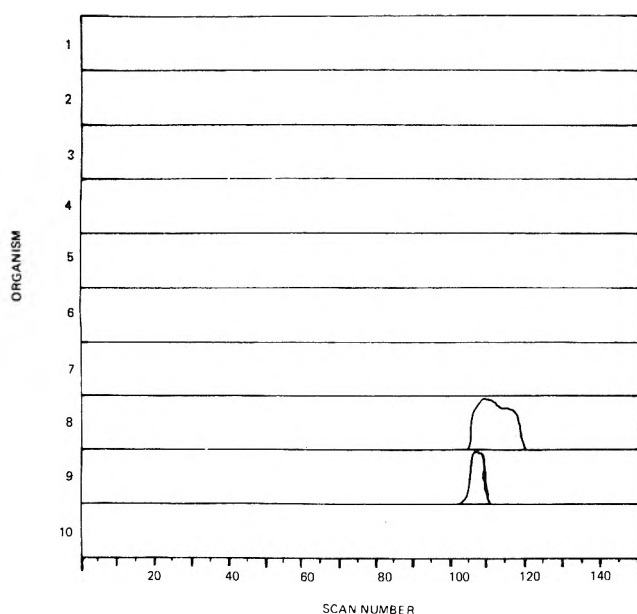
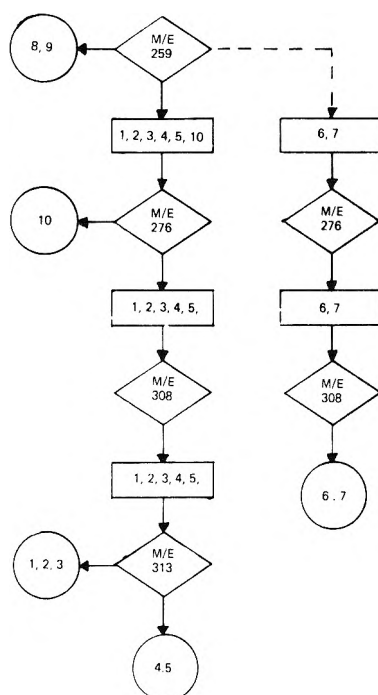
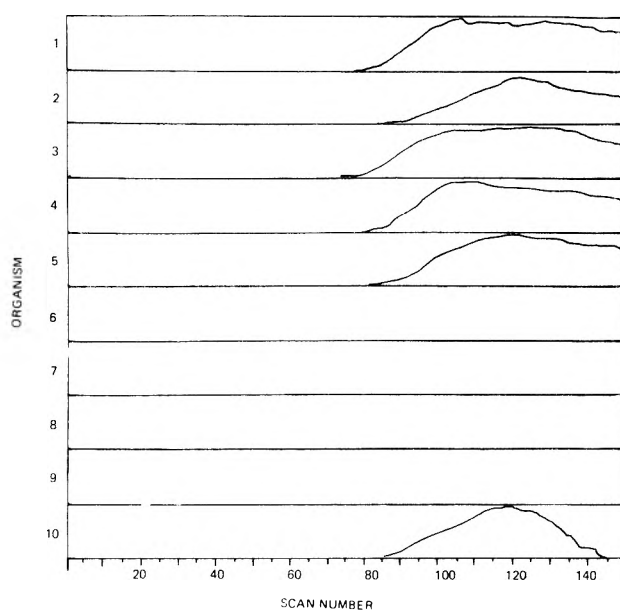
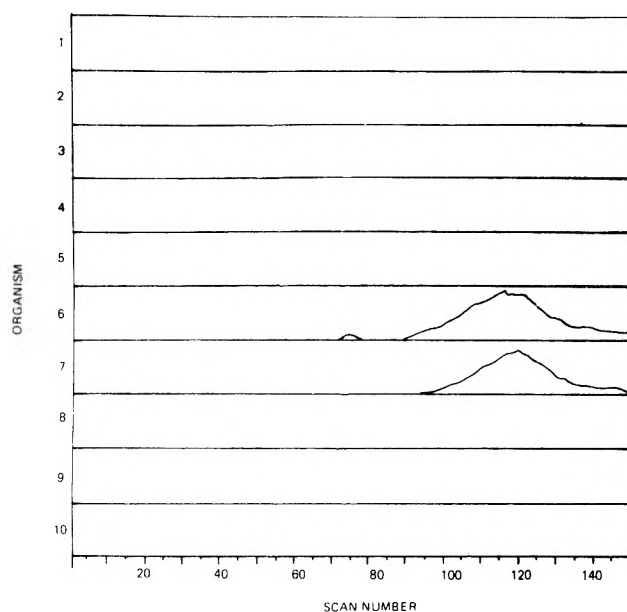
Figure 9. Profiles of ions at  $m/e$  549.

Figure 10. Flow chart for grouping 10 bacteria according to genus using temperature/time profiles.

Nevertheless, several plasticizers exist that would be expected to have the same chemical ionization masses as several of the ions used as characterizers.<sup>17</sup> The most likely interfering plasticizer is butylbenzylphthlate, molecular weight 312. The interference would occur at  $m/e$  313, a mass that was used to separate the *Escherichia* organisms from the *Pseudomonas* organisms. The estimated boiling point of butylbenzylphthlate is 227 °C at 1 Torr; this temperature is reached at about the 90th scan under the experimental conditions used. There are no features common to all of the profiles at  $m/e$  313 to indicate a particular single compound evolving at about the 90th scan. Since the single maximum for organism 2 and the lower temperature maximum for organism 1 that occur at

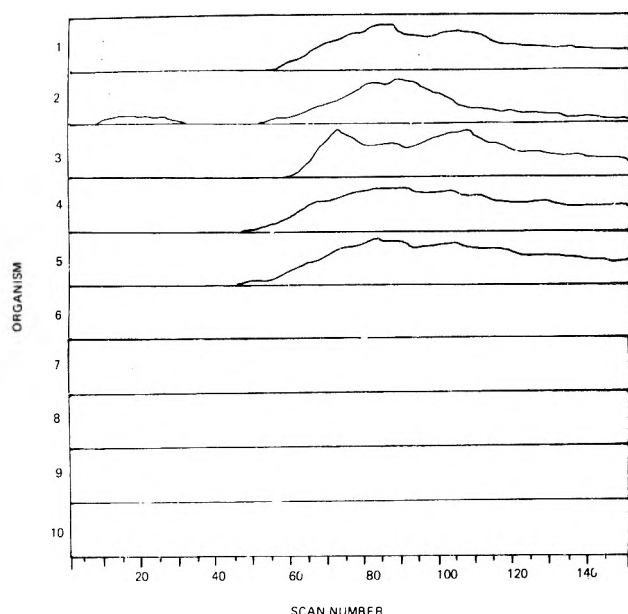
Figure 11. Profiles for ions at  $m/e$  276.Figure 12. Profiles of ions at  $m/e$  308.

about the 90th scan do not coincide with each other when superimposed, it appears unlikely that they have a common origin in such a single simple contaminant.

The long-term repeatability of the results from linear programmed thermal degradation mass spectrometric (LPTD-MS) analysis of bacteria was established by repeating the analyses many times during the course of a year. During this time, the detailed procedures for the method were developed, and so the location of specific maxima shifted, but the overall shapes of specific ion profiles were the same. Having developed the methodology, the reproducibility of a particular analysis was of a very high order. This was tested using the *Citrobacter freundii* organisms grown on blood agar plates. Sample cells prepared in this way will constitute a more severe test of reproducibility since relatively small numbers of cells were harvested from portions of a single plate. This allowed a greater opportunity for variations to appear than with a large mass of cells spun down together.

TABLE II: Correlation Coefficients for Replicate Runs of *Citrobacter freundii*

Replicate no.	1	2	3	4	5	Av
1	1.000					
2	0.969	1.000				
3	0.971	0.978	1.000			
4	0.984	0.985	0.987	1.000		
5	0.936	0.948	0.972	0.975	1.000	
Av	0.983	0.987	0.994	0.998	0.978	1.000
1	1.000					
2	0.930	1.000				
3	0.965	0.960	1.000			
4	0.946	0.961	0.994	1.000		
5	0.979	0.906	0.976	0.961	1.000	
Av	0.980	0.968	0.996	0.990	0.981	1.000

Figure 13. Profiles for ions at  $m/e$  313.

Reproducibility of temperature/time profiles at various masses was shown by calculating linear correlation coefficients between each of several replicate profiles and an averaged profile. A vector representative of a particular profile in a given replicate was produced by taking the ion intensity at every tenth scan number above the 60th, and normalizing each point in the vector to the base ion for that entire run. The vectors formed in this way for each of the replicates were then used to produce an average vector. Linear correlation coefficients between each replicate and all other replicates and the average vector were then calculated. This was done for several mass numbers for the *Citrobacter freundii* samples. Table II shows the results for two different mass numbers,  $m/e$  259 and 261. These results are in a format that is symmetrical about the diagonal with the number located at the intersection of any row and column representing the value of the linear correlation coefficient for those two runs, e.g., the value of the linear correlation coefficient for the second and third replicates at  $m/e$  259 is 0.978. The linear correlation coefficient of each replicate with the average vector is given in the row labeled average. The linear correlation coefficients of each of these replicates both with the average value and with each of the other replicates is seen to be very high. The existence of these high values of correlation coefficients demonstrates that the

LPTD-MS method is capable of giving a high order of reproducibility to determinations, and therefore the quality of bacterial identification based upon a number of characteristic profiles can be expected to be high. The fact that this high degree of reproducibility was obtained from organisms harvested from a small section of an agar plate increases the confidence one has in the ability to easily grow bacterial organisms using a generally accepted method for preparation.

The purpose of this work was to demonstrate the feasibility of identifying various bacterial organisms by use of ion intensity profiles produced in the course of an LPTD-MS analysis. This goal has clearly been achieved. The degree of separation between several closely related organisms has been demonstrated to be high, and the separation has been shown to be relatively free from the most likely source of interfering masses. The degree of separation, while being high, has been shown to have a relationship with the taxonomy of the bacteria studied. Organisms known to be related to each other have been shown to have points of commonality in the ion profiles generated. Finally, the type of data generated in an LPTD-MS analysis have been shown to be very reproducible insofar as the linear correlation coefficients between replicate runs and the average of several runs agree with each other.

NOTE ADDED IN PROOF: It has been brought to our attention that some work related to the present research was reported at the 2d Western Regional Meeting of the American Chemical Society (Oct, 1966) and reviewed briefly.<sup>18</sup> This earlier work is not cited in *Chemical Abstracts* nor in any of the other literature searched in conjunction with the present work. The results obtained by Friedman et al. were quite different than those obtained in this work since they were working with the low mass products of air pyrolysis. The earlier work resulted in observing few qualitative differences between six different bacterial samples, and the results from any bacterial pyrolysis were difficult to reproduce.

**Acknowledgments.** We are grateful to Scientific Research Instruments Corporation for financial support of this work. We wish also to acknowledge helpful discussions about the calculations of correlation coefficients with Professor F. W. Lampe of Pennsylvania State University and Dr. Gordon J. Fergusson of Scientific Research Instruments, as well as to thank Mr. Brian A. Jerome for help in data acquisition.

## References and Notes

- (1) S. T. Cowan, "Manual for the Identification of Medical Bacteria", Cambridge University Press, New York, N.Y., 1965.
- (2) R. E. Strange, *Adv. Microbiol. Phys.*, **88**, 105 (1972).



- (3) W. J. Russell, J. F. Zettler, G. C. Blanchard, and E. A. Boling, "New Approaches to the Rapid Identification of Microorganisms", C. Tiborilini, Wiley, New York, N.Y., 1975, pp 393-406.
- (4) P. D. Zeman, *Anal. Chem.*, **24**, 1709 (1952).
- (5) E. Reiner, *Nature (London)*, **206**, 1272 (1965).
- (6) E. Reiner and W. H. Ewing, *Nature (London)*, **217**, 191 (1968).
- (7) E. Reiner, J. J. Hicks, R. E. Beam, and H. L. David, *Am. Rev. Respir. Dis.*, **101**, 656 (1971).
- (8) P. G. Vincent and M. L. Kulik, *Appl. Microbiol.*, **20**, 957 (1970).
- (9) H. L. C. Meuzelaar and P. G. Kistemaker, *Anal. Chem.*, **45**, 587 (1973).
- (10) H. R. Schulten, H. D. Becky, H. L. C. Meuzelaar, and A. J. H. Boerboom, *Anal. Chem.*, **45**, 191 (1973).
- (11) J. P. Anhalt and C. Fenselau, *Anal. Chem.*, **47**, 219 (1975).
- (12) B. D. Mitchell and A. C. Birnie, "Differential Thermal Analysis", R. C. McKenzie, Ed., Academic Press, London, 1970, Chapter 24.
- (13) C. B. Murphy, ref 12, Chapter 23.
- (14) E. K. Gibson and S. M. Johnson, *Thermochim. Acta*, **4**, 49 (1972).
- (15) A. L. Yergey, F. W. Lampe, M. L. Vestal, E. J. Gilbert, and G. J. Fergusson, "Gassification of Fossil Fuels under Oxidative, Reductive and Pyrolytic Conditions", Final Report to EPA, Project No. 68-02-0206 (U.S. Government Access: EPA-650/2-73-042).
- (16) S. R. Prescott, J. E. Campana, P. C. Jurs, T. H. Risby and A. L. Yergey, *Anal. Chem.*, **48**, 827 (1976).
- (17) "Modern Plastics Encyclopedia", McGraw-Hill, New York, N.Y., 1946, pp 460-477.
- (18) H. L. Friedman, G. A. Griffith, and H. W. Goldstein in "Thermal Analysis", Vol. 1, R. F. Schwenker, Jr., and P. D. Garn, Ed., Academic Press, New York, N.Y., 1969, p 405.

## Arrival Time Distributions in High Pressure Mass Spectrometry. 5. Effect of $E/P$ on Measured Apparent Heats and Entropies of Reaction

G. G. Melsels,\* R. K. Mitchum,<sup>†</sup> and J. P. Freeman<sup>‡</sup>

Department of Chemistry, University of Nebraska—Lincoln, Lincoln, Nebraska 68588 (Received May 25, 1976)

Publication costs assisted by the University of Nebraska

The temperature dependence of the equilibrium involving the proton transfer between methane and carbon dioxide and their protonated analogues has been investigated at a series of values of the field strength  $E/P$ . The apparent values of  $\Delta S$  and  $\Delta H$  were found to depend on  $E/P$ ; experimental uncertainty in the former was too large to establish systematic trends. The latter decreased approximately linearly with  $E/P$ ; limiting values of  $\Delta H = -1.58 \pm 0.06$  kcal/mol and  $\Delta S = 1.7 \pm 0.3$  eu are in good agreement with those obtained by flowing afterglow and ICR techniques.

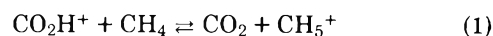
### Introduction

High pressure mass spectrometry has been employed extensively in recent years for the measurement of ionic equilibria in the gas phase.<sup>2-4</sup> Values for  $\Delta S$  and  $\Delta H$  are derived from studies of the temperature dependence of the equilibrium constant  $K$ . Such measurements may be subject to systematic errors;<sup>5-7</sup> these fall into two categories. One results from uncertainties in the conditions prevailing in the ion source. These are of interest here. Another is associated with the problems of ion sampling, discrimination, collision induced dissociations, and similar processes which are primarily external to the reaction region.

Two complications exist within the reaction region itself. The first is caused by the time dependence of the approach to equilibrium.<sup>7,8</sup> Time resolved measurements are now accepted as essential. The second difficulty arises from the occasional use of extraction fields in high pressure mass spectrometers of the chemical ionization type, or in drift tube mass spectrometers. It is well known that average ion energies are shifted upward by applied fields and that the ion velocity distributions lose Maxwell-Boltzmann character at higher values of  $E/P$ .<sup>9,10</sup> In this investigation we report our findings on the effect of  $E/P$  on measured values of the equilibrium

constant under conditions where equilibrium is totally achieved.

We have chosen to study the equilibrium



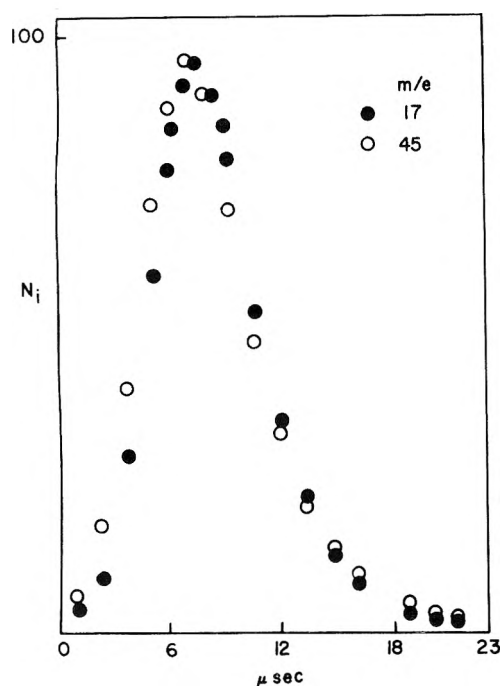
for several reasons. It is one of the earliest studies by high pressure mass spectrometry in the laboratory of Professor Franklin.<sup>11</sup> A careful study of this system has also been made by the flowing afterglow technique,<sup>12</sup> and has received support from another investigation employing ion cyclotron resonance.<sup>13</sup> The previous findings should provide a reliable reference point against which to evaluate our observations. Lastly, the enthalpy change associated with the equilibrium of reaction 1 is relatively small, so that the equilibrium reaction should proceed rapidly and ions should be thermalized quickly. The small exothermicity of the reaction also leads to the hope that processes external to the ion source such as collision induced dissociation, etc., will affect both ions approximately equally in spite of the substantial difference in mass.

### Experimental Section

The experimental procedures have been described previously.<sup>14</sup> Briefly, an Atlas CH-4 mass spectrometer was modified by the installation of a high pressure ion source and differential pumping system. Gases were maintained in sep-

\* Present address: NCTR-FDA, Jefferson, Ark. 72079.

<sup>†</sup> Present address: Department of Chemistry, University of Hawaii, Honolulu, Ha.

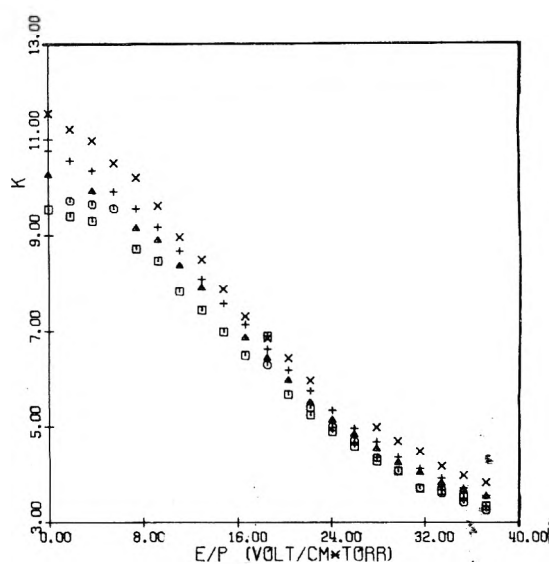


**Figure 1.** Arrival time distributions of  $\text{CO}_2\text{H}^+$  ( $m/e$  45) and  $\text{CH}_5^+$  ( $m/e$  17) at a field strength of  $15.6 \text{ V cm}^{-1} \text{ Torr}^{-1}$ , 441 K, and 0.35 Torr total source pressure containing 10%  $\text{CH}_4$  in  $\text{CO}_2$ ; normalized at maximum.

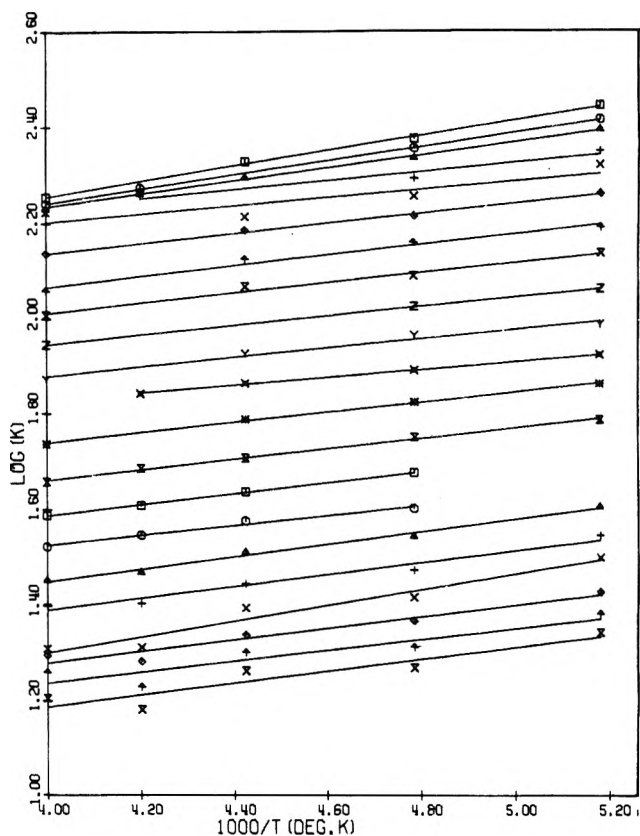
arate 5-l. stainless steel reservoirs; composition and total pressure were established using a Baratron capacitance gauge whose sensing arm was attached directly to the ion source. All experiments were performed at a concentration of ca. 10%  $\text{CO}_2$  in methane. Temperatures of the source block were adjusted by resistance heating and monitored with a calibrated thermistor. Time resolved measurements were made by pulsing the electron gun through the application of a  $0.5\text{-}\mu\text{s}$  pulse to 90% transparent tungsten mesh between the filament and the ion source block to reverse the 3-V negative bias on the screen. The pulse also triggered a time-to-pulse height converter which was terminated upon arrival of an ion at the electron multiplier detector. The arrival time of each single ion appearing at the detector was sorted on a 400-channel TMC pulse height analyzer. A complete arrival time spectrum could usually be accumulated in a period of approximately 10 min. The output of the memory of the analyzer was transferred onto paper tape and eventually processed on an IBM 360 computer. Ion residence times in the source were calculated by subtracting from the arrival times the flight time between the ion source exit and the detector, as described previously.<sup>14</sup>

## Results

Residence time distributions of  $\text{CO}_2\text{H}^+$  and  $\text{CH}_5^+$  were obtained over a range of values of temperature and  $E/P$  ( $\text{V cm}^{-1} \text{ Torr}^{-1}$ ). Representative distributors are given in Figure 1 and demonstrate clearly that the normalized arrival time distributions can be overlaid completely. This was the case at all temperatures and values of  $E/P$  employed in this investigation. Equilibrium measurements were made thereafter in a time averaged (dc) mode and are shown in Figure 2 as a function of  $E/P$  at several temperatures, and in Figure 3 in the form of Van't Hoff plots. It was noted that results were reproducible only when source and supply gases were scrupulously clean and free of moisture.



**Figure 2.** Variation of apparent equilibrium constant  $K_e$  with  $E/P$ ; top to bottom:  $\times$  193 °C;  $+$  209 °C;  $\Delta$ , 226 °C;  $\circ$ , 238 °C;  $\square$ , 250 °C.



**Figure 3.** Van't Hoff plots of  $K_e$  at various field strength.  $E/P$  increases from top to bottom.

## Discussion

Identity of arrival time distributions for two ions so disparate in mass as  $\text{CH}_5^+$  and  $\text{CO}_2\text{H}^+$  is possible only when the proton spends part of its time on methane and part of it on  $\text{CO}_2$  with a substantial number of interchanges, at least 5.<sup>15</sup> It was, therefore, not necessary to rely upon arrival time distributions for the establishment of equilibrium constants. The advantages of dc measurements for evaluating the temperature dependence of the equilibrium position are primarily the

much increased sensitivity and higher signal-to-noise ratio of such measurements, since the continuous measurements provide ion signals several orders of magnitude more intense than those observed in the pulsed mode.

It is evident from Figure 3 that Van't Hoff plots depend on  $E/P$ . Ion behavior in applied fields has been described by the well-established Wannier expression for average ion energies ( $\bar{E}_i$ ),<sup>9</sup> an equation derived on the basis of the retention of a Maxwell-Boltzmann distribution of ion energies:

$$\bar{E}_i = \frac{3}{2}kT_0 + \frac{1}{2}(M_i + M_G)v_d^2 \quad (\text{I})$$

where  $k$  is the Boltzmann constant,  $M_i$  the mass of the ion (g),  $M_G$  the mass of the neutral drift gas,  $v_d$  the drift velocity of the ions in question ( $\text{cm s}^{-1}$ ), and  $T_0$  is the gas temperature (K). This permits a qualitative understanding of the change of  $\Delta H_e$  with  $E/P$ . As  $E/P$  and therefore  $v_d$  increase, the second term on the right-hand side becomes more important, the ion energy becomes greater than that defined by  $T_0$ , and the energy barrier for reaction less important; hence,  $\Delta H_e$  appears to decrease.

Equation I may be developed in an attempt to derive more quantitative insight. Young and Edelson<sup>16</sup> and Parkes<sup>17</sup> have shown that eq I may be used to derive the effective joint temperature  $T_{j,a-B}$  of ion a colliding with neutral B of mass  $M_B$ .

$$T_{j,a-B} = T_0 + M_B v_d^2 / 3k \quad (\text{II})$$

The drift velocity  $v_d$  is given by<sup>18</sup>

$$v_d = 2.79 K_a^0 E T_0 / P \quad (\text{III})$$

where  $K_a^0$  is the reduced mobility which, for ion a drifting in a mixture of neutrals A and B of mole fraction composition  $X_A$  and  $X_B$ , is given by Blanc's law<sup>19</sup>

$$K_a^0 = [X_A/K_{a-A}^0 + X_B/K_{a-B}^0]^{-1} \quad (\text{IV})$$

where  $K_{a-A}^0$  is the reduced mobility of ion a in the pure gas A. Insertion of eq III and IV into eq II yields

$$T_{j,e-B} = T_0 \{ 1 + 2.59 M_B / k [X_A/K_{a-A}^0 + X_B/K_{a-B}^0]^{-2} T_0 (E/P)^2 \} \quad (\text{V})$$

where  $M_B$  is in grams.

The term in parentheses is a correction factor to  $T_0$ . It can be estimated by inserting the relationship<sup>18</sup>

$$K^0 = 35.9 / \sqrt{\alpha \mu} \quad (\text{VI})$$

where  $\alpha$  is the polarizability in Bohr radii cubed and  $\mu$  the reduced mass; eq VI is based on the Langevin drift theory.  $T_j$  differs from  $T_0$  by more than 10% for  $\text{CH}_5^+$  drifting in  $\text{CH}_4/\text{CO}_2$  mixtures when  $E/P$  exceeds ca.  $5 \text{ V cm}^{-1} \text{ Torr}^{-1}$  (at 500 K).

$T_{j,a-B}$  is not the same as  $T_{j,b-A}$ . When two ions considerably different in mass drift in a mixture and when the mean ion energy exceeds the thermal energy greatly, the effective temperature of the two ions will not be the same; in our system, it will be approximately 50% greater for the reverse reaction of the equilibrium described by reaction 1 at high fields. That is, the effective joint temperatures are not the same for the forward and reverse reactions. This is a complication only when both reactions have finite activation energies.

An attempt to interpret the field dependence of results quantitatively can be based on the operational definitions of enthalpy  $\Delta H_e$  and entropy  $\Delta S_e$  which are derived from Van't Hoff plots, assuming the applicability of the standard thermodynamic relationship

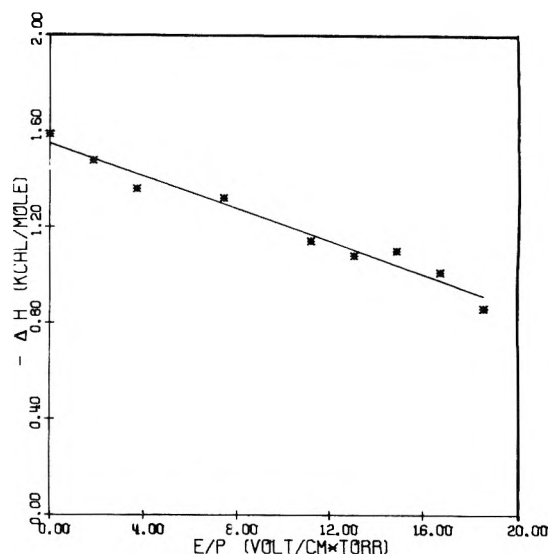


Figure 4. Apparent heat of reaction  $\Delta H_e$  and its dependence on  $E/P$ .

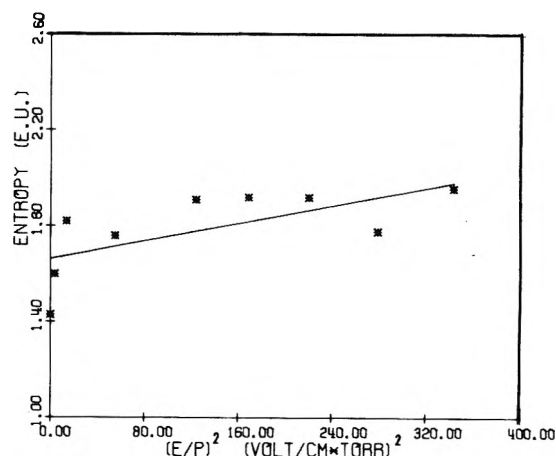


Figure 5. Apparent heat of reaction  $\Delta S_e$  and its dependence on  $E/P$ .

$$\ln K_e = \Delta S_e / R - \Delta H_e / RT_e \quad (\text{VII})$$

The subscript e indicates that the quantities derived do not necessarily correspond to the true thermodynamic ones. Clearly, eq V can represent translational energy only. Insertion of  $T_{j,a-B}$  from eq V for  $T_e$  in eq VII is simplified since the forward reaction should not have an activation energy. One may then identify a with  $\text{CH}_5^+$ , A with  $\text{CH}_4$ , and B with  $\text{CO}_2$ .

There is, of course, a serious difficulty inherent in such an approach. The derivation of the drift temperature leading to eq V is based not only on the assumption that translational Maxwell-Boltzmann distributions are preserved for ions, but disregards entirely energy transfer into internal modes. Yet the use of eq V as a "temperature" assumes that  $T_{j,a-B}$  describes the population of all energy states of the ion. At best one may therefore expect any quantitative relationships to reflect only qualitative trends, and dependencies on "effective" temperatures much weaker than those expected for thermodynamic temperature changes of the same magnitude. These complications are well known.<sup>16,17,20,21</sup>

At field strengths less than about  $5 \text{ V cm}^{-1} \text{ Torr}^{-1}$ , binomial expansion of the full equation and neglect of higher terms leads to

$$\ln K_e = \Delta S/R + [2.59\Delta H M(\text{CO}_2)/R] \\ \times [X(\text{CH}_4)/K^0(\text{CH}_5^+ \text{ in } \text{CH}_4) \\ + X(\text{CO}_2)/K^0(\text{CH}_5^+ \text{ in } \text{CO}_2)]^{-2} [E/P]^2 - \Delta H/RT_0 \quad (\text{VIII})$$

One would expect from eq VIII that the slope of a Van't Hoff plot should yield the thermodynamic value of  $\Delta H$  even in the presence of low fields while  $\Delta S$  should be weakly dependent on  $E/P$ . This is not supported by our results (Figures 4 and 5); while  $\Delta S$  may indeed vary somewhat with  $E/P$ , the magnitude of the expected change is too small to be detected reliably.  $\Delta H_e$ , however, appears to be quite sensitive to the presence of applied fields in sharp contrast to eq VIII.

Two explanations are possible. The first relies on experimental uncertainty and a systematic error in obtaining the slope of Van't Hoff plots. Linear dependence is forced upon these curves, and it may well be that the change in slope is an artifact. It is more probable that the nonadherence to eq VIII reflects the inadequacy of the assumptions underlying the derivations.

$\Delta H_e$  and  $\Delta S_e$  extrapolate smoothly to  $E/P = 0$ , where their values of  $\Delta H^\circ = -1.54 \pm 0.06$  kcal/mol and  $\Delta S^\circ = 1.7 \pm 0.3$  eu are in excellent agreement with  $\Delta H^\circ = -1.5$  kcal/mol and  $\Delta S^\circ = 1.5$  eu obtained by flowing afterglow<sup>12</sup> and ICR<sup>13</sup> techniques; at higher field strength, our equilibrium constant is also in good agreement with that reported by Kasper and Franklin.<sup>11</sup> We must conclude, however, that the evaluation of energy dependent phenomena such as equilibrium constants and rate constants and resulting derivation of heats of reaction and activation energies in high pressure sources which employ external fields in the reaction region are subject to systematic error unless the field strength approaches zero.

**Acknowledgments.** This investigation was supported in part by the United States Energy Research and Development Administration and by the D. J. Brown Fund of the University of Nebraska. We are sincerely grateful for this assistance.

## References and Notes

- (1) This paper was presented in part at the 22nd Annual Meeting on Mass Spectrometry and Allied Topics, Philadelphia, Pa., May 1974.
- (2) (a) P. Kebarle and E. W. Godbole, *J. Chem. Phys.*, **39**, 1131 (1963); (b) P. Kebarle in "Ion-Molecule Reactions", J. L. Franklin, Ed., Plenum Press, New York, N.Y., 1972, Chapter 7.
- (3) D. P. Beggs and F. H. Field, *J. Am. Chem. Soc.*, **93**, 1567, 1576 (1971).
- (4) S. L. Bennet and F. H. Field, *J. Am. Chem. Soc.*, **94**, 5186 (1972).
- (5) C. Chang, G. J. Sroka, and G. G. Meisels, *Int. J. Mass Spectrom. Ion Phys.*, **11**, 367 (1973).
- (6) C. Chang, G. G. Meisels, and J. A. Taylor, *Int. J. Mass Spectrom. Ion Phys.*, **12**, 411 (1973).
- (7) A. J. Cunningham, J. D. Payzant, and P. Kebarle, *J. Am. Chem. Soc.*, **94**, 7627 (1972).
- (8) G. G. Meisels, G. J. Sroka, and R. K. Mitchum, *J. Am. Chem. Soc.*, **96**, 5045 (1974).
- (9) G. H. Wannier, *Bell Syst. Tech. J.*, **32**, 170 (1953).
- (10) S. B. Woo and S. F. Wong, *J. Chem. Phys.*, **55**, 3531 (1971).
- (11) S. F. Kasper and J. L. Franklin, *J. Chem. Phys.*, **56**, 1156 (1972).
- (12) R. S. Hemsworth, H. W. Rundle, D. K. Bohme, H. I. Schiff, D. B. Dunkin, and F. C. Fehsenfeld, *J. Chem. Phys.*, **59**, 61 (1973).
- (13) R. H. Staley and J. L. Beauchamp, *J. Chem. Phys.*, **62**, 1998 (1975).
- (14) G. Sroka, C. Chang, and G. G. Meisels, *J. Am. Chem. Soc.*, **94**, 1052 (1972).
- (15) G. Sroka, C. Chang, and G. G. Meisels, *J. Chem. Phys.*, **55**, 5154 (1971).
- (16) C. E. Young and W. E. Falconer, *J. Chem. Phys.*, **57**, 918 (1972).
- (17) D. A. Parkes, *Trans. Faraday Soc.*, **67**, 711 (1971).
- (18) E. W. McDaniel, "Collision Phenomena in Ionized Gases", Wiley, New York, N.Y., 1964, Chapter 9.
- (19) A. Blanc, *J. Phys. Radium*, **7**, 825 (1908).
- (20) S. P. Hong and S. B. Woo, *J. Chem. Phys.*, **57**, 2593 (1972).
- (21) W. Lindinger, D. L. Albritton, C. J. Howard, F. C. Fehsenfeld, and E. E. Ferguson, *J. Chem. Phys.*, **63**, 5220 (1975).

## Thermochemistry of Alkyl Ions

Alan Goren and Burnaby Munson\*

Department of Chemistry, University of Delaware, Newark, Delaware 19711 (Received November 12, 1975)

Equilibrium experiments on hydride transfer reactions of tertiary alkyl ions and tertiary hydrocarbons have been made by high pressure mass spectrometry which give differences in hydride affinities of *tert*-butyl, *tert*-pentyl, and *tert*-hexyl ions. Good agreement is noted with previous work. The hydride affinities and heats of formation of the tertiary ions decrease with increasing molecular weight of the ions. The hydride affinities appear to approach a lower limit of 229 kcal/mol. From these data and ionization potentials of tertiary alkyl radicals, it is suggested that there is a small decrease in the dissociation energies of tertiary C-H bonds with increasing chain length. The literature data for secondary alkyl ions suggest a similar decrease toward a limit in hydride affinities of 246 kcal/mol with increasing chain length of the ions.

The thermochemistry of alkyl and other hydrocarbon ions has been studied since the early days of mass spectrometry. A group contributions method for estimating heats of formation of gaseous ions was proposed many years ago<sup>1</sup> which has been very helpful in estimating heats of formation of higher molecular weight ions for which data are not available. Accurate data for key compounds are essential for this procedure. Extensive calculations are now being made for heats

of formation of alkyl ions<sup>2</sup> and the accuracy of experimental data is not always sufficient to test these calculations.<sup>3</sup>

Recent measurements have been reported on reversible gaseous ionic reactions of tertiary alkyl ions with tertiary alkanes and thermochemical data have been obtained from the temperature coefficients of the equilibrium constants.<sup>4</sup> Few data from equilibrium measurements are available for comparison, however, and significant discrepancies have been

noted in the data for the ionic heats of reaction of cluster (or solvated) ions obtained by different workers.<sup>5</sup> A high degree of precision can be obtained for differences in heats of formation of gaseous ions from equilibrium measurements; however, it is advisable to obtain data on different instruments and by somewhat different techniques to assess the accuracy of these differences in heats of formation.

We wish to report the results of our experiments on equilibrium among hydride ions and heats of formation of gaseous tertiary alkyl ions. These results will be compared with other data and used to estimate heats of formation of other alkyl ions.

## Experimental Section

All experiments were performed on a duPont (CEC) 21-110B mass spectrometer which had been modified previously for chemical ionization studies.<sup>6</sup> Other modifications were made to allow these experiments in equilibria to be made.

The path length for the ions (the distance between the electron entrance hole and the ion exit hole) was increased to 1.5 cm. The areas of the electron entrance and ion exit holes were reduced: the electron entrance was a channel 0.07 cm in diameter  $\times$  0.15 cm, and the ion exit hole was a pinhole ( $1 \times 10^{-3}$  cm<sup>2</sup>) in 0.0025-cm stainless steel. The source connections were made more vacuum tight. A preheating zone (a coiled loop, 20 cm of 0.06-cm i.d. stainless steel tubing) was added as a connection between the glass inlet lines and the source. Separate heaters and thermocouples were used for the source and for this preheating zone. The glass inlet lines to the mass spectrometer (200 cm of 0.4-cm i.d. tubing) were heated in five separate sections, each with a separate thermocouple for temperature measurement. A grid (100 lines/in. molybdenum screen) was placed between the focus plates and the ion exit plate of the source. A bias of a few volts was maintained between this grid and the ion exit plate of the source to give reasonable ion currents. For these studies the bias voltage had no effect on the distribution of the ions. We hope, therefore, that we have greatly reduced the likelihood of collisionally induced decompositions in the region immediately outside the source of the mass spectrometer.<sup>5,6b</sup> These alkyl ions are not very susceptible to collisionally induced decompositions and the decomposition products, if any, of the higher alkyl ions will not be of the same mass as the lower alkyl ions. No evidence was noted for collisionally induced decompositions of these tertiary alkyl ions in the pure gases under our experimental conditions.

2-Methylpropane, research grade, 99.96%, was purchased from Matheson Gas Products. 2-Methylbutane, 2- and 3-methylpentane, and 2- and 3-methylhexane were all obtained from the Aldrich Chemical Co. The stated purities of the hydrocarbons decreased with increasing molecular weight, but the purities were all greater than 99%. No significant impurities were detected except for an ion of  $m/e$  101 in 2-methylhexane. This ion was not detected in the samples which had been extracted with concentrated H<sub>2</sub>SO<sub>4</sub> which were used in these experiments.

The equilibria were studied in two ways. In one set of experiments, a fixed pressure of one compound was maintained in the source by a pressure from one large volume manifold and a smaller amount of a second gas was introduced from a separate manifold. The pressures were read directly from a quartz spiral Bourdon gage which is attached to the source. In the other set of experiments, mixtures of constant composition were introduced from a single manifold at different pressures. The latter procedure gave somewhat more precise

results and was used most often, but the same results were obtained from both techniques.

The reactions were studied at pressures of 0.4–2.0 Torr and at temperatures of 90–280 °C. The temperatures are probably correct to  $\pm 5$  °C. The glass inlet lines, the preheater, and the source were maintained at the same ( $\pm 2$  °C) temperatures. About 30 min was allowed for temperature equilibration after each change. The residence time of the gas in the source itself is only of the order of a few tenths of a second, but the residence time of the gas in the entire heated zone is a few seconds.

Experimental values were calculated for the ratio,  $K = (\text{MH})I_{\text{N}^+}/(\text{NH})I_{\text{M}^+}$ , as functions of either total or partial pressures at different temperatures. The heats of reaction were determined from the slopes of the van't Hoff plots ( $\log K$  vs.  $1/T$ ) for data taken from the pressure region for which  $K$  was independent of pressure. The heats of reaction thus obtained were not sensitive functions of pressure and  $\Delta H$  was essentially independent of pressure above 1 Torr.

The experiments were performed without any repeller potential in the source, although a small ( $<4$  V) repeller potential had no effect on the apparent equilibrium constants. If we use the Langevin treatment to calculate the mobilities of hydrocarbon ions in hydrocarbon gases, and therefore the residence times of the ions in our source,<sup>7</sup> we obtain values of several hundred microseconds in our source at pressures of 1 Torr for an assumed maximum field strength of 1 V/cm. These times are longer than those reported previously by Field and co-workers<sup>4a</sup> for a continuous source because of our longer path length and smaller field strength. These ionic residence times are comparable to those reported previously for equilibrium measurements in high pressure mass spectrometers.<sup>4b,c,8</sup>

## Results and Discussion

Typical data for the pressure dependence of  $K$  are shown in Figure 1 for the 2-methylpropane/3-methylpentane system and typical data for the temperature dependence of  $K$  are shown in Figure 2 for the 2-methylpropane/2-methylbutane system.

Table I gives the reactions and derived heat of reaction data for some of the systems that were studied. The data are internally consistent since  $\Delta H(a) = \Delta H(b) - \Delta H(c)$  from Hess's law, and  $\Delta H(a) = -2.8 \pm 0.2$  kcal/mol and  $\Delta H(b) - \Delta H(c) = -2.7$  kcal/mol. Similarly  $\Delta H(a) = \Delta H(d) - \Delta H(e)$  and  $\Delta H(d) - \Delta H(e) = -2.1$  kcal/mol. The error limits in Table I are those obtained from the analysis of the data, but  $\pm 0.5$  kcal/mol would probably be a somewhat more realistic estimate.

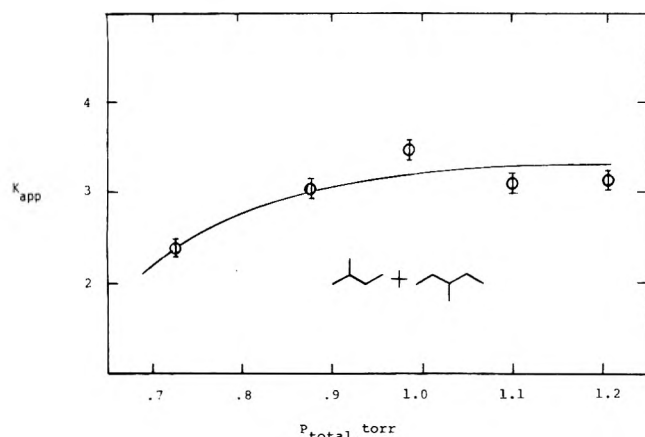
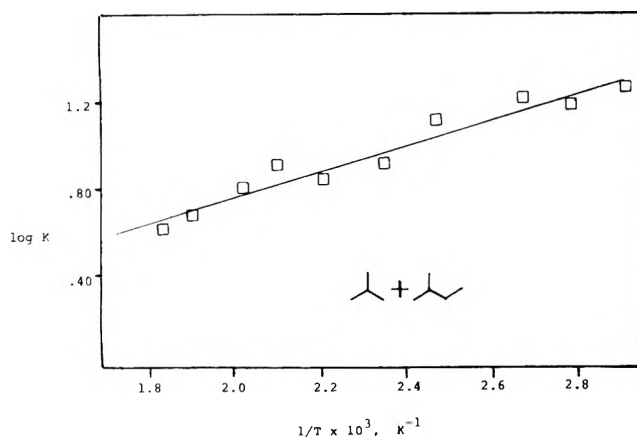
There are few data with which we can compare our numbers. For reaction a, Solomon and Field<sup>4a</sup> obtained a value of  $-3.6$  kcal/mol and Solomon, Meot-Ner, and Field<sup>4b</sup> obtained a value of  $-3.3$  kcal/mol. If one considers the present state of the art of measurement of equilibrium constants for gaseous ionic reactions, the agreement among these numbers is very good. The differences are probably within the experimental errors of the measurements. Earlier data gave  $-7 \pm 5$  kcal/mol<sup>3</sup> for the heat of this reaction.

Solomon and Field have recently reported values for the heats of reaction for (b) and (d) from their pulsed measurements as  $-3.8$  and  $-4.8$  kcal/mol.<sup>4c</sup> The agreement between their results and ours is satisfactory.

These values for the heats of reaction are the best indications of the small differences in stabilities of the ions. Based on the idea that the "stabilities" of all tertiary alkyl ions are the same, one would expect the heats of reaction of these hydride transfer reactions to be zero. That they are small and

TABLE I: Thermochemistry of Hydride Transfer Reactions

	Reaction	$\Delta H$ , kcal/mol	$\Delta S$ , gibbs/mol
a		$-2.80 \pm 0.20$	$-1.81 \pm 0.49$
b		$-4.60 \pm 0.22$	$-3.81 \pm 0.47$
c		$-1.86 \pm 0.25$	$-0.05 \pm 0.70$
d		$-3.85 \pm 0.45$	$-1.74 \pm 0.94$
e		$-1.79 \pm 0.21$	$-1.22 \pm 0.41$

Figure 1.  $K_{\text{apparent}}$  vs.  $P$ .Figure 2.  $\log K$  vs.  $1/T$  for 2-methylpropane/2-methylbutane mixture.

negative for the specified reactions indicates that there is a slight increase in "stability" with increasing molecular weight in the homologous series.

Table I also shows the entropy changes for these reactions. The values are all small. They are not internally consistent to a high degree since  $\Delta S(b) - \Delta S(c) = \Delta S(a)$ ;  $\Delta S(b) - \Delta S(c) = -3.8$  gibbs/mol and  $\Delta S(a) = -1.8$  gibbs/mol. Similarly  $\Delta S(d) - \Delta S(e) = \Delta S(a)$  and  $\Delta S(d) - \Delta S(e) = -0.5$  gibbs/mol. Solomon and Field<sup>4a</sup> reported  $-2.3$  gibbs/mol and Solomon, Meot-Ner, and Field<sup>4b</sup> reported  $-2.3$  gibbs/mol for the entropy change for reaction a. Benson<sup>9</sup> indicates that errors associated with  $\Delta S$  values obtained from van't Hoff plots are often  $\pm 2$  gibbs/mol. Consequently we feel that the entropy changes for these reactions are indistinguishable from zero.

Solomon and Field<sup>4c</sup> also consider that the entropy changes for reactions b and d are essentially zero. Entropy changes of essentially zero have been reported for a few simple proton transfer reactions.<sup>10,11</sup>

It is the expectation of these equilibrium studies that one obtain heats of formation of gaseous ions with a higher degree of accuracy than that previously observed. It is essential, however, that an accurate reference value be obtained. The obvious reference ion for these measurements is  $t\text{-C}_4\text{H}_9^+$ .

Until recently the accepted value for  $\Delta H_f(t\text{-C}_4\text{H}_9^+)$  was 176 kcal/mol,<sup>3</sup> a value which was based on  $\text{IP}(t\text{-C}_4\text{H}_9) = 171.1 \pm 1.6$  kcal/mol<sup>12</sup> and  $\Delta H_f(t\text{-C}_4\text{H}_9) = 4.5$  kcal/mol.<sup>13</sup> This value of the ionization potential of the  $t\text{-C}_4\text{H}_9$  radical has been superseded by a more recent value,  $\text{IP}(t\text{-C}_4\text{H}_9) = 159.9 \pm 1.1$  kcal/mol.<sup>14</sup> Lossing and Semeluk<sup>14</sup> used  $\Delta H_f(t\text{-C}_4\text{H}_9) = 6.8 \pm 1$  kcal/mol<sup>15</sup> to obtain  $\Delta H_f(t\text{-C}_4\text{H}_9^+) = 166.6 \pm 1.6$  kcal/mol. The value of 6.8 kcal/mol for  $\Delta H_f(t\text{-C}_4\text{H}_9)$  used by Lossing and Semeluk was based on the work of Teranishi and Benson,<sup>16</sup>  $D(t\text{-C}_4\text{H}_9\text{-H}) = 90.9$  and  $\Delta H_f(t\text{-C}_4\text{H}_9) = 6.7$  kcal/mol. These data have since been reinterpreted to give  $D(t\text{-C}_4\text{H}_9\text{-H}) = 91.8 \pm 1.2$  kcal/mol and  $\Delta H_f(t\text{-C}_4\text{H}_9) = 7.6 \pm 1.2$  kcal/mol.<sup>17</sup> The previously reported value of 166.6 kcal/mol<sup>14</sup> should be raised to  $167.4 \pm 1.6$  kcal/mol.

Lossing and Semeluk report a value of 10.56 eV for  $\text{AP}(t\text{-C}_4\text{H}_9^+, \text{neo-C}_5\text{H}_{12})$ <sup>14</sup> which is the same as a previous photoionization value for  $\text{AP}(t\text{-C}_4\text{H}_9^+, \text{neo-C}_5\text{H}_{12})$ <sup>18</sup> of  $10.55 \pm 0.005$  eV. Use of this value gives  $\Delta H_f(t\text{-C}_4\text{H}_9^+) = 169.7 \pm 1.0$  kcal/mol with  $\Delta H_f(\text{CH}_3) = 34.0 \pm 1.0$  kcal/mol.<sup>15,17</sup> Another value for  $\Delta H_f(t\text{-C}_4\text{H}_9)$  has been proposed recently,  $9.3 \pm 1.4$  kcal/mol,<sup>19</sup> and using this value and the new value for  $\text{IP}(t\text{-C}_4\text{H}_9)$ , we obtain  $\Delta H_f(t\text{-C}_4\text{H}_9^+) = 169.1 \pm 1.8$  kcal/mol, the value chosen by Solomon and Field.<sup>4c</sup>

The *tert*-butyl ion is a key compound for the determination of heats of formation of gaseous ions and it is disconcerting that there is a 2 kcal/mol spread in the reliable values. There are no obvious reasons for choosing one value over the other and the uncertainties of the values overlap each other. The average of these three values of  $\Delta H_f(t\text{-C}_4\text{H}_9^+)$  is 168.7 kcal/mol. This value is sufficiently close to that chosen by Solomon and Field<sup>4c</sup> that we will use their choice for  $\Delta H_f(t\text{-C}_4\text{H}_9^+)$  to preclude the appearance of a third value in the literature.


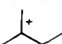
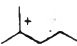
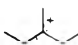
A brief consideration of eq 1 shows that the heat of reaction

$$\Delta H(298) = \Delta H(T) + \int_{298}^T \{ [C_p(i\text{-C}_5\text{H}_{12}) - C_p(i\text{-C}_4\text{H}_{10})] - [C_p(t\text{-C}_5\text{H}_{11}^+) - C_p(t\text{-C}_4\text{H}_9^+)] \} dt \quad (1)$$

should be independent of temperature. The heat capacities of the tertiary alkyl ions are not known; however, an analysis of thermochemical data for homologous compounds and the group contributions method for estimating thermochemical

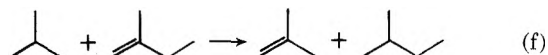


TABLE II: Heats of Formation of Tertiary Alkyl Ions

Ion	$\Delta H_f^\circ$ , kcal/mol, 298 K			NSRDS- 26 <sup>d</sup>
	This work <sup>a</sup>	FS <sup>b</sup>	L <sup>c</sup>	
	169.1 <sup>f</sup>	169.1 <sup>f</sup>	167 (169) <sup>e</sup>	176
	161.5 ± 0.5	161.1	161 (161) <sup>e</sup>	164
	155.0 ± 0.5	155.6	155 (156) <sup>e</sup>	
	156.0 ± 0.5	155.3		

<sup>a</sup> Heat of formation data for neutral compounds are taken from ref 20, which are the same as the data for these compounds given in ref 3 and were taken from the table compiled by the American Petroleum Institute, Project 44. Calculated from data of Table I. <sup>b</sup> Reference 4c. Slightly different values (±0.1 kcal/mol) were used for the heats of formation of some of the hydrocarbons, D. W. Scott, *J. Chem. Phys.*, **60**, 3144 (1974). <sup>c</sup> Reference 22. Data are obtained from IP's of tertiary radicals and assumption that  $D(t\text{-T-H}) = 92$  kcal/mol for all tertiary C-H bonds. <sup>d</sup> Reference 3. <sup>e</sup> See text. <sup>f</sup> Reference value, see text.

properties<sup>1,20,21</sup> indicates that the integrand in eq 1 should be very small. The difference in heat capacities of butane and pentane is small and should be very nearly the same as the difference in heat capacities of the butyl and pentyl ions. For a similar reaction involving neutral hydrocarbons, eq f, the



integrated heat capacity term analogous to that in eq 1 is less than 0.1 kcal/mol for  $\Delta T = 200^\circ\text{C}$ .

Table II shows the derived values for the heats of formation of *tert*-alkyl ions and comparisons with other data. The error limits are estimated values and not the standard deviations of experimental data. The value for  $t\text{-C}_5\text{H}_{11}^+$  is obtained from the direct equilibrium measurement only and does not include the indirect values obtained from combinations of (b) and (c) and (d) and (e) because of the larger experimental uncertainties associated with these differences. The values for the isomeric  $t\text{-C}_6\text{H}_{13}^+$  ions are the averages of the values obtained from  $t\text{-C}_4\text{H}_9^+$  and  $t\text{-C}_5\text{H}_{11}^+$ . The agreement among the three recent measurements in this table is very good.

The differences in heats of formation between the 2-methyl-2-butyl ion and the 2-methyl-2-propyl ion (−7.6, −8.0, and −6 kcal/mol) and the difference in heats of formation between the 2-methyl-2-pentyl ion and the 2-methyl-2-butyl ion (−6.5, −5.5, and −6 kcal/mol) represent the changes in heat of formation per methylene group in a homologous series. This methylene increment should be compared with the value of −5.0 kcal/mol for the alkanes.<sup>1,20,21</sup> Solomon and Field noted this difference previously.<sup>4a</sup> However, if one examines the data from which this value of −5.0 kcal/mol per  $\text{CH}_2$  group is obtained, it is apparent that it is true only for fairly long chains and that the increment per  $\text{CH}_2$  group only approaches −5.0 kcal/mol as the chain length increases.<sup>20</sup> Heat of formation data for homologous series of molecular ions of alcohols, aldehydes, methyl ketones, primary amines, and alkylbenzenes<sup>3</sup> show that replacement of H by  $\text{CH}_3$  (or insertion of a methylene group) decreases the heats of formation of the ions by substantially more than 5 kcal/mol when the substitution is near the presumed charge center of the ions. However, as the chain length increases, the methylene incre-

ment approaches a value of −5 kcal/mol. Although there are not enough data to justify an extrapolation, we feel that there is a trend in the present ionic data and that the methylene increment for higher homologues in this series would be −5 kcal/mol.

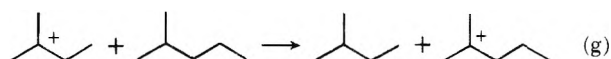
There are few data with which direct comparisons of our values can be made. However, for reaction a we can obtain the following relation:

$$\Delta H(\text{a}) = D(t\text{-C}_5\text{H}_{11}\text{-H}) - D(t\text{-C}_4\text{H}_9\text{-H}) + \text{IP}(t\text{-C}_5\text{H}_{11}) - \text{IP}(t\text{-C}_4\text{H}_9) \quad (2)$$

The difference in bond dissociation energies for two tertiary C-H bonds is generally assumed to be zero, primarily because of the absence of data. Tsang has reported, however, that  $D(t\text{-C}_5\text{H}_{11}\text{-H}) - D(t\text{-C}_4\text{H}_9\text{-H})$  is 1.3 kcal/mol.<sup>19</sup> The difference in ionization potentials may be calculated from the data of Lossing<sup>22</sup> as −1.8 kcal/mol. The calculated value of  $\Delta H(\text{a})$  from these literature data, then, is −0.5 kcal/mol (probably ±0.5 kcal/mol). This value may be compared with the experimental values of −2.8, −3.3, and −3.6 (av = −3.2) kcal/mol obtained from the ionic equilibrium measurements. It is obvious that there is an inconsistency in the data. If the experimental difference in the bond dissociation energies is correct, then consistency with the ionic equilibrium data requires that  $\text{IP}(t\text{-C}_5\text{H}_{11})$  be 0.20 eV lower than  $\text{IP}(t\text{-C}_4\text{H}_9)$  rather than the reported value of 0.06 eV.<sup>22</sup> If the bond dissociation energies of the two tertiary C-H bonds are the same, then  $\text{IP}(t\text{-C}_5\text{H}_{11})$  must be 0.14 eV lower than  $\text{IP}(t\text{-C}_4\text{H}_9)$  rather than the reported value of 0.06 eV<sup>22</sup> for consistency with the ionic equilibrium data. If the difference in ionization potentials is correct, then  $D(t\text{-C}_5\text{H}_{11})$  is 1.4 kcal/mol less than  $D(t\text{-C}_4\text{H}_9)$  rather than 1.3 kcal/mol higher, as reported.<sup>19</sup>

An examination of the available data on the effects of structural variations on ionization potentials of molecules and radicals<sup>3,22-24</sup> indicates to us that a value of 0.20 eV for the difference between ionization potentials of  $t\text{-C}_4\text{H}_9$  and  $t\text{-C}_5\text{H}_{11}$  is larger than one should expect. Since we feel that our value for  $\Delta H(\text{a})$  is correct within ±0.5 kcal/mol, we conclude that the previously reported difference in dissociation energies of tertiary C-H bonds in 2-methylpropane and 2-methylbutane is incorrect. The accuracy of the ionization potential data is not sufficient to allow us to distinguish between the other two cases.

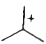
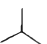
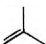
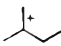
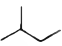
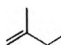
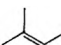
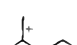
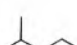
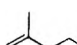
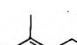
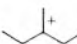

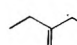
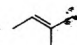
Using the average values of hydride affinities of  $t\text{-C}_5\text{H}_{11}^+$  and  $t\text{-C}_4\text{H}_9^+$  in Table III we calculate the heat of reaction of the tertiary pentyl ion with 2-methylpentane, reaction g, to



be −1.3 kcal/mol, with a probably maximum error of ±0.5 kcal/mol. If the dissociation energies of the two tertiary C-H bonds are identical, then  $\text{IP}(t\text{-C}_6\text{H}_{13})$  must be 0.06 eV lower than  $\text{IP}(t\text{-C}_5\text{H}_{11})$ , instead of 0.03 eV as reported.<sup>22</sup> If the ionization potentials are correct, then we estimate that  $D(t\text{-C}_6\text{H}_{13}\text{-H}) - D(t\text{-C}_5\text{H}_{11}\text{-H})$  is −0.6 kcal/mol.

A very reasonable extrapolation of our data suggests that the reaction of the tertiary hexyl ions with 2-methylhexane would be thermoneutral to 0.5 kcal/mol exothermic. Very recently, Field and co-workers have obtained data of heats of formation of *tert*-heptyl ions which indicate that the reaction of the 2-methylpentyl ion with 2-methylhexane is zero within an experimental error of ±0.5 kcal/mol.<sup>25</sup> With the reported value of  $-0.7 \pm 1$  kcal/mol for  $\text{IP}(t\text{-C}_7\text{H}_{15}) - \text{IP}(t\text{-C}_6\text{H}_{13})$ , we estimate that  $D(t\text{-C}_7\text{H}_{15}\text{-H}) = D(t\text{-C}_6\text{H}_{13}\text{-H})$  within the estimated error of ±0.5 kcal/mol.

TABLE III: Proton and Hydride Affinities<sup>a</sup>

MH <sup>+</sup>	$\Delta H_f$	H <sup>+</sup> A(MH <sup>+</sup> )	MH <sub>2</sub>	PA(M)		M
	169.1	234.4 (235.5) <sup>e</sup>		194.0 (192.0) <sup>e</sup>		
	161.1	231.2 <sup>b</sup> (232.3) <sup>e</sup>		197.4 (195.4) <sup>e</sup>	195.9 (193.9) <sup>e</sup>	 
	155.0	229.9 <sup>c</sup> (231.0) <sup>e</sup>		199.7 (197.7) <sup>e</sup>	197.9 (195.9) <sup>e</sup>	 
	155.7	229.9 <sup>d</sup> (231.0) <sup>e</sup>		199.2 (197.1) <sup>e</sup>	197.6 (195.4) <sup>e</sup>	 

<sup>a</sup>  $H^+A(MH^+) \equiv \Delta H_f(MH^+) + \Delta H_f(H^-) - \Delta H_f(MH_2) = D(MH^+ - H^-)$ .  $PA(M) \equiv \Delta H_f(M) + \Delta H_f(H^+) - \Delta H_f(MH^+) = D(M - H^+)$ . All numerical values in kcal/mol.  $\Delta H_f$  data for alkanes and alkenes taken from ref 20.  $\Delta H_f(H^+, 298\text{ K}) = 367.19\text{ kcal/mol}$  from, D. R. Stull and H. Prophet, (JANAF Tables) *Natl. Stand. Ref. Data Ser., Natl. Bur. Stand., No. 37* (1971). The difference between this value and the value of 365.6 kcal/mol obtained from ref 30 is the inclusion of integrated heat capacity terms, treating  $H^+$ , and  $e^-$  as monatomic gases.  $\Delta H_f(H^-, 298\text{ K}) = 33.2\text{ kcal/mol}$  from JANAF Tables. The difference between this value and the value of 34.7 kcal/mol reported elsewhere (ref 30) is the inclusion of integrated heat capacity terms treating  $H^-$  and  $e^-$  as monatomic gases. <sup>b</sup> The three reported values of  $\Delta H(a)$  are  $-3.6$ ,<sup>4a</sup>  $-3.3$ ,<sup>4b</sup> and  $-2.8\text{ kcal/mol}$ , with an average value of  $-3.2\text{ kcal/mol}$ .  $\Delta H_f$  and PA values are calculated from this  $H^+A$  value. <sup>c</sup> Our value for  $\Delta H(b)$  is  $-4.6\text{ kcal/mol}$  from the direct measurement and  $-5.1\text{ kcal/mol}$  from the indirect method of (a) + (c). These values are combined with  $-3.8\text{ kcal/mol}$ <sup>4c</sup> to give the average value of  $-4.5\text{ kcal/mol}$ .  $\Delta H_f$  and PA values are calculated from this  $H^+A$  value. <sup>d</sup> Our value for  $\Delta H(d)$  is  $-3.8\text{ kcal/mol}$  from the direct measurement and  $-5.0\text{ kcal/mol}$  from the indirect method of (a) + (e). These values are combined with  $-4.8\text{ kcal/mol}$ <sup>4c</sup> to give the average value of  $-4.5\text{ kcal/mol}$ .  $\Delta H_f$  and PA values are calculated from this  $H^+A$  value. <sup>e</sup> An alternative calculation of hydride affinity and proton affinity uses  $\Delta H_f(H^+, 0\text{ K}) = 365.24\text{ kcal/mol}$  and  $\Delta H_f(H^-, 0\text{ K}) = 34.24\text{ kcal/mol}$  with  $\Delta H_f(\text{ion}, T)$  in which  $T$  is nominally 298 K. This usage is inconsistent thermodynamically. However, it has the advantage of being conceptually similar to the definition of ionization potential in which the leaving electron is considered to have no kinetic energy. In this calculation the ion and neutral molecule are considered at a given temperature, but  $H^+$  and  $H^-$  are presumed to have no kinetic energy. These values are those in parentheses. There is yet no agreement on the definition and usage of proton and hydride affinities. Another value which has been used is  $\Delta H_f(H^+) = 366\text{ kcal/mol}$ .

The data on heats of formation of tertiary alkyl ions of Lossing which are listed in Table II are based on ionization potentials of the radicals and a constant value of 92.0 kcal/mol for the dissociation energies of all tertiary C-H bonds. If the dissociation energies of the tertiary C-H bonds vary in the manner which we have suggested, then the value of  $\Delta H_f(t\text{-C}_5\text{H}_{11}^+) = 161\text{ kcal/mol}$  must be lowered by 1.4 kcal/mol and the value of  $\Delta H_f(t\text{-C}_6\text{H}_{13}^+) = 155\text{ kcal/mol}$  must be lowered by 0.7 kcal/mol. These corrections lessen the agreement of the data obtained by the two techniques. However, if the higher values of Tsang<sup>19</sup> for  $\Delta H_f(t\text{-C}_4\text{H}_9)$  and  $D(t\text{-C}_4\text{H}_9\text{-H})$  are used, then each of Lossing's values must be raised by 1.7 kcal/mol. The results of these two corrections are the values in parentheses in Table II. The agreement between the ionic equilibrium data and the ionization potential data is excellent.

Although additional experiments by other techniques are necessary to confirm these suggestions, it appears likely to us that there are small structural effects on bond dissociation energies of tertiary C-H bonds. The same phenomena which cause the structural effects on ionization potentials of radicals and hydride affinities of ions should have an effect on dissociation energies of C-H bonds.

The hydride affinities of ions are better measures of the relative stabilities of ions than the heats of formation<sup>26</sup> since the heats of formation will decrease with increasing chain length. The heats of reaction for hydride transfer reactions are expressed as differences in the hydride affinities of the two ions

$$\Delta H(a) = H^+A(t\text{-C}_5\text{H}_{11}^+) - H^+A(t\text{-C}_4\text{H}_9^+) \quad (3)$$

Consequently, the differences in hydride affinities can be obtained directly and accurately from the experimental data. The hydride affinity of  $t\text{-C}_4\text{H}_9^+$  is obtained from the defini-

tion and the selected value  $\Delta H_f(t\text{-C}_4\text{H}_9^+) = 169.1\text{ kcal/mol}$ . The hydride affinities of the other ions are obtained by averaging the heats of reaction reported in Table I equally with those values reported previously. The heats of formation and proton affinities are then obtained from the hydride affinities. The data are summarized in Table III.


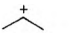
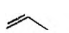
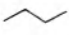
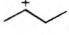
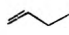
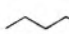
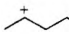


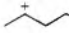

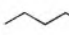
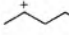

The differences in the stabilities of these tertiary alkyl ions are small and it appears that the hydride affinities of the tertiary alkyl ions are approaching a limiting value. We would estimate that the hydride affinity of tertiary heptyl ions would be about 229–230 kcal/mol and that the higher tertiary alkyl ions would have hydride affinities of about 229 kcal/mol.

Data have been reported previously which suggested that the proton affinities of a few classes of oxygenated compounds increased with increasing chain length and reached a limit after the insertion of only a few methylene groups into the chain.<sup>27</sup> The data in Table III suggest a similar trend. If the hydride affinities of the alkyl ions reach a constant value, then the proton affinities of the associated alkenes must also reach a constant value.

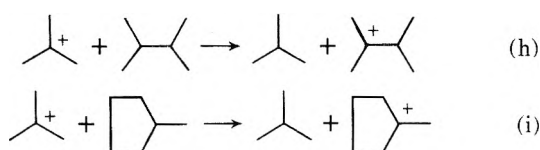
From the data of Table III, we would predict that the hydride affinities of all other tertiary aliphatic hexyl ions would be 230 kcal/mol. Additional experiments were performed on mixtures of isobutane and 2,3-dimethylbutane and on mixtures of isobutane and methylcyclopentane. The results of these experiments are not given in Table I because the apparent equilibrium constants for the hydride transfer reactions in these systems did not achieve the same constancy that was noted for the reactions listed in Table I.  $\Delta H$  was not, however, a sensitive function of pressure for these reactions.

$\Delta H$  values were obtained for the following two hydride transfer reactions:

TABLE IV: Thermochemical Data for Secondary Alkyl Ions<sup>a</sup>

H-A(MH <sup>+</sup> )	MH <sub>2</sub>	MH <sup>+</sup>	ΔH <sub>f</sub> (MH <sup>+</sup> )	M	PA(M)
250			192 <sup>c</sup>		180
246			183 <sup>c</sup>		184
247			173 ± 3 <sup>d</sup> 179 <sup>b</sup>		183
246			171 ± 2 <sup>d</sup> 173 <sup>b</sup>		184
246			162 <sup>d</sup> 168 <sup>b</sup>		184

<sup>a</sup> All data in kcal/mol. The uncertainties represent the spread among the different measurements of these values. Heat of formation data for neutral compounds are taken from ref 20. ΔH<sub>f</sub>(H<sup>+</sup>) and ΔH<sub>f</sub>(H<sup>-</sup>) are taken from JANAF Tables (see footnotes, Table III). <sup>b</sup> From ref 22. Heats of formation of the secondary radicals calculated using  $D(s-C_nH_{2n+1}-H) = 95$  kcal/mol. The values of hydride affinities in this reference are 1.5 kcal/mol higher than those in this table because of different choice in ΔH<sub>f</sub>(H<sup>-</sup>), 34.7 kcal/mol (see footnotes, Table III). <sup>c</sup> Reference 14. <sup>d</sup> Reference 3.



ΔH(h) = -5.2 ± 0.5 kcal/mol and ΔH(i) = -4.1 ± 0.8 kcal/mol. Solomon and Field have reported a value of -5.4 for ΔH(h),<sup>4c</sup> and -6.5 kcal/mol for ΔH(i).<sup>28</sup> From the data of Table III on hydride affinities of hexyl ions, the heats of reaction were predicted to be -4.5 kcal/mol. The agreement of our data with the data of Solomon and Field<sup>2</sup> is satisfactory. The agreement of the data with the simple predictions indicates that there are no major interactions which must be considered for hydrocarbons with adjacent tertiary C-H bonds and that there is no significant strain energy in the methyl cyclopentyl ion, ΔH(strain) < 1 kcal/mol.

Experiments were also done with mixtures of 2-methylpropane or 2-methylbutane and 2-methylhexane or 3-methylhexane. The experimental heats of reaction give heats of formation for these *tert*-heptyl ions of 140 kcal/mol and hydride affinities of 219 kcal/mol. Solomon and Field<sup>4c</sup> reported values of about 135 kcal/mol for some *tert*-heptyl ions. These values for the heats of formation of the *tert*-heptyl ions are 10–15 kcal/mol lower than values expected from extrapolation of the data of Table III.

Recent ionization potential measurements indicated that the heat of formation of the 2-methyl-2-hexyl ion was 150 kcal/mol and its hydride affinity was 231 kcal/mol<sup>22</sup> in good agreement with an extrapolation of the data of Table III. Very recently, however, Meot-Ner, Solomon, and Field<sup>25</sup> have reported new experiments on equilibria which involve the *tert*-heptyl ions in which they observe thermal decomposition of heptyl ions at high temperatures. Their new values for the heats of formation of *tert*-heptyl ions are about 150 kcal/mol in agreement with the ionization potential data and the trends indicated in Table III.

Because of the likelihood of isomerization of secondary alkyl ions to the more stable tertiary structures, it is unlikely that equilibrium measurements will be possible for most secondary ions. However, the trends observed for the tertiary ions should be useful for predictions of secondary and primary alkyl ions. Some thermochemical data are available from the literature for secondary ions and are summarized in Table IV for heats of formation, hydride affinities, and proton affinities.

Following Lossing and Semeluk,<sup>1c</sup> we have reassigned the structures of the alkyl ions produced by photoionization of the

*n*-alkanes as secondary rather than primary as was done previously<sup>3</sup> to obtain the data reported in Table IV. We have chosen the ionization potential measurements of Lossing and co-workers<sup>14,22</sup> as the most consistent set of data to discuss. The accuracy of the data does not warrant any attempt to distinguish among isomeric secondary ions. The heats of formation of the ions decrease in this homologous series as one would expect. There is also a small decrease in hydride affinities of the ions, and a small increase in the proton affinities of the 1-alkenes. It seems reasonable that the latter two quantities should reach limiting values and should be unaffected by subsequent increases in chain length. From these data, we suggest that the hydride affinities of the secondary pentyl and of the higher alkyl ions is 246 ± 1 kcal/mol and that the proton affinities of the 1-alkenes is 184 ± 1 kcal/mol. The proton affinities of the *cis*-2-alkenes (which may be used as models for cyclic olefins) are about 2 kcal/mol lower than the proton affinities of the 1-alkenes.

If we consider that the secondary ions are good models for the cyclohexyl ions, then from Table IV we would estimate that the hydride affinity of the cyclohexyl ion is 246 kcal/mol and therefore that ΔH<sub>f</sub>(c-C<sub>6</sub>H<sub>11</sub><sup>+</sup>) = 183 kcal/mol. One could not estimate the heat of formation of the cyclohexyl ion from the heat of formation of the secondary alkyl ions by any group contributions method because no data exist on the contribution for a ring. The available data for the heat of formation of the cyclohexyl ion are relatively old electron impact data and range from 180 to 195 kcal/mol.<sup>3</sup> The direct value for ΔH<sub>f</sub>(c-C<sub>6</sub>H<sub>11</sub><sup>+</sup>) obtained from IP(c-C<sub>6</sub>H<sub>11</sub>) = 7.66 ± 0.05 eV<sup>29</sup> and ΔH<sub>f</sub>(c-C<sub>6</sub>H<sub>11</sub>) = 13.9 kcal/mol<sup>30</sup> is 190 kcal/mol. If this experimental value is correct, then the difference between our estimated value and the experimental value, 7 kcal/mol, may be attributable to strain energy in the ion.

No significant strain energy was noted for the tertiary methylcyclopentyl ion in the hydride transfer equilibrium experiments. It is known that the *sec*-butyl ion undergoes rapid hydride abstraction reactions with cyclohexane;<sup>31</sup> consequently, the hydride affinity of the cyclohexyl ion must be less than the hydride affinity of the *sec*-butyl ion, 246 kcal/mol. CI spectra have been obtained of methylcyclohexane with isobutane; therefore, the hydride affinity of the tertiary methylcyclohexyl ion is less than the hydride affinity of the *tert*-butyl ion, 234.5 kcal/mol, and no significant strain energy exists in this ion.

Consequently, we feel that either the reported ionization potential of the cyclohexyl radical is about 0.3 eV too high or that the heat of formation of the cyclohexyl radical and the

dissociation energy of the  $c\text{-C}_6\text{H}_{11}\text{-H}$  bond are too high. An estimate of the ionization potential of the cyclohexyl radical from thermochemical considerations gave a value of  $7.2 \pm 0.1$  eV.<sup>32</sup> Lossing<sup>33</sup> has remeasured the ionization potential of the cyclohexyl radical as 7.34 eV and therefore  $\Delta H_f(c\text{-C}_6\text{H}_{11}^+) = 183$  kcal/mol, and no significant strain energy need be considered for the ion.

Equation 3 shows that the heat of reaction for hydride transfer reactions can be estimated directly from the hydride affinities of the ions involved in the reactions. Similarly, it can be shown that heats of reaction for proton transfer reactions can be estimated directly from the proton affinities of the neutral molecules. The example of cyclohexyl ions just mentioned indicates that it may frequently be easier to estimate the hydride affinities of the ions (or the proton affinities of the neutral molecules) than it is to estimate the heats of formation of the ions themselves, particularly for complex ions. In addition, heats of formation of gaseous molecules are seldom available for complex molecules.

Consider the case of the steroidal hydrocarbon, cholestane. This compound has four rings and several tertiary hydrogens. Reliable data are not available for the heat of formation of the gaseous molecule, nor are any ionization potentials available for the molecule or  $(M - H)$  radicals. One could not estimate the heat of formation of the cholestanyl ions from a group contributions method because of the absence of data for multi-ring systems. Consequently, one could not predict the thermochemistry of proton or hydride transfer reactions with any of the common chemical ionization reactant ions. However, from the data of Table III we could easily determine that the hydride affinity of the cholestanyl ion is less than the hydride affinity of  $t\text{-C}_4\text{H}_9^+$ . Hydride abstractions of  $t\text{-C}_4\text{H}_9^+$  with cholestane will be exothermic and should be rapid. One would not predict an exothermicity greater than a few kcal/mol; consequently, the product ions should be formed with little excess energy and should not decompose to any significant extent. The isobutane chemical ionization mass spectrum of cholestane has been obtained, and it consists of essentially one peak,  $(M - H)^+$ , in agreement with expectations.<sup>34</sup>

**Acknowledgments.** The authors are grateful to Dr. D. P. Ridge for helpful discussions, to Dr. F. H. Field for information prior to publication, and to Dr. F. P. Lossing for the communication of some unpublished work.

## References and Notes

- (1) (a) J. L. Franklin, *Ind. Eng. Chem.*, **41**, 1070 (1949); (b) J. L. Franklin, *J. Chem. Phys.*, **21**, 2029 (1953).
- (2) J. A. Pople, *Int. J. Mass Spectrom. Ion Phys.*, **19**, 89 (1976).
- (3) J. L. Franklin, J. G. Dillard, H. M. Rosenstock, J. T. Bero, K. Draxl, and F. H. Field, *Natl. Stand. Ref. Data Ser., Natl. Bur. Stand.*, **No. 26** (1969).
- (4) (a) J. J. Solomon and F. H. Field, *J. Am. Chem. Soc.*, **95**, 4483 (1973); (b) J. J. Solomon, M. Meot-Ner, and F. H. Field, *ibid.*, **96**, 3723 (1974); (c) J. J. Solomon and F. H. Field, *ibid.*, **97**, 2625 (1975).
- (5) See K. Hiraoka and P. Kebarle, *J. Am. Chem. Soc.*, **97**, 4179 (1975).
- (6) (a) J. A. Michnowicz, Ph.D. Thesis, University of Delaware, 1972; (b) A. Goren, B. Munson, and Y. Shimizu, *Int. J. Mass Spectrom. Ion Phys.*, **21**, 73 (1976).
- (7) W. McDaniel, "Collision Phenomena in Ionized Gases", Wiley-Interscience, New York, N.Y., 1964, Chapter 9.
- (8) J. W. Long and J. L. Franklin, *Int. J. Mass Spectrom. Ion Phys.*, **12**, 403 (1973).
- (9) S. W. Benson, "Thermochemical Kinetics", Wiley, New York, N.Y., 1968.
- (10) R. S. Hemsworth, H. W. Rundle, D. K. Bohme, H. I. Schiff, D. B. Dunkin, and F. C. Fehsenfeld, *J. Chem. Phys.*, **59**, 61 (1973).
- (11) J. P. Briggs, R. Yamdagni, and P. Kebarle, *J. Am. Chem. Soc.*, **94**, 5128 (1972).
- (12) F. P. Lossing, P. Kebarle, and J. B. DeSousa, *Adv. Mass Spectrom.*, **1**, 431 (1959).
- (13) M. Szwarc, *Discuss. Faraday Soc.*, **10**, 336 (1951).
- (14) F. P. Lossing and G. P. Semeluk, *Can. J. Chem.*, **48**, 955 (1970).
- (15) J. A. Kerr, *Chem. Rev.*, **66**, 465 (1966).
- (16) H. Teranishi and S. W. Benson, *J. Am. Chem. Soc.*, **85**, 2887 (1963).
- (17) D. M. Golden and S. W. Benson, *Chem. Rev.*, **69**, 125 (1969).
- (18) B. Steiner, C. F. Giese, and M. G. Ingraham, *J. Chem. Phys.*, **34**, 189 (1961).
- (19) W. Tsang, *J. Phys. Chem.*, **76**, 143 (1972).
- (20) D. R. Stull, E. F. Westrum, Jr., and G. C. Sinke, "The Chemical Thermodynamics of Organic Compounds", Wiley, New York, N.Y., 1969.
- (21) S. W. Benson, "Thermochemical Kinetics", Wiley, New York, N.Y., 1968.
- (22) F. P. Lossing and A. Maccoll, *Can. J. Chem.*, in press.
- (23) F. P. Lossing and J. C. Traeger, *Int. J. Mass Spectrom. Ion Phys.*, **19**, 9 (1976).
- (24) A. G. Harrison, "Mass Spectrometry of Organic Radicals", in "Mass Spectrometry of Organic Ions", F. W. McLafferty, Ed., Academic Press, New York, N.Y., 1963, p. 207.
- (25) M. Meot-Ner, J. J. Solomon, and F. H. Field, *J. Am. Chem. Soc.*, **98**, 1025 (1976).
- (26) (a) R. W. Taft, R. H. Martin, and F. W. Lampe, *J. Am. Chem. Soc.*, **87**, 2490 (1965); (b) T. B. McMahon, R. J. Blint, D. P. Ridge, and J. L. Beauchamp, *ibid.*, **94**, 8934 (1972).
- (27) J. Long and B. Munson, *J. Am. Chem. Soc.*, **95**, 2427 (1973).
- (28) J. J. Solomon and F. H. Field, Paper presented at 23rd Conference on Mass Spectrometry, Houston, Tex., May, 1975.
- (29) R. F. Pottier, A. G. Harrison, and F. P. Lossing, *J. Am. Chem. Soc.*, **83**, 3204 (1961).
- (30) K. W. Egger and A. T. Cocks, *Helv. Chim. Acta*, **56**, 1516 (1973).
- (31) P. Ausloos, S. G. Lias, and A. A. Scala, *Adv. Chem. Ser.*, **No. 58**, 264 (1966).
- (32) A. G. Harrison, C. D. Finney, and J. A. Sherck, *Org. Mass Spectrom.*, **5**, 1313 (1971).
- (33) F. P. Lossing, private communication.
- (34) J. L. Smith and W. J. A. Vanden Heuvel, *Anal. Lett.*, **5**, 51 (1972).

# The Nominal Butyl Ester Ion in the Mass Spectra of Long-Chain *n*-Alkyl Esters

Seymour Meyerson,\* E. S. Kuhn,

Research Department, Standard Oil Company (Indiana), Naperville, Illinois 60540

Imre Puskas, and E. K. Fields

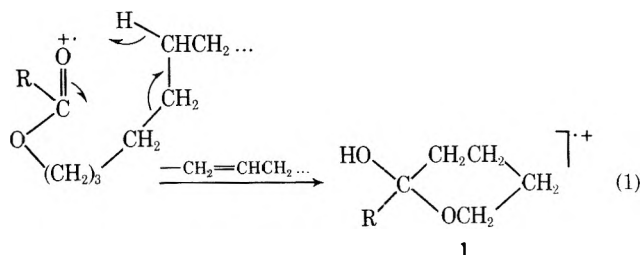
Research and Development Department, Amoco Chemicals Corporation, Naperville, Illinois 60540 (Received June 9, 1976)

Publication costs assisted by the Standard Oil Company (Indiana) and Amoco Chemicals Corporation

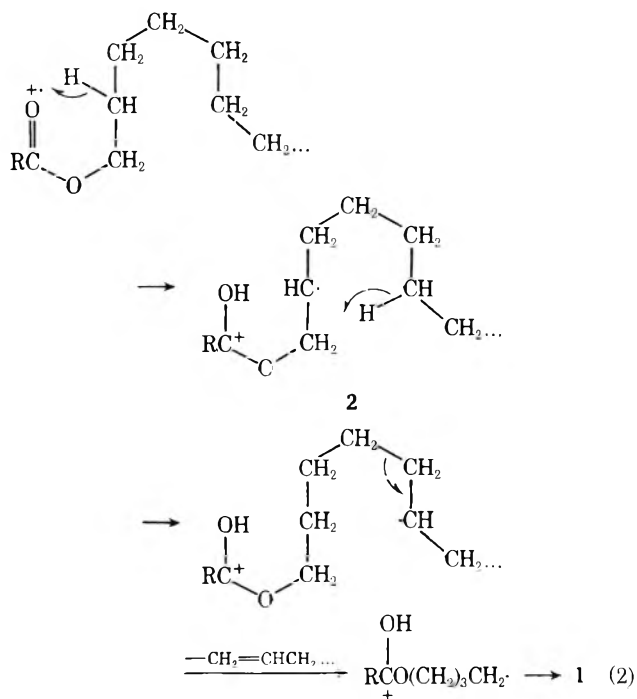
The mass spectra of *n*-alkyl carboxylates in which the alkyl group contains seven or more carbons show a characteristic peak at the mass of the molecular ion of the corresponding butyl ester. Intensity is generally low, of the order of a few hundredths to a few tenths percent of total ion intensity. However, it is comparatively free of interferences and substantially more intense than peaks corresponding to higher and lower homologues. Hence it is a useful feature for qualitative identification. We have explored the origins of this peak in the spectrum of *n*-octadecyl benzoate, employing deuterium labeling, precise-mass measurement, and metastable scanning. The greater part of the intensity appears to arise by a reaction sequence initiated by the familiar  $\gamma$ -hydrogen migration to the carbonyl oxygen, followed by a second hydrogen migration from C-6 to C-2,  $\beta$  cleavage of the bond between C-4 and C-5, and stabilization by a third hydrogen migration probably from C-3 to the carbonyl oxygen. Some 20% of the observed intensity apparently stems from one of a family of reactions giving rise to a homologous series of  $(M^+ - C_k H_{2k})$  fragments via nonspecific hydrogen abstraction and  $\beta$  carbon-carbon bond cleavage.

Ryhae and Stenhagen called attention a number of years ago to a low-intensity but characteristic feature of the mass spectra of long-chain *n*-alkyl esters of carboxylic acids—a peak at the mass ( $M/z$ ,  $z = 1$ ) of the molecular ion of the corresponding butyl ester.<sup>1</sup> They observed such a peak in the spectra of docosyl formate, acetate, propanoate, butanoate, and heptanoate at masses 102, 116, 130, 144, and 186, respectively. Intensity at these masses ranged from 0.1 to 0.4% of total ion intensity, greater by factors of 2 to 10 than at masses corresponding to higher and lower homologues of this ion. More recently, in a study of long-range intramolecular interactions,<sup>2</sup> we noted the corresponding peaks in the mass spectra of several long-chain *n*-alkyl esters of aromatic acids. Thus, benzoates, trimellitic anhydride esters, trimellitimidates, *n*-alkylmethyl iso- and terephthalates, and 4-*n*-alkyl 1,2-dimethyl trimellitates show the peak at masses 178, 248, 247, 236, and 294, respectively. Our own files of reference spectra and a literature search<sup>3</sup> revealed further examples and demonstrated that the peak is characteristic of *n*-alkyl esters in which the alkyl group contains seven or more carbons. Although intensity is generally only a few hundredths to a few tenths percent of total ion intensity, the absence of interferences and, except in special cases,<sup>2</sup> the much lower intensity of homologous ions make this feature easy to detect and useful for qualitative identification.

Hydrogen migration from C-6 to the carbonyl oxygen, rupture of the bond between C-4 and C-5, and formation of a new bond between C-4 and the carbonyl carbon to give 1 (path 1) have been suggested to account for this peak.<sup>1</sup> How-



ever, the implied ten-membered cyclic transition state offers no obvious driving force for so specific a process. The same overall effect might, alternatively, be rationalized in terms of initiation by the ubiquitous  $\gamma$ -hydrogen migration to the carbonyl oxygen,<sup>4-6</sup> followed by hydrogen migration from C-6 to C-2, as in 2,  $\beta$  cleavage with respect to the radical center on C-6 and, presumably, some further step such as ring closure to 1 to yield a configuration that is better stabilized than a primary free radical (path 2). The intermediate hydrogen

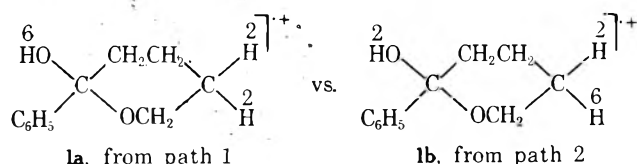


migration involves a six-membered cyclic transition state, and resembles the series of 1,5 migrations that have been proposed to account for the 4-carbon periodicity of intensity maxima

in the  $\text{CH}_3\text{OCO}(\text{CH}_2)_m^+$  peak series in the spectra of long-chain methyl *n*-alkanoates.<sup>7</sup>

Our spectrum of *n*-octadecyl-6,7-*d*<sub>2</sub> benzoate<sup>2b</sup> (isotopic composition: 7% *d*<sub>0</sub>, 18% *d*<sub>1</sub>, 63% *d*<sub>2</sub>, 6% *d*<sub>3</sub>, 4% *d*<sub>4</sub>, 1% *d*<sub>5</sub>, 1% *d*<sub>6</sub>; see Experimental Section) shows retention of one deuterium atom in about 32% of the nominal butyl benzoate ions; the spectra of *n*-octadecyl-9,10-*d*<sub>2</sub> and -9,10,12,13-*d*<sub>4</sub> benzoates show no retention in these ions. These data are in accord with retention of one hydrogen from C-6, as required by either of the postulated reaction paths. A substantial fraction of the fragment ions of mass 14 u greater, presumably the next higher homologue, also retains one deuterium atom in the spectrum of the 6,7-*d*<sub>2</sub> benzoate but not in those of the 9,10-*d*<sub>2</sub> and 9,10,12,13-*d*<sub>4</sub> benzoates. We infer that the label retained in this case comes most likely from C-7; we have not, however, pursued the question.

Better to define the chemistry involved and, in particular, to distinguish between the two suggested paths leading to the nominal butyl benzoate ion, we have prepared *n*-octadecyl-2,2-*d*<sub>2</sub> benzoate and studied the behavior of this compound under electron impact in conjunction with that of the unlabeled and the 6,7-*d*<sub>2</sub> analogues. Either path 1 or path 2 should yield a product  $\text{C}_{11}\text{H}_{14}\text{O}_2^+$  containing one hydrogen atom originally from C-6 and both atoms originally from C-2, but in differing positions:



We postulated that 1 might break down further by losing  $\text{H}_2\text{O}$  and that cyclohexanol might serve as a model for the mechanism of the dehydration step. The spectrum shows a peak at the appropriate mass, 160, although it is lower in intensity by a factor of about 10 than the  $\text{C}_{11}\text{H}_{14}\text{O}_2^+$  peak at 178. Elimination from cyclohexanol under electron impact has been studied extensively.<sup>8</sup> The preferred process there is 1,4 elimination, which accounts for some 40% of total  $\text{H}_2\text{O}$  loss; 1,3 elimination accounts for most of the remainder. Thus, one might anticipate that structure 1a containing a deuterium atom from C-6 should lose the label almost quantitatively in eliminating water; the same species containing two deuterium atoms from C-2 should lose one of the two in some 40% of the reacting ions. Structure 1b containing a label from C-6 should lose it in perhaps 20% of the reacting ions; the same species containing two deuterium atoms from C-2 should lose one of them almost quantitatively and both in 20% of the reacting ions.

We used precise-mass measurement, at a resolution of 10 000 (10% valley definition), to confirm the elemental compositions of ions under study and to distinguish among isobaric species containing zero, one, and two oxygen atoms. Quantitative separation of isobaric ions containing the same number of oxygen atoms and differing in elemental composition only by virtue of isotopic content— $2\text{H}$  vs.  $\text{D}$  (0.0015 u),  $^{12}\text{CD}$  vs.  $^{13}\text{CH}$  (0.0029 u),  $^{12}\text{CH}$  vs.  $^{13}\text{C}$  (0.0045 u)—would require resolution beyond the capability of our instrument. We therefore measured peak intensities for isotopic analysis of fragment ions of interest also at a resolution of 10 000 and made the necessary corrections for natural heavy-isotopic species with the help of standard abundance tables<sup>9</sup> as in low-resolution work. Parent-daughter relationships as revealed by decomposition of metastable ions in the first field-

free region of a double-focusing instrument were determined by the usual procedure of focusing on a fragment-ion peak, then holding the magnetic field and the electric-sector voltage constant and scanning the ion-accelerating voltage to increasing values ("metastable scanning").<sup>10</sup> In the spectra obtained when sample was introduced via the heated batch inlet system,<sup>2</sup> intensities of the peaks with which we were concerned were generally too low to yield the information now sought. These intensities were increased by probe injection of the sample directly into the source and by increasing amplification of the multiplier output by 10× or 100× via a Keithley Model 427 current amplifier, replacing the amplifier furnished as original equipment. The probe was not heated directly but was in thermal contact with the source. To make each series of measurements, source temperature was set initially at 180 °C and was increased in small increments as needed to maintain an approximately constant ion-beam current; at about 220 °C, the beam current dropped suddenly to a very low value, signaling depletion of the sample.

These procedures magnified the peaks of interest to a useful level. At the same time, however, they also magnified a great many additional peaks that were so weak as to be easily ignored in the spectra as measured in our earlier work.<sup>2</sup> In particular, the  $\text{C}_{11}\text{H}_{14}\text{O}_2^+$  and  $\text{C}_{11}\text{H}_{12}\text{O}^+$  peaks at respective masses 178 and 160 in the spectrum of the unlabeled ester were now clearly seen to be accompanied by peaks at adjacent masses, assuring interferences in the spectra of the labeled esters, and at masses corresponding to higher and lower homologues of  $\text{C}_{11}\text{H}_{14}\text{O}_2^+$ , revealing as an illusion, at least in part, the unique role we had attributed initially to this ion in the spectrum.

## Results and Discussion

Precise-mass measurement at masses 178 and 160 in the spectrum of unlabeled *n*-octadecyl benzoate confirmed the expected elemental compositions, as shown in Table I. Metastable scanning, as described above, of the ions of masses 160 and 178 identified the respective precursor masses as 178 and 374, as postulated. Thus the reaction sequence is established as:

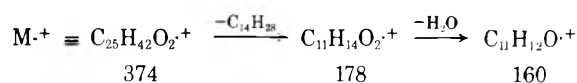


Table II displays the results of a typical scan through the regions around masses 178 and 160 in the spectrum of unlabeled *n*-octadecyl benzoate under conditions that cleanly separate the components containing zero, one, and two oxygen atoms at each nominal mass. All but 0.4% of total intensity at mass 178 and 100.0% of that at 160 are attributable to the components of interest, the ions containing two and one oxygen atoms, respectively. The  $\text{C}_{11}\text{H}_{14}\text{O}_2^+$  ion at 178 is accompanied by  $\text{C}_{11}\text{H}_{13}\text{O}_2^+$  at 177; the intensities attributable to dioxy ions at 179 and 180 are almost entirely accounted for by naturally occurring heavy-isotopic species. The  $\text{C}_{11}\text{H}_{12}\text{O}^+$  ion at 160 is accompanied by other monoxy ions at 159, 161, and 162.

The peak intensities assigned to dioxy species in the immediate vicinity of mass 178, as shown in Table II, were corrected for natural heavy-isotopic contributions and normalized to a total intensity of 100 for these peaks alone; those assigned to monoxy species in the vicinity of mass 160 were treated likewise. The resulting intensity distributions are shown in Table III, along with the corresponding distributions



**TABLE I: Precise-Mass Measurements at Masses 178 and 160 in Mass Spectrum of *n*-Octadecyl Benzoate**

Measured mass	Assignment		Discrepancy, ppm
	Formula	Mass	
178.0985	C <sub>11</sub> H <sub>14</sub> O <sub>2</sub> <sup>+</sup>	178.0994	5
160.0891	C <sub>11</sub> H <sub>12</sub> O <sup>+</sup>	160.0838	2

**TABLE II: Peak Intensities<sup>a</sup> in the Regions Around Masses 178 and 160 in Mass Spectrum of *n*-Octadecyl Benzoate**

Nominal Mass	No. of oxygen atoms		
	0	1	2
182	1320	0	2
181	900	0	4
180	500	0	20
179	26	0	172
178	6	0	1360
177	12	6	132
166	800	0	2
165	60	0	26
164	10	0	194
163	8	8	1030
162	2	36	14
161	10	36	6
160	0	216	0
159	12	38	0

<sup>a</sup> Expressed in mm as measured on analog record.**TABLE III: Normalized<sup>a</sup> Isotope-Corrected Intensity Distributions in Selected Regions<sup>b</sup> of Mass Spectra of *n*-Octadecyl Benzoates**

Mass	Unlabeled	2,2- <i>d</i> <sub>2</sub>	6,7- <i>d</i> <sub>2</sub>
180		54	
179		37	28
178	91	8	65
177	9	1	7
163		1	
162	11	25	11
161	3	50	21
160	73	19	55
159	13	5	13

<sup>a</sup> Normalized to a total of 100 in each of the two mass regions independently. <sup>b</sup> Only dioxy ions are included in the 177-to-180 mass region, and only monooxy ions in the 159-to-163 mass region.

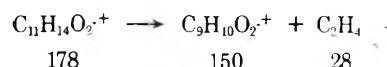
derived from the spectra of the two labeled *n*-octadecyl benzoates.

As an aid to estimate and thereby to correct for interferences, we performed metastable scans on the peak at mass 177 and on those at 159, 161, and 162 in the spectrum of the unlabeled benzoate. The scan of the mass 177 peak showed one intense metastable peak, corresponding to the molecular ion, mass 374, as precursor. The ion of mass 159 was found to stem from precursors of masses 177, 374, and 356 ( $M^+ - H_2O$ ); 161, from 179 (presumably denoting loss of  $H_2O$  from the heavy-isotopic analogue of C<sub>11</sub>H<sub>14</sub>O<sub>2</sub><sup>+</sup>); and 162, from 180, 192, and 374. Precise-mass measurement on the peaks at 192, 164, 150, and 136 identified the respective ions as C<sub>12</sub>H<sub>16</sub>O<sub>2</sub><sup>+</sup>, C<sub>10</sub>H<sub>12</sub>O<sub>2</sub><sup>+</sup>, C<sub>9</sub>H<sub>10</sub>O<sub>2</sub><sup>+</sup>, and C<sub>8</sub>H<sub>8</sub>O<sub>2</sub><sup>+</sup>, homologues of

**TABLE IV: C<sub>11</sub>H<sub>14</sub>O<sub>2</sub><sup>+</sup>, C<sub>11</sub>H<sub>13</sub>O<sub>2</sub><sup>+</sup>, and Their Homologues in the Mass Spectrum of *n*-Octadecyl Benzoate**

Mass	Ion	Rel intensity
206	C <sub>13</sub> H <sub>18</sub> O <sub>2</sub> <sup>+</sup>	0.011
192	C <sub>12</sub> H <sub>16</sub> O <sub>2</sub> <sup>+</sup>	0.082
178	C <sub>11</sub> H <sub>14</sub> O <sub>2</sub> <sup>+</sup>	0.47
164	C <sub>10</sub> H <sub>12</sub> O <sub>2</sub> <sup>+</sup>	0.034
150	C <sub>9</sub> H <sub>10</sub> O <sub>2</sub> <sup>+</sup>	0.11
136	C <sub>8</sub> H <sub>8</sub> O <sub>2</sub> <sup>+</sup>	0.056
122	C <sub>7</sub> H <sub>6</sub> O <sub>2</sub> <sup>+</sup>	5.31
205	C <sub>13</sub> H <sub>17</sub> O <sub>2</sub> <sup>+</sup>	0.005
191	C <sub>12</sub> H <sub>15</sub> O <sub>2</sub> <sup>+</sup>	0.033
177	C <sub>11</sub> H <sub>13</sub> O <sub>2</sub> <sup>+</sup>	0.039
163	C <sub>10</sub> H <sub>11</sub> O <sub>2</sub> <sup>+</sup>	0.30
149	C <sub>9</sub> H <sub>9</sub> O <sub>2</sub> <sup>+</sup>	0.093
135	C <sub>8</sub> H <sub>7</sub> O <sub>2</sub> <sup>+</sup>	0.30
123	C <sub>7</sub> H <sub>7</sub> O <sub>2</sub> <sup>+</sup>	100.0

C<sub>11</sub>H<sub>14</sub>O<sub>2</sub><sup>+</sup> at 178. Similar measurements identified the major or sole components at 191, 177, 163, 149, and 135 as C<sub>12</sub>H<sub>15</sub>O<sub>2</sub><sup>+</sup>, C<sub>11</sub>H<sub>13</sub>O<sub>2</sub><sup>+</sup>, C<sub>10</sub>H<sub>11</sub>O<sub>2</sub><sup>+</sup>, C<sub>9</sub>H<sub>9</sub>O<sub>2</sub><sup>+</sup>, and C<sub>8</sub>H<sub>7</sub>O<sub>2</sub><sup>+</sup>, respectively. Returning to metastable scanning of homologues of C<sub>11</sub>H<sub>14</sub>O<sub>2</sub><sup>+</sup> and C<sub>11</sub>H<sub>13</sub>O<sub>2</sub><sup>+</sup>, we arrived at the molecular ion as the common precursor of all the members examined of both series: the ions of masses 206, 192, 164, 150, 136, and 122; and 205, 191, 163, 149, and 135. The only other metastable peak of substantial intensity so found corresponds to the process:



Weaker metastable peaks pinpointed 163, 177, and 191 as the masses of additional precursors of the ion of mass 135. Our failure to detect contributing reactions of C<sub>11</sub>H<sub>14</sub>O<sub>2</sub><sup>+</sup> homologues may reflect simply their lower abundances than that of C<sub>11</sub>H<sub>14</sub>O<sub>2</sub><sup>+</sup> in the total ion population. Thus, C<sub>11</sub>H<sub>14</sub>O<sub>2</sub><sup>+</sup> was now clearly seen to be only one member, although the most abundant one except for the benzoic acid radical cation of mass 122, of a homologous series of ions arising predominantly by loss of olefin molecules from the molecular ion of *n*-octadecyl benzoate. Similarly, C<sub>11</sub>H<sub>13</sub>O<sub>2</sub><sup>+</sup> of mass 177 was seen to be a member of a second homologous series arising predominantly by loss of alkyl radicals from the molecular ion. Peak intensities corresponding to these two homologous series of ions, corrected for naturally occurring heavy-isotopic species, are shown in Table IV. The intensity scale here is defined by assigning a value of 100.0 to the intensity of C<sub>7</sub>H<sub>7</sub>O<sub>2</sub><sup>+</sup>, the most abundant ion in the spectrum of *n*-octadecyl benzoate.

With the help of one further piece of data, the isotopic composition of the *n*-octadecyl-2,2-*d*<sub>2</sub> ester—9% *d*<sub>0</sub>, 36% *d*<sub>1</sub>, and 55% *d*<sub>2</sub> (see Experimental Section)—we could now proceed to estimate the isotopic composition of the C<sub>11</sub>H<sub>14</sub>O<sub>2</sub><sup>+</sup> and C<sub>11</sub>H<sub>12</sub>O<sup>+</sup> ions.

If the original tagged atoms in the 2,2-*d*<sub>2</sub> ester are retained quantitatively in C<sub>11</sub>H<sub>13</sub>O<sub>2</sub><sup>+</sup> and no isotope effects intervene, the 9 intensity units assigned to this ion—as shown in Table III at mass 177 in the spectrum of the unlabeled ester—will be distributed in the spectrum of the 2,2-*d*<sub>2</sub> ester as 5 units at 179, 3 at 178, and 1 at 177. Removing these contributions from the intensities listed for the 2,2-*d*<sub>2</sub> ester and renormalizing gives for the isotopic distribution of C<sub>11</sub>H<sub>14</sub>O<sub>2</sub><sup>+</sup>:

Mass	No. of D atoms	%
180	2	59
179	1	35
178	0	6

This distribution agrees well with that of the molecular ions and hence indicates quantitative retention of the hydrogen atoms on C-2. Moreover, such internal consistency supports the assumption of quantitative retention of the original C-2 hydrogens in  $C_{11}H_{13}O_2^+$ . Taking the mass 177 intensity of the 6,7- $d_2$  ester at face value and ignoring possible isotope effects, we conclude that 7 units of the  $C_{11}H_{13}O_2^+$  ions are unlabeled and assume arbitrarily that the remaining 2 units are singly labeled. Removing these contributions from the intensities listed for the 6,7- $d_2$  species and renormalizing yields for the isotopic distribution of  $C_{11}H_{14}O_2^+$ :

Mass	No. of D atoms	%
179	1	31
178	0	69

This distribution agrees with the estimate of 32% deuterium retention arrived at earlier without benefit of high-resolution measurements. Within the limitations imposed by the presence of isotopic impurities in the 6,7- $d_2$  ester and of a possible small isotope effect, in view of the implied competition between migration of deuterium and protium atoms from C-6, the distribution found is in good accord with the expectation that one hydrogen atom from C-6 is retained in  $C_{11}H_{14}O_2^+$ , as required by either reaction path 1 or 2.

The 159-to-163 mass region involves greater uncertainties. In the spectrum of the 2,2- $d_2$  ester, the 5 units at 159 are clearly attributable to  $C_{11}H_{11}O^+$ , 1 unit at 163 to  $C_{11}H_{13}DO^+$ , 10 units at 162 to  $C_{11}H_{14}O^+$ . We arbitrarily assign 3 units at 161 to  $C_{11}H_{13}O^+$ . In view of the parallel origins of  $C_{11}H_{11}O^+$  and  $C_{11}H_{12}O^+$  by loss of  $H_2O$  from  $C_{11}H_{13}O_2^+$  and  $C_{11}H_{14}O_2^+$ , respectively, we assume that the ratio of singly to doubly labeled  $C_{11}H_{11}O^+$  at 160 and 161, respectively, is identical with the corresponding ratio of  $C_{11}H_{12}O^+$  species at 161 and 162. Calculation of the isotopic distribution of  $C_{11}H_{12}O^+$  ions is then straightforward. In the spectrum of the 6,7- $d_2$  ester,  $C_{11}H_{11}O^+$ ,  $C_{11}H_{13}O^+$ , and  $C_{11}H_{14}O^+$  are evidently free of deuterium, and the residual intensities at 160 and 161 define the isotopic distribution of  $C_{11}H_{12}O^+$  ions. The distributions that result are:

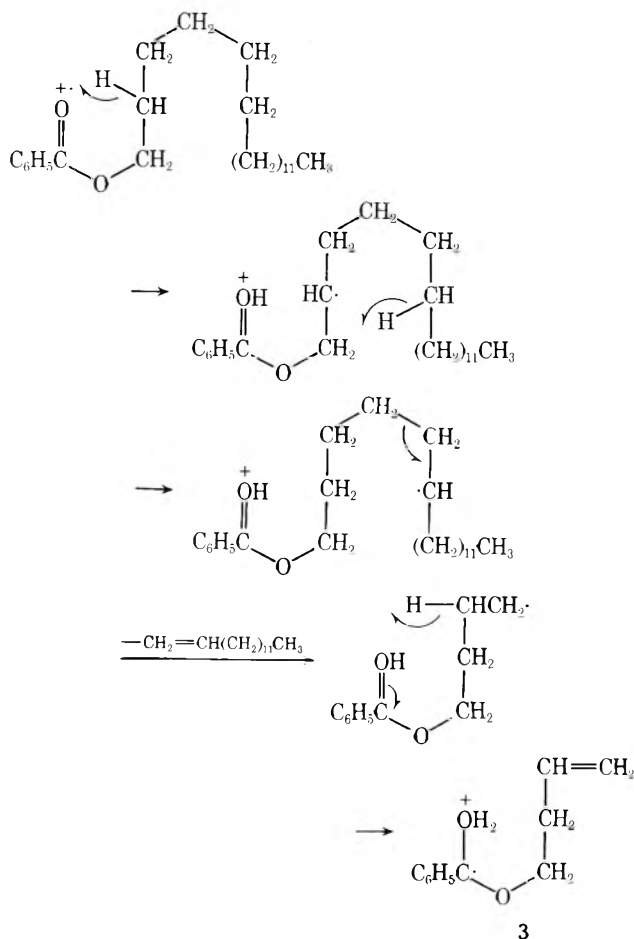
	2,2- $d_2$ ester	6,7- $d_2$ ester
$d_2$	20	
$d_1$	62	25
$d_0$	18	75

If one assumes that  $C_{11}H_{12}O^+$  arises solely by dehydration of  $C_{11}H_{14}O_2^+$  and that isotope effects are negligible, these isotopic distributions in conjunction with those of the corresponding  $C_{11}H_{14}O_2^+$  ions lead to the following conclusions: (a) the hydrogen atom originally from C-6 is lost as part of the  $H_2O$  molecule in  $(31 - 25)/31 = 19\%$  of the reacting ions; (b) one hydrogen atom originally from C-2 is lost similarly in  $(59 - 20)/59 = 66\% \approx 2(35 - [62 - 39])/35 = 69\%$  of the reacting ions; (c) in none of the reacting ions are both C-2 hydrogen atoms lost.

These conclusions are compatible with neither of the two

suggested reaction paths as written. The small fraction of C-6 hydrogen lost as part of the water molecule rules out a major contribution from path 1. Our failure to find evidence for any appreciable loss of both C-2 hydrogens would seem to rule out structure 1 as an intermediate. If one assumes that hydrogen atoms from C-2 and C-6 are in no case lost together, the data can furnish a basis for a plausible rationale. One of the three hydrogens is incorporated in the water molecule lost from 85 to 88% of reacting  $C_{11}H_{14}O_2^+$  ions, close enough to 100% that we can take this as an acceptable material balance within the uncertainties associated with unknown, but most likely small,<sup>11</sup> isotope effects and the approximations made in estimating isotopic distributions. The data can then be accounted for by assuming that both paths 1 and 2, modified to omit ring closure to 1, contribute, with the second water hydrogen coming from another position, most likely C-3, whence hydrogen migration might be assisted by  $\beta$  activation by the radical center on C-4.

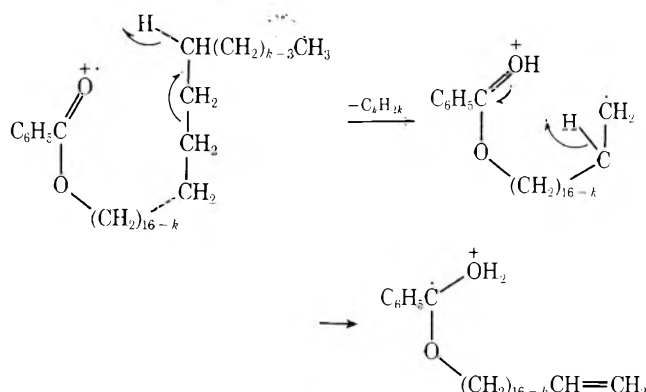
We thus conclude that the 70–80% of reacting  $C_{11}H_{14}O_2^+$  ions that lose C-2 hydrogen most likely arise by path 2, but with stabilization of the intermediate primary radical via a third hydrogen migration step:



Insofar as one can judge from the product of subsequent dehydration, this appears to be the specific process chiefly responsible for the nominal butyl ester ion that prompted this inquiry. Our data do not, of course, rule out possible contributions from structures isomeric to 3 that do not break down further by loss of water. The minimum chain-length requirement of seven carbons follows directly from the central role of hydrogen migration from C-6. Many systems are known in which otherwise nonspecific migration drops sharply in

probability or even vanishes at the terminal carbon.<sup>2,5,12-14</sup> The source of this effect is presumably the difference between the dissociation energies of primary and secondary carbon-hydrogen bonds,<sup>15</sup> which would make the second migration step in path 2 endothermic by some 2–3 kcal/mol in a hexyl ester, whereas it is approximately thermoneutral in a heptyl or longer ester.

The ~20% of reacting  $C_{11}H_{14}O_2^{+}$  ions that lose C-6 hydrogen most probably arise by hydrogen migration directly from C-6 to the carbonyl oxygen, as in path 1, also modified to incorporate stabilization via 3. This contribution to the  $C_{11}H_{14}O_2^{+}$  yield is presumably the counterpart of the observed higher and lower homologues arising by a sequence of nonspecific hydrogen abstraction and  $\beta$  carbon-carbon bond cleavage, with stabilization via a second hydrogen migration step:



Such a sequence requires retention of a hydrogen atom from C-7 in  $C_{12}H_{16}O_2^{+}$ , the next higher homologue of  $C_{11}H_{14}O_2^{+}$ , and is therefore supported by our observation that a substantial part of the  $C_{12}H_{16}O_2^{+}$  yield from *n*-octadecyl-6,7- $d_2$  benzoate contains deuterium. As we suggested in another similar system,<sup>2</sup>  $\beta$  cleavage on the far side of the radical site would effect loss of an alkyl radical, and may well be the source of the observed  $C_{11}H_{13}O_2^{+}$  and its homologues. The relatively high abundance of  $C_{10}H_{11}O_2^{+}$  in this series, as seen in Table IV, is then readily accounted for, because it is the product of the reaction sequence initiated by abstraction from C-2, the most favored position. Low-yield reactions involving such intramolecular nonspecific abstraction from an alkyl chain have been reported as contributors to the mass spectra of aldehydes,<sup>5b,12</sup> ketones,<sup>16</sup> acids,<sup>17</sup> nitriles,<sup>18</sup> and ethers,<sup>19</sup> as well as esters.<sup>2,13,14</sup>

The nominal butyl ester ion—at least the bulk of those ions that react further by  $H_2O$  loss before departing the ion source and hence contribute to the normal  $C_{11}H_{12}O^{+}$  peak in the mass spectrum—appears to comprise a new member of the growing family of products of reaction sequences initiated by  $\gamma$ -hydrogen abstraction by a carbonyl oxygen atom.<sup>4-6,20</sup> Cyclization apparently plays an important part in stabilization of fragment ions in some systems,<sup>21</sup> but it seems to be less frequently preferred by the reacting molecules than by authors trying to rationalize molecular behavior.

## Experimental Section

Mass spectra were measured initially on a DuPont Model 21-104 instrument, using electrical scanning, with the inlet system at 250–280° and the source at 250°. All subsequent measurements, as described above, were made on a CEC Model 21-110b instrument, using probe injection in most cases.

*n*-Octadecyl Benzoates. Preparation of *n*-octadecyl- $d_0$  and

6,7- $d_2$  benzoates has been reported.<sup>2b</sup> The isotopic analysis of the latter<sup>2b</sup> was derived from measurements on the  $C_{18}H_{36}^{+}$  peaks rather than  $M^{+}$ , because the  $C_{18}H_{36}^{+}$  data agreed well with those on the  $M^{+}$  peaks of the stearic acid-6,7- $d_2$  from which the ester had been made and with those on both the  $M^{+}$  and  $C_{18}H_{36}^{+}$  peaks of 4-*n*-octadecyl-6,7- $d_2$  trimellitate anhydride made from the same stearic acid. An estimate of the isotopic distribution based on the  $M^{+}$  peaks of the labeled benzoate was apparently slightly distorted by contributions from protonated ester arising from a bimolecular process.<sup>22</sup>

To prepare *n*-octadecyl-2,2- $d_2$  benzoate, commercial USP grade stearic acid was labeled in the  $\alpha$  position by heating for 2 days with 98%  $D_2SO_4$  in a sealed tube at 105–110 °C,<sup>23</sup> and this procedure was then repeated three times. The extent of exchange was monitored by recovering the stearic acid after each treatment and measuring its isotopic composition by mass spectrometry; the fourth treatment had no detectable effect on isotopic composition. Finally, the recovered stearic acid was recrystallized twice from ethanol to remove palmitic and eicosanoic acid impurities. The product melted at 69 °C (lit. mp,<sup>24</sup> unlabeled stearic acid, 70 °C). The  $M^{+}$  peaks in the 70-eV mass spectrum gave the isotopic distribution: 9%  $d_0$ , 36%  $d_1$ , 55%  $d_2$ . The labeled stearic acid (1.33 g) was added to a stirred refluxing mixture of 0.88 g of lithium aluminum hydride and freshly purified tetrahydrofuran. Refluxing was continued for 10 min, after which the heat was turned off and the mixture stirred for an additional hour. The excess lithium aluminum hydride was decomposed by cautious addition of methanol, followed by aqueous methanol. Solvents were removed by vacuum distillation, and the residue was extracted repeatedly with ether. Removal of the ether from the extract left a solid which was recrystallized from methanol to give octadecanol-2,2- $d_2$ , mp 57 °C (lit. mp,<sup>25</sup> unlabeled octadecanol, 58 °C). Equimolar quantities of the labeled octadecanol and benzoyl chloride were dissolved in anhydrous pyridine-benzene mixture and stirred at room temperature for 1 h. The solvent and the volatile pyridine hydrochloride were removed at 0.5 Torr by increasing the temperature to 210 °C, leaving the crude ester as a residue. This was recrystallized from methanol-chloroform to give *n*-octadecyl-2,2- $d_2$  benzoate, mp 42–44 °C (lit. mp,<sup>2b</sup> unlabeled *n*-octadecyl benzoate, 42.5–44.0 °C). Isotopic composition estimated from the peaks in the molecular-ion region of the 70-eV spectrum showed slightly higher enrichment than that found for the stearic acid-2,2- $d_2$ . In our experience, protonated molecules stemming from bimolecular processes occur commonly in the spectra of long-chain alkyl esters,<sup>22</sup> and we found clear evidence for such species in the spectra of both the unlabeled and 6,7- $d_2$  octadecyl benzoates. We therefore took the isotopic composition found for the stearic acid-2,2- $d_2$  as our best estimate for the octadecyl-2,2- $d_2$  benzoate as well. Substantial loss of label in the reaction leading to  $C_{18}H_{36}^{+}$  ruled out measurements on this ion for isotopic analysis of the octadecyl-2,2- $d_2$  ester, in contrast to the corresponding 6,7- $d_2$ , 9,10- $d_2$  and 9,10,12,13- $d_4$  esters.<sup>2b</sup>

## References and Notes

- (1) R. Ryhage and E. Stenhagen, *Ark. Kem.*, **14**, 483 (1959).
- (2) (a) S. Meyerson, I. Puskas, and E. K. Fields, *Adv. Mass Spectrom.*, **6**, 17 (1974); (b) *J. Am. Chem. Soc.*, **95**, 6056 (1973).
- (3) See especially A. G. Sharkey, J. L. Shultz, and R. A. Friedel, *Anal. Chem.*, **31**, 87 (1959).
- (4) S. Meyerson, *Int. J. Mass Spectrom. Ion Phys.*, **1**, 309 (1968).
- (5) (a) C. Fenselau, J. L. Young, S. Meyerson, W. R. Landis, E. Selke, and L. C. Leitch, *J. Am. Chem. Soc.*, **91**, 6847 (1969); (b) S. Meyerson, C. Fenselau, J. L. Young, W. R. Landis, E. Selke, and L. C. Leitch, *Org. Mass Spectrom.*, **3**, 689 (1970).

- (6) For a pertinent recent review, see D. G. I. Kingston, J. T. Bursey, and M. M. Bursey, *Chem. Rev.*, **74**, 215 (1974).
- (7) G. Spittler, M. Spittler-Friedmann, and R. Houriet, *Monatsh. Chem.*, **97**, 121 (1966); see also D. H. Hunneman and W. J. Richter, *Org. Mass Spectrom.*, **6**, 909 (1972).
- (8) C. G. Macdonald, J. S. Shannon, and G. Sugowdz, *Tetrahedron Lett.*, 807 (1963); H. Budzikiewicz, Z. Pelah, and C. Djerassi, *Monatsh. Chem.*, **95**, 158 (1964); M. M. Green and J. Schwab, *Tetrahedron Lett.*, 2955 (1968); R. S. Ward and D. H. Williams, *J. Org. Chem.*, **34**, 3373 (1969); M. M. Green, R. J. Cook, J. M. Schwab, and R. B. Roy, *J. Am. Chem. Soc.*, **92**, 3076 (1970); J. L. Holmes, D. McGillivray, and R. T. B. Rye, *Org. Mass Spectrom.*, **7**, 347 (1973).
- (9) J. H. Beynon and A. E. Williams, "Mass and Abundance Tables for Use in Mass Spectrometry", Elsevier, New York, N.Y., 1963.
- (10) J. H. Futrell, K. R. Ryan, and L. W. Sieck, *J. Chem. Phys.*, **43**, 1832 (1965); K. R. Jennings, *ibid.*, **43**, 4176 (1965); S. Meyerson, R. W. Vander Haar, and E. K. Fields, *J. Org. Chem.*, **37**, 4114 (1972).
- (11) M. M. Green, J. M. Moldowan, M. W. Armstrong, T. L. Thompson, K. J. Sprague, A. J. Hass, and J. J. Artus, *J. Am. Chem. Soc.*, in press.
- (12) R. J. Liedtke and C. Djerassi, *J. Am. Chem. Soc.*, **91**, 6814 (1969); K. Christiansen, V. Mahadevan, C. V. Viswanathan, and R. T. Holman, *Lipids*, **4**, 421 (1969); A. G. Harrison, *Org. Mass Spectrom.*, **3**, 549 (1970).
- (13) J. Cable and C. Djerassi, *J. Am. Chem. Soc.*, **93**, 3905 (1971).
- (14) For a closely analogous photochemical example, see R. Breslow and M. A. Winnik, *J. Am. Chem. Soc.*, **91**, 3083 (1969); R. Breslow and P. C. Scholl, *ibid.*, **93**, 2331 (1971).
- (15) See, for example, F. O. Rice and T. A. Vanderslice, *J. Am. Chem. Soc.*, **80**, 29 (1958); A. A. Zavitsas, *ibid.*, **94**, 2779 (1972); A. A. Zavitsas and A. A. Melikian, *ibid.*, **97**, 2757 (1975).
- (16) W. Carpenter, A. M. Duffield, and C. Djerassi, *J. Am. Chem. Soc.*, **90**, 160 (1968).
- (17) N. C. Rol, *Recl. Trav. Chim. Pays-Bas*, **84**, 413 (1965).
- (18) A. Beugelmans, D. H. Williams, H. Budzikiewicz, and C. Djerassi, *J. Am. Chem. Soc.*, **86**, 1386 (1964); W. Carpenter, Y. M. Sheikh, A. M. Duffield, and C. Djerassi, *Org. Mass Spectrom.*, **1**, 3 (1968).
- (19) M. A. Winnik, C. K. Lee, and P. T. Y. Kwong, *J. Am. Chem. Soc.*, **96**, 2901 (1974).
- (20) Cf. P. J. Derrick, A. M. Falick, A. L. Burlingame, and C. Djerassi, *J. Am. Chem. Soc.*, **96**, 1054 (1974); R. P. Morgan and P. J. Derrick, *J. Chem. Soc., Chem. Commun.*, 836 (1974).
- (21) See, for example, W. J. Baumann, A. J. Aasen, J. K. G. Kramer, and R. T. Holman, *J. Org. Chem.*, **38**, 3767 (1973).
- (22) F. W. McLafferty, *Anal. Chem.*, **29**, 1782 (1957); J. H. Beynon, "Mass Spectrometry and Its Applications to Organic Chemistry", Elsevier, New York, N.Y., 1960, pp 275 ff; K. Biemann, "Mass Spectrometry. Organic Chemical Applications", McGraw-Hill, New York, N.Y., 1962, p 55.
- (23) W. E. van Heyningen, D. Rittenberg, and R. Schoenheimer, *J. Biol. Chem.*, **125**, 495 (1938).
- (24) "Beilstein's Handbuch der Organischen Chemie", Vol. 2, III, Springer-Verlag, West Berlin, 1960, p 991.
- (25) "Beilstein's Handbuch der Organischen Chemie", Vol. 1, III, Springer-Verlag, West Berlin, 1958, p 1834.

## The Thermochemistry of $C_2H_4O^+$ Ions

John L. Holmes,\* J. K. Terlouw,<sup>1</sup>

Chemistry Department, University of Ottawa, Ottawa, Canada K1N 6N5

and F. P. Lossing\*

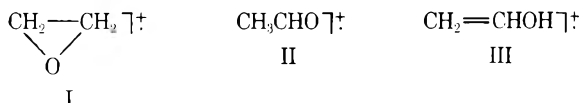
Division of Chemistry, National Research Council of Canada, Ottawa, Canada K1A 0R6 (Received May 11, 1976)

Publication costs assisted by the National Research Council of Canada

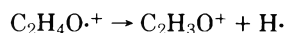
The heat of formation of the molecular ion of vinyl alcohol has been measured by an electron impact method to be 181 kcal/mol. The heat of formation of the transient neutral molecule is estimated to be  $-26.5$  kcal/mol, whence the ionization potential is  $9.0 \pm 0.15$  eV. The significance of these results is discussed with particular regard to some recent metastable ion studies and to the generation of  $C_2H_4O^+$  ions in the mass spectra of aliphatic aldehydes.

### Introduction

In a recent paper<sup>2</sup> it was shown that the three isomeric  $C_2H_4O^+$  ions (I–III) can unequivocally be identified by the



characteristic metastable peaks accompanying their fragmentation by H atom loss:



Two further forms of  $C_2H_4O^+$  were observed in these experiments but their structures were not confirmed. Although the ionic heats of formation of I and II are well-established, there is no reliable value for III since the parent neutral molecule cannot be isolated. However, the unequivocal participation of III in certain ionic fragmentations<sup>2</sup> provides a means of deriving its heat of formation as a fragment ion.

In this paper we report measurements of the heats of formation of  $C_2H_4O^+$  ions I and II by direct ionization of parent molecules, and III as a primary fragment ion in decompositions of known mechanism.

### Experimental Section

All compounds were of research grade purity or were purified by glc. Metastable peak measurements were performed on a G.E.C.-A.E.I. MS902S mass spectrometer. The electron impact apparatus comprising an electrostatic electron monochromator<sup>3</sup> together with a quadrupole mass spectrometer and minicomputer data system<sup>4</sup> has been described elsewhere.

### Results and Discussion

The ionization potentials (IP) of ethylene oxide and acetaldehyde measured in this work are in close agreement with those obtained in photoionization studies.<sup>5</sup> These IP and the derived heats of formation for structures I and II are given in

TABLE I: Heat of Formation of  $C_2H_4O^+$  Molecular Ions

Precursor molecule		Neutral fragment	AP( $C_2H_4O^+$ ), eV	$\Delta H_f(C_2H_4O^+)$ , kcal/mol
Structure	$\Delta H_f$ , kcal/mol			
	-12.6 <sup>a</sup>		10.57	231
CH <sub>3</sub> CHO	-39.7 <sup>a</sup>		10.23	196
	-32.2 <sup>b</sup>	C <sub>2</sub> H <sub>4</sub>	9.87	182
CH <sub>2</sub> =CHOC <sub>2</sub> H <sub>5</sub>	-33.6 <sup>a</sup>	C <sub>2</sub> H <sub>4</sub>	10.19	189
CH <sub>3</sub> (CH <sub>2</sub> ) <sub>2</sub> CHO	-48.9 <sup>a</sup>	C <sub>2</sub> H <sub>4</sub>	10.52	181
(CH <sub>3</sub> ) <sub>2</sub> CHCH <sub>2</sub> CHO	-56.5 <sup>c</sup>	C <sub>3</sub> H <sub>6</sub>	10.57	182
CH <sub>3</sub> CH <sub>2</sub> OH	-56.2 <sup>a</sup>	H <sub>2</sub>	≤ 10.45 <sup>d</sup>	≤ 185 <sup>d</sup>
	-59 <sup>e</sup>	CH <sub>2</sub> O	10.30	204.5
	-71.1 <sup>a</sup>	CH <sub>2</sub> O	10.87	205.5

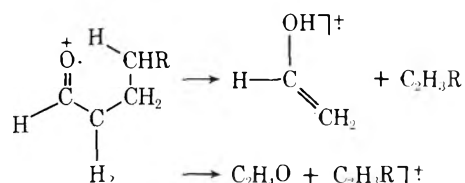
<sup>a</sup> Reference 6. <sup>b</sup> Derived from  $\Delta H_f(\text{cyclobutane}) - 6.78 \text{ kcal/mol}$ <sup>6</sup> and the average of the differences  $\Delta H_f(\text{cyclopentane}) - \Delta H_f(\text{cyclopentanal}) = 39.5 \text{ kcal/mol}$  and  $\Delta H_f(\text{cyclohexane}) - \Delta H_f(\text{cyclohexanal}) = 38.9 \text{ kcal/mol}$ . <sup>c</sup>  $\Delta H_f(\text{isovaleraldehyde})$  taken as  $\Delta H_f(\text{valeraldehyde}) - 2 \text{ kcal/mol}$ .<sup>6</sup> <sup>d</sup> Long-tailed curve, suggesting upper limit only. <sup>e</sup> From  $\Delta H_f(\text{liquid}) = -71.3 \text{ kcal/mol}$ <sup>6</sup> and estimated  $\Delta H(\text{vapor}) = +12 \text{ kcal/mol}$ .

Table I. Also given are the appearance potentials (AP) and derived heats of formation for  $C_2H_4O^+$  ions formed as a fragment in the elimination of a neutral olefin (or H<sub>2</sub>) from five compounds in which the metastable peak characteristics have indicated that the vinyl alcohol ion was produced.<sup>2</sup> The data show that the  $C_2H_4O^+$  ion formed in these processes is nearly 50 kcal/mol more stable than I and 14 kcal/mol more stable than II. Since the AP may include some kinetic energy, the preferred value for  $\Delta H_f(C_2H_4O^+)$  will lie at or below the lower end of the range shown in Table I. We propose therefore that  $\Delta H_f(\text{vinyl alcohol}^+) = 181 \text{ kcal/mol}$ . Although neutral vinyl alcohol cannot be isolated, its heat of formation can be assessed using simple additivity. For example, the effect on  $\Delta H_f$  of substituting vinyl for ethyl in straight-chain compounds is  $+30.0 \pm 2.0 \text{ kcal/mol}$ ;<sup>6</sup> thus going from ethanol ( $\Delta H_f = -56.2 \text{ kcal/mol}$ ) to vinyl alcohol leads to  $\Delta H_f$  for the latter  $= -26.2 \pm 2.0 \text{ kcal/mol}$ . Similarly, the effect of substituting hydroxyl for methyl in *n*-alkanes is  $-31.5 \pm 0.2 \text{ kcal/mol}$ ; thus going from propene ( $\Delta H_f = -4.9 \text{ kcal/mol}$ ) to vinyl alcohol,  $\Delta H_f$  for the latter  $= -26.6 \pm 0.2 \text{ kcal/mol}$ . A reasonable value for  $\Delta H_f(\text{vinyl alcohol})$  is therefore  $-26.5 \pm 2.0 \text{ kcal/mol}$ . From  $\Delta H_f(\text{vinyl alcohol}^+) = 181 \text{ kcal/mol}$ , the IP for this compound is derived to be  $9.0 \pm 0.15 \text{ eV}$ .

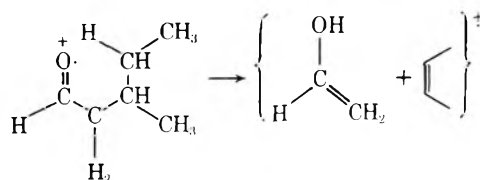
Note that the last two compounds in Table I produce  $C_2H_4O^+$  ions with  $\Delta H_f$ 's which are above those of the vinyl alcohol and acetaldehyde molecular ions, but below that for ethylene oxide. The metastable peaks for H atom loss for these two ions were clearly both of the vinyl alcohol type.<sup>2</sup> The metastable peaks for their formation from their precursor molecular ions were of Gaussian shape, showing that no significant reverse activation energy was involved. We tentatively propose therefore that the  $C_2H_4O^+$  ion in these two cases may be a fourth structural species, which however decomposes over the same potential energy surface as does the vinyl alcohol ion and thus produces a similar metastable peak for H atom loss.

The present result for the IP of vinyl alcohol has particular relevance to the long-standing controversy concerning charge location and the mechanism of ion rearrangement in olefin elimination from the molecular ion of aliphatic aldehydes. This reaction generates two pairs of partners:  $C_2H_4O^+$  of structure III plus a neutral olefin, and an olefin ion plus a

neutral  $C_2H_4O$ . The reaction is believed to proceed via a six-membered intermediate:



The most recent experiments are a field ionization kinetic (FIK) study by Morgan and Derrick.<sup>7</sup> These authors showed that at times in excess of 20 ps (following ionization)  $C_2H_4O^+$  was the favored product in the  $\gamma$ -hydrogen rearrangement of 1-hexanal, whereas for 3-methylpentanal the  $C_4H_8^+$  ion predominated. For both molecules the  $C_2H_4O^+/C_4H_8^+$  ratio fell steeply between 20 ps and the microsecond region, more sharply in the case of the branched aldehyde. It was argued that the suppression of  $C_2H_4O^+$  in 3-methylpentanal supported the proposed mechanism in which  $\gamma$ -hydrogen transfer and  $\beta$  cleavage occur as discrete steps, not as a concerted reaction. They also proposed that on  $\beta$  cleavage the charge is retained by the product of lowest ionization potential. Two estimates for the ionization potential of III were then available, namely, 9.5 eV by Meyerson and McCallum<sup>8</sup> and a more recent estimate of 9.25 eV by Bentley and Johnstone.<sup>9</sup> Thus, in the case of 3-methylpentanal, Morgan and Derrick suggested that vinyl alcohol and but-2-ene (IP 9.13 eV)<sup>5</sup> compete for the charge with the latter succeeding. Note that for this molecule the hydrocarbon can be produced directly, without hydrogen rearrangement:



In contrast, 1-hexanal without hydrogen rearrangement would give but-1-ene, whose IP, 9.58 eV, exceeded the estimates for vinyl alcohol. Hence the larger ratio for  $C_2H_4O^+/C_4H_8^+$  compared with that for the branched aldehyde would be ex-

plained. For 1-hexanal, however, the ratio falls appreciably below a value of unity at times exceeding  $\sim 100$  ps and this was interpreted as an indication that hydrogen rearrangement yielded but-2-ene at these longer times.

From the previous<sup>2</sup> and present results there can be little doubt that the charged  $C_2H_4O$  species is indeed ion III. This ion is not converted into any of its isomeric forms up to its threshold for H atom loss. Much of the argument of Morgan and Derrick rests on the assumption that the ionization potential for vinyl alcohol is larger than that of but-2-ene. This is not in agreement with the present findings. However, their observations can be better analyzed by consideration of the thermochemistry of the possible pairs of products, rather than the ionization potential alone. The pairs are listed below, with individual heats of formation, and the sum for the product pairs. Reactions involving the more energetic ionic forms I and II are clearly not competitive, and have not been included.

	$\Delta H_f(\text{products}),$ kcal/mol	
$C_6H_{12}O^+ \rightarrow CH_2CHOH^+ + CH_2=CHCH_2CH_3$	181	(1)
	(181) (0)	
$\rightarrow CH_2CHOH^+ + CH_3CH=CHCH_3$	179	(2)
	(-2)	
$\rightarrow CH_2CHOH + CH_2=CHCH_2CH_3^+$	194.5	(3)
	(-26.5) (221)	
$\rightarrow CH_2CHOH + CH_3CH=CHCH_3^+$	181.5	(4)
	(208)	
$\rightarrow CH_3CHO + CH_2=CHCH_2CH_3^+$	181	(5)
	(-39.7)	
$\rightarrow CH_3CHO + CH_3CH=CHCH_3^+$	168	(6)

Reactions 1–4 are those considered by Morgan and Derrick.<sup>7</sup> However, if the hydrogen rearrangement generating but-2-ene from 1-hexanal is a reasonable proposition, one should also allow the analogous rearrangement to give the most stable neutral  $C_2H_4O$  species, acetaldehyde, as in reactions 5 and 6. It can be seen that reaction 6 is much less endothermic than reactions 1–5, and under conditions where sufficient time is available for rearrangement it will predominate. Thus for 1-hexanal, reaction 1 will give way to reactions 2 or 5 and finally to reaction 6 at increasing times. Similarly, for 3-methylpentanal reaction 4 competes favorably with reaction 2 at short times, but will be overtaken by reaction 6 at longer times. The great decrease in the  $C_2H_4O^+/C_4H_8^+$  ratio with time for both molecules is thereby explained.

It is necessary to show that there is no significant barrier, such as a reverse activation energy, to the occurrence of reaction 6. The appearance potential for  $C_4H_8^+$  from 1-hexanal

( $\Delta H_f(g) = -59.4$  kcal/mol)<sup>10</sup> was measured to be 9.89 eV, compared with the calculated heat of reaction 6, 9.87 eV. Since the calculated appearance potential for the other reactions generating  $C_4H_8^+$  (reactions 3, 4, and 5) are in excess of 10.4 eV, it appears that there is no significant impediment to the occurrence of reaction 6 on the time scale of these measurements (residence time in the ion source 30  $\mu$ s).<sup>11</sup> This is confirmed by the presence of a weak metastable peak of Gaussian shape having a small  $T_{0.5} = 0.019$  eV, indicating the absence of any reverse activation energy.

The appearance potential of  $C_2H_4O^+$  ion from 1-hexanal was found to be about 10.7 eV, the uncertainty arising from its rather gradual onset. The calculated appearance potential for reactions 1 and 2 are  $\sim 10.4$  eV. Formation of acetaldehyde or ethylene oxide ions would require an AP of 11.0 and 12.5 eV, respectively. No metastable peak could be discerned for this fragmentation in the first field free region indicating that this reaction does not occur to any appreciable extent on the microsecond time scale. This observation is in keeping with the appearance potential measurements.

Very similar observations were recorded for 3-methylpentanal. (AP  $m/e$  44 = 10.88 eV, calcd for [vinyl alcohol] $^+$ ) and but-2-ene =  $10.42 \pm 0.1$  eV; AP  $m/e$  56 = 9.86 eV, calcd for [but-2-ene] $^+$  and  $CH_3CHO = 9.96 \pm 0.1$  eV.)<sup>12</sup> Again the formation of  $m/e$  56 was accompanied by a metastable peak ( $T_{0.5} = 0.012$  eV) and none was observed for  $C_2H_4O^+$  production.

**Acknowledgments.** J.L.H. wishes to thank the National Research Council of Canada for continuing support of this research. J.K.T. thanks the Netherlands Organization for the Advancement of Pure Research (Z.W.O.) for a Fellowship during the tenure of which this work was initiated.

## References and Notes

- (1) Permanent address: Analytical Chemistry Laboratory, University of Utrecht, Croesestraat 77A, Utrecht, The Netherlands.
- (2) J. L. Holmes and J. K. Terlouw, *Can. J. Chem.*, **53**, 2076 (1975).
- (3) K. Maeda, G. P. Semeluk, and F. P. Lossing, *Int. J. Mass Spectrom. Ion Phys.*, **1**, 395 (1968).
- (4) F. P. Lossing and J. C. Traeger, *Int. J. Mass Spectrom. Ion Phys.*, **19**, 9 (1976).
- (5) J. L. Franklin, J. G. Dillard, H. M. Rosenstock, J. T. Herron, K. Draxl, and F. H. Field, *Natl. Stand. Ref. Data Ser., Natl. Bur. Stand.*, **No. 26**, (1969).
- (6) J. D. Cox and G. Pilcher, "Thermochemistry of Organic and Organometallic Compounds," Academic Press, New York, N.Y., 1970.
- (7) R. P. Morgan and P. J. Derrick, *Chem. Commun.*, 836 (1974).
- (8) S. Meyerson and J. D. McCollum, *Adv. Anal. Chem. Instrum.*, **2**, 179 (1963).
- (9) T. W. Bentley and R. A. W. Johnstone, *Adv. Phys. Org. Chem.*, **8**, 242 (1970).
- (10) D. R. Stull, E. F. Westrum, Jr., and G. C. Sinke, "The Chemical Thermodynamics of Organic Compounds," Wiley, New York, N.Y., 1969.
- (11) The alternative fragmentation yielding  $C_3H_6O^+$  and  $C_3H_6$  has a minimum (calcd) AP of 10.6 eV.
- (12) The uncertainty in the calculated AP lies in the estimate for  $\Delta H_f(3\text{-methylpentanal}) = -61 \pm 2$  kcal mol<sup>-1</sup>.

## Thermodynamic Properties of Dilute Sulfuric Acid and the Potential of the Lead Sulfate–Lead Electrode

Kenneth S. Pitzer

Department of Chemistry and Material and Molecular Research Division of the Lawrence Berkeley Laboratory, University of California, Berkeley, California 94720 (Received June 18, 1976)

Publication costs assisted by the Energy Research and Development Administration

The 1934 data of Shrawder and Cowperthwaite for the cell  $\text{Pt}, \text{H}_2|\text{H}_2\text{SO}_4(m)|\text{PbSO}_4, \text{Pb}, \text{Hg}$ , which have been generally ignored, are shown to yield valuable information about the properties of sulfuric acid in the range below 0.02 M and to give probably the best available value for the potential of the lead–lead sulfate electrode.

In 1934 Shrawder and Cowperthwaite<sup>1</sup> published measurements of the potential of the cell  $\text{Pt}, \text{H}_2|\text{H}_2\text{SO}_4(m)|\text{PbSO}_4, \text{Pb}, \text{Hg}$  over the range 0.001–0.02 M and 0–50 °C. These data seem ideally suited to the determination of the thermodynamic properties of sulfuric acid below 0.02 M since the  $\text{HSO}_4^-$  is almost all dissociated in the most dilute solutions whereas it is roughly half dissociated at higher concentration. Surprisingly, neither the original authors nor anyone else to my knowledge has ever published a straightforward analysis of these measurements without unnecessary involvement of other data. Shrawder and Cowperthwaite used, in their own interpretation, the dissociation constants of Hamer<sup>2</sup> for  $\text{HSO}_4^-$  which have since been shown to be inaccurate. Subsequently, this work seems to have been ignored in consideration of the activity of sulfuric acid until Lilley and Briggs<sup>3</sup> showed that, in the range of overlap (0.01–0.02 M), the Shrawder and Cowperthwaite results were in excellent agreement with those of Covington et al.<sup>4</sup> However, both Latimer<sup>5</sup> and Ives and Smith<sup>6</sup> listed electrode potentials based upon Shrawder and Cowperthwaite's data.

Thus, it seems desirable to treat the Shrawder and Cowperthwaite data with a reasonable Debye–Hückel function including the limiting law but, so far as possible, without other assumptions which would bias the resulting standard cell potential and the implied solute standard state.

While the dissociation constant for  $\text{HSO}_4^-$  will enter the calculation, its value may be interlocked with assumptions about the activity coefficients of ions and, therefore, not be unambiguous.

### Calculations

In addition to the measured cell potentials, Shrawder and Cowperthwaite<sup>1</sup> report the following quantity (actually its negative since they wrote the cell in the opposite direction):

$$E^\circ = E - (RT/2F) \ln (4m^2m_2) \quad (1a)$$

$$= E^\circ - (3RT/2F) \ln \gamma_{\pm} \quad (1b)$$

Here  $m$  is the gross molality of the acid and  $m_2$  is the molality of sulfate near the lead sulfate electrode assuming complete dissociation of  $\text{HSO}_4^-$  but also recognizing the solubility of lead sulfate.

For activity coefficients in this dilute range our assumed expression is

$$\ln \gamma_i = -z_i^2 A_\phi [I^{1/2}/(1 + bI^{1/2}) + (2/b) \ln (1 + bI^{1/2})] \quad (2)$$

where  $z_i$  is the number of charges on the  $i$ th ion and  $A_\phi$  the Debye–Hückel parameter. This expression was derived recently<sup>7a</sup> from the Debye–Hückel distribution and the “pressure” equation of modern statistical mechanics. Use of the original Debye–Hückel expression

$$\ln \gamma_i = -z_i^2 A_\phi I^{1/2}/(1 + \rho I^{1/2}) \quad (3)$$

would give substantially the same results. Here  $A_\phi = 3A_\phi$ . The assumed distance of closest interionic approach leads formally to the same value for  $b$  or  $\rho$ , but it is well-known that this feature of the theory is oversimplified and that  $b$  (or  $\rho$ ) is best treated as an empirical parameter with a value near unity.

The bisulfate dissociation is given by the expression

$$K_2 = \frac{(2m - m_3)(m - m_3)}{m_3} \frac{\gamma_{\text{H}}\gamma_{\text{SO}_4}}{\gamma_{\text{HSO}_4}} \quad (4)$$

where  $m_3$  is the molality of  $\text{HSO}_4^-$ ,  $(2m - m_3)$  that of  $\text{H}^+$ , and  $(m - m_3)$  that of  $\text{SO}_4^{2-}$ . Then the stoichiometric activity coefficient  $\gamma_{\pm}$  is

$$\gamma_{\pm}^3 = \frac{(2m - m_3)^2(m - m_3)}{4m^3} \gamma_{\text{H}}^2\gamma_{\text{SO}_4}$$

The effect of higher terms in the activity coefficient expressions would be small in this concentration range. While we<sup>7</sup> have used  $b = 1.2$  as a standard value in the expression in eq 2 when higher terms for short-range interactions are included, we explore the possible effects of such interactions by variation in  $b$ .

An iterative procedure was followed with an initial value  $K_2$  and of  $m_3$  assumed. First  $m_3$  is iteratively refined to fit eq 4 with activity coefficients determined by eq 2 and with  $I = 3m - 2m_3$ . Next eq 1b, 2, and 5 yield a value of  $E^\circ$ . This process is repeated with adjusted values of  $K_2$  until the minimum in standard deviation of  $E^\circ$  is located.

It was found that excellent agreement could be obtained except for the most dilute solutions at the higher temperatures where there was a moderate but systematic deviation. This is not surprising since these are the conditions where solubility of lead sulfate is expected to have the greatest effect. Although a correction was made<sup>1</sup> for the most obvious effect of this solubility, there are other effects which cannot readily be predicted. Hence it seemed best to ignore the values for 0.001 M at and above 25 °C and those for 0.002 M at 37.5 and 50 °C.

The results for 25 °C with a range of values of  $b$  are given in Table I. The fit is excellent with a standard deviation of only



**TABLE I: Parameters of Activity Coefficient Equations Fitted to Cell Potentials for 25 °C**

$b$	$-\ln K_2$	$\sigma(E)/\text{mV}$	$-E^\circ/\text{mV}$	$\gamma_{\pm}(m = 0.01)$
0.8	4.23	0.06 <sub>6</sub>	350.97	0.538
1.0	4.27	0.05 <sub>3</sub>	351.07	0.537
1.2	4.30	0.04 <sub>5</sub>	351.14	0.536
1.5	4.35	0.03 <sub>5</sub>	351.28	0.534
2.0	4.41	0.03 <sub>4</sub>	351.43	0.532
3.0	4.50	0.05 <sub>2</sub>	351.64	0.529

**TABLE II: Standard Potentials and Activity Coefficients at Various Temperatures (with  $b = 1.2$ )**

$t, ^\circ\text{C}$	$-E^\circ/\text{mV}$	$\gamma_{\pm}(m = 0.01)$	$-\ln K_2$
0.0	327.78	0.616	3.39
12.5	339.21	0.575	3.88
25.0	351.14	0.536	4.30
37.5	363.7	0.494	4.69
50.0	377.5	0.445	5.14

0.05 mV. While the smallest  $\sigma$  was found for  $b = 2.0$ , the minimum is very broad and one cannot select a precise value for  $b$  on this basis. The absolute values for  $E^\circ$  (which include the correction factor  $1 \text{ Int } V = 1.000 \text{ 33 Abs } V$ ) are not independent of  $b$ , but the uncertainty is quite small. Likewise the effect of  $b$  on  $\gamma_{\pm}$  is small at 25 °C.

In contrast the variation in  $K_2$  with  $b$  is substantial. There is an intrinsic redundancy between  $b$  and  $K_2$  which cannot be resolved from these data, at least. Hence it is meaningless to compare  $K_2$  values from different sources unless the assumed activity coefficient expressions are considered simultaneously.

Although the optimum  $b$  for 25 °C is greater than 1.2, that value, used elsewhere<sup>7</sup> as a standard, is within the acceptable range and was used for treatment of the data at other temperatures. The results are given in Table II. Activity coefficients at other molalities can be obtained, either from the parameters and eq 2, 4, and 5, or by correcting the originally published values<sup>1</sup> by the same ratio as for 0.01 M.

The values of  $K_2$  in Table II have meaning only in relation to eq 2 and the value  $b = 1.2$  used there. The effect of reasonable variation of  $b$  on  $E^\circ$  and  $\gamma_{\pm}$  is small at 25 °C as shown in Table I and is even less at lower temperatures (only 0.1 mV at 0 °C). At higher temperatures the uncertainties become considerably greater with an uncertainty of 1 mV or more for  $E^\circ$  at 50 °C.

The temperature coefficient of the  $K_2$  values in Table II corresponds to a  $\Delta H$  of dissociation of about  $-6 \text{ kcal/mol}$  at 25 °C. This is somewhat larger the value  $-5.2$  from both calorimetry<sup>8</sup> and other sources.<sup>9</sup> However this value of  $-6 \text{ kcal/mol}$  is much more nearly correct than the value  $-2.2$  implied by the dissociation constants of Hamer<sup>2</sup> which Shrawder and Cowperthwaite used in their own analysis of these data.

## Discussion

The primary conclusion of this work is that the Shrawder and Cowperthwaite<sup>1</sup> results, which have been ignored in most studies of sulfuric acid, should be included in determining the properties in the dilute region. Except for the most dilute points at the higher temperatures, these data are quite consistent with generally established equations for activity coefficients and the dissociation of  $\text{HSO}_4^-$  ion.

The  $E^\circ$  value at 25 °C from Table I may be taken as  $-351.3 \pm 0.3 \text{ mV}$ . For comparison one may consider two values from combinations of other cells. Briggs and Lilley<sup>10</sup> obtain  $-352.6 \pm 0.4 \text{ mV}$  from determinations involving a membrane electrode for  $\text{Ca}^{2+}$  in cells with  $\text{CaCl}_2$  and the  $\text{AgCl}$ ,  $\text{Ag}$  electrode and with  $\text{CaSO}_4$ , and the  $\text{PbSO}_4$ ,  $\text{Pb}$ ,  $\text{Hg}$  electrode. Combination of the  $E^\circ$  values for the  $\text{AgX}$ ,  $\text{Ag}$  electrodes,<sup>7</sup> the cells<sup>7</sup>  $\text{Hg}, \text{Zn}|\text{ZnX}_2(m)|\text{AgX}, \text{Ag}$  (with  $\text{X} = \text{Cl}$  and  $\text{Br}$ ), and the cell<sup>11</sup>  $\text{Hg}, \text{Zn}|\text{ZnSO}_4(m)|\text{PbSO}_4, \text{Pb}, \text{Hg}$  yield values in the range  $-349.4$  to  $-350.2 \text{ mV}$ . In view of the possible accumulation of error in combinations of data from several cells, the result for the single cell discussed in this paper seems preferable at or below 25 °C.

At higher temperatures, the interpretation of the results of Shrawder and Cowperthwaite becomes more ambiguous; hence indirect measurements of the  $\text{PbSO}_4$ ,  $\text{Pb}$  potential could yield a more accurate value and could then be used together with the present data to obtain a more accurate description of the properties of dilute sulfuric acid.

As noted above, the values of the dissociation constant  $K_2$  for  $\text{HSO}_4^-$  are interlocked with assumptions about activity coefficients of the ions. Covington et al.<sup>4</sup> recognized this situation in their recent discussion. For 25 °C they recommend  $0.0106 \pm 0.0009$  for  $K_2$  although their own experimental results indicate a slightly higher range  $0.0111 \pm 0.0006$ . These authors used eq 3 with  $\rho$  values from 1.0 to 1.7 for activity coefficients of the ions. The results of Table I correspond to  $K_2 = 0.0125 \pm 0.001$  with a wider range of values of  $b$  than was used for  $\rho$ . While our value of  $K_2$  is higher, there is no conflict when uncertainties in interpretation are considered.

**Acknowledgment.** This research was sponsored by the Energy Research and Development Administration.

## References and Notes

- (1) J. Shrawder and I. A. Cowperthwaite, *J. Am. Chem. Soc.*, **56**, 2340 (1934).
- (2) W. J. Hamer, *J. Am. Chem. Soc.*, **56**, 860 (1934).
- (3) T. H. Lilley and C. C. Briggs, *Electrochim. Acta*, **20**, 257 (1975).
- (4) A. K. Covington, J. V. Dobson, and Lord Wynne-Jones, *Trans. Faraday Soc.*, **61**, 2050, 2057 (1965).
- (5) W. M. Latimer, "Oxidation States of the Elements and Their Potentials in Aqueous Solution", 2d ed, Prentice-Hall, New York, N.Y., 1952, p 154.
- (6) D. J. G. Ives and F. R. Smith, in "Reference Electrodes", D. J. G. Ives and G. J. Janz, Ed., Academic Press, New York, N.Y., 1961, Chapter 8.
- (7) (a) K. S. Pitzer, *J. Phys. Chem.*, **77**, 268 (1973); (b) K. S. Pitzer and G. Mayorga, *ibid.*, **77**, 2300 (1973).
- (8) K. S. Pitzer, *J. Am. Chem. Soc.*, **59**, 2365 (1937).
- (9) See C. W. Davies, H. W. Jones, and C. B. Monk, *Trans. Faraday Soc.*, **48**, 921 (1952), for a summary.
- (10) C. C. Briggs and T. H. Lilley, in press.
- (11) K. S. Pitzer, *J. Chem. Soc., Faraday Trans. 2*, **68**, 101 (1972).

# Unimolecular Thermal Decomposition Reactions of Gaseous Carbonium Ions

M. Meot-Ner and F. H. Field\*

The Rockefeller University, New York, New York 10021 (Received February 2, 1976)

Publication costs assisted by the National Science Foundation

$C_7$  carbonium ions are observed to undergo thermally activated endothermic unimolecular decomposition reactions:  $C_7H_{15}^+ \rightarrow C_4H_9^+ + C_3H_6$ .  $C_8$ – $C_{10}$  carbonium ions also decompose by analogous reactions with the loss of an olefin. All possible decompositions which lead to an ionic product which is  $C_4H_9^+$  or larger and a neutral olefin which is  $C_3H_6$  or larger are observed. Decomposition reactions were observed between 480 and 600 K and third body pressures of 0.5–3.0 Torr. Reaction rates are  $1 \times 10^3$ – $20 \times 10^3$  s $^{-1}$ . The rate constants increase with increasing third-body pressure, i.e., the reactions are the "fall-off" region of unimolecular kinetics. This is further demonstrated by the Arrhenius activation energies,  $E_a^\circ \approx 13$  kcal/mol, which are about 10 kcal/mol lower than the endothermicities for the decomposition reactions.

## Introduction

Thermally activated unimolecular decomposition and rearrangement of gaseous molecules constitute a class of thoroughly investigated chemical reactions.<sup>1</sup> Little, however, is known about thermally activated unimolecular reactions of gaseous ions, although the decomposition of energetic ions, such as those formed by electron impact, has been the subject of much work.

The introduction of pulsed high-pressure mass spectrometric techniques enables us to monitor the concentration of ions in a reaction system as a function of reaction time. This method allows accurate measurement of the decomposition kinetics of thermalized gaseous ions without need to resort to assumptions about ion residence times and spatial ion distributions which were required in previous work using continuous ionization techniques.<sup>2</sup>

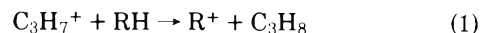
The present work constitutes the first investigation of the thermal decomposition of gaseous ions, in this case of tertiary  $C_7$  to  $C_{10}$  carbonium ions, by the pulsed high-pressure mass spectrometric method. These reactions are both of basic interest as fast thermal decomposition reactions, with half-lives of  $10^{-3}$  to  $10^{-5}$  s, and of applied interest because of their relation to the catalytic cracking of hydrocarbons in the petroleum industry.

## Experimental Section

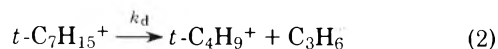
The present measurements were performed on The Rockefeller University Chemical Physics mass spectrometer used in the pulsed mode.<sup>3</sup> Gas mixtures of 1% of a  $C_7$ – $C_{10}$  hydrocarbon in propane and occasionally in  $i$ - $C_4H_{10}$  or in a mixture of 10% NO in  $N_2$  are introduced into the ion source and ionized by a 20- $\mu$ s pulse of 600-V electrons. Ion intensities as a function of reaction time are followed on a multichannel analyzer whose sweep through 256 10- $\mu$ s wide channels is initiated by a pulse synchronous with the rising edge of the bombarding electron pulse. In the propane–heptane mixtures the major peaks observed were at  $m/e$  43 ( $C_3H_7^+$ ),  $m/e$  99 ( $(M-H)^+$ ), and  $m/e$  57 (the  $((M-H)-C_3H_6)^+$  decomposition product, i.e.,  $C_4H_9^+$ ). In the case of  $C_8$  hydrocarbons, the  $((M-H)-C_4H_8)^+$  decomposition product, and in  $C_9$  and  $C_{10}$  hydrocarbons, the  $((M-H)-C_5H_{10})^+$  and  $((M-H)-C_6H_{12})^+$  ions were also observed.

Ions generated by the electron beam react very rapidly in primary reactions with propane to yield mostly the  $C_3H_7^+$

reactant ion, as is used in chemical ionization. The resultant  $C_3H_7^+$  react with the higher hydrocarbons in the reaction

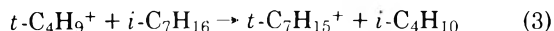


The rate constants for reaction 1 are in the order of  $5$ – $10 \times 10^{-10}$  cm $^3$ /mol s, and the half-life for these reactions under our conditions is  $\approx 5$   $\mu$ s. Consequently, all primary ions of interest disappear in less than 50  $\mu$ s. After this time the only reaction seen is the decomposition of the  $C_7$ – $C_{10}$   $R^+$  carbonium ions to form the product ions in a reaction with first-order or pseudo-first-order kinetics. Sample kinetic plots for the reaction



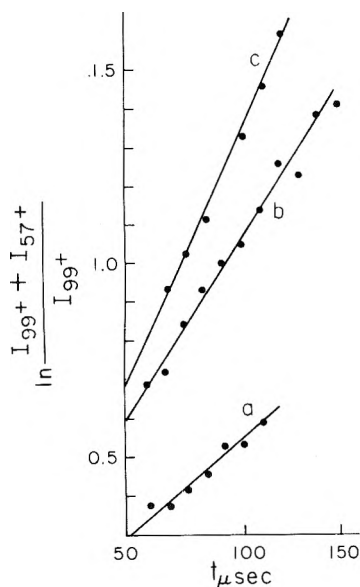
are shown in Figure 1. The reproducibility of the rate constants obtained from plots such as these is about  $\pm 10\%$ . In the context of the present work it should be noted that under our experimental conditions the concentration of ions is much smaller than that of the neutral molecules, and all ion–molecule reactions exhibit pseudo-first-order kinetics. Consequently, the pseudo-first-order nature of the reaction does not imply that the reaction is unimolecular. Investigations of the order of the reaction requires pressure studies (see below).

A possible kinetic complication in our work could have arisen from the transfer reaction



in which the product ion of reaction 2 regenerates the reactant  $C_7H_{15}^+$  ion. From previous kinetic studies,<sup>4</sup> the rate constants for such reactions at 500 K are on the order of  $10^{-12}$  cm $^3$ /mol s. Under our conditions ( $i\text{-}C_7H_{16}$ )  $\approx 10^{14}$  mol/cm $^3$ , and the rate of reaction 3  $\leq 10^2$  s $^{-1}$ . Thus the rate of the transfer reaction is at least 10–100 times slower than the observed decomposition rates and does not effect our measured rates significantly. The excellent linearity of the decomposition kinetic plots (Figure 1) also indicates that this opposing reaction 3 is not significant. Furthermore, we checked that a fivefold decrease in the concentration of  $i\text{-}C_7H_{16}$  did not affect the measured decomposition rate of  $C_7H_{15}^+$  beyond the experimental error limit of 10% on the rate constants. This indicated that reaction 3, which is first order in ( $i\text{-}C_7H_{16}$ ), is not significant.

Some of our measurements were carried out in field-free conditions and some requiring higher sensitivity with repeller fields of 2 V (5 V/cm). In control experiments we found no



**Figure 1.** Kinetic plots from a pressure study for the reaction  $C_7H_{15}^+ \rightarrow C_4H_9^+ + C_3H_6$ , in a mixture of 1% 2-methylhexane in propane at 537 K, with total pressure of (a) 0.75 Torr, (b) 1.45 Torr, (c) 2.5 Torr.

effect of the repeller field on the measured decomposition rate constants.

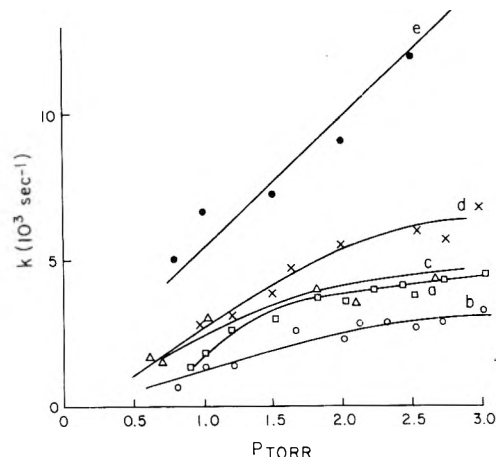
The carrier gas used was Matheson Research Grade  $C_3H_8$  (99.9% pure); all hydrocarbons were at least 99% pure.

## Results

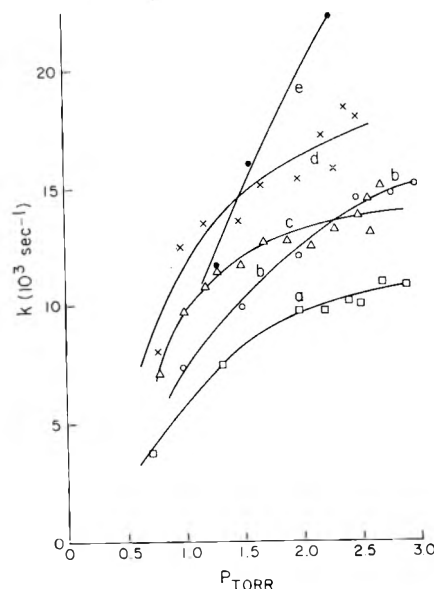
**1. Pressure Dependence of the Decomposition Rate Constants.** The phenomenon of the falloff of rate constants of thermal unimolecular neutral reactions at low pressures where the rate of activation is slow compared with the reaction rate has been investigated thoroughly both experimentally and theoretically.<sup>1</sup> We have extended such studies to gaseous ions, and the pressure dependences of the decomposition rates of five heptyl ions at 503 and 537 K are shown in Figures 2 and 3. Obviously, the decomposition rates of these ions exhibit falloff with decreasing pressure. The falloff rates of the ion decomposition rate constants are similar to the rate of falloff of unimolecular neutral reactions with pressure. For example, the rate of decomposition of cyclobutane at 722 K decreases by a factor of 1.9 over a tenfold drop in pressure; the isomerization rate of methyl isocyanide at 503 K decreases by a factor of 6.3 over a tenfold decrease in pressure in the falloff region (ref 1, pp 248 and 254). By comparison, the decomposition rate of the 2,4-dimethylpentyl ion at 537 K decreases by a factor equivalent to 6.3 over a tenfold decrease in pressure; the decomposition rate of the 2,2,3-trimethylbutyl ion decreases by a factor of 4.6 over a tenfold decrease in pressure.

At the lower part of our pressure range the decomposition reactions seem to reach the low-pressure limit, and the decomposition rate constants,  $k_d$ , are directly proportional to the total pressure. As the pressure increases the slopes of the plots of  $k_d$  vs.  $P$  decrease and the rate constants seem to enter the transition region from second-order kinetics toward the high pressure limit of unimolecular behavior. However, in our accessible pressure range the slopes of the plots of  $k_d$  vs.  $P$  do not level off to zero and the high pressure limit is not reached.

**2. The Temperature Dependence of Decomposition Rate Constants.** Comparison of the corresponding plots in Figures 2 and 3 shows the marked increase of the decomposition rates



**Figure 2.** Pressure dependences of the decomposition rate constants of  $C_7H_{15}^+$  ions formed in 1% heptane in propane at 503 K for the following heptanes: (a) 2-methylhexane, (b) 2,2,3-trimethylbutane, (c) 3-ethylpentane, (d) *n*-heptane, (e) 2,4-dimethylpentane.



**Figure 3.** Pressure dependences of the decomposition rates of  $C_7$  carbonium ions plotted in Figure 2 at 537 K.

with increasing temperature. Sample Arrhenius plots illustrating the temperature dependences of these decomposition reactions at third body (propane) densities of  $1.6 \times 10^{16}$  and  $4.4 \times 10^{16}$  mol/cm<sup>3</sup> are shown in Figure 4. The Arrhenius activation energies obtained from the slopes of these plots are summarized in Table I. The activation energies are seen to increase with increasing bath gas pressure. Comparison with the calculated endothermicities of the decomposition reactions (Table I) shows that the Arrhenius activation energies are significantly lower than the endothermicities at both densities. This can be interpreted as further indication that the rate constants are below their high-pressure limit throughout our pressure range (see Discussion section).

**3. Effects of the Reactant Gas.** In order to establish that the reactions observed are indeed thermal unimolecular decomposition reactions, it is important to establish that the identity of the carrier gas does not effect substantially the decomposition process. Some effect of the carrier gas on the decomposition rates is expected, however, because of the different

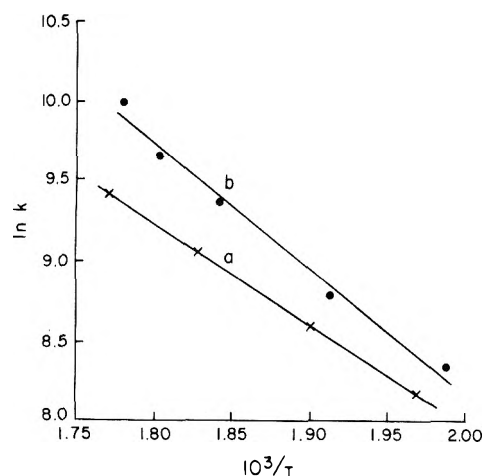


Figure 4. Arrhenius plots for the decomposition of the  $C_7H_{15}^+$  ion formed in a mixture of 1% 2-methylhexane in propane at a total particle density of (a)  $1.6 \times 10^{16}$  mol/cm<sup>3</sup> and (b)  $4.4 \times 10^{16}$  mol/cm<sup>3</sup>.

efficiencies of different bath gas molecules to activate the decomposing ions. To investigate the effect of the ionizing agent and bath gas we measured some decomposition rates of the heptyl ions generated from 2-methylhexane in  $N_2 + 10\%$  NO as carrier gas; in this mixture  $NO^+$  is the ionizing agent. We also made some qualitative observations in  $i-C_4H_{10}$ .

Fast ion mobility and consequent short ion residence times in the  $N_2 + NO$  carrier made quantitative measurements difficult. At 537 K, 2.5 Torr total pressure, we obtained a decomposition rate for the  $C_7H_{15}^+$  ion generated from 2-methylhexane of  $k = (15.0 \pm 3.0) \times 10^3 s^{-1}$ , as compared with  $10.4 \times 10^3 s^{-1}$  obtained for the same ion in propane. At 503 K,  $P = 1.0$  Torr we obtained in  $N_2 + NO$  for the same ion  $k = (5.5 \pm 2) \times 10^3$ , as compared with  $2.0 \times 10^3$  in propane. At 556 K,  $P = 2.5$  Torr,  $k = (16.3 \pm 5) \times 10^3$  in  $N_2 + NO$  compared with  $k = 18.0 \times 10^3$  in propane.

In  $i-C_4H_{10}$  as carrier gas, decomposition reactions yielding  $C_4H_9^+$  cannot be measured directly since the product ion is indistinguishable from the *tert*-butyl ions formed from  $i-C_4H_{10}$ . However, with partially deuterated 2-methylhexane in isobutane at 600 K we observed  $C_4D_nH_{9-n}^+$  ions whose isotopic distribution agreed with the isotopic distribution of

the  $C_7D_nH_{15-n}^+$  ions. Evidently decomposition reactions of the heptyl ions occur also with  $i-C_4H_{10}$  as the carrier gas.

Reaction 1, which generates the  $C_7H_{15}^+$  ions, is exothermic by 19–23 kcal/mol (depending on the  $C_7$  ion). The analogous reaction involving  $NO^+$  is exothermic by 14–18 kcal/mol; the analogous reaction involving the  $t-C_4H_9^+$  instead of  $C_3H_7^+$  is exothermic by 4–8 kcal/mol. The fact that the  $C_7H_{15}^+$  ions generated in all of these reactions decompose under similar conditions at similar rates indicates that the decomposing species are thermalized heptyl ions in each case.

4. *Decomposition of  $C_8$ – $C_{10}$  Carbonium Ions.* Although most of the work in the present study concerned  $C_7$  ions, it is of interest to see how molecular size effects the decomposition of carbonium ions. Experiments showed that decomposition of ions with six or less carbon atoms does not occur up to 600 K. However, decomposition is observed in all carbonium ions with seven or more carbon atoms. This observation is compatible with the experience of the ease of cracking of  $C_7$  and higher hydrocarbons in petroleum refining.

In the present study we observed decomposition of some  $C_8$ – $C_{10}$  carbonium ions in propane as carrier gas. The processes observed and some kinetic values obtained are shown in Table II. The sum of the decomposition rates of each of the ions into its products is similar to the rates observed for the decomposition of  $C_7$  ions. Pressure studies on the 2-methylheptyl ion showed that its decomposition rate increases linearly with bath gas density between 1.6 to 4.4 mol/cm<sup>3</sup>, i.e., the reaction is at its low pressure limit in this range. Temperature studies at  $(C_3H_8) = 1.6$  mol/cm<sup>3</sup> gave  $E_a = 16.7$  kcal/mol for its decomposition both to the *tert*-butyl and *tert*-pentyl ions. Neither pressure nor the temperature seemed to effect the ratio of the rates of the two decomposition reactions.

Our observations on the thermal decomposition of carbonium ions can be summarized by saying that all possible decomposition processes are observed, provided the ionic product is not smaller than  $C_4H_9^+$  and the neutral olefinic fragment is not smaller than  $C_3H_6$ .

## Discussion

The present study is aimed at the investigation of thermal unimolecular reactions. Variation of the bath gas produced some evidence that we are indeed observing the decomposition

TABLE I: Kinetic Parameters for the Decomposition of  $C_7$  Carbonium ions at 503 and 537 K

Reactant <sup>a</sup>	Product <sup>a</sup>	$k_{503}, 10^3 s^{-1} b$		$k_{537}, 10^3 s^{-1}$		$E_a, kcal/mol$		$\Delta H_f, kcal/mol^c$
		$[M]_l$	$[M]_h$	$[M]_l$	$[M]_h$	$[M]_l$	$[M]_h$	
1.		2.2	6.2	11.8	17.8	13.9		<sup>d</sup>
2.		2.8	4.2	6.0	10.6	12.9	15.6	23.0
3.		3.8	5.5	9.5	13.8	12.9	16.0	26.0
4.		5.2	11.7	11.1	24.2	12.0		25.6
5.		0.9	3.0		8.8		16.0	29.5

<sup>a</sup>The structures shown are the ions corresponding to the  $C_7$  hydrocarbon from which they were produced by reaction 1. The actual structure of the decomposing and product ions and neutral species is not known. <sup>b</sup> $M_l$  and  $M_h$  indicate the lower ( $1.6 \times 10^{16}$  mol/cm<sup>3</sup>) and higher ( $4.4 \times 10^{16}$  mol/cm<sup>3</sup>) propane bath gas densities at which these rate constants were obtained. <sup>c</sup> $\Delta H_f$  calculated for the reactant ions shown in column 2 and products in column 3.  $\Delta H_f$  for the heptyl ions was obtained from M. Meot-Ner and F. H. Field, unpublished results;  $\Delta H_f$  = 169.1 and  $\Delta H_f$  = 4.9 kcal/mol were used.

<sup>d</sup>Accurate value for  $\Delta H_f$  () is not known; also, the decomposing ions are possibly rearranged, tertiary structures.

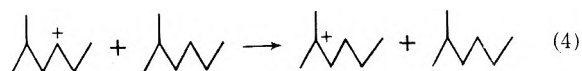
TABLE II: Decomposition Reactions of Some  $C_8$ – $C_{10}$  Carbonium Ions

Reactant <sup>a</sup>	Products	$k_{503}^b$ $10^3 \text{ s}^{-1}$	$k_{571}^b$ $10^3 \text{ s}^{-1}$
	$C_4H_9^+ + C_4H_8$		4.3
	$C_5H_{11}^+ + C_3H_6$		5.7
	$C_4H_9^+ + C_4H_8$	1.8	5.7
	$C_5H_{11}^+ + C_3H_6$	1.8	5.7
	$C_4H_9^+ + C_5H_{10}$	1.4	3.7
	$C_5H_{11}^+ + C_4H_8$	2.5	5.7
	$C_6H_{13}^+ + C_3H_6$	2.0	2.9
	$C_4H_9^+ + C_6H_{12}$		1.5
	$C_5H_{11}^+ + C_5H_{10}$		1.8
	$C_6H_{13}^+ + C_4H_8$		2.3

<sup>a</sup>The structures shown indicate the structure of the hydrocarbon from which the ion was derived. The actual structures of the ions are not known. <sup>b</sup> $(C_3H_8) = 1.6 \times 10^{16} \text{ mol/cm}^3$ .

of thermal ions. Here we shall present some further arguments to this effect.

Our kinetic plots, as shown in Figure 1, are based on ions which reside in the source 50–200  $\mu\text{s}$  after the incidence of the ionizing electron beam. The lower limit of third-body densities in our experiments is  $\approx 10^{16} \text{ mol/cm}^3$ . With ion–molecule collision rates on the order of  $10^{-9} \text{ cm}^3/\text{mol s}$ , a heptyl ion will have undergone 500 or more collisions with propane molecules before decomposition. This should be more than sufficient to dissipate the excess energy imparted to the heptyl ions in the ionizing reaction 1. Also, if secondary, rather than tertiary heptyl ions are generated in reaction 1, they would have undergone 10–100 collisions with the parent heptane compound in 50  $\mu\text{s}$ . Judging by existing knowledge of the relation between exothermicity and reaction rate in  $H^-$  transfer in hydrocarbons,<sup>7</sup> bimolecular hydride transfer from secondary to tertiary positions of the type



which is exothermic by  $\approx 15 \text{ kcal/mol}$ ,<sup>6</sup> should proceed near unit efficiency. The decomposing ions must therefore be tertiary heptyl ions.

The structure of the decomposing ions cannot be identified by our mass spectrometric technique. Some hints concerning the structures of the ions may be, however, inferred from the kinetic data. The fact that the decomposition kinetics of  $(M-1)^+$  ions obtained in our study from  $n$ -alkanes is not much different from the decompositions of tertiary ions (obtained in our study from the hydrocarbons containing tertiary hydrogens) indicates that the secondary ions have probably also rearranged to tertiary structures before decomposing. Such rearrangements are well known in solution. The isomeric identity of the decomposing tertiary ions is not known. It is quite possible that rearrangements proceed with rates comparable to or larger than decomposition and the structures of the ions do not always correspond to the original heptane. In

fact, decomposition of the 3-ethylpentyl ion to a *tert*-butyl ion and propane certainly requires skeletal rearrangements. If decomposition by fission  $\beta$  to the charge is assumed, skeletal rearrangement of all but the 2-methylhexyl ions is necessary. These rearrangements may precede or be concerted with the decomposition process. Gaumann et al.<sup>7</sup> have studied the loss of propane from energetic 1-heptyl ions and found evidence for extensive rearrangement possibly with ring formation in the process.

The results of Figures 1–4 and Table I show that the decomposition rates and pressure dependencies are not identical for all  $C_7$  ions, and consequently, that all ions did not rearrange to a common species prior to fragmentation. However, the decomposition rates and, in particular, activation energies are very similar for all isomers and it is possible that the decomposition process itself proceeds through a common intermediate. In this case, the differences in decomposition kinetics reflect the differences in the rate the different isomers reach this common intermediate. Studies with labeled compounds should be helpful to decide these questions.

A quantity of major interest in unimolecular reactions is the energy barrier for the reaction. Experimentally this may be measured by the activation energy at the high pressure limit  $E_a^\infty$ . Unfortunately, however, the Arrhenius activation energy at low pressures, to which our experiments are limited,  $E_a^\circ$ , is smaller than the energy barrier because of the role of activation from internal degrees of freedom. For example, the Kassel expression connecting the two quantities is<sup>8</sup>

$$E_a^\circ = E_a^\infty - (s-1)kT \quad (5)$$

where  $s$  is the total number of oscillators in the decomposing molecule; in practice,  $s$  is only a fraction of this number. Although the limitations of Kassel's equation are well known, it gives a measure of the order of magnitude of the effect of activation from internal degrees of freedom. In our case, the total number of internal degrees of freedom is  $3N-6=60$ ;  $60RT$  at 500 K is 60 kcal/mol, so that the measured value of  $E_a^\circ = 13 \text{ kcal/mol}$  may correspond to an energy barrier of up to 73 kcal/mol. In any event, our measured values of  $E_a^\circ$  are significantly smaller than the energy barriers for decomposition, which are equal at least to the endothermicities of the decomposition processes, i.e., 23–30 kcal/mol.

## Conclusions

Gaseous carbonium ions  $C_nH_{2n-1}^+$  are observed to undergo, between 480 and 600 K, thermal decomposition to form smaller carbonium ions with the loss of an olefin  $C_mH_{2m}$ .

Reactions occur if and only if the fragment ion is  $C_4H_9^+$  or larger and the neutral olefinic product is  $C_3H_6$  or larger; all reactions obeying these conditions are observed. The kinetics exhibit behavior characteristic of unimolecular decomposition in neutral molecules: the rate constant decreases at low pressures; the Arrhenius activation energy is smaller than the energy barrier for the reaction; and the activation energy increases with increasing pressure.

Extension of the study of thermal unimolecular reactions to ions offers several benefits. Since the concentration of the ions and of their decomposition products is very small, many kinetic complications common in pyrolysis studies are avoided. Because of the facility of data acquisition by mass spectrometry, the collection of large amounts of data is possible. This should help to clarify structure–reactivity correlations, to examine the value of theoretical models, and to

measure efficiencies of energy transfer processes from various bath gases. It is especially important that these studies be extended to higher pressures to obtain  $E_a^\infty$  and the energy barriers to the decomposition of gaseous ions, since this is a quantity of great importance in ion chemistry.

**Acknowledgments.** This research was supported in part by a grant from the National Science Foundation. We thank Mr. R. Ciccarone for performing many of the measurements reported in this paper.

## References and Notes

- (1) P. J. Robinson and K. A. Holbrook, "Unimolecular Reactions", Wiley-Interscience, London, 1972.
- (2) F. H. Field, *J. Am. Chem. Soc.*, **91**, 2827 (1969).
- (3) (a) J. J. Solomon, M. Meot-Ner, and F. H. Field, *J. Am. Chem. Soc.*, **96**, 3727 (1974); (b) Detailed description is given in M. Meot-Ner, Ph.D. Thesis, The Rockefeller University, New York, N.Y., 1975.
- (4) M. Meot-Ner and F. H. Field, *J. Chem. Phys.*, **64**, 277 (1976).
- (5) P. Ausloos and S. G. Lias in "Ion-Molecule Reactions", Vol. II, J. L. Franklin, Ed., Plenum Press, New York, N.Y., 1972, p 707.
- (6) F. P. Lossing, private communication.
- (7) A. Fiaux, B. Wirtz, and T. Gausmann, *Helv. Chim. Acta*, **57**, 525 (1974).
- (8) R. P. Wayne, in "Comprehensive Chemical Kinetics", C. H. Bamford and D. F. H. Tipper, Ed., Elsevier, New York, N.Y., 1969, p 270.

## Consistency between Kinetics and Thermodynamics

M. Boudart

Department of Chemical Engineering, Stanford University, Stanford, California 94305 (Received February 6, 1976)

If an expression is known or postulated for the rate of a chemical reaction in the forward direction, what are the thermodynamic restrictions on the form of the rate expression for the reverse direction? Is there a relationship between rate constants in both direction and the equilibrium constant of the reaction? This question has been considered by a number of authors<sup>1-6</sup> but perhaps with a lack of generality or rigor. The purpose of the present note is to take advantage of work by Temkin<sup>7,8</sup> that bears directly on this problem to clarify a situation which is of great practical interest.

Consider a sequence of  $s$  steps, open or closed, the sum of which represents a stoichiometric equation for reaction proceeding at a net rate  $r$ . If the rate of each step is denoted by  $r_i$  in the forward direction and by  $r_{-i}$  in the reverse direction, with  $i = 1, 2, \dots, s$ , we can write the identity:

$$(r_1 - r_{-1})r_2r_3 \dots r_s + r_{-1}(r_2 - r_{-2})r_3 \dots r_s + r_{-1}r_2(r_3 - r_{-3}) \dots r_s + \dots + r_{-1}r_2r_3 \dots (r_s - r_{-s}) = r_1r_2r_3 \dots r_s - r_{-1}r_{-2}r_{-3} \dots r_{-s} \quad (1)$$

At the steady state, we may write

$$r_i - r_{-i} = \chi_i r \quad (i = 1, 2, \dots, s) \quad (2)$$

where  $\chi_i$  is the stoichiometric number of step  $i$ .<sup>6</sup>

Substitution of (2) into (1) yields Temkin's general equation for the rate of a single reaction at the steady state:

$$r = \frac{r_1r_2r_3 \dots r_s - r_{-1}r_{-2}r_{-3} \dots r_{-s}}{\chi_1r_2r_3 \dots r_s + r_{-1}\chi_2r_3 \dots r_s + \dots + r_{-1}r_{-2} \dots \chi_s} \quad (3)$$

If any step from left to right is irreversible ( $r_{-i} = 0$ ), the reaction is proceeding irreversibly from left to right at a rate  $r = \bar{r}$ . Similarly, if any step is irreversible when it proceeds from right to left ( $r_i = 0$ ), then  $r = \bar{r}$ . From (3), we get then

$$\bar{r} = (r_1r_2r_3 \dots r_s)/P \text{ and } \bar{r} = (r_{-1}r_{-2}r_{-3} \dots r_{-s})/P \quad (4)$$

where  $P$  is the denominator of eq 3. Thus

$$\bar{r}/\bar{r} = \prod_{i=1}^s r_i/r_{-i} \quad (5)$$

Now, for every elementary process and its reverse which have rates  $r_i$  and  $r_{-i}$  amenable to the equilibrium formulation of transition state theory, we can write:

$$r_i/r_{-i} = \exp(A_i/RT) \quad (6)$$

where  $A_i$  is the affinity of step  $i$  in the forward direction, equal to  $-\Delta G_i$ , the Gibbs free energy of reaction.

With (6), (5) becomes

$$\bar{r}/\bar{r} = \exp\left(\sum_{i=1}^s A_i/RT\right) \quad (7)$$

Now, the average stoichiometric number of the reaction  $\bar{\chi}$  is defined, following Temkin,<sup>7</sup> as

$$\bar{\chi} = \sum_{i=1}^s \chi_i A_i / \sum_{i=1}^s A_i = A / \sum_{i=1}^s A_i \quad (8)$$

where  $A$  is the total affinity for the overall reaction

$$A = \sum_{i=1}^s \chi_i A_i \quad (9)$$

I have shown elsewhere<sup>6</sup> that  $\bar{\chi}$  retains its meaning at equilibrium.

Substitution of (8) into (7) yields the relation equivalent to (6) but applicable to a single reaction instead of an elementary step:

$$\bar{r}/\bar{r} = \exp(A/\bar{\chi}RT) \quad (10)$$

It must be noted that  $\bar{\chi}$  depends on composition and, therefore, may change with extent of reaction. If there exists a rate-determining step (subscript  $l$ ) so that  $A_i \approx 0$  except for  $i = l$ , it is clear that  $\bar{\chi} = \chi_l$ , and eq (10) becomes

$$\bar{r}/\bar{r} = \exp(A/\chi_l RT) \quad (11)$$

whereas eq 5 simplifies to

$$\bar{r}/\bar{r} = r_l/r_{-l} \quad (12)$$

since  $r_i \approx r_{-i}$  except for  $i = l$ . Equation 11 due to Horiuti<sup>2</sup> is a particular case of Temkin's eq 10.

There is little incentive to go beyond the statements of eq 10 and 11. Both express, with rigor and generality, the expected consistency between thermodynamic requirements and kinetic formalisms. Indeed since  $r = \bar{r} - \tilde{r}$  or  $r = \tilde{r}[1 - (\bar{r}/\tilde{r})]$ , we must have for any acceptable rate law:

$$r = \tilde{r}[1 - \exp(-A/\bar{\chi}/RT)] \quad (13)$$

The expression between brackets can be considered as a thermodynamic potential factor.<sup>9</sup>

However, because of previous results in the literature, it is useful to show that, with certain reasonable assumptions, eq 10 gives

$$\bar{k}/\tilde{k} = K^{1/\bar{\chi}} \quad (14)$$

where  $K$  is the equilibrium constant of the overall reaction and  $\bar{k}$  and  $\tilde{k}$  are suitably defined, overall rate constants for the forward and reverse rates of the single reaction. Indeed, from thermodynamics

$$A = A^\circ - RT \ln \prod_{j=1}^c (B_j)^{\nu_j} \quad (15)$$

where  $A^\circ$  is the standard affinity for the reaction

$$0 = \sum_{j=1}^c \nu_j B_j \quad (16)$$

where  $\nu_j$  is the stoichiometric coefficient of component  $B_j$  in the stoichiometric equation for reaction between  $c$  components, counted as positive for a product and negative for a reactant. The concentration of  $B_j$  in the thermodynamically ideal system is  $(B_j)$ . Besides

$$A^\circ = RT \ln K \quad (17)$$

Substitution of (15) and (17) into (11) gives

$$\tilde{r}/\bar{r} = \left[ K \prod_{j=1}^c (B_j)^{-\nu_j} \right]^{1/\bar{\chi}} \quad (18)$$

Now, let us assume, as is found frequently in catalytic reactions, that  $\tilde{r}$  and  $\bar{r}$  can be expressed as follows:

$$\tilde{r} = \tilde{k} \prod_{j=1}^c (B_j)^{\tilde{\alpha}_j} / \varphi \quad (19)$$

$$\bar{r} = \bar{k} \prod_{j=1}^c (B_j)^{\bar{\alpha}_j} / \varphi \quad (20)$$

where  $\tilde{k}$  and  $\bar{k}$  are functions of temperature only,  $\tilde{\alpha}_j$  and  $\bar{\alpha}_j$  are orders of reaction which may be positive, negative, or zero.

The function  $\varphi$ , like the polynomial  $P$  of eq 4, may be a function of both temperature and concentration.

Then, eq 18 becomes, with substitution of (19) and (20)

$$(\tilde{k}/\bar{k}) \prod_{j=1}^c (B_j)^{\tilde{\alpha}_j - \bar{\alpha}_j} = K^{1/\bar{\chi}} \left[ \prod_{j=1}^c (B_j)^{-\nu_j} \right]^{1/\bar{\chi}} \quad (21)$$

Now on the left-hand side,  $\tilde{k}/\bar{k}$  is a function of temperature only, while the product is a function of concentrations only if the orders of reaction are "good" orders, i.e., they do not depend on temperature. On the right-hand side,  $K^{1/\bar{\chi}}$  depends only on temperature, at least in a field of compositions where  $\bar{\chi}$  is approximately constant, whereas the product depends only on composition, at least if  $\bar{\chi}$  is a "good" average stoichiometric number, i.e., is independent of temperature.

Therefore:

$$(\tilde{k}/\bar{k})(K^{-1/\bar{\chi}}) = \prod_{j=1}^c (B_j)^{[-(\nu_j/\bar{\chi}) - \tilde{\alpha}_j + \bar{\alpha}_j]} = \text{constant} \quad (22)$$

where the constant is a pure number which must be unity, since for (22) to be true for arbitrary values of the independent concentrations, all exponents of the concentrations must be equal to zero. Hence, we can write eq 14 within the approximations mentioned. This is the general form of a relation which many authors have written in different ways, as an expression of the consistency requirement between kinetics and thermodynamics. Its obtention from Temkin's general equation in the form of (18) is trivial. Nevertheless, it may clarify some obscure or less general statements in the literature.<sup>1-6</sup> If the system is thermodynamically nonideal, all concentrations should be replaced by activities and  $\tilde{k}/\bar{k}$  may now contain some activity coefficients of transition states which are composition dependent but only slightly so compared to the exponential temperature dependence of the rate constants. Thus within that additional approximation, the result expressed by eq 14 above remains valid.

## References and Notes

- (1) K. G. Denbigh, "The Principles of Chemical Equilibrium", University Press, Cambridge, 1961, p 442.
- (2) J. Horiuti, *J. Catal.*, **1**, 199 (1962).
- (3) E. H. Blum and R. Luus, *Chem. Eng. Sci.*, **19**, 322 (1964).
- (4) R. Aris, "Elementary Chemical Reactor Analysis", Prentice Hall, Englewood Cliffs, N.J., 1969, p 56.
- (5) P. Van Rysselberghe, *Chem. Eng. Sci.*, **22**, 706 (1967).
- (6) M. Boudart, in "Physical Chemistry: An Advanced Treatise", Vol. 7, H. Eyring, W. Jost, and D. Henderson, Eds., Academic Press, New York, N.Y., 1975, Chapter 7, p 353.
- (7) M. I. Temkin, *Dokl. Akad. Nauk SSSR*, **152**, 153 (1963).
- (8) M. I. Temkin, *Int. Chem. Eng.*, **11**, 709 (1971).
- (9) J. Happel, *Catal. Rev.*, **6**, 221 (1972).



## Terminal Ions in Weak Atmospheric Pressure Plasmas. Applications of Atmospheric Pressure Ionization to Trace Impurity Analysis in Gases

M. W. Siegel and W. L. Fite\*

Extranuclear Laboratories, Incorporated, Pittsburgh, Pennsylvania 15238 (Received July 26, 1976)

Publication costs assisted by Extranuclear Laboratories Incorporated

The realization that terminal ion spectra in a weak plasma are often dominated by ions characteristic of minute trace impurities has led to the development of atmospheric pressure weak plasma ion sources for mass spectrometry (API-MS). In addition to their application in analytical tasks, these ion sources may prove useful in the study of ion-molecule reactions at high pressure. The quiescent ion spectrum in an API-MS employing a  $^{63}\text{Ni}$   $\beta$ -ray primary ionization source interfaced to a positive/negative ion mass spectrometer system is discussed for the cases of  $\text{N}_2$ , Ar, and air as carrier gases. The effects of carrier gas impurities, especially  $\text{H}_2\text{O}$ , are discussed and demonstrated experimentally. The API source is modeled in terms of engineering parameters and the rate constants for charge transferring processes, electron attachment, and recombination. The model is shown to predict quiescent spectra in agreement with experimental results. Response as an analytical detector for trace sample species is modeled, and the model found to agree with experimental results with respect to sensitivity and dynamic range. Illustrative data are presented and discussed for response to  $\text{SF}_6$ , Freons 11, 12, 13, 21, 22, and 23, vinyl chloride ( $\text{HC}=\text{CCl}$ ), NO, and  $\text{SO}_2$ . By the exponential dilution technique calibrated sensitivities to the 10 ppt level are demonstrated for appropriately responding species. This limit is shown to be set by wall retention and desorption in the dilution vessel, and sub part-per-trillion sensitivity may be extrapolated in the absence of these effects. Preliminary data obtained with a gas chromatograph-atmospheric pressure ionizer-mass spectrometer system are presented and discussed.

### I. Introduction

In a weak plasma formed in an appropriately inert carrier gas, the direction of ion-molecule reactions between primary ions and trace impurities is often toward terminal ions characteristic of the trace impurities rather than the major component. Thus in nominal "ultra high purity"  $\text{N}_2$  or Ar, virtually all of the positive ions are accounted for by  $\text{H}_2\text{O}^+$ ,  $\text{H}_3\text{O}^+$ ,  $\text{NO}^+$ ,  $\text{O}_2^+$ , and their clusters with  $\text{H}_2\text{O}$  and  $\text{N}_2$  or Ar; also a portion of the negative charge is usually carried by  $\text{O}_2^-$  and  $\text{Cl}^-$  in preference to thermal electrons. Only extensive in situ cleaning of the carrier gas, along with high temperature bakeout of the gas handling system and the plasma confining walls, can reduce the impurity content, of which water is usually the major offender, to a sufficiently low level that the primary (major gas component) ions and their clusters can be seen.

This sensitivity to trace contaminants suggests that a weak plasma in an appropriately cleaned inert gas at atmospheric pressure will be a highly efficient region in which to ionize trace constituents for analytical mass spectrometric detection.<sup>1</sup> A virtue of keeping the plasma relatively weak, as by using a  $\beta$ -radioactive source rather than an electrical discharge for the primary ionization, is that the ion density can be small enough to be comparable to part-per-trillion impurity molecule densities, so that even when only low level impurities are present, impurity molecule ions dominate the terminal ion spectrum. When interesting species present in only trace concentration in the neutral fraction comprise essentially the total population in the ionized fraction interpretation of trace effects is obviously simplified.

In comparison with low pressure electron impact ion sources, a high pressure plasma ion source is selective rather than universal, the ionization efficiency for a given component of a mixture depending on the major species and often deli-

cately on the trace components as well. Trace species may form negative ions by attachment of thermal electrons, or by charge-transferring reactions with uninteresting impurity negative ions (e.g.,  $\text{O}_2^-$ ), or they may form positive ions by successfully competing directly or indirectly with the uninteresting impurity species (e.g.,  $\text{H}_2\text{O}$ ) for the available positive charge. Since many species of atmospheric, environmental, and biological interest are interesting precisely because they are strong electron acceptors or strong proton acceptors, the terminal ion spectrum will be dominated by those species whose neutral precursors are interesting rather than merely numerous.

The efficiency (ions out per sample molecule in) of an atmospheric pressure ionizer with the appropriate combination of carrier and trace sample is easily shown to be very nearly equal to the ratio of the rate constant for trace molecule ionization (by ion-molecule reactions) to the rate constant for neutralization of the resulting ion (by recombination).<sup>2,3</sup> This ratio is typically of the order of  $10^{-3}$ , but in selected cases might be as high as  $10^{-1}$ . The numerical result is practically independent of engineering details, which in lower pressure devices effectively limits efficiency by increasing the relative importance of technical loss mechanisms such as sample pumpout before ionization and ion diffusion to walls before extraction. Furthermore, this efficiency, being limited by the nature of the rate constants rather than by engineering details, is probably the best that can be obtained in any realistic number density sensitive ionizer, and is certainly the best that can be obtained in any true plasma ion source.

For these reasons atmospheric pressure ionization (API) sources for mass spectrometry have recently been developed by several groups, including Horning et al.,<sup>1,4-8</sup> Reid et al.,<sup>9</sup> Harden et al.,<sup>10,11</sup> and ourselves.<sup>2,3,12,13</sup> Sensitivities approaching  $10^{-16}$  mol for batch samples and approaching 1 part

in  $10^{12}$  for gas phase trace components have been demonstrated. These results are in good agreement with the theoretical net ionization efficiency of  $10^{-3}$  when combined with an instrument efficiency of  $10^{-3}$  for extraction, mass analysis with adequate resolution, and detection, the latter factor being close to a realistic engineering limit.<sup>2</sup>

Carrier gases which have received the most attention to date are  $N_2$ , Ar, air, and various mixtures of interest for reasons relevant to gas chromatography and chemical ionization techniques. Most of our effort has been devoted to  $N_2$ , which is the only one sufficiently inexpensive at reasonable purity (because it is available as liquid  $N_2$  boiloff) that it is practical to use at large flow rates for continuous periods of several weeks, the time scale required for ultimate removal of internally adsorbed impurity materials. In contrast to other workers, we have, by rigorous attention to these time-consuming cleaning procedures, succeeded in observing the primary ion spectra under conditions where the total ion density is the order of  $10^8 \text{ cm}^{-3}$  at atmospheric pressure. This ion concentration (per unit gas density) is only two to three orders of magnitude larger than in the natural ionosphere.

Most of the specific data discussed herein concerns those results in an  $N_2$  carrier. We also briefly discuss results with Ar, used primarily to check the correctness of proposed cluster identifications and because of its applications in gas chromatography, and air, used to gain some preliminary impressions about the prospects for eventual applications of API-MS to direct atmospheric monitoring.

## II. Kinetics of Quiescent and Responding States

In a really pure carrier gas which does not form negative ions, the quiescent state of the ionization chamber plasma in an API source consists of an equilibrium distribution of carrier gas ions and a thermal electron cloud. The qualifying assumptions which go with this statement are that the gas transit time through the ionization volume is long compared to the equilibration time for the relevant ion-molecule reactions, and that there are no strong electric fields in the ionization volume. These conditions are satisfied in the first instance by practical ion source volumes ( $10 \text{ mm}^3$ – $1 \text{ cm}^3$ ) and practical gas flow rates into fast but not heroic vacuum pumps, and in the second instance by gentle ionization sources, such as low energy  $\beta$ -radiation at 1–10 mCi activity. They exclude the case of atmospheric pressure ionization via a corona discharge, as discussed by Carroll et al.,<sup>8</sup> where the intense ionization rate may be valuable for certain analytical problems, but where the strong fields employed mean that nonequilibrium ion distributions are observed.

The atmospheric pressure ionization device, some of whose engineering details are discussed below, can for present purposes be thought of as an atmospheric pressure gas volume containing a radioactive source of a sufficiently gentle nature that all of the ionizing radiation energy is dissipated in the gas volume. An appropriate choice is  $^{63}\text{Ni}$ , with a 66-keV (maximum energy)  $\beta$  ray and no  $\gamma$ . Sample material is supplied to the ionization volume in a carrier gas whose optimum choice depends in part on the specific sample material of interest. Nitrogen is a good general choice. Carrier gas, un-ionized sample material, and the terminal ions flow from the ionization volume via a sampling aperture into a suitable vacuum system containing the ion mass analysis apparatus.

The expected total ion density, more-or-less independent of mass spectral details, is determined by the radioactive source activity, the geometry, and the values of positive ion-electron and positive ion-negative ion recombination rates.

A detailed discussion applicable to the present apparatus has been recently given elsewhere.<sup>3</sup> We repeat only the principal points. The 1-mCi  $^{63}\text{Ni}$  source produces about  $2 \times 10^{11}$  ion pairs  $\text{s}^{-1} \text{ cm}^{-3}$ . This ion production rate is balanced by ion loss rates for gas flow ( $F \approx 0.3 \text{ cm}^3 \text{ s}^{-1}$ ), diffusion ( $D \approx 0.1 \text{ cm}^2 \text{ s}^{-1}$ ), and recombination ( $R_0 \approx 10^{-6} \text{ cm}^3 \text{ s}^{-1}$ ). Dissociative recombination rates between positive ions and electrons are about the same order of magnitude as phenomenological two-body rates for three-body positive ion-negative ion recombination at atmospheric pressure, these being an order of magnitude larger than direct mutual neutralization between positive and negative ions.<sup>14</sup> Thus it is often possible to drastically simplify the solution of complicated sets of rate equations by assuming, as a sufficiently good approximation, a single "universal" recombination rate constant of about  $10^{-6} \text{ cm}^3 \text{ s}^{-1}$ .

The quiescent state rate equations for ion and electron density where only one type of primary ion is made and there is no negative ion are simply

$$\frac{dn_+}{dt} = S - \frac{F}{V}n_+ - \frac{D_+}{r_0^2}n_+ - R_0n_+n_e \quad (1a)$$

and

$$\frac{dn_e}{dt} = S - \frac{F}{V}n_e - \frac{D_e}{r_0^2}n_e - R_0n_+n_e \quad (1b)$$

where  $S$  is the above  $2 \times 10^{11} \text{ cm}^{-3} \text{ s}^{-1}$  source function,  $V$  is the source volume ( $\approx 0.1 \text{ cm}^3$ ), and  $r_0$  is a characteristic length ( $\approx 0.2 \text{ cm}$ ) determined by the geometry of the active volume. Naïve solution of these two equations on the assumption that  $D_+$  and  $D_e$  are characteristic of electrostatically free ions and electrons indicates that as a result of the assumed more rapid diffusion of electrons the positive ion density is several hundred times the thermal electron density. However, the numerical size of the individual densities is sufficiently large that we can conclude that plasma effects are important (the Debye length<sup>15</sup> is small compared to the source dimensions), so that diffusion is ambipolar with both positive ions and electrons characterized by an effective diffusion constant  $D_A \approx 2D_+$ ,<sup>16</sup> and the positive ion density must be approximately equal to the electron density.

Under these conditions the equilibrium ion and electron densities are easily shown to be only weakly influenced by the flow and diffusion rates, being effectively given by

$$n_0 \approx \sqrt{S/R_0} \quad (2)$$

which evaluates to about  $4 \times 10^8 \text{ cm}^{-3}$ . The flow "loss" of approximately  $10^8 \text{ s}^{-1}$  of either sign is, of course, the current of either sign into the mass spectrometer vacuum. This theoretically estimated current, about  $10^{-11} \text{ A}$ , is confirmed by total current measurements in vacuo.

The total charge density of either sign is determined, under constant primary ionization rate conditions, by the relevant recombination rate, and shows the expected small but systematic dependence on the nature of the negative charge carriers, i.e., electrons or negative ions. Since positive ion-electron recombination rates are systematically about an order of magnitude larger than positive ion-negative ion recombination rates, the total charge density of either sign should and does increase by about a factor of 3 when passing from the electron-dominated to negative-ion-dominated (saturated) regimes. This effect is somewhat enhanced by the increased diffusion rate (by a factor of 2) in the electron-dominated limit as compared to the negative-ion-dominated limit.

In the presence of trace impurities, the primary ions and

electrons may rapidly transfer their charge to the impurities, forming characteristic positive or negative ions, or both. In the approximation that total charge density of either sign remains relatively constant independent of spectral details (i.e., that there is a "universal" recombination rate) the positive or negative sample ion densities formed in one-step processes are determined by the rate equations

$$dn_A^+/dt = A_+(n_0 - n_A^+)n_A - R_0n_A^+n_0 \quad (3a)$$

or

$$dn_A^-/dt = A_-(n_0 - n_A^-)n_A - R_0n_A^-n_0 \quad (3b)$$

where  $n_0$  is the nearly constant charge density ( $\sqrt{S/R_0}$  above),  $n_A$ ,  $n_A^+$ , and  $n_A^-$  are densities of neutral, positive ion, and negative ion sample species, and  $A_+$  and  $A_-$  are the rate constants for positive and negative ion formation from sample molecules.

The steady state solutions are

$$n_A^\pm = \frac{A_\pm}{R_0} n_A \left( 1 + \frac{A_\pm n_A}{R_0 n_0} \right)^{-1} \quad (4a)$$

which it is convenient to expand as

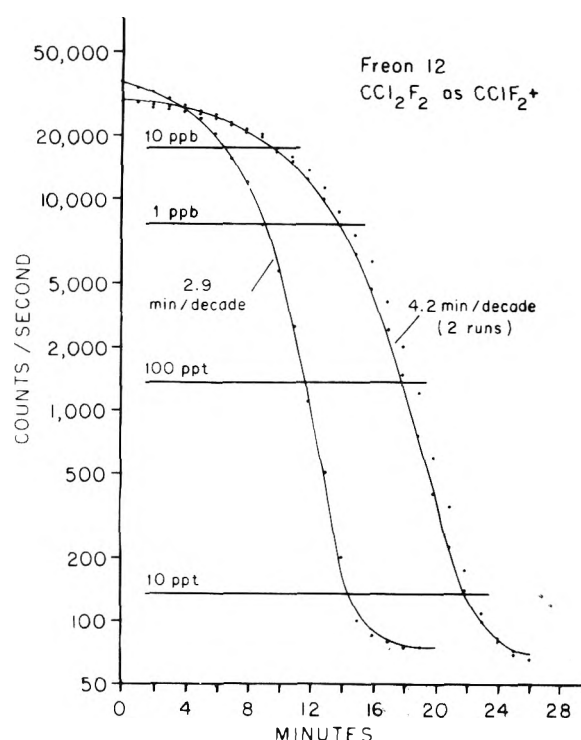
$$n_A^\pm = \frac{A_\pm}{R_0} n_A \left( 1 - \frac{A_\pm n_A}{R_0 n_0} + \left( \frac{A_\pm n_A}{R_0 n_0} \right)^2 - \dots \right) \quad (4b)$$

Since typical ion-molecule and effective electron attachment rates for strongly responding sample materials are of the order of  $10^{-9} \text{ cm}^3 \text{ s}^{-1}$ , the ratio  $A_\pm/R_0$  is the order of  $10^{-3}$ . For small impurity concentrations it follows that  $n_A^\pm/n_A \approx 10^{-3}$ . This ratio of sample ion-to-sample molecule density is essentially the ratio of ion lifetime against recombination to neutral lifetime against ionization, and is thus the best that can be obtained in a plasma ion source. Despite the simplicity of this derivation, we find that it is frequently not appreciated that in the small sample regime the "sensitivity" of a plasma ion source is practically independent of the reactant ion density; any change in ionization rate is exactly cancelled by a corresponding change in recombination rate.

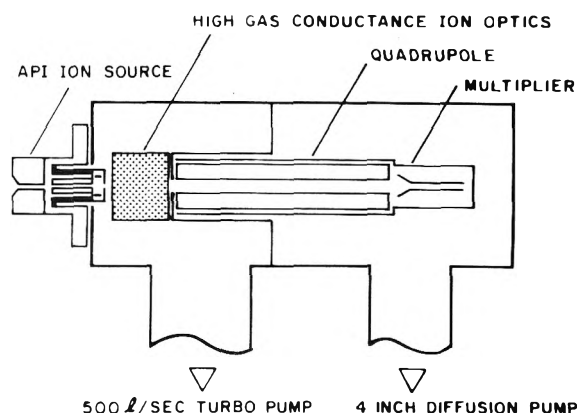
What the reactant ion density does determine is the range of validity of the linear response approximation, i.e., the dynamic range of the ion source. Using the numerical parameters of this example, a 10% deviation from linearity is expected with  $(n_A/n_0) \approx 10^2$ , corresponding to a sample molecular concentration at atmospheric pressure of about 1 ppb. Figure 1 shows experimental results confirming this expectation. The sample is  $\text{CCl}_2\text{F}_2$  (Freon 12) introduced into an exponential dilution flask at an initial concentration of 1 ppm. Response (as the ion  $\text{CClF}_2^+$ ) is shown at two flow rates, i.e., two dilution time constants. It is seen that response is practically saturated above a few parts per billion and becomes approximately linear below a few hundred part per trillion. Below 10 ppt the response falls off anomalously slowly with time, this effect probably being due to slow desorption of sample adsorbed on the dilution vessel and tubing walls. Details of this experimental technique are discussed in section IV.1.

### III. Apparatus

Figure 2 is a schematic diagram of the atmospheric pressure ionization mass spectrometer. This apparatus is functionally similar to an earlier one previously described in detail.<sup>2,3</sup> The API source was originally designed for chemical analysis of trace organic materials in microliter solvent aliquots by direct syringe injection and vaporization in the ionization volume.<sup>1</sup> To facilitate the present set of experiments a 1-l dilution flask



**Figure 1.** Exponential dilution signal obtained from Freon 12 ( $\text{CCl}_2\text{F}_2$ ) sample observed as  $\text{CClF}_2^+$ . Shown with two dilution time constants (2.9 min/decade and 4.2 min/decade). Carrier gas is  $\text{N}_2$  at  $200^\circ \text{C}$ .



**Figure 2.** Schematic diagram of atmospheric pressure ionization mass spectrometer system. The first vacuum stage (ion optics) normally operates at  $4 \times 10^{-4}$  Torr with a 50- $\mu\text{m}$  diameter aperture in the API source. The second vacuum stage (mass analysis) normally operates at  $2 \times 10^{-6}$  Torr.

has been placed in the carrier gas line. Sample gas may thus be introduced to the carrier stream at an initial part-per-million level and effectively observed to the fractional part-per-trillion level by exponential decay with a time constant the order of 100 s. An additional direct gas mixing inlet in the API source is now used for connection of a gas chromatograph.

Carrier gas is supplied to the API in excess at slightly above atmospheric pressure, and allowed to overflow to the laboratory atmosphere, thereby permitting dynamic sealing and essentially constant pressure operation at various total flow rates. A pinhole aperture (typically 25–50  $\mu\text{m}$  in diameter) connects the ionization volume to the first vacuum stage, held at approximately  $3 \times 10^{-4}$  Torr when loaded by the gas flow of approximately  $0.3 \text{ atm cm}^3/\text{s}$ . At this intermediate pressure the ion-molecule mean free path is large enough (a few cen-

timeters) that electrostatic optics can efficiently separate the ions from the gas jet, and focus them through a differential pumping aperture into the mass filter in the second vacuum stage. The mass filter and particle multiplier-type detector are maintained by the second stage pump at about  $2 \times 10^{-6}$  Torr during normal operation.

The ionization chamber is a bullet shaped volume approximately 4 mm in diameter and 3 mm long, conically tapered for an additional 1 mm to meet the pinhole aperture. The chamber is machined in a self-gasketing copper disk, then gold plated. To minimize periodic cleaning problems and the possibility of radioactive contamination buildup, this part is disposable. The  $^{63}\text{Ni}$  is plated on one side of a  $50\text{ }\mu\text{m}$  thick  $\times 2.5\text{ mm} \times 6\text{ mm}$  platinum foil,<sup>17</sup> and the foil rolled into a "C" to fit the chamber. The inlet end of the chamber is a precision bore quartz capillary tube coated on the end with gold (by the resin bonding technique<sup>18</sup>). This design allows the ionization chamber to float electrically while still safely accepting a variety of grounded sample insertion devices, including syringe needles for liquid samples. The 1-mCi  $^{63}\text{Ni}$  activity is about 30% of the maximum activity which could be accommodated on the foil area without saturation due to self-absorption.<sup>19</sup> The entire device is regularly baked at  $400\text{ }^\circ\text{C}$  in situ, extended high temperature baking being the only realistic final cleaning procedure.

The cleaned and dried carrier gas is heated to operating temperature by requiring it to flow through a low conductance 60-cm length path internal to the heated ion source housing before it reaches the ionization volume. A total carrier gas flow of  $1$  to  $10\text{ cm}^3\text{ s}^{-1}$  is used, of which approximately  $0.3\text{ cm}^3\text{ s}^{-1}$  constitutes the flow through the ionization chamber into the vacuum system, the remainder being divided between several overflow paths designed to provide continual internal flushing and dynamic sealing. The total flow can result from the summing of several gas sources, such as a GC flow and a make-up flow of clean carrier gas.

In the intermediate pressure chamber a lens system designed for high gas conductance is used to electrostatically separate ions from the gas jet and focus them into a differential pumping aperture constituting the entrance aperture of the mass filter. Seven potentials are employed to bias the ionization volume, to provide the required extraction field, as three lens voltages, as an ELFS<sup>20</sup> bias, and to adjust the potential on the axis on the mass filter. Several of these elements could be operated at ground potential with only a modest loss in transmission. An ohmically heated filament is situated at a suitable position in the lens array, and with an alternative set of lens potentials the focusing array can be used as an electron bombardment ionizer, this facility being convenient for checking mass calibration with organic reference compounds.

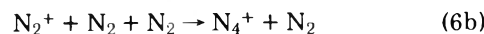
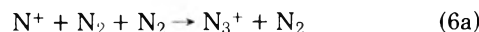
The mass filter is a 8.525-mm pole diameter quadrupole 22 cm in length and equipped with an RF/DC field separation element (ELFS)<sup>20</sup> to improve transmission and resolution. An on-axis saturated high-gain continuous dynode electron multiplier is used for ion counting. Ratemeter conversion of the electronically discriminated and standardized pulses is used to generate a simulated analog signal which drives an oscilloscope display and chart recorder. Digital counters are used to obtain ultimate signal-to-noise ratio on low intensity mass peaks observed in a multiple ion detection mode. An off-axis low-gain continuous dynode electron multiplier is also provided, it being useful for current amplification under the occasional circumstances where the incident count rate may exceed the capability of the high-gain multiplier.

#### IV. Terminal Ion Spectra

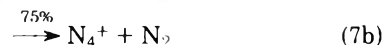
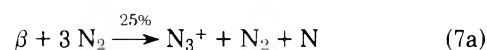
The primary ionizing events in an  $\text{N}_2$  carrier gas produce  $\text{N}^+$  and  $\text{N}_2^+$  in a 1:3 branching ratio<sup>21</sup> via



The clustering reactions



proceed with rate constants of  $1.8 \times 10^{-29}\text{ }^{22}$  and  $5 \times 10^{-29}\text{ }^{23}\text{ cm}^6\text{ s}^{-1}$ , respectively, and have resulting characteristic times under  $10^{-10}\text{ s}$  at atmospheric pressure. Recombination with electrons and impurity negative ions, and charge transfer to impurity molecules, are sufficiently slow compared with the clustering rate that we may treat  $\text{N}_3^+$  and  $\text{N}_4^+$  as pseudo-primary ions:



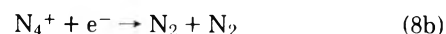
The higher clustering reactions proceed slowly if at all at  $200\text{ }^\circ\text{C}$ , and the observed  $\text{N}_5^+$ ,  $\text{N}_7^+$ , ... and  $\text{N}_6^+$ ,  $\text{N}_8^+$ , ... series are assumed to originate in the free jet expansion into the mass spectrometer vacuum system.<sup>24</sup>

We have already shown on very general grounds that for the source strength and geometrical conditions typical of the API device the technical loss mechanisms (diffusion and flow) are negligible compared to recombination and reaction losses. With this simplification we now consider the problem of determining the relative concentrations of  $\text{N}_3^+$  and  $\text{N}_4^+$  under ideally clean circumstances, where these pseudo-primary ions are lost only to recombination.

The relevant recombination mechanisms are the two-body processes



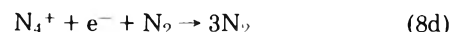
with a  $4.4 \times 10^{-7}\text{ }^{25}\text{ cm}^3\text{ s}^{-1}$  rate constant at  $200\text{ }^\circ\text{C}$ , and



with a  $1.3 \times 10^{-6}\text{ }^{26}\text{ cm}^3\text{ s}^{-1}$  rate constant at  $200\text{ }^\circ\text{C}$ , and the three-body processes

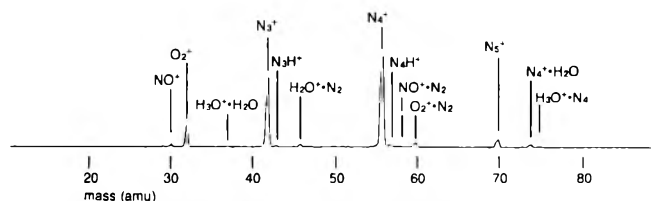


and

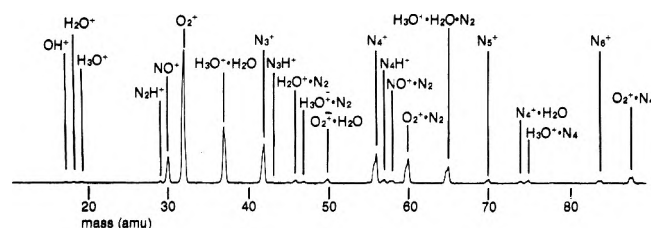


The three-body recombination rates are published only as generic values assumed approximately valid for all clustered species recombining via the mediation of atomic, polar, or nonpolar buffers.<sup>27</sup> The recommended universal rate constant for processes mediated by  $\text{N}_2$  is  $1.6 \times 10^{-26}\text{ cm}^6\text{ s}^{-1}$  at  $200\text{ }^\circ\text{C}$ , which is equivalent to a phenomenological two-body rate constant, at our working pressure and temperature, of  $2.5 \times 10^{-7}\text{ cm}^3\text{ s}^{-1}$ . The sum of two- and three-body rates are thus estimated at effective two-body rates of  $R_3 = 6.9 \times 10^{-7}\text{ cm}^3\text{ s}^{-1}$  for  $\text{N}_3^+$  and  $R_4 = 1.5 \times 10^{-6}\text{ cm}^3\text{ s}^{-1}$  for  $\text{N}_4^+$ .

Solution of the steady state rate equations



**Figure 3.** Quiescent spectrum of very dry  $N_2$  carrier gas at 200 °C, positive ions. The  $N_4^+$  peak amplitude is about 7000 counts  $s^{-1}$ .



**Figure 4.** Quiescent spectrum of moderately dry  $N_2$  carrier gas at 350 °C, positive ions. Increased temperature (cf. Figure 3) increases the  $H_2O$  level. The  $O_2^+$  peak amplitude is about 9500 counts  $s^{-1}$ .

$$d[N_3^+]/dt = 0 = 0.25 - R_3[N_3^+][e] \quad (9a)$$

and

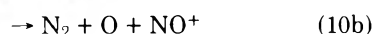
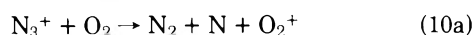
$$d[N_4^+]/dt = 0 = 0.75 - R_4[N_4^+][e] \quad (9b)$$

gives

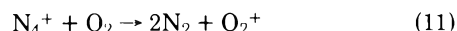
$$\frac{[N_3^+]}{[N_4^+]} = \frac{1}{3} \frac{R_4}{R_3} = 0.72$$

We have recently succeeded in preparing sufficiently pure carrier gas and a sufficiently clean ionization volume that their spectra are dominated by  $N_3^+$  and  $N_4^+$ , with the remaining ions being attributable to traces of  $O_2$  and  $H_2O$ . Under these circumstances the observed ratio of  $N_3^+$  to  $N_4^+$  is in agreement with the calculated value. Spectra demonstrating very dry and moderately dry conditions are shown in Figures 3 and 4.

The major impurity ions are then  $O_2^+$  and  $NO^+$  and their clusters with  $N_2$ , indicating that the most important residual impurity is  $O_2$ . The relevant reactions are



and



The total rate constant for (10) is reported as  $1 \times 10^{-10} \text{ }^{28} \text{ cm}^3 \text{ s}^{-1}$ , with assumed roughly equal branching. The rate constant for (11) is reported as  $4 \times 10^{-10} \text{ }^{29} \text{ cm}^3 \text{ s}^{-1}$ . Assuming roughly equal recombination rates for  $O_2^+$  and  $NO^+$ , and roughly equal concentrations of  $N_3^+$  and  $N_4^+$ , allows us to estimate (by inspection of (10a), (10b), and (11) and their respective rate constants) that  $[NO^+]/[O_2^+] \approx 0.1$ , which is in agreement with the data. In practice the ratio is somewhat dependent on other impurity levels, but is always of order-of-magnitude  $10^{-1}$ .

The published rate constant for (10) is stated to include a third channel<sup>28</sup>



from which we expect to observe  $NO_2^+$  at mass 46. We do see an ion at mass 46 and its clusters with  $(N_2)_n$  but their intensity

is strongly correlated to trace levels of  $H_2O$  (as indicated by  $H_3O^+ \cdot H_2O$ ) and not to  $O_2$ . We believe this ion is actually  $N_2 \cdot H_2O^+$  and not  $NO_2^+$ . As further confirmation, we observe that at increased  $O_2$  concentrations (as indicated by  $O_2^+$ ),  $O_2^+$  and  $NO^+$  rise together, but the mass 46 peak decreases and a mass 50 peak ( $H_2O^+ \cdot O_2$ ) appears. Also, at higher  $H_2O$  concentrations masses 17, 18, and 19 ( $OH^+$ ,  $H_2O^+$ ,  $H_3O^+$ ) rise, and so do  $(46) \cdot (N_2)_n$  and  $(47) \cdot (N_2)_n$ . This correlation further encourages us to believe that masses 46 and 47 are  $H_2O^+ \cdot N_2$  and  $H_3O^+ \cdot N_2$ .

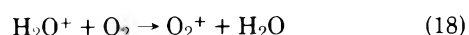
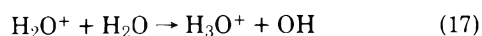
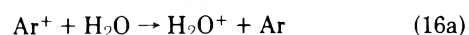
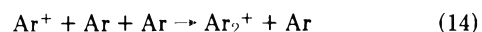
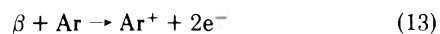
Also correlated with the water concentration when it is at a very low level are the minor peaks at masses 19, 57, and  $(57) \cdot (N_2)_n$ . We attribute these to protonated  $N_2$  clusters formed by reaction of  $N_4^+$  with  $H_2O$ :



Let us summarize the observations in dry  $N_2$  before discussing Ar and air under dry conditions and  $N_2$ , Ar, and air under wet conditions:

The major terminal positive ions in a weak plasma in  $N_2$  are  $N_3^+$  and  $N_4^+$  in roughly equal concentration. Trace impurities of  $O_2$  lead to  $O_2^+$  and  $NO^+$ , but probably not  $NO_2^+$ . Trace impurities of  $H_2O$  lead to  $H_3O^+ \cdot H_2O$ ,  $H_3O^+$ ,  $H_2O^+$ ,  $OH^+$ , the series  $H_2O^+ \cdot (N_2)_n$  and  $H_3O^+ \cdot (N_2)_n$ , and the protonated  $N_2$  cluster series  $(N_2)_n \cdot H^+$ , the order stated roughly corresponding to decreasing  $H_2O$  concentration. Trace impurities of  $H_2O$  in a spectrum otherwise dominated by  $O_2^+$  and  $NO^+$ ,  $N_3^+$ , and  $N_4^+$  appear as  $O_2^+ \cdot H_2O \cdot (N_2)_n$  rather than  $H_3O^+ \cdot H_2O \cdot (N_2)_n$ . Also, trace impurities of  $O_2$  appear in the negative ion spectrum as  $O_2^-$ .

With dried Ar carrier gas (welding grade rather than UHP) the major impurities are  $O_2$ ,  $H_2O$ , and  $N_2$ . Typical mass spectra with low and moderate  $H_2O$  concentrations in Ar are shown in Figures 5 and 6. The low water concentration spectrum is reasonably straightforward, dominated by  $O_2^+$ ,  $OH^+$ ,  $N_2H^+$ ,  $N_3H^+$  (?) at mass 43,  $H_3O^+ \cdot N_2$  at mass 47, and their clusters with Ar. Also seen are smaller quantities of  $H_3O^+$  and  $N_2^+$ , and much smaller quantities of  $O^+$  (?) at mass 16,  $H_2O^+$ ,  $NO^+$  at mass 30,  $Ar^+$ , and an ion at mass 31, and clusters of the major ions with Ar. The higher water concentration spectra are more complicated (perhaps due in some part to the higher temperature used to increase the water concentration), containing in addition to the ions seen in the dry spectrum primarily  $H_3O^+ \cdot H_2O$  and  $O_2H^+$  (?) at mass 33. The relative intensity of the  $OH^+$  and  $H_3O^+$  ions are interchanged with respect to the very dry condition, and the  $N_2H^+$  intensity is very much diminished. At the same time the relative and absolute intensities of the ions at masses 43 and 47, which we believe are  $N_3H^+$  and  $H_3O^+ \cdot N_2$ , are practically unchanged, an observation we find difficult to reconcile with the dramatic change in  $OH^+$ . We speculate that the major observations with dry Ar carrier can be accounted for by the reactions



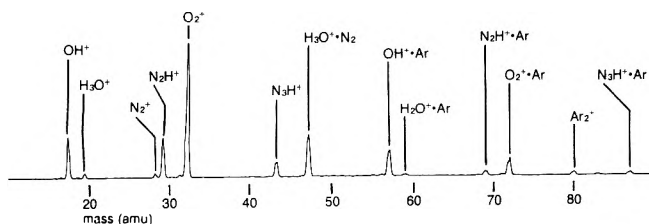


Figure 5. Quiescent spectrum of very dry Ar carrier gas at 200 °C, positive ions. The  $O_2^+$  peak amplitude is about 10 000 counts  $s^{-1}$ .

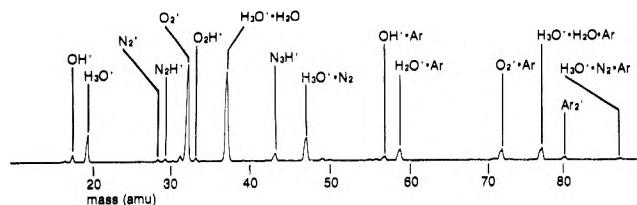
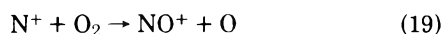


Figure 6. Quiescent spectrum of moderately dry Ar carrier gas at 400 °C, positive ions. Increased temperature (cf. Figure 5) increases the  $H_2O$  level. The  $O_2^+$  peak amplitude is about 8000 counts  $s^{-1}$ .

with rate constants of approximately  $5 \times 10^{-11}$ ,  $3.0 \times 10^{-9}$ ,  $1.4 \times 10^{-9}$ ,  $1.8 \times 10^{-9}$ ,  $3.2$  and  $2.0 \times 10^{-10}$   $cm^3 s^{-1}$  for (15), (16), (17), and (18), respectively. The likely proton donor for formation of  $N_2H^+$ ,  $N_3H^+$ , and  $N_4H^+$  is  $ArH^+$ .

In relatively dry air (which we have run at somewhat lower temperatures than  $N_2$  and Ar, typically 125 °C vs 200 to 400 °C) the dominant positive ions are  $O_4^+$ , mass 47 (which in this case we are confident is  $H_3O^+ \cdot N_2$ ),  $O_2^+ \cdot H_2O$ ,  $NO^+$ ,  $O_2^+$ ,  $H_3O^+ \cdot H_2O$ ,  $N_2H^+$ , and clusters of these ions with  $N_2$  and  $O_2$ . In air  $NO^+$  is significantly larger than  $O_2^+$ , in contrast to the situation in  $N_2$ . This is expected, since in air the primary  $N^+$  ions have a significant probability of reacting with  $O_2$  via

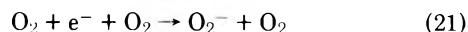


in competition with the clustering reaction (6a). The published rate constant is  $2.8 \times 10^{-10}$   $cm^3 s^{-1}$ . The analogous reaction

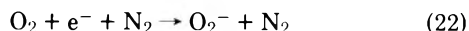


has a much smaller rate constant,  $1.1 \times 10^{-12}$   $cm^3 s^{-1}$ , but the reaction is still very fast at atmospheric pressure in air and it too should contribute to the large  $NO^+$  concentration. The positive ion spectrum in moderately dry air is shown in Figure 7.

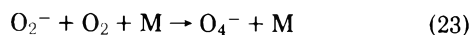
An additional feature of air as a carrier gas is that there is a rich negative ion spectrum, the largest fraction of the negative charge being carried by  $O_4^-$ . The negative ion spectrum in moderately dry air is shown in Figure 8. The relevant reactions are



with a rate constant  $1.4 \times 10^{-29}$   $cm^6 s^{-1}$



with a rate constant of  $1.1 \times 10^{-31}$   $cm^6 s^{-1}$ , and



with a rate constant of  $3.5 \times 10^{-31}$   $cm^6 s^{-1}$ .

After  $O_4^-$  and  $O_2^-$  the highest negative ion concentrations under dry conditions are at masses 60, 76, 92. We believe these to be due to

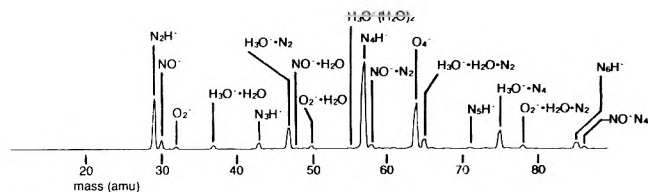


Figure 7. Quiescent spectrum of moderately dry air carrier gas at 125 °C, positive ions. The  $N_4H^+$  peak amplitude is about 7000 counts  $s^{-1}$ .

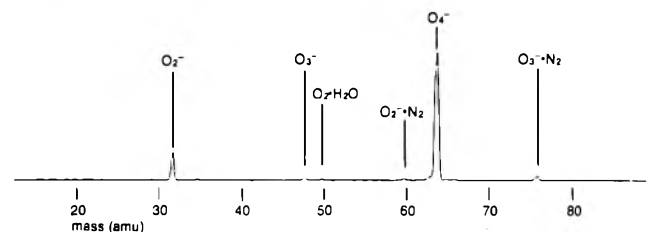
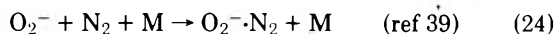
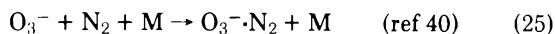


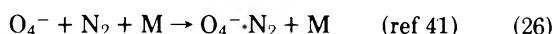
Figure 8. Same conditions as Figure 7, negative ions. The  $O_4^-$  peak amplitude is about 95 000 counts  $s^{-1}$ . The total negative ion signal in this spectrum is about equal to the total positive ion signal in Figure 7 when the many small positive ion peaks (including higher mass clusters) are included in the sum.



giving  $O_2^- \cdot N_2$  at mass 60



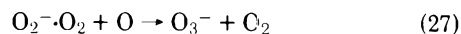
giving  $O_3^- \cdot N_2$  at mass 76, and



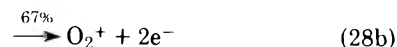
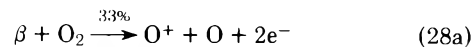
giving  $O_4^- \cdot N_2$  at mass 92.

We recognize that the ions at masses 60 and 76 may be  $CO_3^-$  and  $CO_4^-$  coming from reactions of  $O_3^-$  and  $O_4^-$  with a small  $CO_2$  impurity, but at present we believe this is not the case. The question will ultimately be settled by careful measurement of the isotopic peaks at masses 61 and 77 (1.1% of the main peaks due to  $^{13}C$  if  $CO_2$  is present) and at masses 62 and 78 (due to differing  $^{18}O$  components in  $CO_3^-$  and  $O_2^- \cdot N_2$  and in  $CO_4^-$  and  $O_3^- \cdot N_2$ ).

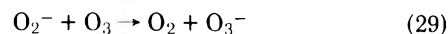
The  $O_3^-$  required for (25) is observed at mass 48 at about 2% the  $O_2^-$  concentration. It may be formed (among several possible routes) via



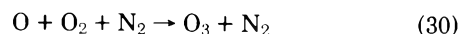
with a rate constant of  $4 \times 10^{-10}$   $cm^3 s^{-1}$ . The O can come from the primary ionization



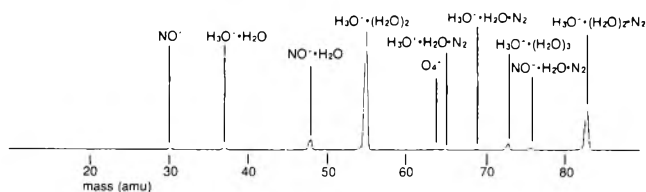
with a 1:2 branching ratio,<sup>43</sup> and from processes such as (19).  $O_3^-$  may also be formed by charge transfer to  $O_3$  via



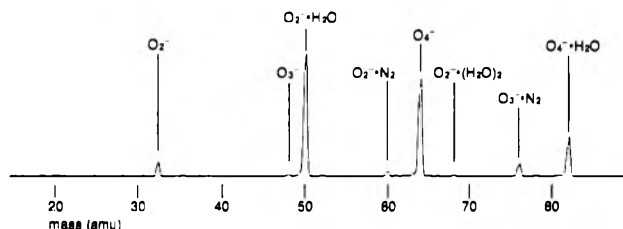
with a rate constant of  $4 \times 10^{-10}$   $cm^3 s^{-1}$ . The  $O_3$  can originate by several routes in the neutral chemistry, for example



with a rate constant of  $6 \times 10^{-34}$   $cm^6 s^{-1}$ .



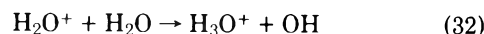
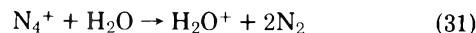
**Figure 9.** Quiescent spectrum of moderately wet air carrier gas at 125 °C, positive ions. The water content is controlled by mixing a small flow of very wet N<sub>2</sub> with a larger flow of dry air. The H<sub>3</sub>O<sup>+</sup>·(H<sub>2</sub>O)<sub>2</sub> peak amplitude is about 16 000 counts s<sup>-1</sup>.



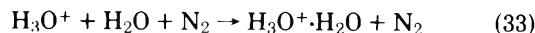
**Figure 10.** Same conditions as Figure 9, negative ions. The O<sub>2</sub><sup>-</sup>·H<sub>2</sub>O peak amplitude is about 45 000 counts s<sup>-1</sup>. The total negative ion signal in this spectrum is about equal to the total positive ion signal in Figure 9 when the many small positive ion peaks (including higher mass clusters) are included in the sum.

It is important to emphasize that all of the above discussion relating to the quiescent spectrum in N<sub>2</sub>, Ar, and air describes observations under conditions that we believe to be uniquely clean and dry. Where we have made comparisons between our “wet” and “dry” conditions, “wet” meant “a significant fraction of the total ions, perhaps 15%, was H<sub>3</sub>O<sup>+</sup>·H<sub>2</sub>O,” and “dry” meant “we saw practically no H<sub>3</sub>O<sup>+</sup>·H<sub>2</sub>O, certainly no more than 0.1% of the total ions”. We now discuss results obtained under “very wet” conditions, where we have intentionally reintroduced H<sub>2</sub>O to the carrier gas in order to duplicate our earlier conditions, which we believe are the conditions still prevailing in all other laboratories doing API work. Spectra showing these wet conditions have been published previously, and we show typical examples of positive and negative ion spectra in wet air in Figures 9 and 10.

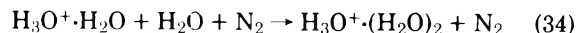
As previously discussed, our early API efforts<sup>2,3</sup> indicated, in agreement with the conclusions of earlier observers,<sup>1</sup> that the indicators of a clean carrier gas and ionization volume would be a hydrated-hydronium cluster spectrum (whatever the inert carrier gas) in the positive ion mode and no ions at all in the negative mode, i.e., the negative charge cloud residing in thermal electrons. This level of cleanliness is actually reached with relatively modest effort, through material choice and handling techniques comparable to those used in ultra-high vacuum applications combined with a few days of high temperature in situ cleanup.<sup>3</sup> As an analytical tool in a broad range of applications, this may turn out to be a circumstance beyond which it is pointless to continue cleanup efforts, because no matter how dry the quiescent spectrum a certain amount of water will accompany all real samples. For example, we now find that in connecting a gas chromatograph outlet to the API source the spectrum is always instantly restored to the water dominated status, from which it may take several hours to recover after the GC is disconnected. This remains true even after the column and fittings have been processed at high temperature and high carrier flow rate for several weeks. Thus while it remains fundamentally interesting to continue investigating the limiting cases, it is of practical value to catalogue the details of the normal, i.e., very wet operating state. The clustering sequence has been described<sup>46</sup> as



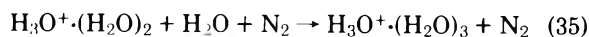
$$k = 1.8 \times 10^{-9}, \text{ ref 47}$$



$$k = 3.4 \times 10^{-27}, \text{ ref 48}$$



$$k = 2.3 \times 10^{-27}, \text{ ref 48}$$



$$k = 2.4 \times 10^{-24}, \text{ ref 48}$$

and so on.

Reaction 33 has a phenomenological two-body rate constant the order of  $7 \times 10^{-8} \text{ cm}^3 \text{ s}^{-1}$  at atmospheric pressure, and (34), (35), etc., are only slightly slower. This is consistent with the observation that the H<sub>2</sub>O<sup>+</sup> concentration usually exceeds the H<sub>3</sub>O<sup>+</sup> concentration, (32) being a relatively slow bottleneck maintaining a high H<sub>2</sub>O<sup>+</sup> concentration. [In the early stages of cleanup the mass 18 peak may be misleading, because room air always contains enough ammonia (enhanced by the presence of people) to dominate the spectrum until thoroughly cleaned up. Inspection of mass 30–40 region is in such cases instructive, because peaks at masses 35 and 36 (NH<sub>4</sub><sup>+</sup>·NH<sub>3</sub> and NH<sub>4</sub><sup>+</sup>·H<sub>2</sub>O) serve to diagnose ammonia.]

The remaining interesting ions in the wet spectrum with N<sub>2</sub> and Ar carrier are generally only clusters with the carrier, and some NO<sup>+</sup>. The NO<sup>+</sup> probably originates via previously mentioned mechanisms involving the O<sub>2</sub> impurity (and thus may be a useful indicator of O<sub>2</sub> even in a wet environment) but we cannot rule out the possibility that mechanisms requiring only H<sub>2</sub>O may be sufficient.

A striking feature of the moderately wet air positive ion spectrum as compared to the moderately dry air case is the absence of N<sub>2</sub>H<sup>+</sup> and other protonated nitrogen ions. At H<sub>2</sub>O concentrations below 10 ppb N<sub>2</sub>H<sup>+</sup> is essentially a terminal ion, while at higher concentrations proton transfer to H<sub>2</sub>O produces H<sub>3</sub>O<sup>+</sup> in parallel with (31). The resulting positive ion distribution is similar to that in wet N<sub>2</sub>, the intense H<sub>3</sub>O<sup>+</sup>·(H<sub>2</sub>O)<sub>*n*</sub>·A<sub>*m*</sub> clusters tending to involve A = N<sub>2</sub> rather than O<sub>2</sub>. In the negative ion spectrum quite the opposite is true, the major difference between the dry and wet negative ion spectra being the appearance of large O<sub>2</sub><sup>-</sup>·H<sub>2</sub>O and O<sub>4</sub><sup>-</sup>·H<sub>2</sub>O concentrations. This is of course not surprising, since in the negative ion spectrum the H<sub>2</sub>O clusters to existing ions, while the positive ion spectrum is dominated by H<sub>2</sub>O-related ions to which carrier gas molecules cluster. It is also interesting that while the O<sub>3</sub><sup>-</sup> and O<sub>2</sub><sup>-</sup>·N<sub>2</sub> concentrations are relatively unaffected by the H<sub>2</sub>O concentration, O<sub>3</sub><sup>-</sup>·N<sub>2</sub> and O<sub>4</sub><sup>-</sup>·N<sub>2</sub> concentrations are significantly enhanced.

We might summarize the state of our understanding of the quiescent terminal ion spectra as “the end of the beginning”. We are now confident that we can exercise sufficient control over the carrier gas condition that we will be able to begin with a pure pseudo-primary ion distribution (N<sub>3</sub><sup>+</sup>, N<sub>4</sub><sup>+</sup>) in N<sub>2</sub> and add H<sub>2</sub>O, O<sub>2</sub>, etc., in a sufficiently systematic way that the full dynamics can be developed.

#### IV. Illustrative Examples of API Response to Trace Samples

The impetus for the development of API-MS can be traced to the biomedical community, whose spokespersons express an apparently limitless need to press ever lower the minimum detectable samples of numerous complex organic materials,



including drugs, hormones, pesticides and other poisons, etc. Using a case-by-case approach, extremely high sensitivity in both negative and positive ion modes has been demonstrated to a broad and more-or-less random assortment of these materials. The Baylor group, under E. C. Horning, has published extensively in this area,<sup>1,4-8</sup> and we have reported results on several compounds.<sup>2,3,12</sup>

We have chosen to devote the bulk of our efforts to more fundamental investigations involving simpler species, particularly those which may for one reason or another be of atmospheric interest. In these cases the potential exists for comparison with and extension perhaps of existing rate constant data. Under these circumstances it is also realistic to expect that experimental results will be useful in checking theoretical models and scaling relationships, through which optimum approaches to specific biomedical problems may be developed. In this section we discuss some of our illustrative results with a variety of relatively simple but still relevant sample species.

1. *Sulfur Hexafluoride*.  $\text{SF}_6$  is a useful initial example because direct electron attachment to form  $\text{SF}_6^-$  is the only process which need be considered, there is no competing negative ion (in a clean ion source), and the positive ion spectrum is to a good approximation unaffected by this attachment process. The response test, as shown in Figure 11, is performed by injecting 1  $\mu\text{l}$  of  $\text{SF}_6$  mixed with 9  $\mu\text{l}$  of air into the 1-l exponential dilution flask discussed previously. The decay of the  $\text{SF}_6^-$  signal is plotted as a function of time. The initial concentration is taken to be 1 ppm (approximately  $2 \times 10^{13} \text{ cm}^{-3}$ ), and the dilution time constant is measured on the straight line portion of the semilog decay plot. The resulting time constant (182 s) is in agreement with the approximate value obtained by dividing the known flask volume by the estimated total flow rate. A direct measurement of the flow rate is precluded by the contamination the necessary apparatus would introduce. The validity of this method is confirmed by varying the flow rate, thus changing the time constant, and observing that the absolute signal vs calculated concentration plot is independent of the flow rate.

The general form of the data is obviously that required by the simple theory of section II. At low sample concentration the signal is linear in concentration, and at high concentration the signal saturates. From eq 4a the time dependence of the relative signal can be written as

$$\frac{n^-(t)}{n^-(0)} = \frac{K + 1}{K + e^{-\alpha t}} \quad (36)$$

where

$$K = \frac{A_- n_A^0}{R_0 n_0} \quad (37)$$

and

$$n_A(t) = n_A^0 e^{-\alpha t} \quad (38)$$

$A_-$  is the attachment rate,  $R_0$  the (assumed constant) recombination rate,  $n_A^0$  the initial sample concentration,  $n_0$  the (assumed constant) total ion concentration, and  $\alpha$  the dilution time constant. A good fit to the data is obtained, as shown, with  $K = 200$ . No attempt has been made to optimize the fit, an approximate value of  $K$  being sufficient for our purposes. This value of  $K$  is consistent with  $A_- = 4 \times 10^{-9}$ ,  $R_0 = 10^{-6}$ ,  $n_A^0 = 2 \times 10^{13}$ , and  $n_0 = 4 \times 10^8$ , all of which are reasonable estimates of the actual rate constants and operating parameters.

The approach of the signal to a constant value at concen-

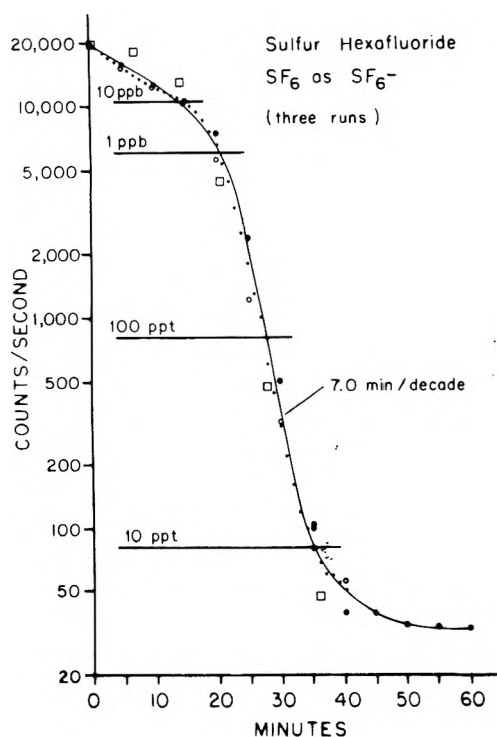


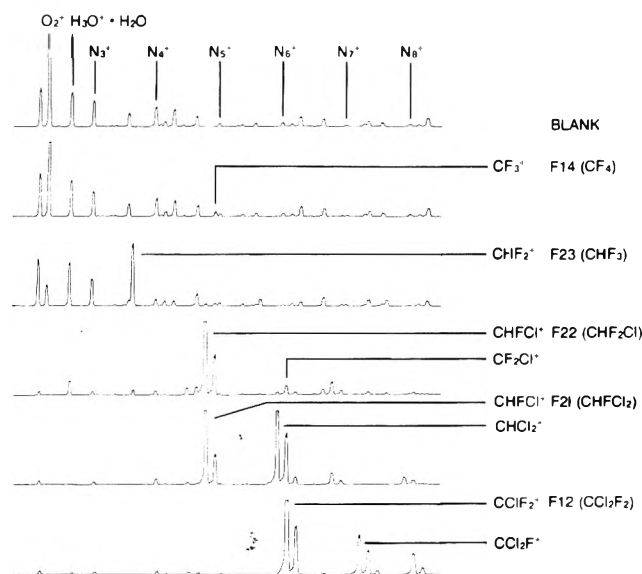
Figure 11. Exponential dilution signal obtained from  $\text{SF}_6$  sample observed as  $\text{SF}_6^-$ . The dilution time constant is 7 min/decade. Carrier gas is  $\text{N}_2$  at 200 °C. Squares show approximate fit with  $K = 200$  (see text).

trations nominally below about 10 ppt is attributed to slow desorption of some fraction of the sample initially adsorbed on the dilution vessel and tubing walls. The required desorption rate to maintain 10 ppt in the carrier stream is about  $4 \times 10^6 \text{ cm}^{-2} \text{ s}^{-1}$ , or approximately one monolayer in 7 years. After a test like this one, residual sample is seen indefinitely and is removed only by an overnight bakeout of the dilution vessel at 300–400 °C.

2. *Freons*. Detection prospects for trace quantities of fluorochlorocarbons has received considerable recent attention because of their postulated effect on the stratospheric ozone layer.<sup>51</sup> It is well known that these compounds are detected with very high sensitivity by the gas chromatographic electron capture detector (ECD),<sup>52</sup> and it would thus be expected that similar sensitivity should be seen with API-MS. [A recent discussion of the similarities and differences between ECD and API is given in ref 3.]

In the negative ion API mode the fluorochlorocarbons respond sensitively but ambiguously, since the only observed negative ion is  $\text{Cl}^-$ , which has numerous sources. Negative ion GC-API-MS in this application might be useful, but perhaps no more so than straightforward ECD technique.

In the positive ion API mode the fluorochlorocarbons respond sensitively and unambiguously, each giving a characteristic positive ion signature of large fragments, each generally the parent molecule less one halogen atom. Figure 12 shows a sequence of response tests in the form of broad spectral scans showing the quiescent spectrum and response to the fluorocarbons F14 ( $\text{CF}_4$ ) and F23 ( $\text{CHF}_3$ ), and the fluorochlorocarbons F22 ( $\text{CHF}_2\text{Cl}$ ), F21 ( $\text{CH}_2\text{FCl}_2$ ), and F12 ( $\text{CCl}_2\text{F}_2$ ). These spectra were each collected by introducing 10  $\mu\text{l}$  of the vapor into the dilution flask, so the concentration at the beginning of each scan was 10 ppm. The scan and dilution rates were such that by the end of each scan the



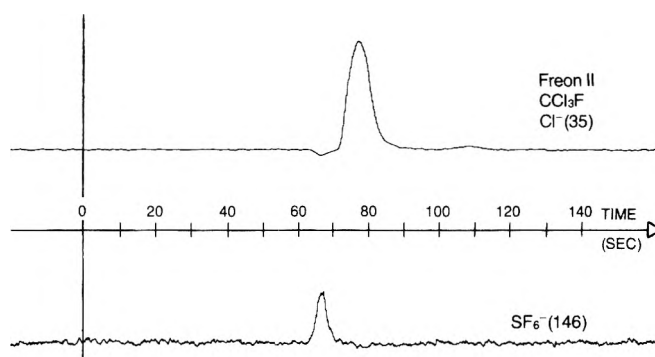
**Figure 12.** API-MS spectra showing quiescent spectrum of  $N_2$  carrier gas at 200 °C, and response spectra to Freons 14, 23, 22, 21, and 12. All spectra are recorded at the same sensitivity, where full scale deflection (the saturated  $O_2^+$  in the blank, the saturated  $CHF_3^{35}Cl^+$  peaks, etc.) is 10 000 counts  $s^{-1}$ .

concentration dropped to a few hundred parts per billion. Since response is essentially saturated in this concentration regime, discrimination across the scan is relatively small.

The blank spectrum shows that the API is moderately dry, with  $H_3O^+ \cdot H_2O$  accounting for about 15% of the total ions. The  $CF_4$  spectrum shows a small response at  $CF_3^+$ , and no detectable perturbation to the quiescent spectrum. The  $CHF_3$  spectrum shows a distinctly stronger response, the major ion in the spectrum becoming  $CHF_2^+$ , with a small  $CF_3^+$  peak also appearing. The quiescent spectrum is distinctly perturbed, the major changes being a drastic reduction in  $O_2^+$  and easily observable reductions in  $N_4^+$  and  $O_2^+ \cdot N_2$ . As compared to the fluoromethanes, the fluorochloromethanes F22, F21, and F12 are detected with dramatic sensitivity. The  $CHF_2Cl$  is seen as  $CHFC1^+$ , which accounts for about 75% of the total positive ions, and also less intensely as  $CF_2Cl^+$ . The  $CHFC1_2$  is seen dominating the spectrum as  $CHFC1^+$  and  $CHCl_2^+$  with about equal intensity. The  $CCl_2F_2$  is seen dominating the spectrum as  $CClF_2^+$  and somewhat less strongly as  $CCl_2F^+$ .

The ultimate potential sensitivity to the fluorochlorocarbons is exemplified by the data of Figure 1, which has been briefly discussed earlier. In the absence of the surface effects noted above, signal-to-noise in the present configuration is sufficient that a detection limit under 1 ppt should be feasible with multiple ion detection and counting instrumentation. There has been no attempt in these preliminary tests to optimize the temperature, pressure, quiescent spectrum, or any other parameters. Operating conditions are our standard 200 °C, 1 atm, with moderately dry  $N_2$  carrier; optimization might well lead to a somewhat lower limit.

As an example of some of our initial and very preliminary results with GC-API-MS, we show in Figure 13 the separation of F11 ( $CCl_3F$ ) detected as  $Cl^-$  and  $SF_6$  detected as  $SF_6^-$  using a multiple ion monitoring technique to demultiplex the individual signals onto separate chart recorder channels. The sample was 1  $\mu$ l of air containing approximately 1 ppm each of F11 and  $SF_6$ , corresponding to about 45 fmol (6 pg) of each constituent. The coupling between GC output and API inlet was of a temporary nature for evaluation purposes, and this

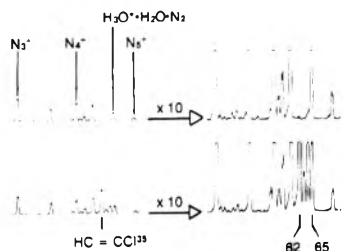


**Figure 13.** Gas chromatograph API-MS multiple ion detection response to a 1- $\mu$ l air sample containing 1 ppm Freon 11 detected as  $Cl^-$  and 1 ppm  $SF_6$  detected as  $SF_6^-$ . Effective sample size after correction for splitting loss (see text) is 0.6 pg of each material. The steps seen on the large  $Cl^-$  peak are due to the sample-and-hold circuits in the MID demultiplexer. Baselines are offset to compensate for time-independent  $Cl^-$  and  $SF_6^-$  signals due to slow desorption of previous large samples. The dip in  $Cl^-$  when  $SF_6^-$  appears is due to competition between the time-resolved  $SF_6^-$  and the time-independent  $Cl^-$ . Note the appearance of a small  $Cl^-$  peak at about 110 s, due to an unidentified impurity.

set up resulted in transfer of no more than 10% of the GC flow into the API active volume. Thus the response seen is to no more than 0.6 pg of each constituent.

Furthermore, in addition to producing a continual stream of  $H_2O$  vapor, the column in its present condition produces a continual stream of an unidentified substance generating  $Cl^-$  in the API, resulting in a  $Cl^-$  baseline which had to be offset by approximately 10 times the height of the  $Cl^-$  peak from the F11. The existence of this baseline is evidenced by the baseline dip in the  $Cl^-$  trace when the  $SF_6^-$  peak appears, this being due to competition for the total available electron charge. The  $SF_6^-$  baseline noise is due to a similar offset due to a continual  $SF_6$  bleed from the column, this being traceable to an earlier test with a very large  $SF_6$  sample. Somewhat higher gain in the  $SF_6^-$  channel emphasizes the noise level. In short, conditions for this test were very far from optimum, and we reemphasize that this is a very preliminary demonstration. The peaks are nevertheless well separated, and seen with a signal-to-noise sufficiently good that even the weaker, noisier component ( $SF_6^-$ ) could have been clearly seen at approximately the 100 fg level.

3. *Vinyl Chloride (Ethylene Monochloride)*. Vinyl chloride, the stock material used in the manufacture of polyvinyl chloride plastics, has been identified as carcinogenic.<sup>53</sup> The reported detection limit for this material by flame ionization detection gas chromatograph is 50 ppb in a 1- $cm^3$  air sample.<sup>54</sup> It appears not to respond in the ECD. To evaluate the potential for API-MS detection of vinyl chloride, a 50 ppb concentration in  $N_2$  was prepared by diluting 20:1 the flow from a 1 ppm vinyl chloride in  $N_2$  tank with the  $N_2$  carrier gas flow feeding the API. Figure 14 shows the quiescent spectrum in the mass region encompassing  $N_3^+$  through  $N_5^+$ , and the spectrum of the sample flow in the same mass region. The sample is seen as  $C_2HCl^+$  at masses 62 and 64 and as  $C_2HCl \cdot H^+$  at masses 63 and 65. The signal at mass 65 is obscured by the  $H_3O^+ \cdot H_2O \cdot N_2$  peak, but this is the smallest of the four relevant mass peaks. Considering only the information available in the mass 62 peak, the signal seen corresponds to a count rate of 3500  $s^{-1}$ . Since there is no significant interfering mass peak at 62 amu, and the dark rate is below 10  $s^{-1}$ , a 1-ppb sample concentration could be observed with a signal-to-noise ratio of 7 or better. No attempt was made to optimize operating conditions during this test.



**Figure 14.** API-MS response to vinyl chloride ( $\text{HC}=\text{CCI}$ ) as  $\text{HC}=\text{CCI}^+$  and  $\text{HC}=\text{CCI}-\text{H}^+$ . The upper spectra show the quiescent carrier gas spectrum,  $\text{N}_2$  at  $200^\circ\text{C}$ . The lower spectra show the result of adding 50 ppb of vinyl chloride to the flow.

**4. Nitric Oxide and Sulfur Dioxide.** As examples of simple molecular species of interest as automobile emissions we have examined the API-MS response to NO and  $\text{SO}_2$ . Nitric oxide is observed as  $\text{NO}^+$  and sulfur dioxide is observed as  $\text{HSO}_2^+$ . In each of these cases the present detection limit is set by interfering species in the quiescent spectrum. In the case of NO as  $\text{NO}^+$ , the quiescent spectrum already contains a significant  $\text{NO}^+$  peak due to ion molecule reactions between carrier gas primary ions and  $\text{N}_2$  and  $\text{O}_2$ , as discussed previously. In the case of  $\text{HSO}_2^+$ , at mass 65, the  $\text{H}_3\text{O}^+\cdot\text{H}_2\text{O}\cdot\text{N}_2$  peak interferes. Nevertheless detection of both these species at the small part-per-million level is straightforward. The exponential dilution signal in each case levels off to the background level at a sample concentration of a few hundred parts per billion. The statistical noise on the interfering background peaks is a few percent with a 1-s integrating time (i.e., the count rates are a few thousand per second), and the statistical noise exceeds the dark counting rate by an order of magnitude. With appropriate integrating and subtraction procedures it should be possible to extend the detection limits for NO and  $\text{SO}_2$  to a few tens of parts per billion.

## V. Summary, Conclusions, and Future Prospects

The terminal ion spectrum in a weak atmospheric pressure plasma has been demonstrated to be highly sensitive to the presence of trace levels of appropriately active species, and the plasma has thus been identified as an efficient region in which to ionize selected trace samples species for mass spectrometric analysis. It has been shown that the ionization efficiency of a practical ion source operating on this principle is almost entirely determined by the relevant rates for primary ionization, ion-molecule reactions and electron attachment, and recombination, and is insensitive to the technical loss mechanisms determined by engineering details. The response of an API-MS system has been compared with predictions based on known reaction mechanisms and rate constants, and agreement between theory and experiment has been shown to be good. This makes obvious the possibility of using an API-MS system for fundamental ion-molecule reaction studies at high pressure, as well as for the originally intended task of high sensitivity impurity analysis. The API-MS combination has been shown with several relevant sample types to provide a sensitivity capability unmatched by any other concentration-sensitive ionization source. The feasibility of interfacing a gas chromatograph to an API-MS has been demonstrated in a preliminary fashion with extremely encouraging results. The availability of chromatographic pre-separation techniques is particularly appreciated in API-MS because of its diminished sensitivity to components of an unseparated mixture due to their competition for the essentially fixed total available charge.

Much of the data presented is of a preliminary nature, and much of it has a technical orientation aimed at demonstrating carrier gas purity effects. The API-MS field has passed from infancy to childhood with our recent demonstration that with appropriate technique it is possible to obtain sufficient gas purity that primary ions dominate the observed spectrum. We are about to enter a stage in which minute impurity effects can be quantitatively investigated by controlled reintroduction of relevant impurities. We expect the results will be useful both in generating high pressure reaction rate data, and in identifying and developing secondary processes to extend ultra-high sensitivity analytical capability to additional species.

**Acknowledgments.** We acknowledge numerous useful discussions with D. I. Carroll and I. Dzidic. The GC-API-MS data were obtained with the invaluable assistance of Ms. Zorah Curry. This research has been supported by Extranuclear Laboratories, Inc.

## References and Notes

- (1) E. C. Horning, M. G. Horning, D. I. Carroll, I. Dzidic, and R. N. Stillwell, *Anal. Chem.*, **45**, 936-943 (1973).
- (2) M. McKeown and M. W. Siegel, *Am. Lab.*, **91** (Nov 1975).
- (3) M. W. Siegel and M. McKeown, *J. Chromatogr.*, **122**, 397-413 (1976).
- (4) E. C. Horning, M. G. Horning, D. I. Carroll, R. N. Stillwell, and I. Dzidic, *Life Sci.*, **13**, 1331-1346 (1973).
- (5) D. I. Carroll, I. Dzidic, R. N. Stillwell, M. G. Horning, and E. C. Horning, *Anal. Chem.*, **46**, 706-709 (1974).
- (6) E. C. Horning, D. I. Carroll, I. Dzidic, K. D. Haegele, M. G. Horning, and R. N. Stillwell, *J. Chromatogr. Sci.*, **12**, 725-729 (1974).
- (7) I. Dzidic, D. I. Carroll, R. N. Stillwell, and E. C. Horning, *Anal. Chem.*, **47**, 1308-1312 (1975).
- (8) I. Dzidic, D. I. Carroll, R. N. Stillwell, and E. C. Horning, *Anal. Chem.*, **48**, 1763-1768 (1976).
- (9) N. M. Reid, J. B. French, C. C. Poon, and J. A. Buckley, Proceedings of the 24th Annual Conference of the American Society for Mass Spectrometry, San Diego, Calif., May 1976, Paper S10, in press.
- (10) C. S. Harden and T. C. Imeson, Proceedings of the 9th Army Scientific Conference, West Point, N.Y., June 1974, pp 415-429.
- (11) T. C. Imeson and C. S. Harden, Edgewood Arsenal Technical Report EATR 4642 (May 1972).
- (12) M. W. Siegel, Abstracts of the 1976 Pittsburgh Conference on Analytical Chemistry and Applied Spectroscopy, Cleveland, Ohio, March 1976, Papers 358 and 359.
- (13) M. W. Siegel, Proceedings of the 24th Annual Conference of the American Society for Mass Spectrometry, San Diego, Calif., May 1976, Paper S11, in press.
- (14) M. H. Bortner and T. Baurer, Ed., "Defense Nuclear Agency Reaction Rate Handbook", 2d ed, M. A. Biondi, Chapter 16, "Charged-Particle Recombination Processes", pp 16-1 to 35, especially Table 16-1.
- (15) E. W. McDaniel, "Collision Phenomena in Ionized Gases", Wiley, New York, N.Y., 1964, Appendix I, p 693.
- (16) Reference 15, p 512.
- (17) New England Nuclear, Boston, Mass., Model NER-9991.
- (18) Englehard Minerals and Chemicals Corp., East Newark, N.J.
- (19) D. Reader, New England Nuclear, private communication.
- (20) W. L. Fite, *Rev. Sci. Instrum.*, **47**, 326-330 (1976). ELFS is an acronym for Extranuclear Laboratories Field Separation.
- (21) D. Rapp, D. D. Briglia, and P. Englander-Golden, *J. Chem. Phys.*, **42**, 4081 (1965).
- (22) J. T. Moseley, R. M. Snuggs, D. W. Martin, and E. W. McDaniel, *Phys. Rev.*, **178**, 240 (1969); also D. K. Bohme, D. B. Dunkin, F. C. Fehsenfeld, and E. E. Ferguson, *J. Chem. Phys.*, **51**, 863 (1969).
- (23) T. M. Miller, J. T. Moseley, D. W. Martin, and E. W. McDaniel, *Phys. Rev. Lett.*, **21**, A3 (1968).
- (24) J. A. Laurmann, Ed., "Rarefied Gas Dynamics", Vol. I, Academic Press, New York, N.Y., 1963.
- (25) M. H. Bortner, R. H. Kummier, and T. Baurer, ref. 4, Chapter 24, "Summary of Suggested Rate Constants", 24-7.
- (26) W. H. Kasner and M. A. Biondi, *Phys. Rev.*, **137**, A317 (1965); also R. Hackam, *Planet. Space Sci.*, **13**, 667 (1965).
- (27) Reference 25, p 24-6.
- (28) D. B. Dunkin, F. C. Fehsenfeld, A. L. Schmeltekopf, and E. E. Ferguson, *J. Chem. Phys.*, **54**, 3817 (1971).
- (29) Deleted in revision.
- (30) P. Warneck, *J. Chem. Phys.*, **46**, 513 (1967); also N. G. Adams, D. K. Bohme, D. B. Dunkin, and F. C. Fehsenfeld, *J. Chem. Phys.*, **52**, 1951 (1970).
- (31) C. J. Howard, H. W. Rundle, and F. Kaufman, *J. Chem. Phys.*, **55**, 4772 (1971).

- (32) A. Good, D. A. Durden, and P. Kebarle, *J. Chem. Phys.*, **52**, 212, 222 (1970).
- (33) E. E. Ferguson, *Rev. Geophys.*, **5**, 305 (1967); also F. C. Fehsenfeld, A. L. Schmeltekopf, and E. E. Ferguson, *J. Chem. Phys.*, **46**, 2802 (1967).
- (34) D. B. Dunkin, F. C. Fehsenfeld, A. L. Schmeltekopf, and E. E. Ferguson, *J. Chem. Phys.*, **49**, 1365 (1968); also R. Johnsen, H. L. Brown, and M. A. J. Biondi, *ibid.*, **52**, 5080 (1970).
- (35) W. L. Fite, *Can. J. Chem.*, **47**, 1797 (1969); also E. E. Ferguson, *Rev. Geophys.*, **5**, 305 (1967).
- (36) J. L. Pack and A. V. Phelps, *J. Chem. Phys.*, **44**, 1870 (1966); **45**, 4316 (1966); also A. V. Phelps, *Can. J. Chem.*, **47**, 1783 (1969).
- (37) Deleted in revision.
- (38) J. L. Pack and A. V. Phelps, *Bull. Am. Phys. Soc.*, **16**, 214 (1971); also D. A. Parkes, *Trans. Faraday Soc.*, **67**, 711 (1971).
- (39) N. G. Adams, D. K. Bohme, D. B. Dunkin, F. C. Fehsenfeld, and E. E. Ferguson, *J. Chem. Phys.*, **52**, 3133 (1970).
- (40) The three-body clustering rate for  $N_2$  to  $O_3^-$  appears not to have been measured.
- (41) The three-body clustering rate for  $N_2$  to  $O_4^-$  appears not to have been measured.
- (42) F. C. Fehsenfeld, E. E. Ferguson, and D. K. Bohme, *Plant. Space Sci.*, **17**, 1759 (1969).
- (43) R. T. Brackmann and W. L. Fite, *Phys. Rev.*, **113**, 815–816 (1959).
- (44) E. E. Ferguson, *Can. J. Chem.*, **47**, 1815 (1969).
- (45) F. Kaufman, and J. R. Kelso, *Discuss. Faraday Soc.*, **37**, 26 (1974); *J. Chem. Phys.*, **46**, 4541 (1967).
- (46) A. Good, D. A. Durden, and P. Kebarle, *J. Chem. Phys.*, **52**, 212 (1970).
- (47) A. Good, D. A. Durden, and P. Kebarle, *J. Chem. Phys.*, **52**, 212, 222 (1970); also W. L. Fite, *Can. J. Chem.*, **47**, 1797 (1969).
- (48) A. Good, D. A. Durden, and P. Kebarle, *J. Chem. Phys.*, **52**, 212, 222 (1970).
- (49) Deleted in revision.
- (50) Deleted in revision.
- (51) R. J. Cicerone, R. S. Stolarski, and S. Walters, *Science*, **185**, 1165–1167 (1974). Also M. J. Molina and R. S. Rowland, *Nature (London)*, **249**, 810–812 (1974).
- (52) E. P. Grimsrud and R. A. Rasmussen, *Atmos. Environ.*, **9**, 1010–1013 (1975). Also references therein.
- (53) Federal Register **39**, 16897 (May 19, 1974).
- (54) F. Debbrecht and E. M. Neel. Proceedings of a Specialty Conference, New Jersey Institute of Technology, Newark, N.J., March 22–23, 1976, Technomic Publishing Co., Westport, Conn., p 113.

## Collision Induced Singlet to Triplet Transition of Methylene.

### 2. Numerical Tests of Two Theories<sup>†</sup>

Kenneth C. Kulander<sup>†</sup> and John S. Dahler\*

Departments of Chemistry and Chemical Engineering, University of Minnesota, Minneapolis, Minnesota 55455 (Received March 16, 1976)

Publication costs assisted by the Petroleum Research Fund

The inert gas catalyzed reaction  $CH_2(^1A_1) + X \rightarrow CH_2(^3B_1) + X$  has been studied using two different models for the process. The first is a direct, single collision mechanism. The second involves a collision complex intermediate. Both methods assume that the transition occurs via the spin-orbit coupling in methylene when the catalyst atom induces a degeneracy between adiabatic vibrational levels of the two electronic states. Vibrational energy levels and wave functions for the bending mode of  $CH_2$  and  $CD_2$  in the  $^1A_1$  and  $^3B_1$  states have been constructed. Also calculated are potential energy surfaces (using the Gordon–Kim method) for the interactions of singlet and triplet methylene with He, Ne, Ar, and Kr. Both models predict rates in order-of-magnitude agreement with experiment and also predict the final triplet state will be vibrationally excited.

### 1. Introduction

In a recent investigation<sup>1</sup> Chu and Dahler (CD) proposed that the (thermal) collision induced singlet to triplet transition of methylene is a simple, direct reaction which proceeds via a well-defined transition state. According to this theory the role of the chemically inert “catalyst” is to collisionally induce a degeneracy between adiabatic singlet ( $^1A_1$ ) and triplet ( $^3B_1$ ) vibronic levels. This degeneracy results from the unequal interaction of the atom with the two electronic states of the radical. This rate-determining step is followed by a spin-orbit coupled singlet to triplet transition which subsequently is stabilized by the lifting of the degeneracy which accompanies the continuing relative motion of catalyst and radical.

In the theory of Chu and Dahler it is assumed that the reactive event is a catalyst–radical collision with a trajectory which pierces the singlet–triplet “crossing surface” only twice, first as the particles approach one another and then again as they retreat. However, due to the existence of attractive

long-range forces—the van der Waals and dipole-induced dipole interactions—it may be possible to form a loosely bound collision complex. For this to occur the relative translational kinetic energy of the colliding catalyst–radical pair must be transformed into internal rotational or vibrational energy. The complex then will dissociate at some later time when this excess energy once again finds its way back into the mode associated with relative motion of catalyst and radical.

If the life of the complex is very long, the crossing surface for the singlet to triplet transition will be pierced many times before it dissociates. Consequently, the probability of reaction may be greatly enhanced over that associated with the single pass, direct reaction mechanism. Furthermore, if the lifetime of this resonance is sufficiently great, the system will lose all memory of how the complex was formed. Under these circumstances one can use the statistical approximations familiar from the RRKM theory of unimolecular reactions to predict whether dissociation will result in the formation of a triplet or a singlet radical.

A theory of this type has been used by Tully<sup>2</sup> to explain the collisional quenching by  $N_2$  of the  $^1D$  state of atomic oxygen,

<sup>†</sup> Present address: Science Research Council, Daresbury Laboratory, Warrington WA4 4AD, England.

e.g., the reaction  $\text{N}_2 + \text{O}(^1\text{D}) \rightarrow \text{N}_2 + \text{O}(^3\text{P})$ . It was remarkably successful in accounting for the experimental observations of this spin-forbidden molecular collision process and recently<sup>3</sup> has been applied with equal success to a number of other, similar systems. Therefore, it is only natural that we should investigate the applicability of this theory to the collision induced singlet to triplet transition of methylene.

The purpose of the present investigation is to test numerically the predictions of these two theories, the direct reaction mechanism of CD and the collision complex mechanism due to Tully. Many of the calculations involved are common to both models. We begin by considering the CD theory and then in section 4 present calculations based upon the Tully theory.

## 2. The Direct Reaction Model

To transform this mechanism into a mathematical theory Chu and Dahler invoked the following simplifying assumptions:

(1) Thermal collisions perturb the catalyst (an inert gas atom) so slightly that its (electronic) state is unaltered.

(2) The vibrational Hamiltonian operator for the methylene radical is unchanged by the approach of the catalyst particle, i.e., the vibrational levels themselves are not collisionally distorted.

(3) The portion of the collision trajectory along which there is a significant probability of transition is so short that rotation of the radical can be neglected during this part of the collision.

(4) The duration of the transition is so short that the subsequent unbending of the radical (from its singlet angle of  $104^\circ$  to the triplet angle of  $140^\circ$ ) plays no part in determining the rate of reaction.

(5) The Born-Oppenheimer separation of electronic and nuclear motions is valid. The vibration of the radical is treated quantum mechanically whereas classical mechanics is used to describe the relative motion of catalyst and radical.

(6) The reactant radical is in the ground vibrational level of the singlet ( $^1\text{A}_1$ ) manifold. The basis for this assumption is the experimental observation that the rate of reaction is independent of the source (ketene or diazomethane) of singlet radicals. Due to the large splitting between vibrational levels at thermal energies only the lowest level will be significantly populated.

Because the electronic charge distributions of the singlet and triplet states differ from one another, so also will the catalyst-radical interaction energies,  $V(^1\text{A}_1; \mathbf{r})$  and  $V(^3\text{B}_1; \mathbf{r})$ . Here  $\mathbf{r}$  denotes the vector (see Figure 1) extending from the carbon atom of  $\text{CH}_2$  to the catalyst. In the course of a binary collision the energy gap between a given pair of singlet and triplet vibronic levels will change continuously from the asymptotic value of  $\Delta W_{mn}^0 = W_m^0(^1\text{A}_1) - W_n^0(^3\text{B}_1)$  to  $\Delta W_{mn}(\mathbf{r}) = \Delta W_{mn}^0 + \Delta V(\mathbf{r})$  wherein  $\Delta V(\mathbf{r}) = V(^1\text{A}_1; \mathbf{r}) - V(^3\text{B}_1; \mathbf{r})$ . In some cases this gap size may shrink to zero so that for an instant of time the two levels become degenerate. The conditions for this to happen depend not only upon the specific pair of levels that is being considered but also upon the relative orientation of the two interacting species. According to the mechanism proposed by Chu and Dahler the vibronic transition  $\text{CH}_2(^1\text{A}_1; m = v_1, v_2, v_3) \rightarrow \text{CH}_2(^3\text{B}_1; n = v_1', v_2', v_3')$  can occur only at points  $\mathbf{r}_0$  which lie very near to the "crossing surface",  $\mathcal{S}_{mn}^0$ , defined by  $\Delta W_{mn}(\mathbf{r}_0) = 0$ . The "activation energy" required for preparation of this transition state is equal to  $E_1(\mathbf{r}_0) = V(^1\text{A}_1; \mathbf{r}_0)$ , the value of the adiabatic X-

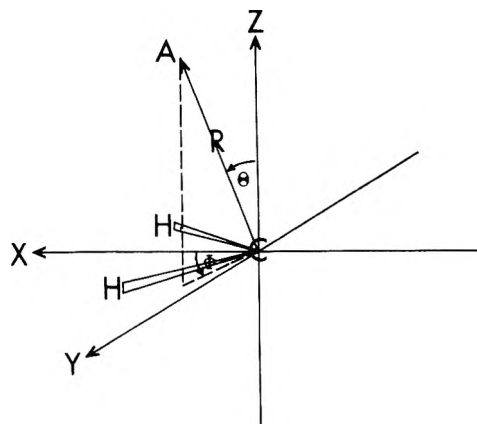


Figure 1. Coordinate system used. The x axis bisects the H-C-H angle and the methylene lies within the xy plane. The location of the catalyst is denoted by point A. The vector  $\mathbf{r} = (r, \theta, \phi)$  extends from the carbon atom to A.

$\text{CH}_2(^1\text{A}_1)$  potential at the point where the collision trajectory pierces the crossing surface.

From the theory of Landau and Zener the probability for reaction to occur is given by  $P(v) = 2e^{-\gamma} (1 - e^{-\gamma})$  where  $\gamma_{mn}(v, \mathbf{r}_0) = v_{mn}(\mathbf{r}_0)/v$  and

$$v_{mn} = 2\pi\hbar^{-1} |\langle ^3\text{B}_1, n | V_{\text{SO}} | ^1\text{A}_1, m \rangle|^2 / \Delta F(\mathbf{r}_0) \quad (1)$$

Here  $v$  is the relative speed of the two colliding species,  $\Delta F(\mathbf{r}) = \partial \Delta V(\mathbf{r}) / \partial r$ , and  $V_{\text{SO}}$  is the spin-orbit interaction. With the above assumptions each matrix element of this operator can be written as the product of an electronic factor  $v_{\text{SO}}$  and a vibrational overlap integral  $S_{mn}$ .

By the application of transition state theory Chu and Dahler obtained for the specific rate (of a particular singlet to triplet vibronic transition) the formula

$$k_{mn}(\beta) = \int \int_{\mathcal{S}_{mn}^0} d\mathcal{S} (\dot{r}_{\text{rot}} / \dot{r}_{\text{rot}}^{\text{CH}_2}) p_{mn} \exp[-\beta E_1(\mathbf{r}_0)] \quad (2)$$

Here  $\dot{r}_{\text{rot}} / \dot{r}_{\text{rot}}^{\text{CH}_2} = (\Gamma_1^* \Gamma_2^* \Gamma_3^* / \Gamma_1 \Gamma_2 \Gamma_3)^{1/2}$  is the ratio of the rotational partition function of the X- $\text{CH}_2$  "transition complex" to that of the free, singlet methylene radical. The quantities  $\Gamma_j^*(\mathbf{r}_0)$  and  $\Gamma_j$  are the principal moments of inertia of these two objects. Finally

$$p_{mn}(\beta, \mathbf{r}_0) = \int_0^\infty dv v P_{mn} \exp\left(-\beta \frac{M}{2} v^2\right) / \int_0^\infty dv \exp\left(-\beta \frac{M}{2} v^2\right) \quad (3)$$

with  $M = m_X m_{\text{CH}_2} / (m_X + m_{\text{CH}_2})$ .

The evaluation of the specific rate given by the formula 2 involves a number of calculations, each of which can sensitively affect the final outcome. Since CD's prime objective was to test the viability of their mechanism, they did not refine these calculations. However once their relatively crude calculations had succeeded in establishing the plausibility of the proposed mechanism, it then became imperative that a more careful calculation be performed. This has been the purpose of the investigation reported here. Each step of the calculation done by CD has been refined and performed much more accurately. From this we find that although the calculations of CD were quite crude and, in some instances, grossly inaccurate, their final conclusions concerning the acceptability of the proposed reaction mechanism are confirmed by our closer and more rigorous scrutiny.

We conclude this section with an outline of how the present

and previous calculations differ from one another and then give in section 3 a more detailed account of the current investigation.

(i) From the vibronic spectra of the methylene radical one obtains the energy gaps  $\Delta W_{mn}^0 = \epsilon_m(^1A_1) - \epsilon_n(^3B_1) + \Delta u^0$ . Here  $\epsilon_m(^1A_1)$  and  $\epsilon_n(^3B_1)$  are vibrational energies while  $\Delta u^0$  denotes the difference between the electronic energies of the singlet and triplet states. CD applied the harmonic oscillator approximation to obtain these vibrational energies. Instead of this we have used recent ab initio calculations of the angle dependence of electronic energy to construct a bending mode vibrational Hamiltonian for the methylene radical. (Because the symmetric and antisymmetric stretching modes are so much stiffer than the bending mode, we can completely ignore their contributions to the rate). The vibrational energies and the associated eigenfunctions then were obtained by numerical methods.

(ii) From these same vibrational eigenfunctions we have computed the values of the Franck-Condon overlap integrals  $S_{mn}$ . The results gotten in this way differ greatly from the average value of  $S \approx 0.1$  suggested by Chang and Basch<sup>4</sup> and used by CD in their earlier calculations.

(iii) CD used for  $v_{SO}$ , the electronic matrix element of the spin-orbit interaction operator, a value ( $9.18 \times 10^{-15}$  erg) appropriate to an isolated carbon atom. Here we use the theoretical value of  $1.595 \times 10^{-15}$  erg ( $8.031 \text{ cm}^{-1}$ ) which recently was reported by Langhoff.<sup>5</sup>

(iv) CD used for  $p_{mn}$  the approximate value of  $2v_{mn}$ . We have eliminated this approximation by directly evaluating the integral (3).

(v) The adiabatic catalyst-radical interactions  $V(^1A_1; \mathbf{r})$  and  $V(^3B_1; \mathbf{r})$  were computed by CD from an adaptation of the Fermi-Thomas statistical theory of pseudopotentials which had been developed by Gombas<sup>6</sup> and applied by Baylis<sup>7</sup> to the calculation of atom-atom interactions. It is not known whether this theory gives reliable predictions for cases such as those involved here. Furthermore, CD used in their calculations very crude methylene wave functions.

The present calculations are based upon accurate methylene wave functions constructed by Schaefer.<sup>8</sup> For the potential functions we have used a modification of the much tested Gordon-Kim theory.<sup>9</sup> This theory and the Schaefer wave functions provide what we believe to be are very reliable estimates for the factors  $\Delta F$  that occur in the Landau-Zener formula 1, for the activation energies  $E_1(\mathbf{r}_0)$ , and for the "crossing surfaces",  $S_{mn}^0$ , defined by  $\Delta W_{mn}(\mathbf{r}_0) = 0$ .

(vi) Finally, we have made a more thorough study than did CD of the angle dependence of the integrand of the formula 2 for  $k_{mn}$ . This information allows us to estimate the value of the integral with greater accuracy.

### 3. Calculations Based Upon the Direct Reaction Model

**3.1. Vibronic States of Methylene.** Several investigations<sup>10</sup> have been made of how the electronic energy of methylene depends upon the angle  $\theta$  of the H-C-H bending mode. The best of these studies appears to be that of Staemmler<sup>11</sup> who (as had others before him) used in his calculations a fixed CH bond length,  $R_{CH}$ , equal to  $2.1 a_0$ . From Staemmler's results<sup>27</sup> we have constructed bending mode vibrational wave functions and eigenvalues for the  $^1A_1$  and  $^3B_1$  states.

The Hamiltonian operator for this bending motion can be written in the form

$$H_{\text{vib}} = -\frac{\hbar^2}{2\mu R_{CH}^2} \frac{d^2}{d\theta^2} + V(\theta) \quad (4)$$

**TABLE I: Numerical Values of the Born-Oppenheimer Potentials for the Methylene Bending Mode<sup>a</sup>**

	$^3B_1$	$^1A_1$
<i>A</i>	1.27(-2)	6.25(-2)
<i>B</i>	1.04(-2)	2.37(-2)
<i>C</i>	-2.95(-2)	-8.28(-2)
$\theta$	$V(\theta)$	$V(\theta)$
90	8.39	-34.01
105	-5.37	-37.01
120	-11.78	-32.92
135	-12.14	-23.38
150	-8.29	-12.33
165	-2.93	-3.61
180	0.0	0.0

<sup>a</sup> Parameters for the analytical fit (eq 5). Energies are in kcal/mol [ $1.27(-2) = 1.27 \times 10^{-2}$ ].

with  $\mu = \mu_0[1 + m_H(m_C + m_H)^{-1} \cos \theta]$  and where  $\mu_0 = \frac{1}{2}m_H(m_C + m_H)(m_C + 2m_H)^{-1}$ . Here  $m_C$  and  $m_H$  are the masses of the carbon and hydrogen atoms, respectively. In Table I we have collected Staemmler's numerical values for the potential functions (Born-Oppenheimer electronic energy eigenvalues) specific to the  $^1A_1$  and  $^3B_1$  states of methylene. These data can be fitted quite well to the analytic forms

$$V(\theta) = (\theta - 180^\circ)^2[A + C \exp\{-B|\theta - 180^\circ|\}] \quad (5)$$

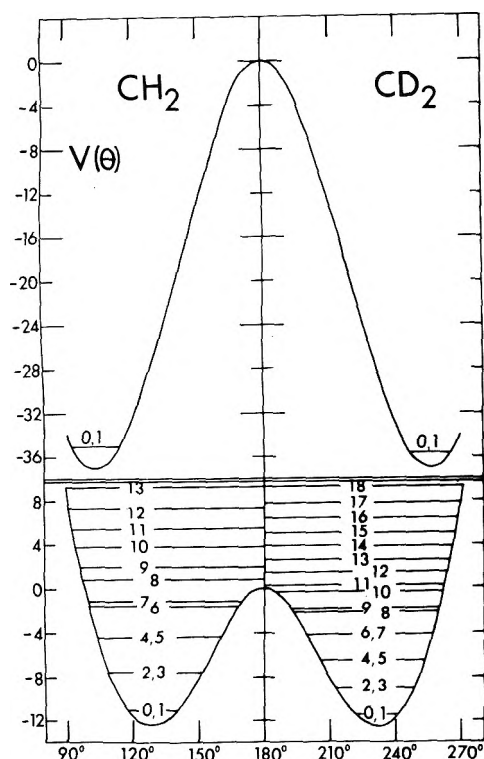
The values of the parameters *A*, *B*, and *C* associated with the two electronic states are included in Table I.

We have used a finite difference boundary value method (and a grid of 899 points)<sup>12</sup> to compute the 20 lowest lying states of  $^3B_1$  and the 2 lowest of  $^1A_1$ . The vibrational spectra obtained in this way are shown in Figure 2 for CH<sub>2</sub> and CD<sub>2</sub>. Because the potentials  $V(\theta)$  exhibit double minima, several of the low lying levels are doubly degenerate—to within the numerical accuracy of our calculations. For convenience we set  $\cos \theta$  in  $\mu$  equal to its average value of zero and so replaced  $\mu$  with  $\mu_0$ . To the Born-Oppenheimer approximation the electronic states of CD<sub>2</sub> and CH<sub>2</sub> are identical. Therefore, to determine the bending mode spectra for CD<sub>2</sub> we had only to replace  $m_H$  in  $\mu$  with  $m_D$ , the mass of a deuteron.

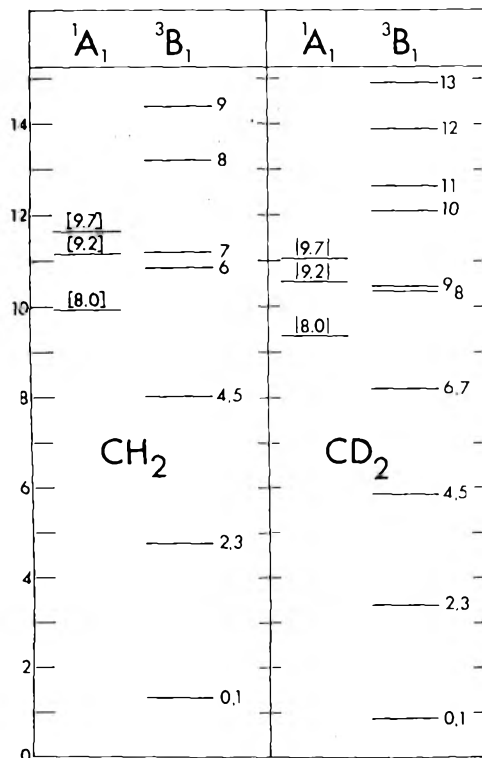
There is uncertainty and considerable controversy<sup>13</sup> over the size of the gap,  $\Delta u^0$ , between the minima of the  $^3B_1$  and  $^1A_1$  potential energy curves. It will be recalled that the reaction mechanism proposed by Chu and Dahler hinges upon a collision induced shift of the two vibronic manifolds. Therefore, the asymptotic positioning of these manifolds, which is fixed by the value  $\Delta u^0$ , will sensitively affect where crossings of the triplet and singlet potential energy surfaces occur. Because of this sensitivity and also because of the current lack of agreement about the  $^3B_1 - ^1A_1$  energy gap we have calculated rates of reaction for three estimates of  $\Delta u^0$ : (1) the most recent "experimental" value of 8.0 kcal/mol due to Frey;<sup>14</sup> (2) the most recent (and lowest result ever gotten from an ab initio calculation) theoretical value of 9.2 kcal/mol obtained by Staemmler;<sup>11</sup> and (3) the theoretical estimate of 9.7 kcal/mol proposed by Harrison.<sup>13</sup>

From Figure 3 one can see where, for each assumed value of  $\Delta u^0$ , the energy of the initial (ground vibrational) singlet state of CH<sub>2</sub> (and CD<sub>2</sub>) lies in relation to the array of unperturbed triplet vibronic energy eigenvalues. Because a catalyst atom interacts differently with singlet and triplet CH<sub>2</sub> (or CD<sub>2</sub>) the arrangements of states shown in these two figures





**Figure 2.** Bending mode vibrational levels of  $\text{CH}_2$  (left side of well) and of  $\text{CD}_2$  (right side). The upper curve is for the  $^1A_1$  electronic state and the lower for  $^3B_1$ . Energy is in kcal/mol and  $180^\circ$  corresponds to the linear configuration.



**Figure 3.** Location of the lowest vibrational energy level of  $\text{CH}_2(^1A_1)$  relative to triplet levels for three different singlet-triplet splittings (indicated by the brackets on the left side). Positions for  $\text{CD}_2$  on right.  $v_2$  is the bending mode vibrational quantum number. Energies are in kcal/mol.

will alter as the catalyst draws near to the radical. Singlet-triplet degeneracies invariably arise provided that the catalyst-radical separation is made sufficiently small. The most important of these degeneracies couple the initial singlet state to those members of the  $^3B_1$  manifold which are its immediate (energetic) neighbors in the asymptotic, precollision configuration. For example, with an asymptotic splitting of  $\Delta u^0 = 8.0$  kcal/mol we see from Figure 3 that the most likely nonadiabatic transitions of  $\text{CH}_2$  are those which will populate either the  $v_2' = 6$  or the almost degenerate  $v_2' = 4, 5$  levels of the triplet. One also can extract from this figure the magnitudes of the energy shifts needed to produce these degeneracies. In Table II we have listed values of the asymptotic energy gaps  $\Delta W_{mn}^0 = \epsilon_m(^1A_1) - \epsilon_n(^3B_1) + \Delta u^0$  for those transitions which contribute the most to the rate of the singlet to triplet transitions.

The transition probabilities for these nonadiabatic events are dependent upon the associated Franck-Condon factors. To calculate the values of these overlap integrals we use the numerical eigenfunctions of the vibrational energy operator  $H_{\text{vib}}$ . These bending mode Franck-Condon factors will differ from zero only for states with equal parities. Furthermore, the lowest of the  $^1A_1$  vibronic levels is doubly degenerate, with one symmetric and one antisymmetric state (vibrational states with even and odd parities, respectively). The first of these is used to calculate the Franck-Condon factors associated with transitions to triplet vibrational states of positive parity whereas the second is used in conjunction with triplet states of odd parity. For the transitions of interest to us the numerical values of the Franck-Condon factors are assembled in Table III.

The vibrational energies reported here differ significantly from those computed by CD on the basis of the harmonic oscillator model and the force constants reported by Bender et al. Furthermore, each of the Franck-Condon factors presented in Table III exceeds by more than an order of magnitude the average value of 0.01 suggested by Chang and Basch<sup>4</sup> and used by Chu and Dahler.

**3.2. Electronic States of Methylene.** The shapes of the electron distributions are quite different for the singlet and triplet ( $^1A_1$  and  $^3B_1$ ) states of methylene. The dominant contributors to these two states are the MO configurations  $^1A_1[(1a_1)^2(2a_1)^2(1b_2)^2(3a_1)^2]$  and  $^3B_1[(1a_1)^2(2a_1)^2(1b_2)^2(3a_1)(1b_1)]$ , respectively. The major component of the  $3a_1$  MO is a  $2p_x$  AO centered on the carbon atom (see Figure 1 for an illustration of the coordinate system used) and the  $1b_1$  MO can be identified with a carbon  $2p_z$  AO.

At small separations the electronic energy of the methylene-catalyst pair will be dominated by the repulsive contribution due to overlap of the two charge distributions. Consequently, when the catalyst approaches the radical along the body-fixed  $z$  axis the interaction will be more repulsive for the triplet than for the singlet. These unequal interactions produce upward shifts of the triplet vibronic manifold relative to the singlet. As the catalyst draws closer still a separation will be reached at which the ground vibrational level of the singlet state becomes degenerate with the vibrationally excited triplet level which lay immediately beneath it in the initial, unperturbed state. A similar argument leads to the conclusion that as the catalyst approaches the radical along the negative  $x$  axis there will be an oppositely directed relative shift of the singlet and triplet manifolds. In this case it is the charge cloud of the singlet state which overlaps more strongly with that of the incident catalyst atom and here the tendency is to develop a degeneracy between the initial singlet level and the vibra-



**TABLE II: Asymptotic Energy Gaps  $\Delta W_{mn}^0$  (in kcal/mol) and Cap Parameters of the Crossing Surfaces for Three Singlet-Triplet Splittings<sup>a</sup>**

	Axis	$\Delta W^0$	$\theta$	$\Omega$
Case 1. $\Delta u^0 = 8.0$ kcal/mol				
CH <sub>2</sub>	z	1.9	25	0.6
	x	-0.9	30	0.8
CD <sub>2</sub>	z	1.15	25	0.6
	x	-2.0	20	0.4
Case 2. $\Delta u^0 = 9.2$ kcal/mol				
CH <sub>2</sub>	z	0.3	>40	>1.5
	x	-0.05	>40	>1.5
CD <sub>2</sub>	z	0.1	>40	>1.5
	x	-1.55	20	0.4
Case 3. $\Delta u^0 = 9.7$ kcal/mol				
CH <sub>2</sub>	z	0.45	40	1.5
	x	-1.55	20	0.4
CD <sub>2</sub>	z	0.6	40	1.5
	x	-1.05	25	0.6

<sup>a</sup> The angle  $\theta$  is in degrees.**TABLE III: Franck-Condon Factors,  $S_{v'v''}$ , for the Important Vibronic Transitions<sup>a</sup>**

	$v_2(^1A_1)$	$v_2(^3B_1)$	$S_{v'v''}$
CH <sub>2</sub>	1	5	0.23
	0	6	0.16
	1	7	0.19
	0	8	0.12
CD <sub>2</sub>	1	7	0.19
	0	8	0.15
	1	9	0.16
	0	10	0.10

<sup>a</sup>  $v_2$  and  $v_2'$  are the bending vibrational quantum numbers for the initial and final levels, respectively.

tionally excited triplet level that lay immediately above it at infinite separation.

In either event, further crossings are possible but they will occur at smaller catalyst-radical separations and so tend to be energetically unfavored. The activation energy for one of these nonadiabatic events is the energy needed to bring the catalyst and radical so close together that this crossing of potential energy surfaces occurs. Thus, the activation energy is equal to the value of the catalyst-singlet potential at the point on the crossing surface. For catalyst-radical orientations other than the two already mentioned the differences between the electronic distributions of the singlet and triplet are far less pronounced. Therefore, curve crossing (if it occurs at all) will take place only at very small separations. Since the activation energies associated with these small separations are so very large the corresponding parts of the crossing surface cannot be reached in thermal collisions. For this reason the portions of the crossing surface where reaction is likely to occur are confined to the vicinities of the  $z$  and minus  $x$  axes. This directionality was predicted by Chu and Dahler and supported by their crude calculations of the adiabatic energy surfaces. In the following section we describe the methods by which we have constructed much more reliable estimates for these interactions. There too shall we devote considerable attention to the variations of activation energy and rate with the relative orientation of catalyst and radical.

**3.3. Gordon-Kim Potentials of Interaction.** Recent studies<sup>15</sup> have shown that the Gordon-Kim (GK) electron gas model provides a reasonably reliable and remarkably inexpensive method for calculating interactions between closed shell systems. Furthermore, the modifications of this model suggested by Rae<sup>16</sup> and by Cohen and Pack<sup>17</sup> apparently have succeeded in increasing its dependability without adding significantly to the expense or effort of the enterprise. Therefore, we have chosen to apply these methods to  $\text{CH}_2(^1A_1) + \text{X}$  and  $\text{CH}_2(^3B_1) + \text{X}$  with X taken to be one of the inert gas atoms, namely, X = He, Ne, Ar, or Kr.

Since the electronic state of the triplet has two unpaired electrons, one really should modify the calculational procedure accordingly. However, Gordon and Kim<sup>18</sup> found that these modifications do not increase the dependability and so we have chosen to proceed as though these electrons were paired.

The GK method uses the undistorted electronic density distributions of the isolated species to calculate the Coulomb interaction between the two. The kinetic, exchange, and correlation energies also can be computed from these undistorted densities provided that one adopts the formulas derived from the uniform electron gas model. We have obtained from Schaefer electronic wave functions for the  $^1A_1$  and  $^3B_1$  states of methylene. The electronic ground state is represented by a single configuration natural orbital wave function. The wave function for the excited, singlet state consists of two configurations of natural orbitals. The orbital occupancies for these two states are  $^3B_1[(1a_1)^2(2a_1)^2(1b_2)^2(3a_1)(1b_1)]$  and  $^1A_1[(1a_1)^2(2a_1)^2(1b_2)^2(3a_1)^2 + (1a_1)^2(2a_1)^2(1b_2)^2(1b_1)^2]$ , respectively. The wave function for the singlet state consists almost entirely of the first configuration, with the second contributing only a few percent. Therefore, it is reasonable to expect that the small admixture of the second configuration will not alter significantly the strong directionality of the reaction surface which was obtained by Chu and Dahler on the basis of a single configuration approximation to the  $^1A_1$  state. This expectation is confirmed by the present calculation.

Wave functions for the inert gas atoms were taken from the Clementi.<sup>19</sup>

The GK potentials have been calculated using a program written by Green<sup>20</sup> and modified according to the prescription provided by Cohen and Pack. These modifications involve corrections due to self-exchange and procedures for incorporating long-range interactions. The GK interaction can be written as the sum,  $V = V_{\text{COUL}} + V_{\text{KE}} + V_{\text{EX}} + V_{\text{CORR}}$ , of four parts. Here

$$V_{\text{COUL}} = \sum_a \sum_b \frac{Z_a Z_b}{|\mathbf{R}_a - \mathbf{R}_b|} + \sum_a Z_a \int d\mathbf{r} \frac{\rho_B(\mathbf{r})}{|\mathbf{R}_a - \mathbf{r}|} + \sum_b Z_b \int d\mathbf{r} \frac{\rho_A(\mathbf{r})}{|\mathbf{R}_b - \mathbf{r}|} + \int d\mathbf{r}_1 \int d\mathbf{r}_2 \frac{\rho_A(\mathbf{r}_1)\rho_B(\mathbf{r}_2)}{|\mathbf{r}_1 - \mathbf{r}_2|} \quad (6)$$

denotes the Coulomb interaction between two systems A and B.  $Z_a$  and  $\mathbf{R}_a$  are the nuclear charge and position of atom a of system A;  $Z_b$  and  $\mathbf{R}_b$  are defined similarly. The symbols  $\rho_A$  and  $\rho_B$  represent the electronic charge densities of the two systems.

According to the uniform electron gas approximation the kinetic, exchange, and correlation energies each can be written in the form

$$V_i = \int d\mathbf{r} [\rho_{AB} E_i(\rho_{AB}) - \rho_A E_i(\rho_A) - \rho_B E_i(\rho_B)] \quad (7)$$

with  $i = \text{KE, EX, or CORR}$ .  $\rho_{AB}$ , the electronic density for the AB system, is set equal to the sum of densities,  $\rho_A + \rho_B$ , of the

separate species. Finally, GK give for the energy densities  $E_i$  the formulas

$$E_{\text{KE}}(\rho) = \frac{3}{10} (3\pi^2)^{2/3} \rho^{2/3}$$

$$E_{\text{EX}}(\rho) = -\frac{3}{4} \left(\frac{3}{\pi}\right)^{1/2} \rho^{1/3} \quad (8)$$

and

$$E_{\text{CORR}} = 0.0311 \ln r_S - 0.048 + 0.009 r_S \ln r_S - 0.01 r_S$$

$$r_S \leq 0.7$$

$$= -0.06156 + 0.01898 \ln r_S \quad 0.7 < r_S < 10$$

$$= -0.438 r_S^{-1} + 1.325 r_S^{-3/2} - 1.47 r_S^{-2} - 0.4 r_S^{-5/2}$$

$$r_S \geq 10$$

wherein  $r_S = (3/4\pi\rho)^{1/3}$ .

Roe<sup>16</sup> has argued that the exchange energy calculated in this way includes a self-exchange part which can be corrected by replacing  $V_{\text{EX}}(\text{GK})$  with

$$V_{\text{EX}}(\text{GKR}) = (1 - 8\delta/3 + 2\delta^2 - \delta^4/3) V_{\text{EX}}(\text{GK})$$

Here  $\delta$  satisfies the equation  $(4N)^{-1} = \delta^3 - 9\delta^4/8 + \delta^6/4$  with  $N$  taken equal to the total number of electrons in the combined AB system.

Finally, the correlation energy computed according to the GK prescription does not include the long-range dispersion interaction,  $V_{\text{DISP}}$ . According to Cohen and Pack<sup>17</sup> the way to handle this is by modifying the GK correlation energy as follows:<sup>28</sup>

$$V_{\text{CORR}}(\text{GKCP}; R) = V_{\text{DISP}}(R) \quad R \geq R_c$$

$$= [V_{\text{DISP}}(R_c)/V_{\text{CORR}}(\text{GK}; R_c)]$$

$$\times V_{\text{CORR}}(\text{GK}; R) \quad R < R_c \quad (9)$$

Here  $R_c$  is the separation at which the function  $V_{\text{CORR}}(\text{GK}; R) - V_{\text{DISP}}(R)$  exhibits a minimum.

We have assumed for the dispersion energy the expression  $V_{\text{DISP}}(R) = -C_6 R^{-6}$  and for the van der Waals coefficient we have used the formula

$$C_6 = 3\alpha_{\text{CH}_2}\alpha_{\text{X}}I_{\text{CH}_2}I_{\text{X}}/2(I_{\text{CH}_2} + I_{\text{X}}) \quad (10)$$

For  $\alpha_{\text{CH}_2}$ , the polarizability of methylene, we have taken the value of  $8.73 a_0^3$  which can be gotten by using simple empirical rules for adding bond polarizabilities.<sup>21</sup> Values of  $\alpha_{\text{X}}$  were extracted from the tabulations of Fraga.<sup>22</sup> For  $I_{\text{CH}_2}$ , the ionization potential of methylene, we used the value of 10.4 eV reported by Harrison and Allen.<sup>23</sup> The ionization potentials of the inert gas atoms were obtained from Moore.<sup>24</sup>

In all the cases considered by Cohen and Pack the values of  $V_{\text{CORR}} - V_{\text{DISP}}$  invariably were positive. However, we occasionally have encountered negative values for this function. Whenever this happened we abandoned the Cohen and Pack procedure and elected instead to shift the values of the dispersion interaction rather than those of the GK correlation potential, i.e., in place of (9) we used

$$V'_{\text{CORR}}(\text{GKCP}; R) = [V_{\text{CORR}}(\text{GK}; R_c)/R_c^{-6}] R^{-6} \quad R \geq R_c$$

$$= V_{\text{CORR}}(\text{GK}; R) \quad R < R_c \quad (9')$$

In some cases this leads to "corrected" van der Waals coefficients,  $C'_6 = -R_c^{-6} V_{\text{CORR}}(\text{GK}; R_c)$  which are as much as three times greater than those computed from formula 10. As we soon shall see, there is some evidence that this scheme pro-

**TABLE IV: Total Argon-Methylene Electronic Interaction Energies Using (1) the Methods of Gordon and Kim,  $E(\text{GK})$ ; (2) Including the Rae Correction  $E(\text{GKR})$ ; and (3) Including the Long-Range Interactions Obtained by Using the Methods of Cohen and Pack,  $E(\text{GKRCP})$ <sup>a</sup>**

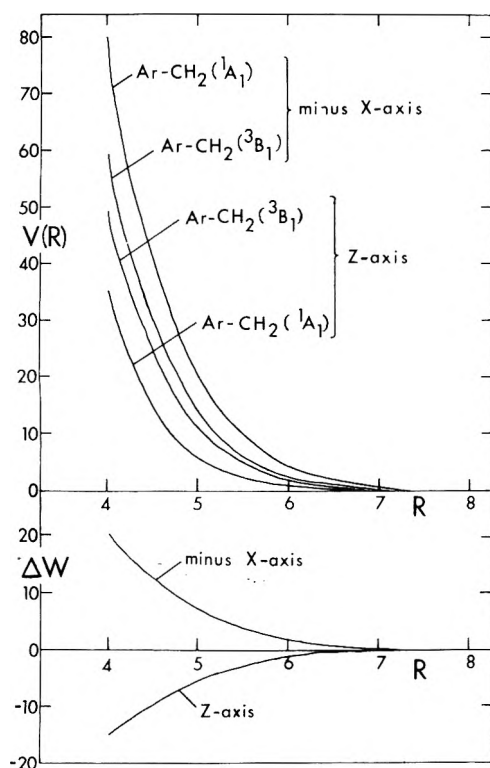
$R$	$E(\text{GK})$	$E(\text{GKR})$	$E(\text{GKRCP})$
<b><math>\text{CH}_2(^1\text{A}_1)</math>, Singlet</b>			
3	130.71	183.75	182.07
4	20.74	35.685	35.032
5	1.984	5.853	5.617
6	0.257	0.687	0.594
7	-0.209	0.010	-0.060
8	-0.071	-0.023	-0.075
<b><math>\text{CH}_2(^3\text{B}_1)</math>, Triplet</b>			
3	132.46	202.11	202.11
4	27.53	49.87	49.87
5	4.187	10.951	10.951
6	0.052	1.974	1.974
7	-0.298	0.230	0.209
8	-0.155	-0.017	-0.053

<sup>a</sup> The argon atom is on the body-fixed  $z$  axis at a distance  $R$  (in bohr) from the carbon atom. Energies are in kcal/mol.

duces more accurate estimates for the long-range tails of the potential functions. However, because these changes are significant only at very large separations they actually have very little effect upon our estimates of the reaction rate.

We adopted this particular alternative to the Cohen-Pack prescription because our confidence was greater in the GK estimate for the correlation energy than in our own relatively crude calculation of the dispersion energy. Thus, we have retained only the first term from the expression  $V_{\text{DISP}}(\text{CP}; R) = -C_6 R^{-6} - C_8 R^{-8} - C_{10} R^{-10}$  used by Cohen and Pack and even then we were forced to rely on the semiempirical formula 10 for the value of  $C_6$ . To gain some feeling for the magnitudes of the terms that have been neglected let us consider the interaction of two argon atoms. In this case  $C_6 = 67.7$ ,  $C_8 = 1280$ , and  $C_{10} = 30\,000$ . For  $R = 6$  (a typical value of  $R_c$ ) the values of  $-C_6 R^{-6}$  and of  $V_{\text{DISP}}(\text{CP}; R)$  are equal to -0.00147 and -0.00271, respectively. Therefore, for separations within this range the higher order terms of the asymptotic series are not at all negligible. Our procedure compensates for this by increasing the numerical value of the  $C_6$ , van der Waals coefficient. There is a second fault to be found with our estimate of the long-range interaction. For the cases of interest to us here (in contrast to those considered by Cohen and Pack) there are dipole-induced dipole interactions and these give rise to additional potential energy contributions proportional to  $R^{-6}$  which are not accounted for by the dispersion theory formula 10.

A detailed account of our numerical results will be given only for the system  $\text{Ar}-\text{CH}_2$ . These are representative of what we have obtained for the other inert gases and for  $\text{CD}_2$  as well. Values of the argon-methylene singlet ( $^1\text{A}_1$ ) interaction energy are listed in Table IV for positions of the argon atom along the body-fixed  $z$  axis. Results obtained from three different approximations are given. The entries labeled GK were calculated without modifying either the exchange or correlation energies. Those with the label GKR incorporate Rae's correction to the exchange energy and so are considerably more repulsive. Finally, the entries in the column headed GKRCP include the Rae correction as well as the Cohen-Pack modification of the correlation energy. The last of these three is



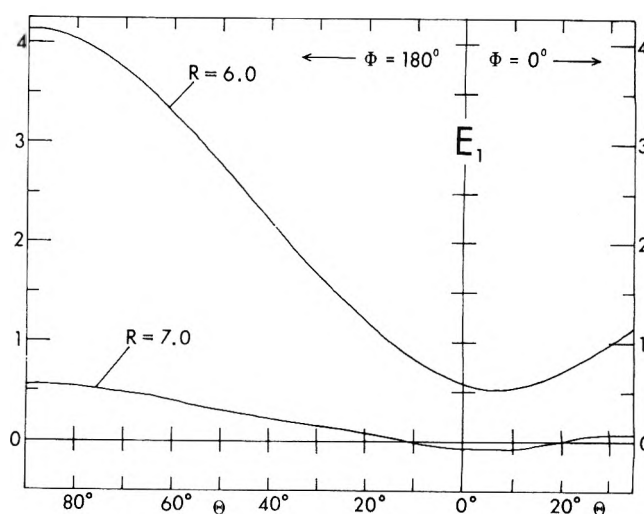
**Figure 4.** Upper portion of diagram displays the total Ar-CH<sub>2</sub> interaction energy (in kcal/mol) as a function of  $R$  (in bohr) for the states and orientations indicated. All states become slightly attractive at large  $R$  to an extent which cannot be seen on this scale. Lower portion shows the dependence of the induced shift,  $\Delta W$ , for the two orientations (same units).

expected to be the most reliable. Table IV contains analogous information about the argon-methylene triplet ( $^3B_1$ ) interaction.

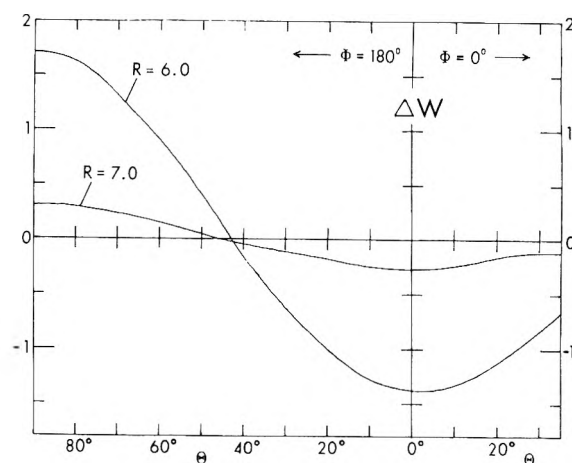
The curves of Figure 4 show the variations of the singlet and triplet interaction energies as the argon atom is moved along the body-fixed  $z$  and minus  $x$  axes. The qualitative features of these potentials clearly conform to our earlier expectations.

The difference between the singlet and triplet potentials of interaction is equal to the collision induced relative shift of the vibronic manifolds. Values of this difference, plotted as functions of the displacement along the coordinate axes, also are displayed in Figure 4. The orientation dependence of the activation energy and the induced shift for configurations in the body-fixed  $xz$  plane are plotted in Figures 5 and 6, respectively. The coordinates used to specify these orientations are depicted in Figure 1.

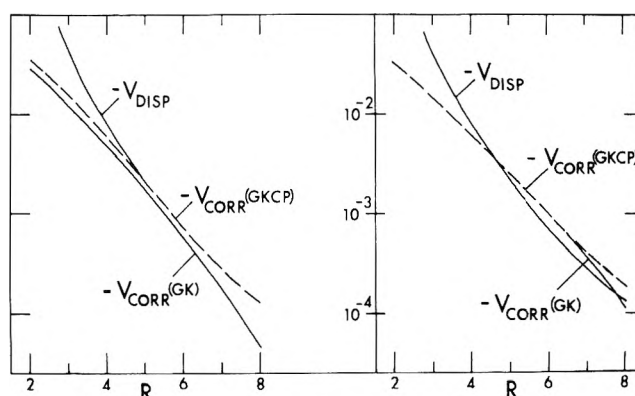
Finally, Figure 7 has been included in order to illustrate how the modifications of the correlation energy actually are carried out. According to the Cohen-Pack prescription the values of the short-range correlation energy are shifted in order that they join smoothly and continuously with the long-range dispersion energy. Figure 7a shows how this is done for Ar-CH<sub>2</sub>( $^1A_1$ ) when the atom is located on the  $z$  axis.  $V_{\text{CORR}}(\text{GK}; R)$  is the correlation energy calculated according to the uniform electron gas model. The adjusted correlation energy is labeled  $V_{\text{CORR}}(\text{GKCP}; R)$ . As one can see from Figure 7b the situation is quite different for the case of Ar-CH<sub>2</sub>( $^3B_1$ ). Here we "shift" the dispersion energy curve until it fits smoothly into the curve of the correlation energy. The effect of this shift is to increase the value of the van der Waals coefficient from 33.4 to 45.3 (in units of  $a_0^6$ ).



**Figure 5.** Orientation dependence of the activation energy for points in the  $xz$  plane for fixed catalyst-radical separations,  $R$ . The  $z$  axis corresponds to  $\theta = 0^\circ$ , and the minus  $x$  axis to  $\theta = 90^\circ$  at the far left of the figure. Energies in kcal/mol and distances in bohr.



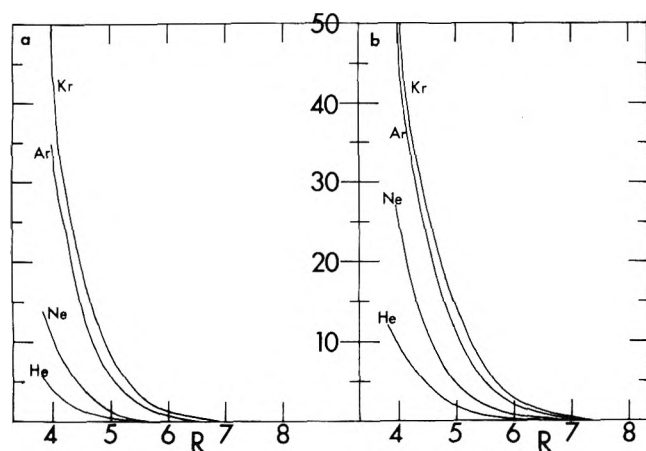
**Figure 6.** Orientation dependence of the induced shift (in kcal/mol).



**Figure 7.** (a) Cohen-Pack correction to the correlation energy (dashed curve) as given by eq 9. Energy in au. (b) Modified Cohen-Pack correction to the correlation energy (dashed curve) as given by eq 9'. Energy in au.

Figure 8 shows how the energies of interaction with singlet and triplet methylene vary—for each of the four inert gases—as the atom is moved along the  $z$  axis.

**3.4. Reaction Rates.** It has been mentioned previously that calculations were performed for the three values 8.0, 9.2, and



**Figure 8.** (a) Catalyst dependence of the interaction energy with methylene in the  $^1A_1$  state. The catalyst is on the body-fixed  $z$  axis. Energy in kcal/mol and distance in bohr. (b) Same as (a) but for the  $^3B_1$  state.

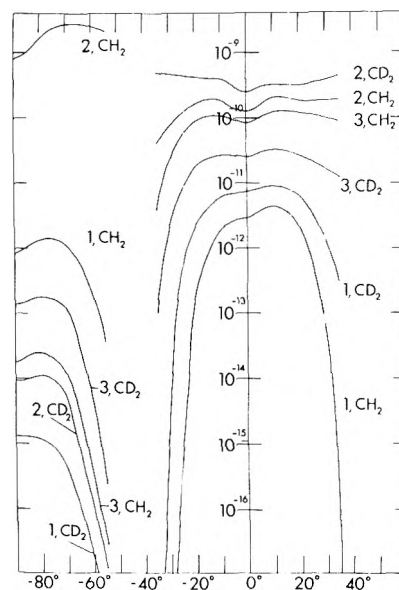
9.7 kcal/mol of the singlet-triplet electronic energy gap  $\Delta u^0$ . For each value of this parameter estimates can be made for the asymptotic values  $\Delta W_{mn}^0 = \epsilon_m(^1A_1) - \epsilon_n(^3B_1) + \Delta u^0$  of the energy differences between various pairs of singlet and triplet vibronic levels. Then, from a knowledge of the adiabatic interaction potentials  $V(^1A_1; \mathbf{r})$  and  $V(^3B_1; \mathbf{r})$  one can construct for each value of  $\Delta W_{mn}^0$  the locus of points  $\mathbf{r}_0^{mn} \equiv (r_0, \theta_0, \phi_0)$  for which  $\Delta W_{mn}^0 + \Delta V(\mathbf{r}_0^{mn}) = 0$ . This is the procedure that generates the crossing surfaces,  $\mathcal{S}_{mn}^0$ .

For most pairs of states and for most relative orientations ( $\theta_0, \phi_0$ ) the values of the activation energy  $E_1(\mathbf{r}_0^{mn}) = V(^1A_1; \mathbf{r}_0^{mn})$  greatly exceed that of  $\beta^{-1} = k_B T$ . This is very important because the rate of the singlet to triplet reaction will be dominated by those vibronic transitions  $\text{CH}_2(^1A_1; 0, 0, 0) \rightarrow \text{CH}_2(^3B_1; 0, \nu_2', 0)$  for which the values of  $\beta E_1(\mathbf{r}_0)$  are of the order of unity. (Here  $\nu_2'$  is the vibrational quantum number associated with the  $\text{CH}_2$  bending mode.) Because there is a large spacing (relative to the value of  $\beta^{-1}$ ) between neighboring states of the triplet vibronic manifold, only one or at most two of these levels ever contribute significantly to the rate of reaction. (The values of  $\Delta W_{mn}^0$  for these pairs of states are presented in Table II. Entries with positive values refer to situations where the energy of the initial singlet state lies above that of the triplet. For negative values of  $\Delta W_{mn}^0$  the triplet, final state lies above the singlet. Transitions of these two types are favored by collisions in which the catalyst lies along the body-fixed  $z$  and minus  $x$  axes, respectively.)

Already we have learned that the parts of the crossing surfaces where reaction is favored lie near the  $z$  and minus  $x$  axes of the body fixed frame of reference. Therefore, it is sensible to use the mean value theory to express the rate given by (2) in the form  $k_{mn}^x + 2k_{mn}^z$ . Here the quantities  $k_{mn}^v$  (with  $v = x, z$ ) are defined by

$$k_{mn}^v = A_v \left\{ \frac{f_{\text{rot}}^v(\mathbf{r}_0)}{f_{\text{rot}}^{\text{CH}_2}} \rho_{mn}(\mathbf{r}_0) \exp\{-\beta E_1(\mathbf{r}_0)\} \right\}_{\mathbf{r}_0 = \mathbf{r}_0^v} \quad (11)$$

and  $\mathbf{r}_0^x = (r_{0x}, \pi/2, \pi)$  and  $\mathbf{r}_0^z = (r_{0z}, 0, 0)$ .  $r_{0x}$  and  $r_{0z}$  are the distances to the crossing surface measured along the minus  $x$  and  $z$  axes, respectively. Finally, the magnitude of  $A_x = \Omega_x r_{0x}^{-2}$  (and of  $A_z = \Omega_z r_{0z}^{-2}$ , analogously) equals the size of the region on the crossing surface to which can be assigned (in the sense of the mean value theorem) the value of the rate at  $\mathbf{r}_0^x$ . We effectively replace the actual crossing surface by a spherical cap which extends to an angle  $\theta_x$  off the minus  $x$  axis. The solid angle subtended by this cap is given by  $\Omega_x = 2\pi(1$



**Figure 9.** Orientation dependence for the rate (integrand of eq 2) in  $\text{cm}^3 \text{s}^{-1}$ . Curves labeled 1, 2, and 3 correspond to  $\Delta u^0 = 8.0, 9.2, \text{ and } 9.7$  kcal/mol, respectively. The  $z$  axis corresponds to  $\theta = 0^\circ$ , and the minus  $x$  axis to the left side of the figure. Points on the left contribute to  $k_x$  and those in the center to  $k_z$ .

$-\cos \theta_x$ ). The quantities  $\Omega_z$  and  $\theta_z$  are similarly defined and related to one another.

To determine the numerical values of  $\theta_x$  and  $\theta_z$  we calculated the rate (integrand of formula 2) at various points on the crossing surface for the Ar-methylene system. In Figure 9 we have plotted these rates for points on the crossing surface in the  $xz$  plane. The rates (for both  $\text{CH}_2$  and  $\text{CD}_2$ ) for the three asymptotic splittings considered are displayed: the labels 1, 2, and 3 refer to the values of  $\Delta u^0 = 8.0, 9.2, \text{ and } 9.7$  kcal/mol, respectively. As expected the rates generally diminish as the point on the crossing surface moves away from the  $z$  or minus  $x$  axes. The slight increases of rate in the immediate vicinity of the axes are due to the increased density of rotational states of the complex for these less symmetric configurations. For the cases with very small asymptotic gaps (e.g., for 2,  $\text{CD}_2$  where  $\Delta W^0 = 0.1$  kcal/mol this decrease occurs much farther from the axes. The decreases associated with displacements in others directions from the axes are similar but typically (for a given splitting) slightly slower than those shown. From these calculations we determined the values of  $\theta_x$  and  $\theta_z$  that are shown in Table II along with the corresponding values of  $\Omega_x$  and  $\Omega_z$ .

For the cases with small gaps ( $<0.5$  kcal/mol) the rates are orders of magnitude larger than experiment. At room temperature at least half the collisional orientations will be reactive. For larger gaps the calculated rates agree well with experiment and only 15–20% of the surface is accessible. This directionality was predicted by CD, although it turns out to be somewhat less pronounced than they had expected. The area of these caps will depend slightly on the particular catalyst atom since the densities of rotational states are greater for the heavier species. Believing this effect to be small we have calculated the overall rates for all catalysts using the cap sizes determined for argon. These results are presented in Table V along with the parameters which characterize the crossing surface on the  $z$  and minus  $x$  axes. These rates depend on the value assumed for the energy gap  $\Delta u^0$  and also upon the choice of the catalyst species  $X = \text{He, Ne, Ar, Kr}$ . This table also contains the values of the vibrational quantum

**TABLE V: Rates for Collision Induced Singlet to Triplet Transition in CH<sub>2</sub> and CD<sub>2</sub> (in cm<sup>3</sup> s<sup>-1</sup>) Using the Direct Reaction Model<sup>a</sup>**

		$v_{2x}'$	$v_{2z}'$	$r_{0x}$	$r_{0z}$	$E_{1x}$	$E_{1z}$	$ \Delta F(\mathbf{r}_0^x) $	$ \Delta F(\mathbf{r}_0^z) $	$k_x$	$k_z$	$k$
$\Delta u^0 = 8.0$ kcal/mol												
CH <sub>2</sub>	He	6	5.4	5.4	4.7	1.9	1.0	1.6	2.2	1.4(-13)	5.4(-13)	7.6(-13)
	Ne	6	5.4	5.9	5.4	1.8	0.5	1.7	3.1	6.3(-13)	3.6(-12)	4.8(-12)
	Ar	6	5.4	6.4	5.8	2.1	1.0	1.5	2.7	7.2(-13)	2.9(-12)	4.1(-12)
	Kr	6	5.4	6.6	5.9	2.0	1.5	1.5	2.0	1.0(-12)	2.2(-12)	4.1(-12)
CD <sub>2</sub>	He	8	6.7	4.8	5.0	5.2	0.4	3.1	1.7	1.1(-16)	1.1(-12)	1.3(-12)
	Ne	8	6.7	5.4	5.6	4.5	0.2	3.6	2.1	1.3(-15)	5.1(-12)	6.1(-12)
	Ar	8	6.7	5.9	6.1	4.7	0.4	3.1	1.8	1.9(-15)	6.6(-12)	7.9(-12)
	Kr	8	6.7	6.0	6.2	5.0	0.6	2.6	1.7	1.8(-15)	7.2(-12)	8.6(-12)
$\Delta u^0 = 9.2$ kcal/mol												
CH <sub>2</sub>	He	7	6	6.8	5.8	-0.1	0.03	0.1	0.6	1.6(-10)	1.5(-11)	2.8(-10)
	Ne	7	6	7.2	6.3	0.1	0.01	0.1	0.7	4.2(-10)	4.8(-11)	7.7(-10)
	Ar	7	6	7.7	7.0	0.1	-0.02	0.2	0.5	5.1(-10)	1.3(-10)	1.2(-9)
	Kr	7	6	7.9	7.0	0.0	-0.03	0.1	0.6	8.4(-10)	1.4(-10)	1.7(-9)
CD <sub>2</sub>	He	10	9	5.0	6.4	3.6	-0.02	2.4	0.25	1.7(-15)	3.0(-11)	9.0(-11)
	Ne	10	9	5.6	6.8	3.5	-0.02	3.0	0.25	6.0(-15)	1.0(-10)	3.0(-10)
	Ar	10	9	6.0	7.4	3.6	-0.07	2.5	0.24	9.6(-15)	2.2(-10)	6.6(-10)
	Kr	10	9	6.2	7.6	3.8	-0.1	2.2	0.24	1.0(-14)	3.0(-10)	9.0(-10)
$\Delta u^0 = 9.7$ kcal/mol												
CH <sub>2</sub>	He	8	7	5.0	5.6	3.6	0.08	2.4	0.9	3.3(-15)	9.6(-12)	2.9(-11)
	Ne	8	7	5.6	6.2	3.5	0.02	3.0	0.8	1.2(-14)	4.5(-11)	1.4(-10)
	Ar	8	7	6.0	6.7	3.6	0.03	2.5	0.7	1.9(-14)	8.4(-11)	2.5(-10)
	Kr	8	7	6.2	6.8	3.8	0.05	2.2	0.9	2.0(-14)	8.1(-11)	2.4(-10)
CD <sub>2</sub>	He	10	9	5.2	5.5	2.6	0.1	1.9	1.0	1.2(-14)	3.6(-12)	1.1(-11)
	Ne	10	9	5.8	6.0	2.2	0.05	2.0	1.2	9.0(-14)	1.2(-11)	3.6(-11)
	Ar	10	9	6.3	6.6	2.4	0.1	1.8	1.0	1.2(-13)	2.5(-11)	7.5(-11)
	Kr	10	9	6.5	6.7	2.1	0.1	1.6	1.0	3.3(-13)	2.8(-11)	8.4(-11)

<sup>a</sup> See the text for definitions of tabulated parameters.

number  $v_{2z}'$  of the final, triplet state bending mode. Also included are the coordinate values  $r_{0x}$  and  $r_{0z}$  of the crossing surface,  $E_{1x}$  and  $E_{1z}$  the corresponding values of the activation energy, and  $\Delta F_1(\mathbf{r}_0^{\nu})$ ; with  $\nu = x, z$ , the difference of slopes of the adiabatic potential energy functions at the location of the crossing surface. Distances are recorded in units of bohrs ( $a_0$ ), energies in kilocalories per mole, and specific rates in (centimeters)<sup>3</sup>(second)<sup>-1</sup>.

The integral  $p_{mn}$  defined by (3) can be expressed as the product of the approximation,  $2v_{mn}$ , used by CD and a "correction factor"

$$C(E) = (\pi E)^{-1/2} \int_0^1 dx g(x; E) [1 - g(x; E)]$$

with

$$g(x; E) = \exp\{-[E(1 - \ln x)^{-1}]^{1/2}\}$$

which depends upon the value of the dimensionless variable  $E_{mn} = \beta(M/2)v_{mn}^2$ . For values of the coupling matrix element of interest to us here, the value of  $C(E)$  never differs from unity by more than 2 or 3%.

#### 4. The Collision Complex Model

According to the statistical theory<sup>2</sup> the cross section for the singlet to triplet transition can be decomposed into the product

$$\sigma(E) = \sigma_{cc}(E) \int dJ \rho(J) P(E, J) \quad (12)$$

of the cross section,  $\sigma_{cc}(E)$ , for complex formation with a second factor which is equal to the fraction of these capture

events that produce triplet radicals. Here  $E$  denotes the total energy of the catalyst-radical pair (measured relative to the energy of the initial, singlet vibronic state),  $J$  the total angular momentum of the complex, and  $\rho(J)$  the unit normalized distribution of this angular momentum. Finally, the fraction  $P(E, J)$  is related by the formula

$$P(E, J) = \Delta_2(E, J) / [\Delta_1(E, J) + \Delta_2(E, J)] \quad (13)$$

to the rates,  $\Delta_1$  and  $\Delta_2$ , at which a complex (formed in a collision with energy  $E$  and angular momentum  $J$ ) decays into the entrance and triplet channels, respectively. In the usual formulation of the statistical theory these rates are identified with the rates of transmission through certain "critical configurations"—in our case the singlet-triplet crossing surface and the configuration at which "capture" occurs. Tully expresses these rates in the form

$$\Delta_i(E, J) = \int_0^{E-B_i(J)} d\epsilon_i \Gamma_i(\epsilon_i) N_i(W_i) / h N^*(W^*) \quad (14)$$

where  $\epsilon_i$  is the energy of translation along the reaction coordinate at the location of critical configuration  $i$ .  $W_i$  and  $W^*$  are the energies available for distribution among the "active modes" of the critical configuration  $i$  and among those of the collision complex.  $N_i$  and  $N^*$  are the corresponding densities of internal states. According to the classical (RRK) theory  $N_i(W_i) = W_i^{s_i-1}$  where  $s_i$ , the effective number of oscillators associated with the configuration  $i$ , is equal to the sum of the number of vibrational modes plus one-half the number of active rotations. In the present case this prescription yields  $s_i = 9/2$ . By energy conservation  $W_i = E - B_i(J) - \epsilon_i$  where

TABLE VI: Constants Used in Collision Complex Model Calculation<sup>a</sup>

	$\alpha$	$m$	IP	$\mu(\text{CH}_2\text{-X})$	$\mu(\text{CD}_2\text{-X})$	$C_6$
CH <sub>2</sub>	8.78	14.0	10.4			
CD <sub>2</sub>	8.78	16.0	10.4			
He	1.40	4.0	24.6	3.11	3.20	4.94
Ne	2.69	20.2	21.6	8.27	8.93	9.14
Ar	11.01	39.9	15.8	10.38	11.42	33.4
Kr	16.75	83.8	14.0	12.02	13.43	48.4

<sup>a</sup> Dipole polarizability,  $\alpha$  (a.u.<sup>3</sup>); masses,  $m$  (amu); ionization potentials, IP (eV); reduced masses,  $\mu$  (amu); and van der Waals coefficients,  $C_6$  (au a.u.<sup>6</sup>).

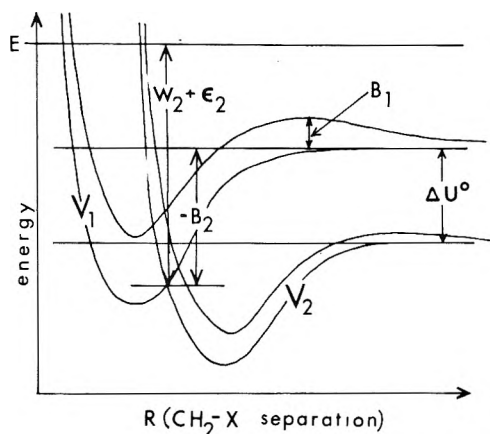


Figure 10. Schematic representation of "critical configurations",  $R_1$  and  $R_2$  in collision complex model. Curves  $V_1$  and  $V_2$  represent initial and final potential energy surfaces. Other quantities are defined in the text.

$B_i$  is the value of the effective potential energy for the critical configuration  $i$ . The quantity  $\Gamma_i(\epsilon_i)$  which appears in (14) is the probability that the complex will decay to products when it reaches the critical configuration  $i$ .

A schematic representation of these various energies and configurations is presented in Figure 10. The initial state potential energy curve (which actually is a surface) is labeled  $V_1$ .  $V_2$  is the potential associated with the vibronically excited triplet, final state. The dashed curve lying above  $V_1$  represents the effective potential  $V_1 + J^2/2MR^2$ . The "capture radius"  $R_1$  is the separation at which this effective potential exhibits a local maximum. Because this capture radius is expected to be rather large, its value can be estimated by neglecting the short-range interactions and replacing  $V_1(R)$  with the dispersion energy  $V_{\text{DISP}} = -C_6R^{-6}$ . To this approximation one finds that the value of the effective potential at the local maximum is equal to  $B_1(J) = J^3(54C_6M^3)^{-1/2}$ . For energies in excess of this maximum the transmission coefficient  $\Gamma_1$  will be equal to unity.

For given  $E$  the complex can reach this critical configuration only if the angular momentum is less than  $J_{\text{max}}(E) = (54C_6M^3E^2)^{1/6}$ . Tully assumes that each collision which reaches this configuration results in capture and so obtains the formula  $\sigma_{\text{cc}}(E) = (\pi/2mE)J_{\text{max}}^2(E)$  for the capture cross section.

The second critical configuration occurs at the location  $R_2 (= r_{0x} \text{ or } r_{0z})$  of the singlet-triplet crossing surface. In terms of this separation the critical potential  $B_2(J)$  is given by  $E_1(R_2) + J^2/2MR_2^2$  where  $E_1(\mathbf{r}) \equiv V(^1A_1; \mathbf{r})$  is the adiabatic interaction energy for the catalyst with methylene in the singlet state. The decay process associated with this second critical configuration is the spin-orbit coupled singlet to

TABLE VII: Rates of Singlet-to-Triplet Transition (in  $\text{cm}^3 \text{s}^{-1}$ ) of Methylene for Thermal Collisions with Inert Gas Atoms as Calculated from the Collision Complex Model<sup>a</sup>

	Catalyst	$\Delta u^0 = 8.0$	9.2	9.7
CH <sub>2</sub>	He	4.4(-15)	1.2(-12)	6.2(-13)
	Ne	2.7(-14)	1.6(-12)	1.5(-12)
	Ar	5.8(-15)	5.3(-12)	2.1(-12)
	Kr	1.6(-15)	5.5(-12)	1.4(-12)
CD <sub>2</sub>	He	5.2(-14)	6.9(-12)	4.1(-13)
	Ne	1.5(-13)	7.6(-12)	6.3(-13)
	Ar	8.1(-14)	2.4(-11)	7.1(-13)
	Kr	3.8(-14)	3.5(-11)	7.4(-13)

<sup>a</sup> Rates presented are for three singlet-triplet splittings (in kcal/mol) [ $4.4(-15) = 4.4 \times 10^{-15}$ ].

triplet transition. Therefore, it is sensible to select for  $\Gamma_2$  the Landau-Zener approximation  $1 - \exp(-\gamma)$  with  $\gamma_{mn} = v_{mn}/v_2 \equiv v_{mn}/(2\epsilon_2/M)^{1/2}$ .

With these assumptions and approximations the specific rate

$$k(\beta) = (8/\pi M)^{1/2} \beta^{3/2} \int_0^\infty dE E \sigma(E) \exp(-\beta E)$$

assumes the form

$$k(\beta) = [8\pi(\beta/M)^3]^{1/2} \int_0^\infty dE \exp(-\beta E) \times \int_0^{J_{\text{max}}(E)} dJ J [9A|E - E_1 - J^2/2MR_2^2|^4] [9A|E - E_1 - J^2/2MR_2^2|^4 + \{E - (54C_6M^3)^{-1/2} J^3\}^2]^{-1} \quad (15)$$

The quantities  $A = (M/2)^{1/2} v_{mn}$  and  $E_1(r)$  which appear in this formula are to be evaluated at a point  $\mathbf{r}_0 = (R_2, \theta_0, \phi_0)$  on the crossing surface.

This integral was evaluated numerically for CH<sub>2</sub> and CD<sub>2</sub> in combination with each of the inert gases He, Ne, Ar, and Kr, and for the same three values of  $\Delta u^0$  (8.0, 9.2, and 9.7 kcal/mol) used in conjunction with the CD theory. The values of the parameters needed for these calculations are compiled in Table VI. The van der Waals coefficients  $C_6$  were generated from formula 10. Values of other parameters such as locations of the crossing surfaces, activation energies, Franck-Condon factors, and  $\Delta F$  have been reported earlier in the paper.

The rate constants presented in Table VII were calculated for the critical configuration  $\mathbf{r}_0^z = (r_{0z}, 0, 0)$ . Rates calculated for the critical configuration  $\mathbf{r}_0^x = (r_{0x}, \pi/2, \pi)$  generally were found to be much smaller because of the correspondingly larger values of the activation energy. The only exception to this was when  $\Delta u^0 = 9.2$  kcal/mol and  $\Delta W_{17^0} = -0.05$  kcal/

mol, in which case the rates for the two critical configurations were of comparable magnitudes.

## 5. Discussion of Results

The thermal rates for the He and Ar collision induced singlet-to-triplet transition of methylene have been observed by several investigators. Eder and Carr<sup>25</sup> report that the rate with Ar is three times larger than with He in the case of CH<sub>2</sub> and 1.5 times larger in the case of CD<sub>2</sub>. The rate for CD<sub>2</sub> with He is faster by a factor of 3 than for CH<sub>2</sub>. Similar results were obtained by Braun, Bass, and Pilling<sup>26</sup> who reported the rates for CH<sub>2</sub> with He and Ar to be  $(3.0 \pm 0.7) \times 10^{-13}$  and  $(6.7 \pm 1.3) \times 10^{-13}$  cm<sup>3</sup> s<sup>-1</sup>, respectively.

We have found that the direct reaction model and the collision complex model both are very sensitive to the asymptotic energy spacing between the initial and final vibronic levels. Changes of these spacings can result in orders of magnitude shifts of the overall reaction rates. Our results reveal that singlet-triplet splittings do exist for which each of these models is capable of reproducing the experimental observations. Thus, reasonably good agreement was obtained with the direct reaction model for a splitting of 8.0 kcal/mol and with the collision complex model for a splitting of 9.2 kcal/mol. However, for most choices of the singlet-triplet energy gap neither of these theories correctly predicts the experimentally observed isotope or catalyst dependences of the rates. If one adds to these the criterion that the theory also generate rates of the correct order of magnitude, then the range of "acceptable"  $\Delta u^0$  values is even more severely limited. Indeed, it can be seen from Figure 3 that there is a chance for the direct reaction model to satisfy all three of these requirements only if  $\Delta u^0$  lies near one of the values 1.0, 8.0, or 10.2 kcal/mol. The reason for this is that quite large singlet-triplet vibronic energy spacings are needed to produce rates as small as those observed. In fact it seems likely that the value of 10.2 kcal/mol also must be rejected because it probably would generate unacceptably large rates. We have not considered splittings in excess of 12 kcal/mol because the theoretical (variational) estimates of Staemmler and others<sup>10,11,13,23</sup> are understood to provide upper bounds to the value of  $\Delta u^0$ . Even if one is hesitant to accept this direct reaction model (or the collision complex model either) as a suitable tool for identifying the correct value of  $\Delta u^0$  our discussion here will have served to draw attention to how very sensitively the theoretical predictions depend on the value of this parameter. Furthermore, it is interesting to note that if one accepts this theory, then observation of the vibrational states of the product triplet radicals would permit a rather direct determination of  $\Delta u^0$ . The theory predicts that only one or two such levels should be significantly populated.

Because no strongly attractive short-range interactions are involved the methylene-inert gas systems considered here differ significantly from those to which the collision complex model previously has been applied. Nevertheless, it is not beyond the reach of imagination that a loosely bound CH<sub>2</sub>-X complex might persist long enough to satisfy the criteria for applicability of the Tully theory. Our classical treatment of the density of states is a severe approximation. Furthermore, because the available energies are so small our use of classical statistics to treat the breakup of the complex may introduce serious errors. The striking prediction of this classical treatment is that the complex is far less likely to undergo a singlet-to-triplet transition than it is to reemerge into the entrance channel. Because of this the probability that complex formation will result in a singlet-triplet transition actually

is much less (rates smaller by two orders of magnitude) than that such a transition takes place in a single, direct collision. Rather than the expected enhancement due to multiple crossings of the transition zone, we obtain instead a significant diminution. However, our calculations clearly indicate that the mechanism of complex formation cannot be discounted and that it may contribute significantly to the overall rate.

NOTE ADDED IN PROOF: Since the calculation's reported here were completed and this article submitted for publication two new experimental determinations of the methylene singlet-triplet splitting have appeared in the literature. The first of these by Simons and Curry<sup>28</sup> reported a value of  $8.3 \pm 1.0$  kcal/mol, which agreed very well with what then was accepted widely by both experimentalists and theoreticians to be the true splitting. It also agreed nicely with our rate-constant-determined value of 8.0 kcal/mol.

The second paper caught us by surprise. From a quite convincing analysis of photoelectron experiments on CH<sub>2</sub><sup>-</sup>, Zittel et al.<sup>30</sup> determined the level splitting to be  $19.5 \pm 0.7$  kcal/mol. Since this differs so much from the previously accepted range of values we had performed no calculations for level splittings of this size. However, despite this lack of specific calculations there are reasons for expecting that the theories presented here still may predict rates in substantial agreement with experiment even with this new value for the level splitting. Thus, in order that the rates predicted by the collision complex model be as large as those observed experimentally it is sufficient that  $\Delta u^0$  be such that it result in asymptotic gaps which are sufficiently small. This possibility is by no means precluded by the value of  $\Delta u^0 = 19.5$  kcal/mol.

On the other hand, the direct mechanism will overestimate the rates of reaction unless the spacings between adjacent vibronic levels of the singlet manifold are quite large. From our calculations it was estimated that for CH<sub>2</sub> this spacing must exceed 2.5 kcal/mol. We find (see our Figure 2) as do Zittel et al. (see their Figure 3) that the level splitting in this region is somewhat greater than 2 kcal/mol. Indeed, the spacings generated by Zittel et al. appear to be larger than ours. It is to be expected that the actual potential curve will not remain parabolic as the vibrational energy increases; H-H repulsion must cause a more rapid rise as the H-C-H bond angle diminishes. Also, the Franck-Condon factors we have calculated for transitions to the upper levels (for CH<sub>2</sub>:  $S_{1,1,3} = 0.038$  and  $S_{0,1,4} = 0.023$ ) are almost an order of magnitude smaller than those for the transitions reported in this paper. Therefore, it is quite possible that we would obtain agreement with experiment for a value of  $\Delta u^0$  near 19.5 kcal/mol. We believe that the existence of this new, unexpectedly large value of the splitting alters in no significant way the conclusions reached in the present paper. It remains clear that a marked improvement on our results can be obtained only by including a more rigorous treatment of the collision dynamics. Such calculations are now being considered.

*Acknowledgments.* We are deeply indebted and grateful to Kei-May Lau for computational assistance. To Professor H. F. Schaeffer, III, go our sincere thanks for the methylene wave functions used in this study. Also we thank Professor D. G. Truhlar for the use of his finite difference boundary value method program and for the help he gave to us in running it. Finally, we appreciate the advice concerning Gordon-Kim potentials which was provided to us by Dr. Russell T Pack.

Acknowledgment is made to the National Science Foundation and to the donors of the Petroleum Research Fund,



administered by the American Chemical Society, for partial support of this research.

## References and Notes

- <sup>†</sup> A preliminary report of this work appeared in K. C. Kulander and J. S. Dahler, *Chem. Phys. Lett.*, **41**, 125 (1976).
- (1) M. Y. Chu and J. S. Dahler, *Mol. Phys.*, **27**, 1045 (1974); paper 1 in this series.
- (2) J. C. Tully, *J. Chem. Phys.*, **61**, 61 (1974); see also G. E. Zahr, R. K. Preston, and W. H. Miller, *J. Chem. Phys.*, **62**, 1127 (1975).
- (3) J. C. Tully, *J. Chem. Phys.*, **62**, 1893 (1975).
- (4) T. Y. Chang and H. Basch, *Chem. Phys. Lett.*, **5**, 147 (1970).
- (5) S. R. Langhoff, *J. Chem. Phys.*, **61**, 3881 (1974).
- (6) P. Gombas, "Pseudopotentials", Springer-Verlag, New York, N.Y., 1967.
- (7) W. E. Baylis, *J. Chem. Phys.*, **51**, 2665 (1969).
- (8) S. V. O'Neil, H. F. Schaefer, III, and C. F. Bender, *J. Chem. Phys.*, **55**, 162 (1971).
- (9) R. G. Gordon and Y. S. Kim, *J. Chem. Phys.*, **56**, 3122 (1972); Y. S. Kim and R. G. Gordon, *ibid.*, **61**, 1 (1974).
- (10) J. F. Harrison, *J. Am. Chem. Soc.*, **93**, 4112 (1971); C. F. Bender, H. F. Schaefer, III, D. R. Franceschetti, and L. C. Allen, *ibid.*, **94**, 6888 (1972); P. J. Hay, W. J. Hunt, and W. A. Goddard, *Chem. Phys. Lett.*, **13**, 30 (1972); and especially ref 23 for earlier work.
- (11) V. Staemmler, *Theor. Chim. Acta*, **31**, 49 (1973).
- (12) D. G. Truhlar, *J. Comp. Phys.*, **10**, 123 (1972). Professor Truhlar supplied us with his program for these calculations.
- (13) J. F. Harrison, *Acc. Chem. Res.*, **7**, 378 (1974).
- (14) H. M. Frey, *J. Chem. Soc., Chem. Commun.*, **18**, 1024 (1972).
- (15) S. Green, B. J. Garrison, and W. A. Lester, Jr., *J. Chem. Phys.*, **63**, 1154 (1975), and references therein.
- (16) A. I. M. Rae, *Chem. Phys. Lett.*, **18**, 574 (1973).
- (17) J. S. Cohen and R. T. Pack, *J. Chem. Phys.*, **61**, 2372 (1974).
- (18) Y. S. Kim and R. G. Gordon, *J. Chem. Phys.*, **60**, 1842 (1974).
- (19) E. Clementi, *IBM J. Res. Develop.*, **9**, 2 (1965).
- (20) S. Green and R. G. Gordon, Program 251, Quantum Chemistry Program Exchange (QCPE), Indiana University, Bloomington, Ind.
- (21) J. O. Hirschfelder, C. F. Curtiss, and R. B. Bird, "Molecular Theory of Liquids and Gases", Wiley, New York, N.Y., 1954, p 951.
- (22) J. Thorhallsson, C. Fisk, and S. Fraga, *Theor. Chim. Acta*, **10**, 388 (1968).
- (23) J. F. Harrison and L. C. Allen, *J. Am. Chem. Soc.*, **91**, 807 (1969).
- (24) C. Moore, Ed., *Natl. Bur. Stand., Circ. No. 467*, Vol. 1 (1949).
- (25) T. W. Eder and R. W. Carr, *J. Chem. Phys.*, **53**, 2258 (1970).
- (26) W. Braun, A. M. Bass, and M. Pilling, *J. Chem. Phys.*, **52**, 5131 (1970).
- (27) We have used the energies from Staemmler's best SCF calculations, namely, his basis set C.
- (28) Here and throughout this section we use symbols such as  $V_{\text{CORR}}(R)$  and  $V_{\text{EX}}(R)$  to denote the functional dependence of the interaction energy contributions upon the catalyst-radical separation  $|r| \equiv R$  for a fixed relative orientation of the two species.
- (29) J. W. Simons and R. Curry, *Chem. Phys. Lett.*, **28**, 171 (1976).
- (30) P. F. Zittel, G. B. Ellison, S. V. O'Neil, E. Herbst, W. C. Lineberger, and W. P. Reinhardt, *J. Am. Chem. Soc.*, **98**, 3732 (1976).

## Application of a Modified Elastic Spectator Model to Proton Transfer Reactions in Polyatomic Systems

M. L. Vestal,\* A. L. Wahrhaftig, and J. H. Futrell

Department of Chemistry, University of Utah, Salt Lake City, Utah 84112 (Received March 8, 1976)

Publication costs assisted by the Petroleum Research Fund

A simplified elastic spectator model is applied to the interpretation of crossed-beam data on the proton transfer reactions  $\text{H}_3^+(\text{D}_2, \text{H}_2)\text{D}_2\text{H}^+$ , and isotopic analogues, and  $\text{H}_3^+(\text{N}_2, \text{H}_2)\text{N}_2\text{H}^+$ . This model employs two-body central force trajectories for reactants and products connected by the assumption that reaction occurs by a stripping mechanism at a hard-sphere barrier. It accounts satisfactorily for the observed product center-of-mass angular distributions and average relative translational energies at reactant relative translational energies of 2.5 eV and greater. At lower relative translational energies some discrepancies are observed, and the model does not account for the observed product relative translational energy distributions. The apparent success of this grossly oversimplified model indicates that the major features of the product distributions are largely determined by the kinematics and the long-range interactions and that the effects of the orientation dependent short-range interactions are apparent only in the product relative translational energy distributions and as the source of the discrepancies observed at low energies.

## Introduction

A complete theoretical treatment of the proton transfer reactions involving a triatomic ion and a diatomic molecule, such as those described previously,<sup>1</sup> requires a detailed knowledge of the nine-dimensional potential surface for the five atom system. Unfortunately, only fragmentary information is presently available; and even if the surfaces were completely known, the calculation of a sufficient number of trajectories to characterize the reaction would be an enormous task.

Reactions which involve the transfer of a relatively light particle from one heavy particle to another, e.g., proton or hydrogen atom transfer, have been extensively studied in

crossed-beam experiments. These reactions have often been found to occur by a direct mechanism even at near thermal energies, and the observed product scattering distributions correspond, approximately, to those predicted by extensions of the "spectator stripping" model.<sup>2</sup>

In this paper a "modified stripping" model is applied to the interpretation of experimental data on proton transfer reactions involving a triatomic ion and a diatomic molecule. This model incorporates some of the concepts employed previously in the elastic spectator model of Herschbach,<sup>3</sup> the "modified" stripping model of Wolfgang et al.,<sup>4</sup> and the impulsive reaction model of Chang and Light.<sup>5</sup>

In a previous paper<sup>1</sup> we noted that the average product

energies observed for the reaction  $\text{H}_3^+(\text{D}_2, \text{H}_2)\text{D}_2\text{H}^+$ , and its isotopic analogues, were in accord with those expected for an elastic spectator model. The present work was undertaken to explore whether such a simplified model could account, at least semiquantitatively, for the major features observed in the product intensity distributions.

The model consists of two-body central force trajectories for reactants and products connected by the assumption that reaction occurs by a stripping mechanism at a hard-sphere barrier. In the stripping mechanism the relative translational energy and orbital angular momentum of the transferred particle (averaged over all possible reactant orientations) are transformed, respectively, into internal energy and angular momentum of the product, and the products are elastically scattered from the hard-sphere barrier. This assumption, in effect, ignores the effects that reactant orientation and orientation dependent forces have, both on the probability of reaction and on the resulting product scattering. If these factors have a small effect on the observed differential reaction cross sections, and if the stripping model is approximately correct, then the model should predict at least the gross features of the product scattering, such as the center-of-mass angular distributions and the average relative translational energies. Conversely, agreement between experiment and the predictions of this simple model implies that the experimental data contain very little information concerning the details of the interaction.

### The Modified Elastic Spectator Model

The development of this model from earlier direct interaction models is described elsewhere.<sup>6</sup> In this section a brief recapitulation of the conceptual basis of the model is given together with a summary of the simplifying approximations and the resulting equations. In this discussion we will refer to the metathetical reaction



but will allow either A or C (or both) to represent molecules. In general, any of the species may be ionic, but for the present application the transferred particle B is a proton and A and C are neutral.

The modified elastic spectator model, in common with many other direct interaction models, is derived from a rudimentary extension of the classical optical potential model for elastic scattering.<sup>3</sup> The reactants A + BC are assumed to approach the region of chemical interaction along a two-body central force trajectory specified by a spherically symmetric potential function  $V(r)$ , impact parameter  $b$ , and kinetic energy  $T$ . At a critical separation,  $r_c$  (measured from A to the center of mass of BC), a fraction  $P(b, T)$  of these collisions lead to reaction. The products AB + C depart from the corresponding critical separation of products,  $r'_c$  (measured from C to the center of mass of AB), along another two-body trajectory determined by potential function  $V'(r)$ , impact parameter  $b'$ , and kinetic energy  $T'$ . The differential scattering cross sections for elastic and reactive scattering then are given by

$$I_E(\chi) = [1 - P(b, T)] 2\pi b \, db/d\omega \quad (1)$$

$$I_R(\chi') = P(b', T') 2\pi b' \, db'/d\omega' \quad (2)$$

where  $\chi$  and  $\chi'$  are the elastic and reactive scattering angles and

$$d\omega = 2\pi \sin \chi \, d\chi \quad (3)$$

$$d\omega' = 2\pi \sin \chi' \, d\chi' \quad (4)$$

are the corresponding solid-angle elements in the center of mass (CM) system. In reactive collisions the scattering angle is the sum of contributions from the reactant and product portions of the trajectory

$$\chi' = \chi_r(b, T) + \chi_p(b', T') \quad (5)$$

The lack of a third contribution representing the ABC complex makes apparent the direct character of this model. Application of classical two-body collision mechanics gives explicit expressions for the scattering angles

$$\chi_r = \frac{\pi}{2} - b \int_{r_c}^{\infty} [1 - V(r)/T - b^2/r^2]^{-1/2} dr/r^2 \quad (6)$$

$$\chi_p = \frac{\pi}{2} - b' \int_{r'_c}^{\infty} [1 - V'(r)/T' - b'^2/r^2]^{-1/2} dr/r^2 \quad (7)$$

To complete the model further assumptions are required to specify the potentials,  $V(r)$  and  $V'(r)$ , the reaction probability functions,  $P(b, T)$ , the critical reaction distance,  $r_c$ , and the relationship of  $r_c$ ,  $b$ , and  $T$ , to  $r'_c$ ,  $b'$ , and  $T'$ . The assumptions made in the development of the elastic spectator model are the following:

(1) The difference between the barycentric distances  $r_{A-BC}$  and  $r_{AB-C}$  at the critical reaction distance is neglected.

(2) The reactants are assumed to be in their ground electronic states and the internal vibrational and rotational energy of the reactants is neglected.

(3) The reaction occurs by a stripping mechanism at  $r_c$  with elastic scattering of the spectator C from a "hard sphere" potential barrier.

(4) The orbital angular momentum of the products is equal to the initial orbital angular momentum of C and A averaged over all possible orientations of BC.

(5) The potential functions  $V(r)$  and  $V'(r)$  are given by the ion-induced dipole expression.

(6) The fraction of collisions producing reaction,  $P(b, T)$ , is uniform for all impact parameters  $b \leq b_m(T)$  where  $b_m(T)$  is that maximum impact parameter for which the reactants can surmount the rotational barrier and reach the critical distance  $r_c$ .

With the exceptions of (1) and (4) these assumptions are identical with those made in the impulsive reaction model of Chang and Light,<sup>5</sup> which was developed for the triatomic system  $\text{Ar}^+ + \text{H}_2$  and included the arbitrary assumption of a linear collision complex. For the five atom systems considered in this work, a large number of reactant orientations in the collision complex is possible. Since the intermediate range forces between closed shell reactants appear to be nearly spherically symmetric, it seems more appropriate here to make the opposite assumption that reaction is independent of reactant orientation. Thus, assumptions (1) and (4) correspond to ignoring the role that reactant orientation may play in determining the scattering of products.

Applying assumptions (1) through (4) the following relationships between parameters determining the reactant and product trajectories are obtained:

$$r'_c = r_c \quad (8)$$

$$T' = [T - V(r_c)] \cos^2 \beta + V'(r_c) \quad (9)$$

$$b' = b(T/T')^{1/2} \cos \beta \quad (10)$$

where

$$\cos^2 \beta = (m_A m_C)/m_{AB} m_{BC} \quad (11)$$

According to assumption (5) the potentials are given by

$$V(r) = -\alpha e^2/2r^4 \quad (12)$$

$$V'(r) = -\alpha' e^2/2r^4 \quad (13)$$

where  $\alpha$  is the polarizability of the neutral reactant,  $\alpha'$  is the polarizability of the neutral product, and  $e$  is the electronic charge. The maximum impact parameter for reaction  $b_m(T)$  of assumption (6) is then given by

$$b_m(T) = \begin{cases} r_c(4T_c/T)^{1/4} & \text{when } T \leq T_c \\ r_c(1 + T_c/T)^{1/2} & \text{when } T > T_c \end{cases} \quad (14)$$

where

$$T_c = \alpha e^2/2r_c^4 \quad (16)$$

The translational exoergicity,  $Q$ , and the final internal energy of the products,  $W'$ , are given by

$$Q = (T' - T) = -T \sin^2 \beta - V(r_c) \cos^2 \beta + V'(r_c) \quad (17)$$

$$W' = -Q - \Delta E \quad (18)$$

The orbital angular momentum of the products is given by

$$\bar{L}' = \bar{L} \cos^2 \beta \quad (19)$$

and the rotational angular momentum of the product AB is

$$\bar{J}' = \bar{L} \sin^2 \beta \quad (20)$$

In the foregoing we have assumed, following Chang and Light,<sup>5</sup> that the overall reaction endoergicity,  $\Delta E$ , is subtracted from the internal energy of the products and has no effect on the final translational energy. There appears to be no a priori reason to assume that this is generally true for the impulsive reaction mechanism, since the factors governing the distribution of the energy of reaction between internal and translational modes are determined by details of the interaction which are ignored in the impulsive model. It appears that any partitioning is possible.

This completes the definition of the modified elastic spectator model. The relative translational energy of the products is given by eq 9 and the product scattering angle by eq 5-7 with the appropriate substitutions from eq 8-13. Substituting these results into eq 2 gives the differential reaction cross section. As in elastic scattering the scattering angles calculated from eq 5 to 7 range from  $+\pi$  to  $-\infty$ , while the observable center of mass polar scattering angles lie between 0 and  $\pi$ . Thus, the final result for the differential cross section for product scattered at an observable angle between  $\chi$  and  $\chi + d\chi$  is given by

$$\frac{d\sigma}{d\chi} = 2\pi I(\chi) \sin \chi = 2\pi \frac{\sum P(b_i) b_i}{\left| \frac{d\chi_i'}{db_i} \right|_{b_i}} \quad (21)$$

where

$$\chi = |\chi'(b_i) + 2\pi k| \quad (22)$$

and  $k$  is zero or an integer which causes eq 22 to yield a value of  $\chi$  between 0 and  $\pi$ . The summation in eq 21 is carried over all  $b_i$  for which eq 22 yields the same value of  $\chi$ .

The only adjustable parameter in this model is the critical reaction distance,  $r_c$ . In the calculations based on this model we shall attempt to fit all of the data on the  $H_3^+ + D_2$  and  $D_3^+ + H_2$  reactions with a single, physically reasonable value of this parameter.

## Computer Programs

The calculations of differential reaction cross sections based on the modified elastic spectator model were carried out on a PDP-11/45 computer<sup>7</sup> using a Fortran program called SCAT which was developed explicitly for these calculations. The input data to the program consist of the parameters characterizing the potential functions,  $V(r)$  and  $V'(r)$ , e.g., the polarizabilities of the neutral reactant and product,  $\alpha$  and  $\alpha'$ , respectively; the relative translational energy of the reactants,  $T$ ; the masses of A, B, and C; the endoergicity of the reaction,  $E$ ; the critical distance for reaction,  $r_c$ ; and the number of trajectories to be calculated,  $N$ .

The program first calculates the maximum impact parameter for reaction,  $b_m$ , as given by eq 14 or 15; the relative translational energy of the products,  $T'$ , eq 9; and the internal energy of the products,  $W'$ , eq 18. If either  $T'$  or  $W'$  is found to be negative, the values are printed and further calculation is aborted with an indication to the operator that the reaction is not possible under the conditions given.

If both  $T'$  and  $W'$  are nonnegative, the program then proceeds to the trajectory calculations. These calculations are performed for each of  $N$  different values of the impact parameter ranging from zero to  $b_m$  in regular increments,  $\Delta b$ , where  $\Delta b = b_m/N$ . The trajectory calculation consists of the numerical integration of the expressions for the reactant and product deflection angles,  $\chi_r$  and  $\chi_p$ , given by eq 6 and 7, respectively, to yield finally the scattering angle  $\chi'(b)$  as given by eq 5 for each value of the impact parameter. In some cases the quantity under the radical in the calculation of  $\chi_p$ , eq 7, may become negative, indicating that the products cannot surmount the rotational barrier and separate. When this occurs, the trajectories are counted as unreactive according to this direct mechanism, although at low energies reaction might occur by a long-lived complex mechanism.

The values of  $\chi'(b)$  resulting from successful reaction trajectories are converted to the corresponding observable scattering angle,  $\chi$ , by the transformation given in eq 22. The calculation of differential cross sections is accomplished by dividing the range of possible scattering angles ( $0^\circ \leq \chi \leq 180^\circ$ ) into finite intervals; for the present work  $10^\circ$  intervals were used. A function  $f(m)$  is constructed which gives the differential cross section for product scattered between  $\chi_m$  and  $\chi_{m+1}$ . For each calculated value  $\chi(b)$  the value of  $m$  is found such that

$$\chi_m \leq \chi < \chi_{m+1} \quad (23)$$

and the value of the corresponding element,  $f(m)$ , is increased by the appropriate finite difference cross section

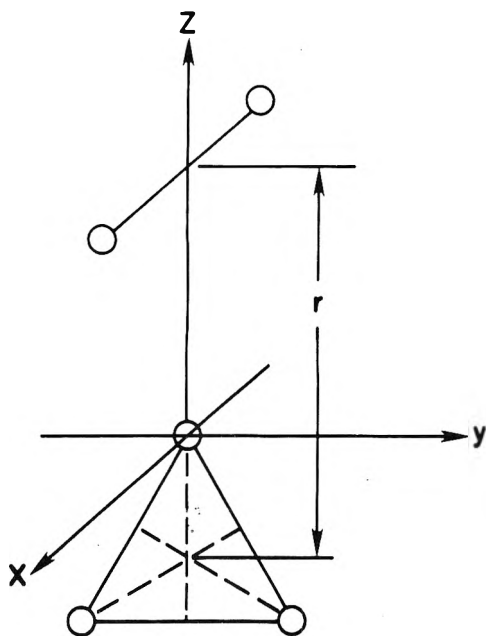
$$\Delta\sigma = 2\pi P(b) b \Delta b \quad (24)$$

After all  $N$  trajectories have been calculated, the function  $f(m)$  is proportional to the finite difference cross section for scattering product between  $\chi_m$  and  $\chi_{m+1}$ , that is

$$\Delta\sigma(\chi_m)/\Delta\chi = f(m)/\Delta\chi \quad (25)$$

where  $\chi_m = m\Delta\chi$ . The accuracy of this approximation to the differential cross section is limited only by the coarseness of the intervals taken and the total number of trajectories calculated.

The reaction probability is taken as unity for  $b \leq b_m$ , where the maximum impact parameter,  $b_m(T)$ , is given by either eq 14 or 15. The output from the program includes the product deflection function,  $\chi'(b)$ , for each impact parameter for which the trajectory is calculated; the difference cross section,  $f(m)$ ,



**Figure 1.** Equilibrium  $C_{2v}$  geometry for  $H_5^+$ . The dimensions of the  $H_3^+$  and  $H_2$  fragments are essentially unperturbed. The distance  $r$  between the center of mass of the  $H_3^+$  and  $H_2$  fragments is the internuclear distance employed in the spherically symmetric potentials used in the modified elastic spectator model.

for scattering between  $\chi_m$  and  $\chi_{m+1}$ ; the difference cross section,  $g(m)$ , for scattering per unit solid angle at the angle between  $\omega_m$  and  $\omega_{m+1}$ , given by

$$g(m) = f(m)/2\pi \sin(\chi_m') \quad (26)$$

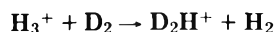
where

$$\begin{aligned} \chi_m' &= (\chi_m + \chi_{m+1})/2 \\ \omega_m &= 2\pi \sin(\chi_m') \end{aligned} \quad (27)$$

The output also includes the relative translational energy of the products,  $T'$ , the internal energy of the products,  $W'$ , and the total reaction cross section,  $\sigma$ , given by

$$\sigma = \sum f(m) \quad (28)$$

where the summation is carried over the range of  $m$  corresponding to the total range of  $\chi$  ( $0 \leq \chi \leq \pi$ ).



In the calculations for this reaction and its isotopic analogues, we have neglected the small zero point energy differences and treated the reactions as thermoneutral. The polarizabilities<sup>8</sup> of  $D_2$  and  $H_2$  are taken as  $0.93 \times 10^{-24} \text{ cm}^3$  which give for the ion-induced dipole potentials

$$V(r) = V'(r) = -5.8/r^4 \quad (29)$$

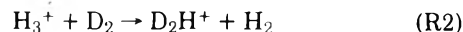
where  $r$  is in Å, and  $V$  in eV.

Several recent theoretical calculations on the equilibrium energy and geometry of  $H_5^+$  have been reported in the literature.<sup>9-11</sup> The equilibrium geometry of  $H_5^+$  was found to be an elongated tetrahedron having the  $C_{2v}$  symmetry shown in Figure 1. According to these results  $H_5^+$  is a loosely bound ion cluster consisting of an almost unperturbed  $H_3^+$  bound to an  $H_2$  molecule mainly by the ion-induced dipole attraction. The calculated equilibrium distance between the centers of mass of the  $H_3^+$  ion and the  $H_2$  molecule is  $2.1 \pm 0.2 \text{ Å}$ , and the binding energy is  $0.25 \pm 0.15 \text{ eV}$ , where the variations indicate

the range of results obtained by different methods of calculation.

Salmon and Poshusta<sup>9</sup> suggest that the relative motions of the  $H_3^+$  and  $H_2$  are free except for the small barriers due to the weak ion-induced dipole attraction. This implies that  $H_2$  should be considered as distributed on a sphere about  $H_3^+$  with only a slight maximum probability at the calculated geometry. Since orientation of the partners apparently has little effect on the interaction potential, the use of spherically symmetric potentials in the scattering calculations should be a reasonable approximation at distances comparable to the equilibrium separation and larger.

The first series of calculations based on the modified elastic spectator model were performed for the reaction



which was most extensively studied experimentally in this work. The difference cross sections,  $\Delta\sigma/\Delta\chi$ , were calculated using program SCAT at angular increments,  $\Delta\chi$ , of  $10^\circ$  for several assumed values of  $r_c$ . The experimental relative differential cross section results for comparison were obtained, as described in a preceding paper,<sup>1</sup> by integrating the intensity contour diagrams over the relative translational energy, multiplying the resulting intensity,  $I(\chi)$ , by  $\sin \chi$ , and renormalizing. In comparing the calculated and experimental results both sets of data are given in arbitrary units with the maximum differential cross section, as a function of  $\chi$ , set equal to 100.

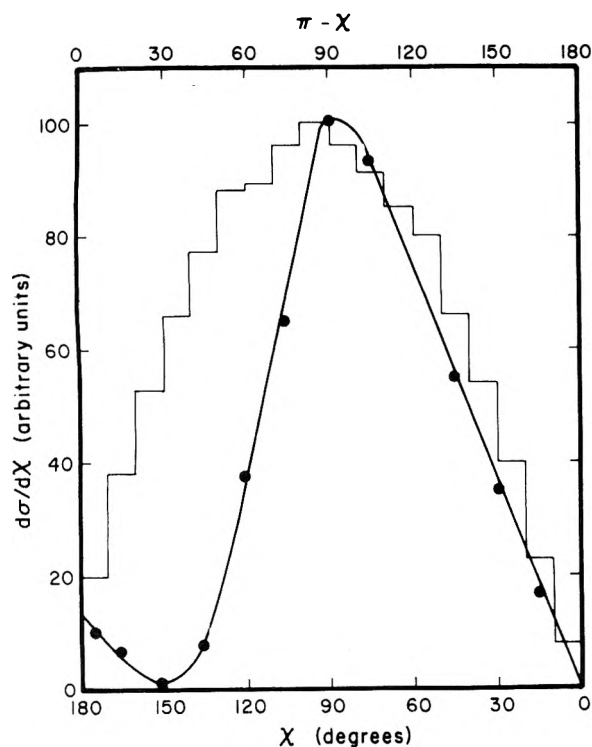
The best agreement between the calculated and experimental results were obtained assuming a critical reaction distance,  $r_c$ , of  $2.0 \text{ Å}$ , although small variations about this value (ca.  $\pm 0.1 \text{ Å}$ ) causes no significant perturbation relative to experimental uncertainties. This critical distance implies that the relative translational energy of the products is given by

$$T' = [T - V(r_c)] \cos^2 \beta + V'(r_c) = 8/15T - 0.17 \quad (30)$$

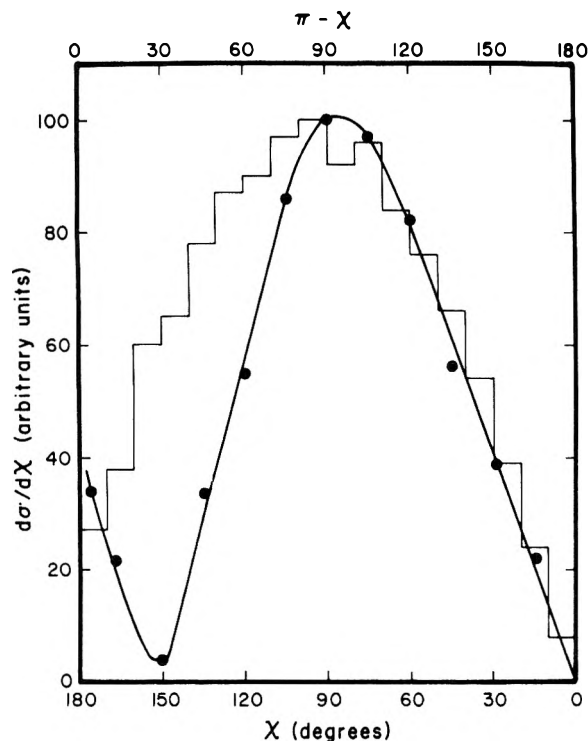
which is 0.17 eV less than that for pure spectator stripping.

Comparisons between calculated and experimental differential cross sections are shown in Figures 2-7. At relative translational energies of 2.5 eV and above, Figures 2-5, the agreement in the rebound direction ( $\chi < 90^\circ$ ) is excellent. This implies that for  $b \leq r_c/\sqrt{2}$  the assumption that the reaction probability,  $P(b)$ , is a constant is satisfactory. However, in the stripping direction the agreement is not generally as good in that the calculated cross sections are significantly larger in the region,  $180^\circ \geq \chi \geq 90^\circ$ . Part of this discrepancy is undoubtedly due to the experimental artifact associated with the "droop" in the retarding potential energy analyzer transmission function discussed in the earlier paper. To ascertain the extent to which this discrepancy was due to this experimental difficulty, an experiment was done using a deflection type energy analyzer which gives the differential energy spectrum directly.<sup>14</sup> The differential cross section data obtained from this experiment at a relative translational energy of 5.9 eV are shown in Figure 4, where the results are compared with calculated results at 5.9 eV and with the earlier experimental results, at 5.2 eV, obtained using the retarding potential analyzer. Except in the region near  $\chi = 150^\circ$ , where the results obtained in the earlier experiment are substantially too low, the two experimental results are in good agreement. The small discrepancy between calculated and experimental results in Figure 4 appears to represent a genuine difference between the predictions of the model and the experimental results.

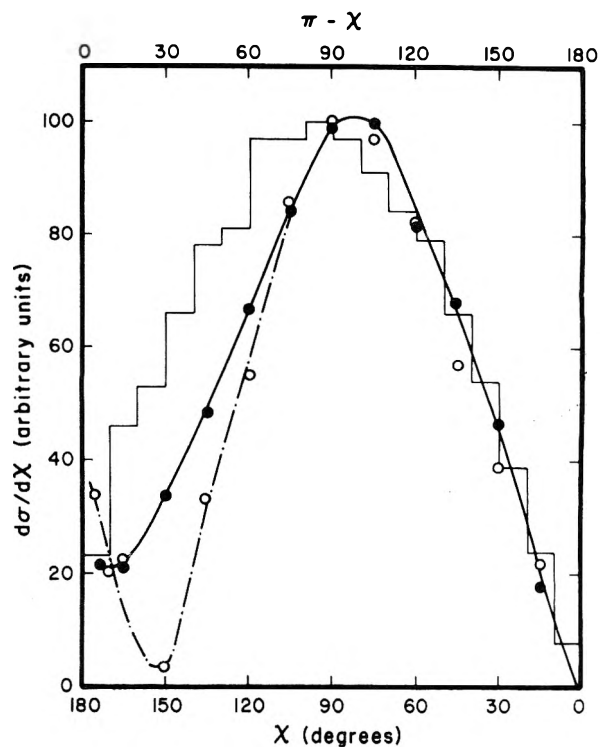
At a relative translational energy of 2.5 eV, Figure 5, the



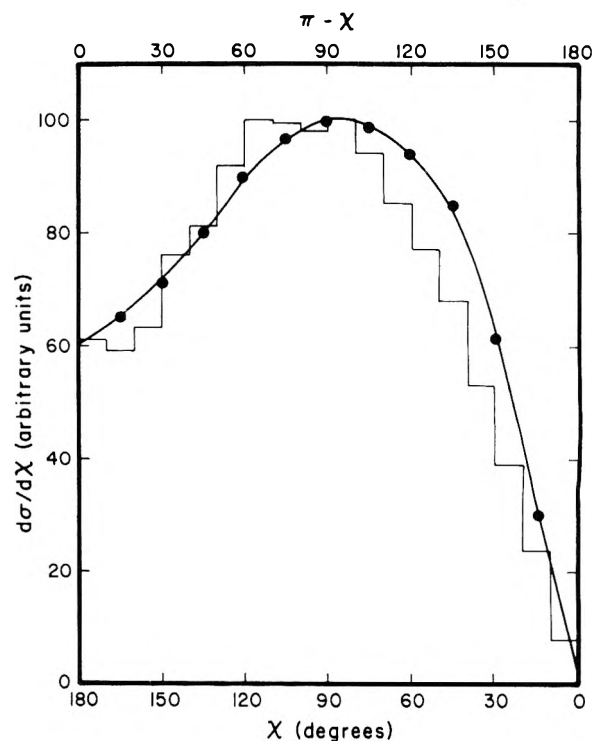
**Figure 2.** Relative differential cross section  $d\sigma/d\chi$  as a function of center of mass scattering angle  $\chi$  for the reaction  $\text{H}_3^+ + \text{D}_2 \rightarrow \text{D}_2\text{H}^+ + \text{H}_2$  at a reactant translational energy of 8.2 eV. The histogram represents the results of calculations based on the modified elastic spectator model, and the data points represent the experimental results.



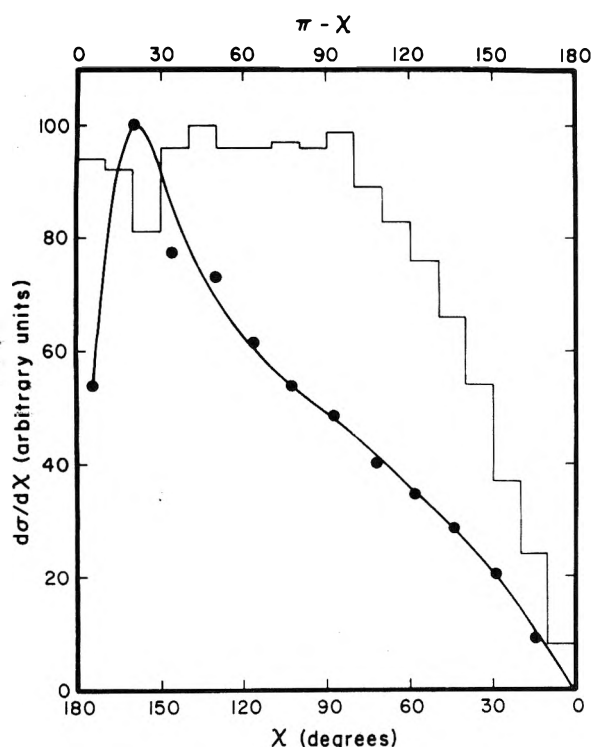
**Figure 3.** Relative differential cross section  $d\sigma/d\chi$  as a function of center of mass scattering angle  $\chi$  for the reaction  $\text{H}_3^+ + \text{D}_2 \rightarrow \text{D}_2\text{H}^+ + \text{H}_2$  at a reactant translational energy of 5.2 eV. The histogram represents the results of calculations based on the modified elastic spectator model, and the data points represent the experimental results.



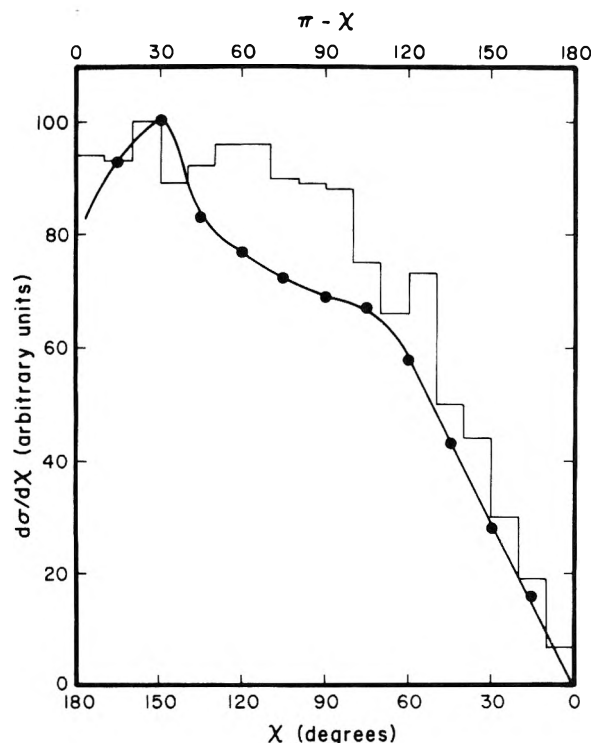
**Figure 4.** Relative differential cross section  $d\sigma/d\chi$  as a function of center of mass scattering angle  $\chi$  for the reaction  $\text{H}_3^+ + \text{D}_2 \rightarrow \text{D}_2\text{H}^+ + \text{H}_2$  at a reactant relative translational energy of 5.9 eV. The histogram represents the results of calculations based on the modified elastic spectator model, and the data points —O— represent the experimental results obtained using the differential energy analyzer described in Appendix I of the previous paper. —O— gives the data obtained with the retarding potential energy analyzer at 5.2 eV.



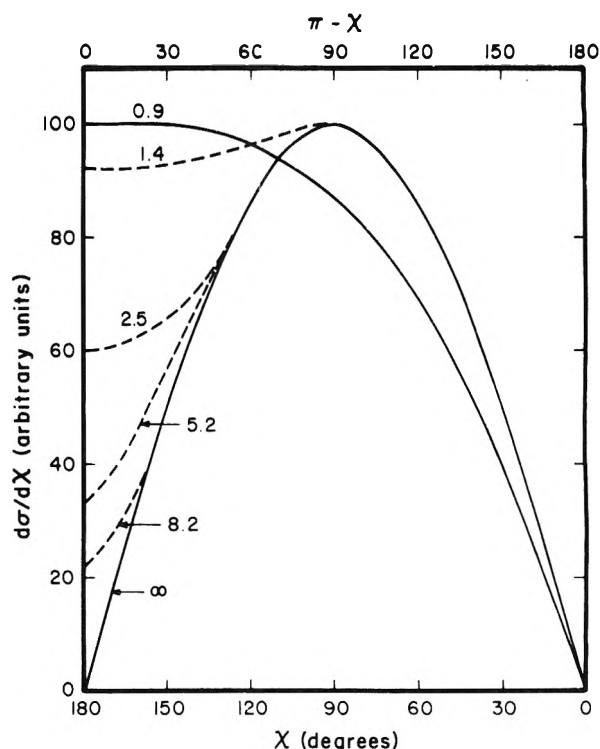
**Figure 5.** Relative differential cross section  $d\sigma/d\chi$  as a function of center of mass scattering angle  $\chi$  for the reaction  $\text{H}_3^+ + \text{D}_2 \rightarrow \text{D}_2\text{H}^+ + \text{H}_2$  at a reactant translational energy of 2.5 eV. The histogram represents the results of calculations based on the modified elastic spectator model, and the data points represent the experimental results.



**Figure 6.** Relative differential cross section  $d\sigma/d\chi$  as a function of center of mass scattering angle  $\chi$  for the reaction  $\text{H}_3^+ + \text{D}_2 \rightarrow \text{D}_2\text{H}^+ + \text{H}_2$  at a reactant translational energy of 1.4 eV. The histogram represents the results of calculations based on the modified elastic spectator model, and the data points represent the experimental results.



**Figure 7.** Relative differential cross section  $d\sigma/d\chi$  as a function of center of mass scattering angle  $\chi$  for the reaction  $\text{H}_3^+ + \text{D}_2 \rightarrow \text{D}_2\text{H}^+ + \text{H}_2$  at a reactant translational energy of 0.9 eV. The histogram represents the results of calculations based on the modified elastic spectator model, and the data points represent the experimental results.



**Figure 8.** Summary of the relative differential cross sections  $d\sigma/d\chi$  as functions of center of mass scattering angle  $\chi$  for the reaction  $\text{H}_3^+ + \text{D}_2 \rightarrow \text{D}_2\text{H}^+ + \text{H}_2$  calculated using the modified elastic spectator model. The numbers labeling the curves correspond to the relative translational energy of the reactants. The curve corresponding to infinite energy for this model is identical with that predicted by using a simple hard-sphere potential.

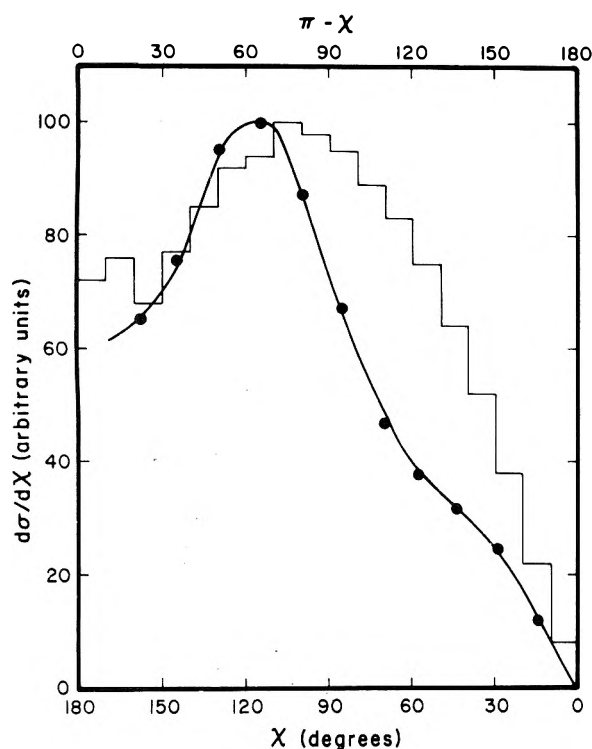
agreement between calculated and experimental differential cross sections is excellent at all scattering angles. At the lower energies, 1.4 eV shown in Figure 6, and 0.9 eV shown in Figure 7, the agreement is significantly poorer.

The shapes of the curves in the rebound direction ( $\chi < 90^\circ$ ) are in reasonable agreement (after appropriate renormalization) but the experimental results show a maximum which is somewhat suggestive of a classical rainbow in elastic scattering. This behavior is not predicted by the modified elastic spectator model using the ion-induced dipole potential to represent the interaction.

The predictions of the model are summarized in Figure 8. As the relative translational energy becomes large compared to  $|V(r_c)|$  the distribution of differential cross sections approaches that for elastic scattering from a hard sphere given by

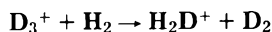
$$d\sigma/d\chi = 2\pi I_0 \sin \chi \quad (31)$$

where  $I_0$  is a constant.<sup>15</sup> At lower energies the large impact parameter trajectories, which are able to reach the critical reaction distance,  $r_c$ , due to the attractive long-range potential, yield an increasing contribution to the scattering in the stripping direction. At 0.9 eV (for  $r_c = 2.0 \text{ \AA}$ ) orbiting begins to occur for the largest impact parameters, that is  $\pi - \chi$  becomes less than  $-\pi$ . As the energy is further decreased orbiting occurs for an increasingly large fraction of the impact parameters until at 0.36 eV products formed by this mechanism cannot separate (i.e., the product relative translational energy becomes negative) and this model must be abandoned in favor of a long-lived complex model. The precise quantitative behavior predicted from this model depends, of course, on the



**Figure 9.** Relative differential cross section  $d\sigma/d\chi$  as a function of center of mass scattering angle  $\chi$  for the reaction  $D_3^+ + H_2 \rightarrow H_2D^+ + D_2$  at a reactant translational energy of 2.4 eV. The histogram represents the results of calculations based on the modified elastic spectator model, and the data points represent the experimental results.

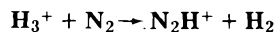
value of  $r_c$  chosen, but the qualitative behavior is independent of that choice.



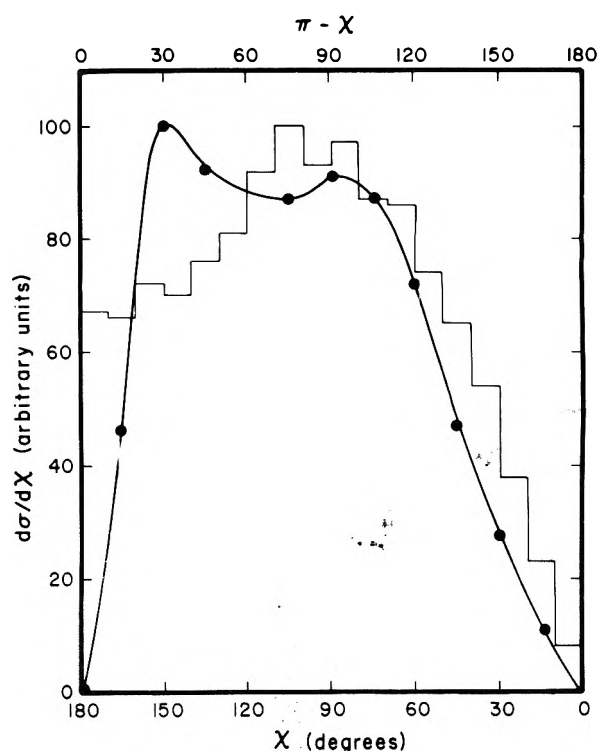
Differential reaction cross section distributions for this reaction were calculated using the same models and potential functions employed for the proton transfer from  $H_3^+$  to  $D_2$ . At a reactant relative translational energy of 2.4 eV fair agreement with experiment was obtained. Results of the calculation are compared to the experimental results in Figure 9. At lower translational energies, for example, 0.6 eV, the model predicts that the final translational energy of products given by

$$T' = [T - V(r_c)] \cos^2 \beta + V'(r_c) \\ = [0.6 + 0.36](1/3) - 0.36 = -0.04 \quad (32)$$

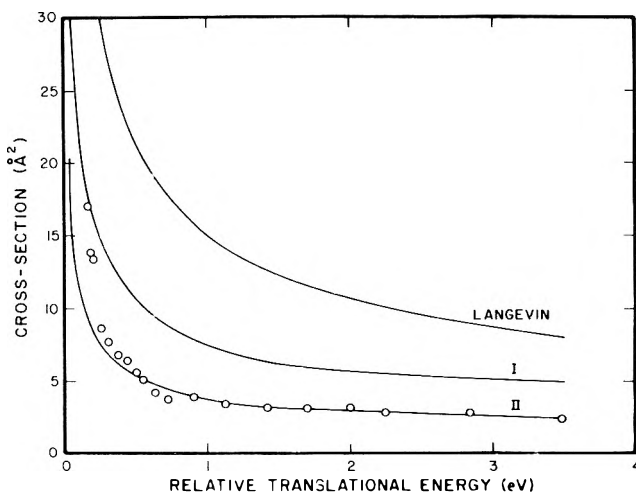
is less than zero, indicating that reaction is impossible by this mechanism, and requiring that the reaction occur by a long-lived intermediate complex mechanism. The experimental results indicate that orbiting collisions predominate but that a small direct component is also present.



The results of a calculation for this reaction, with  $r_c = 2.0 \text{ \AA}$ , are compared with experiment in Figure 10. While the two results are in good agreement in the rebound direction, serious discrepancies occur in the stripping direction. Experimentally we find a very low intensity at the spectator stripping point ( $\chi = 180^\circ$ ) with a maximum at  $\chi = 150^\circ$ , in qualitative disagreement with the calculated distribution. Also, experimentally the most probable product relative translational energy



**Figure 10.** Relative differential cross section  $d\sigma/d\chi$  as a function of center of mass scattering angle  $\chi$  for the reaction  $H_3^+ + N_2 \rightarrow N_2H^+ + H_2$  at a reactant translational energy of 8.3 eV. The histogram represents the results of calculations based on the modified elastic spectator model and the data points represent the experimental results.



**Figure 11.** Absolute reaction cross sections for the reaction  $H_3^+ + D_2 \rightarrow D_2H^+ + H_2$ . The data points represent the experimental work of Clow and Tiernan<sup>12</sup> and the curves labeled I and II correspond to calculations using the modified elastic spectator model with the reaction probability,  $P(b)$ , equal to 0.5 and 0.25, respectively. The cross section calculated from the Langevin model is shown for comparison.

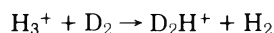
is 5.4 eV in good agreement with the spectator stripping value, while the model gives the substantially higher value of 6.2 eV.

### Absolute Cross Sections

In the experimental work described in the previous paper<sup>1</sup> absolute cross sections were not obtained. Recently, Clow and



Tiernan<sup>13</sup> used a tandem mass spectrometer to measure the absolute cross section for the reaction



as a function of translational energy. Their results are compared with the predictions of the modified elastic spectator model in Figure 11. Curve I is the result predicted by the model assuming that  $P(b) = 0.5$  for  $b \leq b_m$  and curve II is a similar result but for  $P(b) = 0.25$  for  $b \leq b_m$ . At relative translational energies above ca. 0.5 eV the experimental results are in excellent agreement with curve II, but at lower energies the experimental cross sections are significantly larger, at the lowest energy, approaching agreement with curve I. This change occurs in the energy range in which the model calculations predict the onset of orbiting and seems to indicate a transition from a direct mechanism to a long-lived complex mechanism. Considering the symmetry between reactants and products for this reaction, a reaction probability of 0.5 is certainly reasonable for a long-lived complex mechanism. The lower value of the reaction probability for the direct mechanism may reflect the average fraction of reactant orientations which correspond to a reactive configuration.

### Summary

The modified elastic spectator model described in this paper yields angular distributions in reasonable agreement with experimental results for proton transfer reactions involving the  $\text{H}_5^+$  intermediate. The relative translational energies of the products predicted by the model are in good agreement with the average product translational energies observed in the experiments, but the model does not predict the observed broad distributions of product energies.<sup>1</sup> In every case the agreement between the calculated and experimental differential cross sections is fairly good for products scattered in the rebound direction ( $\chi < 90^\circ$ ); however, in the stripping direction ( $\chi > 90^\circ$ ) some significant discrepancies are observed. The relative translational energy at which the experimental angular distributions indicate a transition from a "direct" mechanism to a long-lived orbiting "complex" is in good agreement with predictions of the model.

It appears that the discrepancies between the experimental results and the model calculations are due to the effects of reactant orientation and orientation-dependent forces which are only important in a rather small reactant zone corresponding to barycentric distances comparable to, or less than, the equilibrium distance in the  $\text{H}_5^+$  intermediate complex. At greater separation the use of two-body central force trajectories appears to be a satisfactory approximation. Furthermore, the assumption that the reaction probability depends only on the impact parameter,  $b$ , and is constant for  $b \leq b_{\text{max}}$ , is satisfactory for "hard" collisions involving small impact parameters and relatively high energies. For "softer" collisions the reaction probability obviously depends on both the impact parameter and the orientation of the reactants.

Moreover, at all relative translational energies and impact parameters, the product relative translational energies are determined by the orientation dependent interactions occurring within the reaction zone. One-dimensional calculations, such as those presented in this paper, provide no information about the details of these short-range interactions, but do serve to separate out the effects controlled primarily by the kinematics and the long-range interactions.

A complete interpretation of crossed-beam data involving these polyatomic systems obviously will require calculation of trajectories on the appropriate  $n$ -dimensional potential surfaces. The present study shows that these calculations may be restricted to the region in which the short-range interactions occur. Moreover, the success or failure of such calculations must be judged on their ability to account for the details of the product distributions which are clearly due to the short-range orientation dependent interactions. The approximate agreement obtained with the present simplified model shows that accurate prediction of angular distributions and average product energies may be achieved without reference to a detailed potential surface, consequently we may conclude that prediction of these properties by a potential surface calculation is a necessary but not a sufficient condition for assessing the validity of the calculation.

**Acknowledgment.** Acknowledgment is made to the donors of the Petroleum Research Fund, administered by the American Chemical Society, for support of this research.

### References and Notes

- (1) M. L. Vestal, C. R. Blakley, P. W. Ryan, and J. H. Futrell, *J. Chem. Phys.*, in press.
- (2) For reviews and references to the original literature see J. Dubrin and M. J. Henchman, *MTP Int. Rev. Sci., Ser. One*, **9**, 213 (1972); B. H. Mahan, *MTP Int. Rev. Sci., Ser. Two*, **9**, (1974).
- (3) D. R. Herschbach, *Appl. Opt. Suppl.*, **2**, 128 (1965); D. R. Herschbach, *Adv. Chem. Phys.*, **10**, 319 (1966); C. M. Connally and E. A. Gislason, *Chem. Phys. Lett.*, **14**, 103 (1972); J. L. Kinsey et al., *J. Chem. Phys.*, **64**, 1914 (1976).
- (4) Z. Herman, J. Kerstetter, T. Rose, and R. Wolfgang, *J. Chem. Phys.*, **46**, 2844 (1967).
- (5) D. T. Chang and J. C. Light, *J. Chem. Phys.*, **52**, 5687 (1969).
- (6) M. L. Vestal, Ph.D. Dissertation, University of Utah, 1975.
- (7) Model PDP-11/45 by Digital Equipment Corp., Maynard, Mass.
- (8) Landolt-Bornstein, "Zahlenwerte und Funktionen", Springer, Vol. I, Berlin, 1951, part 3, p 510; Moelwyn-Hughes, "Physical Chemistry", Pergamon Press, London, 1957, p 373.
- (9) W. I. Salmon and R. D. Posusta, *J. Chem. Phys.*, **59**, 4867 (1973).
- (10) J. Easterfield and J. W. Linnett, *Chem. Commun.*, **64** (1970).
- (11) J.-T. J. Huano, M. F. Schwartz, and G. V. Pfeiffer, *J. Chem. Phys.*, **56**, 755 (1972).
- (12) A. Henglein, *J. Phys. Chem.*, **76**, 3883 (1972).
- (13) R. P. Clow, T. O. Tiernan, and B. M. Hughes, paper presented at the 22nd Annual Conference on Mass Spectrometry and Allied Topics, Philadelphia, Pa., May 1974.
- (14) See the Appendix of ref 1 for experimental details.
- (15) For comparisons between experiment and calculations we have used  $d\sigma/d\chi$ , the differential cross section per radian, rather than the more conventional  $d\sigma/d\Omega$ , the differential cross section per steradian. Since  $d\sigma/d\chi$  is proportional to the fraction of the total cross section corresponding to scattering between  $\chi$  and  $\chi + d\chi$ , provided there is no dependence on the azimuthal angle, it allows the comparisons to be made with equal weighting at all scattering angles.

## Reactions of Saturated Hydrocarbons in the Presence of Deuterium on Evaporated Iron Films

Robert S. Dowie, Charles Kemball, and David A. Whan\*

Department of Chemistry, University of Edinburgh, Edinburgh, Scotland, EH9 3JJ (Received February 9, 1976)

The reactions of *n*-butane, propane, ethane, and methane have been studied in the presence of deuterium on evaporated films of iron at temperatures such that exchange and, except in the case of methane, hydrogenolysis could be observed. Results indicated that the hydrocarbons interacted strongly with the catalyst surface such that exchanged products tended to be perdeuterioalkanes and the predominant product of hydrogenolysis was perdeuteriomethane. These observations suggest that the desorption of single carbon entities as methane may be the rate-determining step in *n*-butane and propane hydrogenolysis.

### Introduction

In comparison with metals such as platinum and nickel, and with the notable exception of ammonia synthesis, reactions on iron catalysts have aroused little interest. Much of this lack of interest may be due to the inability of iron to catalyze simple reactions of hydrocarbons, such as exchange with deuterium, in a temperature range where other metals have considerable activity. This has been attributed to the ease with which iron dissociatively, and irreversibly, adsorbs hydrocarbons.<sup>1</sup> On raising an iron catalyst to a sufficiently high temperature for hydrogenolysis to occur it has been found that the rate of the reaction of ethane<sup>2</sup> displays a positive dependence on hydrogen pressure, in contrast to the negative dependence shown by most other metals: this observation may also be interpreted on the assumption that hydrocarbon radicals are tightly held on an iron surface.

The ability of a gas chromatograph-mass spectrometer combination to determine the isotopic contents of products of hydrogenolysis at low conversions when carbon-carbon bonds are broken in the presence of deuterium is of little value as an aid to interpreting mechanism if the rate of exchange of the reactant is fast in comparison with the rate of hydrogenolysis, as has been shown to be the case with platinum.<sup>3</sup> Preliminary results<sup>4</sup> confirmed our assumptions that, because of the poor ability of iron to cause exchange at low temperatures, it might be a metal on which unambiguous results could be obtained in the region where hydrogenolysis occurs.

### Experimental Section

The apparatus used for this work has been described elsewhere.<sup>5</sup> Essentially, it consisted of a static reaction system of volume  $2.44 \times 10^{-4} \text{ m}^3$  coupled by means of a gas sampling valve to a Perkin-Elmer Type F11 gas chromatograph. The normal reaction mixture was  $427 \text{ N m}^{-2}$  of hydrocarbon and  $4.91 \text{ kN m}^{-2}$  of deuterium, measured at 273 K. This corresponded to  $2.76 \times 10^{19}$  molecules of hydrocarbon in the reaction vessel and a deuterium to hydrocarbon ratio of 11.5:1.

By means of an evacuated gas sampling valve quantities of material, up to ~2.5% of the contents of the reaction vessel, could be withdrawn and analyzed by gas chromatography on a column of bis(2-methoxyethyl) adipate (13.5%) and di-2-ethylhexyl sebacate (6.5%) on 60-80 mesh Chromosorb P at room temperature. The effluent from the chromatographic

column could be directed either to a flame ionization detector or, through a sintered glass molecular separator, to an A.E.I. MS20 Rapide mass spectrometer.

For experiments involving only chromatography the integrated areas of peaks produced by the flame ionization detector were used to calculate product distributions at different extents of reaction. Results are presented in terms of the carbon present in molecules in the gas phase. Mass spectral data from the GC-MS studies were corrected for background, naturally occurring isotopes and for fragmentation of molecules within the ion source of the mass spectrometer as has been described.<sup>3</sup> To allow for partial separation of the isotopic hydrocarbons in the chromatographic column summation of the intensities for each mass number was carried out for each compound emerging from the column.<sup>5</sup>

Methane, ethane, and deuterium (99.5%) were supplied by Cambrian Chemicals, Ltd. Propane and *n*-butane were obtained from Phillips Petroleum Co. and were of research grade. All gases were further purified either by distillation from liquid nitrogen traps, in the case of hydrocarbons, or diffusion through a heated palladium-silver alloy thimble in the case of deuterium or hydrogen.

The iron wire from which films (8-16 mg) were prepared was Johnson Matthey Specpure grade with total impurities less than 15 parts/10<sup>6</sup>. It was used in the form of a 15-cm wire with a diameter of 0.4 mm. The wire was outgassed at a current of 2.5 A for 30 min, after taking the metal through the  $\alpha\gamma$  phase transition to facilitate the removal of dissolved species, prior to evaporation at 3.6 A for 8 min onto the walls of the reaction vessel maintained at 273 K. The pressure in the reaction vessel during evaporation was  $<10^{-4} \text{ N m}^{-2}$ . Films had a geometric area of  $110 \text{ cm}^2$  and would be expected to have a roughness factor of about 2.

### Results

The reactions of *n*-butane, propane, ethane, and methane were studied at temperatures between 386 and 602 K. At these temperatures methane underwent exchange with deuterium while the higher hydrocarbons simultaneously exchanged and were hydrogenolyzed.

Information about the initial rates of each reactant as a function of temperature is presented in Figure 1 in the form of Arrhenius plots. The figure shows that the reactivity for hydrogenolysis increases as the number of carbon atoms in the

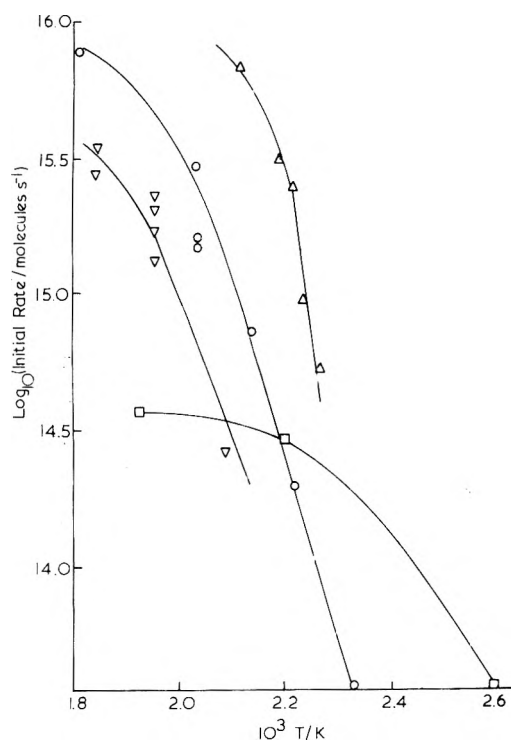


Figure 1. Arrhenius plots for the hydrogenolysis of *n*-butane ( $\Delta$ ), propane (O), and ethane ( $\nabla$ ) and exchange of methane ( $\square$ ) with deuterium on evaporated films.

molecule increases. A marked "turning over" of the Arrhenius plots at higher temperatures was observed and the temperature of the onset of curvature decreased with increase in the number of carbon atoms in the reactant. In all experiments the total amount of carbon in the gas phase fell slightly with time. Loss of carbon was confirmed by heating a used catalyst in hydrogen, after removal of the reaction mixture, when the production of methane was detected.

It was observed that catalyst activities were reduced if films were allowed to remain at reaction temperature prior to admission of reactants. For example, in the case of the reaction of ethane at 513 K the activity of the catalyst was reduced by a factor of 10 when the film was allowed to stand for 30 min before being contacted with the reactants.

The principal product of hydrogenolysis for all reactants was methane. In the case of *n*-butane the amount of methane produced increased from 88% of the products at 443 K to 95% at 483 K at points in the reactions where 10% of the reactant had been consumed. A typical experiment, showing the course of the hydrogenolysis of *n*-butane, is presented in Figure 2. With propane as reactant methane was the almost exclusive product, the ethane concentration at no time rising to more than 0.5% of the total carbon in the system.

Exchange of reactant with deuterium proceeded concurrently with hydrogenolysis. Typical values for the ratio of the rates of disappearance of reactant by hydrogenolysis (yielding mainly  $\text{CD}_4$ ) to exchange (yielding mainly mono- and perdeuterio reactant) were 1.0 for butane and 2.0 for propane at about 455 K and 6 for ethane at 513 K. Clearly exchange is relatively more important the larger the hydrocarbon. By extrapolating the selectivities for each isotopic species to zero conversion, see Figure 3, it was established, in the case of *n*-butane, that only *n*-butane- $d_1$  and *n*-butane- $d_{10}$  were formed initially in the approximate ratio of 1:4. Butane with deuterium numbers other than 1 or 10, formed later in the experi-

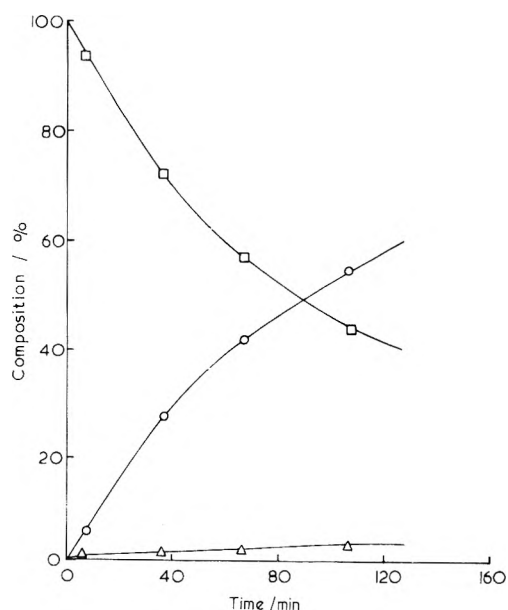


Figure 2. A typical reaction of *n*-butane on an iron film at 473 K:  $\square$ , *n*-butane; O, methane;  $\Delta$ , ethane.

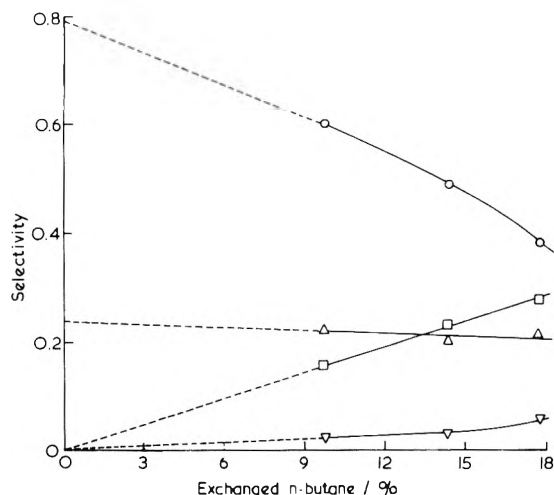


Figure 3. Isotopic content of *n*-butane with extent of reaction at 458 K: O, *n*-butane- $d_{10}$ ;  $\Delta$ , *n*-butane- $d_1$ ;  $\square$ , *n*-butane- $d_9$ ;  $\nabla$ , *n*-butane- $d_2$ .

ment, may be attributed to successive visits to the catalyst and the dilution of the deuterium pool by hydrogen. In the reaction of propane an analysis of the initial products of exchange showed that the main product was  $\text{C}_3\text{D}_8$  with approximately 10% of  $\text{C}_3\text{H}_7\text{D}$  and  $\text{C}_3\text{HD}_7$ . The only initial product formed by the exchange of ethane was  $\text{C}_2\text{D}_6$ .

The initial deuterium contents of the products of hydrogenolysis were also determined by extrapolation to zero time. In all cases perdeuterio material was the only product detected.

The use of the combined GC-MS technique made possible a comparative study of the behavior of several hydrocarbons in a single experiment, both with respect to hydrogenolysis and exchange. Such an experiment is particularly straightforward on iron where the main product of the hydrogenolysis is methane. The hydrogenolysis of a mixture containing approximately  $430 \text{ N m}^{-2}$  of each of *n*-butane, propane, and ethane on a 16-mg iron film at 513 K is shown in Figure 4. It is seen that the order of reactivity of the hydrocarbons was

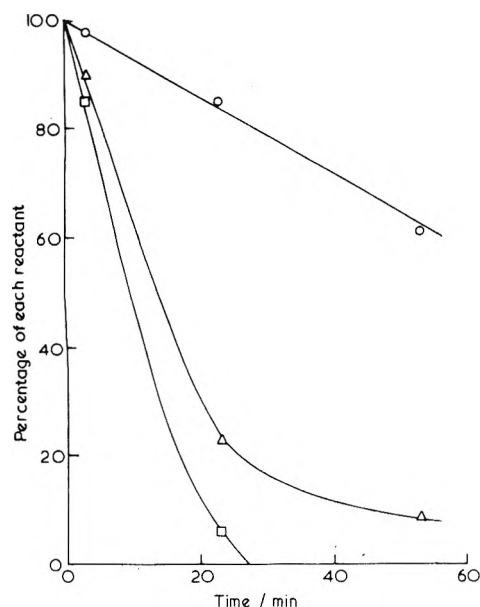


Figure 4. Reaction of  $430 \text{ N m}^{-2}$  of each of *n*-butane ( $\square$ ), propane ( $\Delta$ ), and ethane ( $\circ$ ) at 513 K.

*n*-butane > propane > ethane which is in agreement with the order when each reactant was used individually. Because the total hydrocarbon pressure in this experiment was much larger than with a normal reaction mixture it was studied with an overall deuterium to hydrocarbon ratio of only 3.8 to 1. This reduced ratio resulted in a substantial loss of carbon to the catalyst as reaction proceeded. Initially determined isotopic contents of the exchanged reactants in this experiment, and of the methane produced by hydrogenolysis, were not significantly different from those determined from the reactions of each hydrocarbon separately.

In contrast with previous findings,<sup>7</sup> the exchange of methane with deuterium on iron films was observed by continuous mass spectrometric analysis at temperatures between 385 and 523 K. Rates of reaction were slow and decreased with time at all temperatures, see Figure 1. The initial product distribution showed that only perdeuteriomethane was produced by the exchange reaction.

## Discussion

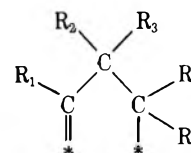
Iron does not catalyze the low temperature exchange reaction of hydrocarbons.<sup>7,9</sup> Adsorption of hydrocarbons on iron is known to occur at low temperatures<sup>10</sup> and thus the absence of exchange indicates that desorption of these molecules is not rapid. On raising the temperature exchange is observed to commence as soon as the products of hydrogenolysis, almost exclusively methane, are detected. This suggests that desorption of methane releases sites on the surface on which a further reactant molecule may adsorb.

Results show that the predominant products of exchange of *n*-butane, propane, and ethane with deuterium are the mono- or perdeuterio species. The  $d_1$  product must arise via the reversible formation of an adsorbed alkyl radical which, on leaving the surface, collects a deuterium atom in place of the hydrogen atom lost during adsorption. The formation of a significant percentage of the  $d_1$  product shows that the adsorbed alkyl species is relatively stable. Any alkyl species which do dissociate further become completely exchanged probably by rapid interconversion of various adsorbed species such as the  $\alpha\beta$ -adsorbed species (adsorbed olefin)<sup>9</sup> and the

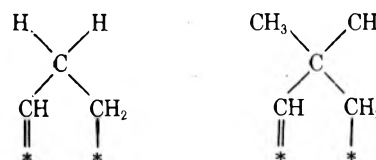
$\alpha\beta\gamma$ -adsorbed species (adsorbed allyl) or of course form hydrogenolysis products if C-C bond rupture occurs.

That the principal product of hydrogenolysis of *n*-butane and propane was methane suggests that the rate of desorption from the surface is slow, in comparison to the rate of fission of carbon-carbon bonds, for the species leading to hydrogenolysis. The surface intermediates responsible for hydrogenolysis must thus be adsorbed less reversibly than those involved in the exchange process with deuterium. This argument cannot be applied to ethane where methane is the only possible product of hydrogenolysis.

It has been suggested<sup>11</sup> that the hydrogenolysis of alkanes higher than ethane on metals proceeds via a species adsorbed at nonadjacent carbon atoms. In particular an  $\alpha\gamma$  adsorbed species has been proposed as a likely intermediate

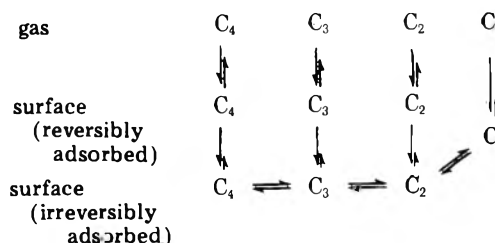


and has been confirmed as the species responsible for the hydrogenolysis of neopentane.<sup>5</sup> An  $\alpha\alpha\gamma$  species will tend to be irreversibly adsorbed on an iron surface and is likely to lead to methane as the principal hydrogenolysis product. It is significant to note that propane and neopentane hydrogenolysis proceed with comparable rates and this may be explained by the similarity, with respect to interaction with the surface, of the  $\alpha\alpha\gamma$  species formed.



The formation of species adsorbed at  $\alpha$  and  $\gamma$  positions is not possible with ethane, where hydrogenolysis probably occurs via an  $\alpha\alpha\beta$  species, and this may be a factor contributing to the low rate of its hydrogenolysis in comparison with higher alkanes.

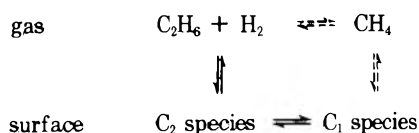
It may be postulated that there exist two main classes of intermediate on the surface of an iron catalyst. The first, leading to exchange, is reversibly adsorbed and the second, responsible for hydrogenolysis, is almost completely irreversibly adsorbed. It is likely that the first species is a precursor of the second. This scheme may be represented as



in which the lengths of the arrows bear some relation to the rates of the various processes. Such a scheme can explain the exchange of the individual reactants and also the observation that the almost exclusive product of hydrogenolysis is perdeuteriomethane. Taking, for example, the reaction of propane, this molecule may exchange by reversible adsorption on the surface. The fraction of the reversibly adsorbed species which further dissociates to become irreversibly adsorbed will suffer fission of a carbon-carbon bond to yield  $C_1$  and  $C_2$

species. The  $C_2$  species will correspond to irreversibly adsorbed ethane which will in turn suffer fission of its carbon-carbon bond to yield methane and will not appear as ethane in the gas phase.

It is necessary to seek an explanation for the observation that the rate of production of methane by hydrogenolysis can exceed the rate of desorption of methane as measured by the rate of methane exchange. Such an explanation may be attempted by employing the concept of "virtual" pressure, first introduced by Tempkin and Pyzhev<sup>12</sup> to account for the observed kinetics of the catalytic decomposition of ammonia, in which the slow step was assumed to be desorption of the product nitrogen. Taking hydrogenolysis of the simplest hydrocarbon, ethane, as an example, the various relevant equilibria which may be established are as follows:



In the present argument it is to be assumed that equilibria represented by continuous arrows are established but, because of the slow desorption of  $C_1$  species, those represented by broken lines are not. This situation would lead to an accumulation of  $C_1$  entities on the surface until a concentration is reached such that it would be in equilibrium with a gas phase pressure of methane equal to that which would be in equilibrium with the ethane and hydrogen present in the system. The "virtual" pressure of methane is thus simply defined as that which would satisfy the two equilibria represented by broken lines.

This argument suggests the surface coverage of  $C_1$  species achieved during hydrogenolysis may be much greater than during methane exchange experiments thus explaining how the rate of production of methane by hydrogenolysis can exceed the rate of methane exchange. It would be expected that the rate of hydrogenolysis should be related to the virtual pressure of methane in equilibrium with the reactant hydrocarbon. In Table I standard equilibrium constants<sup>13</sup> have been used to calculate the pressure of methane which would be in equilibrium with the pressures of hydrocarbon and deuterium employed in the standard reaction mixture. It is seen that the trend in "virtual" pressures is in the same direction as the trend in observed rates of hydrogenolysis.

The exchange of methane on deuterium has not previously been observed on iron film catalysts. That the exclusive product of exchange currently reported is the perdeuterio molecule suggests that the methyl radical, in contrast to higher alkyl radicals, has little stability on the metal surface and rapidly interconverts with the  $\alpha\alpha$ , or more highly dissociated, species.

It is interesting to contrast the differences between the behavior of iron, presently reported, and platinum.<sup>3</sup> On platinum it seems that hydrocarbons interact relatively weakly with the metal, as evidenced by hydrogenolyzed products which have suffered fracture of a single carbon-carbon bond. On platinum the rate-determining step is likely to be the fission of carbon-carbon bonds rather than methane desorption. Iron on the other hand tends to interact much

TABLE I: Virtual Pressure of Methane in Equilibrium with 427 N m<sup>-2</sup> of Various Hydrocarbons at 500 K

Equilibrium	$P_{CH_4}$ , atm
$C_2H_6 + H_2 \rightleftharpoons 2CH_4$	69
$C_3H_8 + 2H_2 \rightleftharpoons 3CH_4$	907
$n-C_4H_{10} + 3H_2 \rightleftharpoons 4CH_4$	2729

more strongly with hydrocarbons. At low temperatures the extent of interaction is such that desorption does not occur and at higher temperatures all the hydrogen atoms in a molecule can be replaced by deuterium during a single visit to the catalyst surface. Hydrogenolysis products on iron are almost exclusively perdeuteriomethane suggesting that desorption of methane may be rate determining.

In the present work no attempt has been made to extract information from other than the initial reaction rates and initial product distributions. This is because there is little doubt that the surface of the film was changing as each experiment proceeded. Accumulation of carbonaceous material on the surface was apparent from the loss of total hydrocarbon from the gas phase and was confirmed by the slow liberation of methane when a used catalyst was heated in hydrogen. Loss of metal area due to sintering will also be expected. Evidence tending to indicate this came from the reaction of ethane on a catalyst which had been allowed to stand for 30 min before being contacted with the reactants; this resulted in a 10-fold reduction in rate in comparison to a standard experiment. It is likely that, while part of this decline in activity may be attributed to sintering, some will also be due to contamination of the surface and thus in our opinion extraction of kinetic information, other than at zero time, would be of little value. Similarly, it is not possible from the experiments which have been conducted to rule out some contribution from sintering to the turnover in the Arrhenius plots at higher temperatures.

**Acknowledgments.** The authors acknowledge a grant from the Science Research Council for the purchase of apparatus. R.S.D. thanks the British Petroleum Co., Ltd. for a studentship.

## References and Notes

- (1) J. C. Kempling and D. A. Whan in "Surface and Defect Properties of Solids", Vol. 2, The Chemical Society, London, 1973, pp 99-113.
- (2) J. H. Sinfelt and D. J. C. Yates, *J. Catal.*, **10**, 362 (1968).
- (3) R. S. Dowie, D. A. Whan, and C. Kemball, *J. Chem. Soc., Faraday Trans. 1*, **68**, 2150 (1972).
- (4) R. S. Dowie, M. C. Gray, D. A. Whan, and C. Kemball, *J. Chem. Soc., Chem. Commun.*, 883 (1971).
- (5) R. S. Dowie, C. Kemball, J. C. Kempling, and D. A. Whan, *Proc. R. Soc. London, Ser. A*, **327**, 491 (1972).
- (6) A. S. Porter and F. C. Tompkins, *Proc. R. Soc. London, Ser. A*, **217**, 529 (1953).
- (7) C. Kemball, *Proc. R. Soc. London, Ser. A*, **217**, 376 (1953).
- (8) D. A. Whan and C. Kemball, *Trans. Faraday Soc.*, **61**, 294 (1965).
- (9) J. R. Anderson and C. Kemball, *Proc. R. Soc. London, Ser. A*, **223**, 361 (1954).
- (10) P. G. Wright, P. G. Ashmore, and C. Kemball, *Trans. Faraday Soc.*, **54**, 1962 (1958).
- (11) J. R. Anderson and B. G. Baker, *Proc. R. Soc. London, Ser. A*, **271**, 402 (1963).
- (12) M. I. Tempkin and V. M. Pyzhev, *Acta. Physicochim.*, **12**, 327 (1940).
- (13) Selected Physical and Thermodynamic Properties, American Petroleum Institute Report, 1973, p 750.

# A Study of the Mechanism of (<sup>2</sup>P) Carbon Ion Reactions with Benzene at 1.0–12 eV

Richard D. Smith<sup>1</sup> and James J. DeCorpo\*

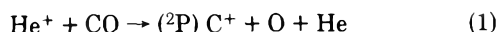
Chemistry Division, Naval Research Laboratory, Washington, D.C. 20375 (Received September 2, 1976)

Publication costs assisted by the Naval Research Laboratory

Branching ratios have been determined for the reactions of ground state (<sup>2</sup>P) <sup>12</sup>C<sup>+</sup> and <sup>13</sup>C<sup>+</sup> ions with benzene over a range of translational energies of 1.0–12 eV. The benzene molecular ion is the principal product (~80%) at all energies. The use of <sup>13</sup>C<sup>+</sup> reactant ions shows that several ionic products (C<sub>3</sub>H<sub>2</sub><sup>+</sup>, C<sub>3</sub>H<sub>3</sub><sup>+</sup>, C<sub>4</sub>H<sub>2</sub><sup>+</sup>, C<sub>4</sub>H<sub>3</sub><sup>+</sup>, and C<sub>5</sub>H<sub>3</sub><sup>+</sup>) incorporate the <sup>13</sup>C reactant nucleus. The amount of <sup>13</sup>C retention for the C<sub>5</sub>H<sub>3</sub><sup>+</sup> product is in excellent agreement with that predicted by a carbon-randomized model. Secondary ion reactions were also studied at higher pressures, however, collisional stabilization of a postulated C<sub>7</sub> intermediate was not observed. The possible relevance to the <sup>14</sup>C<sup>+</sup> ion-accelerator studies of Lemmon and co-workers is discussed.

## Introduction

Studies of reactions of ground state atomic ions are especially interesting since knowledge of the relative translational energy of the collisional partners allows one to fix the total internal energy of the collisional complex within well-defined limits.<sup>2,3</sup> The reactions of carbon ions with hydrocarbon molecules have recently attracted considerable interest.<sup>2–14</sup> Previous work has demonstrated that ground state (<sup>2</sup>P) C<sup>+</sup> ions may be easily prepared by ion–molecule reactions in a mixture of CO and a large excess of He. The mechanism of C<sup>+</sup> ion formation is the dissociative charge reaction from He which is not sufficiently exothermic to produce excited state (<sup>4</sup>P) C<sup>+</sup> ions.<sup>2,4</sup>



The subject of the present report is a study of the ion–molecule reactions of (<sup>2</sup>P) C<sup>+</sup> ions with benzene. The only previous studies of C<sup>+</sup> ion reactions with benzene are the <sup>14</sup>C<sup>+</sup> ion-accelerator experiments of Lemmon and co-workers.<sup>9–13</sup> These previous experiments examined the products of <sup>14</sup>C<sup>+</sup> impact on a solid benzene target at translational energies between 2 eV and 15 keV. Following irradiation the <sup>14</sup>C-labeled products are studied using mainly radiogas chromatographic techniques. While these experiments have provided a wealth of interesting information, they do not provide easily recognized information concerning the initial ion–molecule reaction products or their dependence on internal energy.

In the present study we have used a tandem mass spectrometer to study the reactions of C<sup>+</sup> with C<sub>6</sub>H<sub>6</sub> over the chemically important range of 1–12 eV. Our primary interest was the determination of branching ratios for the initial ion–molecule products and their dependence on translational energy. Both (<sup>2</sup>P) <sup>12</sup>C<sup>+</sup> and (<sup>2</sup>P) <sup>13</sup>C<sup>+</sup> reactions have been studied, allowing an examination of the detailed mechanism of these reactions. The results of a tandem Dempster-ICR study of these reactions at 0.1 eV, reported elsewhere by Smith and Futrell,<sup>15</sup> are compared to the present results and used for extrapolation to thermal energies.

A question of relevance to the ion-accelerator studies of Lemmon and co-workers is whether ion–molecule reactions are important in producing the observed <sup>14</sup>C-labeled products<sup>9–13</sup> and, in particular, if a C<sub>7</sub> ionic species can be formed in the primary ion–molecule encounter. The present results

clearly suggest that a C<sub>7</sub> ionic intermediate does exist and its formation is a significant reaction pathway at low translational energies (≤8 eV).

## Experimental Section

Two mass spectrometers were used in the present study. Also compared are results obtained in a study<sup>15</sup> utilizing a tandem Dempster-ion cyclotron resonance (ICR) mass spectrometer to examine the (<sup>2</sup>P) <sup>12</sup>C<sup>+</sup> and <sup>13</sup>C<sup>+</sup> ion–molecule reactions with C<sub>6</sub>H<sub>6</sub> at near thermal translational energies (~0.1 eV). The tandem quadrupole mass spectrometer used in this work has been described previously<sup>16</sup> and was used to study these reactions between 1 and 12 eV. Finally, a dual high-pressure, electron impact-photoionization mass spectrometer was utilized to study the mechanisms of the secondary ion reactions in benzene at elevated pressures.

In the tandem quadrupole instrument,<sup>16</sup> C<sup>+</sup> ions were generated by 150-eV electron impact on a 10:1 mixture of He:CO. For the results reported in Table I the collision chamber pressure was 0.25 × 10<sup>−3</sup> Torr, assuring that secondary reactions were negligible. The second stage quadrupole mass spectrometer is in-line with the first stage,<sup>16</sup> which may lead to minor discrimination effects against ions resulting from reactions involving little momentum transfer (e.g., charge transfer). The implications of this effect are discussed in the next section.

An additional series of experiments, using the tandem quadrupole instrument, was undertaken at increased collision chamber pressures (1–10 × 10<sup>−3</sup> Torr) to examine the various secondary ion reactions. These experiments were complemented by studies of ion–molecule reactions in benzene, using a dual photoionization-electron impact quadrupole mass spectrometer at pressures between 0.5 × 10<sup>−3</sup> and 0.5 Torr.

## Results

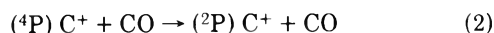
As described previously,<sup>2,4</sup> (<sup>2</sup>P) C<sup>+</sup> ions can be generated by electron impact on CO/He mixtures. Reaction 1 can only yield ground state (<sup>2</sup>P) C<sup>+</sup> ions and has a rate constant of 1.5 × 0.2 × 10<sup>−9</sup> cm<sup>3</sup> molecule<sup>−1</sup> s<sup>−1</sup>.<sup>17</sup> Use of a large excess of helium, and source conditions which require that the average ion undergoes many collisions before leaving the source assures that the mass-selected reactant ions consist entirely of ground state carbon ions.<sup>2</sup> The tandem Dempster-ICR source is a closed “chemical-ionization type” source and meets these

**TABLE I: Product Distributions<sup>a</sup> for the Reactions of (2P)  $^{12}\text{C}^+$  and (2P)  $^{13}\text{C}^+$  Ions with Benzene**

<i>m/e</i>	0.1 eV <sup>b</sup>		1 eV <sup>c</sup>		2 eV <sup>c</sup>		4 eV <sup>c</sup>		8 eV <sup>c</sup>		12 eV <sup>c,d</sup>	
	$^{12}\text{C}^+$	$^{13}\text{C}^+$	$^{12}\text{C}^+$	$^{13}\text{C}^+$	$^{12}\text{C}^+$	$^{13}\text{C}^+$	$^{12}\text{C}^+$	$^{13}\text{C}^+$	$^{12}\text{C}^+$	$^{13}\text{C}^+$	$^{12}\text{C}^+$	$^{13}\text{C}^+$
38					0.9	<0.4	1.4	0.4	1.9	0.8		
39	3	3	6.0	4.6	6.3	5.6	7.4	6.7	7.5	7.6	18	18
40				1.4		1.5		1.7		1.0		
50			0.3	0.2	0.5	0.3	0.7	0.3	2.1	0.7		
51			1.9	1.6	2.1	1.5	2.1	1.7	3.0	4.2	4	3
52			1.9	2.3	1.8	2.6	1.5	2.3	2.6	2.9		1
61									0.6	<0.2		
62							0.6	<0.2	2.6	0.6		
63	14	3	7.0	2.0	6.5	2.0	5.2	1.8	3.3	3.3	3	2
64		11		5.0		4.5		4.1		2.5		1
77			0.5	0.5	0.8	0.9	1.0	0.9	2.0	2.0		
78 <sup>e</sup>	83	83	82.4	82.4	81.1	81.0	80.1	80.1	74.4	74.4	75	75

<sup>a</sup> Corrected for naturally occurring  $^{13}\text{CC}_5\text{H}_6$ . <sup>b</sup> Data obtained by Smith and Futrell (ref 15). <sup>c</sup> Data obtained using the tandem quadrupole mass spectrometer. <sup>d</sup> The 12-eV data have a considerably higher uncertainty (a precision of approximately  $\pm 3\%$  of the total products) due to a decrease in the total product ion intensities. <sup>e</sup> The intensity of *m/e* 78 for  $^{12}\text{C}^+$  and  $^{13}\text{C}^+$  reactant ions always agreed to within 1.5%. The intensity of *m/e* 78 was set equal to facilitate comparisons of the minor product intensities.

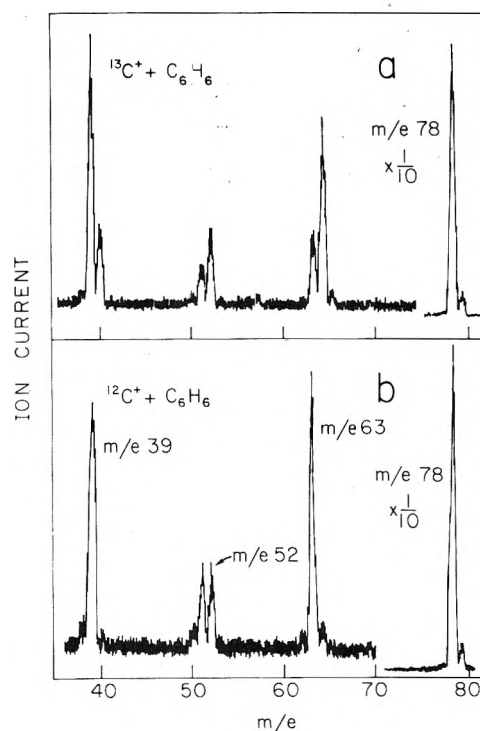
requirements; previous experiments have shown that only (2P)  $\text{C}^+$  ions leave the Dempster source.<sup>2</sup> The tandem quadrupole instrument, however, has a more open source, thus restricting the maximum number of collisions. Thus, it is possible that excited (4P)  $\text{C}^+$  ions may have contributed to the present results. Excited  $\text{C}^+$  ions can result from electron impact on CO (approximately 30–40% may be formed in the 4P state),<sup>18</sup> but may be relaxed in subsequent collisions with CO.



The carbon atom exchange reaction is known<sup>4,19</sup> to occur with a rate constant of  $2 \times 10^{-10} \text{ cm}^3 \text{ molecule}^{-1} \text{ s}^{-1}$ , and is probably important in the relaxation of (4P)  $\text{C}^+$  ions. We estimate that the contribution of (4P)  $\text{C}^+$  ions in the tandem quadrupole experiments may be as large as 5%; the contribution in the tandem Dempster-ICR experiment is  $<1\%$ .<sup>2</sup>

The tandem Dempster-ICR results,<sup>15</sup> at 0.1 eV (laboratory frame) average translational energy, are given in the first column of Table I. The results have a precision of  $\pm 1\%$  of the total products, and an estimated accuracy of  $\pm 5\%$  of the reported values. In a properly conducted tandem Dempster-ICR experiment, mass discrimination and effects resulting from the collision dynamics are usually negligible, and the absolute uncertainty is determined by the accuracy of the calibration procedure and the S/N ratio of the experiment.

The tandem-quadrupole results, for average translational energies of 1–12 eV, are given in Table I. Figure 1 shows typical product ion spectra for the reactions of  $^{12}\text{C}^+$  and  $^{13}\text{C}^+$  ions with benzene at 1 eV obtained by scanning the *m/e* with the second stage quadrupole mass filter. The results in Table I and Figure 1 were obtained at sufficiently low collision chamber pressures ( $2.5 \times 10^{-4}$  Torr) to assure the absence of secondary ion reactions. The fractional abundance of the charge transfer product ( $\text{C}_6\text{H}_6^+$  at *m/e* 78) for  $^{12}\text{C}^+$  and  $^{13}\text{C}^+$  reactant ions agreed to within 1.5%. To simplify the comparison of branching ratios for the minor reaction products, the intensities of the *m/e* 78 product were set equal for both  $^{12}\text{C}^+$  and  $^{13}\text{C}^+$  reactant ions. This correction has a negligible effect on the product distributions and allows a quantitative comparison of branching ratios for  $^{12}\text{C}^+$  and  $^{13}\text{C}^+$  ions. The slight difference in the reactant translational energies for  $^{12}\text{C}^+$  and  $^{13}\text{C}^+$  reactant ions can safely be neglected since it amounts to only 1% of the reported energy.



**Figure 1.** Typical scans of the product ion spectra for the reactions of  $^{13}\text{C}^+$  (a) and  $^{12}\text{C}^+$  (b) ions with benzene at 1-eV average translational energy. These scans were obtained at a collision chamber pressure of  $2.5 \times 10^{-4}$  Torr where secondary ion reactions were negligible.

The absolute accuracy of the tandem quadrupole data is difficult to access due to possible mass discrimination effects in the analyzer (second stage) quadrupole mass filter, as well as problems arising from the collisional dynamics mentioned earlier. For reactions involving a collision complex (with a lifetime longer than rotational period and, hence, momentum transfer), and resulting in ionic products over a narrow mass range, we can safely assume that such effects are negligible. Thus, the  $^{12}\text{C}^+$  and  $^{13}\text{C}^+$  product distributions may be compared quantitatively to determine the extent of  $^{13}\text{C}$  retention in the ionic products. The absolute branching ratios for products having significantly different velocity vectors and *m/e* ratios (e.g.,  $\text{C}_3\text{H}_3^+$  and  $\text{C}_6\text{H}_6^+$ ) may be in error by as much



TABLE II: Standard Heats of Formation (kcal/mol)

Species	$\Delta H_f^a$	Ref
$C_6H_6^+$	233	b
$C_6H_5^+$	266	c
$C_6H_4^+$	$\leq 352$	b
$C_5H_3^+$	$\leq 368$	b
$C_5H_2^+$		
$C_4H_4^+$	281	d
$C_4H_3^+$	$\leq 307$	b
$C_4H_2^+$	337	b
$C_3H_3^+$	256	d
$C_3H_2^+$	$\leq 365$	b
$C^+ (^2P)$	431	b
$C^+ (^4P)$	$\sim 553$	e
$C_6H_6$	19.8	b
$C_4H_4$	69	b
$C_4H_3$		
$C_4H_2$	102	b
$C_3H_4$	45.9	b
$C_3H_3$	80.7	c
$C_3H_2$	113	f
$C_2H_3$	65	b
$C_2H_2$	54.2	b
$C_2H$	112	b
CH	142.4	b
H	52.1	b

<sup>a</sup> Heat of formation in kcal/mol for the lowest energy structure.

<sup>b</sup> Reference 26. <sup>c</sup> Reference 21. <sup>d</sup> Reference 27. <sup>e</sup> Reference 24.

<sup>f</sup> Reference 41.

as 20% of the reported value. These problems, however, have little relevance to our primary interests in this work; the mechanism of the various reaction channels in  $C^+ + C_6H_6$  ion-molecule reactions.

All heats of reaction were calculated from thermodynamic data given in Table II. Unfortunately, accurate heats of formation are not known for a number of species important to this work, and one should note that only upper limits to  $\Delta H_f$  are given for several species.

## Discussion

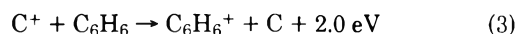
**Reaction Mechanisms.** An examination of the results presented in Table I shows that between 0.1 and 8 eV the following ionic products of primary  $C^+ + C_6H_6$  bimolecular reactions are observed:  $C_6H_6^+$ ,  $C_6H_5^+$ ,  $C_5H_3^+$ ,  $C_5H_2^+$ ,  $C_4H_4^+$ ,  $C_4H_3^+$ ,  $C_4H_2^+$ ,  $C_3H_3^+$ , and  $C_3H_2^+$ . At near thermal translational energies (0.1 eV) only  $C_6H_6^+$ ,  $C_5H_3^+$ , and  $C_3H_3^+$  are observed.<sup>15</sup> At higher kinetic energies both the  $C_6H_6^+$  and  $C_5H_3^+$  ions account for decreasing fractions of the total ion

products, while most remaining products show increasing importance.

Comparison of product distributions for  $^{12}C^+$  and  $^{13}C^+$  reactions can provide important information on the mechanism of these reactions. The results in Table I (and Figure 1) clearly show that there is significant retention of the  $^{13}C^+$  reactant nucleus in several of the ionic products. A useful model for comparison with the fraction of  $^{13}C$  retention in the ionic products is one in which complete carbon atom randomization occurs in the intermediate (a  $C_7$  species such as  $^{13}C^{12}C_6H_6^+$ ) before fragmentation. In Table III we give the experimental fraction of  $^{13}C$  retention divided by the fraction of  $^{13}C$  retention predicted by the carbon-randomized model. Thus, a value of 1.0 corresponds to  $^{13}C$  retention in exact agreement with the carbon-randomized model. Below we discuss the various reactions observed in this work and the possible mechanisms deduced from thermodynamics and the information in Tables I and III.

Table I shows that the  $C_6H_6^+$  ion is the major ionic product over the entire energy range studied, accounting for approximately 80% of the total products at low energies, and apparently a slightly decreasing fraction at higher energies. (It should be noted, however, that tandem mass spectrometers of the "in-line" configuration often discriminate against charge transfer products and that this decrease may be an experimental artifact.) After correction of the  $m/e$  79 intensity for naturally occurring  $^{13}C^{12}C_5H_6^+$ , the results indicate that the  $^{13}C^{12}C_5H_6^+$  product certainly amounts to <1% of the total products. Thus, the  $C_6H_6^+$  ion is apparently due to a simple charge transfer reaction.

The charge transfer reaction



while exothermic, probably does not result in subsequent dissociation of the  $C_6H_6^+$  product unless accompanied by significant conversion of translational to internal energy at higher kinetic energies. A simple charge transfer process, without momentum transfer, will produce  $C_6H_6^+$  ions with approximately 2 eV of internal energy while approximately 4.6 eV is required to observe fragmentation on the experimental time scale ( $\sim 5 \times 10^{-6}$  s) of the tandem quadrupole experiment.<sup>20,21</sup> It should be noted, however, that the considerably longer reaction time in the tandem Dempster-ICR experiment<sup>15</sup> ( $\sim 5 \times 10^{-3}$  s) will often result in lower appearance potentials for the fragmentation of complex ions due to a reduction in the magnitude of the kinetic shift.<sup>22</sup>

Fragmentation of the initial charge transfer product ( $C_6H_6^+$ ) may either result from charge transfer reactions involving significant momentum transfer or from the presence of excited ( $^4P$ ) carbon ions. Only at the highest translation

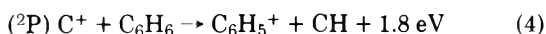
TABLE III: Experimental  $^{13}C$ -Retention Divided by Expectation of a Carbon-Randomized Model<sup>a</sup>

Product ion	0.1 eV	1.0 eV	2.0 eV	4 eV	8 eV
$C_3H_2^+$			$1.6 \pm 0.8$	$1.6 \pm 0.6$	$1.3 \pm 0.8$
$C_3H_3^+$	0–0.5	$0.54 \pm 0.05$	$0.55 \pm 0.10$	$0.54 \pm 0.07$	$0.31 \pm 0.15$
$C_4H_2^+$		$0.5 \pm 0.15$	$0.7 \pm 0.14$	$1.0 \pm 0.4$	$1.1 \pm 0.4$
$C_4H_3^+$		$0.37 \pm 0.12$	$0.5 \pm 0.2$	$0.6 \pm 0.2$	$0.0 \pm 0.4$
$C_4H_4^+$		<0.05	<0.05	<0.10	<0.10
$C_5H_2^+$				$1.0 \pm 0.3$	$0.9 \pm 0.3$
$C_5H_3^+$	$1.01 \pm 0.2$	$1.00 \pm 0.04$	$0.98 \pm 0.07$	$1.04 \pm 0.10$	$1.02 \pm 0.15$
$C_6H_6^+$	<0.05	<0.02	<0.03	<0.03	<0.05

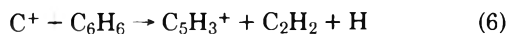
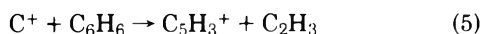
<sup>a</sup> A carbon-randomized model would yield 43, 57, 71, and 86%  $^{13}C$ -retention for  $C_3$ ,  $C_4$ ,  $C_5$ , and  $C_6$  products, respectively.

energies studied (12 eV) does the contribution of dissociative charge transfer from the (<sup>2</sup>P) C<sup>+</sup> appear to amount to more than a few percent. This is not surprising since such charge exchange processes typically have large cross sections and dominate the ion chemistry at high translational energies. Examination of experimental<sup>21,23,24</sup> and calculated<sup>20,21</sup> breakdown curves for benzene shows that charge transfer from the excited (<sup>4</sup>P) state will yield C<sub>6</sub>H<sub>6</sub><sup>+</sup> ions with sufficient internal energy (~7.4 eV) to cause complete dissociation. Quasi-equilibrium theory (QET) calculations<sup>20</sup> suggest C<sub>6</sub>H<sub>5</sub><sup>+</sup> should be the major fragmentation product (76%) with smaller amounts of other species: C<sub>6</sub>H<sub>4</sub><sup>+</sup> (12%), C<sub>5</sub>H<sub>3</sub><sup>+</sup> (1%), C<sub>4</sub>H<sub>4</sub><sup>+</sup> (8%), and C<sub>3</sub>H<sub>3</sub><sup>+</sup> (4%). However, charge exchange breakdown curves for benzene<sup>23</sup> suggest C<sub>4</sub>H<sub>4</sub><sup>+</sup> will be the largest product (~60%) with approximately equal amounts of C<sub>6</sub>H<sub>5</sub><sup>+</sup> and C<sub>3</sub>H<sub>3</sub><sup>+</sup> (each with ~20%), while more reliable photoelectron-photoion coincidence measurements<sup>24</sup> suggest a [C<sub>6</sub>H<sub>5</sub><sup>+</sup>]:[C<sub>4</sub>H<sub>4</sub><sup>+</sup>]:[C<sub>3</sub>H<sub>3</sub><sup>+</sup>] ratio of 2.5:4:1. If the C<sub>6</sub>H<sub>5</sub><sup>+</sup> intensity is due solely to dissociative charge transfer from the <sup>4</sup>P state we may estimate the contribution of this state in the present work at 1–6%. Recent work<sup>21</sup> on the photoionization of benzene, however, also suggests that charge transfer from the <sup>4</sup>P state of C<sup>+</sup> may populate a long-lived electronic state of C<sub>6</sub>H<sub>6</sub><sup>+</sup> which fragments primarily to form the C<sub>4</sub>H<sub>4</sub><sup>+</sup> and C<sub>3</sub>H<sub>3</sub><sup>+</sup> ions. It is interesting to note that the photoelectron spectra of C<sub>6</sub>H<sub>6</sub> shows an absence of structure in the region corresponding to resonant charge transfer with the <sup>4</sup>P state of C<sup>+</sup> (~16.6 eV), in contrast to charge transfer from the <sup>2</sup>P state, which is near resonant with a state at 11.5 eV.

As noted above the small contribution of C<sub>6</sub>H<sub>5</sub><sup>+</sup> may be due to a dissociative charge transfer reaction involving excited (<sup>4</sup>P) C<sup>+</sup> ions. The dissociative charge transfer reaction of (<sup>2</sup>P) C<sup>+</sup> ions is 1.67-eV endothermic. Alternately, this product may result from the exothermic hydride ion abstraction reaction:



The C<sub>5</sub>H<sub>3</sub><sup>+</sup> ionic product of the C<sup>+</sup> + C<sub>6</sub>H<sub>6</sub> reaction is one of the most interesting features of this work. Two possible reactions yielding this product are



Unfortunately, there is no reliable value for the heat of formation of C<sub>5</sub>H<sub>3</sub><sup>+</sup> in the literature. A value based on an appearance potential measurements<sup>26</sup> (368 kcal/mol) would suggest that reaction 6 is 1-eV endothermic while reaction 5 is 0.8-eV exothermic. However, this value for the Δ*H*<sub>f</sub> of C<sub>5</sub>H<sub>3</sub><sup>+</sup> is probably too high and it is likely that both reactions are exothermic.

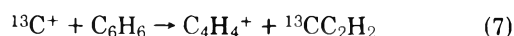
Reaction 6 is probably a more likely source of the C<sub>5</sub>H<sub>3</sub><sup>+</sup> product than reaction 5, due to its analogy with reactions previously reported for C<sup>+</sup> ions with simple hydrocarbon molecules (methane through propane).<sup>2</sup> This previous work suggested a mechanism in which the initial step involved insertion at a C–H or C=C bond. In the case of attack at a C–H bond the adduct was usually postulated to fragment via H-atom elimination at the site of attack followed by a more complex (usually molecular) elimination process. This mechanism has the advantages of H-atom elimination occurring at a site where the excess energy is initially concentrated and yielding a favored even-electron ion (C<sub>7</sub>H<sub>5</sub><sup>+</sup>) in the first dissociation step.

The results in Tables I and III support a mechanism in-

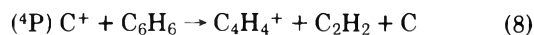
volving a C<sub>7</sub> intermediate species. The results in Table I demonstrate that the relative importance of this reaction decreases with increasing translational energy. Such behavior is typical of reactions involving an intermediate species as opposed to fast (direct) atom or electron transfer mechanisms. More important, however, are results showing considerable <sup>13</sup>C retention in the C<sub>5</sub>H<sub>3</sub><sup>+</sup> product. Table III shows that the ratio of <sup>13</sup>C retention (experimental)/<sup>13</sup>C retention (randomized model) is approximately equal to 1.0 over the entire energy range studied. These results provide strong evidence for the existence of a C<sub>7</sub> intermediate species which undergoes complete carbon atom randomization prior to dissociation to form the C<sub>5</sub>H<sub>3</sub><sup>+</sup> product.

At higher energies C<sub>5</sub>H<sub>2</sub><sup>+</sup> also becomes a significant product. Since the <sup>13</sup>C retention in C<sub>5</sub>H<sub>2</sub><sup>+</sup> is near the statistical prediction (Table III), this product may either result directly from decomposition of the C<sub>7</sub> intermediate or from H-atom elimination from the C<sub>5</sub>H<sub>3</sub><sup>+</sup> product.

The C<sub>4</sub>H<sub>4</sub><sup>+</sup> product is also quite interesting in that the <sup>13</sup>C retention is negligible over the entire energy range (Table III). Since this product cannot result from dissociative charge transfer, which is 2.4-eV endothermic for (<sup>2</sup>P) C<sup>+</sup> ions, C<sub>4</sub>H<sub>4</sub><sup>+</sup> can only be attributed to two possible mechanisms; first, C<sub>4</sub>H<sub>4</sub><sup>+</sup> may be due to the specific reaction

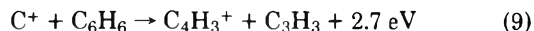


which, unlike all other reactions of (<sup>2</sup>P) C<sup>+</sup> ions, cannot be eliminated on thermodynamic grounds. Using the calculated value of Δ*H*<sub>f</sub> for C<sub>3</sub>H<sub>2</sub> (Table II) reaction 7 is exothermic by 57 kcal/mol. The second possible mechanism is a reaction involving the excited (<sup>4</sup>P) C<sup>+</sup> ions, which were mentioned earlier.

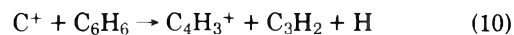


In support of reaction 8, one would predict similar contributions to C<sub>6</sub>H<sub>5</sub><sup>+</sup> and C<sub>3</sub>H<sub>3</sub><sup>+</sup> resulting from dissociative charge transfer from (<sup>4</sup>P) C<sup>+</sup>, as observed. Reaction 7 would be atypical of most carbon ion reactions, in that one usually postulates a reasonably long-lived intermediate for complex molecular eliminations, suggesting a lifetime sufficient for carbon atom randomization. The results in Table III show negligible carbon atom randomization and we presently favor reaction 8 as the source of C<sub>4</sub>H<sub>4</sub><sup>+</sup> ions.

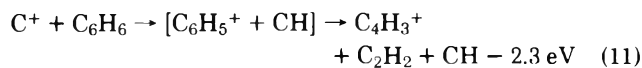
The C<sub>4</sub>H<sub>3</sub><sup>+</sup> product probably results from the following overall reaction



The reaction



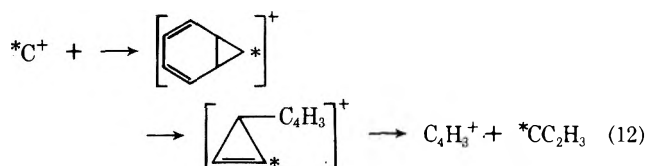
is almost certainly endothermic and may be dismissed at low translational energies. The dissociative hydride ion abstraction



may also be dismissed at low translational energies on thermodynamic grounds. Similarly, all other reactions of <sup>2</sup>P carbon ions are quite endothermic and are unlikely to contribute to C<sub>4</sub>H<sub>3</sub><sup>+</sup> formation.

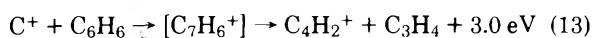
Table III shows that the C<sub>4</sub>H<sub>3</sub><sup>+</sup> ionic product has a ratio of <sup>13</sup>C retention (experimental)/<sup>13</sup>C retention (randomized model) of less than 1.0 from 1 to 8 eV. These results suggest two possible rationalizations. First, the small contribution of excited (<sup>4</sup>P) carbon ions, if present, may undergo a direct re-

action leading to  $C_4H_3^+$  formation. A reaction with a direct first step, such as the dissociative hydride abstraction reaction, will yield  $C_4H_3^+$  ionic products with a total absence of the  $^{13}C$ -isotopic label (the reaction,  $C_6H_5^+ \rightarrow C_4H_3^+ + C_2H_2$  is known to occur.<sup>28</sup> One should also note that  $C_4H_4^+$  ions may eliminate a H atom<sup>28</sup> to form  $C_4H_3^+$ , however,  $C_4H_4^+$  ions formed by a charge transfer from ( $^4P$ )  $C^+$  ions will not have sufficient energy to undergo this reaction unless significant momentum transfer is also involved.) This mechanism, in conjunction with reaction 9, involving C atom randomization can account for the present results. Second, one may postulate a mechanism whereby  $^{13}C$  retention is favored in the  $C_3H_3$  neutral product of reaction 9. Such a mechanism may involve insertion at a C-C bond and formation of a cyclic  $C_3$  species:



Carbon ion attack at C=C double bonds has been postulated previously for  $C^+$  reactions with ethylene and propylene.<sup>2</sup>

The  $C_4H_2^+$  product becomes more important at higher translational energies (Table I), apparently eliminating the reaction

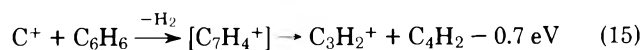


which one would expect to be most important at low energies. Other possible reactions include  $H_2$  loss from  $C_4H_4^+$  and H-atom loss from  $C_4H_3^+$ . Both reactions have been observed as metastable decay channels in the mass spectra of benzene, with kinetic energy releases of 0.32 and 0.066 eV, respectively.<sup>28</sup> The reaction energetics and  $^{13}C$ -labeling results suggest that the most likely source of  $C_4H_2^+$  ions is H-atom elimination from  $C_4H_3^+$ . Results in Table III show a higher  $^{13}C$  retention for the  $C_4H_2^+$  product than observed for the  $C_4H_3^+$  product, however, rather large error limits apply to these measurements and the actual  $^{13}C$  retention may be similar for the  $C_4H_3^+$  and  $C_4H_2^+$  ions.

The situation for the  $C_3H_3^+$  and  $C_3H_2^+$  ionic products is quite similar to that observed for the  $C_4$  ionic products. The  $C_3H_3^+$  products may either result from a complex process involving a  $C_7$  intermediate, with a second contribution due to dissociative charge transfer from ( $^4P$ )  $C^+$  ions, or a more specific complex process favoring  $^{13}C$  retention in the neutral product. We favor the former mechanism since our earlier assumption of  $C_4H_4^+$  ions formed by dissociative charge transfer from ( $^4P$ )  $C^+$  ions would suggest a similar contribution of  $C_3H_3^+$  ion. Reaction 14 is the most likely process yielding  $^{13}C$ -labeled  $C_3H_3^+$  products.



The  $C_3H_2^+$  product shows a high degree of  $^{13}C$  retention, possibly even greater than predicted for a carbon randomized  $C_7$  intermediate species. Possible reactions to rationalize these of reaction 14 and reaction 15.



## Secondary Reactions

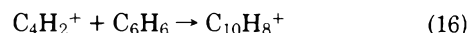
Experiments at elevated collision chamber pressures ( $1-10 \times 10^{-3}$  Torr) in the tandem quadrupole apparatus were un-

dertaken to determine the major products resulting from secondary ionic reactions. The major ionic species detected at  $m/e$  values greater than the benzene molecular ion ( $m/e$  78) were  $C_7H_8^+$  ( $m/e$  92),  $C_9H_9^+$  ( $m/e$  117),  $C_{10}H_8^+$  ( $m/e$  128),  $C_{10}H_9^+$  ( $m/e$  128), and  $C_{12}H_{12}^+$  ( $m/e$  156).

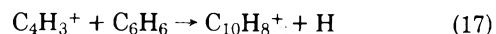
Experiments were also conducted in a dual photoionization-electron impact mass spectrometer using pure benzene at pressures between  $0.5 \times 10^{-3}$  and 0.5 Torr. At low pressures the photoionization of benzene, using a xenon rare gas resonance lamp (1295.6 Å, 9.57-eV ionizing radiation), produces only the  $C_6H_6^+$  ion. At elevated pressures  $C_7H_8^+$  and  $C_{12}H_{12}^+$  ions are observed. The  $C_7H_8^+$  ion is apparently produced by an efficient charge transfer reaction to a small toluene impurity and has been observed in previous studies.<sup>29,30</sup> The  $C_{12}H_{12}^+$  ion and its formation in benzene is well established and has been the subject of several studies.<sup>23-38</sup> The important point is that the  $C_7H_8^+$  and  $C_{12}H_{12}^+$  ions observed in the present study may be ascribed to reactions of  $C_6H_6^+$  with the toluene impurity and benzene, respectively.

We have also used electron impact ionization to study the ion-molecule reactions in benzene at elevated pressures. These results are in essential agreement with previous studies<sup>31-37</sup> and show a variety of secondary reaction products. The principle ions resulting from electron impact on benzene ( $C_6H_6^+$ ,  $C_6H_5^+$ ,  $C_5H_3^+$ ,  $C_4H_4^+$ ,  $C_4H_3^+$ ,  $C_4H_2^+$ ,  $C_3H_3^+$ , and  $C_3H_2^+$ ) are quite similar to those observed for the reaction of  $C^+$  ions with benzene. At elevated pressures, however, there is at least one notable difference in the secondary ion spectra. While the  $C_{10}H_9^+$  and  $C_{10}H_8^+$  species are observed in both spectra,  $C_9H_9^+$  is a major ion in the  $C^+ + C_5H_6$  secondary ion spectra, but is significant in electron impact spectra of benzene only at low temperatures and much higher pressures.<sup>34</sup>

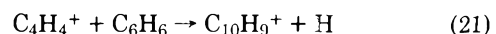
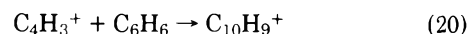
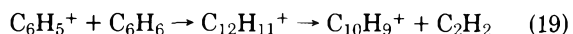
Possible reactions for formation of the  $C_{10}H_8^+$  product may include either the condensation reaction



or elimination of an H atom or  $H_2$  molecule from an intermediate.

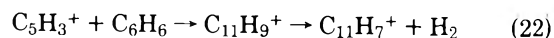


In pure benzene Lifshitz and Reuben<sup>38</sup> rule out reaction 16 since fragmentation of the  $C_{10}H_8^+$  species was not detected, and favor reaction 17. Formation of  $C_{10}H_9^+$  may be attributed to one of the following reactions



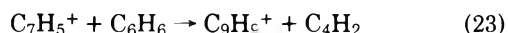
The second step in reaction 19 has been observed as a metastable transition by Lifshitz and Reuben<sup>38</sup> and must be considered a viable pathway.

The secondary reactions ultimately leading to formation of the  $C_9H_9^+$  species cannot be unambiguously determined from the present work. Since the  $C_5H_3^+$  ion intensity decreases with increasing pressure one would suspect this species might be involved, however, previous work suggests  $C_5H_3^+$  undergoes reaction

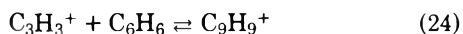


which was not observed in the present study. Two possible rationalizations may be suggested. One involves a reaction of

the postulated  $C_7H_5^+$  intermediate (which may alternately decomposes to yield the  $C_5H_3^+$  product)



and the second involves formation of  $C_3H_3^+$  ions which readily undergo the association reaction with benzene, as previously observed<sup>34</sup> at low temperatures ( $\sim 100^\circ\text{C}$  and 0.5 Torr).



It is interesting to note that the van't Hoff plot for reaction 24 was reported<sup>34</sup> to exhibit anomalous behavior. It should be noted that this discussion does not consider the possibility that ions resulting from the  $C^+ + C_6H_6$  reaction may be isomeric to ions formed by electron impact on benzene. Obviously, additional experiments are necessary to unravel the complex secondary ion processes observed in this system.

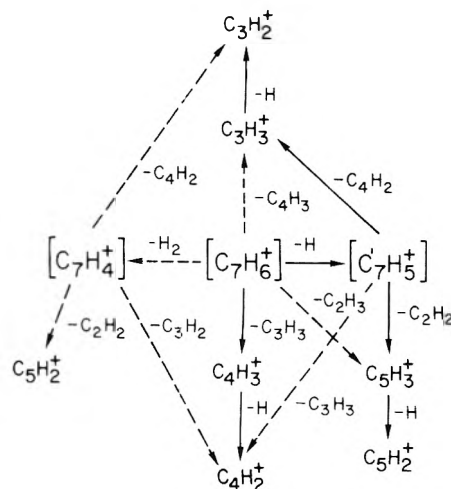
## Conclusions

For the reaction of (2P)  $C^+$  ions with benzene this work has shown that 85–90% of the total reaction may be attributed to direct processes not involving a carbon-randomized intermediate. The major reaction pathway ( $\sim 80\%$ ) is a simple charge exchange process.

This study has also shown that a significant fraction of the total reaction appears to involve a carbon-randomized  $C_7$  intermediate species. This  $C_7$  intermediate accounts for approximately 15% of the total reaction at 0.1 eV and about 11% between 1 and 8 eV. In Figure 2 we summarize the various dissociation reactions possible for  $C_7$  intermediates resulting from the  $C^+ + C_6H_6$  reaction. The reactions which we consider most likely are indicated by solid arrows, less likely reactions are denoted by dashed arrows. It is emphasized that subsequent experiments or new thermodynamic information may require altering features of this reaction scheme, however, the present results clearly show the existence of  $C_7$  intermediate species in the reaction of carbon ions with benzene.

The present results have interesting implications for the ion-accelerator experiments of Lemmon and co-workers.<sup>9–14</sup> After extended periods of  $^{14}\text{C}^+$  bombardment on benzene from 2 eV to 15 keV, Lemmon has found a number of labeled  $^{14}\text{C}$  products (benzene, toluene, cycloheptatriene, phenylacetylene, biphenyl, diphenylmethane, and phenylcycloheptatriene). While it is not possible to establish a direct relationship between the present study and work of Lemmon et al., a few comments are in order. First, disregarding the obvious problem of comparison of gas and solid phase reactions (and assuming a collision limited reaction rate for the initial step), it appears that a large fraction of the  $^{14}\text{C}^+$  ions ( $\sim 80\%$ ) will undergo charge exchange on impact. The subsequent reactions leading to  $^{14}\text{C}$ -labeled products will be those of carbon atoms with benzene; "hot"  $^{11}\text{C}$  atom reactions with benzene have been studied previously.<sup>39</sup> The present results also show that there will be a small, but apparently increasing, contribution at higher energies of the hydride ion abstraction reaction. Thus,  $^{14}\text{CH}$  radicals very likely play a role in the ion-accelerator experiments, where they may also be formed by C atom reactions.<sup>9,40</sup>

While charge transfer leading to C-atom formation is major reaction of  $C^+$  with benzene, the present results clearly indicate that a  $C^+$  ion reaction with benzene, to yield a  $C_7$  intermediate, may also occur in the ion-accelerator experiments. If these  $C_7$  intermediates undergo similar dissociations in the solid benzene matrix then one expects that  $^{14}\text{C}$ -labeled  $C_3H_3^+$ ,  $C_4H_3^+$ , and  $C_5H_3^+$  species will be formed. Secondary ion reactions in the solid phase will probably be limited to simple



**Figure 2.** Reaction scheme for the dissociation of the  $C_7$  intermediate species formed in approximately 10–15% of the  $C^+ + C_6H_6$  collisions. The solid arrows correspond to reaction pathways which we assume to be most likely.

condensation reactions yielding  $C_9H_9^+$ ,  $C_{10}H_9^+$ , and  $C_{11}H_9^+$ ; the ultimate neutral products are presently a matter of speculation. One should also note that the reaction scheme illustrated in Figure 2 would also result in a number of  $^{14}\text{C}$ -labeled neutral products ( $C_4H_2$ ,  $C_3H_3$  and  $C_2H_2$ ). It is also possible that the  $C_7$  intermediate will be stabilized (probably as  $C_7H_5^+$ ) by rapid energy transfer in the solid benzene matrix. This product, before or after charge neutralization, may be involved in the formation of labeled products<sup>9,14</sup> (possibly toluene, cycloheptatriene, diphenylmethane, or phenylcycloheptatriene) which have been attributed<sup>9,10</sup> to a  $C_7$  intermediate. The possible role of ion-molecule reactions in the radiolysis of benzene has been discussed previously by Wexler and Clow.<sup>33</sup>

While the present experiments may have interesting implications for the ion-accelerator experiments, the number of unknown factors and the complexity of processes occurring in the ion-accelerator experiments preclude complete understanding of the importance of ion-molecule reactions. The unknown factors include the abundance of excited (4P)  $C^+$  ions and the rate constants and branching ratios for (4P)  $C^+$  reactions. Other factors of importance (and less easily measured) include the rate of charge neutralization. Other results of the ion-accelerator experiments, such as observation of a  $^{14}\text{C}$ -labeled benzene product, formed with equal efficiency at 2 eV to 5 keV, are difficult to understand.<sup>10</sup> The present experiments have found no evidence for a  $^{13}\text{C}$ -labeled  $C_6$  ionic product of the  $^{13}\text{C}^+ + C_6H_6$  reaction.

The present study has provided information on the mechanism of  $C^+$  ion reactions with benzene at translational energies of 1.0–12 eV. This study has provided evidence for a  $C_7$  carbon-randomized intermediate species in 10–15% of the reactive collisions. Further experiments are planned to determine the branching ratios for excited (4P)  $C^+$  ions and to attempt the collisional stabilization of the  $C_7$  intermediate species. We also plan additional studies of  $^{12}\text{CH}^+$  ( $^{13}\text{CH}^+$ ) and  $^{12}\text{CH}_2^+$  ( $^{13}\text{CH}_2^+$ ) ion-molecule reactions with benzene.

**Acknowledgments.** We thank Dr. W. N. Allen and Professor F. W. Lampe for helpful discussions and technical assistance in the tandem quadrupole experiments. We are also indebted to Dr. J. R. Wyatt for assistance in construction of the NRL photoionization mass spectrometer.

## References and Notes

- (1) NRC-NRL Resident Research Associate 1975–1976. Present address: Radiological Sciences, Battelle-Northwest, Richland, Washington, 99352.
- (2) R. D. Smith and J. H. Futrell, *J. Chem. Phys.*, **65**, 2574 (1976).
- (3) R. D. Smith, J. J. DeCorpo, W. N. Allen, and F. W. Lampe, *J. Chem. Phys.*, **65**, 3665 (1976).
- (4) V. G. Anicich, W. T. Huntress, and J. H. Futrell, *Chem. Phys. Lett.*, **40**, 233 (1976).
- (5) P. S. Wilson, R. W. Rozett, and W. S. Koski, *J. Chem. Phys.*, **52**, 5321 (1970).
- (6) P. S. Wilson, R. W. Rozett, and W. S. Koski, *J. Chem. Phys.*, **53**, 3494 (1970).
- (7) P. S. Wilson, R. W. Rozett, and W. S. Koski, *J. Chem. Phys.*, **53**, 1276 (1970).
- (8) E. Lindemann, R. W. Rozett, and W. S. Koski, *J. Chem. Phys.*, **57**, 803 (1972).
- (9) R. M. Lemmon, *Acc. Chem. Res.*, **6**, 65 (1973).
- (10) R. M. Lemmon and W. R. Erwin, *Sci. Am.*, **232**, 72 (1975).
- (11) H. M. Pohlit, T. Lin, W. Erwin, and R. M. Lemmon, *J. Am. Chem. Soc.*, **91**, 5425 (1969).
- (12) H. M. Pohlit, T. Lin, W. Erwin, and R. M. Lemmon, *J. Am. Chem. Soc.*, **91**, 5421 (1969).
- (13) H. M. Pohlit, W. Erwin, T. Lin, and R. M. Lemmon, *J. Phys. Chem.*, **75**, 2521 (1972).
- (14) J. Lintermans, W. Erwin, and R. M. Lemmon, *J. Phys. Chem.*, **76**, 2521 (1972).
- (15) R. D. Smith and J. H. Futrell, *Int. J. Mass Spectrom. Ion Phys.*, to be submitted for publication.
- (16) T.-Y. Yu, T. M. H. Cheng, V. Kempter, and F. W. Lampe, *J. Phys. Chem.*, **76**, 3321 (1972).
- (17) J. B. Laudenslager, W. T. Huntress, and M. T. Bowers, *J. Chem. Phys.*, **61**, 4600 (1974).
- (18) (a) E. Lindholm, *Adv. Chem. Ser.*, **58**, 1 (1966); (b) R. C. C. Lao, R. W. Rozett, and W. S. Koski, *J. Chem. Phys.*, **49**, 4202 (1968).
- (19) W. D. Watson, V. G. Anicich, and W. T. Huntress, *Astrophys. J.*, in press.
- (20) (a) M. Vestal and G. Lerner, ARL Report No. 67-0014, Johnston Laboratory, Baltimore, Md., 1967; (b) M. L. Vestal, in "Fundamental Processes in Radiation Chemistry", P. Ausloos, Ed., Interscience, New York, N.Y., 1968.
- (21) H. M. Rosenstock, J. T. Larkins, and J. A. Walker, *Int. J. Mass Spectrom. Ion Phys.*, **11**, 309 (1973).
- (22) (a) R. D. Smith, Ph.D. Dissertation, University of Utah, 1975; (b) R. D. Smith and J. H. Futrell, *Org. Mass Spectrom.*, **11**, 445 (1976).
- (23) (a) B. O. Jonsson and E. Lindholm, *Ark. Fys.*, **39**, 65 (1969); (b) E. Lindholm, in "Ion-Molecule Reactions", J. L. Franklin, Ed., Plenum Press, New York, N.Y., 1962, p. 448.
- (24) J. H. D. Eland, R. F. Rey, H. Schulte, and B. Brehm, *Int. J. Mass Spectrom. Ion Phys.*, **21**, 209 (1976).
- (25) D. W. Turner, C. Baker, and C. R. Brundle, "Molecular Photoelectron Spectroscopy", Wiley-Interscience, New York, N.Y., 1970.
- (26) J. L. Franklin, J. G. Dillard, H. M. Rosenstock, J. T. Herron, K. Drazl, and F. H. Field, *Natl. Stand. Ref. Data Ser., Natl. Bur. Stand.*, **No. 26** (1969).
- (27) H. M. Rosenstock, private communication.
- (28) C. H. Ottinger, *Z. Naturforsch.*, **202**, 1229 (1965).
- (29) F. H. Field, P. Hamlet, and W. F. Libby, *J. Am. Chem. Soc.*, **89**, 6035 (1967).
- (30) L. W. Sieck and R. Gorden, Jr., *Int. J. Mass Spectrom. Ion Phys.*, **19**, 269 (1976).
- (31) E. G. Jones, A. K. Bhattacharya, and T. O. Tiernan, *Int. J. Mass Spectrom. Ion Phys.*, **17**, 147 (1975).
- (32) S. Wexler and L. G. Pobo, *J. Phys. Chem.*, **74**, 257 (1970).
- (33) S. Wexler and R. P. Clow, *J. Am. Chem. Soc.*, **90**, 3940 (1968).
- (34) F. H. Field, P. Hamlet, and W. F. Libby, *J. Am. Chem. Soc.*, **91**, 2839 (1969).
- (35) J. A. D. Stockdale, *J. Chem. Phys.*, **58**, 3881 (1973).
- (36) V. G. Anicich and M. T. Bowers, *J. Am. Chem. Soc.*, **96**, 1279 (1974).
- (37) A. Aiardini-Guidoni and F. Zocchi, *Trans. Faraday Soc.*, **64**, 2342 (1968).
- (38) C. Lifshitz and B. G. Reuben, *J. Chem. Phys.*, **50**, 951 (1969).
- (39) T. Rose, C. MacKay, and R. Wolfgang, *J. Am. Chem. Soc.*, **89**, 1529 (1967).
- (40) W. R. Erwin, B. E. Gordon, and R. M. Lemmon, *J. Phys. Chem.*, **80**, 1852 (1976).
- (41) W. J. Hehre, J. A. Pople, W. A. Lathan, L. Radom, E. Wasserman, and Z. R. Wasserman, *J. Am. Chem. Soc.*, **98**, 4378 (1976).

## Role of Impact Parameters in Branching Reactions. Chemical Accelerator Study of the Reactions of $\text{Kr}^+$ with Methane

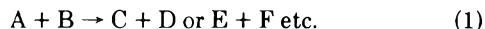
J. R. Wyatt,<sup>†</sup> L. W. Strattan,<sup>‡</sup> and P. M. Hierl\*

Department of Chemistry, University of Kansas, Lawrence, Kansas 66045 (Received January 19, 1976)

The dynamics of the exoergic ion-molecule reactions  $\text{Kr}^+(\text{CH}_4, \text{CH}_3)\text{KrH}^+$ ,  $\text{Kr}^+(\text{CH}_4, \text{H}_2)\text{KrCH}_2^+$ , and  $\text{Kr}^+(\text{CH}_4, \text{H})\text{KrCH}_3^+$  were studied over the relative reactant translational energy range 0.5–10 eV by chemical accelerator techniques. Results of the kinematic measurements are reported as scattering intensity contour maps in Cartesian velocity space. In addition, excitation functions (integral reactive cross sections vs. collision energy) are reported for the three reactions and for  $\text{Kr}^+(\text{CD}_4, \text{CD}_3)\text{KrD}^+$ . The kinematic results are compared to those predicted by standard models for direct reactions. The cross sections are discussed in terms of the apparent difficulty in converting large amounts of reactant orbital angular momentum into product rotation in the absence of strong angle-dependent forces. Both of the kinematic results and the cross sections support the hypothesis that the impact parameter plays a major role in determining reaction channels in direct reactions.

### I. Introduction

An important problem in chemical kinetics is the prediction of which products will be formed when a given pair of reactants can form two or more sets of products, as in



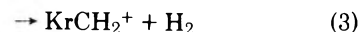
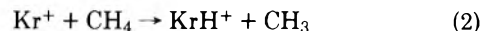
The customary approach is to assume that the reactants form an intermediate complex,  $(\text{AB})^*$ , and that competition between the various reaction channels is determined by the relative rates of unimolecular decomposition of the complex to form the various sets of products. It is further assumed that the lifetime of  $(\text{AB})^*$  is sufficiently long to permit a redistribution of the excess energy among the various internal degrees of freedom. Then the probability of any decay mode of the complex will be independent of the mode of formation, and the relative rates of decomposition can be calculated from statistical considerations. The general conclusion of the statistical theory is that the reaction will predominantly follow the most exoergic channel.<sup>1</sup>

On the other hand, an increasing body of experimental data has indicated that certain reactions (e.g., reactions of fast hydrogen atoms with saturated hydrocarbons,<sup>2</sup> reactions of alkali atoms with halogens,<sup>3</sup> and many ion-molecule reactions<sup>4</sup>) proceed by a direct mechanism rather than by the formation of a long-lived complex. Since the duration of the collision is usually less than  $10^{-13}$  s in direct reactions, there is no opportunity for the redistribution of energy within the collision complex. Clearly, statistical theories of unimolecular decomposition are inapplicable in such reactions.<sup>5</sup>

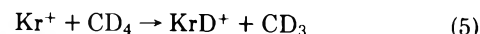
The question then arises, what controls the relative yields of the various products in direct reactions? For such reactions Wolfgang postulated that the reaction path is determined by steric factors, i.e., by the impact parameter and the angle of collision.<sup>2</sup> While hot hydrogen data are consistent with such a concept, the evidence is circumstantial in nature, being based primarily upon ratios of product yields and relative rates. Consequently, it has been impossible in the past to determine rigorously whether a particular yield pattern is due

primarily to steric factors or to other considerations such as bond energies and inertial effects.<sup>6</sup>

In the hope of obtaining more direct experimental information on the factors determining product yields, the competing ion-molecule reactions



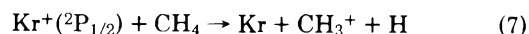
were studied at collision energies over the range 0.5 to 10 eV (CM). Velocity and angular distributions of the ionic products have been measured by chemical accelerator techniques. Excitation functions (reaction cross sections as a function of collision energy) were also obtained for these three reactions and for the reaction



As reported in a preliminary communication,<sup>7</sup> the results strongly support the hypothesis that, in direct reactions, factors such as the impact parameter determine the reaction channel followed in a given collision.

Reactions 2–4 have previously been studied by high pressure mass spectrometry.<sup>8</sup> With an ion exit energy of 2.5 eV, the following rate constants were obtained:  $k_2 = 1.22 \times 10^{-11}$ ,  $k_3 = 1 \times 10^{-12}$ , and  $k_4 = 3 \times 10^{-12}$  cm<sup>3</sup>/mol s.<sup>8a</sup> The  $\text{KrCH}_2^+$  ion has also been reported by Koski.<sup>8b</sup>

The dominant reactions occurring in  $\text{Kr}^+ - \text{CH}_4$  mixtures are the asymmetric charge exchange reactions:<sup>8,9</sup>



Thermal energy rate constants of  $1.1 \times 10^{-9}$  and  $2 \times 10^{-9}$  cm<sup>3</sup>/mol s have been reported<sup>9g</sup> for reactions 6 and 7, respectively.

### II. Experimental Section

**A. Apparatus.** The instrument used in this study is a single-beam collision chamber type of chemical accelerator with product velocity and angular analysis.  $\text{Kr}^+$  ions, formed by impact of 35-eV electrons, are focused into a nearly monoenergetic beam of variable energy (0.5–100 eV LAB) by a system

<sup>†</sup> Present address: Naval Research Laboratory, Washington, D.C. 20371.

<sup>‡</sup> Present address: Department of Chemistry, Emory University, Atlanta, Ga.

of electrostatic lenses. This collimated beam passes through the collision chamber containing the  $\text{CH}_4$  at a pressure of about  $10^{-3}$  Torr (i.e., under single collision conditions). The ion gun can be rotated about the center of the collision chamber, permitting the fixed detector to measure scattered products at various angles. Those ions leaving the collision chamber at the selected angle pass through a rectangular detection slit (typical resolution is  $1^\circ$  in the horizontal plane and  $4^\circ$  in the vertical), a parallel plate retarding potential energy analyzer, and a set of strong focusing quadrupole lenses. Mass analysis of the ions is performed with the 30 cm,  $90^\circ$  deflection magnetic sector analyzer of a Nuclide mass spectrometer from which the conventional ion source and accelerating electrodes have been removed. The individual components of this instrument have been described in detail elsewhere.<sup>10,11</sup>

Because the primary ion beam was not mass selected, it contained a mixture of krypton isotopes whose relative intensities are presumably determined by their natural abundance. The most abundant isotope,  $^{84}\text{Kr}$  (56.9%), was utilized in the study of reaction 2. The second most abundant isotope,  $^{86}\text{Kr}$  (17.4%), was used in studying the other reactions.

**B. Internal States of the Reactants.** The  $\text{Kr}^+$  is produced by impact of 35-eV electrons, so that the primary ion beam contains no doubly charged ions and about 1.5% of high energy metastable ions.<sup>12</sup> Nearly all (98.5%) of the  $\text{Kr}^+$  ions, therefore, are in the  $^2\text{P}$  state and are presumably distributed statistically in a 2:1 ratio between the  $J = 3/2$  and the  $J = 1/2$  levels,<sup>13</sup> which differ in energy by 0.66 eV.<sup>14</sup>

The neutral target gas is assumed to be in thermal equilibrium, so that the internal energy of the methane is determined by its temperature (85  $^\circ\text{C}$  under the conditions of the experiment). Nearly all of the  $\text{CH}_4$  molecules, therefore, are in their ground vibrational state. The most probable rotational state is  $J = 9$ , which corresponds to an energy of about 0.015 eV. Consequently, most of the energy available to the reaction products is derived from the heat of reaction plus the initial translational energy in the center-of-mass (CM) system.

**C. Heats of Reaction.** Intermolecular potentials for  $\text{KrH}^+$  have been derived from experiments on the elastic scattering of protons on krypton. Weise et al.<sup>15</sup> obtained a value of  $4.45 \pm 0.10$  eV for the well depth,  $D_e$ , while Rich et al.<sup>16</sup> reported a value of 4.6 eV. Assuming that the zero point vibrational energy of  $\text{KrH}^+$  is 0.16 eV, equal to that of the isoelectronic molecule  $\text{HBr}$ ,<sup>17</sup> one obtains for the dissociation energy  $D_0(\text{Kr}-\text{H}^+)$  values of 4.29 and 4.44 eV from the two scattering experiments. These values are in good agreement with the value of 4.38 eV recently obtained from flowing afterglow studies of the equilibrium between  $\text{KrH}^+$  and  $\text{H}_3^+$  in  $\text{Kr}-\text{H}_2$  mixtures.<sup>18</sup> Using the latter value for  $D_0(\text{Kr}-\text{H}^+)$  and taking  $D_0(\text{H}-\text{CH}_3) = 4.47$  eV,<sup>19</sup> reaction 2 is exothermic by  $0.3 \pm 0.1$  eV when the  $\text{Kr}^+$  is in the  $^2\text{P}_{3/2}$  ground state.

Holtz and Beauchamp<sup>20</sup> have reported a value of  $10.37 \pm 0.65$  eV for the heat of formation of  $\text{KrCH}_3^+$ , which, in conjunction with the thermodynamic data listed in Table I, yields a value of  $0.61 \pm 0.65$  for the exothermicity of reaction 4. The corresponding values for the bond strengths are  $D_0(\text{Kr}^+-\text{CH}_3) = 5.03 \pm 0.65$  eV and  $D_0(\text{Kr}-\text{CH}_3^+) = 0.91 \pm 0.65$  eV.

Thermodynamic data on  $\text{KrCH}_2^+$  are not available, but if one assumes that  $D_0(\text{Kr}^+-\text{CH}_2) = D_0(\text{Kr}^+-\text{CH}_3) = 5.03$  eV,<sup>23</sup> reaction 3 is found to be exothermic by  $1.34 \pm 0.65$  eV. This corresponds to  $D_0(\text{Kr}-\text{CH}_2^+) = 2.56 \pm 0.65$  eV.

### III. Results

**A. Excitation Functions.** Integral reaction cross sections,  $\sigma_R$ , are calculated from the equation

TABLE I: Heats of Formation  $\Delta H^\circ_{298}$

Species	$\Delta H^\circ_{298}$ , eV	Ref
H	2.26	19
$\text{CH}_2$	$2.86 \pm 0.22$	19
$\text{CH}_3$	$1.43 \pm 0.09$	19
$\text{CH}_4$	-0.78	21
$\text{Kr}^+(^2\text{P}_{3/2})$	14.00	14
$\text{Kr}^+(^2\text{P}_{1/2})$	14.66	14
$\text{CH}_2^+$	14.44	22
$\text{CH}_3^+$	11.28	22
$\text{KrH}^+$	$11.49 \pm 0.10$	a
$\text{KrCH}_2^+$	$11.88 \pm 0.65$	b
$\text{KrCH}_3^+$	$10.37 \pm 0.65$	20

<sup>a</sup> Derived from the value  $D_0(\text{Kr}-\text{H}^+) = 4.38$  eV.<sup>18</sup> <sup>b</sup> Derived under the assumption  $D_0(\text{Kr}^+-\text{CH}_2) = D_0(\text{Kr}^+-\text{CH}_3) = 5.03$  eV.

$$\sigma_R = \frac{I_C/I_A}{n_B L} K(T) \quad (8)$$

where  $I_C$  is the total reactively scattered product ion intensity,  $I_A$  is the transmitted primary ( $\text{Kr}^+$ ) ion intensity,  $n_B$  is the number density of methane in the collision chamber, and  $L$  is the collision path length. Any attenuation of the reactant and product beams is corrected by the term

$$K(T) = \frac{T \ln T}{T - 1} \quad (9)$$

where  $T = I_A/I_A^0$ , the transmission.<sup>11</sup> As before,<sup>10,11</sup> the ratio of total ion intensities is given by

$$\frac{I_C}{I_A} = \frac{I_C(0^\circ)K_C}{I_A(0^\circ)K_A} K_1 K_2 \quad (10)$$

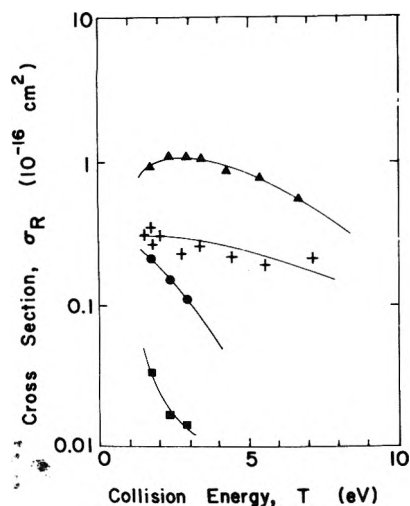
where  $I_C(0^\circ)$  and  $I_A(0^\circ)$  are the observed ion intensities at the angular maximum,  $K_C$  and  $K_A$  correct for differences in collection efficiency caused by differences in angular distributions,  $K_1$  corrects for differences in multiplier gain, and  $K_2$  corrects for any broadening of the mass spectral peak of ions formed with a wide distribution of kinetic energies.

Because the small cross sections for these reactions resulted in very low product ion intensities, the quantities  $K_1$  and  $K_2$  could not be measured directly and were therefore assumed to equal unity. This assumption is consistent with results obtained in previous studies of other reactions and is not expected to introduce an error of more than a few percent. The correction factor  $K_C/K_A$  was obtained by integration of the observed laboratory angular distributions.<sup>11</sup> The experimental uncertainty in  $\sigma_R$  is judged to be  $\pm 50\%$ . The excitation functions ( $\sigma_R$  vs.  $E$ ) for reactions 2–5 are presented in Figure 1.

**B. Kinematic Data.** Angular ( $\theta$ ) distributions in the laboratory (LAB) system are obtained for the ionic species  $\text{Kr}^+$ ,  $\text{KrH}^+$ ,  $\text{KrCH}_2^+$ , and  $\text{KrCH}_3^+$  by recording the appropriate ion signal while rotating the ion gun about the center of the collision chamber. Because the detector views a decreasing fraction of the collision path length with increasing scattering angle, the observed ion signal at each LAB angle is divided by the path length subtended by the detector at that angle.<sup>11</sup> The resulting angular distributions,  $I_L(\theta, \Phi = 0^\circ)$ , which are normalized to unity at the angular maximum, represent the relative ion intensity scattered through a LAB angle  $\theta$  in the plane  $\Phi = 0^\circ$  from a reaction path of unit length.

The stopping potential curves obtained at various angles are first scaled to reflect the total relative intensity at that angle and are then differentiated to yield the energy distri-





**Figure 1.** Integral reaction cross sections,  $\sigma_R$ , vs. CM collision energy,  $T$ , for the reactions of  $\text{Kr}^+$  with  $\text{CH}_4$  to produce  $\text{KrH}^+$  (triangles),  $\text{KrCH}_2^+$  (circles), and  $\text{KrCH}_3^+$  (squares), and with  $\text{CD}_4$  to produce  $\text{KrD}^+$  (crosses). The lines drawn through the data points represent an empirical best fit to the experimental data.

bution at that angle,  $I_L(E, \theta, \Phi = 0^\circ)$ . These energy distributions are converted to velocity distributions by multiplying each point by the corresponding LAB velocity  $v$  in accord with the transformation<sup>24</sup>

$$I_L(E, \theta, \Phi) dE d\Omega = I_L(v, \theta, \Phi) dv d\Omega \quad (11)$$

These LAB cross sections,  $I_L(v, \theta, \Phi)$ , are converted to probabilities in Cartesian velocity space according to the transformation

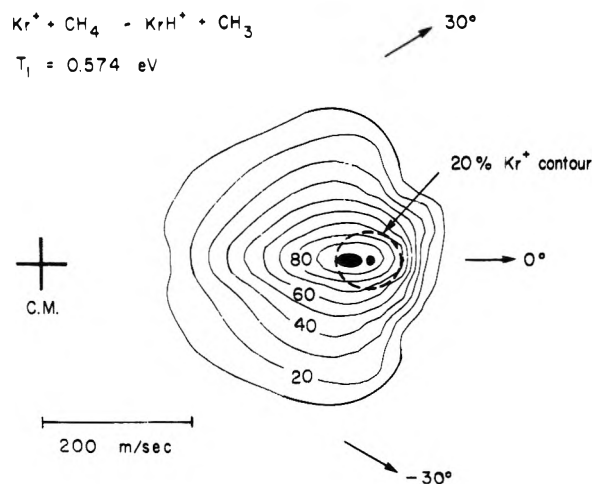
$$P_C(v_x, v_y, v_z) = v^{-2} I_L(v, \theta, \Phi) \quad (12)$$

where  $P_C$  represents the probability of finding product in a given volume of velocity space.<sup>25</sup> These probabilities are then scaled, with the highest intensity arbitrarily set equal to 100. A plot of the appropriate contours on a velocity vector diagram produces a map of relative intensities as seen by a detector sensitive to particles in an element  $dv_x dv_y dv_z$  of velocity space. Such velocity vector diagrams have been constructed to present Cartesian probabilities for the formation of  $\text{KrH}^+$  (Figures 2–4),  $\text{KrCH}_2^+$  (Figures 5 and 6), and  $\text{KrCH}_3^+$  (Figures 7 and 8) at several energies of the  $\text{Kr}^+$  beam.

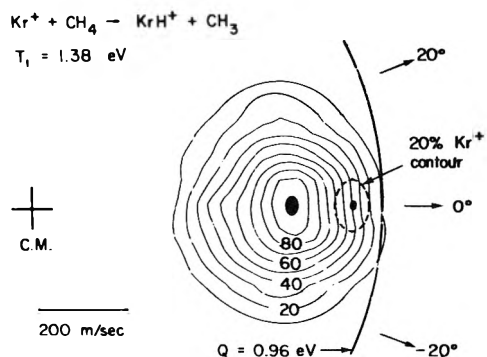
As an alternative to the construction of the complete velocity vector diagram, simply the position of maximum product ion intensity was determined. The product energy distribution was measured at the LAB angle of maximum product intensity and then converted to the corresponding Cartesian velocity spectrum by multiplying the intensity at each point (i.e., energy) by the overall Jacobian factor of  $1/v$ . The velocity corresponding to the peak in this velocity spectrum was then used to calculate the translational exoergicity  $Q$  (defined as the net difference between the final and initial translational energies) and the ratio of the LAB velocity of the ionic product to the LAB velocity of the incident ion,  $v_{\text{KrY}^+}/v_{\text{Kr}^+}$  (where Y is H,  $\text{CH}_2$ , or  $\text{CH}_3$ ). The most probable values of the translational exoergicity and the velocity ratio are plotted vs. the CM collision energy in Figures 9–12.

#### IV. Discussion

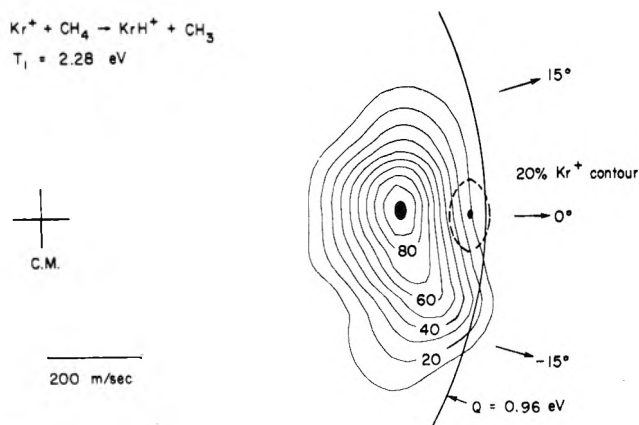
A.  $\text{KrH}^+$  and  $\text{KrD}^+$ . Integral reaction cross sections for reaction 2,  $\sigma_2$ , are on the order  $1 \text{ \AA}^2$  at collision energies  $< 4 \text{ eV}$



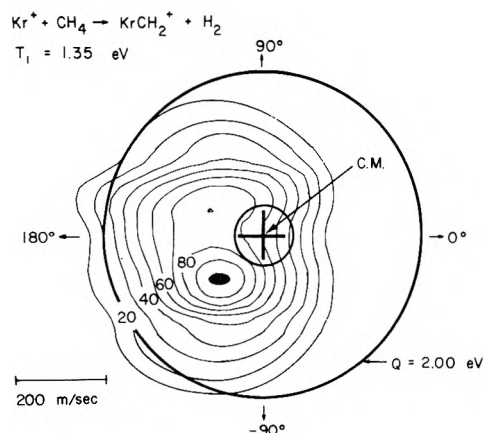
**Figure 2.** Product probability distribution  $P_C(u, \theta)$  for reaction 2 at the collision energy  $T = 0.574 \text{ eV}$  (CM). The  $\text{KrH}^+$  intensities, normalized to 100 at the position of maximum intensity, are shown relative to the Cartesian system  $P_C$ . Arrows represent scattering angle with respect to the center of mass (marked C.M.). The dashed oval represents the 20% contour line for the reactant  $\text{Kr}^+$ . At this collision energy the maximum possible  $\text{KrH}^+$  velocity (calculated from  $Q_{\text{max}} = 0.96 \text{ eV}$ ) is  $720 \text{ m/s}$  and thus falls beyond the range of velocities displayed in this figure. Because no  $\text{KrH}^+$  intensity was observed behind the center of mass, this region of velocity space has been omitted from Figures 2–4.



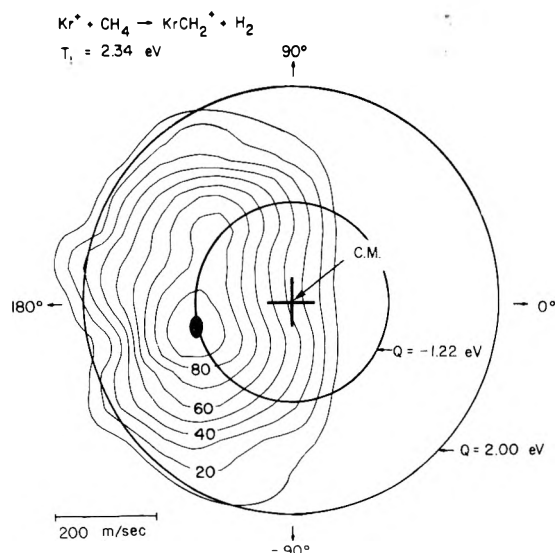
**Figure 3.** Product probability ( $P_C$ ) distribution for reaction 2 at the collision energy  $T = 1.38 \text{ eV}$  (CM). The arc marked  $Q = 0.96 \text{ eV}$  represents the maximum possible  $\text{KrH}^+$  velocity, which is limited by the reaction exothermicity and reactant excitation.



**Figure 4.** Product probability distribution for reaction 2 at the collision energy  $T = 2.28 \text{ eV}$ .



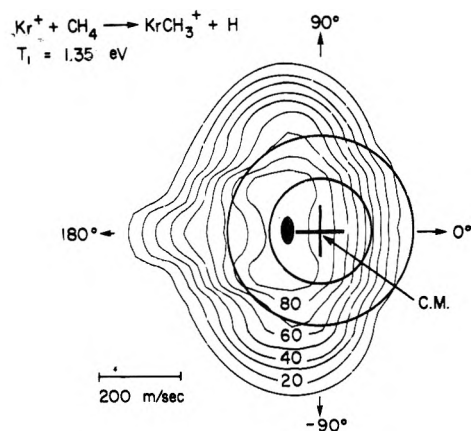
**Figure 5.** Product probability distribution for reaction 3 at the collision energy  $T = 1.35$  eV. The circle marked  $Q = 2.00$  indicates the maximum possible  $\text{KrCH}_2^+$  velocity consistent with conservation of energy. The smaller unmarked circle about the center-of-mass (CM) indicates the minimum  $\text{KrCH}_2^+$  velocity consistent with product stability.



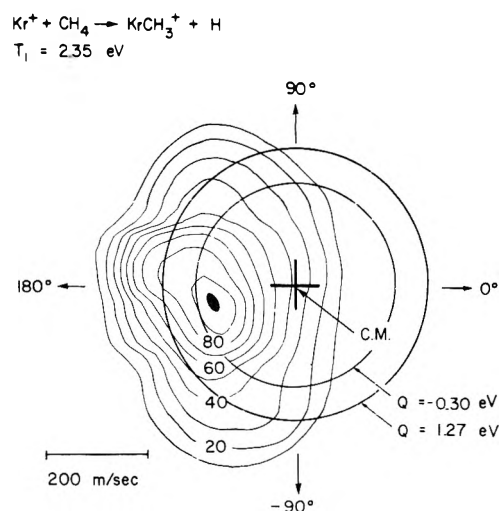
**Figure 6.** Product probability distribution for reaction 3 at the collision energy  $T = 2.34$  eV. The circle marked  $Q = 2.00$  eV indicates the maximum possible  $\text{KrCH}_2^+$  velocity consistent with conservation of energy, and the smaller circled marked  $Q = -1.22$  eV indicates the minimum  $\text{KrCH}_2^+$  velocity consistent with product stability. Product intensity within the inner circle is presumably a consequence of internal excitation of the  $\text{H}_2$  product and/or the finite resolution of the instrument.

and decrease at higher energies (see Figure 1). They are thus comparable in magnitude to the cross sections found for H-atom abstraction from  $\text{CH}_4$  by  $\text{Ar}^+$  ( $\sigma_{\text{max}} \sim 0.25 \text{ \AA}^2$ )<sup>11</sup> and by  $\text{N}_2^+$  ( $\sigma_{\text{max}} \sim 0.7 \text{ \AA}^2$ ).<sup>26</sup> As reported previously, the excitation functions for these two reactions maximize at about 5 eV (CM) and decrease at lower collision energies, appearing to possess a threshold at  $\sim 0.1$  eV. The present study does not extend to sufficiently low collision energies to determine if the excitation function for reaction 2 also exhibits such threshold behavior.

The cross section for the abstraction of a D atom from  $\text{CD}_4$  by  $\text{Kr}^+$  is appreciably smaller than that for H-atom abstraction from  $\text{CH}_4$ , with  $\sigma_5 \sim 1/3\sigma_2$  over the energy range studied. A similar isotope effect favoring abstraction of H over D has also been observed in the reactions of  $\text{Ar}^+$  and  $\text{N}_2^+$  with  $\text{CH}_4$ ,  $\text{CH}_2\text{D}_2$ , and  $\text{CD}_4$ .<sup>11,26,27</sup>



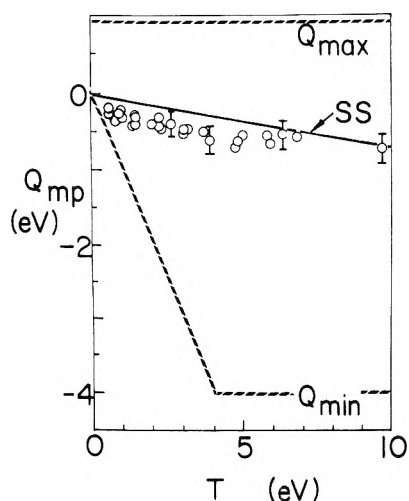
**Figure 7.** Product probability distribution for the ionic product of reaction 4 at the collision energy  $T = 1.35$  eV. The large circle about the center of mass (CM) represents the maximum  $\text{KrCH}_3^+$  velocity consistent with conservation of energy (i.e.,  $Q = 1.27$  eV). The smaller circle represents the minimum  $\text{KrCH}_3^+$  velocity consistent with product stability ( $Q = -0.30$  eV).



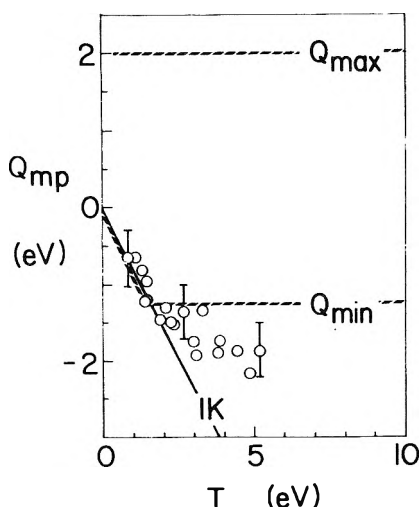
**Figure 8.** Product probability distribution for the ionic product of reaction 4 at the collision energy  $T = 2.35$  eV. The circles labeled  $Q = -0.30$  eV and  $Q = 1.27$  eV represent the minimum and maximum product velocities, respectively, allowed by energetic considerations. Observation of product intensity not within the allowed annular ring presumably results from finite instrumental resolution and/or an error in the value of  $\Delta H_{298}^\circ(\text{KrCH}_3^+)$  used to calculate  $Q_{\text{min}}$  and  $Q_{\text{max}}$ .

The integral cross sections for reaction 2 are smaller, by as much as an order of magnitude at low energies, than the cross sections for the reaction  $\text{Kr}^+(\text{H}_2, \text{H})\text{KrH}^+$ .<sup>28</sup> This is presumed to be a consequence of competition from the fast charge transfer reactions occurring in the methane system (reactions 6 and 7). The total cross section for charge exchange in  $\text{Kr}^+ - \text{CH}_4$ ,  $\sigma_6 + \sigma_7$ , is about  $40 \text{ \AA}^2$  over the energy range covered in the present study.<sup>9b</sup>

As shown in Figures 2–4, the  $\text{KrH}^+$  product is strongly scattered in the forward direction (i.e., in the same direction as the incident  $\text{Kr}^+$ ). The observation that the product is asymmetrically distributed about  $\pm 90^\circ$  in the CM system is a clear indication that, even at the lowest energy for which a complete  $\text{KrH}^+$  velocity vector distribution was measured (0.57 eV CM), the contribution of any long-lived intermediate is small, and that the abstraction of an H atom from  $\text{CH}_4$  by  $\text{Kr}^+$  is dominated by a direct mechanism (i.e., an impulsive



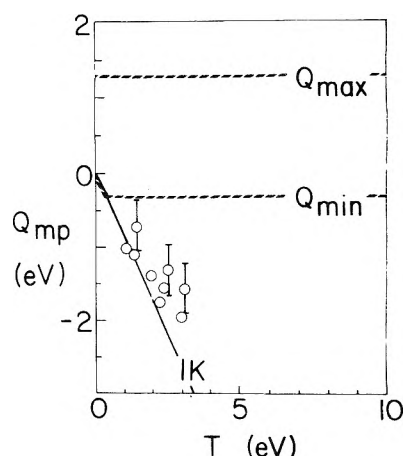
**Figure 9.** Most probable translational exoergicity,  $Q_{mp}$ , vs. collision energy,  $T$ , for the reaction  $\text{Kr}^+(\text{CH}_4, \text{CH}_3)\text{KrH}^+$ . The lines labeled  $Q_{max}$  and  $Q_{min}$  represent 0 and 100% conversion of available energy to product excitation, respectively. The prediction of the spectator stripping model is shown by the solid line labeled SS. Estimated experimental uncertainties in  $Q_{mp}$  are indicated by error bars for several selected points.



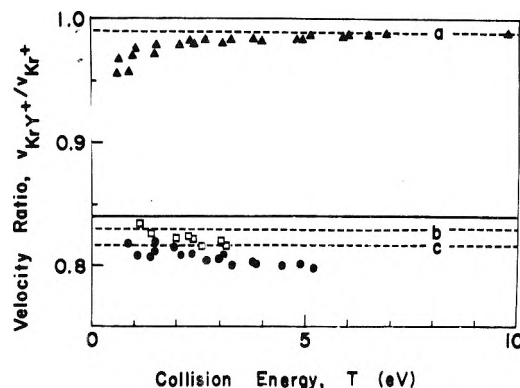
**Figure 10.** Most probable translational exoergicity,  $Q_{mp}$ , vs. collision energy,  $T$ , for the reaction  $\text{Kr}^+(\text{CH}_4, \text{H}_2)\text{KrCH}_2^+$ . The prediction of the ideal knockout model, eq 20, is shown by the solid line labeled IK. Estimated experimental uncertainties are indicated by error bars for certain selected points.

type of interaction occurring on a time scale comparable to one rotational period, which is on the order of  $10^{-13}$  s at these energies).<sup>29</sup> Similar behavior has been observed in chemical accelerator studies of H-atom abstraction from  $\text{CH}_4$  by  $\text{Ar}^+$  and by  $\text{N}_2^+$ .<sup>24,26,27,30</sup>

While the  $\text{KrH}^+$  distribution clearly remains forward peaked as the collision energy is decreased, there is increased broadening of the distribution and the formation of a low-velocity tail extending toward the center of mass (see Figure 2). Again, similar behavior has been observed for the analogous reactions of  $\text{Ar}^+$  and  $\text{N}_2^+$  with  $\text{CH}_4$  and has been interpreted as an indication of increased interaction between the incident ion and the  $\text{CH}_3$  group at the lower collision energies, with a possible transition from a direct mechanism at higher energies to a long-lived complex mechanism at the very lowest energies ( $T \leq 0.1$  eV CM).<sup>24,26,30</sup> The tentative conclusion that  $\text{KrCH}_4^+$



**Figure 11.** Most probable translational exoergicity,  $Q_{mp}$ , vs. collision energy,  $T$ , for the reaction  $\text{Kr}^+(\text{CH}_4, \text{H})\text{KrCH}_3^+$ . The prediction of the ideal knockout model, eq 20, is shown by the solid line labeled IK. Estimated experimental uncertainties are indicated by error bars for certain selected points.



**Figure 12.** Ratio of the most probable LAB velocity of the product ion to that of the reactant ion vs. collision energy for the reactions of  $\text{Kr}^+$  with  $\text{CH}_4$  to produce  $\text{KrH}^+$  (triangles),  $\text{KrCH}_2^+$  (circles), and  $\text{KrCH}_3^+$  (open squares). The dashed line labeled a represents the prediction of the spectator stripping model, eq 15, for  $\text{KrH}^+$ . The dashed lines labeled b and c are the predictions of the ideal knockout model, eq 19, for the formation of  $\text{KrCH}_3^+$  and  $\text{KrCH}_2^+$ , respectively. The solid horizontal line indicates the velocity ratio that would result if the product ion's velocity spectrum peaked at the center of mass velocity.

was observed<sup>28a</sup> in high pressure mass spectrometric studies of  $\text{Kr}-\text{CH}_4$  mixtures lends support to this interpretation.

The fact that  $\text{KrH}^+$  is scattered through relatively small angles ( $<30^\circ$ ) in the CM suggests that H-atom abstraction, at least at the collision energies employed in this study, occurs principally in grazing encounters resulting from moderately large impact parameter collisions.<sup>31</sup>

The observed energy partitioning is consistent with this suggestion. The translational exoergicity,  $Q$ , defined as the difference between the final and initial translational energies

$$Q = T' - T \quad (13)$$

provides a convenient measure of the partitioning of available energy between internal and translational modes of the products. Conservation of energy requires that the internal energy of the products be given by

$$E_{int}' = E_{int} - \Delta H - Q \quad (14)$$

The internal energy of the reactants,  $E_{int}$ , can be taken as zero or 0.66 eV, depending upon whether the  $\text{Kr}^+$  ion is in the

$^2P_{3/2}$  or the  $^2P_{1/2}$  state, respectively. The heat of reaction,  $\Delta H$ , if taken as  $-0.3$  eV.

The maximum value of  $Q$  occurs when all the available reaction energy (exothermicity plus any reactant excitation) appears as product translation:  $Q_{\max} = 0.96$  eV. A pseudominimum value for  $Q$  can be assigned if we consider the ground state of  $Kr^+$  and assume that all of the product excitation is contained in the ionic product. By requiring that  $E_{\text{int}}' < D_0(Kr-H^+)$  for stable product formation, one obtains  $Q_{\min} = -\Delta H' - D_0(Kr-H^+) = -4.08$  eV. Observation of  $KrH^+$  at  $Q$  values more negative than  $Q_{\min}$  would require that the methyl fragment be preduced with internal excitation.

The  $Q$  values plotted in Figure 9 indicate the "most probable" energy partitioning and its dependence upon collision energy. These data show that the most probable mechanism for  $KrH^+$  formation is one in which there is a net conversion of translational energy (i.e.,  $Q_{\text{mp}} < 0$ ) at all collision energies. Thus, all of the reaction exothermicity plus any reactant excitation is likely to appear as internal excitation of the products. Although  $Q_{\text{mp}}$  becomes more negative (indicating increased internal excitation of the products) as the collision energy  $T$  increases, the relatively slow decrease in  $Q_{\text{mp}}$  with increasing  $T$  shows that most (>90%) of the initial collision energy is retained as product translation. This observation supports the hypothesis that  $KrH^+$  is produced in glancing collisions which transfer little or no momentum to the residual  $CH_3$ .

Indeed, the limiting model for direct reactions of this type, the spectator stripping (SS) mechanism,<sup>32</sup> provides a reasonably good description of the dynamics of  $KrH^+$  formation. This model assumes that the  $Kr^+$  reacts impulsively with the abstracted H atom, stripping it away from the  $CH_4$  in a large impact parameter collision. The  $CH_3$  group acts merely as a spectator to the reaction, proceeding after H-atom abstraction with a velocity unchanged from that of the  $CH_4$  reactant. Since the  $CH_4$  is considered to be stationary in our experiment, conservation of momentum requires that the LAB velocity of the ionic product be a fixed fraction of the LAB velocity of the ionic reactant:

$$\{v_{KrH^+}/v_{Kr^+}\} = (Kr^+)/(KrH^+) \quad (15)$$

where (i) represents the mass of particle i. Experimentally measured values for the velocity ratio (determined from the peak in the Cartesian velocity spectra) are presented graphically in Figure 12. The data agree quite well with the predictions of the SS model at the higher collision energies ( $T > 2$  eV CM). At the lower collision energies the velocity ratios are somewhat smaller than expected on the basis of the SS model, showing that the interaction with the  $CH_3$  group is not negligible and perhaps even indicating a transition from a direct mechanism at high energies to a complex mechanism at low energies.

The SS model predicts that the translational exoergicity will decrease linearly with collision energy:

$$Q_{\text{SS}} = -\frac{(H)(Kr^+ + CH_4)}{(KrH^+)(CH_4)} T = -0.735T \quad (16)$$

when  $^{84}\text{Kr}$  is employed. Comparison with the  $Q$  values derived from the maxima in the Cartesian velocity spectra (Figure 9) show that the SS model consistently overestimates  $Q$  (or, equivalently, underestimates  $E_{\text{int}}'$ ) by about 0.2 eV. Similar behavior was found in the reactions of  $\text{Ar}^+$  and  $\text{N}_2^+$  with  $\text{CH}_4$ .<sup>24,27,30</sup>

Although the present results provide no direct information on the partitioning of internal energy between  $KrH^+$  and  $CH_3$ ,

the close agreement between the experimental data and the SS model make it reasonable to assume the  $E_{\text{int}}'$  is partitioned in a straightforward manner determined by the dynamic features of the reactive collision. Thus, the internal energy of the  $KrH^+$  product will consist of the heat of reaction arising from the energy released in the formation of the new bond, plus the energy of  $Kr^+$  relative to the abstracted atom. Because the interaction with the methyl fragment is relatively weak, the internal excitation of  $CH_3$  will principally be due to the energy difference between planar and  $19^\circ$  tetrahedrally distorted  $CH_3$ , and to the degree relaxation from the latter configuration to the former can occur during the course of the reaction. This energy would amount to several tenths of an electron volt.

The  $KrH^+$  velocity distribution has, of course, a finite width so that reaction at a given collision energy will give rise to products with a range of translational exoergicities (and hence internal energies) distributed about the most probable value reported here. As shown in Figure 4, appreciable  $KrH^+$  intensity is found close to the circle marked  $Q = 0.96$  eV, indicating that some collisions convert all the available energy into product translation and little or none into product excitation. Likewise, product intensity between the maximum and the CM corresponds to greater product excitation than would be deduced from  $Q_{\text{mp}}$ . Nevertheless, at all collision energies studied, the  $KrH^+$  ions are found to be scattered strongly forward of the center of mass, with their most probable velocity approaching ( $T < 2$  eV) or equalling ( $T > 2$  eV) that predicted by the SS model. This observation is interpreted as evidence that most H-atom abstraction reactions occur in grazing collisions arising from moderately large impact parameter collisions.<sup>31</sup>

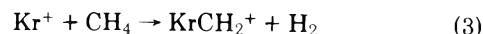
In this regard, it is interesting to note that trajectory studies<sup>33</sup> of the hot-atom reaction



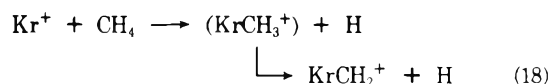
have indicated that this reaction is direct and concerted. A correlation between impact parameter and scattering angle was found, with product distributions peaked sideways or slightly forward at low collision energies and more strongly forward at higher energies, with the mechanism behaving like a stripping reaction when the energy is high enough.<sup>33a</sup>

B.  $KrCH_2^+$  and  $KrCH_3^+$ . The integral cross sections for reactions 3 and 4 are shown in Figure 1. At  $T = 2$  eV,  $\sigma_3$  and  $\sigma_4$  are about  $\frac{1}{3}$  and  $\frac{1}{30}$ , respectively, the size of the  $\sigma_2$ , the cross section for H-atom abstraction. Moreover, the excitation functions for hydrogen displacement decrease more rapidly with increasing collision energy than does the excitation function for abstraction. The finding that the production of  $KrCH_2^+$  is about 6 times as probable as  $KrCH_3^+$  production at low energy is in disagreement with the result of Field et al.,<sup>8a</sup> who found  $KrCH_2^+$  intensity to be only  $\frac{1}{3}$  that of  $KrCH_3^+$ . It is, however, consistent with Koski's observation<sup>8b</sup> of trace amounts of  $KrCH_2^+$  but no detectable  $KrCH_3^+$ .

The double displacement reaction to produce  $KrCH_2^+$  can be postulated as occurring by either of two mechanisms. The first is the concerted displacement of two H atoms as a hydrogen molecule



and the second is a two-step mechanism consisting of single displacement followed by unimolecular decomposition of the excited primary ionic product



Although the neutral product is not detected in the present study, we conclude that reaction 3 is the correct mechanism because reaction 18 is sufficiently endoergic (4.51 eV more endoergic than reaction 3) as to be forbidden over most of the energy range studied, and because no increase in  $\text{KrCH}_2^+$  production is observed at the higher collision energies where the cross section for  $\text{KrCH}_3^+$  production has begun to decrease. The single-step mechanism has also been postulated for the formation of  $\text{CH}_2\text{T}$  arising from hot tritium-methane reactions.<sup>34</sup>

The velocity vector distributions of these ionic products (Figures 5–8) are asymmetric with respect to the center of mass, indicating that the hydrogen displacement reactions also proceed via a direct mechanism over the energy range studied. These distributions, however, peak behind the CM, indicating that displacement occurs via some type of rebound mechanism occurring in small impact parameter collisions.

The same reasoning employed in the discussion of  $\text{KrH}^+$  can be used to assign upper and lower limits for the translational exoergicity of these reactions. With the thermodynamic data of Table I, the resulting limits are (1) for  $\text{KrCH}_2^+$ ,  $Q_{\text{max}} = 2.00$  eV,  $Q_{\text{min}} = -1.22$  eV; (2) for  $\text{KrCH}_3^+$ ,  $Q_{\text{max}} = 1.27$  eV,  $Q_{\text{min}} = -0.30$  eV. As the contour maps show, the product velocity vectors are distributed closer to the circle corresponding to  $Q_{\text{min}}$  than to the one for  $Q_{\text{max}}$ , indicating high internal energy in the products. For  $\text{KrCH}_3^+$  in particular, considerable product intensity is observed within the  $Q_{\text{min}}$  circle; presumably this results from the finite resolution of the instrument and the thermal motion of the target gas.

Values of the most probable translational exoergicity (Figures 10 and 11) show that all of the reaction exothermicity and any reactant excitation, plus the major portion of the initial collision energy, appear as internal excitation of the products. The data for  $\text{KrCH}_2^+$  show that  $Q_{\text{mp}}$  closely follows  $Q_{\text{min}}$ ; for  $\text{KrCH}_3^+$ , however, values of  $Q_{\text{mp}}$  more negative than  $Q_{\text{min}}$  are observed, implying that the  $\text{KrCH}_3^+$  has more than enough energy to dissociate to  $\text{Kr}$  and  $\text{CH}_3^+$ . The Cartesian velocity vector distributions for these ions, however, are rather broad, flat-topped peaks, so there is considerable uncertainty in selecting the most probable velocity (see error bars in Figures 9–11). Moreover, if we had chosen to define  $Q_{\text{mp}}$  in terms of the most probable CM velocity rather than the Cartesian velocity, considerably less negative values of  $Q_{\text{mp}}$  would have resulted. Nevertheless, the conclusion remains that nearly all the available energy is converted to product excitation in the displacement reactions, and that at collision energies above 2 eV this excitation is sufficient to cause product dissociation. This, presumably, is the cause of the relatively marked decrease in the cross sections for these reactions with increasing collision energy (Figure 1).

These findings contrast dramatically with the data for  $\text{KrH}^+$  formation and suggest that displacement occurs principally in small impact parameter encounters that lead to nearly head-on collisions, thus resulting in large angle scattering and high product excitation. Again, this finding parallels the results obtained in the trajectory studies<sup>33</sup> of the reactions of hot T atoms with  $\text{CH}_4$ , which predict that displacement occurs at low impact parameters and large scattering angles.

One of several types of collision models that could produce backward scattering is the billiard-ball or ideal knockout (IK) process.<sup>35</sup> In this model the  $\text{Kr}^+$  projectile ion would collide

impulsively with one hydrogen atom, ejecting it from the  $\text{CH}_4$  molecule. The  $\text{Kr}^+$  ion, its velocity diminished, would then pick up the remaining  $\text{CH}_3$  group to form  $\text{KrCH}_3^+$ . Such a process would presumably occur with greatest probability when the axis of the C–H bond was perpendicular to the velocity vector of the projectile ion and the impact parameter was approximately equal to one-half of the C–H bond distance.

For the general reaction  $X^+ + \text{YZ} \rightarrow \text{XY}^+ + \text{Z}$ , the kinematics of the ideal knockout process predict that, for 180° scattering, the ratio of the LAB velocity of the product ion to that of the projectile ion should depend only upon the masses of the species involved according to the equation

$$\frac{v_{\text{XY}^+}}{v_{X^+}} = \frac{(X)(X - Z)}{(X + Y)(X + Z)} \quad (19)$$

where  $X$  is the mass of the projectile ion,  $Y$  is the mass of the target fragment picked up by the ion, and  $Z$  is the mass of the ejected species. Using  $X = 86$  amu for  $\text{Kr}^+$  and appropriate values for  $Y$  and  $X$ , the velocity ratios predicted by this process are 0.821 for  $\text{KrCH}_2^+$  formation and 0.832 for  $\text{KrCH}_3^+$  formation.

It is also possible to calculate the translational exoergicity. According to the ideal knockout model, this should be the negative of the kinetic energy of the projectile ion ( $X^+$ ) relative to the abstracted group ( $Y$ ), after the projectile has collided elastically with the ejected species ( $Z$ ):

$$Q_{\text{IK}} = - \frac{(Y)(X - Z)^2(X + YZ)}{(X + Y)(X + Z)^2(YZ)} T \quad (20)$$

With  $X = 86$  amu, eq 20 predicts  $Q_{\text{IK}} = -0.813T$  for  $\text{KrCH}_2^+$  formation and  $Q_{\text{IK}} = -0.904T$  for  $\text{KrCH}_3^+$ .

The translational exoergicities and velocity ratios predicted by the ideal knockout model are compared with the experimentally determined values in Figures 10, 11, and 12. Agreement exists only at the lowest collision energies for which data was obtained ( $T \sim 1$  eV), presumably because at higher energies the product excitation predicted by the IK model exceeds that required to cause product dissociation. Previous applications of the IK model to the  $\text{T}-\text{CH}_4$ ,<sup>2b</sup>  $\text{N}_2^+-\text{H}_2$ ,<sup>36</sup> and  $\text{O}^+-\text{H}_2$ <sup>35d</sup> systems have also been unsatisfactory, and reasons for such failure have been discussed.<sup>35d</sup>

The principle of conservation of angular momentum appears to provide a qualitative explanation for several aspects of the  $\text{Kr}^+-\text{CH}_4$  reactions. Let  $\mathbf{L}$  and  $\mathbf{J}$  be the orbital and rotational angular momenta of the reactants, and  $\mathbf{L}'$  and  $\mathbf{J}'$  those of the products. Conservation of angular momentum requires that

$$\mathbf{L} - \mathbf{J} = \mathbf{L}' + \mathbf{J}' \quad (21)$$

The rotational angular momentum of the reactants is small compared to their orbital angular momentum and can be neglected, giving the approximate conservation law  $\mathbf{L} \simeq \mathbf{L}' + \mathbf{J}'$ . Since  $\mathbf{L}$  and  $\mathbf{L}'$  are proportional to the reduced masses of the reactants ( $\mu$ ) and products ( $\mu'$ ), respectively, the disposal of high angular momentum generated in large impact parameter collisions poses a serious problem when  $\mu' \ll \mu$ . For such reactions,  $\mathbf{J}'$  must be large in order to conserve angular momentum if  $\mathbf{L}$  is large. If, however, the potential energy surface does not have strong angle-dependent forces which allow the product to be set into rapid rotation, reaction can occur only if  $\mathbf{L}$  is small.<sup>37</sup>

For the reaction  $\text{Kr}^+(\text{CH}_4, \text{CH}_3)\text{KrH}^+$ , the reduced mass of the products, 12.8 amu, is nearly equal to that of the reactants, 13.4 amu. Because the products can dispose of large

amounts of angular momentum in their orbital motion, reaction can proceed even when  $L$  and hence the impact parameter are large. For the reactions  $\text{Kr}^+(\text{CH}_4, \text{H}_2)\text{KrCH}_2^+$  and  $\text{Kr}^+(\text{CH}_4, \text{H})\text{KrCH}_3^+$ , however, the reduced masses of the products (1.96 and 0.99 amu, respectively) are much smaller than the reactant reduced mass. It appears that large amounts of orbital angular momentum cannot be converted into rotation of the products, and thus these reactions can proceed only when  $L$  and hence the impact parameter are small.

## V. Summary and Conclusions

(1) Reactions 2–4 are dominated by a direct mechanism over the entire energy range studied, 0.5–10 eV CM, with no evidence for the formation of a long-lived collision complex at these energies. Consequently, no strong coupling occurs and statistical theory is inapplicable to these reactions.<sup>5</sup>

(2)  $\text{KrH}^+$  is scattered through small angles with relatively low product excitation, whereas  $\text{KrCH}_2^+$  and  $\text{KrCH}_3^+$  undergo large angle scattering and are formed with internal excitation approaching that required for dissociation. This implies that the opacity functions (reaction probability as a function of impact parameter) are significantly different for these reactions, with abstraction being favored by moderately large impact parameters and displacement being most likely in small impact parameter collisions. This deduction not only accords with one's chemical intuition, but (more significantly) it also is consistent with the need to conserve angular momentum and the difficulty of doing so when the reduced mass of the products is much less than that of the reactants.

(3) The dynamics of these  $\text{X}^+-\text{CH}_4$  reactions (where  $\text{X} = \text{Ar}, \text{Kr}, \text{or } \text{N}_2$ ) are similar to features observed in certain neutral-neutral reactions, principally those involving the reactions of hot T atoms with methane and other simple hydrocarbons. These similarities suggest that certain general characteristics may be common to a wide variety of simple chemical reactions.

**Acknowledgments.** Acknowledgment is made to the donors of the Petroleum Research Fund, administered by the American Chemical Society, for partial support of this research. Additional support was provided by the Research Corporation and by the University of Kansas General Research Fund. We wish to thank Professor R. Sampson and the Kansas Geological Survey for providing the computer program used to construct the intensity contour diagrams.

## References and Notes

- (1) See, for example, R. D. Levine and R. B. Bernstein, "Molecular Reaction Dynamics", Oxford University Press, New York, N.Y., 1974, pp 221–227.
- (2) (a) R. Wolfgang, *Annu. Rev. Phys. Chem.*, **16**, 15 (1965); (b) *Prog. React. Kinet.*, **3**, 97 (1965).
- (3) D. R. Herschbach, *Adv. Chem. Phys.*, **10**, 319 (1966).
- (4) (a) R. Wolfgang, *Acc. Chem. Res.*, **2**, 248 (1969); (b) *ibid.*, **3**, 48 (1970).
- (5) J. C. Light, *Discuss. Faraday Soc.*, **44**, 80 (1967).
- (6) (a) J. W. Root, W. Breckenridge, and F. S. Rowland, *J. Chem. Phys.*, **43**, 3694 (1965); (b) E. Tachikawa, Y.-N. Tang, and F. S. Rowland, *J. Am. Chem. Soc.*, **90**, 3584 (1968); (c) E. Tachikawa and F. S. Rowland, *ibid.*, **90**, 4767 (1968); (d) *ibid.*, **91**, 559 (1969); (e) T. Tominaga and F. S. Rowland, *J. Phys. Chem.*, **72**, 1399 (1968).
- (7) J. R. Wyatt, L. W. Strattan, and P. M. Hierl, *J. Chem. Phys.*, **63**, 5044 (1975).
- (8) (a) F. H. Field, H. N. Head, and J. L. Franklin, *J. Am. Chem. Soc.*, **84**, 1118 (1962); (b) G. R. Hertel and W. S. Koski, *ibid.*, **87**, 1686 (1965).
- (9) (a) C. E. Melton, *J. Chem. Phys.*, **33**, 647 (1960); (b) V. Cermak and Z. Herman, *Nucleonics*, **9**, 16 (1961); (c) G. V. Karachevtsev, M. I. Markin, and V. L. Talrose, *Kinet. Katal.*, **5**, 377 (1964); (d) A. Galli, A. Giardini-Guidoni, and G. G. Volpi, *Nuovo Cimento*, **31**, 1–45 (1964); (e) H. von Koch, *Ark. Fys.*, **28**, 529 (1965); (f) I. Szabo, *ibid.*, **35**, 339 (1967); (g) A. Durden, P. Kebarle, and A. Good, *J. Chem. Phys.*, **50**, 805 (1969); (h) A. J. Masson, Ph.D. Thesis, Brandeis University, 1970.
- (10) P. M. Hierl, L. W. Strattan, and J. R. Wyatt, *Int. J. Mass Spectrom. Ion Phys.*, **10**, 385 (1973).
- (11) J. R. Wyatt, L. W. Strattan, S. Chivalak, and P. M. Hierl, *J. Chem. Phys.*, **63**, 4582 (1975).
- (12) H. D. Hagstrum, *Phys. Rev.*, **104**, 309 (1956).
- (13) For a more detailed discussion of this problem, see ref 9h.
- (14) C. B. Moore, *Natl. Bur. Stand. Circ.*, **No. 467**, Vol. II (1952).
- (15) H. P. Weise, H. U. Mittman, A. Ding, and A. Henglein, *Z. Naturforsch. A*, **26**, 1122 (1971).
- (16) W. G. Rich, S. M. Bobbio, R. L. Champion, and L. D. Doverspike, *Phys. Rev. A*, **4**, 2253 (1971).
- (17) G. Herzberg, "Spectra of Diatomic Molecules", Van Nostrand, Princeton, N.J., 1950, p 534.
- (18) J. D. Payzant, H. I. Schiff, and D. K. Bohme, *J. Chem. Phys.*, **63**, 149 (1975).
- (19) V. I. Vedeneyev, L. V. Gurvich, V. N. Kondrat'yev, V. A. Medvedev, and Ye. L. Frankevich, "Bond Energies, Ionization Potentials, and Electron Affinities", St. Martin's Press, New York, N.Y., 1966.
- (20) D. Holtz and J. L. Beauchamp, *Science*, **173**, 1237 (1971).
- (21) G. N. Lewis and M. Randall, "Thermodynamics", McGraw-Hill, New York, N.Y., 1961, p 682.
- (22) J. L. Franklin, J. G. Dillard, H. M. Rosenstock, J. T. Herron, K. Draxl, and F. H. Field, *Natl. Stand. Ref. Data Ser., Nat. Bur. Stand.*, **No. 26** (1969).
- (23) This assumption seems reasonable when the bond strengths of the isoelectronic molecules  $\text{CH}_2\text{Br}$  and  $\text{CH}_3\text{Br}$  are compared. The dissociation energy of the carbon–bromine bond in methyl bromide is 2.97 eV, while the carbon–bromine bond in methylene bromide is about 0.2 eV stronger.<sup>22</sup>
- (24) J. R. Wyatt, L. W. Strattan, S. C. Snyder, and P. M. Hierl, *J. Chem. Phys.*, **62**, 2555 (1975).
- (25) (a) R. Wolfgang and R. J. Cross, *J. Phys. Chem.*, **73**, 743 (1969); (b) P. M. Hierl, Z. Herman, and R. Wolfgang, *J. Chem. Phys.*, **53**, 660 (1970).
- (26) J. R. Wyatt, L. W. Strattan, S. C. Snyder, and P. M. Hierl, *J. Chem. Phys.*, **64**, 3757 (1976).
- (27) E. A. Gislason, B. H. Mahan, C. W. Tsao, and A. S. Werner, *J. Chem. Phys.*, **50**, 142 (1969).
- (28) J. R. Wyatt, L. W. Strattan, and P. M. Hierl, *J. Chem. Phys.*, **65**, 1593 (1976).
- (29) D. R. Herschbach, *Discuss. Faraday Soc.*, **33**, 149 (1962).
- (30) (a) A. Ding, A. Henglein, D. Hyatt, and K. Lacmann, *Z. Naturforsch. A*, **23**, 2084 (1968); A. Henglein, *J. Chem. Phys.*, **53**, 458 (1958).
- (31) See, for example, ref 1, pp 76–77.
- (32) A. Henglein, K. Lacmann, and G. Jacobs, *Ber. Bunsenges. Phys. Chem.*, **69**, 279, 286, 292 (1965).
- (33) (a) P. J. Kuntz, E. M. Nemeth, J. C. Polanyi, and W. H. Wong, *J. Chem. Phys.*, **52**, 4654 (1970); (b) D. L. Bunker and M. D. Pattengill, *ibid.*, **53**, 3041 (1970); (c) T. Valencich and D. L. Bunker, *ibid.*, **61**, 21 (1974).
- (34) D. Seewald and R. Wolfgang, *J. Chem. Phys.*, **47**, 143 (1967).
- (35) (a) W. F. Libby, *J. Am. Chem. Soc.*, **69**, 2523 (1947); (b) R. J. Cross and R. Wolfgang, *J. Chem. Phys.*, **35**, 2002 (1961); (c) J. C. Light and J. Horrocks, *Proc. Phys. Soc. London*, **84**, 527 (1964); (d) K. T. Gillen, G. H. Mahan, and J. S. Winn, *J. Chem. Phys.*, **58**, 5373 (1973).
- (36) W. R. Gentry, E. A. Gislason, B. H. Mahan, and C. W. Tsao, *J. Chem. Phys.*, **49**, 3058 (1968).
- (37) D. G. Truhlar, *J. Chem. Phys.*, **51**, 4617 (1969); B. H. Mahan, *Acc. Chem. Res.*, **3**, 393 (1970).



## Rate Constants at 297 K for Proton-Transfer Reactions with HCN and CH<sub>3</sub>CN. Comparisons with Classical Theories and Exothermicity

G. I. Mackay, L. D. Belowski,<sup>1</sup> J. D. Payzant,<sup>2</sup> H. I. Schiff, and D. K. Bohme\*<sup>3</sup>

Department of Chemistry and Centre for Research in Experimental Space Science, York University, Downsview, Ontario, M3J 1P3, Canada (Received July 15, 1976)

Publication costs assisted by the National Research Council of Canada

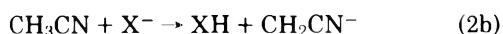
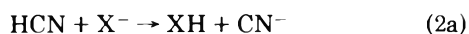
Rate constants for proton-transfer reactions of the type  $XH^+ + HCN (CH_3CN) \rightarrow H_2CN^+ (CH_3CNH^+) + X$  where  $X = H_2, N_2, CO, H_2O$ , and  $CO_2$  and of the type  $HCN (CH_3CN) + X^- \rightarrow CN^- (CH_2CN^-) + XH$  where  $X = H, D, OH, SH, NH_2, C_2H$ , and  $CH_3O$  have been measured at  $297 \pm 2$  K using the flowing afterglow technique. These reactions for which the measured rate constants span a range from  $0.15$  to  $1.5 \times 10^{-8} \text{ cm}^3 \text{ molecule}^{-1} \text{ s}^{-1}$  represent some of the fastest ion-molecule reactions observed to date. The rate constants are compared with the predictions of Langevin, average-dipole-orientation and locked-dipole theories of ion-molecule collisions. The average-dipole-orientation theory provides the most realistic collision rates for these reactions although these appear to be underestimated by  $\sim 10$  to  $\sim 40\%$ . The observed dependence of the efficiency for proton transfer on exothermicity indicates that the assumption of unit reaction probability resident in such comparisons may break down at low exothermicities.

### Introduction

Proton-transfer reactions involving simple molecular systems constitute a large class of ion-molecule reactions which have proven to be most suitable for the testing of the rate predictions of classical theories of ion-molecule collisions. This suitability arises from the expectation that the exothermic transfer of a proton proceeds on essentially every collision. When coupled with this expectation, collision rate theories amount to reaction rate theories so that a comparison of measured reaction rates with calculated collision rates can provide an experimental assessment of the latter.<sup>4</sup> The flowing afterglow measurements previously reported from this laboratory for the transfer of a proton to nonpolar molecules ( $Xe, N_2, CH_4, CO_2$ , and  $C_2H_6$ ), slightly polar molecules ( $NO, CO, N_2O$ :  $\mu_D < 0.2$  D), and moderately polar molecules ( $NH_3$ :  $\mu_D = 1.47$  D,  $H_2O$ :  $\mu_D = 1.84$  D) have indicated that the Langevin<sup>5</sup> and average-dipole-orientation<sup>6-8</sup> theories predict capture rates for collisions of ions with nonpolar and polar molecules, respectively, which often agree, within experimental error, with the measured reaction rates at room temperature.<sup>9,10</sup> In this paper we report further measurements of proton transfer rates and their comparison with the predictions of the various collision theories. The reactions investigated involve highly polar molecules, viz.  $HCN$  ( $\mu_D = 2.98$  D) and  $CH_3CN$  ( $\mu_D = 3.92$  D), which may either accept a proton from an ion



where  $X = H_2, N_2, CO, H_2O, N_2O$ , and  $CO_2$ , or transfer a proton to an ion



where  $X = H, D, SH, OH, NH_2, C_2H$  and  $CH_3O$ .

This study also provided another opportunity to explore the effect of excess energy in the form of reaction exothermicity upon the magnitude of the efficiency for a series of homologous ion-molecule reactions. Our previous investiga-

tions of proton transfer reactions indicated no substantial dependence of the efficiency on the heat of reaction.

### Experimental Section

Rate constants were measured in the usual manner in a flowing afterglow apparatus in which the ions were permitted to thermalize by collisions with a helium or hydrogen buffer gas to the ambient room temperature of  $297 \pm 2$  K before entering the reaction region.<sup>11</sup> Typical operating conditions encompassed total gas pressures,  $P$ , in the range  $0.25$  to  $0.45$  Torr and gas velocities,  $\bar{v}$ , in the range  $8.0$  to  $8.5 \times 10^3 \text{ cm s}^{-1}$ . The reaction length,  $L$ , was  $60$  cm. The accuracy of the rate constant measurements is estimated to be  $\pm 20$  and  $\pm 25\%$  for the  $HCN$  and  $CH_3CN$  reactions, respectively, and the precision was observed to be  $\pm 10\%$ .

The ions  $XH^+$ , where  $X = N_2, CO, CO_2, N_2O$ , and  $H_2O$ , were generated according to the proton transfer reaction



simply by adding the appropriate gas,  $X$ , upstream of the reaction region into a pure hydrogen afterglow in which  $H_3^+$  is the dominant ion.

The negative ions were generated in a helium carrier gas by the impact of electrons ( $\sim 75$  eV) and helium metastables on the appropriate neutral gas:  $H^-$  ( $NH_3$  or  $CH_4$ ),  $D^-$  ( $CD_4$ ),  $OH^-$  ( $H_2O$ ),  $C_2H^-$  ( $C_2H_2$ ),  $NH_2^-$  ( $NH_3$ ),  $CH_3O^-$  ( $CH_3OH$ ).  $H^-$  and  $D^-$  were also produced by the proton-transfer reaction of  $NH_2^-$  with  $H_2$  and  $D_2$ , respectively.

The gases used were helium (Linde, Prepurified Grade, 99.995% He), hydrogen (Linde, Very Dry Grade, 99.95%  $H_2$ ), nitrogen (Matheson, Prepurified Grade, 99.998%  $N_2$ ), carbon monoxide (Matheson, CP Grade, 99.5%  $CO$ ), carbon dioxide (Matheson Coleman Grade, 99.99%  $CO_2$ ), nitrous oxide (Matheson, 98.0%  $N_2O$ ), acetylene (Matheson, Purified Grade, 99.6%  $C_2H_2$ ), methane (Matheson, Ultra High Purify, 99.97%  $CH_4$ ), ammonia (Matheson, anhydrous, 99.99%  $NH_3$ ), distilled water, methanol (BDH Chemicals, Analytical Reagent Grade), and methyl cyanide (Matheson Coleman and Bell, Spectro-quality Grade). The  $HCN$  was prepared by the action of sul-



**TABLE I: Rate Constants (in units of  $10^{-9} \text{ cm}^3 \text{ molecule}^{-1} \text{ s}^{-1}$ ) at  $297 \pm 2 \text{ K}$  for Reactions of the Type  $\text{XH}^+ + \text{Y} \rightarrow \text{YH}^+ + \text{X}$** 

$\text{XH}^+$	$\text{Y}$	$k_{\text{expt}}^a$	$k_{\text{L}}^b$	$k_{\text{LD}}^c$	$k_{\text{ADO}}^d$	$k_{\text{expt}}/k_{\text{ADO}}$	$-\Delta H^\circ_{298},^e$ $\text{kcal mol}^{-1}$
$\text{H}_3^+$	HCN	$7.4 \pm 0.5$ (5)	2.29	18.9	6.48	1.1	$69 \pm 4$
$\text{H}_3\text{O}^+$	HCN	$3.5 \pm 0.5$ (7)	1.13	9.35	3.20	1.1	$5 \pm 2$
$\text{N}_2\text{H}^+$	HCN	$3.2 \pm 0.2$ (5)	1.01	8.35	2.86	1.1	$53 \pm 4$
$\text{HCO}^+$	HCN	$3.0 \pm 0.2$ (3)	1.01	8.35	2.86	1.0	$27 \pm 4$
$\text{H}_3^+$	$\text{CH}_3\text{CN}$	$10 \pm 1$ (9)	2.98	24.5	8.40	1.2	$85 \pm 2$
$\text{H}_3\text{O}^+$	$\text{CH}_3\text{CN}$	$4.7 \pm 0.7$ (18)	1.39	11.4	3.91	1.2	$21 \pm 4$
$\text{N}_2\text{H}^+$	$\text{CH}_3\text{CN}$	$4.1 \pm 0.1$ (2)	1.21	9.98	3.42	1.2	$69 \pm 3$
$\text{HCO}^+$	$\text{CH}_3\text{CN}$	$4.1 \pm 0.4$ (8)	1.21	9.98	3.42	1.2	$43 \pm 3$
$\text{N}_2\text{OH}^+$	$\text{CH}_3\text{CN}$	$3.8 \pm 0.2$ (5)	1.08	8.88	3.05	1.2	$48 \pm 3$
$\text{CO}_2\text{H}^+$	$\text{CH}_3\text{CN}$	$4.1 \pm 0.7$ (5)	1.08	8.88	3.05	1.3	$57 \pm 3$

<sup>a</sup> The mean value and the precision of the measurements. The number of measurements is given in parentheses. The accuracy is estimated to be better than  $\pm 20\%$  (HCN) and  $\pm 25\%$  ( $\text{CH}_3\text{CN}$ ). <sup>b</sup> Langevin theory. <sup>c</sup> Locked-dipole theory. <sup>d</sup> Average-dipole-orientation theory (the  $\cos \theta$  model),  $C = 0.252$ . <sup>e</sup> Proton affinities adopted for the determination of  $\Delta H^\circ_{298}$  are given in Table III.

**TABLE II: Rate Constants (in units of  $10^{-9} \text{ cm}^3 \text{ molecule}^{-1} \text{ s}^{-1}$ ) at  $297 \pm 2 \text{ K}$  for Reactions of the Type  $\text{YH} + \text{X}^- \rightarrow \text{XH} + \text{Y}^-$** 

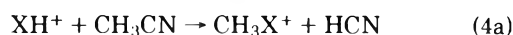
$\text{YH}$	$\text{X}^-$	$k_{\text{expt}}^a$	$k_{\text{L}}^b$	$k_{\text{LD}}^c$	$k_{\text{ADO}}^d$	$k_{\text{expt}}/k_{\text{ADO}}$	$-\Delta H^\circ_{298},^e$ $\text{kcal mol}^{-1}$
HCN	$\text{H}^-$	$15 \pm 2$ (13)	3.82	31.7	10.8	1.4	$50 \pm 2$
HCN	$\text{D}^-$	$9.9 \pm 0.3$ (2)	2.76	22.9	7.8	1.3	$50 \pm 2$
HCN	$\text{NH}_2^-$	$4.8 \pm 0.5$ (8)	1.19	9.85	3.37	1.4	$54 \pm 2$
HCN	$\text{OH}^-$	$4.1 \pm 0.3$ (9)	1.17	9.67	3.31	1.2	$41 \pm 1$
HCN	$\text{C}_2\text{H}^-$	$3.9 \pm 0.2$ (5)	1.05	8.67	2.97	1.3	$29 \pm 4$
HCN	$\text{SH}^-$	$2.9 \pm 0.3$ (2)	0.978	8.10	2.77	1.0	$1.0 \pm 0.2/$
$\text{CH}_3\text{CN}$	$\text{H}^-$	$13 \pm 2$ (8)	5.04	41.5	14.2	0.92	$25 \pm 4$
$\text{CH}_3\text{CN}$	$\text{D}^-$	$9.9 \pm 1.6$ (5)	3.62	29.8	10.2	0.97	$25 \pm 4$
$\text{CH}_3\text{CN}$	$\text{NH}_2^-$	$5.1 \pm 0.2$ (6)	1.47	12.1	4.16	1.2	$29 \pm 4$
$\text{CH}_3\text{CN}$	$\text{OH}^-$	$4.4 \pm 0.2$ (7)	1.44	11.8	4.07	1.1	$16 \pm 4$
$\text{CH}_3\text{CN}$	$\text{C}_2\text{H}^-$	$1.5 \pm 0.2$ (9)	1.27	10.4	3.58	0.42	$4.1 \pm 0.9/$
$\text{CH}_3\text{CN}$	$\text{CH}_3\text{O}^-$	$3.5 \pm 0.3$ (5)	1.19	9.79	3.36	1.0	$6.3 \pm 1.6/$

<sup>a</sup> The mean value and the precision of the measurements. The number of measurements is given in parentheses. The accuracy is estimated to be better than  $\pm 20\%$  (HCN) and  $\pm 25\%$  ( $\text{CH}_3\text{CN}$ ). <sup>b</sup> Langevin theory. <sup>c</sup> Locked-dipole theory. <sup>d</sup> Average-dipole-orientation theory (the  $\cos \theta$  model),  $C = 0.252$ . <sup>e</sup> Proton affinities adopted for the determination of  $\Delta H^\circ_{298}$  are given in Table III. / Based on measurements of the equilibrium constant for the proton transfer reaction, ref 13, and unpublished results from this laboratory.

furic acid on an aqueous solution of KCN,<sup>12</sup> dried by passing it over anhydrous  $\text{CaCl}_2$ , and further purified by distillation in vacuo.

## Results and Discussion

The rate constants measured for reactions of type 1 are summarized in Table I. Their determination from the decay of the primary ion,  $\text{XH}^+$ , was straightforward. Proton transfer was observed to be the dominant ( $>90\%$ ) channel in each case. There were no other obvious primary reaction channels. For several of the reactions with  $\text{CH}_3\text{CN}$  other channels of the type



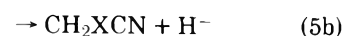
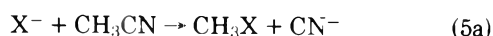
are exothermic but apparently do not compete effectively at room temperature with proton transfer. Secondary reactions of  $\text{H}_2\text{CN}^+$  and  $\text{CH}_3\text{CNH}^+$  were observed to occur at large additions of HCN and  $\text{CH}_3\text{CN}$  and result in the formation of the cluster ions  $\text{H}^+(\text{HCN})_2$  and  $\text{H}^+(\text{CH}_3\text{CN})_2$ , respectively.

The results of the measurements of the rate constants for reactions of type 2 are included in Table II. Proton transfer was again observed to be the dominant reactions channel. For

**TABLE III: Proton Affinities Adopted in the Determination of  $\Delta H^\circ_{298}$** 

$\text{X}$	PA, kcal $\text{mol}^{-1}$	Ref	$\text{X}^-$	PA, kcal $\text{mol}^{-1}$	Ref
$\text{H}_2$	$101 \pm 1$	22	$\text{NH}_2^-$	$404 \pm 1$	27
$\text{N}_2$	$117 \pm 1$	23	$\text{H}^-, \text{D}^-$	$400 \pm 1$	28
$\text{CO}_2$	$129 \pm 2$	23	$\text{OH}^-$	391	28
$\text{N}_2\text{O}$	$138 \pm 2$	23	$\text{C}_2\text{H}^-$	$379 \pm 3$	23
CO	$143 \pm 1$	24	$^-\text{CH}_2\text{CN}$	$375 \pm 3$	23
$\text{H}_2\text{O}$	$165 \pm 3$	25	$\text{SH}^-$	$351 \pm 1$	13
HCN	$170 \pm 3$	26	$\text{CN}^-$	$350 \pm 1$	13
$\text{CH}_3\text{CN}$	$186 \pm 1$	26			

the reactions with HCN and  $\text{CH}_3\text{CN}$  the only product ions observed were  $\text{CN}^-$  and  $\text{CH}_2\text{CN}^-$ , respectively, and there was no evidence for the formation of reactive intermediates. For the reactions of  $\text{X}^-$  with  $\text{CH}_3\text{CN}$  these observations imply that proton transfer dominates at room temperature over nucleophilic displacement of the type



CN<sup>-</sup> was monitored but there was no evidence for its production via reaction 5a which is exothermic for all of the anions investigated. This contrasts the behavior previously observed in this laboratory for the reactions of these anions with halogenated methanes for which displacement was found to be the dominant channel in most instances.<sup>14</sup> Also there was no evidence for the production of H<sup>-</sup> via channel 5b. This channel is athermal for X = H and could not be identified in this case since the mass spectrometer cannot distinguish between reactant and product H<sup>-</sup> ions. However, the experiments with D<sup>-</sup> in which H<sup>-</sup> was monitored showed no evidence for the occurrence of channel 5b.

The proton-transfer reactions of both types 1 and 2 investigated in this study represent some of the fastest ion-molecule reactions observed to date. The rate constants, which have to our knowledge not been determined previously, are generally quite large, spanning the range 0.15 to 1.5 × 10<sup>-8</sup> cm<sup>3</sup> molecule<sup>-1</sup> s<sup>-1</sup>. Only the proton transfer reactions between CH<sub>3</sub>CN and N<sub>2</sub>H<sup>+</sup> and OH<sup>-</sup> were observed previously by Gray<sup>15</sup> in an ion cyclotron resonance spectrometer although their rate constants were not reported.

Included in Tables I and II are the capture rate constants calculated according to three classical models of ion-molecule collisions involving polar and nonpolar molecules. The average-dipole-orientation (ADO) theory of Su and Bowers<sup>6-8</sup> predicts capture rate constants determined by the expression

$$k_{\text{ADO}} = (2\Pi q/\mu^{1/2})[\alpha^{1/2} + C\mu_D(2/\Pi kT)^{1/2}] \quad (6)$$

where  $q$  is the charge on the ion,  $\mu$  is the reduced mass of the reactants,  $\alpha$  is the polarizability, and  $\mu_D$  the permanent dipole moment of the neutral.  $C$  has been parameterized by Su and Bowers<sup>8</sup> to have a value between 0 and 1. Expression 6 reduces to the locked-dipole (LD) limit,  $k_{\text{LD}}$ , when  $C = 1$ .<sup>16,17</sup> The Langevin (L) expression,  $k_{\text{L}}$ , results when  $\mu_D = 0$ .<sup>5</sup> The three classical theories define straight lines on a plot of  $k$  vs.  $\mu^{-1/2}$  for series of homologous reactions of types 1 and 2 for which the neutral substrate remains unchanged. This is illustrated for the reactions with HCN and CH<sub>3</sub>CN in Figures 1 and 2 in which the measured reaction rate constants are compared with the capture rate constants predicted by the three theories. The values for the permanent dipole moments for HCN ( $\mu_D = 2.98$  D) and CH<sub>3</sub>CN ( $\mu_D = 3.92$  D) were taken from the compilation of Nelson et al.<sup>18</sup> The experimental value of  $\alpha = 2.59$  Å<sup>3</sup> was adopted for HCN.<sup>19</sup> The average polarizability of CH<sub>3</sub>CN,  $\alpha = 4.56$  Å<sup>3</sup>, was determined from the average polarizability of its bonds.<sup>19</sup> The appropriate value of  $C = 0.252$  for both HCN and CH<sub>3</sub>CN was determined from the table given by Bass et al.<sup>8</sup> (the  $\cos \theta$  model).

It is evident from the comparisons between reaction and collision rate constants shown in Figures 1 and 2 that the high values of the thermal energy proton-transfer rate constants measured in this study are most adequately accounted for by the average-dipole-orientation theory which attributes 65% of the collision rate for these reactions to ion-permanent dipole interaction. The Langevin theory which ignores ion-permanent dipole interaction clearly underestimates the collision rate whereas the locked-dipole theory appears to overestimate the collision rate. These results reinforce the general observation that ADO theory usually provides the most realistic collision rate for proton transfers.<sup>4</sup>

Notwithstanding the uncertainty in the rate constant measurements, a closer inspection of the values for  $k_{\text{exp}}/k_{\text{ADO}}$  obtained in this study suggests that the ADO theory itself may slightly underestimate the collision rate. 16 of the 22 rate

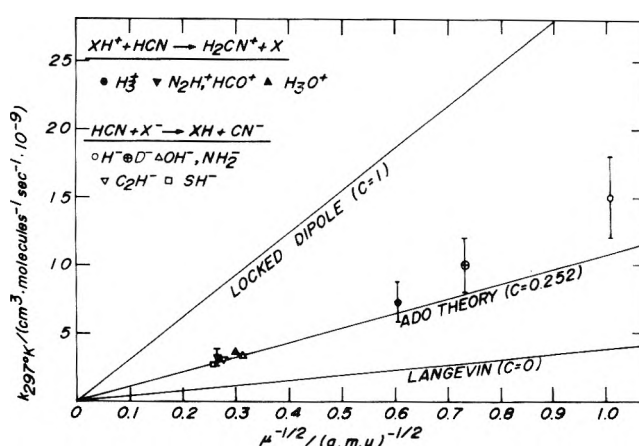


Figure 1. A comparison of measured rate constants with capture rate constants predicted by recent classical theories for proton transfer reactions with HCN ( $\alpha = 2.59$  Å<sup>3</sup>,  $\mu_D = 2.98$  D) at  $297 \pm 2$  K. The solid bars represent the estimated accuracy ( $\pm 20\%$ ) of the measurements.

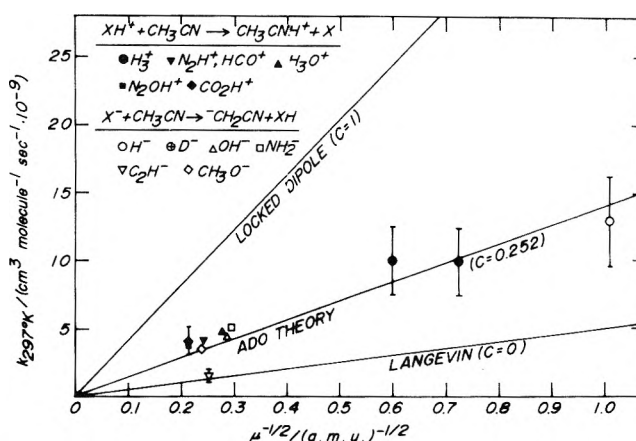


Figure 2. A comparison of measured rate constants with capture rate constants predicted by recent classical theories for proton-transfer reactions with CH<sub>3</sub>CN ( $\alpha = 4.56$  Å<sup>3</sup>,  $\mu_D = 3.92$  D) at  $297 \pm 2$  K. The solid bars represent the estimated accuracy ( $\pm 25\%$ ) of the measurements.

constants measured exceed  $k_{\text{ADO}}$  by at least 10% and as much as 40%. These small differences appear to be significant. A similar disparity has recently been reported by Mackenzie Peers and Muller<sup>20</sup> for positive ion-molecule reactions with dimethyl sulfoxide ( $\alpha = 7.96$  Å<sup>3</sup>,  $\mu_D = 3.96$  D). The rate constants for these reactions measured with a single-source "medium pressure" mass spectrometer were found to exceed the ADO values by  $\sim 30\%$ . Bowers and Su<sup>21</sup> have recently commented on possible shortcomings in their theory and have indicated that more refined calculations will soon be forthcoming. For example, the theoretical model is being extended to include the induced dipole-induced dipole interaction arising from the polarizability of the ion which would lead to an enhanced collision rate. This enhancement is likely to be larger for negative ions. Indeed we observe the largest positive deviations from the ADO predictions for the reactions of anions with HCN, viz. type 2a. An explanation for the smaller deviations observed for the reactions of anions with CH<sub>3</sub>CN, viz. type 2b, can be found in the discussion given below.

Earlier studies of homologous series of proton-transfer reactions have indicated that the assumption of unit reaction efficiency may break down at low reaction exothermicities.<sup>9,10</sup> When this is the case, the measured reaction rate constant will

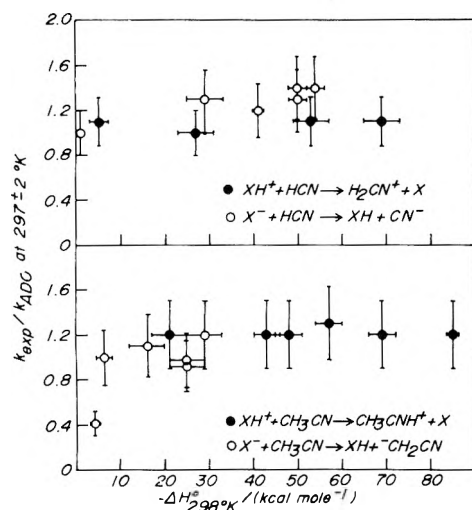


Figure 3. A plot of the ratio of the measured proton-transfer rate constant to the calculated capture (ADO) rate constant as a function of the heat of reaction,  $-\Delta H^\circ_{298}$ .

provide a less meaningful test of collision theory in that it indicates only a lower limit to the collision rate. Comparisons with collision theory should therefore, be confined to those reactions of a homologous series for which  $k_{\text{exp}}/k_{\text{ADO}}$  has been demonstrated to be independent of  $\Delta H^\circ_{298}$ . 15 of the 16 reactions alluded to above fall into this category. Figure 3 explores the variation of reaction efficiency with exothermicity for all of the reactions investigated in this study. The homologous series of proton-transfer reactions of type 1a and 1b show no dependence of  $k_{\text{exp}}/k_{\text{ADO}}$  on the heat of reaction. For the proton-transfer reactions of types 2a and 2b the least exothermic member of each series, viz.  $\text{SH}^- + \text{HCN}$  and  $\text{C}_2\text{H}^- + \text{CH}_3\text{CN}$ , respectively, exhibits the lowest reaction efficiency. For the reactions of type 2a  $k_{\text{exp}}/k_{\text{ADO}}$  becomes independent of  $\Delta H^\circ_{298}$  for values  $\leq -29 \text{ kcal mol}^{-1}$  whereas  $k_{\text{exp}}/k_{\text{ADO}}$  increases gradually for all of the reactions of type 2b for which  $\Delta H^\circ_{298} \geq -29 \text{ kcal mol}^{-1}$ .

**Acknowledgment.** The financial assistance of the National Research Council of Canada is gratefully acknowledged.

## References and Notes

- (1) Present address: Department of Chemistry, University of California, Santa Barbara, Calif. 93106.
- (2) Present address: Department of Chemistry, University of Alberta, Edmonton, Alberta.
- (3) Alfred P. Sloan Research Fellow, 1974–1976.
- (4) D. K. Bohme in "Interactions of Ions with Molecules", P. Ausloos, Ed., Plenum Press, New York, N.Y., 1974.
- (5) G. Gioumousis and D. P. Stevenson, *J. Chem. Phys.*, **29**, 294 (1958).
- (6) T. Su and M. T. Bowers, *J. Chem. Phys.*, **58**, 3027 (1973).
- (7) T. Su and M. T. Bowers, *Int. J. Mass Spectrom. Ion Phys.*, **12**, 347 (1973).
- (8) L. Bass, T. Su, W. J. Chesnavich, and M. T. Bowers, *Chem. Phys. Lett.*, **34**, 119 (1975).
- (9) R. S. Hemsworth, J. D. Payzant, H. I. Schiff, and D. K. Bohme, *Chem. Phys. Lett.*, **26**, 417 (1974).
- (10) D. Betowski, J. D. Payzant, and G. I. Mackay, and D. K. Bohme, *Chem. Phys. Lett.*, **31**, 321 (1975).
- (11) D. K. Bohme, R. S. Hemsworth, H. W. Rundle, and H. I. Schiff, *J. Chem. Phys.*, **58**, 504 (1973).
- (12) G. Brauer, Ed., "Handbook of Preparative Inorganic Chemistry", Academic Press, New York, N.Y., 1965.
- (13) D. Betowski, G. I. Mackay, J. D. Payzant, and D. K. Bohme, *Can. J. Chem.*, **53**, 2365 (1975).
- (14) K. Tanaka, G. I. Mackay, J. D. Payzant, and D. K. Bohme, *Can. J. Chem.*, **54**, 1643 (1976).
- (15) G. A. Gray, *J. Am. Chem. Soc.*, **90**, 6002 (1968).
- (16) T. F. Moran and W. H. Hamill, *J. Chem. Phys.*, **39**, 1413 (1963).
- (17) S. K. Gupta, E. G. Jones, A. G. Harrison, and J. J. Myher, *Can. J. Chem.*, **45**, 3107 (1967).
- (18) R. D. Nelson, D. R. Lide, and A. A. Maryott, *Natl. Stand. Ref. Data Ser., Natl. Bur. Stand.*, **No. 10** (1967).
- (19) J. O. Hirschfelder, C. F. Curtiss, and R. B. Bird, "Molecular Theory of Gases and Liquids", Wiley, New York, N.Y., 1967.
- (20) A. Mackenzie Peers and J. C. Muller, *Int. J. Mass Spectrom. Ion Phys.*, **16**, 321 (1975).
- (21) M. T. Bowers and T. Su in "Interactions of Ions with Molecules", P. Ausloos, Ed., Plenum Press, New York, N.Y., 1974.
- (22) A. J. Duben and J. P. Lowe, *J. Chem. Phys.*, **55**, 4270 (1971).
- (23) Unpublished results from this laboratory.
- (24) P. M. Guyon, W. A. Chupka, and J. Berkowitz, *J. Chem. Phys.*, **64**, 1419 (1976).
- (25) J. Long and B. Munson, *J. Am. Chem. Soc.*, **95**, 2427 (1973).
- (26) M. A. Haney and J. L. Franklin, *J. Phys. Chem.*, **73**, 4328 (1969).
- (27) G. I. Mackay, R. S. Hemsworth, and D. K. Bohme, *Can. J. Chem.*, **54**, 1624 (1976).
- (28) "JANAF Thermochemical Tables", 2d ed, *Natl. Stand. Ref. Data Ser., Natl. Bur. Stand.*, **No. 37**, (1971). 1974 Supplement to *J. Phys. Chem. Ref. Data*, **3**, 311 (1974).

# Photoelectron Spectra of 1,2-Dibromo-1,1-difluoroethane, 1,2-Bromochloroethane, and 1,2-Dichloro-, 1,2-Dibromo-, and 1,2-Diodotetrafluoroethane

F. T. Chau and C. A. McDowell\*

The Department of Chemistry, University of British Columbia, Vancouver 8, British Columbia, Canada V6T 1W5 (Received June 29, 1976)

Publication costs assisted by the National Research Council of Canada

The He I photoelectron spectra of five substituted ethanes, 1,2-dibromo-1,1-difluoroethane, 1,2-bromochloroethane and 1,2-dichloro-, 1,2-dibromo-, and 1,2-diodotetrafluoroethane, are reported. Assuming that Koopmans' theorem holds and also that only the trans rotamers of these molecules give the main features in their spectra, a one-electron molecular orbital model which includes spin-orbit interaction is shown to describe the interaction between the halogen lone pair orbitals.

## Introduction

Rotational isomers of halogenated ethanes have been studied extensively by various physical methods such as infrared and Raman,<sup>1-5</sup> ultrasonic,<sup>6</sup> and microwave spectroscopy.<sup>7</sup> For molecules such as (CH<sub>2</sub>Cl)<sub>2</sub>, (CH<sub>2</sub>Br)<sub>2</sub>, (CH<sub>2</sub>I)<sub>2</sub>, (CF<sub>2</sub>Cl)<sub>2</sub>, (CF<sub>2</sub>Br)<sub>2</sub>, (CF<sub>2</sub>I)<sub>2</sub>, CF<sub>2</sub>BrCH<sub>2</sub>Br, and CH<sub>2</sub>ClCH<sub>2</sub>Br (compounds I–VIII, respectively), the trans form is found to be more stable than the gauche with conformational energy differences<sup>1,2,7</sup>  $\Delta H_{\text{mol}}$  of 1.15, 1.54, 0.44, 0.95, 1.03, and 1.43 kcal/mol for I, II, IV, V, VII, and VIII, respectively. Concentrations of the trans form of I, II, IV, and VIII are, respectively, 77, 90, 52, and 85% and those of V and VII are estimated to be 71 and 74%, respectively, through relation<sup>1</sup> between  $\Delta H_{\text{mol}}$  and the relative concentration of the isomers. Though no such data are available for VI the trans isomer is likely to be more stable than the gauche because of the steric and electrostatic effects in that molecule.

Previously, we reported<sup>8</sup> the photoelectron (PE) spectra of 1,2-dichloro-, 1,2-dibromo-, and 1,2-diodoethanes. A Hückel molecular orbital (MO) method with the inclusion of spin-orbit coupling was used to describe the interaction between the halogen lone pair molecular orbitals (LPMO). In this paper the PE spectra of IV–VIII are presented and a

described earlier<sup>8</sup> are shown in Figures 1 and 2. The observed ionization potentials (IP) are summarized in Table I.

## Method of Calculation

(a) *One-Electron Model for trans-1,2-Dihalotetrafluoroethane (C<sub>2</sub>H<sub>2</sub>F<sub>4</sub>X<sub>2</sub>)*. The four halogen LPMO's of (CF<sub>2</sub>X)<sub>2</sub> are degenerate if they are free from any kind of perturbation effects (see Figure 3 case a). However, these orbitals are shifted to a different extent by both the *through space* and *through bond* interactions.<sup>10</sup> According to a CNDO/2 calculation<sup>11</sup> on IV, the first four highest occupied  $\sigma$  orbitals are  $\sigma_{7a_g}$ ,  $\sigma_{6b_u}$ ,  $\sigma_{6a_g}$ , and  $\sigma_{4b_g}$  in order of increasing IP's. Since only orbitals of same symmetry can have *through bond* interaction, only the LPMO's  $1_{8a_g}$ ,  $1_{7b_u}$ , and  $1_{5b_g}$  are considered to be destabilized by the amount of  $S_{a_g}$ ,  $S_{b_u}$ , and  $S_{b_g}$ , respectively, where  $S_i$  is the parameter for the *through bond* interaction. To simplify the calculations, the interaction between  $1_{8a_g}$  by  $\sigma_{6a_g}$  is neglected. The *through space* interaction parameter,  $d$ , is equal to  $-2S_{\epsilon_p}$ , where  $\epsilon_p$  is the Coulomb integral for the halogen atom.

In addition, the LPMO's can mix with each other through spin-orbit coupling. Using the same spin-orbit operator as Brogli and Heilbronner,<sup>12</sup> a secular equation (eq 1) can be set

$$\begin{vmatrix}
 \epsilon_p + d - \epsilon & 0 & -i\zeta/2 & 0 \\
 0 & \epsilon_p - d - \epsilon & 0 & -i\zeta/2 \\
 -i\zeta/2 & 0 & \epsilon_p + d - \epsilon & 0 \\
 0 & -i\zeta/2 & 0 & \epsilon_p - d - \epsilon \\
 S'_{a_g} & 0 & 0 & 0 \\
 0 & 0 & S'_{b_g} & 0 \\
 0 & 0 & S'_{b_u} & 0 \\
 0 & S'_{b_u} & 0 & 0
 \end{vmatrix}
 = 0
 \quad (1)$$

similar MO treatment is employed. This, of course, assumes that there are no serious deviations from Koopmans' theorem<sup>9</sup> for these molecules. From the MO parameters obtained, some intrinsic molecular properties of these molecules can be obtained. Throughout this work, the trans isomers of all the molecules studied except IV are considered to give rise to the main features in their PE spectra.

## Experimental Section

All the chemicals used were commercially available samples of high purity. The spectra obtained by using the spectrometer

up in accord with the overall interactions for  $1_{8a_g}$ ,  $1_{7b_u}$ ,  $1_{5b_g}$ ,  $1_{5a_u}$ ,  $\sigma_{7a_g}$ ,  $\sigma_{4b_g}$ , and  $\sigma_{6b_u}$  respectively,  $\epsilon_{a_g}$ ,  $\epsilon_{b_g}$ , and  $\epsilon_{b_u}$  are the unperturbed energies of  $\sigma_{7a_g}$ ,  $\sigma_{4b_g}$ , and  $\sigma_{6b_u}$ , respectively,  $S'_i$  is related to  $S_i$  by the equation

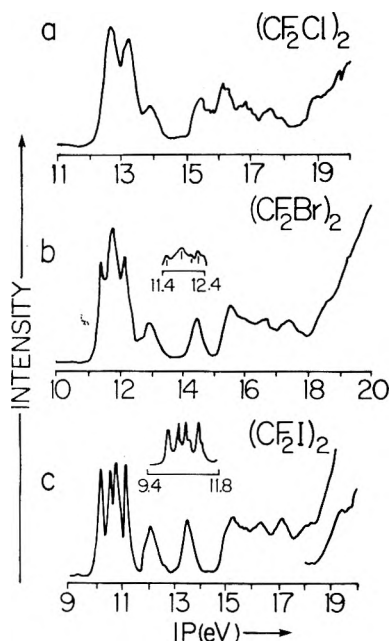
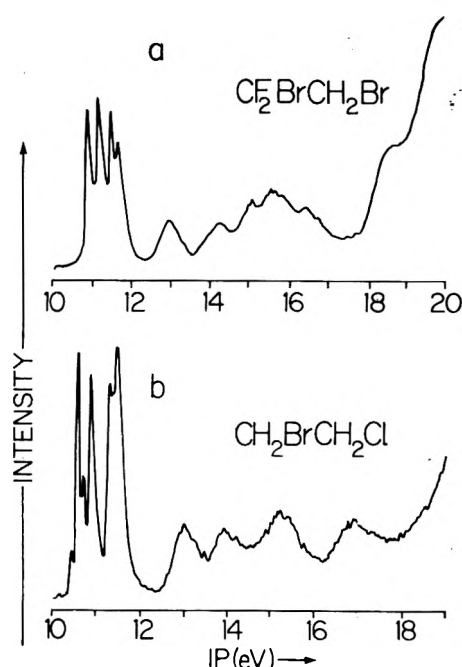
$$S'_i = S_i(S_i + \epsilon_p - \epsilon_i \pm d) \quad (2)$$

with a plus sign for  $1_{8a_g}$  and  $1_{5b_g}$ , and a minus sign for  $1_{5a_u}$  and  $1_{7b_u}$ .  $\zeta$  is the spin-orbit coupling constant which is equal to  $\zeta_x$ , and is taken to be two-thirds of the spin-orbit coupling constant of free halogen atom. The magnitude of  $\zeta$  in (CF<sub>2</sub>X)<sub>2</sub> should be smaller than that in the corresponding (CH<sub>2</sub>X)<sub>2</sub>

TABLE I: Experimental IP's (eV) of (CF<sub>2</sub>Cl)<sub>2</sub>, (CF<sub>2</sub>Br)<sub>2</sub>, (CF<sub>2</sub>I)<sub>2</sub>, (CF<sub>2</sub>I)<sub>2</sub>, CF<sub>2</sub>BrCH<sub>2</sub>Br, and CH<sub>2</sub>BrCH<sub>2</sub>Cl

	(CF <sub>2</sub> Cl) <sub>2</sub>	(CF <sub>2</sub> Br) <sub>2</sub>	(CF <sub>2</sub> I) <sub>2</sub>		CF <sub>2</sub> BrCH <sub>2</sub> Br		CH <sub>2</sub> BrCH <sub>2</sub> Cl
χ <sub>1</sub>	12.47 <sup>c</sup>	11.44	10.11	χ <sub>1</sub>	10.86	χ <sub>1</sub>	10.65
χ <sub>2</sub>	12.82 <sup>c</sup>	11.83	10.44	χ <sub>2</sub>	11.14	χ <sub>2</sub>	10.94
χ <sub>3</sub>	13.06	12.11	10.69	χ <sub>3</sub>	11.46	χ <sub>3</sub>	11.40
χ <sub>4</sub>	13.19	12.21	11.10	χ <sub>4</sub>	11.65	χ <sub>4</sub>	11.52
σ <sub>7a<sub>g</sub></sub>	13.88	13.00 <sup>c</sup>	12.02	σ <sub>10a<sub>-</sub>'</sub>	12.96 <sup>b</sup>	σ <sub>6a<sub>+</sub>'</sub>	13.05
σ <sub>6b<sub>u</sub></sub>	15.43	14.53	13.49	σ <sub>9a<sub>+</sub>'</sub>	14.21 <sup>b</sup>	σ <sub>2a<sub>-</sub>''</sub>	13.94
σ <sub>6a<sub>g</sub></sub>	16.13	15.62	15.24	σ <sub>8a<sub>-</sub>'</sub>	15.06	σ <sub>5a<sub>-</sub>'</sub>	15.24 <sup>b</sup>
σ <sub>4b<sub>g</sub></sub>	16.81	15.99	15.67	σ <sub>5a<sub>-</sub>''</sub>	15.51	σ <sub>4a<sub>+</sub>'</sub>	16.85
σ <sub>4a<sub>u</sub></sub>	17.54	16.61 <sup>b</sup>	16.31	σ <sub>4a<sub>+</sub>''</sub>	16.43		
σ <sub>3b<sub>g</sub></sub>	18.93	17.43 <sup>b</sup>	17.13	σ <sub>3a<sub>-</sub>''</sub>	18.63		
σ <sub>3a<sub>u</sub></sub>	19.6?	18.66 <sup>b</sup>	18.05	σ <sub>7a<sub>-</sub>'</sub>	19.88		
σ <sub>5b<sub>u</sub></sub>			19.37				

<sup>a</sup> Experimental error estimated to be ±0.01 eV, except for those with the superscript b. <sup>c</sup> Uncertainty unknown.

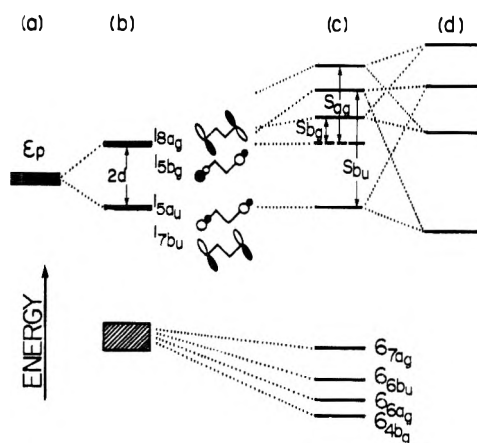
Figure 1. He I PE spectra of (a) (CF<sub>2</sub>Cl)<sub>2</sub>, (b) (CF<sub>2</sub>Br)<sub>2</sub>, and (c) (CF<sub>2</sub>I)<sub>2</sub>.Figure 2. He I PE spectra of (a) CF<sub>2</sub>BrCH<sub>2</sub>Br and (b) CH<sub>2</sub>BrCH<sub>2</sub>Cl.

species because of the mixing of the LPMO's with those of fluorine atoms. In fact, a very small spin-orbit splitting has been observed in the first PE band of CF<sub>3</sub>CF<sub>2</sub>Cl.<sup>13</sup> Since the number of unknown variables,  $\epsilon_p$ ,  $S'_{a_g}$ ,  $S'_{b_u}$ ,  $\epsilon_{a_g}$ ,  $\epsilon_{b_u}$ , and  $\epsilon_{b_g}$  in eq 1 is equal to that of observed IP's,  $\zeta$  is taken to have values of 0,  $\zeta_x/2$ , and  $\zeta_x$ . The other parameters given in Table III are obtained by a trial and error method<sup>8</sup> to give the best fit with the experimental data. It should be mentioned that the symmetry notation A<sub>u</sub> and B<sub>u</sub> used in ref 8 should be read in the reverse as B<sub>u</sub> and A<sub>u</sub>, respectively.

(b) *One-Electron Model of trans-CH<sub>2</sub>BrCH<sub>2</sub>Cl and trans-CF<sub>2</sub>BrCH<sub>2</sub>Br (C<sub>s</sub>)*. Figure 4 shows the qualitative MO diagram of trans-CH<sub>2</sub>BrCH<sub>2</sub>Cl. In this molecule, the Coulomb energies of the bromine atom  $\epsilon_{Br}$  and the chlorine atom  $\epsilon_{Cl}$  are different with  $\epsilon_{Cl} < \epsilon_{Br}$ . The two pairs of doubly degenerate LPMO's (Figure 4 case a) can combine to give orbitals  $1_{7a-}'$ ,  $1_{4a+}''$ ,  $1_{8a+}'$ , and  $1_{3a-}''$ . The subscripts plus and minus mean the in-phase and out-of-phase combinations of the orbitals. The coordinate system used here is the same as that in ref 8. In this case,  $d$  is estimated from the approximation given in ref 14, i.e.

$$d = KS(\epsilon_{Cl}\epsilon_{Br})^{1/2} \quad (3)$$

with  $K$  equal to 2.

Figure 3. Qualitative MO diagram of trans-(CF<sub>2</sub>X)<sub>2</sub> (a) no perturbation, (b) through space interaction, (c) through bond interaction added, and (d) spin-orbit coupling added.

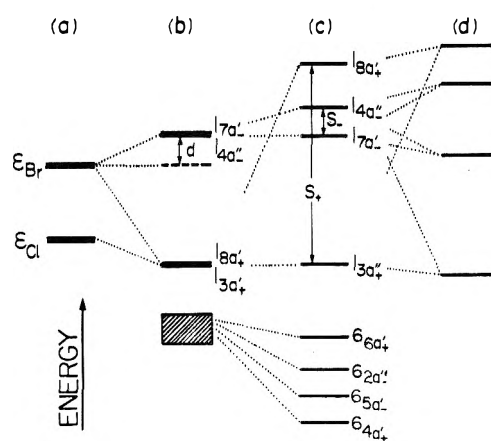
According to a CNDO/BW calculation<sup>15</sup> on the molecule, the first four lone pair IP's in increasing order are related to the  $\sigma$  orbitals,  $\sigma_{6a+}'$ ,  $\sigma_{2a-}''$ ,  $\sigma_{5a-}'$ , and  $\sigma_{4a+}'$ . These  $\sigma$  orbitals can

TABLE II: Calculated MO Parameters (eV) of *trans*-(CF<sub>2</sub>X)<sub>2</sub> and (CH<sub>2</sub>X)<sub>2</sub><sup>a</sup>

	(CF <sub>2</sub> Cl) <sub>2</sub>	(CF <sub>2</sub> Br) <sub>2</sub>			(CF <sub>2</sub> I) <sub>2</sub>			(CH <sub>2</sub> Cl) <sub>2</sub>	(CH <sub>2</sub> Br) <sub>2</sub>	(CH <sub>2</sub> I) <sub>2</sub>
$\zeta$	0.00, 0.035, 0.070	0.00	0.165	0.330	0.00	0.315	0.630	0.070	0.330	0.630
$S$	0.0003	0.0007	0.0007	0.0007	0.0010	0.0010	0.0010	0.0003	0.0005	0.0006
$d$	0.008	0.017	0.017	0.017	0.022	0.022	0.022	0.007	0.011	0.012
$\epsilon_p$	-13.18	-12.20	-12.19	-12.13	-11.08	-11.04	-10.91	-11.82	-10.99	-10.11
$S'_{ag}$	-0.70	-0.78	-0.78	-0.75	-0.95	-0.93	-0.84	-1.05	-0.73	-0.77
$S'_{bu}$	-0.92	-0.94	-0.90	-0.76	-1.25	-1.19	-0.90	-0.96	-0.64	-0.91
$S'_{bg}$	-0.66	-0.52	-0.52	-0.26	-1.29	-1.24	-1.21	-1.06	-0.93	-1.12
$\epsilon_{ag}$	-13.18	-12.26	-12.26	-12.31	-11.07	-11.12	-11.35	-13.09	-12.28	-11.07
$\epsilon_{bu}$	-15.05	-14.14	-14.18	-14.28	-12.83	-12.91	-13.17	-13.95	-13.57	-12.77
$\epsilon_{bg}$	-16.69	-15.92	-15.92	-15.97	-15.31	-15.34	-15.36	-15.02	-14.75	-14.50
$S_{ag}$	+0.70	+0.74	0.74	0.74	0.94	0.88	0.94	0.59	0.33	0.43
$S_{bu}$	+0.38	+0.39	0.35	0.39	0.66	0.59	0.66	0.37	0.15	0.28
$S_{bg}$	+0.12	+0.07	0.07	0.07	0.36	0.33	0.36	0.32	0.22	0.27

<sup>a</sup> These parameters reproduce the observed IP's within experimental error.TABLE III: Calculated MO Parameters (eV) of *trans*-CF<sub>2</sub>BrCH<sub>2</sub>Br, *trans*-CH<sub>2</sub>BrCH<sub>2</sub>Cl, and *gauche* (CF<sub>2</sub>I)<sub>2</sub><sup>a</sup>

	<i>trans</i> -CF <sub>2</sub> BrCH <sub>2</sub> Br			<i>trans</i> -CH <sub>2</sub> BrCH <sub>2</sub> Cl			<i>gauche</i> (CF <sub>2</sub> I) <sub>2</sub>		
$\zeta_{BrH}$	0.00	0.165	0.330	$\zeta_{Br}$	0.33	$\zeta$	0.00	0.315	0.630
$\zeta_{BrF}$	0.00	0.165	0.165	$\zeta_{Cl}$	0.07	$\epsilon_p$	-11.17	-11.17	-11.19
$S$	0.001	0.001	0.001	$S$	0.001	$S_{a-}$	0.19	0.19	0.22
$d$	0.002	0.002	0.001	$d$	0.000	$S_{b-}$	0.79	0.79	0.79
$\epsilon_{BrH}$	-11.46	-11.46	-11.44	$\epsilon_{Br}$	-11.37	$S_{a+}$	0.91	0.91	0.94
$\epsilon_{BrF}$	-11.65	-11.64	-11.64	$\epsilon_{Cl}$	-11.52				
$S'_+$	-1.14	-1.12	-1.12	$S'_+$	-0.95				
$S'_-$	-0.95	-0.94	-0.91	$S'_-$	-1.33				
$\epsilon'_{a+}$	-13.71	-13.72	-13.72	$\epsilon'_{a+}$	-12.46				
$\epsilon'_{a-}$	-12.36	-12.37	-12.41	$\epsilon''_{a-}$	-13.24				
$S_+$	0.50	0.49	0.49	$S_+$	0.59				
$S_-$	0.60	0.59	0.55	$S_-$	0.69				

<sup>a</sup> These parameters reproduce the observed IP's within experimental error.Figure 4. Qualitative MO diagram of *trans*-CH<sub>2</sub>BrCH<sub>2</sub>Cl (a) no perturbation, (b) through space interaction, (c) through bond interaction added, and (d) spin-orbit coupling added.

interact with LPMO's of the same symmetry.<sup>10</sup> Since the energy gap between the LPMO's and  $\sigma_{5a-}$  and  $\sigma_{4a+}$  is large, only  $\sigma_{6a+}$  and  $\sigma_{2a-}$  are considered to mix appreciably with the LPMO's. Under the operation of this perturbation, the ordering of the LPMO's in increasing IP's are (1)  $a_{-}'$ ,  $a_{-}'$ ,  $a_{+}'$ , and  $a_{+}''$ , (2)  $a_{-}''$ ,  $a_{+}'$ ,  $a_{-}'$ , and  $a_{+}'$ , or (3)  $a_{+}'$ ,  $a_{-}''$ ,  $a_{-}'$ , and  $a_{+}''$ . Furthermore, these LPMO's interact with each other via the spin-orbit coupling and the coupling constants are different for chlorine  $\zeta_{Cl}$  and bromine  $\zeta_{Br}$ , with  $\zeta_{Br} > \zeta_{Cl}$ . In ethyl bromide and chloride,<sup>16,17</sup> the first PE bands have a splitting almost equal to  $\zeta_x$  of the bromine atom and the chlorine atom. This reflects that the LPMO's of the halogen atom in ethyl halides are little perturbed by the spin-orbit interaction. This should be true also for CH<sub>2</sub>BrCH<sub>2</sub>Cl. Therefore  $\zeta_{Cl}$  and  $\zeta_{Br}$  are assigned to have values of 0.07 and 0.33 eV, respectively. On the assumption<sup>12</sup> that the electron ejected from the LPMO has  $\beta$  spin only, then the secular determinant corresponding to the above MO model can be written as in eq 4 for  $1_{7a-}$ ,  $1_{8a+}$ ,

$$\begin{vmatrix}
 \epsilon_{Br} + d - \epsilon & 0 & \frac{i}{2}(C_{11}{}^2\zeta_{Br} + C_{12}{}^2\zeta_{Cl}) & 0 & 0 & 0 \\
 0 & \epsilon_{Cl} - d - \epsilon & 0 & \frac{i}{2}(C_{12}{}^2\zeta_{Br} + C_{11}{}^2\zeta_{Cl}) & S_+' & 0 \\
 -\frac{i}{2}(C_{11}{}^2\zeta_{Br} + C_{12}{}^2\zeta_{Cl}) & 0 & \epsilon_{Br} + d - \epsilon & 0 & 0 & S_-' \\
 0 & -\frac{i}{2}(C_{12}{}^2\zeta_{Br} + C_{11}{}^2\zeta_{Cl}) & 0 & \epsilon_{Cl} - d - \epsilon & 0 & 0 \\
 0 & S_+' & 0 & 0 & \epsilon_{a_+}'' - \epsilon & 0 \\
 0 & 0 & S_-' & 0 & 0 & \epsilon_{a_-}'' - \epsilon
 \end{vmatrix} = 0 \quad (4)$$

$1_{4a-}$ ,  $1_{3a+}$ ,  $\sigma_{6a+}$ , and  $\sigma_{2a-}$ , respectively. The coefficients  $C_{11}$  and  $C_{12}$  in the determinant come from the *through space* interaction. Since  $C_{11}$  is found to be much greater than  $C_{12}$  in the calculation,  $C_{11}$  is simply set equal to one, and  $C_{12}$  to zero. Table III lists the calculated MO parameters that reproduce the observed IP's within experimental error. Although there are three possible orderings in the LPMO as mentioned above, the eigenvectors of eq 3 indicate that they all give the same ordering as listed in Table III.

With regard to VII, the interactions between the LPMO's themselves as well as with the  $\sigma$  orbitals are essentially the same as those in VIII. In VII, the Coulomb energy  $\epsilon_{BrH}$  for bromine with hydrogen attached to the same carbon is expected to be higher than  $\epsilon_{BrF}$  for bromine with fluorine attached to the carbon because of the greater electron-withdrawing nature of fluorine. We also assume that  $\zeta_{BrH}$  is greater than  $\zeta_{BrF}$  for the same reason. Since both  $\zeta_F$  and  $\zeta_{Br}$  are unknown for VII,  $\zeta_{BrH}$  and  $\zeta_{BrF}$  are assigned to have values 0,  $\zeta_X/2$ , and  $\zeta_X$  (Table III).

A CNDO/BW calculation<sup>15</sup> on VII indicates that the two highest occupied MO's are  $\sigma_{10a-}$  and  $\sigma_{9a+}$ . The repulsion between these orbitals destabilize  $1_{11a-}$  and  $1_{12a+}$ . Now, there are also three possible orderings in the LPMO, these being the same as those given for VIII. In this case, it is difficult to find the exact orderings owing to the appreciable amount of mixing between the orbitals. The parameters used to reproduce the observed IP's are given in Table III.

## Results and Discussion

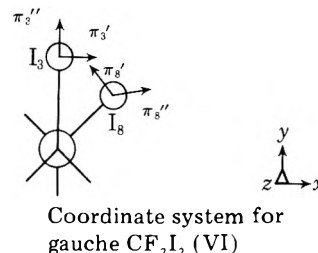
(a) *Interpretation of the Spectra.*  $(CF_2Cl)_2$ ,  $(CF_2Br)_2$ ,  $(CF_2I)_2$ , and  $CF_2BrCH_2Br$ . The He I PE spectra of IV–VII (Figures 1 and 2a) are similar to each other. Each consists of a high-intensity band accompanied by seven or eight broad overlapping bands. These low-intensity bands correspond to ionization of electrons from  $\sigma$  orbitals. The assignment of these IP's (Table I) is based on the relative intensity of the PE bands as well as the result of CNDO/2<sup>11</sup> or CNDO/BW<sup>15</sup> calculations. The MO calculations<sup>11</sup> also show that  $\sigma_{4b_g}$ ,  $\sigma_{4b_u}$ ,  $\sigma_{3b_g}$ , and  $\sigma_{3a_u}$  orbitals of  $(CF_2X)_2$  are mainly composed of fluorine LPMO's.

The first PE band of each of IV–VIII arises from ionization from the four combination of halogen LPMO's which are mixed with each other through interactions mentioned previously. If the population of the trans isomer is very large compared to the gauche form in the vapor phase, this band will give four maxima. However, the spectrum becomes more complicated with an increasing population of the gauche form. In IV, the concentration of the trans rotamer is only slightly higher than that of the gauche. The lowest IP band exhibits a double maxima instead of four bands with not very well-resolved structure. The IP's given in Table I for these peaks are obtained from a band shape analysis which assumed that the trans isomer still gives rise to the main features of the spectrum. However, the uncertainties in the first two IP's are unknown. With regard to V or VII, the situation is less complicated owing to the lower concentration of the gauche form. The first main PE band has four maxima. However, it is impossible to observe peaks from the gauche form as these are buried under those from the trans isomer.

Of all the dihalotetrafluoroethanes studied, only VI gives a well-resolvable structure in the first PE band (Figure 1c). The four sharp and intense peaks in the first band can readily be assigned as arising from the iodine LPMO's of the trans isomer. Each of these peaks is accompanied by a small peak with IP's of 10.21, 10.55, 10.81, and 11.22 eV. A band shape

analysis shows that the intensities of these peaks are almost constant being  $43 \pm 4\%$  of the main peak intensity. It is unlikely that excitation of vibrational modes can account for this intensity. This leads us to suggest that these peaks are mainly contributed from the gauche forms of VI. Assuming the constancy of photoionization cross sections for both isomers as well as the temperature of the collision chamber at 300 K,  $\Delta H_{mol}$  is found to be  $0.92 \pm 0.05$  kcal mol<sup>-1</sup>, compared to 0.95 kcal mol<sup>-1</sup> for V.

$CH_2BrCH_2Cl$ . The He I spectrum of VIII (Figure 2b) is almost the same as that of dihaloethanes.<sup>8</sup> Only four peaks are observable in the region of 12–18 eV. These can be attributed to the ionization of electrons from the  $\sigma$  orbitals. The IP's of these orbitals are somewhere between those of the corresponding orbitals of 1,2-dichloro- and 1,2-dibromoethanes.<sup>5</sup> The first PE band of VIII is similar to that of VI and shows resolvable fine structure. The four sharp peaks come from the LPMO's of the trans isomers. The small peak at 10.50 eV cannot arise from the gauche form of this molecule in accordance with the observations in 1,2-dichloroethane<sup>8</sup> and VI, but rather from an impurity or the fragment  $Br_2$ .<sup>18</sup> The assignment of the peak with an IP of 10.79 eV is not so obvious. The intensity of this peak may partly be enhanced by excitation of  $CH_2$  vibrations, or from ionizations from the LPMO's of the gauche form. On the assumption of the constancy of photoionization cross sections for both isomers, the intensity ratio of the PE bands of the trans and gauche forms is 1:0.2. In fact, a band shape analysis gives a ratio 1:0.3.



(b) *The Orbital Energy in Gauche  $(CF_2I)_2$  ( $C_2$ ).* There are four LPMO's,  $\pi_3'$ ,  $\pi_3''$ ,  $\pi_8''$ , and  $\pi_8'$ , in the gauche form of VI as shown. They can combine spatially with each other to give

$$\begin{aligned} l_{12a+} &= \frac{1}{2}(\pi_3' + \pi_8' + \pi_3'' + \pi_8'') \\ l_{13a-} &= \frac{1}{2}(\pi_3' + \pi_8' - \pi_3'' - \pi_8'') \\ l_{12b+} &= \frac{1}{2}(\pi_3' - \pi_8' + \pi_3'' - \pi_8'') \\ l_{11b-} &= \frac{1}{2}(\pi_3' - \pi_8' - \pi_3'' + \pi_8'') \end{aligned} \quad (5)$$

with

$$\begin{aligned} \pi_3' &= x_3 \\ \pi_3'' &= \frac{1}{3}y_3 - \frac{2\sqrt{2}}{3}z_3 \\ \pi_8' &= \frac{1}{2}x_8 + \frac{\sqrt{3}}{2}y_8 \\ \pi_8'' &= \frac{1}{2\sqrt{3}}x_8 + \frac{1}{6}y_8 + \frac{2\sqrt{2}}{3}z_8 \end{aligned} \quad (6)$$

where  $x_i$  denotes the  $p_x$  orbital of the  $i$ th time.

In addition, some of these LPMO's are destabilized by mixing with  $\sigma$  MO's of proper symmetry. A CNDO/BW calculation<sup>15</sup> on the molecule shows that the first three frontier  $\sigma$  orbitals are  $\sigma_{11a+}$ ,  $\sigma_{10b-}$ , and  $\sigma_{10a-}$  in order of increasing IP's. It is difficult to distinguish the IP's of the  $\sigma$  MO's of the trans



**TABLE IV: Urey-Bradley Force Constants (mdyn/Å) of Trans and Gauche (CH<sub>2</sub>Cl)<sub>2</sub> and (CH<sub>2</sub>Br)<sub>2</sub><sup>a</sup>**

	<i>trans</i> - (CH <sub>2</sub> Cl) <sub>2</sub>	<i>gauche</i> - (CH <sub>2</sub> Cl) <sub>2</sub>	<i>trans</i> - (CH <sub>2</sub> Br) <sub>2</sub>	<i>gauche</i> - (CH <sub>2</sub> Br) <sub>2</sub>
$K_{CC}$	2.99	3.21	2.93	2.96
$K_{CX}$	2.71	2.28	1.97	1.93
$H_{CCX}$	0.19	0.25	0.16	0.15
$F$	0.39	0.23	0.43	0.38

<sup>a</sup>  $K_{CC}$ ,  $K_{CX}$ ,  $H_{CCX}$ , and  $F$  are the C-C stretch, C-X stretch, CCX bending, and nonbonded repulsive force constants, respectively.  $F' = -0.1F$ .

from the *gauche* form owing to the overlapping nature of PE bands in the spectrum. A similar treatment on the *through bond* interaction for *trans*-(CF<sub>2</sub>X)<sub>2</sub> is not applicable in this case. The *through bond* interaction parameter is considered as a diagonal element in the secular equation (eq 7). When the spin-orbit coupling is taken into account, a secular determinant (eq 7) can be set up for  $1_{12a+}$ ,  $1_{13a-}$ ,  $1_{12b+}$ , and  $1_{11b-}$ ,

$$\begin{vmatrix} 1.086\epsilon_p + S_{a+} - \epsilon & 0 \\ 0 & 0.984\epsilon_p + S_{a-} - \epsilon \\ 0 & +i\zeta/6 \\ -i\zeta/6 & 0 \end{vmatrix} = 0$$

respectively. The solutions of eq 7 with  $\zeta = 0.0$ ,  $\zeta_x/2$ , and  $\zeta_x$  are given in Table II. It should be mentioned that the value of  $K$  used here is one,<sup>19</sup> instead of two, in our previous calculation because of unreasonable low value obtained for  $\epsilon_p$  when  $K$  equals to two. In the *trans* isomer, the choice of  $K$  is unimportant owing to the smallness of the *through space* interaction. With  $K$  equal to one, the change in values of the parameters given in Tables II and III is within  $\pm 0.02$  eV.

It is interesting to note that  $\epsilon_p$  for the *gauche* form is lower than for the *trans* form. The same applies to *cis*- and *trans*-1,2-diiodoethylene.<sup>20</sup> It seems that the "effective" electronegativity of the halogen is increased with a larger *through space* interaction. This parallels the results of calculations on the chloro- and bromomethanes.<sup>22</sup>

In 1,2-dichloroethane,<sup>8</sup> the *trans* isomer is found to be more stable which is also the case for the molecular ion.<sup>8</sup> However, the energy difference between the two isomeric ions  $\Delta H_{ion}$  is not known. In VI, both peaks arising from LPMO's of *trans* and *gauche* rotamers are discernible in the PE spectrum. If the energies of the frontier MO's of both isomers are taken to be the same, the *trans* ion is found to be more stable than the *gauche* by 0.14 eV ( $\Delta H_{mol}$  is  $\sim 0.04$  eV from the previous discussion). Taking the difference in  $\epsilon_p$  between the *trans* and *gauche* forms into account,  $\Delta H_{ion}$  is estimated to be 0.06 eV, almost the same as  $\Delta H_{mol}$ . One would expect the difference  $\Delta H_{ion} - \Delta H_{mol}$  is larger in 1,2-dichloroethane or 1,2-bromochloroethane than in fluorinated dihaloethane.

In Tables III and IV, the quantity  $S_i$  for dibromoethane becomes larger with an increasing number of hydrogen replaced by fluorine. The same observation applies to other dihaloethanes and their respective fluorinated derivatives. This is probably due to more high lying  $\sigma$  MO's being available for *through bond* interaction in the fluorinated compounds. It should be noted that our calculations show that the *through bond* interaction is not the same for the *trans* and *gauche* (CF<sub>2</sub>I)<sub>2</sub> but the interaction is greater in the *gauche* form. If the inductive effect is predominated over other effects and also

no rehybridization occurs in the C-X bond of both isomers, we would also expect that the iodine NMR chemical shift will be larger for the *gauche* while the nuclear quadrupole coupling constants are greater for *trans*.

Since we know  $\epsilon_p$  for both *trans* and *gauche* (CF<sub>2</sub>I)<sub>2</sub>, a force constant calculation in simple Urey-Bradley force field<sup>22</sup> was carried out on both isomers of I and II using the frequencies given in ref 23. In the treatment, only the C-C and C-X stretching as well as CCX bending vibrations were considered. Both the **G** and **F** matrices used are the same as those listed in ref 24. Different sets of force constants are used for the two isomers. The force constants shown in Table IV reproduce the observed frequencies to about  $\pm 5\%$  and the notations used have their usual meaning.<sup>22</sup> In general, the nonbonded repulsive force constant  $F$  increases with decreasing interatomic distance between two nonbonded atoms. However, the constant is found to be smaller in *gauche* than in *trans* form for both I and II. This reflects the attractive nature of the halogen atoms in the *gauche* conformer. In VI,  $\epsilon_p$  for the *gauche* form is lower in the two conformers. This implies that the electron is more delocalized over the C-I bond in the *gauche* form if the

$$\begin{vmatrix} 0 & +i\zeta/6 \\ -i\zeta/6 & 0 \\ 0.914\epsilon_p - \epsilon & 0 \\ 0 & 1.016\epsilon_p + S_{b-} - \epsilon \end{vmatrix} = 0 \quad (7)$$

inductive effect only is considered. Therefore, the C-I bond should be stronger in the *gauche* than in the *trans* form. If the same situation occurs in 1,2-dihaloethane, one would expect higher C-X stretching force constant in *gauche* than in *trans* isomer. In fact, the calculated values of  $K_{CX}$  (Table IV) show that this expectation is fulfilled.

## Conclusion

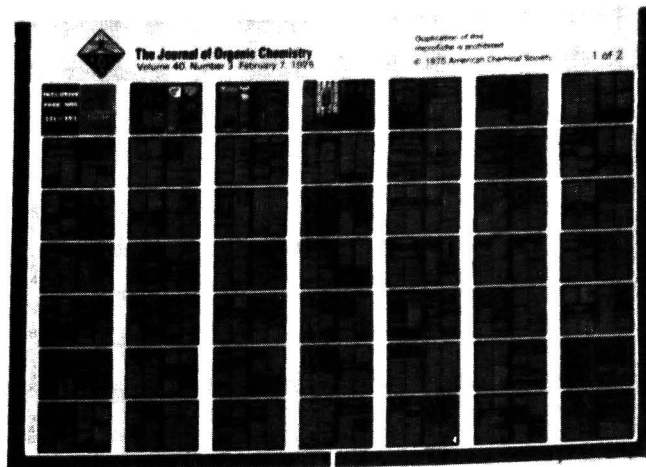
The PE spectra of five substituted ethanes, namely, (CF<sub>2</sub>Cl)<sub>2</sub>, (CF<sub>2</sub>Br)<sub>2</sub>, (CF<sub>2</sub>I)<sub>2</sub>, CH<sub>2</sub>BrCH<sub>2</sub>Cl, and CF<sub>2</sub>BrCH<sub>2</sub>Br, can be interpreted quantitatively by using one-electron models with inclusion of spin-orbit coupling as well as *through bond* and *through space* interactions. In the molecules studied, the *through space* interactions are small compared to the *through bond* interactions which are proportional to energy gap between the two interacting orbitals. With regard to (CF<sub>2</sub>I)<sub>2</sub>, the *gauche* form seems to be observed. Variable temperature PES work is now in progress to determine the conformational energy of the molecule.

**Acknowledgments.** We thank the National Research Council of Canada for generous financial grants. One of us (F.T.C.) thanks the University of British Columbia for an award of a Graduate Fellowship.

## References and Notes

- (1) N. Sheppard, *Adv. Spectrosc.*, **1**, 288 (1959).
- (2) H. P. Buckner and J. R. Nielsen, *J. Mol. Spectrosc.*, **11**, 47 (1963).
- (3) K. Tanabe, *Spectrochim. Acta, Part A*, **28**, 407 (1972).
- (4) R. E. Kagarise, *J. Chem. Phys.*, **26**, 380 (1957).
- (5) R. E. Kagarise and L. W. Daasch, *J. Chem. Phys.*, **23**, 130 (1955).
- (6) K. R. Crook, P. J. D. Park, and E. Wyn-Jones, *J. Chem. Soc. A*, 130 (1969).
- (7) M. Iwasaki, *Bull. Chem. Soc. Jpn.*, **31**, 1071 (1958); **32**, 205 (1959).
- (8) F. T. Chau and C. A. McDowell, *J. Electron Spectrosc.*, **6**, 365 (1975).
- (9) T. Koopmans, *Physica*, **1**, 104 (1934).
- (10) R. Hoffman, *Acc. Chem. Res.*, **4**, 1 (1971); R. Hoffman, A. Imamura, and W. J. Hehre, *J. Am. Chem. Soc.*, **90**, 1499 (1968).
- (11) J. A. Pople and D. L. Beveridge, "Approximate Molecular Orbit Theory".

- McGraw-Hill, New York, N.Y., 1970.
- (12) F. Brogli and E. Heilbronner, *Helv. Chem. Acta*, **54**, 1423 (1971).
- (13) J. Doucet, P. Sauvageau, and C. Sandorfy, *J. Chem. Phys.*, **62**, 355 (1975).
- (14) C. J. Ballhausen and H. B. Gray, "Molecular Orbital Theory", W. A. Benjamin, New York, N.Y., 1965.
- (15) R. J. Boyd and M. A. Whitehead, *J. Chem. Soc., Dalton Trans.*, 73 (1972).
- (16) K. Kimura, S. Katsumata, Y. Achiba, and H. Matsumoto, *Bull. Chem. Soc. Jpn.*, **46**, 373 (1973).
- (17) J. A. Hashmall and E. Heilbronner, *Angew. Chem., Int. Ed. Engl.*, **9**, 305 (1970).
- (18) D. W. Turner, C. Baker, a. D. Baker, and C. R. Brundle, "Molecular Photoelectron Spectroscopy", Wiley, New York, N.Y., 1970.
- (19) R. Hoffman, *J. Chem. Phys.*, **39**, 1397 (1963).
- (20) F. T. Chau and C. A. McDowell, to be submitted for publication.
- (21) R. N. Dixon, J. N. Murrell, and B. Narayan, *Mol. Phys.*, **20**, 611 (1971).
- (22) T. Shimanouchi, *J. Chem. Phys.*, **17**, 245 (1949).
- (23) T. Shimanouchi, *Natl. Stand. Ref. Data Ser., Natl. Bur. Stand.*, **No. 6**, Part 1 (1967).
- (24) S. Mizushima, "Structure of Molecules and Internal Rotation", Academic Press, New York, N.Y., 1954.



# MICROFORMS

American Chemical Society publications in microform

## MICROFILM OR MICROFICHE?

With the ACS microform program you can receive either, or both

### Microfilm

All periodical publications back to volume one

Copying privileges included with current subscriptions

All non-print supplementary materials provided free on microfiche

Archival quality silver halide film supplied as you request; positive or negative; 16 or 35mm; cartridge, reel, or cassette.

For microfilm information:

#### Special Issues Sales

American Chemical Society  
1155 16th Street, N.W.  
Washington, D.C. 20036  
(202) 872-4363

### Microfiche

Current issues of primary journals, beginning with January 1975

Individual issues or full volumes available

Supplementary materials also available on microfiche

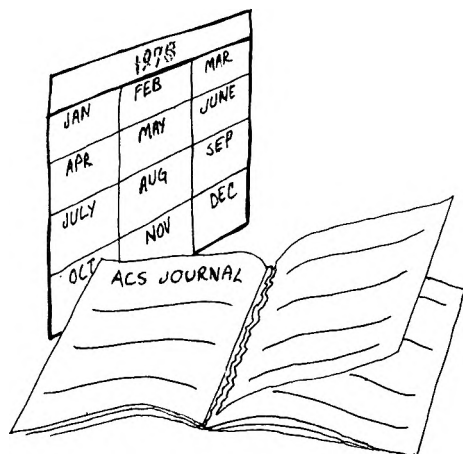
Fiche supplied are archival quality silver halide, negative, 105 x 148mm (4" x 6"); 24x, with eye legible headers, start and end targets, and page numbers

For microfiche information:

#### Business Operations

Books and Journals Division  
American Chemical Society  
1155 16th Street, N.W.  
Washington, D.C. 20036  
(202) 872-4444

# TIMELY TEARSHEETS



Here's an opportunity to choose any article you wish which has been published during the past 12 months in any one of the American Chemical Society journals.\*

The price for this service is very modest—just \$2.50 for the first copy and \$1.25 for each additional copy.

Also, if you wish, you may select articles which have appeared in earlier non-current ACS journal issues, but these will be photocopies rather than tearsheets and an additional 50¢ is required per article.

All you have to do is fill in the order forms below, *include your payment*, mail now, and we'll do the rest.

1. Give complete details for each article. Sorry, we cannot provide a search service.
2. **PRINT** or **TYPE** all information, including label.
3. Make check or money order payable to the AMERICAN CHEMICAL SOCIETY, and mail to: ACS, Business Operations, Books and Journals Division, 1155 16th Street, N.W., Washington, D.C. 20036.

Name \_\_\_\_\_

Address \_\_\_\_\_

City \_\_\_\_\_

State/Zip \_\_\_\_\_

## AMERICAN CHEMICAL SOCIETY JOURNALS TIMELY TEARSHEETS      Order Form

The following article(s) came to my attention in a recent issue of one of the ACS journals. I would like to order the number of tearsheets of each article indicated in the box(es).

ACS Journal \_\_\_\_\_ ☐

Title \_\_\_\_\_

Author(s) \_\_\_\_\_

Issue Date \_\_\_\_\_ Page(s) \_\_\_\_\_

ACS Journal \_\_\_\_\_ ☐

Title \_\_\_\_\_

Author(s) \_\_\_\_\_

Issue Date \_\_\_\_\_ Page(s) \_\_\_\_\_

ACS Journal \_\_\_\_\_ ☐

Title \_\_\_\_\_

Author(s) \_\_\_\_\_

Issue Date \_\_\_\_\_ Page(s) \_\_\_\_\_

\* Copyright restrictions prevent us from providing copies from other than ACS journals

\$2.50 for the first tearsheet.

\$1.25 for each additional tearsheet ordered at the same time.

\$ \_\_\_\_\_  
**Total Enclosed**

These prices do not apply to articles from Chemical Reviews and Journal of Physical and Chemical Reference Data. For information regarding cost of these copies, contact the Books and Journals Division, ACS.



**TIRED of  
searching through  
dozens of  
publications?**

# **WE CAN PUT AN END TO ALL THAT!**

**As an ACS member,  
you may now subscribe to the new,  
semimonthly service called  
ACS CUSTOMIZED ARTICLE SERVICE**

The **key feature** of this service will be a comprehensive selection of **articles of interest to you** from all the ACS journals except C&EN and CHEMISTRY. You'll receive the complete articles (on microfiche) and not a list of references. Along with these you'll receive monthly hard copies of ENVIRONMENTAL SCIENCE & TECHNOLOGY or the JOURNAL OF MEDICINAL CHEMISTRY depending on your choice of subject area. And in addition, we'll send you the semimonthly ACS SINGLE ARTICLE ANNOUNCEMENT.

The number of articles you receive is expected to **average** between 20 to 30 in each semimonthly package. All in all, you'll be getting a really significant amount of information for the modest sum of \$75 a year!

All you have to do to start this valuable service in **January 1977** is to fill out the form at the bottom of this ad and send it back to us today. The **IMPORTANT** thing is to make sure you are one of the charter subscribers to ACS CUSTOMIZED ARTICLE SERVICE. We'll take care of the rest.

**American Chemical Society**  
1155 Sixteenth Street, N.W.  
Washington, D.C. 20036

Yes . . . I would like to start the new service called ACS CUSTOMIZED ARTICLE SERVICE, in January 1977.

	U.S.	PUAS, Canada, Other Nations
One Year	\$75.00/per	\$100.00/per subject
ACS MEMBERS ONLY	subject area	area

Please indicate to which subject area(s) you want to subscribe:

Environmental Chemistry ( )  
Medicinal Chemistry ( )

☐ Please send me information on Microfiche Readers

NAME \_\_\_\_\_

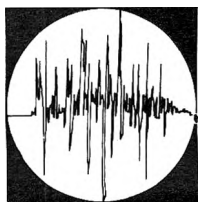
ADDRESS \_\_\_\_\_

CITY \_\_\_\_\_

STATE \_\_\_\_\_

ZIP \_\_\_\_\_

# INSTRUMENTATION IN ANALYTICAL CHEMISTRY



An ACS Reprint Collection comprising 43 articles from Volumes 41-44 of *Analytical Chemistry*. Collected by Alan J. Senzel, Associate Editor of *Analytical Chemistry*.

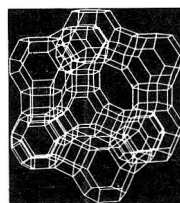
This up-to-date collection of articles provides an extensive and authoritative account of the latest advances in the various fields of instrumentation.

Over forty articles deal with four broad areas of analytical chemistry—spectrometry, chromatography, electrochemistry, and combination and other techniques. Specific topics focus upon instrument design, biomedical instrumentation, pollution measurement devices, and computer applications.

428 pages (1973) Hardback, \$9.95; Paperback, \$5.50. Postpaid in U.S. and Canada, plus 40 cents elsewhere.

Order from:  
**Special Issues Sales**  
**American Chemical Society**  
1155 16th St., N.W.  
Washington, D.C. 20036

# Zeolite Chemistry and Catalysis



Chemists, material scientists, and chemical engineers working in the areas of catalysis and material science related to the petroleum and chemical industry will find this volume a useful and valuable addition to their reference library.

ACS  
MONOGRAPH  
171

Julé A. Rabo,  
Editor

*A comprehensive overview of all important aspects of zeolite catalysis according to structure, chemistry and mechanism, and technology.*

Specific topics include:

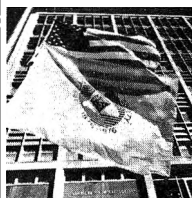
- origin and structure; IR studies of surfaces and surface reactions; stability and ultrastable zeolites
- salt occlusion in zeolite crystals; ESR studies; diffusion; hydrocarbon transformations; molecules containing hetero atoms; metal-containing zeolites
- shape selective catalysis; preparation and performance of cracking catalysts; hydrocracking, isomerization, and other industrial processes

796 pages (1976) clothbound \$65.00  
LC 76-17864 ISBN 0-8412-0276-1

Order from:  
**Special Issues Sales**  
**American Chemical Society**  
1155 Sixteenth St., N.W.  
Washington, D.C. 20036

# A Century of Chemistry

*The Role of Chemists and the American Chemical Society*



Herman Skolnik,  
Chairman, Editorial Board  
Kenneth M. Reese,  
Editor

*An illuminating portrait of the life and times of the world's largest scientific society devoted to a single discipline.*

The book portrays the growth and activities of the ACS in the context of a century that saw two World Wars, the Great Depression, the Cold War, the Space Race, the environmental movement, and numerous scientific and engineering advances.

The volume traces the development of chemical science and technology in the framework of the 27 technical divisions of the Society. It includes a compact, 100-year record of ACS people and events.

*Part One: Historical Perspectives, Chemical Education, Professionalism, Publications, Impact of Government, Public Affairs, Intersociety Relations, Governance, Headquarters Staff and Operations, ACS Divisions and their Disciplines. Part Two: The Record—a list of past presidents, chairmen, members of the board of directors, editors, award winners, and more.*

468 pages (1976) \$15.00 clothbound  
LC 76-6126 ISBN 0-8412-0307-5

**Special Issues Sales**  
**American Chemical Society**  
1155 Sixteenth St., N.W.  
Washington, D.C. 20036

Second  
Series by  
Norman Metzger  
Introduction  
by  
Isaac  
Asimov

men and molecules

A significant and absorbing new book about the latest chemical achievements of the seventies based on interviews with Nobel-Prize-winning scientists, first aired on the radio series "Men & Molecules" sponsored by the American Chemical Society

This fascinating volume tells about some of the extraordinary breakthroughs taking place in laboratories around the world today that will have far-reaching effects on our future lives

Read more about the exciting implications of current research into:

- the riddle of aging
- the quest for molecules which may be the origin of stars and the "soup" in which life began
- Russian water
- the creation of superheavy elements
- the search for neutrinos which may reveal how the sun burns
- the race to synthesize ribonuclease
- genetics, nitrogen fixation, insect chemistry, and polluted oceans

Besides presenting recent discoveries, this compelling book offers valuable insight into the nature of scientific research with its constantly changing "truth." Written in easy-to-follow, non-technical language, it will interest the general reader, scientist, and student who can relate class work to modern-day experiments

246 pages with index & bibliography. Cloth (1972) \$5.95. A Crown Publishers book Postpaid in U.S. and Canada, plus 40¢ elsewhere.

Order from: **Special Issues Sales**  
**American Chemical Society**  
1155 Sixteenth St., N.W.  
Washington, D.C. 20036

# *New Tape Recordings on* **ENERGY**

## ☐ **FUELS FOR THE NEXT 50 YEARS**

A Panel Discussion  
Length: 178 minutes  
7 Speakers—15 Figures  
Price: \$18.00

### **The Panel:**

**G. R. Hill**—Direct Utilization of Coal  
**L. G. Massey**—Gaseous Fuels from Coal and Petroleum  
**E. Gorin**—Liquid Fuels from Coal  
**R. J. Cameron**—Liquid Fuels from Petroleum and Oil Shale  
**T. J. Joyce**—Natural Gas and LNG  
**D. P. Gregory**—Hydrogen, Methanol, and Other Nonconventional Fuels  
**I. Wender**—Fuels from Plant and Waste Materials  
Each speaker briefly discusses his subject; the panel then engages in a freewheeling, give-and-take discussion of the energy problem and suggested solutions.

## ☐ **COAL—NATURE'S BLACK DIAMOND**

Length: 136 minutes  
4 Speakers—61 Figures  
Price: \$18.00

### **The Speakers:**

**R. T. Eddinger**—Coal—Nature's Black Diamond  
**R. F. Moran**—Genesis of a Formed-Coke Process  
**J. F. Jones**—Clean Fuels for Power Generation from High-Sulfur Coals  
**L. Seglin**—The COGAS Process for Pipeline Gas  
This symposium presents a incisive look at coal as a source for synthetic fuels and includes general economic and process details of the COED and COGAS processes.

## **LOW SULFUR LIQUID FUELS FROM COAL**

Length: 148 minutes  
5 Speakers—66 Figures  
Price: \$18.00

### **The Speakers:**

**J. G. Guin**—Photomicrographic Studies of Coal Dissolution  
**H. E. Lebowitz**—Deashing of Coal Liquefaction Products via Partial Deasphalting-Hydrogen Donor Extraction Effluents  
**C. J. Kulik**—Deashing of Coal Liquefaction Products via Partial Deasphalting-Hydrogenation and Hydroextraction Effluents  
**H. P. Malone**—Characterization and Upgrading of Coal Liquids to High Value Fuels and Chemicals

Processes for upgrading liquids extracted from coal are described and first details of a new coal liquefaction process from Gulf Oil are revealed.

## ☐ **THE ROLE OF TECHNOLOGY IN THE ENERGY CRISIS**

Length: 128 minutes  
4 Speakers—60 Figures  
Price: \$18.00

### **The Speakers:**

**H. H. Hasiba**—Contribution of Enhanced Recovery Technology to Domestic Crude Oil  
**R. N. Quade**—Process Applications of Nuclear Heat  
**L. W. Russman**—Engineering Perspective of a Hydrogen Economy  
**A. Decora**—Oil Shale Development and its Environmental Considerations  
In-depth examination of the gains—and problems—which state-of-the art technology will bring if brought to bear on our energy problems.

## ☐ **UNUSUAL FUELS PRODUCTION**

Length: 138 minutes  
5 Speakers—91 Figures  
Price: \$18.00

### **The Speakers:**

**D. L. Klass**—Long-Range Approach to the Natural Gas Shortage Utilizing Nonfossil Renewable Carbon  
**R. G. Sheehan**—Methanol or Ammonia Production from Solid Waste by the City of Seattle  
**W. A. Scheller**—Production of Ethanol and Vegetable Protein by Grain Fermentation  
**P. E. Cassidy**—Use of Methanol as a Motor Fuel  
**W. A. Scheller**—Performance of an Ethanol-Gasoline Blend in Automobiles and Light Trucks

An up-to-date rundown of results achieved in programs to use methanol and ethanol as additives in motor fuel, and details of advanced projects to use solid waste and biomass as sources of fuels.

## **AVAILABLE ON TAPE CASSETTES ONLY**

**PRICES:** \$18.00 per Title (Postpaid)  
\$45.00 Any THREE Titles (Postpaid)

### **ORDER FROM:**

American Chemical Society  
1155 Sixteenth Street, N.W.  
Washington, D.C. 20036  
Dept. AP

NAME: \_\_\_\_\_

ADDRESS: \_\_\_\_\_

City \_\_\_\_\_ State \_\_\_\_\_ Zip \_\_\_\_\_

(Allow 4 to 6 weeks for delivery)



# New... for the Physical Chemist

## HANDBOOK OF CHEMICAL LASERS

Edited by **R.W.F. Gross & J.F. Bott**

Collects and critically reviews all available literature and the entire body of research work in the field of chemical lasers published and performed between 1967 and 1974. Provides a reference sourcebook for the engineers and systems analysts who are going to plan and perform the future development of the field.

744 pp. (0 471 32804-9) 1976 \$39.95

## ADVANCES IN CHEMICAL PHYSICS, Vol. 35

**I. Prigogine & Stuart A. Rice**

CONTENTS: Theories of Chemically Induced Electron Spin Polarization. Kinetic Theory and Rheology of Macromolecular Solutions. Kinetic Theory of Gravitational Systems. Magnetic Circular Dichroism. Time-Dependent Perturbation of a Two-State Quantum System by a Sinusoidal Field.

*Advances in Chemical Physics Series.*

358 pp. (0 471 69937-3) 1976 \$29.75

## ADVANCES IN CHEMICAL PHYSICS, Vol. 34

**I. Prigogine & Stuart A. Rice**

CONTENTS: The Rotation of Molecules in Dense Phases. Roles of Repulsive and Attractive Forces in Liquids: The Equilibrium Theory of Classical Fluids. Recent Advances in the Study of Liquids by X-Ray Diffraction. Diffraction by Molecular Liquids. The Expansion of the Master Equation.

*Advances in Chemical Physics Series.*

324 pp. (0 471 69936-5) 1976 \$28.95

## POINT DEFECTS IN CRYSTALS

**R.K. Watts**

A unified treatment of defects in a variety of semiconducting and other crystals. Provides scientists and engineers with a reference on defect-related electrical and optical properties of crystals, and may also serve as an introductory text on the subject.

approx. 320 pp. (0 471 92280-3) 1977 \$21.95

## SYMMETRY RULES FOR CHEMICAL

### REACTIONS: Orbital Topology and Elementary Processes

**Ralph G. Pearson**

Discusses the detailed paths of important elementary reactions (concerted processes) of both organic and inorganic molecules. The methods used are easiest to apply when at least one element of symmetry persists in going from reactants to products by the specific reaction path. However, rules are also given based on more general topological properties. The book uses a molecular orbital approach throughout, and presents a novel perturbation theory treatment along with many useful methods for estimating the feasibility of a given reaction path.

548 pp. (0 471 01495-8) 1976 \$24.50

## PRINCIPLES OF ULTRAVIOLET PHOTOELECTRON SPECTROSCOPY

**J. Wayne Rabalais**

A detailed presentation of the principles of UV photoelectron spectroscopy in terms of modern chemical physics, i.e., the phenomenon of photoionization and its resulting consequences by means of modern quantum chemical methods. Includes a table of molecules with references to PE spectra as well as numerous illustrations, examples, and mathematical derivations.

approx. 480 pp. (0 471 70285-4) 1976 \$29.95

## TECHNIQUES OF CHEMISTRY, Vol. 8

### Part 2: Solutions and Solubilities

Edited by **Michael R.J. Dack**

A collection of authoritative articles examining the complex subject of solutions in terms of their industrial and biological significance. Covers molecular thermodynamics, solvation of ions, influence of ions, influence of solvents on spectroscopy, chemical technology, molecular complex equilibria, and gases.

499 pp. (0 471 93125-X) 1976 \$34.50

## THE HYDROLYSIS OF CATIONS

**Charles F. Baes, Jr. & Robert E. Mesmer**

A general reference which assists the reader in dealing with the array of hydroxy species that complicate the chemical behavior of metallic elements in aqueous solutions. It critically evaluates information on identities and stabilities of species in solution and the solid hydroxides and oxides produced therefrom.

489 pp. (0 471 03985-3) 1976 \$29.95

## PHOTOCHEMISTRY OF HETEROCYCLIC COMPOUNDS

Edited by **Ole Buchardt**

Offers a comprehensive, varied treatment of heterocyclic reactions and transformations in organic synthesis in a collection of articles by internationally respected authorities. The book affords a quick and easy check of most essential photochemical reactions of heterocyclic types of compounds, and the liberal use of formulae makes rapid scanning convenient. General Heterocyclic Chemistry Series.

622 pp. (0 471 11510-X) 1976 \$49.50

## HANDBOOK OF PROTON IONIZATION HEATS

**James J. Christensen, Lee D. Hansen, & Reed M. Izatt**

An extensive compilation that includes all acids for which  $\Delta H$  values are available (approximately 1,290 entries). Contains a complete listing of the heats of proton ionization,  $\Delta H$ , together with the related thermodynamic quantities,  $pK$ ,  $\Delta S$ , and  $\Delta C_p$ .

269 pp. (0 471 01991-7) 1976 \$22.50

## OPTICAL RESONANCE AND TWO-LEVEL ATOMS

**L. Allen & J.H. Eberly**

This book offers an account of the basic principles behind all quantum optical resonance phenomena—an account unified by its systematic reliance on the two-level model for atoms. It explores the consequences of coupling the Bloch and Maxwell equations at a level suited to the requirements of those interested in laser physics seeking a basic explanation of optical resonance in physical terms.

233 pp. (0 471 02327-2) 1975 \$21.25

Available at your bookstore or write to Nat Bodian, Dept. A 2308-51



## WILEY-INTERSCIENCE

a division of John Wiley & Sons, Inc.

605 Third Avenue, New York, N.Y. 10016

In Canada: 22 Worcester Road, Rexdale, Ontario

Prices subject to change without notice.

A 2308-51